

---

# **The ARCADIA<sup>®</sup> Reactor Analysis System for PWRs Methodology Description and Benchmarking Results**

ANP-10297NP(A)  
Revision 0  
Supplement 1

## **Topical Report**

June 2015

AREVA Inc.

---

(c) 2015 AREVA Inc.

**Copyright © 2015**

**AREVA Inc.  
All Rights Reserved**

### **Nature of Changes**

<b>Item</b>	<b>Section(s) or Page(s)</b>	<b>Description and Justification</b>
1	All	Initial Issue

## Contents

	<u>Page</u>
1.0 INTRODUCTION .....	1-1
1.1 References .....	1-4
2.0 APOLLO2-A METHODOLOGY .....	2-1
2.1 Promethium Branching Ratio Modification .....	2-2
2.2 Cross Section Adjustments .....	2-3
2.3 Impact of the Updates to Promethium Branching Ratio and Cross Section Adjustments on Results .....	2-4
2.4 Enhancements to Gamma Calculation .....	2-8
2.5 Enhancements to Delayed Neutron Data .....	2-9
2.6 New Models .....	2-9
2.6.1 Generation of Spacer Grid Form Functions .....	2-10
2.6.2 Large Core Problems .....	2-11
2.6.3 Surface Spectral History Model .....	2-11
2.7 References .....	2-12
3.0 ARTEMIS™ METHODOLOGY .....	3-1
3.1 Additional Search Algorithms .....	3-1
3.2 Enhanced Dehomogenization Model .....	3-1
3.2.1 Surface Spectral History Model .....	3-2
3.2.2 Multi-group Power Form Functions .....	3-4
3.3 Incorporation of Spectral Cross Section Model .....	3-4
3.4 Update of Steam Tables .....	3-5
3.5 Incorporation of a Spacer Grid Model .....	3-6
3.6 Incorporation of Control Rod Cusping Model .....	3-7
3.7 Incorporation of Time Dependent Inlet Temperature, Inlet Mass Flux and Core Exit Pressure Input .....	3-9
3.8 Incorporation of Non-uniform Inlet Temperature Input in Steady-state and Transient Conditions .....	3-9
3.9 Modifications to Parameter Penalization in Steady-state and Transients .....	3-10
3.10 Incorporation of Optimal Time Step Control During Transient Calculations .....	3-10
3.11 Incorporation of Non-uniform Boron Nodal Distribution Model .....	3-10

3.12	Enhanced Coarse-Fine Mesh Coupling .....	3-11
3.13	Incorporation of Excore Detector Model.....	3-11
3.14	Incorporation of Decay Heat Model .....	3-12
3.15	Modification of the MEDIAN Power Distribution Reconstruction Methodology .....	3-12
3.15.1	Determination of Two-group Optimal Fluxes .....	3-15
3.15.2	Extrapolation of the Nodal Fluxes .....	3-16
3.16	References .....	3-18
4.0	APOLLO2-A RE-VALIDATION .....	4-1
4.1	Critical Experiments .....	4-1
4.1.1	Reactivity .....	4-2
4.1.2	Fission Rate Distribution .....	4-5
4.1.3	Discussion of Results - Critical Experiments .....	4-46
4.2	Integral Experiments .....	4-46
4.3	Spent Fuel Analyses .....	4-48
4.4	References .....	4-53
5.0	ARCADIA® RE-VALIDATION OF CORE BENCHMARKS .....	5-1
5.1	Introduction .....	5-1
5.2	Startup Physics Test Measurement .....	5-6
5.2.1	Startup Physics Summary for Plant A Cycles 1-14 .....	5-7
5.2.2	Startup Physics Summary for Plant B Cycle 1 .....	5-13
5.2.3	Startup Physics Summary for Plant C Cycles 10-18 .....	5-13
5.2.4	Startup Physics Summary for Plant E Cycles 12-17 .....	5-19
5.2.5	Startup Physics Summary for Plant G1 Cycles 26-30 .....	5-19
5.2.6	Startup Physics Summary for Plant G2 Cycles 1-5 .....	5-21
5.2.7	Startup Physics Summary for Plant S1 Cycles 12-14 .....	5-23
5.2.8	Startup Physics Summary for Plant S2 Cycles 12-14 .....	5-27
5.2.9	Startup Physics Summary for Plant T1 Cycles 9-15.....	5-31
5.2.10	Startup Physics Summary for Plant V1 Cycles 18-22 .....	5-36
5.3	Core Follow Measurements .....	5-40
5.3.1	Plant A Cycles 1-14.....	5-41
5.3.2	Plant B Cycle 1.....	5-44
5.3.3	Plant C Cycles 10-18 .....	5-46
5.3.4	Plant E Cycles 12-17.....	5-49
5.3.5	Plant G1 Cycles 26-30 .....	5-49
5.3.6	Plant G2 Cycles 1-5 .....	5-52
5.3.7	Plant S1 Cycles 12-14.....	5-55

5.3.8	Plant S2 Cycles 12-14.....	5-58
5.3.9	Plant T1 Cycles 9-15.....	5-61
5.3.10	Plant V1 Cycles 18-22.....	5-64
5.4	Conclusions .....	5-67
5.5	References .....	5-70
6.0	ADDITIONAL PARAMETER BENCHMARKS.....	6-1
6.1	Cold Critical Benchmarks.....	6-1
6.2	Pseudo-Ejected Rod Worth Benchmarks.....	6-3
6.3	Doppler Benchmarks .....	6-5
6.3.1	Introduction .....	6-5
6.3.2	Doppler Benchmark Conclusions .....	6-8
6.4	References .....	6-8
7.0	VALIDATION FOR TRANSIENT MODEL.....	7-1
7.1	NEACRP Reference Rod Ejection Benchmarks .....	7-1
7.1.1	NEACRP Case Description .....	7-2
7.1.2	NEACRP Results .....	7-2
7.2	ROD DROP TESTS .....	7-18
7.2.1	Rod Drop Test Description .....	7-18
7.2.2	Calculational Model.....	7-18
7.2.3	Results .....	7-19
7.3	SPERT III E-Core REA Benchmarks .....	7-28
7.3.1	Test 60 - HZP.....	7-29
7.3.2	Test 86 - HFP.....	7-30
7.3.3	Conclusion .....	7-31
7.4	Conclusions for Transient Benchmarks .....	7-35
7.5	References .....	7-35
8.0	POWER DISTRIBUTION UNCERTAINTIES .....	8-1
8.1	Introduction .....	8-1
8.2	LOCAL PEAKING UNCERTAINTY .....	8-3
8.2.1	Critical Core Configurations .....	8-3
8.2.2	Multi-Assembly Calculations with APOLLO2-A and ARTEMIS™ .....	8-7
8.2.3	Local Peaking Uncertainty .....	8-20
8.3	INFERRED POWER DISTRIBUTION UNCERTAINTY ANALYSES.....	8-23
8.3.1	MEDIAN with Moveable Fission Detector System.....	8-25

8.3.2	MEDIAN WITH CE Fixed Rhodium Detector System.....	8-30
8.3.3	MEDIAN AMS Reconstruction Methodology .....	8-37
8.3.4	MEDIAN WITH B&W Fixed Rhodium Detector System .....	8-41
8.4	Calculated Power Distribution Uncertainty Analyses (Nuclear Reliability Factors).....	8-48
8.4.1	Global Results.....	8-48
8.4.2	NRF Determination .....	8-54
8.5	Power Distribution Uncertainty Summary .....	8-56
8.6	References .....	8-56
9.0	SAFETY PARAMETER UNCERTAINTIES .....	9-1
9.1	Introduction .....	9-1
9.2	Total Rod Worth.....	9-4
9.3	Isothermal Temperature Coefficient.....	9-6
9.4	References .....	9-9
10.0	SUMMARY AND QUALIFICATION METHOD.....	10-1
10.1	Range of Applicability .....	10-1
10.2	Methods and Qualifications.....	10-3
10.3	Plant Application .....	10-5
10.4	Code Modification Change Process.....	10-5
10.5	Summary .....	10-7
10.6	References .....	10-9
11.0	QA PROGRAM.....	11-1
APPENDIX A	.....	A-1
APPENDIX B	.....	B-1
APPENDIX C	.....	C-1
APPENDIX E	.....	E-1
APPENDIX G1	.....	G1-1
APPENDIX G2	.....	G2-1
APPENDIX S1	.....	S1-1
APPENDIX S2	.....	S2-1
APPENDIX T1	.....	T1-1
APPENDIX V1	.....	V1-1

**List of Tables**

Table 2-1	Cross Section Adjustments Relative to JEFF 3.1.1 Uncertainty Range .....	2-4
Table 4-1	Range of Experimental Conditions .....	4-1
Table 4-2	B&W-1970s Critical Experiments – Reactivity Comparisons .....	4-2
Table 4-3	B&W-1980s Critical Experiments – Reactivity Comparisons .....	4-3
Table 4-4	KRITZ KWU Critical Experiments – Reactivity Comparisons .....	4-4
Table 4-5	EPIPURE Critical Experiments – Reactivity Comparisons .....	4-4
Table 4-6	CAMELEON Critical Experiments – Reactivity Comparisons .....	4-4
Table 4-7	B&W-1970s Fission Rate Distribution Comparisons .....	4-7
Table 4-8	B&W-1980s Fission Rate Distribution Comparisons .....	4-7
Table 4-9	KRITZ KWU Fission Rate Distribution Comparisons .....	4-7
Table 4-10	EPIPURE Fission Rate Distribution Comparisons .....	4-8
Table 4-11	CAMELEON Fission Rate Distribution Comparisons .....	4-8
Table 4-12	Fission Rate Distribution (RMS) Comparisons with ANP-10297P-A .....	4-9
Table 4-13	Reactivity Comparisons to Measurement for VALDUC Critical Experiments .....	4-47
Table 4-14	VALDUC Critical Experiments – Reactivity Difference Comparisons with ANP-10297P-A .....	4-47
Table 4-15	Isotopic Burnup Analysis – UO <sub>2</sub> Concentrations Comparisons (C/M-1)x100% .....	4-50
Table 4-16	Isotopic Burnup Analysis – ERU Concentrations Comparisons (C-M-1)x100% .....	4-51
Table 4-17	Isotopic Burnup Analysis – UO <sub>2</sub> -Gd <sub>2</sub> O <sub>3</sub> Concentrations Comparisons (C-M)x100 .....	4-51
Table 4-18	Isotopic Burnup Analysis – MOX Concentrations Comparisons (C/M-1)x100% .....	4-52
Table 4-19	Isotopic Burnup Analysis – UO <sub>2</sub> APOLLO2-A Results (C/M-1 in %) versus Estimated Uncertainties .....	4-53
Table 4-20	Isotopic Burnup Analysis – MOX APOLLO2-A Results (C/M-1 in %) versus Estimated Uncertainties .....	4-53
Table 5-1	Plant A Comparison of HZP ARO Critical Boron Concentration .....	5-8
Table 5-2	Plant A Comparison of HZP Total Rod Worth .....	5-9



Table 5-3	Plant A Comparison of HZP ARO Isothermal Temperature Coefficient.....	5-9
Table 5-4	Plant B Comparison of HZP ARO Critical Boron Concentration .....	5-13
Table 5-5	Plant B Comparison of HZP Total Rod Worth.....	5-13
Table 5-6	Plant B Comparison of HZP ARO Isothermal Temperature Coefficient.....	5-13
Table 5-7	Plant C Comparison of HZP ARO Critical Boron Concentration .....	5-14
Table 5-8	Plant C Comparison of HZP Total Rod Worth.....	5-14
Table 5-9	Plant C Comparison of HZP ARO Isothermal Temperature Coefficient.....	5-15
Table 5-10	Plant G1 Comparison of HZP ARO Critical Boron Concentration .....	5-20
Table 5-11	Plant G2 Comparison of HZP ARO Critical Boron Concentration .....	5-21
Table 5-12	Plant S1 Comparison of HZP ARO Critical Boron Concentration .....	5-23
Table 5-13	Plant S1 Comparison of HZP Total Rod Worth.....	5-23
Table 5-14	Plant S1 Comparison of HZP ARO Isothermal Temperature Coefficient.....	5-23
Table 5-15	Plant S2 Comparison of HZP ARO Critical Boron Concentration .....	5-27
Table 5-16	Plant S2 Comparison of HZP Total Rod Worth.....	5-27
Table 5-17	Plant S2 Comparison of HZP ARO Isothermal Temperature Coefficient.....	5-27
Table 5-18	Plant T1 Comparison of HZP ARO Critical Boron Concentration.....	5-31
Table 5-19	Plant T1 Comparison of HZP Total Rod Worth.....	5-31
Table 5-20	Plant T1 Comparison of HZP ARO Isothermal Temperature Coefficient.....	5-32
Table 5-21	Plant V1 Comparison of HZP ARO Critical Boron Concentration .....	5-36
Table 5-22	Plant V1 Comparison of HZP Total Rod Worth.....	5-36
Table 5-23	Plant V1 Comparison of HZP ARO Isothermal Temperature Coefficient.....	5-37
Table 5-24	Plant A Comparison of (C-M) RMS Differences for Assembly Average Radial and Core Average Axial Power Distributions.....	5-42
Table 5-25	Plant B Comparison of (C-M) RMS Differences for Assembly Average Radial and Core Average Axial Power Distributions.....	5-45
Table 5-26	Plant C Comparison of (C-M) RMS Differences for Assembly Average Radial and Core Average Axial Power Distributions.....	5-47

Table 5-27	Plant G1 Comparison of (C-M) RMS Differences for Assembly Average Radial and Core Average Axial Power Distributions .....	5-50
Table 5-28	Plant G2 Comparison of (C-M) RMS Differences for Assembly Average Radial and Core Average Axial Power Distributions .....	5-53
Table 5-29	Plant S1 Comparison of (C-M) RMS Differences for Assembly Average Radial and Core Average Axial Power Distributions .....	5-56
Table 5-30	Plant S2 Comparison of (C-M) RMS Differences for Assembly Average Radial and Core Average Axial Power Distributions .....	5-59
Table 5-31	Plant T1 Comparison of (C-M) RMS Differences for Assembly Average Radial and Core Average Axial Power Distributions .....	5-62
Table 5-32	Plant V1 Comparison of (C-M) RMS Differences for Assembly Average Radial and Core Average Axial Power Distributions .....	5-65
Table 5-33	Summary of ARCADIA® Validation and Results .....	5-67
Table 5-34	Results of ARCADIA® Calculations with Startup Physics Test Measurements .....	5-68
Table 5-35	Results of ARCADIA® Calculations with Core Follow Measurements...	5-69
Table 6-1	Cold Critical Benchmark Conditions and Critical Boron Concentration Comparisons .....	6-2
Table 6-2	Cold Critical Benchmark Boron Worth and ITC Comparisons.....	6-2
Table 6-3	Cycle 1 HZP Pseudo-Ejected Rod Worth Measurement Conditions.....	6-4
Table 6-4	Cycle 1 HZP Pseudo-Ejected Rod Worth Comparisons .....	6-5
Table 6-5	DPC Comparisons with Multiple Power Swings .....	6-7
Table 6-6	PC Comparisons with Multiple Power Swings .....	6-7
Table 6-7	DPC Comparisons with Single Power Swing .....	6-7
Table 7-1	Steady State Results for the NEACRP Benchmark .....	7-4
Table 7-2	Transient Results for the NEACRP Benchmark.....	7-5
Table 7-3	Rod Drop Transient Results.....	7-20
Table 7-4	Results of Rod Drop - Synthesis.....	7-21
Table 8-1	Summary of Results of Percent Difference: Observed = $(\text{Calc}/\text{Meas} - 1) \times 100\%$ .....	8-5
Table 8-2	Comparison of Results for Critical Experiments for Local Peaking Uncertainty.....	8-6
Table 8-3	Multi-Assembly Descriptions Using ERU Fuel .....	8-8
Table 8-4	Multi-Assembly Results.....	8-9
Table 8-5	Comparison of Multi-Assembly Statistics .....	8-10

Table 8-6	Global Statistics for MEDIAN with Moveable Fission Detector .....	8-26
Table 8-7	$F_{\Delta H}$ Summary Statistics for MEDIAN with Moveable Fission Detector .....	8-27
Table 8-8	Summary Statistics for MEDIAN with Moveable Fission Detector .....	8-27
Table 8-9	FSA Statistics for MEDIAN with CE Fixed Rhodium Detector.....	8-32
Table 8-10	FR and FZ Statistics for MEDIAN with CE Fixed Rhodium Detector ....	8-32
Table 8-11	$F_R$ Summary Statistics for MEDIAN with CE Fixed Rhodium Detector .....	8-33
Table 8-12	$F_Q$ Summary Statistics for MEDIAN with CE Fixed Rhodium Detector .....	8-33
Table 8-13	Statistics for MEDIAN AMS Detector System .....	8-37
Table 8-14	$F_{\Delta H}$ Summary Statistics for MEDIAN AMS Detector System.....	8-38
Table 8-15	$F_Q$ Summary Statistics for MEDIAN AMS Detector System.....	8-38
Table 8-16	FSA Statistics for MEDIAN with B&W Fixed Rhodium Detector .....	8-42
Table 8-17	FR and FZ Statistics for MEDIAN with B&W Fixed Rhodium Detector .....	8-43
Table 8-18	$F_{\Delta H}$ Summary Statistics for MEDIAN with B&W Fixed Rhodium Detector .....	8-43
Table 8-19	$F_Q$ Summary Statistics for MEDIAN with B&W Fixed Rhodium Detector .....	8-44
Table 8-20	Global Radial Power Statistics.....	8-50
Table 8-21	Global Peak Power Statistics.....	8-51
Table 8-22	Summary $F_{\Delta H}$ Statistics.....	8-55
Table 8-23	Summary $F_Q$ Statistics .....	8-55
Table 8-24	Power Distribution Uncertainty Summary .....	8-56
Table 9-1	Additional Data for Total Rod Worth and ITC used in Determining Safety Parameter Uncertainties .....	9-3
Table 9-2	Total Rod Worth Uncertainty Statistics .....	9-4
Table 9-3	D' Normality Test Statistics for Total Rod Worth Data .....	9-5
Table 9-4	ITC Uncertainty Statistics.....	9-7
Table 9-5	D' Normality Test Statistics for ITC Data.....	9-8
Table 10-1	Operating Cycle Benchmarks .....	10-2
Table 10-2	Methods Qualification Criteria.....	10-4
Table 10-3	Summary of Results.....	10-8

**List of Figures**

Figure 2-1	$k_{\infty}$ Differences Accounting for Modifications to APOLLO2-A .....	2-6
Figure 2-2	W 17X17 with 4.95 wt% $^{235}\text{U}$ Pin Power Differences (%) at 0.50 MWd/kgU and 50.0 MWd/kgU Accounting for Modifications to APOLLO2-A.....	2-7
Figure 2-3	W 17X17 with 4.47 wt% $^{235}\text{U}$ 20X8 + 8X2 Gad Pin Power Differences (%) at 0.50 MWd/kgU and 50.0 MWd/kgU Accounting for Modifications to APOLLO2-A.....	2-7
Figure 2-4	CE 14X14 with 4.11 wt% $^{235}\text{U}$ Pin Power Differences (%) at 0.50 MWd/kgU and 50.0 MWd/kgU Accounting for Modifications to APOLLO2-A.....	2-8
Figure 2-5	Slab Geometry for Generation of Grid Factors .....	2-11
Figure 3-1	ARTEMIS™ Pin Powers ANP-10297P-A (left) and Supplement 1 (right) .....	3-2
Figure 3-2	Axial Power Shape Showing Effect of Spacer Form Functions.....	3-7
Figure 3-3	Nodal Heterogeneity with Partial Control Rod Insertion and Resulting Axial Flux Distribution .....	3-8
Figure 3-4	Partial Currents, $j_g$ .....	3-17
Figure 4-1	B&W 1970's Core XI_2 Fission Rate Comparison (%) .....	4-10
Figure 4-2	B&W 1970's Core XI_6 Fission Rate Comparison (%) .....	4-11
Figure 4-3	B&W 1970's Core XI_8 Fission Rate Comparison (%) .....	4-12
Figure 4-4	B&W 1970's Core XI_11 Fission Rate Comparison (%) .....	4-13
Figure 4-5	B&W 1980's Core 1 Fission Rate Comparison (%).....	4-14
Figure 4-6	B&W 1980's Core 5 Fission Rate Comparison (%).....	4-15
Figure 4-7	B&W 1980's Core 12 Fission Rate Comparison (%).....	4-16
Figure 4-8	B&W 1980's Core 14 Fission Rate Comparison (%).....	4-17
Figure 4-9	B&W 1980's Core 18 Fission Rate Comparison (%).....	4-18
Figure 4-10	B&W 1980's Core 20 Fission Rate Comparison (%).....	4-19
Figure 4-11	KRITZ KWU UWH1 Reference Layout .....	4-20
Figure 4-12	KRITZ KWU UWH1 Reference Fission Rate Comparison (%) – Red Zone .....	4-21
Figure 4-13	KRITZ KWU UWH1 Reference Fission Rate Comparison (%) – Green and Magenta Zones .....	4-22
Figure 4-14	KRITZ KWU UWH1 Reference Fission Rate Comparison (%) – Cyan and Blue Zones .....	4-23

Figure 4-15	EPICURE UH1.2 Reference Layout .....	4-24
Figure 4-16	EPICURE UH1.2 Reference Fission Rate Comparison (%) – Red Zone.....	4-25
Figure 4-17	EPICURE UH1.2 Reference Fission Rate Comparison (%) – Magenta, Green and Blue Zones.....	4-26
Figure 4-18	EPICURE UH1.2, 30% Void Layout.....	4-27
Figure 4-19	EPICURE UH1.2, 30% Void Fission Rate Comparison (%) – Red and Green Zones.....	4-28
Figure 4-20	EPICURE UH1.2, 50% Void Layout.....	4-29
Figure 4-21	EPICURE UH1.2, 50% Void Fission Rate Comparison (%) – Red and Green Zones.....	4-30
Figure 4-22	EPICURE UH1.2, 100% Void Layout.....	4-31
Figure 4-23	EPICURE UH1.2, 100% Void Fission Rate Comparison (%) – Red and Green Zones.....	4-32
Figure 4-24	EPICURE UH1.4 Reference Layout .....	4-33
Figure 4-25	EPICURE UH1.4 Reference Fission Rate Comparison (%) – Red Zone.....	4-34
Figure 4-26	EPICURE UH1.4 Reference Fission Rate Comparison (%) – Green and Blue Zones.....	4-35
Figure 4-27	EPICURE UH1.4 Pyrex Layout.....	4-36
Figure 4-28	EPICURE UH1.4 Pyrex Fission Rate Comparison (%) – Red Zone ....	4-37
Figure 4-29	Pyrex Fission Rate Comparison (%) – Green and Blue Zones.....	4-38
Figure 4-30	EPICURE UH1.4 SS&AIC Layout.....	4-39
Figure 4-31	EPICURE UH1.4 SS&AIC Fission Rate Comparison (%) – Red Zone.....	4-40
Figure 4-32	EPICURE UH1.4, SS&AIC Fission Rate Comparison (%) – Green and Blue Zones.....	4-41
Figure 4-33	CAMELEON 25GT_12GD Fission Rate Comparison (%).....	4-42
Figure 4-34	CAMELEON 13GD Fission Rate Comparison (%).....	4-43
Figure 4-35	CAMELEON 12GD Fission Rate Comparison (%).....	4-44
Figure 4-36	CAMELEON 5GD Fission Rate Comparison (%).....	4-45
Figure 5-1	Plant A HZP ARO Critical Boron Concentration Differences.....	5-10
Figure 5-2	Plant A HZP Total Bank Worth Differences .....	5-11
Figure 5-3	Plant A HZP ARO Isothermal Temperature Coefficient Differences .....	5-12

Figure 5-4	Plant C HZP ARO Critical Boron Concentration Differences .....	5-16
Figure 5-5	Plant C HZP Total Bank Worth Differences .....	5-17
Figure 5-6	Plant C HZP ARO Isothermal Temperature Coefficient Differences .....	5-18
Figure 5-7	Plant G1 HZP ARO Critical Boron Concentration Differences .....	5-20
Figure 5-8	Plant G2 HZP ARO Critical Boron Concentration Differences .....	5-22
Figure 5-9	Plant S1 HZP ARO Critical Boron Concentration Differences.....	5-24
Figure 5-10	Plant S1 HZP Total Bank Worth Differences .....	5-25
Figure 5-11	Plant S1 HZP ARO Isothermal Temperature Coefficient Differences ...	5-26
Figure 5-12	Plant S2 HZP ARO Critical Boron Concentration Differences.....	5-28
Figure 5-13	Plant S2 HZP Total Bank Worth Differences .....	5-29
Figure 5-14	Plant S2 HZP ARO Isothermal Temperature Coefficient Differences ...	5-30
Figure 5-15	Plant T1 HZP ARO Critical Boron Concentration Differences.....	5-33
Figure 5-16	Plant T1 HZP Total Bank Worth Differences.....	5-34
Figure 5-17	Plant T1 HZP ARO Isothermal Temperature Coefficient Differences ...	5-35
Figure 5-18	Plant V1 HZP ARO Critical Boron Concentration Differences.....	5-37
Figure 5-19	Plant V1 HZP Total Bank Worth Differences .....	5-38
Figure 5-20	Plant V1 HZP ARO Isothermal Temperature Coefficient Differences ...	5-39
Figure 5-21	Plant A Cycles 1-14 Comparison of Critical Boron Concentration Differences.....	5-43
Figure 5-22	Plant B Cycle 1 Comparison of Critical Boron Concentration Differences.....	5-45
Figure 5-23	Plant C Cycles 10-18 Comparison of Critical Boron Concentration Differences.....	5-48
Figure 5-24	Plant G1 Cycles 26-30 Comparison of Critical Boron Concentration Differences.....	5-51
Figure 5-25	Plant G2 Cycles 1-5 Comparison of Critical Boron Concentration Differences.....	5-54
Figure 5-26	Plant S1 Cycles 12-14 Comparison of Critical Boron Concentration Differences.....	5-57
Figure 5-27	Plant S2 Cycles 12-14 Comparison of Critical Boron Concentration Differences.....	5-60
Figure 5-28	Plant T1 Cycles 9-15 Comparison of Critical Boron Concentration Differences.....	5-63

Figure 5-29	Plant V1 Cycles 18-22 Comparison of Critical Boron Concentration Differences.....	5-66
Figure 6-1	Test Data Comparisons .....	6-8
Figure 7-1	Power Distribution at Initial Conditions (Plane 6) - Case A1 .....	7-6
Figure 7-2	Power Distribution at time of Maximum Power (Plane 6) - Case A1 .....	7-7
Figure 7-3	Power Distribution at 5 sec (Plane 6) - Case A1 .....	7-8
Figure 7-4	Core Power Fraction – Case A1 .....	7-9
Figure 7-5	Core Average Fuel Temperature – Case A1.....	7-10
Figure 7-6	Core Exit Moderator Temperature – Case A1.....	7-11
Figure 7-7	Core Power Fraction – Case B2 .....	7-12
Figure 7-8	Core Average Fuel Temperature – Case B2.....	7-13
Figure 7-9	Core Exit Moderator Temperature – Case B2.....	7-14
Figure 7-10	Core Power Fraction – Case C1 .....	7-15
Figure 7-11	Core Average Fuel Temperature – Case C1 .....	7-16
Figure 7-12	Core Exit Moderator Temperature – Case C1 .....	7-17
Figure 7-13	Results of Rod Drop Test 1 – 0.7 GWd/mtU, F6K10 (SD bank) .....	7-22
Figure 7-14	Results of Rod Drop Test 2 – 4.34 GWd/mtU, K6F10 (SD bank) .....	7-23
Figure 7-15	Results of Rod Drop Test 3 – 4.34 GWd/mtU, K4F12 (SC bank) .....	7-24
Figure 7-16	Results of Rod Drop Test 4 – 4.34 GWd/mtU, E5L11 (R bank).....	7-25
Figure 7-17	Results of Rod Drop Test 5 – 11.575 GWd/mtU, F6K10 (SD bank) .....	7-26
Figure 7-18	Results of Rod Drop Tests – Synthesis of Deviation on Minimal Derivative of the Nuclear Flux $dP/dt$ .....	7-27
Figure 7-19	SPERT III E-Core Transient Control Rod Worth .....	7-32
Figure 7-20	SPERT III E-Core Test 60 Power Response .....	7-33
Figure 7-21	SPERT III E-Core Test 86 Power Response .....	7-34
Figure 8-1	Colorset 4 at 0.1 GWd/MTU, Pin Power Relative Percent Difference... ..	8-11
Figure 8-2	Colorset 4 at 10.0 GWd/MTU, Pin Power Relative Percent Difference .....	8-12
Figure 8-3	Colorset 4 at 20.0 GWd/MTU, Pin Power Relative Percent Difference .....	8-13
Figure 8-4	Colorset 9 at 0.1 GWd/MTU, Pin Power Relative Percent Difference... ..	8-14
Figure 8-5	Colorset 9 at 10.0 GWd/MTU, Pin Power Relative Percent Difference .....	8-15

Figure 8-6	Colorset 9 at 20.0 GWd/MTU, Pin Power Relative Percent Difference .....	8-16
Figure 8-7	Colorset 24 at 0.1 GWd/MTU, Pin Power Relative Percent Difference .....	8-17
Figure 8-8	Colorset 24 at 10 GWd/MTU, Pin Power Relative Percent Difference .....	8-18
Figure 8-9	Colorset 24 at 20 GWd/MTU, Pin Power Relative Percent Difference .....	8-19
Figure 8-10	Critical Experiments Frequency Distribution versus Normal Distribution .....	8-21
Figure 8-11	Multi-Assembly Problem Frequency Distribution versus Normal Distribution .....	8-22
Figure 8-12	MEDIAN Moveable Fission Detector Radial Frequency Distribution versus Normal Distribution .....	8-28
Figure 8-13	MEDIAN Moveable Fission Detector Frequency Distribution versus Normal Distribution .....	8-29
Figure 8-14	MEDIAN with CE Fixed Rhodium Detector FSA Frequency Distribution versus Normal Distribution .....	8-34
Figure 8-15	MEDIAN with CE Fixed Rhodium FR Frequency Distribution versus Normal Distribution .....	8-35
Figure 8-16	MEDIAN with CE Fixed Rhodium FZ Frequency Distribution versus Normal Distribution .....	8-36
Figure 8-17	MEDIAN AMS Radial Frequency Distribution versus Normal Distribution .....	8-39
Figure 8-18	MEDIAN AMS Peak Frequency Distribution versus Normal Distribution .....	8-40
Figure 8-19	MEDIAN with B&W Fixed Rhodium Detector FSA Frequency Distribution versus Normal Distribution .....	8-45
Figure 8-20	MEDIAN with B&W Fixed Rhodium FR Frequency Distribution versus Normal Distribution .....	8-46
Figure 8-21	MEDIAN with B&W Fixed Rhodium FZ Frequency Distribution versus Normal Distribution .....	8-47
Figure 8-22	All Plants Radial Power Frequency Distribution versus Normal Distribution .....	8-52
Figure 8-23	All Plants Peak Power Frequency Distribution versus Normal Distribution .....	8-53



Figure 9-1	Total Rod Worth Difference Frequency Distribution versus Normal Distribution .....	9-6
Figure 9-2	ITC Difference Frequency Distribution versus Normal Distribution .....	9-9

## Nomenclature

<b>Acronym</b>	<b>Definition</b>
AIC	Silver-Indium-Cadmium
AMS	Aeroball Measurement System
a/o	atom percent
ARO	All Rods Out
ASME	American Society of Mechanical Engineers
B <sub>4</sub> C	Boron Carbide
B&W	Babcock and Wilcox
BLEU	Blended Low Enriched Uranium
BOC	Beginning of Cycle
BOL	Beginning of Life
BP	Burnable Poison
C	Calculated
CBC	Critical Boron Concentration
CE	Combustion Engineering
CEA	Commissariat à l'Energie Atomique
C/M	Calculated to Measured
DOE	U.S. Department of Energy
DOF	Degrees of Freedom
DHO	Dehomogenization
DPC	Doppler Power Coefficient
DTC	Doppler Temperature Coefficient
EFPD	Effective Full Power Days
EOC	End of Cycle
EOL	End of Life
ENU	Enriched Natural Uranium
ERU	Enriched Reprocessed Uranium
FMM	Fuel Management Manual
GWd/t	Gigawatt-days per tonne
HFP	Hot Full Power
HZP	Hot Zero Power
IAPWS	International Association for the Properties of Water and Steam
IFBA	Integral Fuel Burnable Absorber
IRSN	Institute de Radioprotection et de Sûreté Nucléaire

ITC	Isothermal Temperature Coefficient
kgU	Kilograms Uranium
LOCA	Loss of Coolant Accident
LWR	Light Water Reactor
M	Measured
MEDIAN	Measurement Dependent Interpolation Algorithm using NEM
MOC	Middle of Cycle
MOX	Mixed Oxide
MTC	Moderator Temperature Coefficient
MWd	Megawatt Days
MWd/ kgU	Megawatt-days per kilogram uranium
MWd/ mtU	Megawatt-days per metric ton uranium
NEACRP	Nuclear Energy Agency Committee on Reactor Physics
NEM	Nodal Expansion Method
NRC	U.S. Nuclear Regulatory Commission
NRF	Nuclear Reliability Factor
NUREG	U.S. Nuclear Regulatory Commission Report
PC	Power Coefficient
PCM	Percent Change Millirho
PPM	Parts per Million
PWR	Pressurized Water Reactor
QA	Quality Assurance
RAI	Request for Additional Information
RCS	Reactor Coolant System
REA	Rod Ejection Accident
RIA	Reactivity Initiated Accident
RMS	Root Mean Square
RPD	Radical Power Density
SER	Safety Evaluation Report
SHEM	Santamarina Hfaiedh Energy Mesh (APOLLO2-A 281 energy group mesh)
SPERT	Special Power Excursion Reactor Test
SPND	Self-Powered Neutron Detector
SRP	Standard Review Plan
SS	Stainless Steel
TIP	Traveling Incore Probe
TRW	Total Rod Worth

TSC	Time Step Control
UO <sub>2</sub>	Uranium dioxide
W	Westinghouse
WABA	Wet Annular Burnable Absorber
wt% (or w/o)	weight percent
XS	cross section

## ABSTRACT

AREVA's Topical Report ANP-10297P-A, Revision 0, "The ARCADIA<sup>®</sup> Reactor Analysis System for PWRs Methodology Description and Benchmarking Results Topical Report," approved by the NRC, and presents the ARCADIA<sup>®</sup> Code System for evaluation of PWR designs using either steady-state or transient solutions. The ARCADIA<sup>®</sup> Code System can be used to provide core design capability and analyses specific to showing compliance to Chapter 4.2 and Chapter 15 of NUREG-0800.

The analyses based on the ARCADIA<sup>®</sup> Code System are performed based on the APOLLO2-A code for generation of cross sections, assembly discontinuity factors, and heterogeneous form functions; the ARTEMIS<sup>™</sup> 3D core simulator for steady-state and transient calculations and COBRA-FLX<sup>™</sup> for 3D sub-channel by sub-channel in steady-state or transient calculations. The purpose of this supplement is to provide changes and modifications to the ARCADIA<sup>®</sup> code system since the approval of ANP-10297P-A, Revision 0. The supplement provides the impact of these changes on the results of validation and benchmark analyses. Additional benchmarks for cold critical conditions, ERU fuel, transient models and various safety parameters are included. This supplement also describes the enhancements to the MEDIAN power distribution reconstruction methodology for improved treatment of asymmetric detectors and the extension of this methodology in the development of uncertainties to movable fission and fixed rhodium incore detector systems.

The ARCADIA<sup>®</sup> Code System is applicable to PWR designs using either UO<sub>2</sub> or ERU fuel.

## 1.0 INTRODUCTION

By letter dated July 3, 2013, AREVA Inc. (AREVA) submitted the approved version of Topical Report ANP-10297P-A, Revision 0 (Reference 1.1-1). The application methodology and benchmarking results of the ARCADIA<sup>®</sup> code system were evaluated for application to the neutronic design analyses of PWRs, including transient analyses. Changes to this methodology have been made to incorporate new features required to support the development of Non-LOCA methodologies, reduce uncertainties, and extend the benchmark range. Significant changes to the Reference 1.1-1 methodology are presented in this Supplement (Supplement 1). Benchmark and validation cases were evaluated for the intended ARCADIA<sup>®</sup> code system application range. The experimental data and benchmarks were checked for adequacy of the intended application range.

Topical Report ANP-10297P, Revision 0, Supplement 1, henceforth referred to as “Supplement 1,” includes changes and modifications made to the ARCADIA<sup>®</sup> code package in the way of improving and enhancing the code package capabilities and accuracy. The benchmarks presented in Reference 1.1-1 were recalculated and compared to previous results.

Supplement 1 summarizes key aspects of the ANP-10297P-A Topical Report, emphasizing the differences between the current approved methodology and this supplement’s modifications. Supplement 1 highlights the comparisons between the ANP-10297P-A benchmarks results and the recalculated benchmarks results. Additional benchmarks are included to extend the range of applicability of the Reference 1.1-1 methodology.

ARCADIA<sup>®</sup> is an international code package. As such it is a platform designed for applicability to reactor analysis world-wide. Consequently, modifications to the code are necessary to extend applicability to a variety of fuel designs such as Enriched Reprocessed Uranium (ERU) fuel used in Europe and potentially in the U.S. as part of the U.S. Department of Energy's (DOE) BLEU project. These modifications are subject to NRC review and approval. Benchmarks have been added to include the ERU material to the ARCADIA<sup>®</sup> range of applicability.

Code modifications are also needed to support the development of Non-LOCA methodologies based on the transient capabilities of the ARCADIA<sup>®</sup> code system. This provides AREVA the opportunity to transition from existing legacy codes and methodologies to improved codes and methods required to address the updated Standard Review Plan (SRP) Chapter 15 event criteria. These changes are also necessary to address the Reactivity Initiated Accident (RIA) criteria specified in SRP Section 4.2.

Section 2.0 provides a description of the modifications made to the APOLLO2-A computer code, which include implementation of a new processing scheme of the cross-section data library [

].

Section 3.0 provides methodology enhancements to the ARTEMIS<sup>™</sup> 3D nodal simulator. This includes the use of the updated APOLLO-2A cross-section libraries and implementation of an improved pin power reconstruction model and a new spacer grid model.

Section 4.0 addresses the validation cases for the APOLLO2-A code. This section provides a description of the critical experiments, measurement considerations, and discussion of results. It also provides a discussion of integral experiments, including test descriptions, measurements and results. Section 4.3 also addresses the spent fuel analysis. A description of the experimental data is provided, along with comparisons to measurement, isotopic analysis and a discussion of the results.

Section 5.0 provides a confirmation of the ARCADIA<sup>®</sup> code package with the incorporated changes. This section includes recalculation of benchmark comparisons for commercial reactor measurements (e.g. startup physics test measurements and core follow comparisons). An additional reactor benchmark is added which includes ERU fuel.

Section 6.0 provides a description and results of the additions made to the approved Topical Report. These include Doppler Power Coefficient calculations, pseudo-ejected rod worth calculations, and cold critical boron concentration comparisons.

Section 7.0 provides a description as well as validation and verification of the time dependent capabilities of the transient model in the ARCADIA<sup>®</sup> code system. Calculation models are discussed for Rod Drop tests, the SPERT III E-core experiment and the NEACRP UO<sub>2</sub> Control Rod Ejection benchmark. Qualitative and quantitative technical analyses are given for each test. The results of all three calculational models are demonstrated to comply with all regulatory requirements and positions.

Section 8.0 addresses the power distribution uncertainties. Local peaking uncertainties, including critical core configurations and multiple assembly calculations, are discussed as well as the inferred and calculated power distribution uncertainties. The uncertainty analysis presented in Supplement 1 extends the application of the MEDIAN reconstruction methodology, described in Reference 1.1-1 for the Aeroball Measurement System (AMS), to include movable fission and fixed rhodium incore detector systems.



The uncertainty analysis performed in Supplement 1 includes all grid types, including Alloy-718 grids. Therefore, AREVA is requesting that the limitation imposed in the NRC's Safety Evaluation Report (page 28) be removed.

Section 9.0 addresses the uncertainty specific to Total Rod Worth (TRW) and Isothermal Temperature Coefficient (ITC) and results in conformance with regulatory positions and limits. This section provides justification for a change to the uncertainties for these parameters that will be used in safety analyses.

Section 10.0 provides a summary of the ARCADIA<sup>®</sup> code system which defines the range of applicability, specifies the qualification criteria, provides a change process, defines plant application, and includes an overall summary of the topical report. The change process asserts that AREVA can update/modify the codes within the ARCADIA<sup>®</sup> code system. Validation against the qualification criteria are made to ensure the modifications/changes remain within the range of applicability of the approved code system. This change process defines what changes can be made without NRC approval and what code changes would require pre-approval prior to use. This section specifies a notification process to inform the NRC of changes made to ARCADIA<sup>®</sup>.

Section 11.0 defines AREVA's 10CFR50 Appendix B Quality Assurance (QA) program.

## **1.1      *References***

- 1.1-1   Letter, Pedro Salas (AREVA Inc.) to NRC Document Control Desk,  
Publication of ANP-10297(P)-(A), Revision 0, "The ARCADIA<sup>®</sup> Reactor  
Analysis System for PWRs Methodology Description and  
Benchmarking Results Topical Report," July 3, 2013.

## 2.0 APOLLO2-A METHODOLOGY

The approved APOLLO2-A methodology is presented in Section 2.0 of Reference 2.7-1. Modifications to the codes were incorporated since the issuance of Reference 2.7-1. These modifications are documented in this supplement and are categorized as either being enhancements to existing models within the code or addition of new models. The enhancements and new models follow a first principles approach of modeling that have a desirable impact on results.

Model enhancements include:

New models added to APOLLO2-A include:

- Generation of spacer grid form functions
- Large problem capability
- Surface spectral history model

## 2.1 *Promethium Branching Ratio Modification*

Use of the ARCADIA® code system following approval of the Reference 2.7-1 topical report showed [

]. Cross section data were analyzed to determine parameters that could have a potential impact on this behavior. The production of  $^{148m}\text{Pm}$  and its branching ratio were determined to be a potential cause of this behavior.

Radiative capture in  $^{147}\text{Pm}$  can produce either  $^{148}\text{Pm}$  or  $^{148m}\text{Pm}$ . The  $^{148m}\text{Pm}$  branching ratio is the probability that radioactive capture in  $^{147}\text{Pm}$  will produce  $^{148m}\text{Pm}$ . Since  $^{148m}\text{Pm}$  has a much higher capture cross section than the ground state, [

].

A review of current cross section data indicates that the  $^{148m}\text{Pm}$  branching ratio of 0.467 currently in the JEFF 3.1.1 [ ]. It was concluded that a modification to the  $^{148m}\text{Pm}$  branching ratio was justified and a value of [ ] as presented in Reference 2.7-2 was selected. Therefore, the modified branching ratios are:

$^{147}\text{Pm} \rightarrow ^{148}\text{Pm}$  is [ ]

$^{147}\text{Pm} \rightarrow ^{148m}\text{Pm}$  is [ ]

[

]. The same branching ratios were also implemented in ARTEMIS™.

## **2.2      *Cross Section Adjustments***

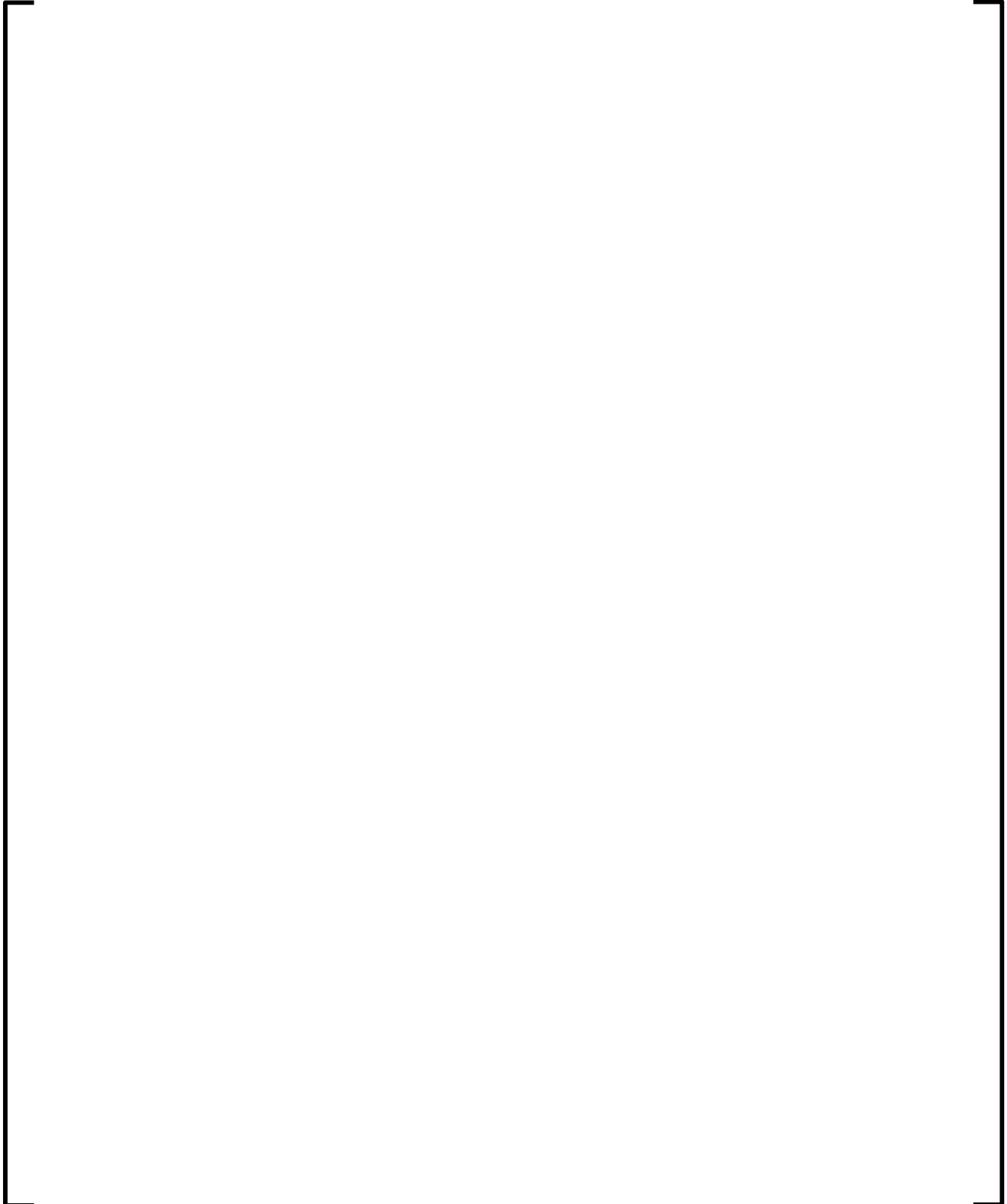


**Table 2-1**  
**Cross Section Adjustments Relative to JEFF 3.1.1 Uncertainty Range**

**2.3      *Impact of the Updates to Promethium Branching Ratio and Cross  
Section Adjustments on Results***

The adjustments made in the Promethium branching ratio (Section 2.1), the inclusion of cross sections adjustments (Section 2.2) are [

].

Further justification of these changes is provided in Section 4.0 where comparisons are made to critical experiments for reactivity and fission rates. Spent fuel analyses are also included in the Section 4.0 validation cases.

**Figure 2-1**  
 **$k^\infty$  Differences Accounting for Modifications to APOLLO2-A**



**Figure 2-2**  
**W 17X17 with 4.95 wt% <sup>235</sup>U Pin Power Differences (%) at 0.50**  
**MWd/kgU and 50.0 MWd/kgU Accounting for Modifications to**  
**APOLLO2-A**

**Figure 2-3**  
**W 17X17 with 4.47 wt% <sup>235</sup>U 20X8 + 8X2 Gad Pin Power Differences**  
**(%) at 0.50 MWd/kgU and 50.0 MWd/kgU Accounting for**  
**Modifications to APOLLO2-A**



**Figure 2-4**  
**CE 14X14 with 4.11 wt%  $^{235}\text{U}$  Pin Power Differences (%) at 0.50**  
**MWd/kgU and 50.0 MWd/kgU Accounting for Modifications to**  
**APOLLO2-A**

**2.4      *Enhancements to Gamma Calculation***

Due to their large free path length, gammas have a smoothing impact on the power density distribution within fuel assemblies. [

]

Total deposited energy is found using the following equation:

All elements of the above equation are straightforward and [

enhanced gamma transport model calculates [

]. The

]

## **2.5      *Enhancements to Delayed Neutron Data***

## **2.6      *New Models***

New models have been added to APOLLO2-A to allow for improvements in the ARTEMIS<sup>™</sup> calculation and to provide a reference solution for certain analyses (e.g., large  $\frac{1}{4}$ -core calculations). These model changes are discussed in this section.

### 2.6.1 Generation of Spacer Grid Form Functions

A model is implemented in APOLLO2-A for the generation of form functions (grid factors) for the treatment of spacer grids in the 3D core simulator ARTEMIS™. The grid factors are generated for application in both steady state and transient core calculations.

The process used to generate these grid factors utilizes the [

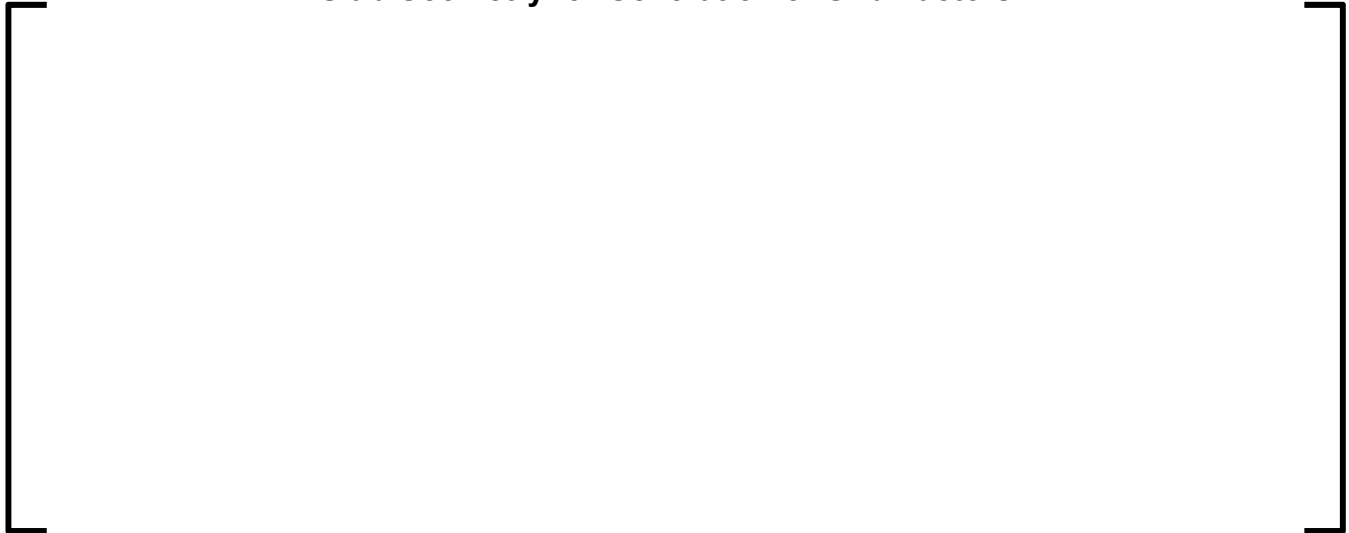
] of APOLLO2-A (typical representation given in Figure 2-5). The calculations are performed in the [

].

Spacer grid factors are [ ] . The form functions are [

].

**Figure 2-5**  
**Slab Geometry for Generation of Grid Factors**



### **2.6.2 Large Core Problems**

The capability has been added to APOLLO2-A to allow for the modeling of large 2D geometries. The capability has been added to allow for configurations of up to 1/4 core pin-by-pin geometry including radial reflectors. This feature can be used for generating reference solutions for comparison to 3D nodal models used in design calculations.

### **2.6.3 Surface Spectral History Model**

Modifications were made to APOLLO2-A to support the Surface Spectral History model in ARTEMIS™. With these modifications, [

].

Tabulated cross section changes are generated for use in the ARTEMIS<sup>™</sup> Surface Spectral History Model. [

]. This is discussed in more detail in Section 3.2.

## 2.7 **References**

- 2.7-1 ANP-10297P-A, Revision 0, The ARCADIA<sup>®</sup> Reactor Analysis System for PWRs Methodology Description and Benchmarking Results Topical Report, February 2013.
- 2.7-2 J. Koning and D. Rochman, Nuclear Data Sheets, Vol. 113, p. 2841 (2012).
- 2.7-3 A. Santamarina, D. Bernard, P. Leconte and J-F. Vidal, Improvement of <sup>238</sup>U Inelastic Scattering Cross-Section for an Accurate Calculation of Large Commercial Reactors, ND2013 proceedings, June 10, 2013.
- 2.7-4 A. Santamarina, D. Bernard, P. Leconte, and J-F. Vidal, Improvement of <sup>238</sup>U Inelastic Scattering XS for an Accurate Calculation of Large Reactors, JEFDOC 1507, JEFF Meeting (Paris), April 17-19, 2013.
- 2.7-5 M. Salvatores and R. Jacqmin, Uncertainty and Target Accuracy Assessment for Innovative Systems using Recent Covariance Data Evaluations, NEA/WPEC-26, ISBN 978-92-64-99053-1, OECD 2008.
- 2.7-6 A. Santamarina, D. Bernard, N. Dos Santos, O. Leray, C. Vaglio and L. Leal, Re-estimation of Nuclear Data and JEFF3.1.1 Uncertainty Calculations, PHYSOR 2012 (Tennessee), April 15-20, 2012.

### **3.0 ARTEMIS™ METHODOLOGY**

The approved ARTEMIS™ methodology is presented in Section 3.0 through Section 5.0 of Reference 3.16-1. Modifications to the code were incorporated after the issuance of Reference 3.16-1. These modifications are either enhancements to existing models within the code or addition of new models and extensions to functionality. The enhancements and new models follow a first principles approach of modeling that have a desirable impact on results. The changes incorporated into ARTEMIS™ are discussed in the following sections.

#### **3.1 *Additional Search Algorithms***

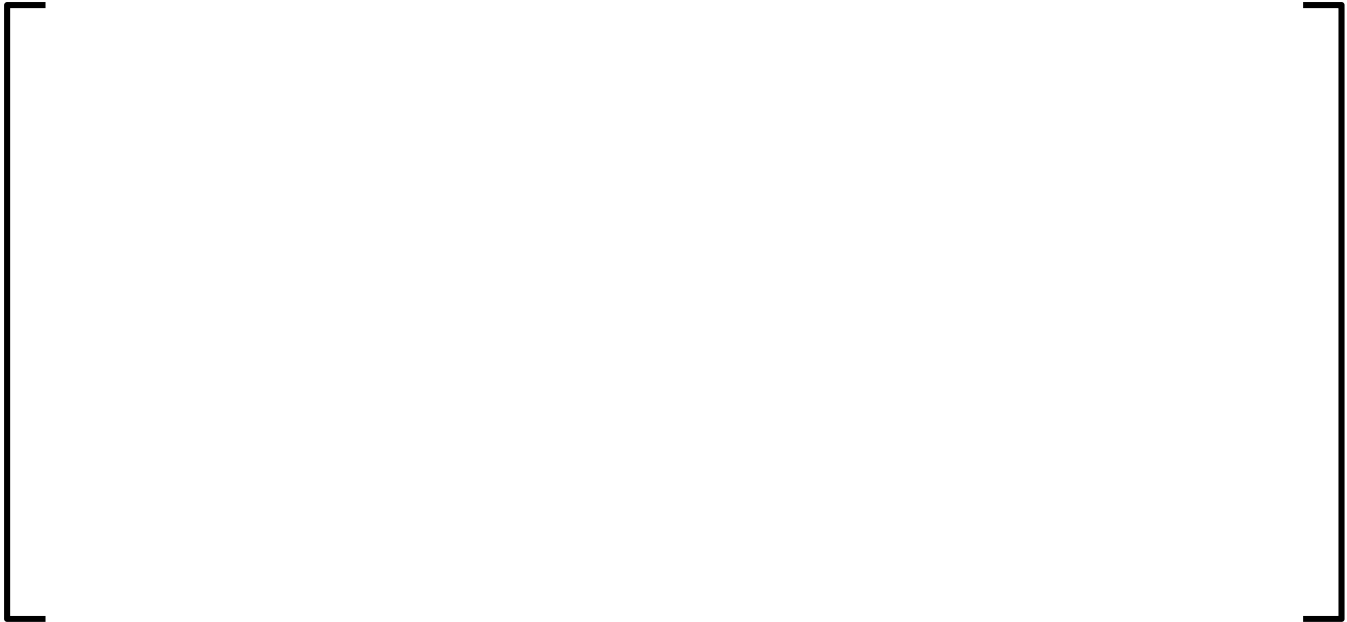
Search algorithms are used in 3D nodal codes to provide the capability to determine core conditions based on many different parameters. Typical search algorithms include boron, power and control rod position. These types of search algorithms already exist in ARTEMIS™. An additional search was added to allow the code to determine the critical condition based on a specified axial offset through adjustment of control rod position or through the imposition of a xenon distribution. The purpose of this search is for the determination of Axial Flux Difference target bands that are used to determine the penalty function in a Power Distribution Control analysis.

#### **3.2 *Enhanced Dehomogenization Model***

The pin reconstruction process was described in Reference 3.16-1, Section 3.7. In extending the application to MOX fuel assemblies, it was observed that improvements to the dehomogenization (DHO) of the nodal data into pin powers were required. [

]. The impact of these models on an assembly pin power distribution are shown in Figure 3-1.

**Figure 3-1**  
**ARTEMIS™ Pin Powers ANP-10297P-A (left) and Supplement 1 (right)**



### 3.2.1 Surface Spectral History Model

The few group nuclear data (cross section, surface and corner discontinuity factors) used in the nodal core simulator are derived from single assembly calculations in an infinite lattice. [

].

The treatment considers the local change in the cross section due to the [

].

A spectral history parameter is defined for each nodal surface and corner as follows:



This approach functionalizes the change in [ ]. The base change in the [ ] is determined using [ ]

[ ]. During the DHO module calculations, the values of [ ] are obtained [ ]

[

].



### 3.2.2 Multi-group Power Form Functions

Pin power reconstruction is performed by [

]. The previous method uses power form functions that are condensed to one energy group. Most of the fissions occur in the thermal energy region but fast fission in  $^{238}\text{U}$  provides a significant contribution as well.

[

]. Consistent with the current application scheme, the power form functions are provided in two energy groups.

### 3.3 Incorporation of Spectral Cross Section Model

To ensure that results from ARTEMIS™ match APOLLO2-A as closely as possible, adjustments are derived by [

]. The spectral cross section model accounts for the differences of the [

] that are stored in the cross section library.

The spectrum adjustment factors are defined as:

The superscript 0 denotes the reference state and the superscript 1 denotes the perturbed state. [

].

The model is applicable to all PWR fuel.

### **3.4      *Update of Steam Tables***

Reference 3.16-1 uses the ASME 1967 (IFC-67 formulation) water properties. Water properties have been updated to the latest version of the IAPWS-IF97 “Thermodynamic Properties of Water and Steam.”

### **3.5      *Incorporation of a Spacer Grid Model***

The spacer grid model uses the form functions (grid factors) generated with the APOLLO2-A lattice code as discussed in Section 2.6.1 of this supplement. These form functions are applied after pin reconstruction on power density and group fluxes. [

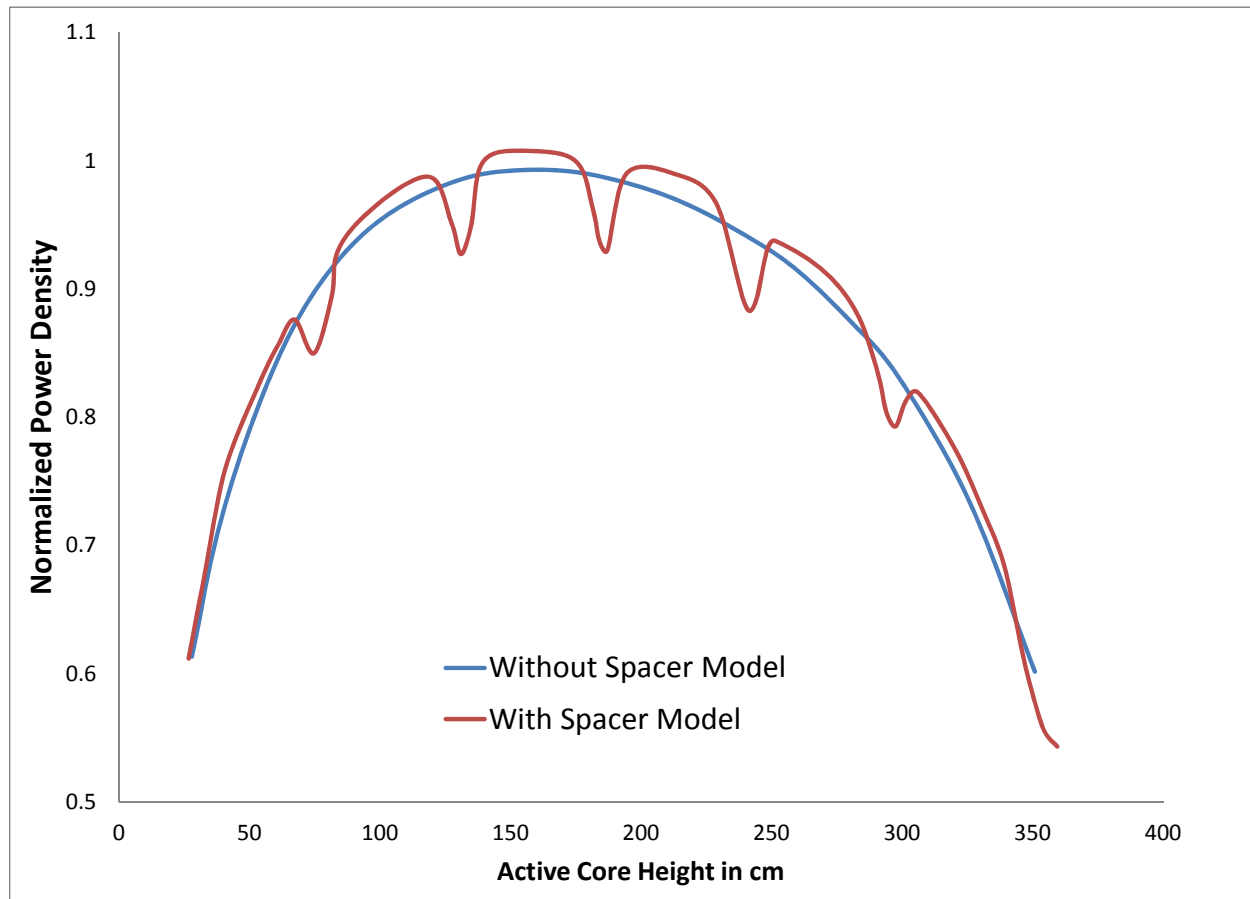
].

A comparison of an axial power shape with and without the spacer form functions applied is provided in Figure 3-2.

[

].

**Figure 3-2**  
**Axial Power Shape Showing Effect of Spacer Form Functions**

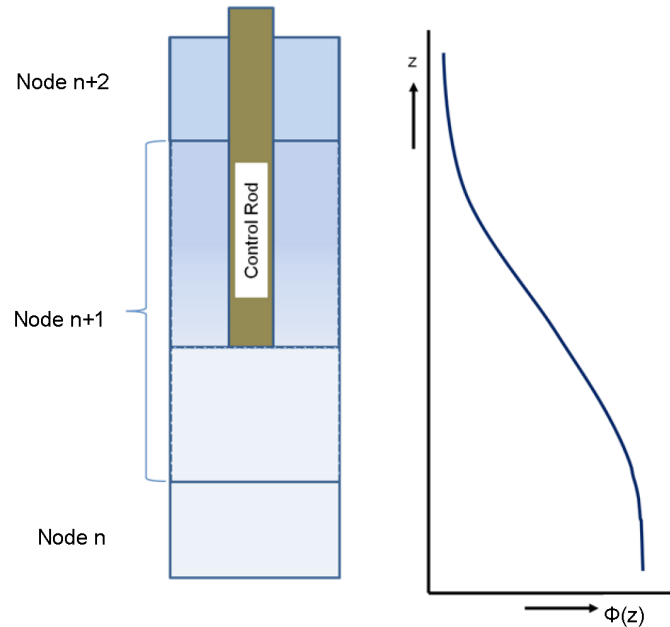


### 3.6 *Incorporation of Control Rod Cusping Model*

Control rod movement in PWRs is either continuous or performed in small discrete steps (e.g. 0.64 in). In nodal coarse mesh calculations, this leads to axial heterogeneities where nodes can be partially rodged, see Figure 3-3. The 'cusping' effect appears when performing a pure volume weighting of the cross sections of the unrodged and the rodged part of the partially rodged nodes. [

].

**Figure 3-3**  
**Nodal Heterogeneity with Partial Control Rod Insertion and Resulting**  
**Axial Flux Distribution**



The implemented model [ ] used in  
 ARTEMIS™ by [ ]  
 [ ].

For two heterogeneous zones in a node, the following equation applies:

$$[ ]$$

Reformulation of the rightmost term [ ]:

This cross section is then used in the nodal balance equation.

### **3.7 *Incorporation of Time Dependent Inlet Temperature, Inlet Mass Flux and Core Exit Pressure Input***

In preparation for using the ARCADIA® code system for transient analyses, it is necessary to allow for input of time dependent inlet temperature, inlet mass flux and core exit pressure to an ARTEMIS™ calculation. This enables ARTEMIS™ to incorporate the data from an approved system code (e.g., S-RELAP5) either through direct coupling or through input of the forcing functions. ARTEMIS™ will use this data to perform 3D neutronics, sub-channel wise thermal-hydraulic and pin-wise thermal-mechanical calculations for the transient (e.g., locked rotor or complete loss of flow).

### **3.8 *Incorporation of Non-uniform Inlet Temperature Input in Steady-state and Transient Conditions***

Input of non-uniform core inlet temperature distributions that may occur in PWRs in steady-state or transient conditions is available and essential for modeling asymmetric events. To capture the correct temperature inlet conditions from non-uniform system conditions (e.g., Main Steam Line Break), ARTEMIS™ has the option available to input asymmetric inlet temperature distributions. This input may be entered manually or passed automatically, linking ARTEMIS™ to a qualified system analysis code (e.g., S-RELAP5).

### **3.9      *Modifications to Parameter Penalization in Steady-state and Transients***

Parameter penalization is essential for conservative safety analyses. Penalization of sensitive parameters is necessary for applying appropriate biasing and implementing uncertainties in development and application of transient analyses based on a 3D approach. This set of modifications to ARTEMIS™ not only allows adjustments of reactivity parameters (e.g., MTC, DTC and rod worth) but also allows for penalization of thermal-hydraulics and thermal-mechanical parameters.

#### **3.10      *Incorporation of Optimal Time Step Control During Transient Calculations***



#### **3.11      *Incorporation of Non-uniform Boron Nodal Distribution Model***



### **3.12      *Enhanced Coarse-Fine Mesh Coupling***

Internal coupling was implemented into ARTEMIS™. This allows the efficient coupling of the 3D nodal solution to the reconstructed 3D pin-wise data at each time step. The pin powers and pin burnups are determined by the DHO. [

] An internal coupling process is now available which allows an efficient and robust evaluation of reconstructed 3D pin-wise / sub-channel wise conditions at each time step.

[

]

### **3.13      *Incorporation of Excore Detector Model***

An excore detector response model has been incorporated in ARTEMIS™. The excore response model uses a set of excore weighting factors input by core location. The weighting factors are the weighted averages of the neutron source terms, and are determined using discrete ordinate transport theory techniques. ARTEMIS™ uses these weighting factors to calculate the excore detector response. The ARTEMIS™ excore detector responses are used to support setpoint analyses and are used in transient analyses for the determination of trip times. A temperature decalibration model is part of the excore detector response model. The decalibration is based on core average temperature and only intended for use in core monitoring.



Implementation of an excore detector model allows for determination of excore signals in either static or time dependent calculations. The model uses weighted averages of the neutron source terms. Assembly weighting factors are determined using discrete ordinate transport theory techniques and are input by core location. The excore detector model also allows for an adjustment to the excore detector signals based on core average temperature.

### **3.14      *Incorporation of Decay Heat Model***

ARTEMIS™ will be used as the core model for many transient analysis calculations. This will either be done stand-alone (e.g., rod ejection) or coupled to an approved code (e.g., S-RELAP5). To accommodate this, a decay heat model was incorporated into ARTEMIS™. This model is based on Reference 3.16-2. The decay heat model can be used in either steady-state or transient analyses. It is applied in the determination of the initial conditions of a transient and for follow-up of the decay heat through the progress of the transient.

### **3.15      *Modification of the MEDIAN Power Distribution Reconstruction Methodology***

The MEDIAN power distribution reconstruction methodology is presented in its entirety in this section. The provided methodology incorporates modifications to the methodology used in Reference 3.16-1. [

].

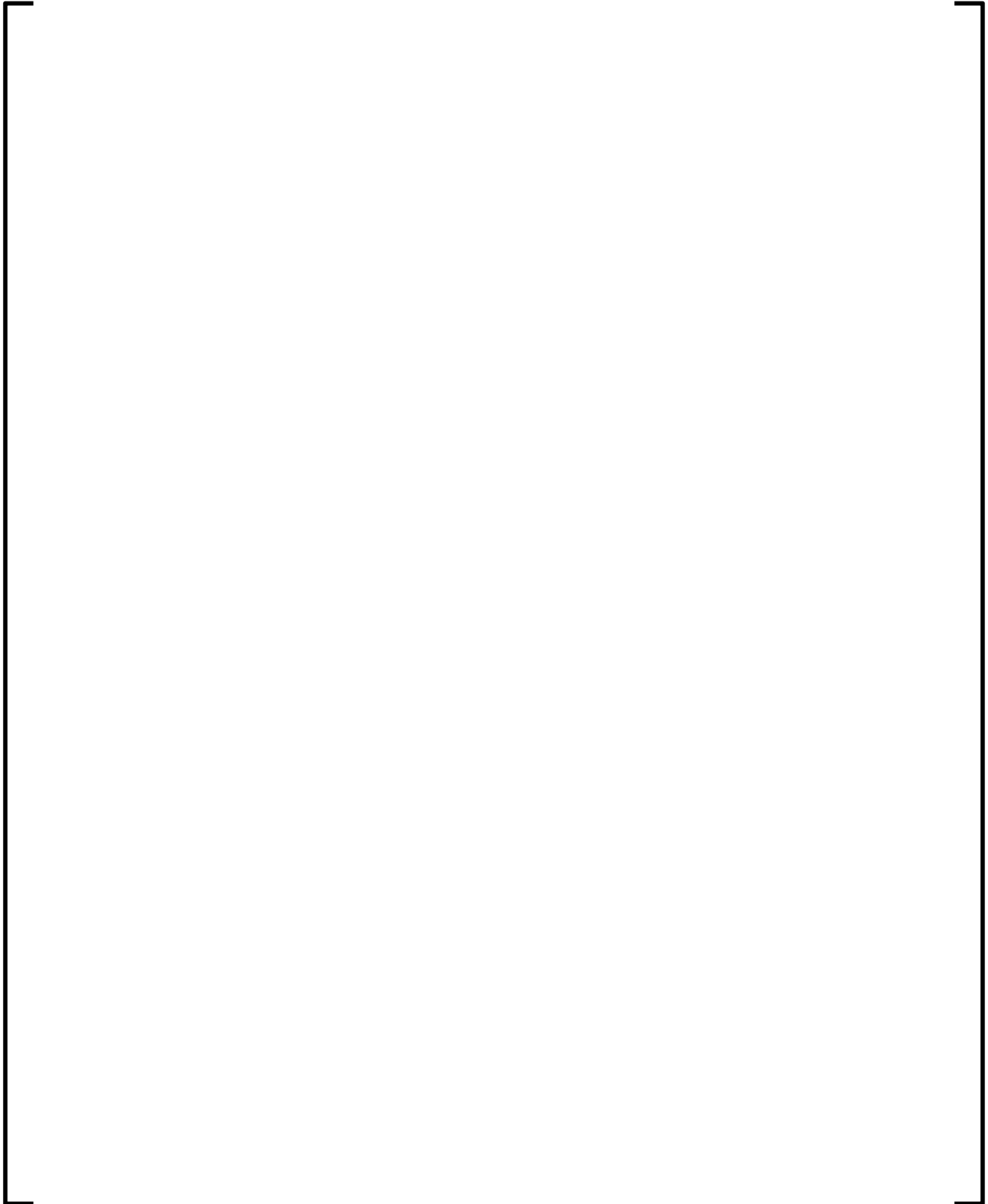
The modified methodology is now applicable to incore detector systems that are fixed, movable or aeroball, full length or axially segmented.

During plant operation, three dimensional core power distributions are periodically derived from a combination of measured and calculated data. This determined power distribution is an inferred power distribution which provides powers for all core locations as opposed to a measured distribution that considers only detector locations.

ARTEMIS™ is capable of providing theoretical 3D detector signals and pin-wise distributions of power, burnup and group fluxes as a function of operational history of the reactor. The MEDIAN module of ARTEMIS™ performs calculations based on measurement and [

]. The pin values are generated using the standard pin reconstruction technique in ARTEMIS™. [

].



### **3.15.1 Determination of Two-group Optimal Fluxes**

### **3.15.2 Extrapolation of the Nodal Fluxes**

**Figure 3-4**  
**Partial Currents,  $j_g$**

### **3.16     *References***

- 3.16-1 ANP-10297P-A, Revision 0, The ARCADIA<sup>®</sup> Reactor Analysis System for PWRs Methodology Description and Benchmarking Results Topical Report, February 2013.
- 3.16-2 ANSI/ANS-5.1-2005, American National Standard, Decay Heat Power in Light Water Reactors, American Nuclear Society, April 2005.

## 4.0 APOLLO2-A RE-VALIDATION

Re-validation of APOLLO2-A consists of comparisons of calculated results to measurements (physical validation). Comparisons are made with critical experiments (reactivity and fission rates), integral experiments, and spent fuel isotopics.

Modeling and scope of the validation comparisons are similar to that presented in Reference 4.4-1, Section 6.0.

### 4.1 *Critical Experiments*

Reference 4.4-1, Section 6.2 describes several sets of critical experiments used to validate APOLLO2-A. These consisted of several international experimental programs, including Babcock and Wilcox (B&W) in the US, KRITZ in Sweden, and two experimental programs – EPICURE and CAMELEON – from the Commissariat à l’Energie Atomique (CEA) in France. All of these critical experiments are UO<sub>2</sub> fueled experimental reactors.

A total of 46 critical configurations were included in Reference 4.4-1, Section 6.2. The range of experimental conditions is shown in Table 4-1. While this table defines the range of the critical experiment, the range of applicability of APOLLO2-A is not restricted to the confines of this table. APOLLO2-A does not employ any empirical models to extrapolate beyond the ranges listed in the table and hence is not vulnerable to extrapolation errors.

**Table 4-1**  
**Range of Experimental Conditions**

--	--



#### 4.1.1 Reactivity

Each experiment is described in Section 6.2 of Reference 4.4-1. Reactivity comparisons between calculated and measured values are summarized in Table 4-2 through Table 4-6. The calculated-to-measured (C-M) results in these tables are expressed in pcm, computed as  $(C-M) \times 10^5$ .

An estimated uncertainty of [ ] for the reactivity of [ ] fueled critical experiments was provided in Reference 4.4-1, response to RAI 60. This value combined both measurement and engineering uncertainties and was calculated by CEA based on sensitivity calculations for the EPICURE and CAMELEON critical configurations.

**Table 4-2**  
**B&W-1970s Critical Experiments – Reactivity Comparisons**

**Table 4-3**  
**B&W-1980s Critical Experiments – Reactivity Comparisons**

**Table 4-4**  
**KRITZ KWU Critical Experiments – Reactivity Comparisons**

**Table 4-5**  
**EPICURE Critical Experiments – Reactivity Comparisons**

**Table 4-6**  
**CAMELEON Critical Experiments – Reactivity Comparisons**

#### 4.1.2 Fission Rate Distribution

Comparisons of calculated to measured fission rate distributions were performed when possible since fission rate measurements were provided for a limited set of critical experiment configurations. These results contain fuel pins with a wide range of relative pin power levels.

Table 4-7 through Table 4-11 provide the results for each of the configurations where comparisons were performed. The results shown are the RMS of the relative pin fission rate differences expressed in percent as well as predicted and measured peak pin fission rate locations, peak pin fission rate differences and maximum, minimum fission rate differences.

Fission rate distribution maps are provided for each configuration for which measurements were provided in Figure 4-1 through Figure 4-36. Due to their size, maps for EPICURE and KRITZ configurations are split into smaller maps. In these cases a description of the complete map is presented first with the definition of the zones that are used for the smaller maps.

For KRITZ, the layout has changed from figures presented in Reference 4.4-1, response to RAI 15. A full core layout is provided and the normalization was slightly changed, leading to slight variations in measured values. For EPICURE UH1.2, 30% Void, UH1.4, Pyrex, and UH1.4, SS & AIC configurations, the figures contain one additional point than did the figures in Reference 4.4-1.

The fission rate distributions are relative to an average assembly fission rate of 1.0. Unlike fission rate distribution maps provided in Reference 4.4-1, response to RAI 15 and Section 12.2.1, no data is included for Gad rod locations in Figure 4-5 through Figure 4-10. Pin powers in the Gad rods locations are below 0.8 and are not used in calculating the statistics for each experiment.

Estimated uncertainties for the fission rate measurements were provided in Reference 4.4-1, response to RAI 60. For the KRITZ KWU configuration, the estimated uncertainty was [            ]. For the EPICURE and CAMELEON experiments, the estimated uncertainty was [            ]. For the B&W 1970s experiments, the [       ] uncertainties were [       ] (Configuration XI\_2), [       ] (Configuration XI\_6), [       ] (Configuration XI\_8) and [       ] (Configuration XI\_11). For the B&W 1980s experiments, the [       ] uncertainties were [       ] for Core 1 and [       ] for all other configurations (Cores 5, 12, 14, 18 and 20).

The RMS values are presented in Table 4-7 through Table 4-11. There are no configurations that exceed a [       ] RMS difference. Only one configuration from the B&W 1970's experimental program has a C/M comparison in which the absolute value of a single pin error exceeds [       ].

Table 4-12 provides a comparison between the average and peak RMS results presented in Reference 4.4-1 and Supplement 1.

**Table 4-7**  
**B&W-1970s Fission Rate Distribution Comparisons**

**Table 4-8**  
**B&W-1980s Fission Rate Distribution Comparisons**

**Table 4-9**  
**KRITZ KWU Fission Rate Distribution Comparisons**

**Table 4-10**  
**EPIPURE Fission Rate Distribution Comparisons**

**Table 4-11**  
**CAMELEON Fission Rate Distribution Comparisons**

**Table 4-12**  
**Fission Rate Distribution (RMS) Comparisons with ANP-10297P-A**



**Figure 4-1**  
**B&W 1970's Core XI\_2 Fission Rate Comparison (%)**



**Figure 4-2**  
**B&W 1970's Core XI\_6 Fission Rate Comparison (%)**



**Figure 4-3**  
**B&W 1970's Core XI\_8 Fission Rate Comparison (%)**



**Figure 4-4**  
**B&W 1970's Core XI\_11 Fission Rate Comparison (%)**



**Figure 4-5**  
**B&W 1980's Core 1 Fission Rate Comparison (%)**



**Figure 4-6**  
**B&W 1980's Core 5 Fission Rate Comparison (%)**

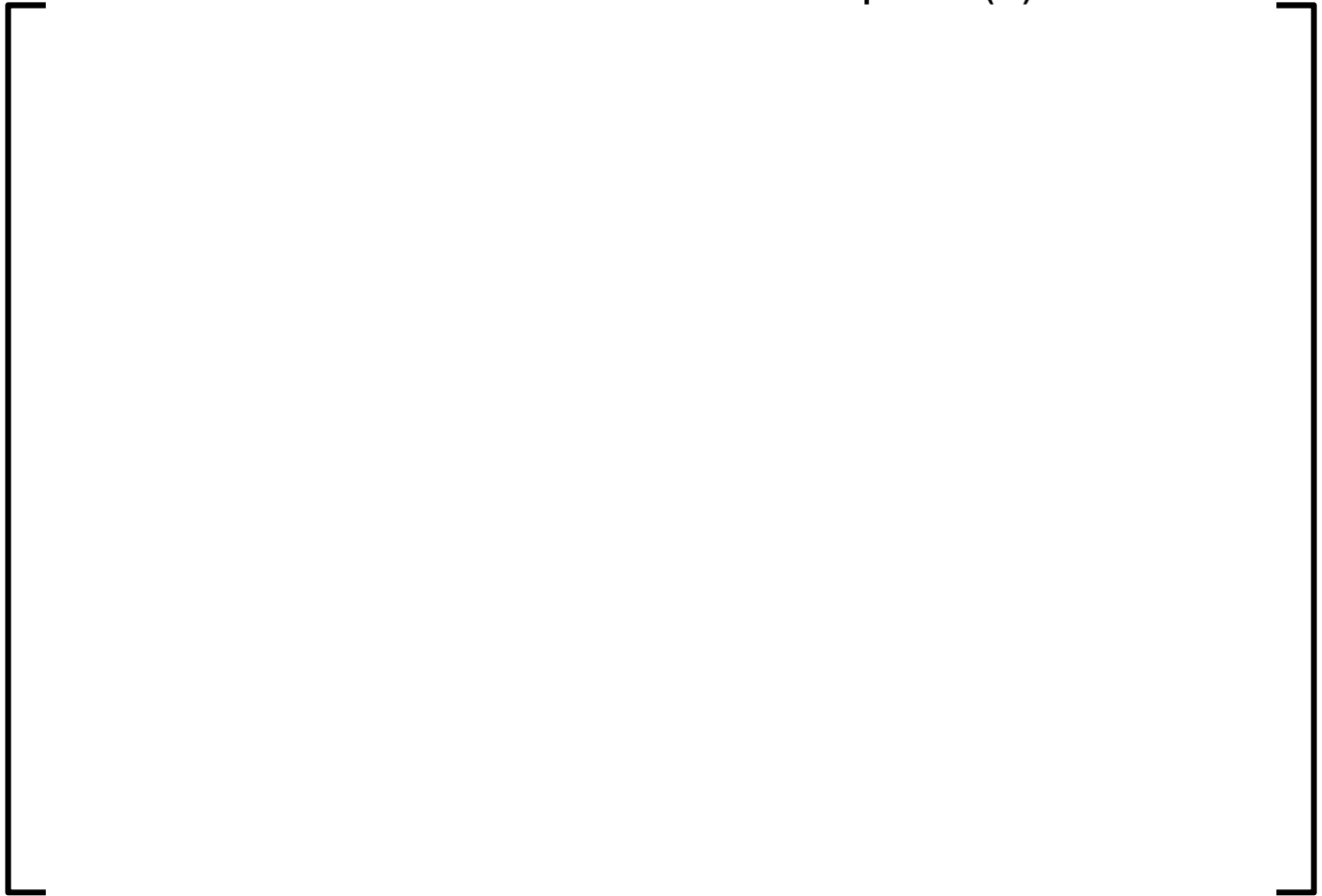


**Figure 4-7**  
**B&W 1980's Core 12 Fission Rate Comparison (%)**

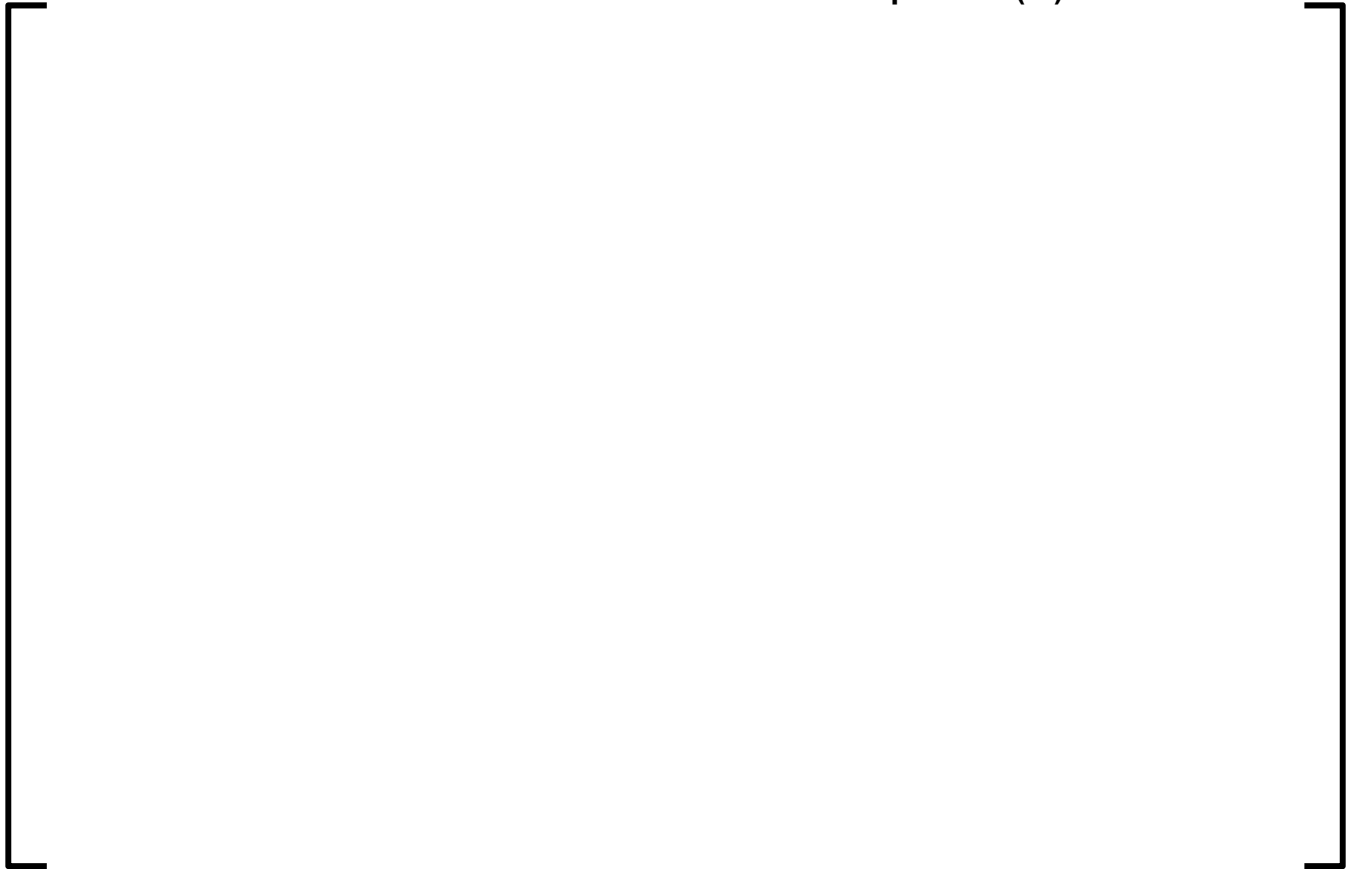


**Figure 4-8**  
**B&W 1980's Core 14 Fission Rate Comparison (%)**





**Figure 4-9**  
**B&W 1980's Core 18 Fission Rate Comparison (%)**



**Figure 4-10**  
**B&W 1980's Core 20 Fission Rate Comparison (%)**



**Figure 4-11**  
**KRITZ KWU UWH1 Reference Layout**

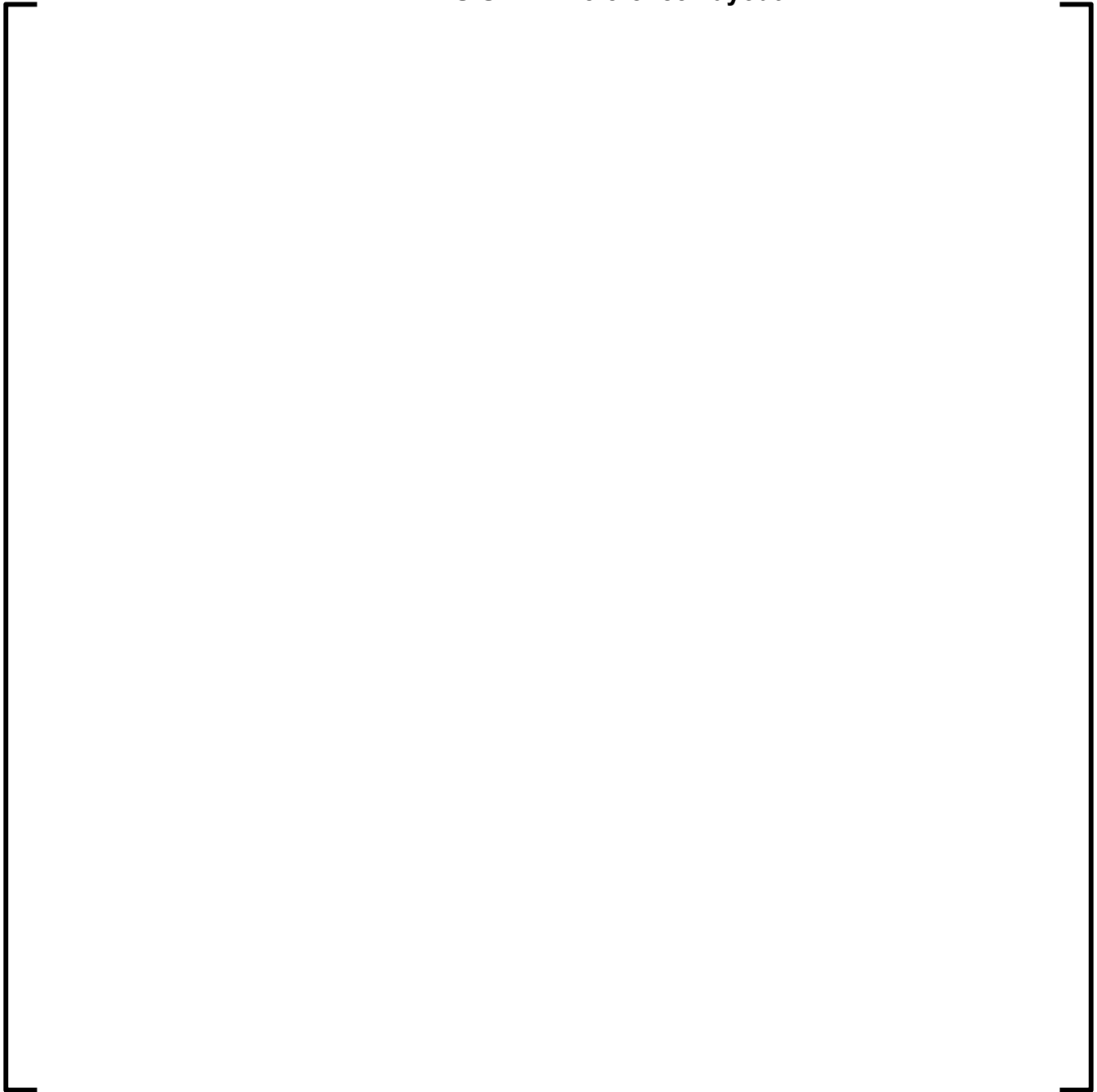


**Figure 4-12**  
**KRITZ KWU UWH1 Reference Fission Rate Comparison (%) –**  
**Red Zone**

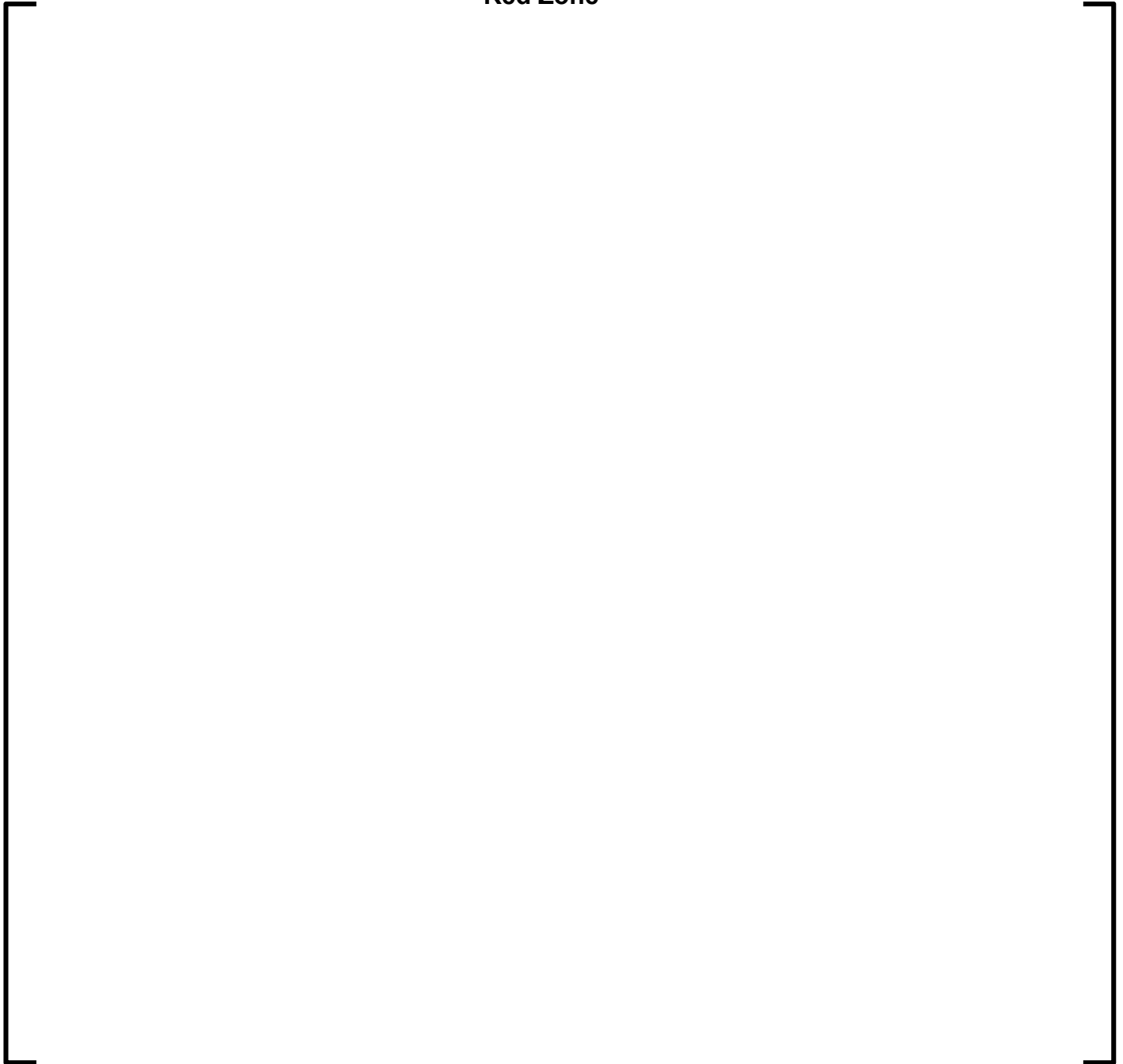


**Figure 4-13**  
**KRITZ KWU UWH1 Reference Fission Rate Comparison (%) –**  
**Green and Magenta Zones**

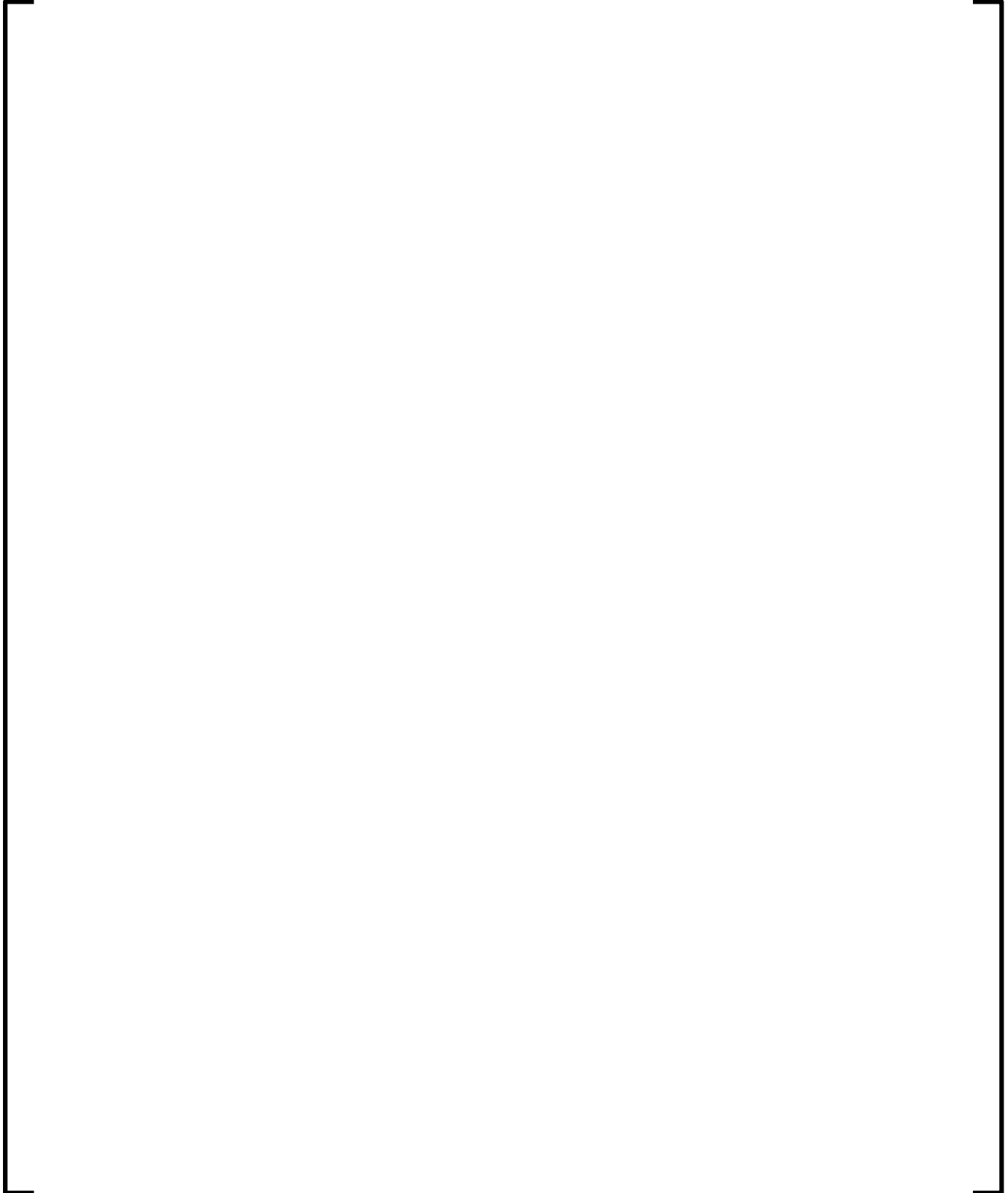


**Figure 4-14**  
**KRITZ KWU UWH1 Reference Fission Rate Comparison (%) –**  
**Cyan and Blue Zones**

**Figure 4-15**  
**EPIPURE UH1.2 Reference Layout**

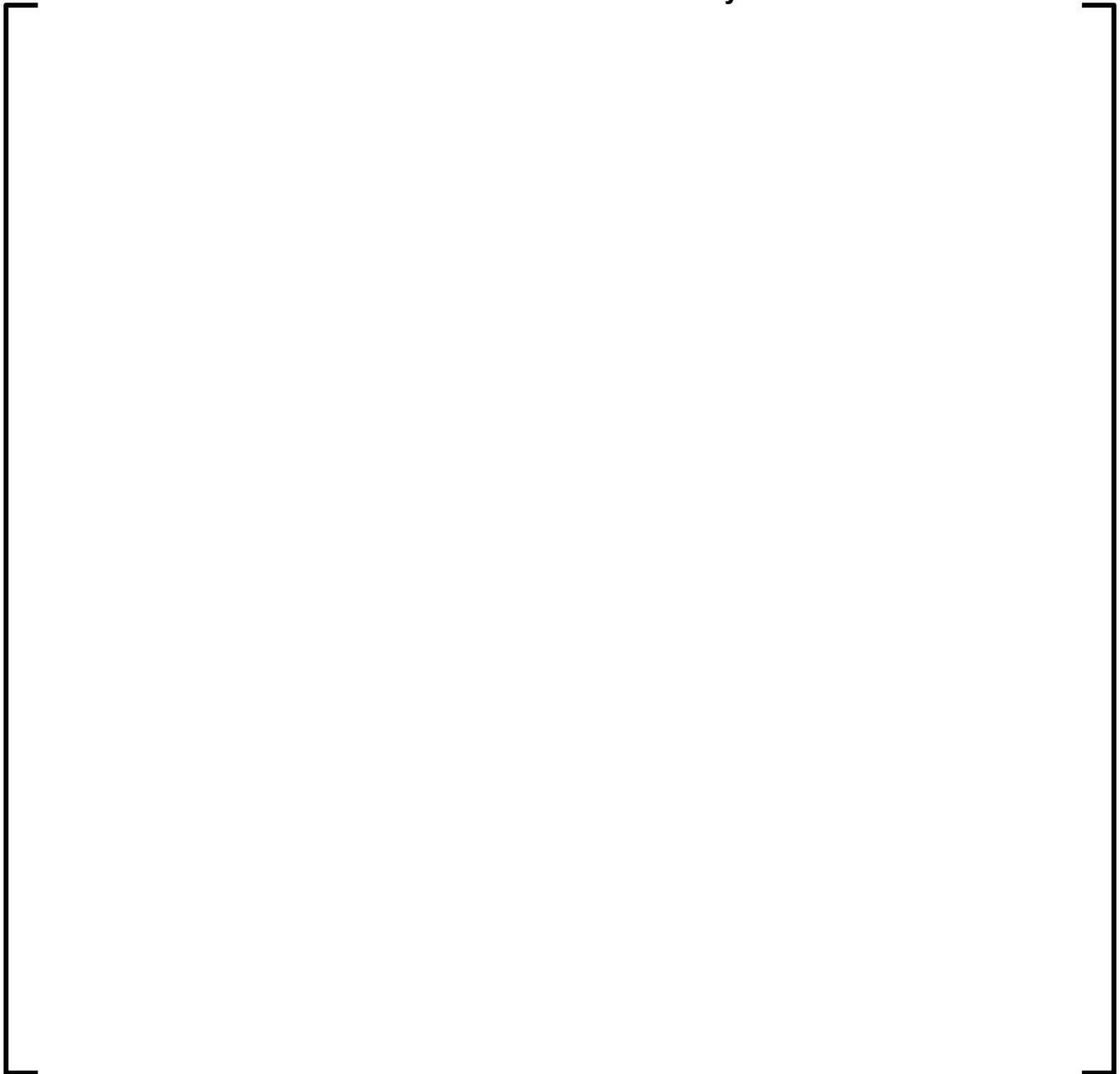


**Figure 4-16**  
**EPIQUIRE UH1.2 Reference Fission Rate Comparison (%) –**  
**Red Zone**





**Figure 4-17**  
**EPIASURE UH1.2 Reference Fission Rate Comparison (%) –**  
**Magenta, Green and Blue Zones**



**Figure 4-18**  
**EPICURE UH1.2, 30% Void Layout**

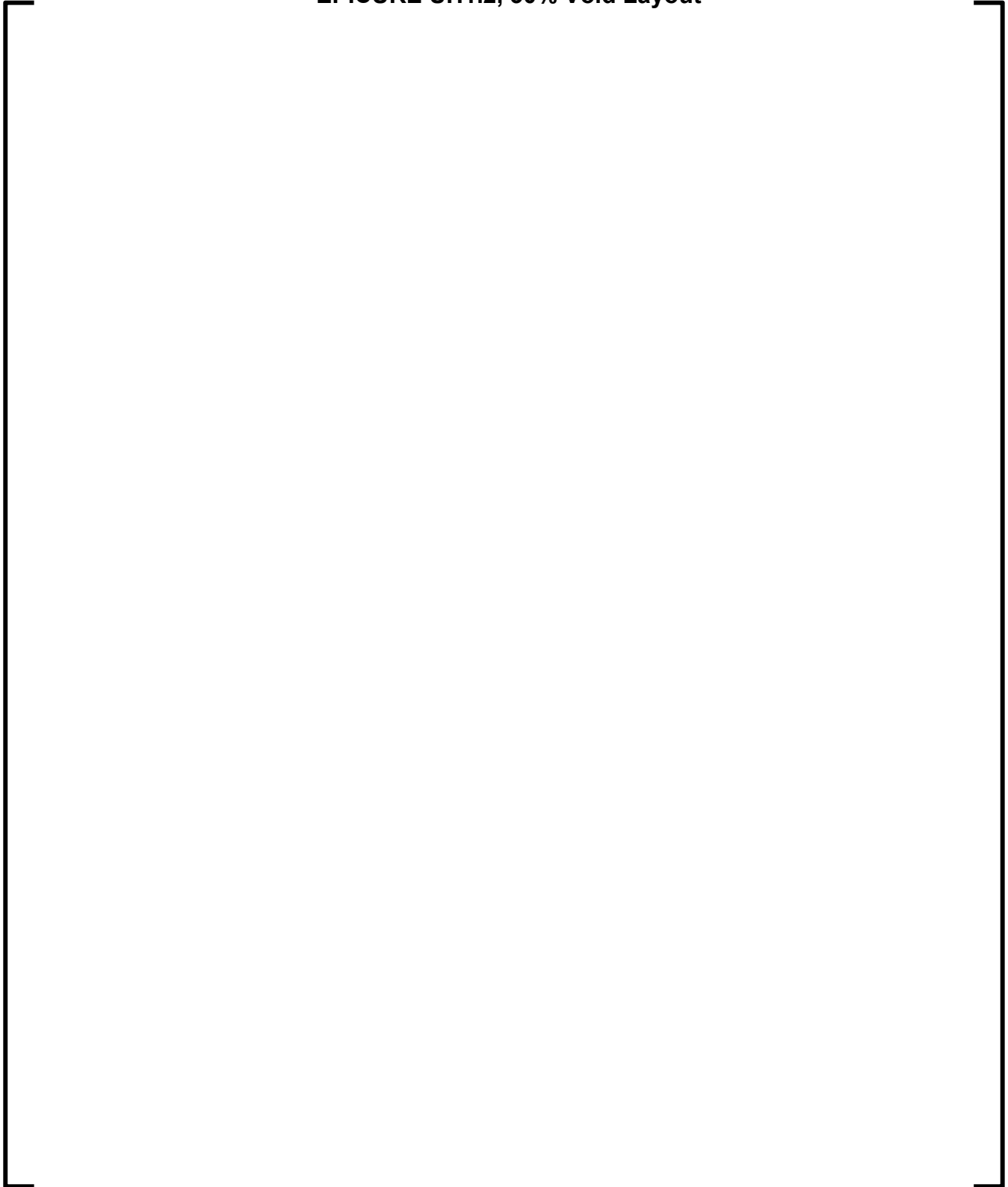


**Figure 4-19**  
**EPIQUIRE UH1.2, 30% Void Fission Rate Comparison (%) –**  
**Red and Green Zones**

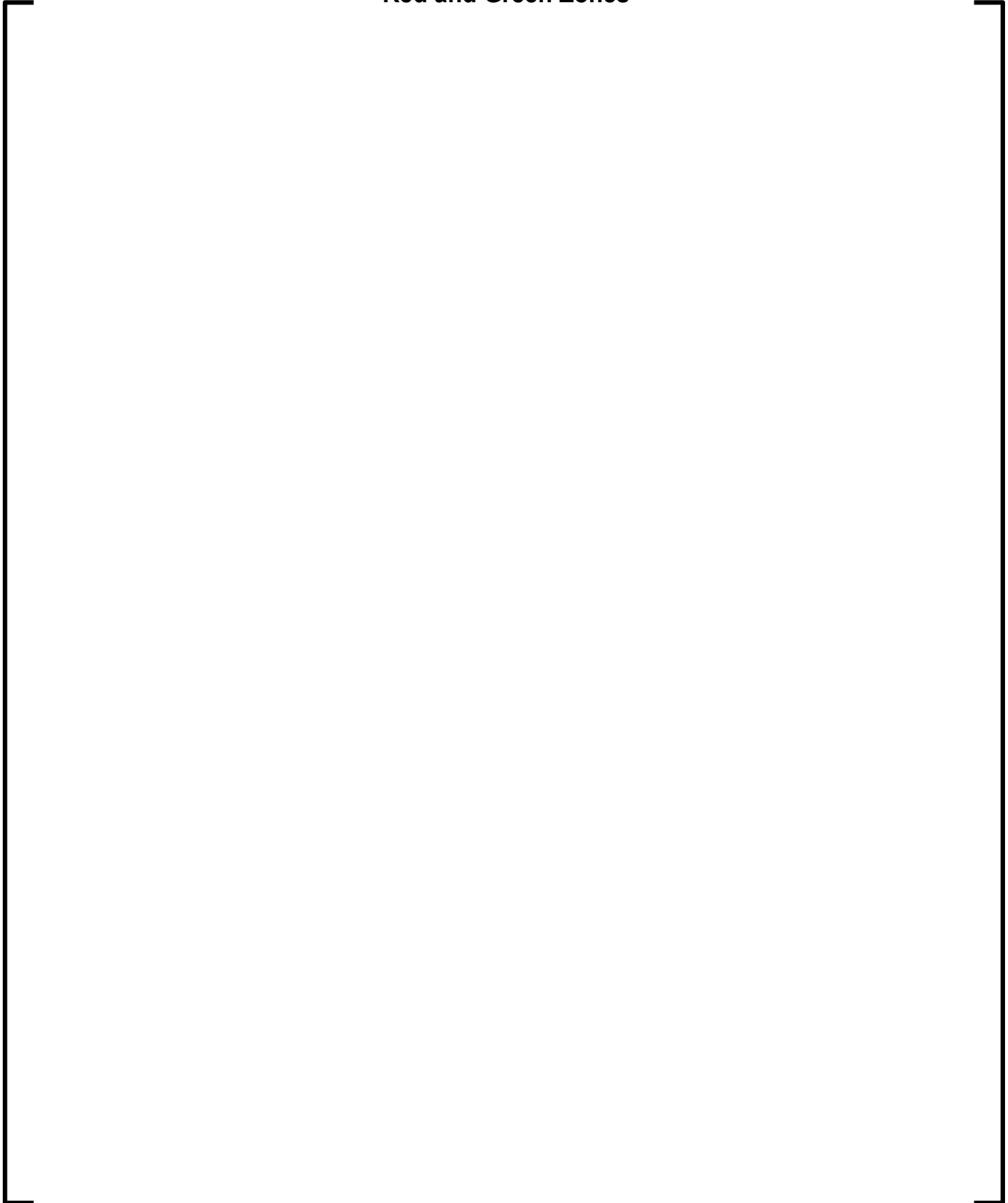


**Figure 4-20**  
**EPICURE UH1.2, 50% Void Layout**

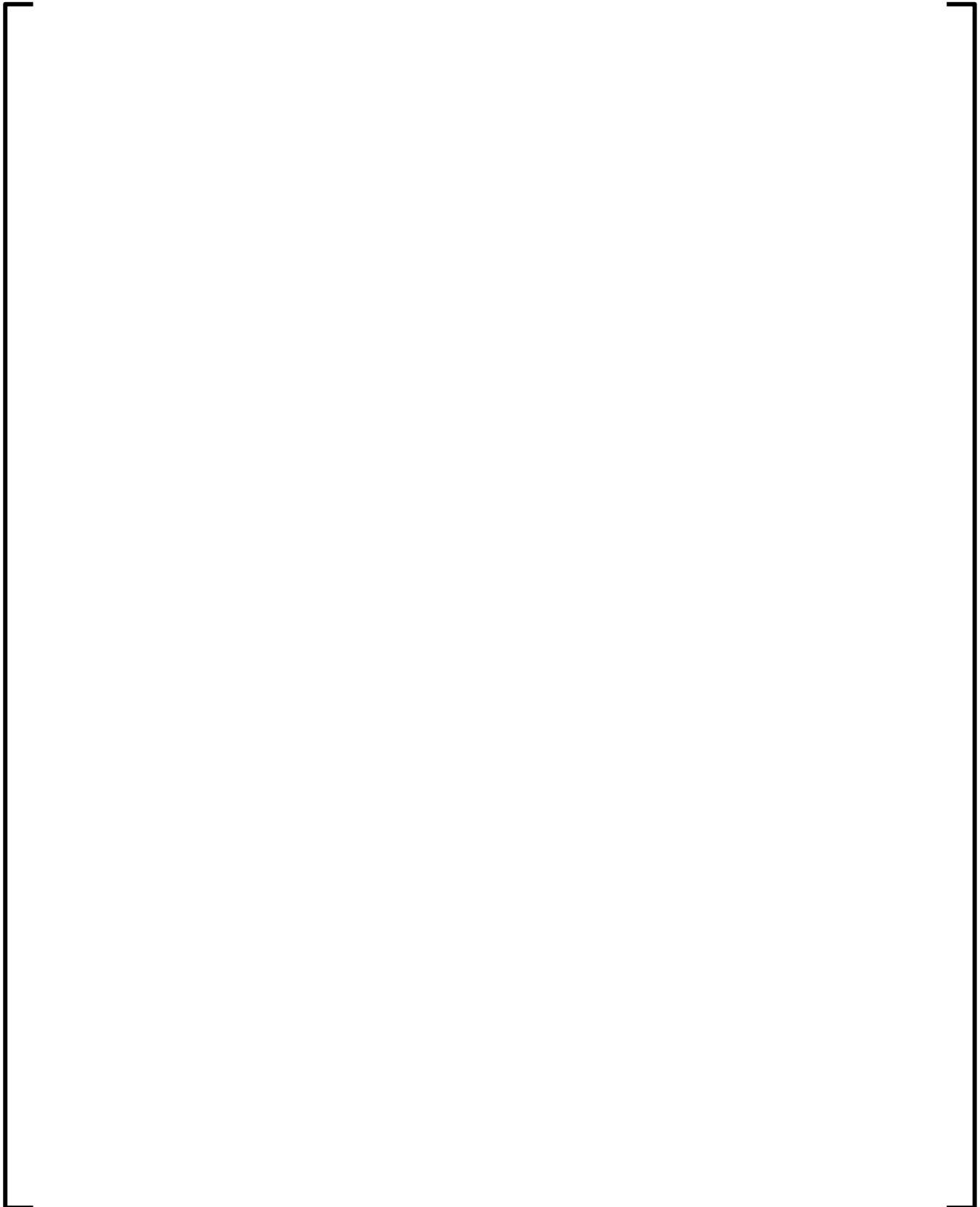


**Figure 4-21**  
**EPIQUIRE UH1.2, 50% Void Fission Rate Comparison (%) –**  
**Red and Green Zones**

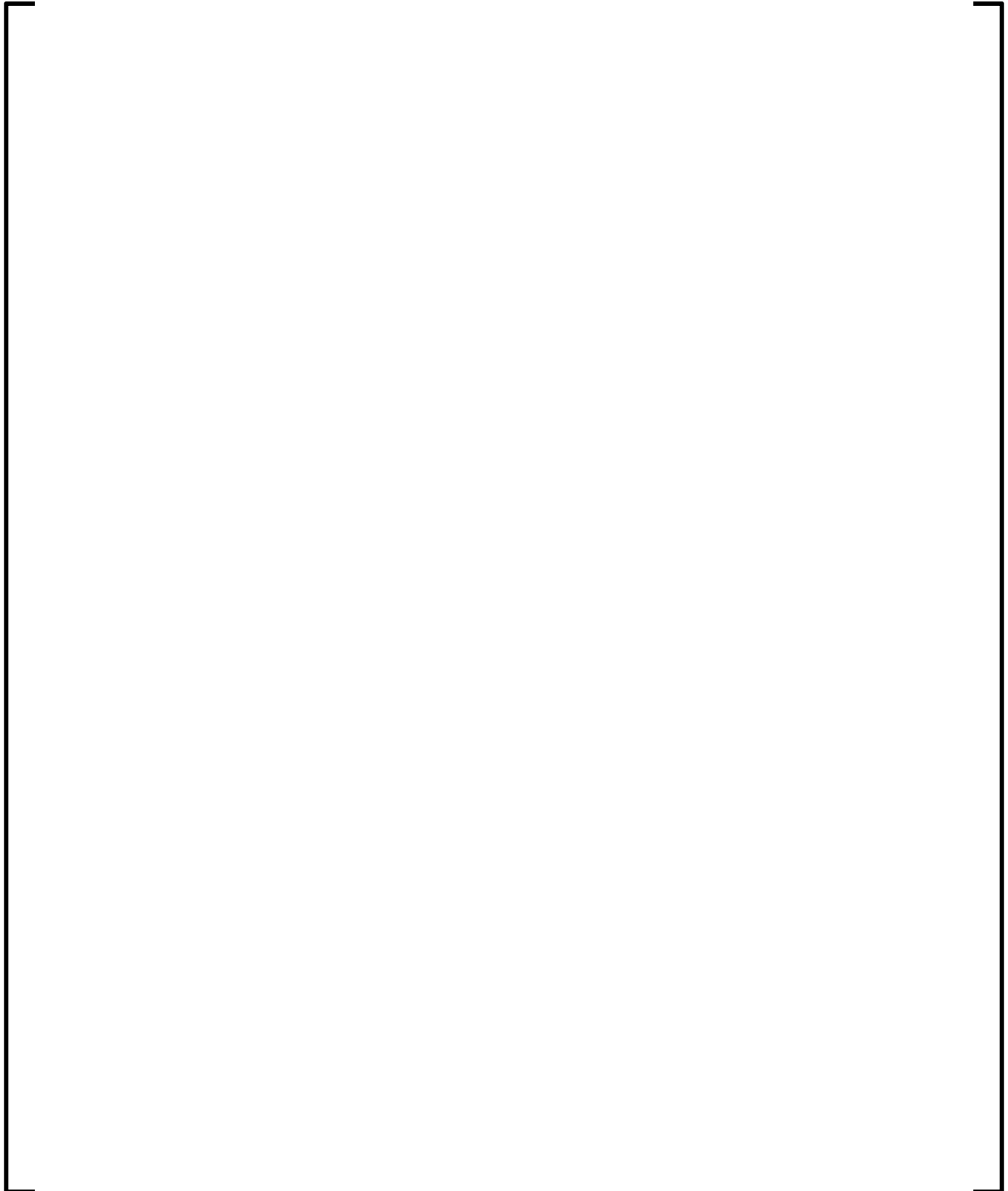


**Figure 4-22**  
**EPIASURE UH1.2, 100% Void Layout**

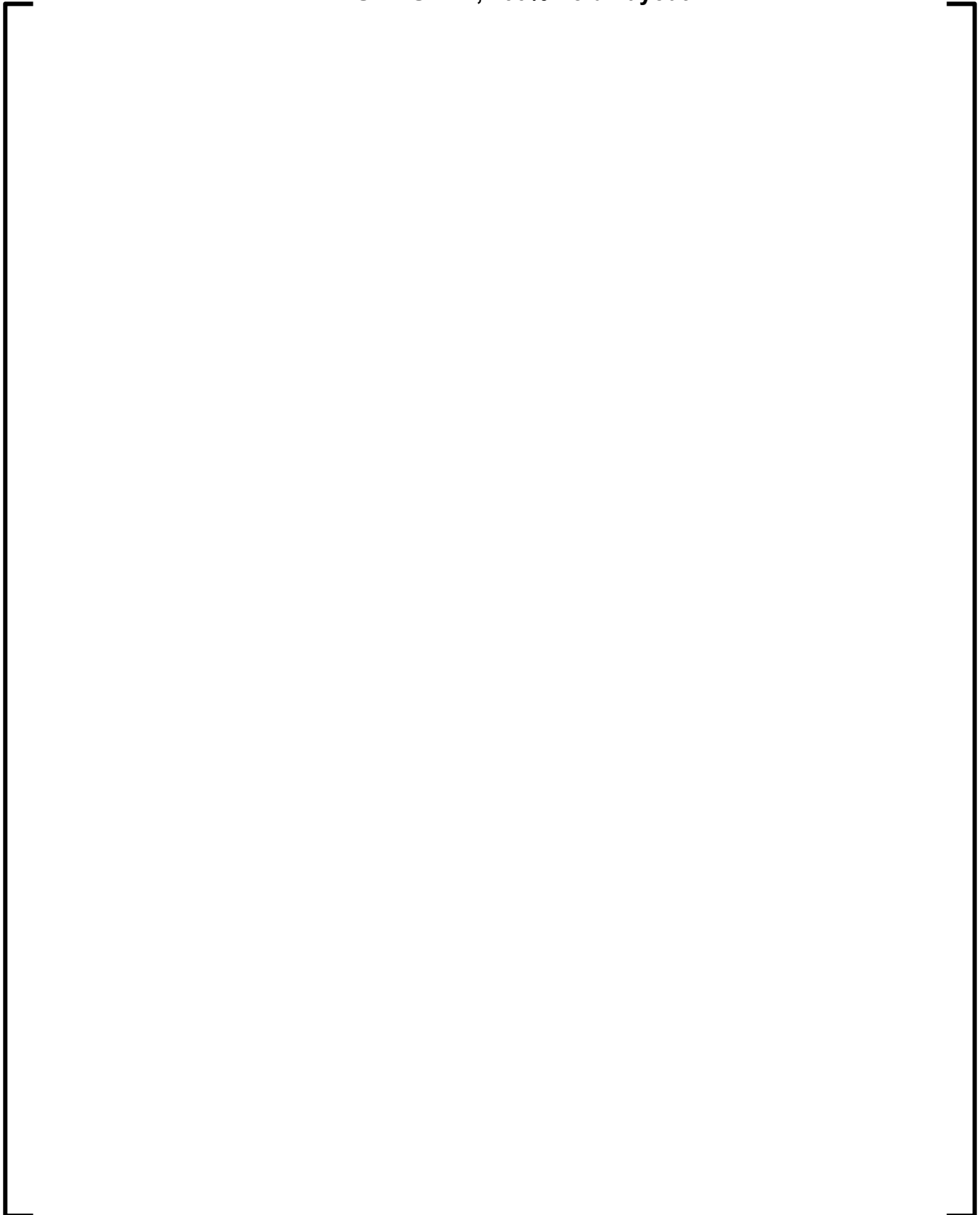


**Figure 4-23**  
**EPIPURE UH1.2, 100% Void Fission Rate Comparison (%) –**  
**Red and Green Zones**

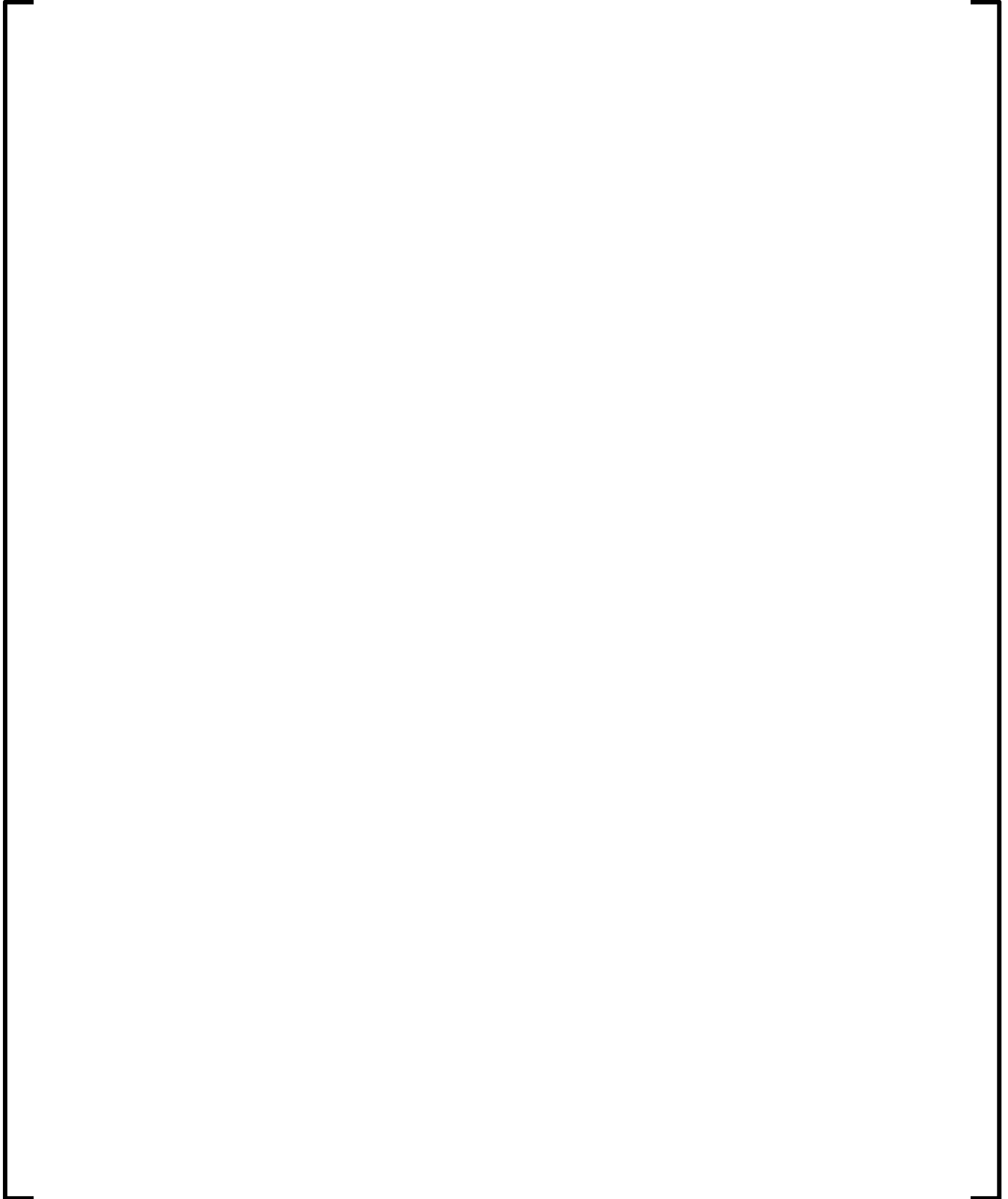


**Figure 4-24**  
**EPIPURE UH1.4 Reference Layout**

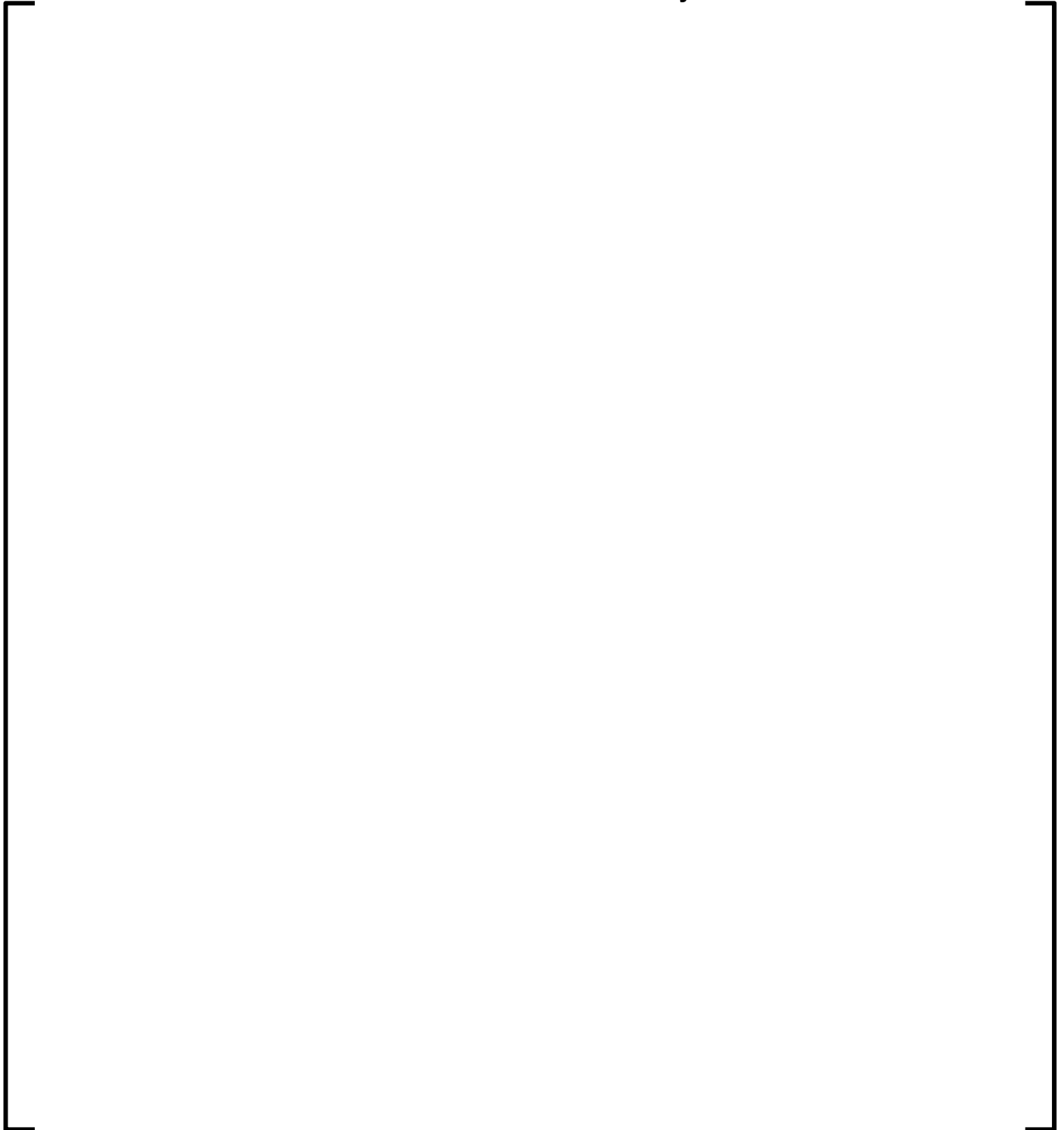




**Figure 4-25**  
**EPIQUIRE UH1.4 Reference Fission Rate Comparison (%) –**  
**Red Zone**



**Figure 4-26**  
**EPIPURE UH1.4 Reference Fission Rate Comparison (%) –**  
**Green and Blue Zones**

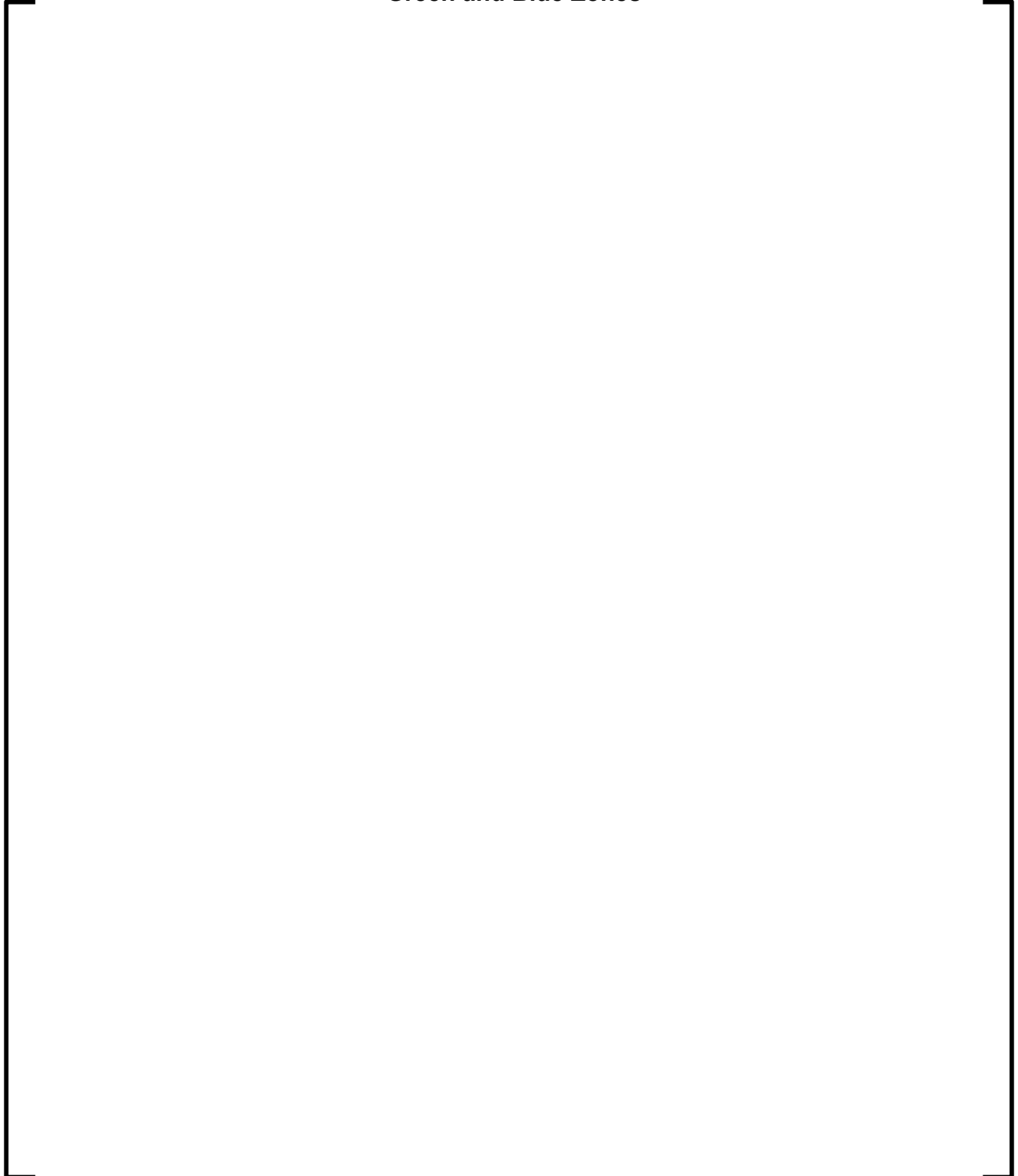


**Figure 4-27**  
**EPICURE UH1.4 Pyrex Layout**

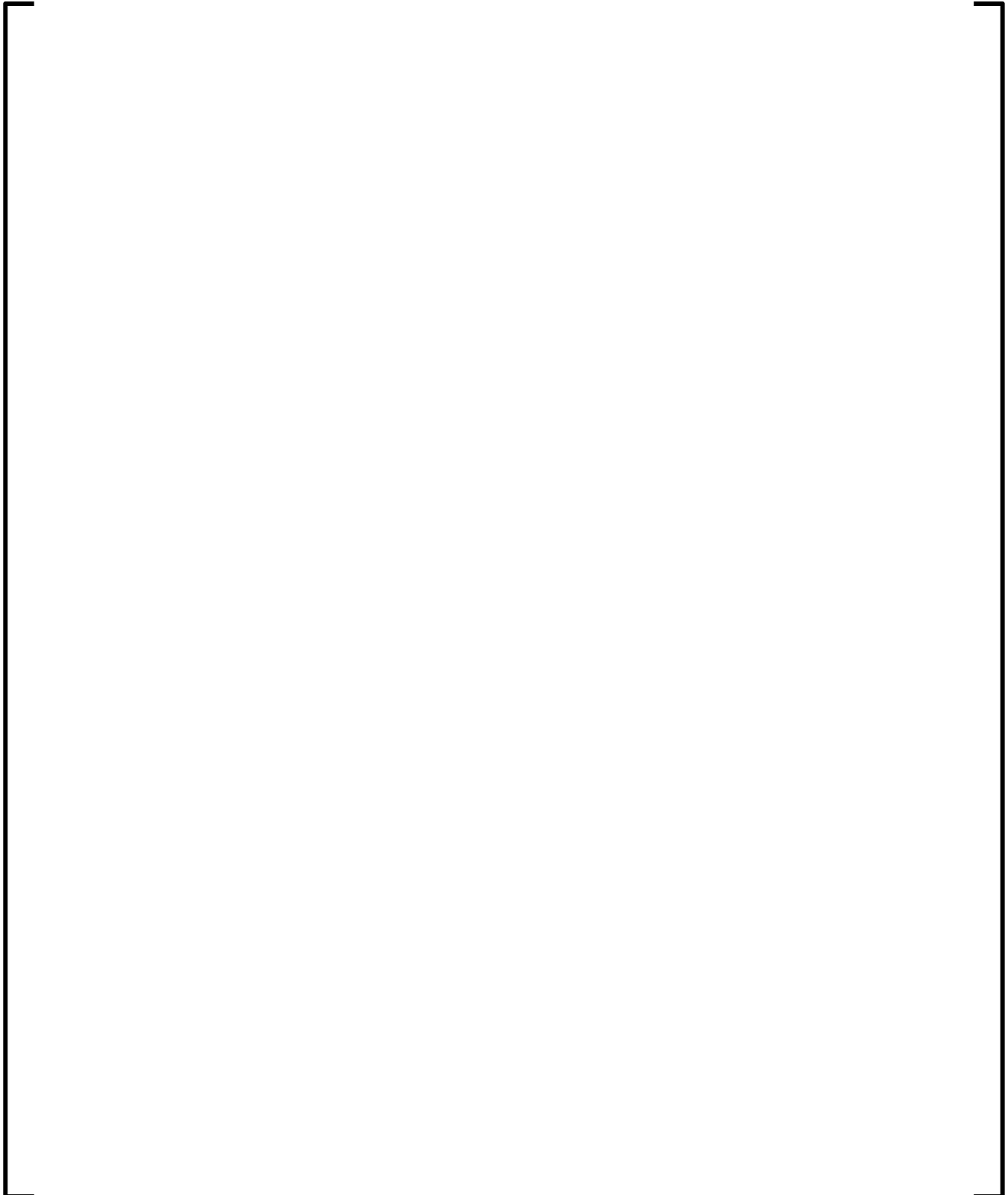


**Figure 4-28**  
**EPIPURE UH1.4 Pyrex Fission Rate Comparison (%) –**  
**Red Zone**



**Figure 4-29**  
**Pyrex Fission Rate Comparison (%) –**  
**Green and Blue Zones**

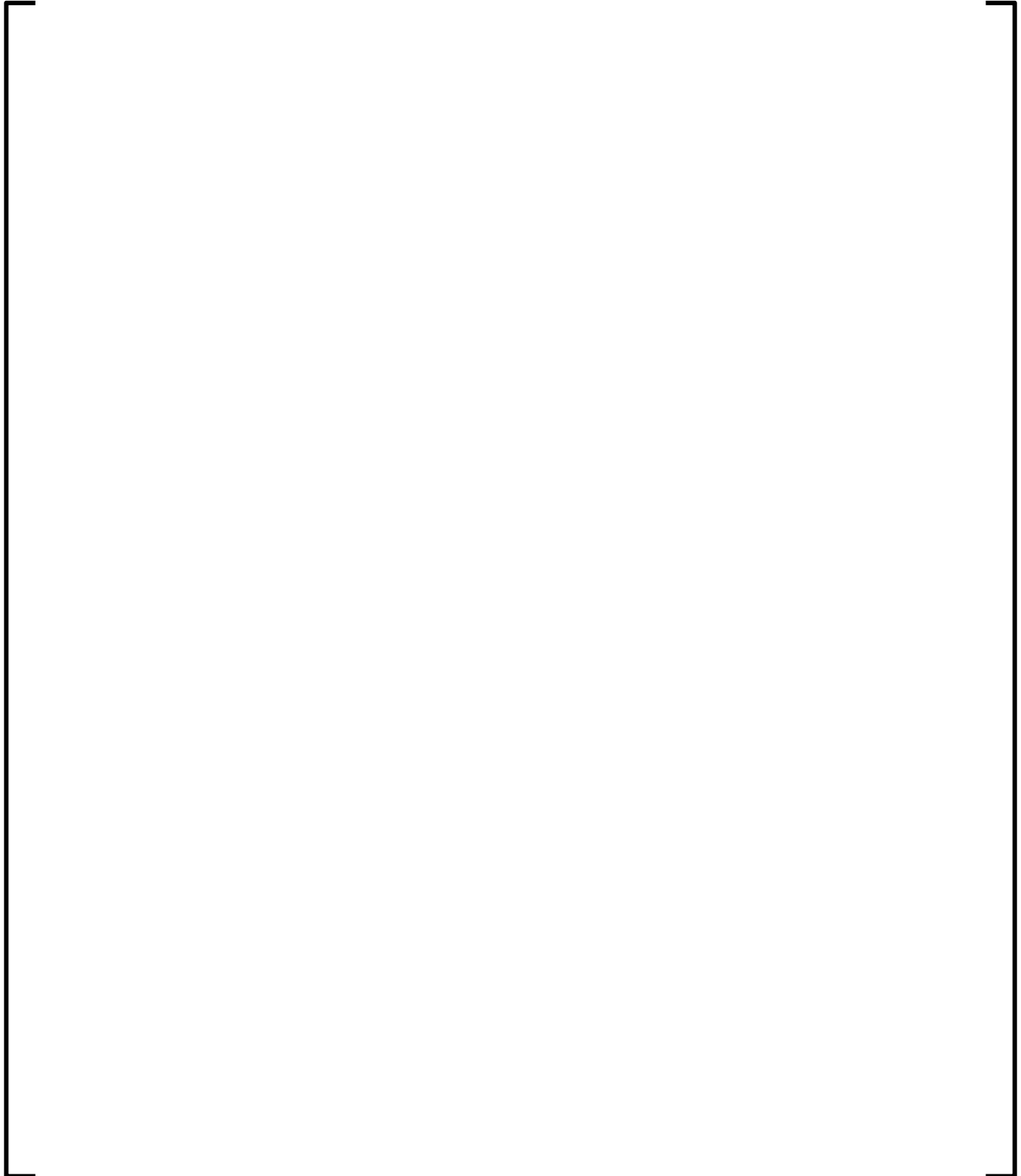


**Figure 4-30**  
**EPICURE UH1.4 SS&AIC Layout**

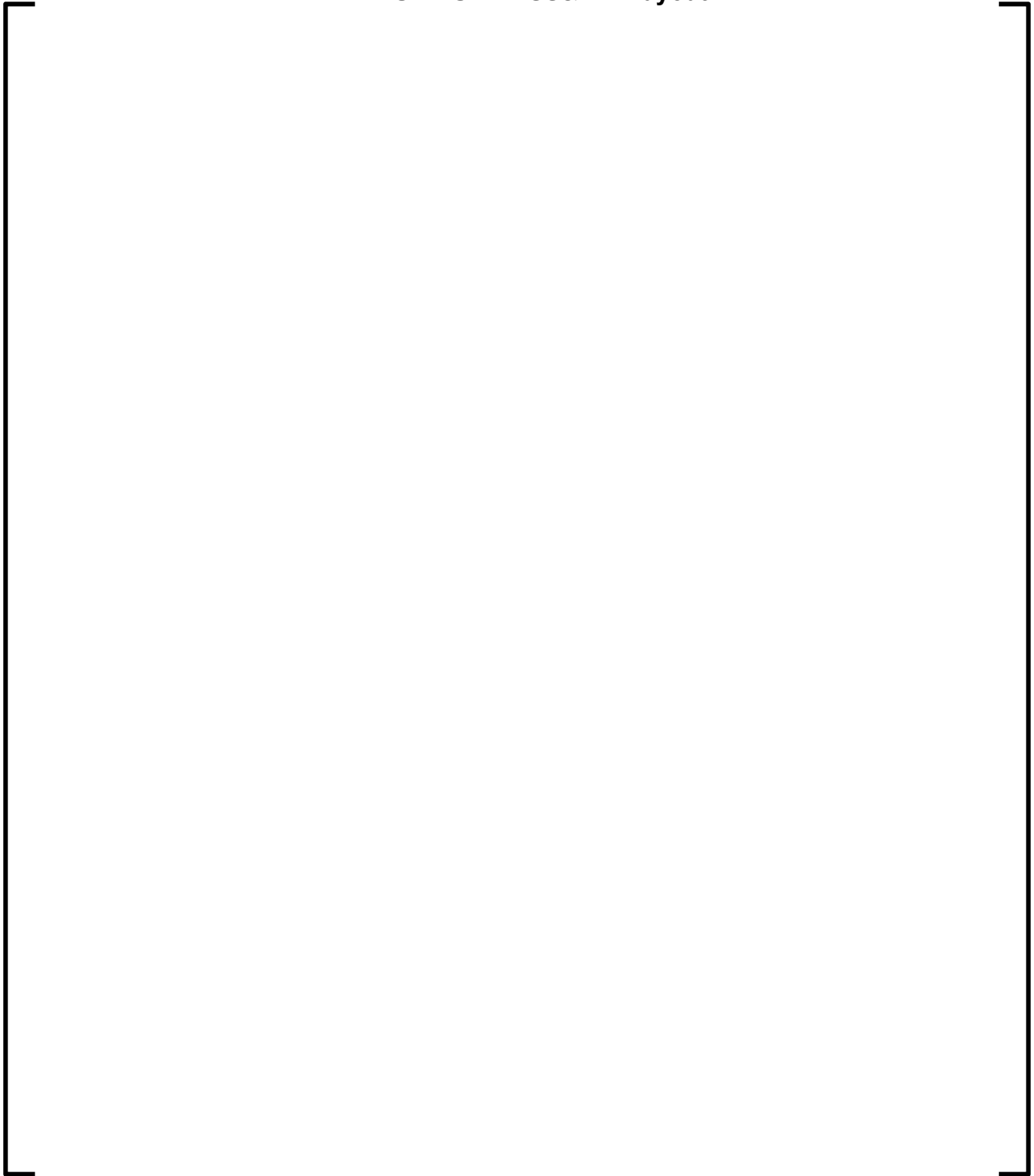


**Figure 4-31**  
**EPIASURE UH1.4 SS&AIC Fission Rate Comparison (%) –**  
**Red Zone**



**Figure 4-32**  
**EPIPURE UH1.4, SS&AIC Fission Rate Comparison (%) –**  
**Green and Blue Zones**

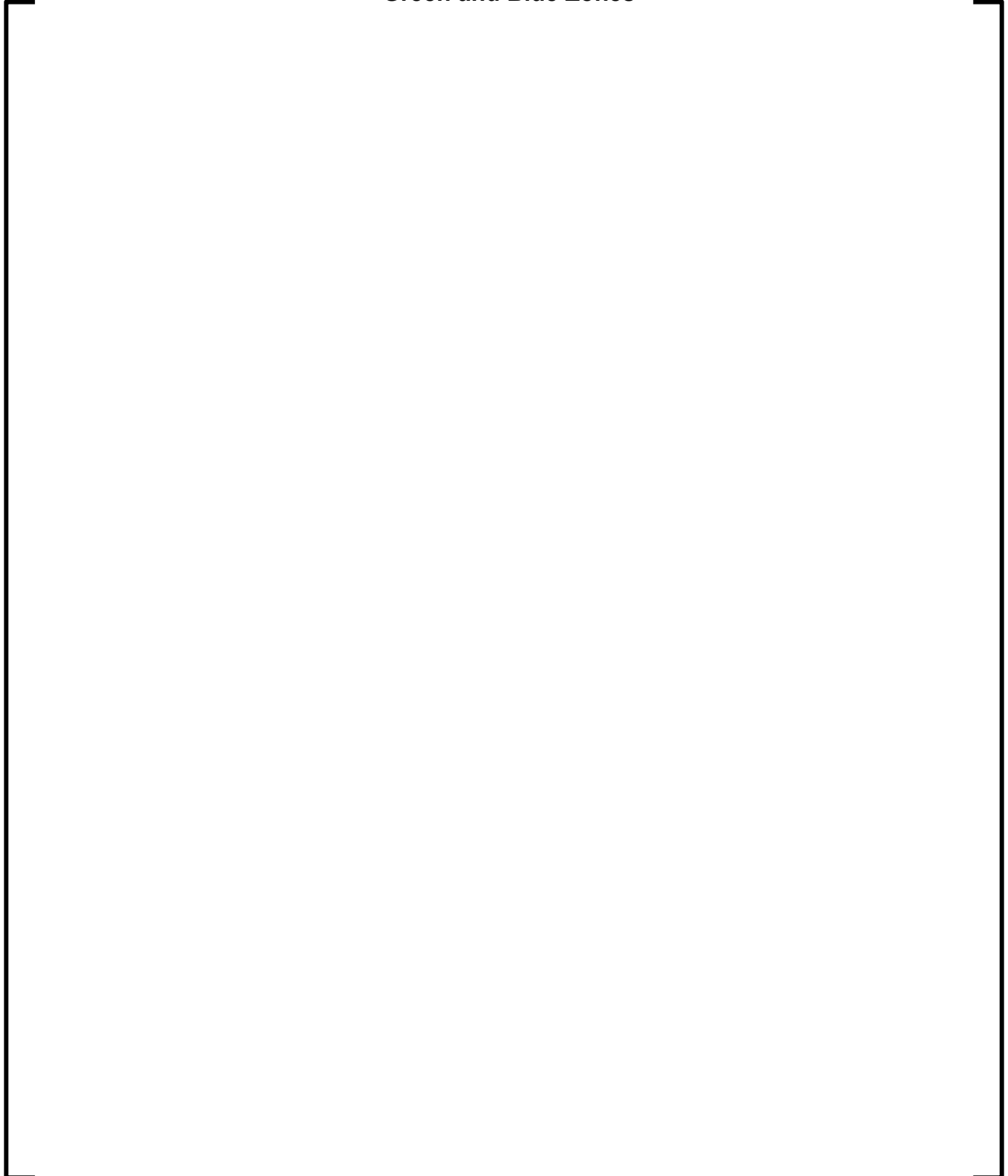




**Figure 4-33**  
**CAMELEON 25GT\_12GD Fission Rate Comparison (%)**



**Figure 4-34**  
**CAMELEON 13GD Fission Rate Comparison (%)**



**Figure 4-35**  
**CAMELEON 12GD Fission Rate Comparison (%)**



**Figure 4-36**  
**CAMELEON 5GD Fission Rate Comparison (%)**



### 4.1.3 Discussion of Results - Critical Experiments

The comparison results provided in Sections 4.1.1 and 4.1.2 of this supplement show good agreement of the calculations with the measurements. For the results related to criticality, APOLLO2-A overestimated the  $k_{\text{eff}}$  of the analyzed experiments by an average of [ ] pcm with a standard deviation of [ ] pcm. This over-estimation is consistent with the changes made to the APOLLO2-A code.

The fission rate distributions also showed good agreement with the measurements; none of the experiments showed a discrepancy of more than [ ] RMS.

These results confirm the ability of APOLLO2-A to accurately calculate the reactivity and fission rate distribution of fuel pin lattices.

## 4.2 Integral Experiments

Reference 4.4-1, Section 6.3 presented a description and results of the VALDUC integral experiments. These experiments were performed by CEA and the Institut de Protection et de Sûreté Nucléaire, now the Institut de Radioprotection et de Sûreté Nucléaire (IRSN) in 1978 at CEA's experiment criticality facility in Valduc, France.

Reactivity measurement comparisons are presented in Table 4-13 as  $((C-M) * 10^5)$  expressed in pcm. Table 4-14 shows comparisons of the reactivity difference results with those presented in Reference 4.4-1.

Table 4-13 shows good agreement of the calculations with the measurements; APOLLO2-A underestimated the  $k_{\text{eff}}$  of the analyzed experiments by an average of [ ] pcm with a standard deviation of [ ] pcm.

**Table 4-13**  
**Reactivity Comparisons to Measurement for VALDUC Critical**  
**Experiments**

--	--

**Table 4-14**  
**VALDUC Critical Experiments – Reactivity Difference Comparisons**  
**with ANP-10297P-A**

--	--

### 4.3 *Spent Fuel Analyses*

Reference 4.4-1, Section 6.4 presented the benchmarking of APOLLO2-A against fuel isotopic evolution during irradiation in a reactor core. Measured samples come from several different power plants in France and Switzerland, covering UO<sub>2</sub>, Enriched Recycled Uranium (ERU), UO<sub>2</sub>-Gd<sub>2</sub>O<sub>3</sub> and MOX fuel types. Burnups ranged from 3 to 71 GWd/t. Experiments from which the samples were taken were well described in Reference 4.4-1.

The averaged results are presented in Table 4-15 through Table 4-18 as (C/M-1), in % for all sample types except the UO<sub>2</sub>-Gd<sub>2</sub>O<sub>3</sub> samples. For UO<sub>2</sub>-Gd<sub>2</sub>O<sub>3</sub> samples, the averaged results are presented as (C-M)\*100 since the relative differences are not pertinent when low concentrations are considered. For low concentrations, use of relative differences incorrectly indicates that significant differences exist when the differences are actually insignificant since these isotopes have almost completely been depleted.

Also included in these tables are the results presented in Reference 4.4-1. It was shown in Reference 4.4-1, response to RAI 18 that the high importance isotopes are, as expected, for Uranium and Plutonium. Data for all isotopics are similar between the supplement and Reference 4.4-1 results.

The results presented for the high importance spent fuel isotopics show good agreement between the calculated and the measured values. Considering the importance on reactivity of the different isotopes and the uncertainties associated with the modeling of the irradiation and with the measurements, the overall comparisons of APOLLO2-A results to measurements are considered acceptable.

Uncertainties associated with the spent fuel isotopics were estimated in Reference 4.4-1, response to RAI 60. It is noted that for the spent fuel analysis, two types of uncertainties are considered: modeling uncertainties and measurement uncertainties. These values are presented in Table 4-19 along with the current results for these isotopes. In all cases, the accuracy of APOLLO2-A is within two standard deviations of the expected accuracy between the model and the measured values.

A similar analysis is presented for MOX fuel in Table 4-20. The combined uncertainties for the four isotopes having the most impact on reactivity ( $^{239}\text{Pu}$ ,  $^{240}\text{Pu}$ ,  $^{241}\text{Pu}$  and  $^{241}\text{Am}$ ) from Reference 4.4-1, response to RAI 60, are also shown in Table 4-20. In all cases, the accuracy of APOLLO2-A is within two standard deviations of the expected accuracy between the model and the measured values.



**Table 4-15**  
**Isotopic Burnup Analysis – UO<sub>2</sub> Concentrations Comparisons**  
**(C/M-1)x100%**

**Table 4-16**  
**Isotopic Burnup Analysis – ERU Concentrations Comparisons**  
**(C-M-1)x100%**

**Table 4-17**  
**Isotopic Burnup Analysis – UO<sub>2</sub>-Gd<sub>2</sub>O<sub>3</sub> Concentrations**  
**Comparisons (C-M)x100**

**Table 4-18**  
**Isotopic Burnup Analysis – MOX Concentrations Comparisons**  
**(C/M-1)x100%**

**Table 4-19**  
**Isotopic Burnup Analysis – UO<sub>2</sub> APOLLO2-A Results (C/M-1 in %)**  
**versus Estimated Uncertainties**

**Table 4-20**  
**Isotopic Burnup Analysis – MOX APOLLO2-A Results (C/M-1 in %)**  
**versus Estimated Uncertainties**

#### **4.4      *References***

- 4.4-1    ANP-10297P-A, Revision 0, The ARCADIA® Reactor Analysis System for PWRs Methodology Description and Benchmarking Results Topical Report, February 2013.

## **5.0 ARCADIA® RE-VALIDATION OF CORE BENCHMARKS**

### **5.1 *Introduction***

Reference 5.5-1 provided validation of the ARCADIA® code system through cycle benchmarks for nine commercial plant/fuel types. Comparisons to startup physics testing as well as core follow data were provided. Validation criteria were based on the ANSI/ANS-19.6.1 standard in Reference 5.5-2.

The nine plants are identified below. Detailed descriptions of the cycles used in the validation are provided in Section 10.2.1 of Reference 5.5-1.

#### **Plant A Cycles 1-14**

Plant Type: Westinghouse reactor containing 157 assemblies  
Fuel Type: 17x17 array with 24 guide tubes/1 guide tube with instrument  
Detector: Moveable fission probe

#### **Plant B Cycle 1**

Plant Type: Westinghouse reactor containing 157 assemblies  
Fuel Type: 17x17 array with 24 guide tubes/1 guide tube with instrument  
Detector: Moveable fission probe

#### **Plant C Cycles 10-18**

Plant Type: Combustion Engineering reactor containing 217 assemblies  
Fuel Type: 14x14 array with 4 large guide tubes/1 large guide tube with instrument  
Detector: Fixed Rhodium SPNDs

#### **Plant G1 Cycles 26-30**

Plant Type: Siemens reactor containing 177 assemblies  
Fuel Type: 15x15 array with 19 guide tubes/1 guide tube with instrument  
Detector: Aeroball (Vanadium)

#### **Plant G2 Cycles 1-5**

Plant Type: Siemens – KONVOI reactor containing 193 assemblies  
Fuel Type: 18x18 array with 23 guide tubes/1 guide tube with instrument  
Detector: Aeroball (Vanadium)

#### **Plant S1 Cycles 12-14**

Plant Type: Westinghouse reactor containing 193 assemblies  
Fuel Type: 17x17 array with 24 guide tubes/1 guide tube with instrument  
Detector: Moveable fission probe

**Plant S2 Cycles 12-14**

Plant Type: Westinghouse reactor containing 193 assemblies

Fuel Type: 17x17 array with 24 guide tubes/1 guide tube with instrument

Detector: Moveable fission probe

**Plant T1 Cycles 9-15**

Plant Type: Babcock & Wilcox reactor containing 177 assemblies

Fuel Type: 15x15 array with 16 guide tubes/1 guide tube with instrument

Detector: Fixed Rhodium SPNDs

**Plant V1 Cycles 18-22**

Plant Type: Westinghouse reactor containing 157 assemblies

Fuel Type: 15x15 array with 20 guide tubes/1 guide tube with instrument

Detector: Moveable fission probe

New results for the benchmark calculations for these plants using APOLLO2-A cross sections and ARTEMIS™ are provided in this section.

An additional plant is benchmarked which will extend the applicability range of benchmarks to include Enriched Reprocessed Uranium (ERU) fuel. This plant is referred to as Plant E. The benchmarked cycle descriptions for this plant are provided below:

**Plant E Cycles 12-17**

Plant Type: Westinghouse reactor containing 157 assemblies

Fuel Type: 17x17 array with the Westinghouse guide tube configuration shown in Appendix E, Figure E 5.1 1.

Detector: Moveable fission probe

**Plant E Cycle 12**

This cycle design loaded 40 fresh fuel assemblies including:

- 36 Enriched Reprocessed Uranium (ERU) at 3.707 wt% <sup>235</sup>U
- 4 Enriched Natural Uranium (ENU) at 3.7 wt% <sup>235</sup>U.

The burned fuel assemblies included:

- 44 once-burnt ERU assemblies at 3.705 wt%  $^{235}\text{U}$
- 8 twice-burnt ERU assemblies at 3.698 and 3.71 wt%  $^{235}\text{U}$
- 33 twice-burnt ENU assemblies at 3.7 wt%  $^{235}\text{U}$
- 8 thrice-burnt ERU assemblies at 3.698 wt%  $^{235}\text{U}$
- 20 thrice-burnt ENU assemblies at 3.7 wt%  $^{235}\text{U}$
- 4 fourth-burnt ENU assemblies at 3.7 wt%  $^{235}\text{U}$ .

No gadolinia-bearing fuel rods were used in the fresh fuel. Cycle 12 operated to approximately 12,078 MWd/MTU.

### **Plant E Cycle 13**

This cycle contained

- 44 fresh ERU assemblies at 3.692 wt%  $^{235}\text{U}$ .

The burned fuel assemblies included:

- 36 once-burnt ERU assemblies at 3.707 wt%  $^{235}\text{U}$
- 4 once-burnt ENU assemblies at 3.7 wt%  $^{235}\text{U}$
- 44 twice-burnt ERU assemblies at 3.705 wt%  $^{235}\text{U}$
- 1 twice-burnt ENU assemblies at 3.7 wt%  $^{235}\text{U}$
- 28 thrice-burnt ENU assemblies at 3.7 wt%  $^{235}\text{U}$ .

No gadolinia-bearing fuel rods were used in the fresh fuel. Cycle 13 operated to approximately 10,808 MWd/MTU.

**Plant E Cycle 14**

This cycle contained

- 40 fresh ERU assemblies at 3.945 wt%  $^{235}\text{U}$ .

The burned fuel assemblies included:

- 44 once-burnt ERU assemblies at 3.692 wt%  $^{235}\text{U}$
- 33 twice-burnt ERU assemblies at 3.707 wt%  $^{235}\text{U}$
- 4 twice-burnt ENU assemblies at 3.7 wt%  $^{235}\text{U}$
- 28 thrice-burnt ERU assemblies at 3.705 wt%  $^{235}\text{U}$
- 4 thrice-burnt ENU assemblies at 3.7 wt%  $^{235}\text{U}$
- 4 fourth-burnt ENU assemblies at 3.7 wt%  $^{235}\text{U}$ .

No gadolinia-bearing fuel rods were used in the fresh fuel. Cycle 14 operated to approximately 11,080 MWd/MTU.

**Plant E Cycle 15**

This cycle contained

- 40 fresh ENU assemblies at 3.7 wt%  $^{235}\text{U}$ .

The burned fuel assemblies included:

- 40 once-burnt ERU assemblies at 3.945 wt%  $^{235}\text{U}$
- 44 twice-burnt ERU assemblies at 3.692 wt%  $^{235}\text{U}$
- 1 twice-burnt ENU assembly at 3.7 wt%  $^{235}\text{U}$
- 28 thrice-burnt ERU assemblies at 3.707 wt%  $^{235}\text{U}$
- 4 thrice-burnt ENU assemblies at 3.7 wt%  $^{235}\text{U}$ .



No gadolinia-bearing fuel rods were used in the fresh fuel. Cycle 15 operated to approximately 11,271 MWd/MTU.

### **Plant E Cycle 16**

This cycle contained

- 40 ERU at 4.01 wt%  $^{235}\text{U}$ .

The burned fuel assemblies included:

- 40 once-burnt ENU assemblies at 3.7 wt%  $^{235}\text{U}$
- 40 twice-burnt ERU assemblies at 3.945 wt%  $^{235}\text{U}$
- 1 twice-burnt ERU assemblies at 3.707 wt%  $^{235}\text{U}$
- 32 thrice-burnt ERU assemblies at 3.692 wt%  $^{235}\text{U}$
- 4 thrice-burnt ENU assemblies at 3.7 wt%  $^{235}\text{U}$ .

No gadolinia-bearing fuel rods were used in the fresh fuel. Cycle 16 operated to approximately 10,397 MWd/MTU.

### **Plant E Cycle 17**

This cycle contained

- 40 ENU at 3.7 wt%  $^{235}\text{U}$ .

The burned fuel assemblies included:

- 40 once-burnt ERU assemblies at 4.01 wt%  $^{235}\text{U}$
- 40 twice-burnt ENU assemblies at 3.7 wt%  $^{235}\text{U}$
- 37 thrice-burnt ERU assemblies at 3.707 and 3.945 wt%  $^{235}\text{U}$ .

No gadolinia-bearing fuel rods were used in the fresh fuel. Cycle 17 operated to approximately 10,920 MWd/MTU.

## 5.2 ***Startup Physics Test Measurement***

Startup physics test predictions are compared to the available measured data at beginning-of-cycle for each cycle of each plant/fuel type. The parameters and criteria compared are:

1. All rods out critical boron concentration

Criterion: Calculated within  $\pm 50$  ppm of measured or  $\pm 500$  pcm equivalent

2. Individual control bank worths

Criterion: Individual bank worths calculated within  $\pm 15\%$  or  $\pm 100$  pcm of measured, whichever is larger

3. Total control bank worth

Criterion: Total bank worth calculated within  $\pm 10\%$  of measured

4. All rods out isothermal temperature coefficient

Criterion: Calculated within  $\pm 2$  pcm/ $^{\circ}\text{F}$  of measured

The above list of parameters is representative of startup physics test data typically available from commercial U.S. reactors at zero power conditions; however, some of the cycles analyzed were for European plants, which have different startup criteria. Certain startup physics test data were not available for those plants. Criteria for the parameters are based on the recommended test criteria provided in Reference 5.5-2.

Comparisons of ARCADIA<sup>®</sup> calculations with measured results for startup physics test measurements are summarized in Table 5-33 and Table 5-34. Measured data has been adjusted to reflect the ARCADIA<sup>®</sup> delayed neutron parameters, where available.

### **5.2.1 Startup Physics Summary for Plant A Cycles 1-14**

Comparisons of ARCADIA<sup>®</sup> calculations with measured results are summarized in Appendix A, Table A 5.2.1-1 through Table A 5.2.1-17. All data are within the Section 5.2 acceptance criteria except for the Cycle 5 total rod worth. [

].

Comparisons between the data supplied in Reference 5.5-1, Section 10.3.1 and those provided in this supplement are given in Table 5-1 through Table 5-3 and Figure 5-1 through Figure 5-3.

**Table 5-1**  
**Plant A Comparison of HZP ARO Critical Boron Concentration**

<sup>a</sup> Using the  $\pm 500$  pcm equivalent criterion for Cycles 7 and 8 results in limits of  $\pm 78$  ppm and  $\pm 80$  ppm, respectively.

**Table 5-2**  
**Plant A Comparison of HZP Total Rod Worth**

--

**Table 5-3**  
**Plant A Comparison of HZP ARO Isothermal Temperature Coefficient**

--

**Figure 5-1**  
**Plant A HZP ARO Critical Boron Concentration Differences**

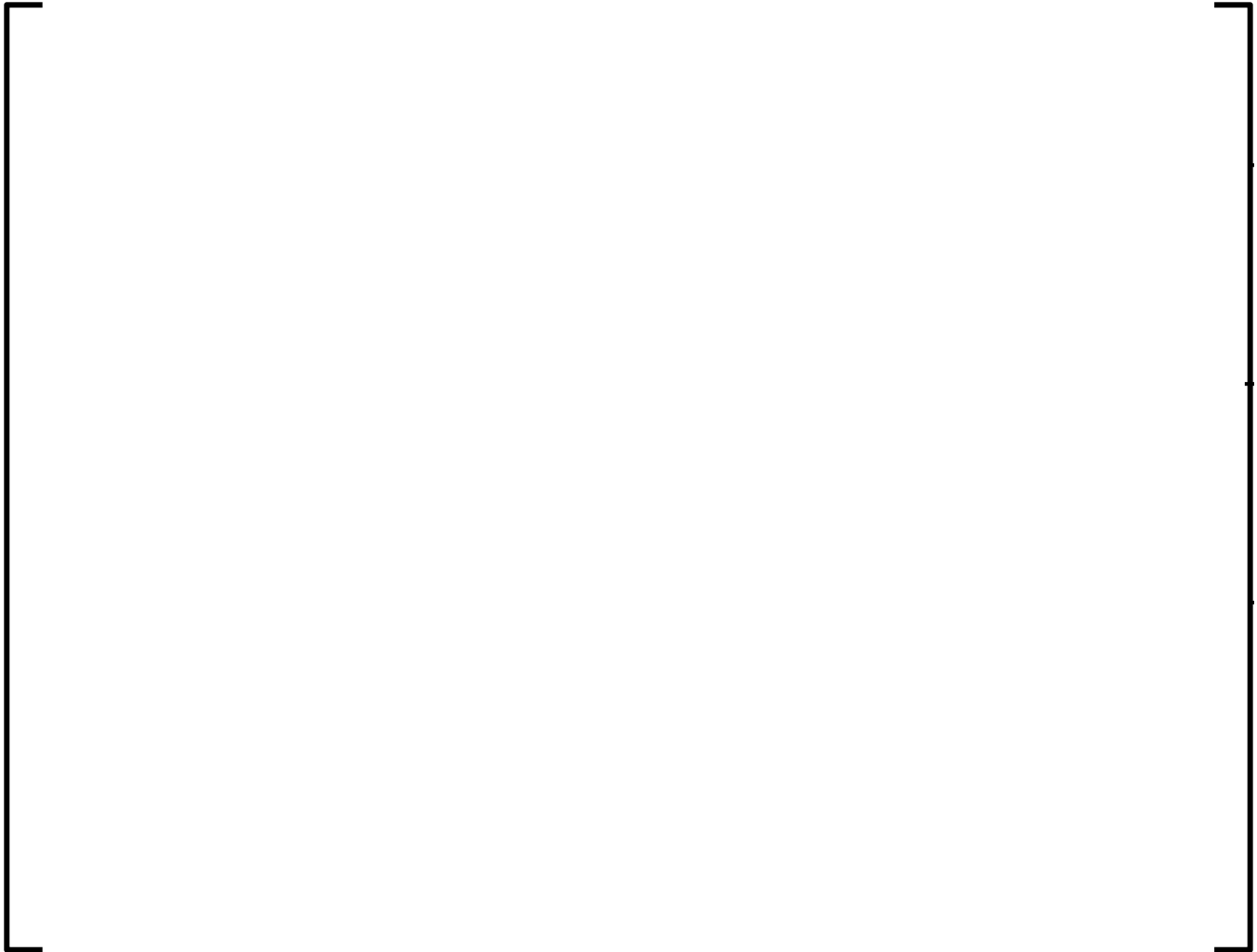
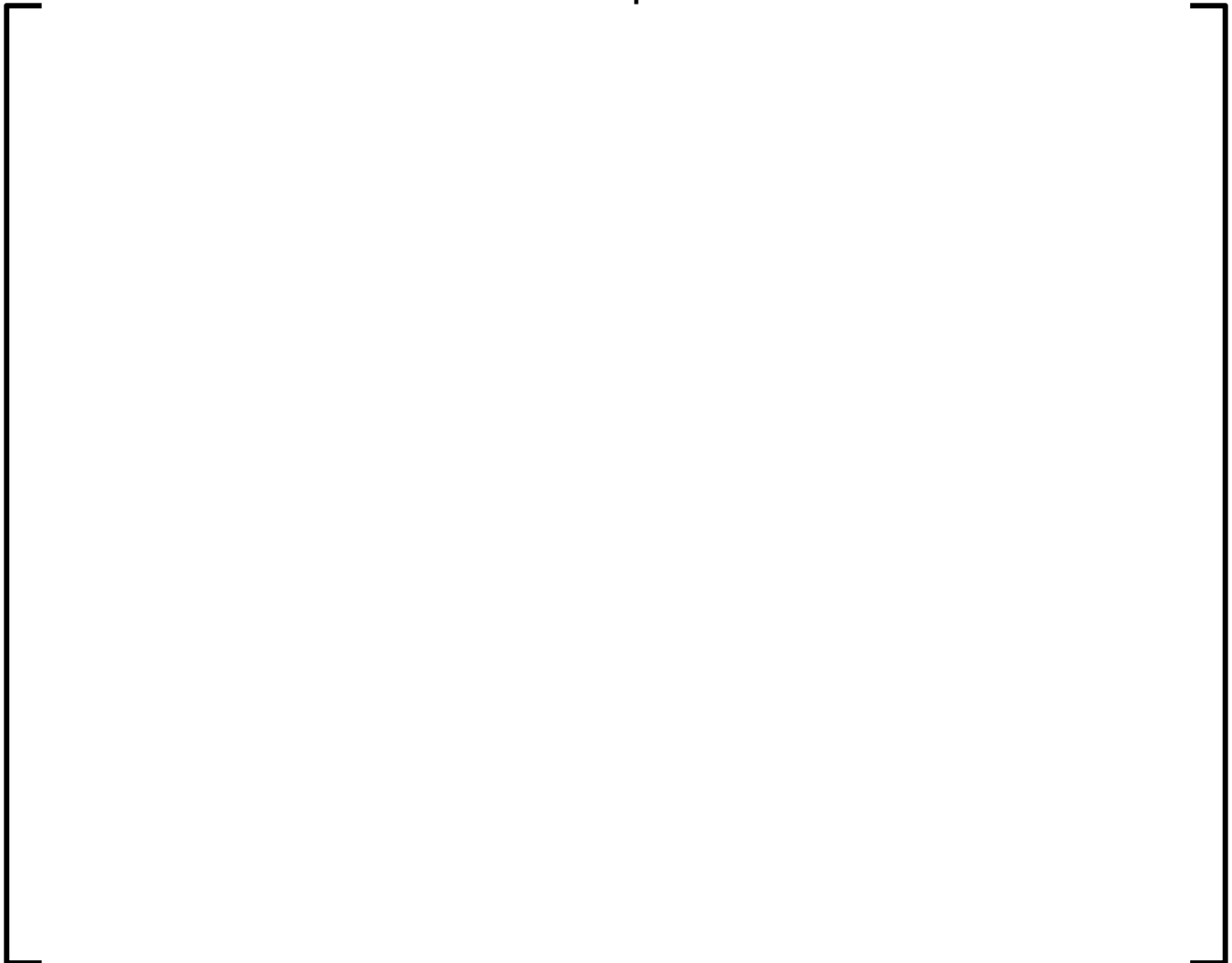


**Figure 5-2**  
**Plant A HZP Total Bank Worth Differences**



**Figure 5-3**  
**Plant A HZP ARO Isothermal Temperature Coefficient Differences**





## 5.2.2 Startup Physics Summary for Plant B Cycle 1

Comparisons of ARCADIA<sup>®</sup> calculations with measured results are summarized in Appendix B, Table B 5.2.2-1 through Table B 5.2.2-4. All data are within the Section 5.2 acceptance criteria.

Comparisons between the data supplied in Reference 5.5-1, Section 10.3.2 and those provided in this supplement are given in Table 5-4 through Table 5-6.

**Table 5-4**  
**Plant B Comparison of HZP ARO Critical Boron Concentration**

**Table 5-5**  
**Plant B Comparison of HZP Total Rod Worth**

**Table 5-6**  
**Plant B Comparison of HZP ARO Isothermal Temperature Coefficient**

## 5.2.3 Startup Physics Summary for Plant C Cycles 10-18

Comparisons of ARCADIA<sup>®</sup> calculations with measured results are summarized in Appendix C, Table C 5.2.3-1 through Table C 5.2.3-11. All data are within the Section 5.2 acceptance criteria. Measured values for individual bank worths and total bank worth were not available for Cycle 18.

Comparisons between the data supplied in Reference 5.5-1, Section 10.3.3 and those provided in this supplement are given in Table 5-7 through Table 5-9 and Figure 5-4 through Figure 5-6.

**Table 5-7**  
**Plant C Comparison of HZP ARO Critical Boron Concentration**

<sup>a</sup> Data not at ARO

**Table 5-8**  
**Plant C Comparison of HZP Total Rod Worth**

**Table 5-9**  
**Plant C Comparison of HZP ARO Isothermal Temperature Coefficient**

<sup>a</sup> Data not at ARO

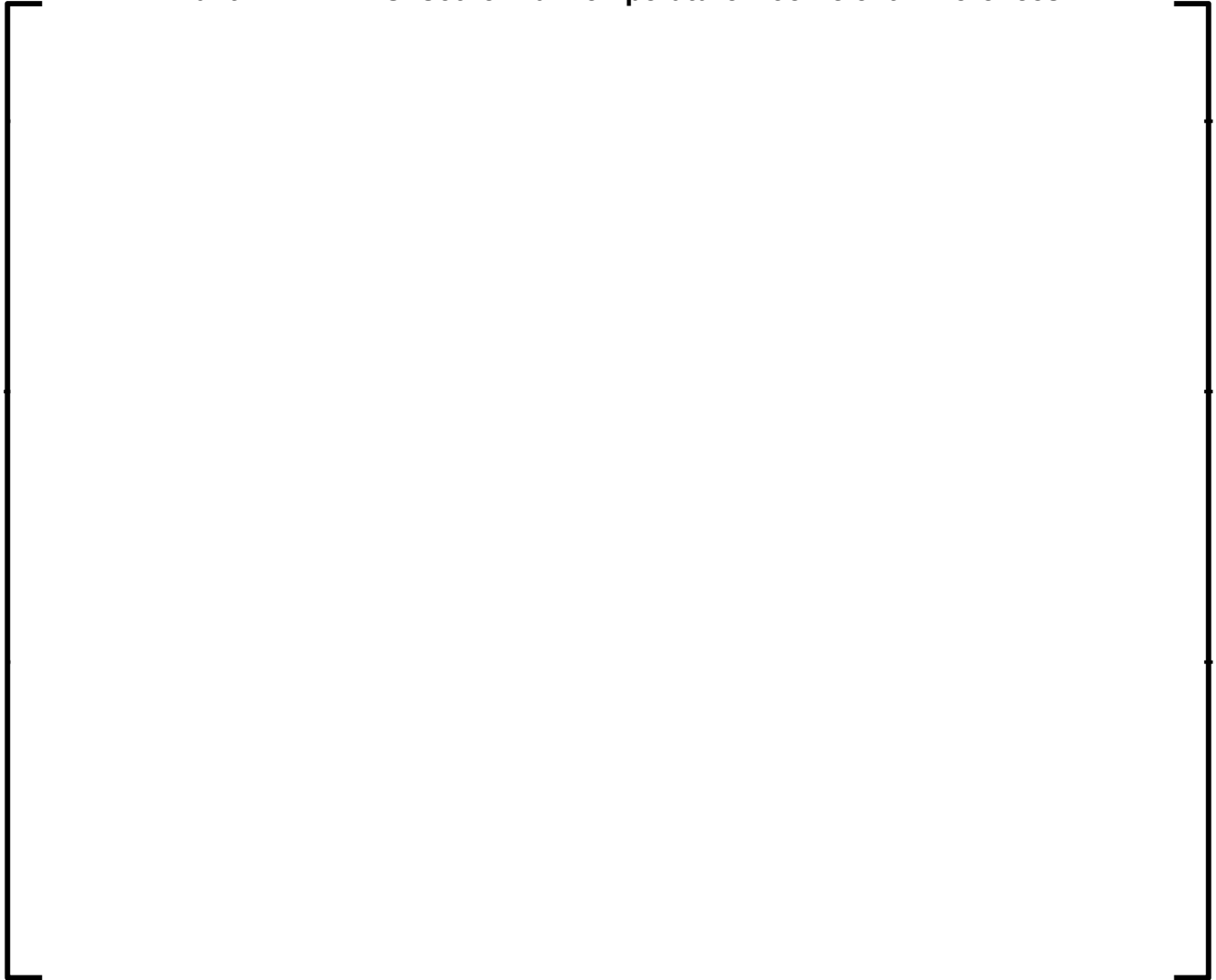
**Figure 5-4**  
**Plant C HZP ARO Critical Boron Concentration Differences**



**Figure 5-5**  
**Plant C HZP Total Bank Worth Differences**



**Figure 5-6**  
**Plant C HZP ARO Isothermal Temperature Coefficient Differences**



#### **5.2.4 Startup Physics Summary for Plant E Cycles 12-17**

Comparisons of ARCADIA<sup>®</sup> calculations with measured results are summarized in Appendix E, Table E 5.2.4-1 through Table E 5.2.4-9. All differences for HZP ARO critical boron concentration, HZP ARO ITC and HZP total rod worth are within the Section 5.2 acceptance criteria.

The results of this plant are new to Supplement 1. Therefore, no comparisons to Reference 5.5-1 can be made.

#### **5.2.5 Startup Physics Summary for Plant G1 Cycles 26-30**

Critical boron concentration comparisons at HZP, ARO conditions of ARCADIA<sup>®</sup> calculations with measured results for all five cycles can be found in Appendix G1, Table G1 5.2.5-1. All data are within the Section 5.2 acceptance criteria. For Plant G1, control rod bank worth measurements at HZP and isothermal temperature coefficients at HZP are not available.

Comparisons between the data supplied in Reference 5.5-1, Section 10.3.4 and those provided in this supplement are given in Table 5-10 and Figure 5-7.

**Table 5-10**  
**Plant G1 Comparison of HZP ARO Critical Boron Concentration**

**Figure 5-7**  
**Plant G1 HZP ARO Critical Boron Concentration Differences**





### 5.2.6 Startup Physics Summary for Plant G2 Cycles 1-5

Critical boron concentration comparisons at HZP, ARO conditions of ARCADIA® calculations with measured results for all five cycles can be found in Appendix G2, Table G2 5.2.6-1. All data are within the Section 5.2 acceptance criteria. For Plant G2, control rod bank worth measurements at HZP and isothermal temperature coefficients at HZP are not available.

Comparisons between the data supplied in Reference 5.5-1, Section 10.3.5 and those provided in this supplement are given in Table 5-11 and Figure 5-8.

**Table 5-11**  
**Plant G2 Comparison of HZP ARO Critical Boron Concentration**

--	--

**Figure 5-8**  
**Plant G2 HZP ARO Critical Boron Concentration Differences**



## **5.2.7 Startup Physics Summary for Plant S1 Cycles 12-14**

Comparisons of ARCADIA® calculations with measured results are summarized in Appendix S1, Table S1 5.2.7-1 through Table S1 5.2.7-6. All data are within the Section 5.2 acceptance criteria.

Comparisons between the data supplied in Reference 5.5-1, Section 10.3.6 and those provided in this supplement are given in Table 5-12 through Table 5-14 and Figure 5-9 through Figure 5-11.

**Table 5-12**  
**Plant S1 Comparison of HZP ARO Critical Boron Concentration**

**Table 5-13**  
**Plant S1 Comparison of HZP Total Rod Worth**

**Table 5-14**  
**Plant S1 Comparison of HZP ARO Isothermal Temperature Coefficient**

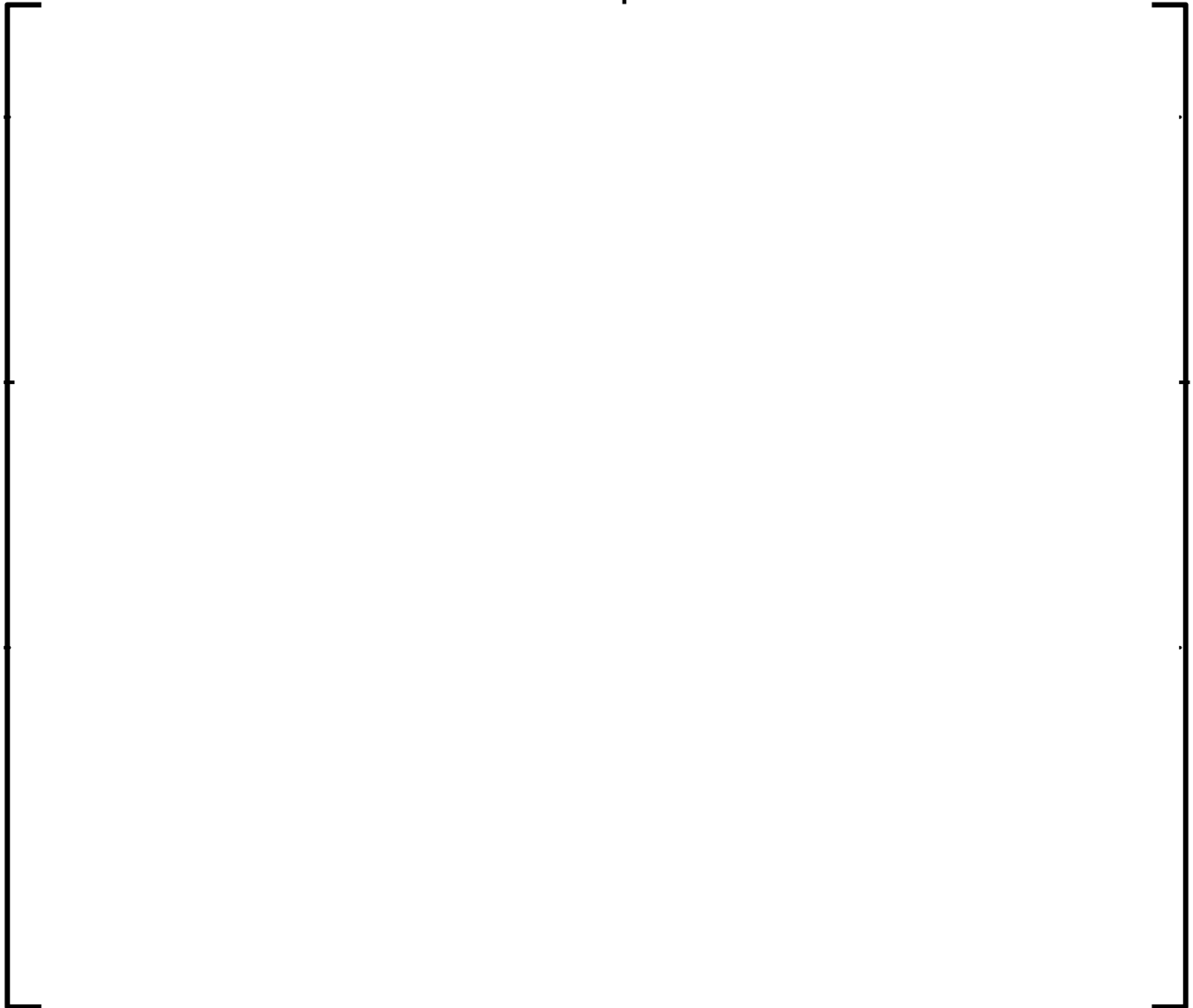
**Figure 5-9**  
**Plant S1 HZP ARO Critical Boron Concentration Differences**



**Figure 5-10**  
**Plant S1 HZP Total Bank Worth Differences**



**Figure 5-11**  
**Plant S1 HZP ARO Isothermal Temperature Coefficient Differences**



## 5.2.8 Startup Physics Summary for Plant S2 Cycles 12-14

Comparisons of ARCADIA® calculations with measured results are summarized in Appendix S2, Table S2 5.2.8-1 through Table S2 5.2.8-6. All data are within the Section 5.2 acceptance criteria.

Comparisons between the data supplied in Reference 5.5-1, Section 10.3.7 and those provided in this supplement are given in Table 5-15 through Table 5-17 and Figure 5-12 through Figure 5-14.

**Table 5-15**  
**Plant S2 Comparison of HZP ARO Critical Boron Concentration**



**Table 5-16**  
**Plant S2 Comparison of HZP Total Rod Worth**



**Table 5-17**  
**Plant S2 Comparison of HZP ARO Isothermal Temperature Coefficient**



**Figure 5-12**  
**Plant S2 HZP ARO Critical Boron Concentration Differences**





**Figure 5-13**  
**Plant S2 HZP Total Bank Worth Differences**



**Figure 5-14**  
**Plant S2 HZP ARO Isothermal Temperature Coefficient Differences**



### **5.2.9 Startup Physics Summary for Plant T1 Cycles 9-15**

Comparisons of ARCADIA® calculations with measured results are summarized in Appendix T1, Table T1 5.2.9-1 through Table T1 5.2.9-10. All data are within the Section 5.2 acceptance criteria.

Comparisons between the data supplied in Reference 5.5-1, Section 10.3.8 and those provided in this supplement are given in Table 5-18 through Table 5-20 and Figure 5-15 through Figure 5-17.

**Table 5-18**  
**Plant T1 Comparison of HZP ARO Critical Boron Concentration**

**Table 5-19**  
**Plant T1 Comparison of HZP Total Rod Worth**

**Table 5-20**  
**Plant T1 Comparison of HZP ARO Isothermal Temperature**  
**Coefficient**

--	--

**Figure 5-15**  
**Plant T1 HZP ARO Critical Boron Concentration Differences**



**Figure 5-16**  
**Plant T1 HZP Total Bank Worth Differences**

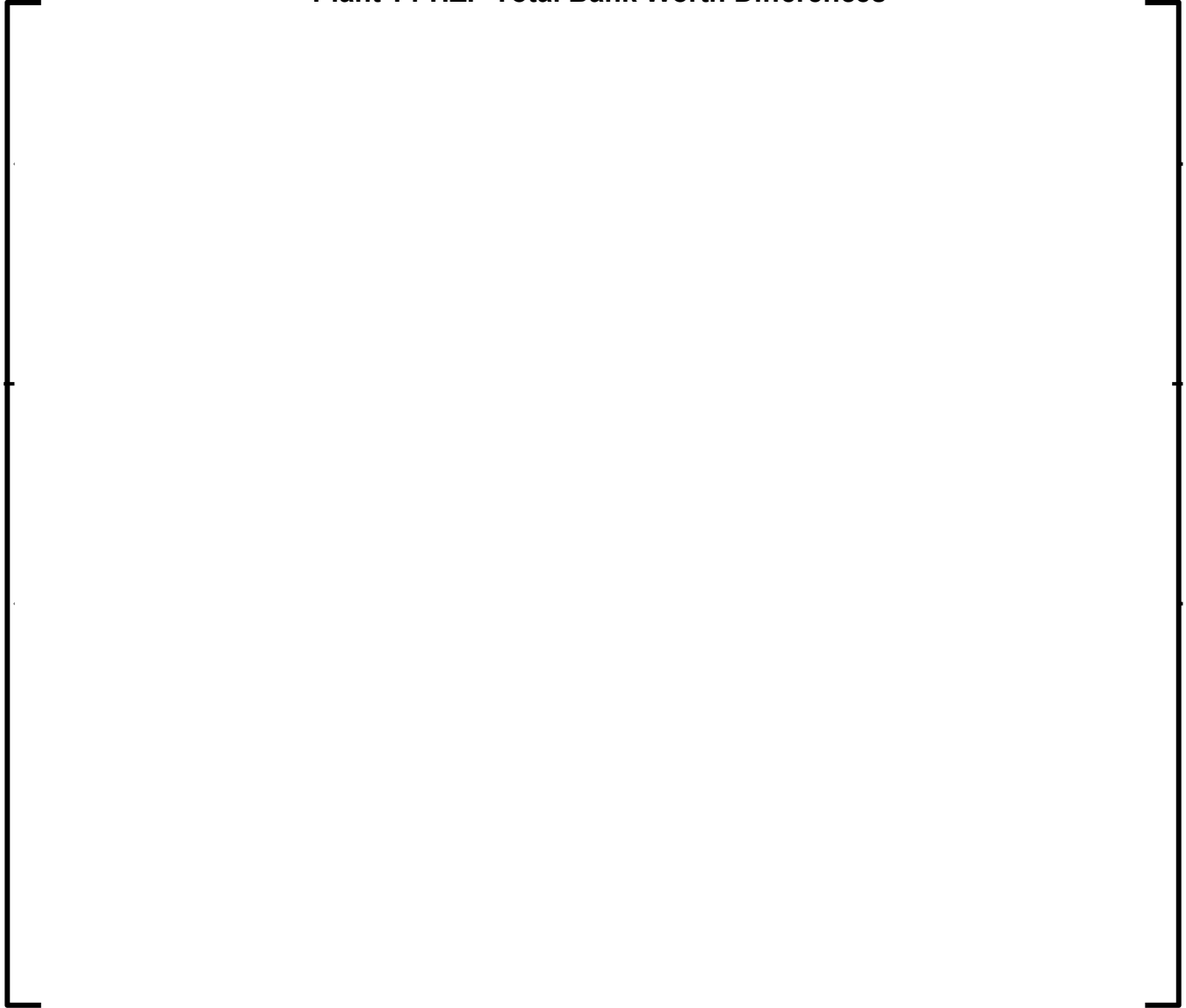


**Figure 5-17**  
**Plant T1 HZP ARO Isothermal Temperature Coefficient Differences**



### 5.2.10 Startup Physics Summary for Plant V1 Cycles 18-22

Comparisons of ARCADIA® calculations with measured results are summarized in Appendix V1, Table V1 5.2.10-1 through Table V1 5.2.10-8. All data are within the Section 5.2 acceptance criteria.

Comparisons between the data supplied in Reference 5.5-1, Section 10.3.9 and those provided in this supplement are given in Table 5-21 through Table 5-23 and Figure 5-18 through Figure 5-20.

**Table 5-21**  
**Plant V1 Comparison of HZP ARO Critical Boron Concentration**

[illegible]

**Table 5-22**  
**Plant V1 Comparison of HZP Total Rod Worth**

[ ]



**Table 5-23**  
**Plant V1 Comparison of HZP ARO Isothermal Temperature**  
**Coefficient**



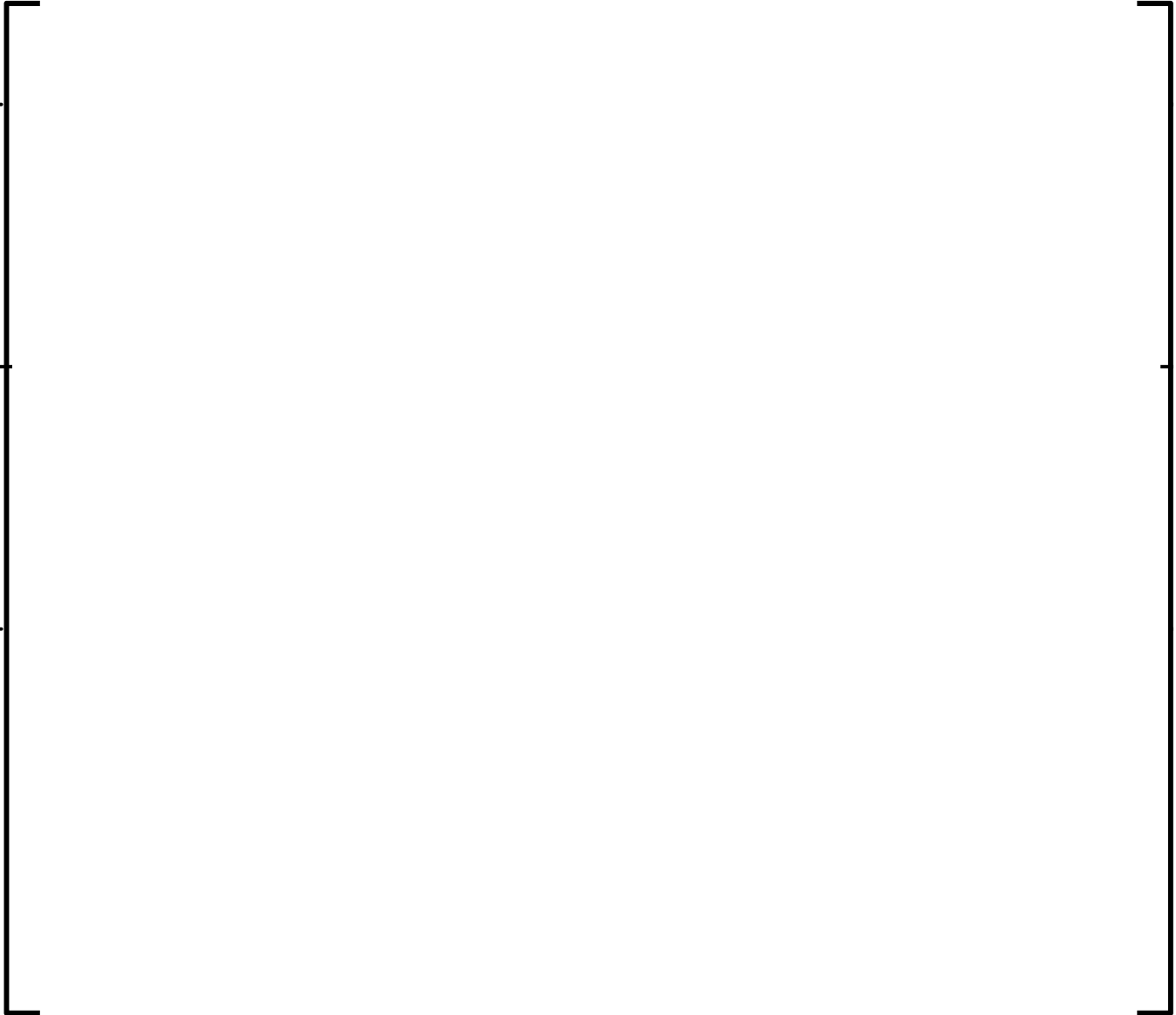
**Figure 5-18**  
**Plant V1 HZP ARO Critical Boron Concentration Differences**



**Figure 5-19**  
**Plant V1 HZP Total Bank Worth Differences**



**Figure 5-20**  
**Plant V1 HZP ARO Isothermal Temperature Coefficient Differences**



### 5.3 Core Follow Measurements

Core follow comparisons are made to the available measured data for each plant/fuel type at, or near, hot full power. The parameters compared are:

1. Critical boron concentration

Criterion: Calculated within  $\pm 50$  ppm of measured or  $\pm 500$  pcm equivalent.

Comparisons are performed for a minimum of one measured data point per 30 effective full power days (EFPD) throughout the cycle.

2. Assembly average power distributions

Criterion: The root mean square (RMS) \* 100 of the absolute difference between calculated and measured assembly powers is  $< 5.0$  for each comparison map.

At least three comparisons maps are provided per cycle, corresponding to the beginning-, middle-, and end-of-cycle conditions. These comparisons are made on a full core basis.

3. Core average axial power distributions

Criterion: The root mean square (RMS) \* 100 of the absolute difference between calculated and measured core-average axial powers is  $< 5.0$  for each map.

Measured boron concentration and power distribution data are typically available from commercial reactors at full power conditions as a function of cycle burnup. The criteria for the parameters are based on the recommended test criteria provided in Reference 5.5-2.

Comparisons to assembly average and core average axial power distributions were provided in Reference 5.5-1, Section 10.4 for all benchmark plants and cycles discussed above. For Supplement 1, these comparisons are provided for each plant but only for the cycles considered in the power distribution uncertainty analysis discussed in Section 8.0 of this supplement. Sufficient data is available from this more limited set of data to show that ARCADIA® is capable of accurately predicting both the assembly average and core average axial power distributions.

### **5.3.1 Plant A Cycles 1-14**

Results for Plant A Cycles 1-14 are within the applicable Section 5.3 acceptance criteria for HFP measured boron concentrations, core-average axial power distributions, and radial power distributions.

The HFP ARO critical boron concentration as a function of fractional cycle length is shown in Appendix A Figure A 5.3.1-1 to Figure A 5.3.1-14. A summary plot of the boron differences are provided in Appendix A Figure A 5.3.1-15 as a function of absolute burnup. Assembly power distribution comparisons are presented in Appendix A Figure A 5.3.1-16 to Figure A 5.3.1-27. Axial power distributions are shown in Appendix A Figure A 5.3.1-28 to Figure A 5.3.1-39.

Comparisons between the boron differences supplied in Reference 5.5-1, Section 10.4.1 and those provided in this supplement are shown in Figure 5-21.

Comparisons between the RMS values for the assembly average and axial power distributions supplied in Reference 5.5-1, Section 10.4.1 and those provided in this supplement are given in Table 5-24. For Reference 5.5-1, the INPAX-W methodology with no spacer grid model was used for the power distribution comparisons. For this supplement, the power distribution comparisons are performed with the MEDIAN methodology and include the spacer grid model.

**Table 5-24**  
**Plant A Comparison of (C-M) RMS Differences for Assembly Average**  
**Radial and Core Average Axial Power Distributions**

**Figure 5-21**  
**Plant A Cycles 1-14 Comparison of Critical Boron Concentration**  
**Differences**



### 5.3.2 Plant B Cycle 1

Measured HFP critical boron comparisons are available only at seven points throughout Cycle 1 for Plant B. All available HFP CBC data was used in the comparisons. Results for Plant B Cycle 1 are within the applicable Section 5.3 acceptance criteria for HFP measured boron concentrations, core-average axial power distributions, and radial power distributions.

The HFP ARO critical boron concentration as a function of fractional cycle length is shown in Appendix B Figure B 5.3.2-1. A summary plot of the boron differences are provided in Appendix B Figure B 5.3.2-2 as a function of absolute burnup. Assembly power distribution comparisons are presented in Appendix B Figure B 5.3.2-3 to Figure B 5.3.2-5. Axial power distributions are shown in Appendix B Figure B 5.3.2-6 to Figure B 5.3.2-8.

Comparisons between the boron differences supplied in Reference 5.5-1, Section 10.4.2 and those provided in this supplement are shown in Figure 5-22.

Comparisons between the RMS values for the assembly average and axial power distributions supplied in Reference 5.5-1, Section 10.4.2 and those provided in this supplement are given in Table 5-25. For Reference 5.5-1, the INPAX-W methodology with no spacer grid model was used for the power distribution comparisons. For this supplement, the power distribution comparisons are performed with the MEDIAN methodology and include the spacer grid model.



**Table 5-25**  
**Plant B Comparison of (C-M) RMS Differences for Assembly Average**  
**Radial and Core Average Axial Power Distributions**

**Figure 5-22**  
**Plant B Cycle 1 Comparison of Critical Boron Concentration**  
**Differences**

### 5.3.3 Plant C Cycles 10-18

Results for Plant C Cycles 10-18 are within the applicable Section 5.3 acceptance criteria for HFP measured boron concentrations, core-average axial power distributions, and radial power distributions.

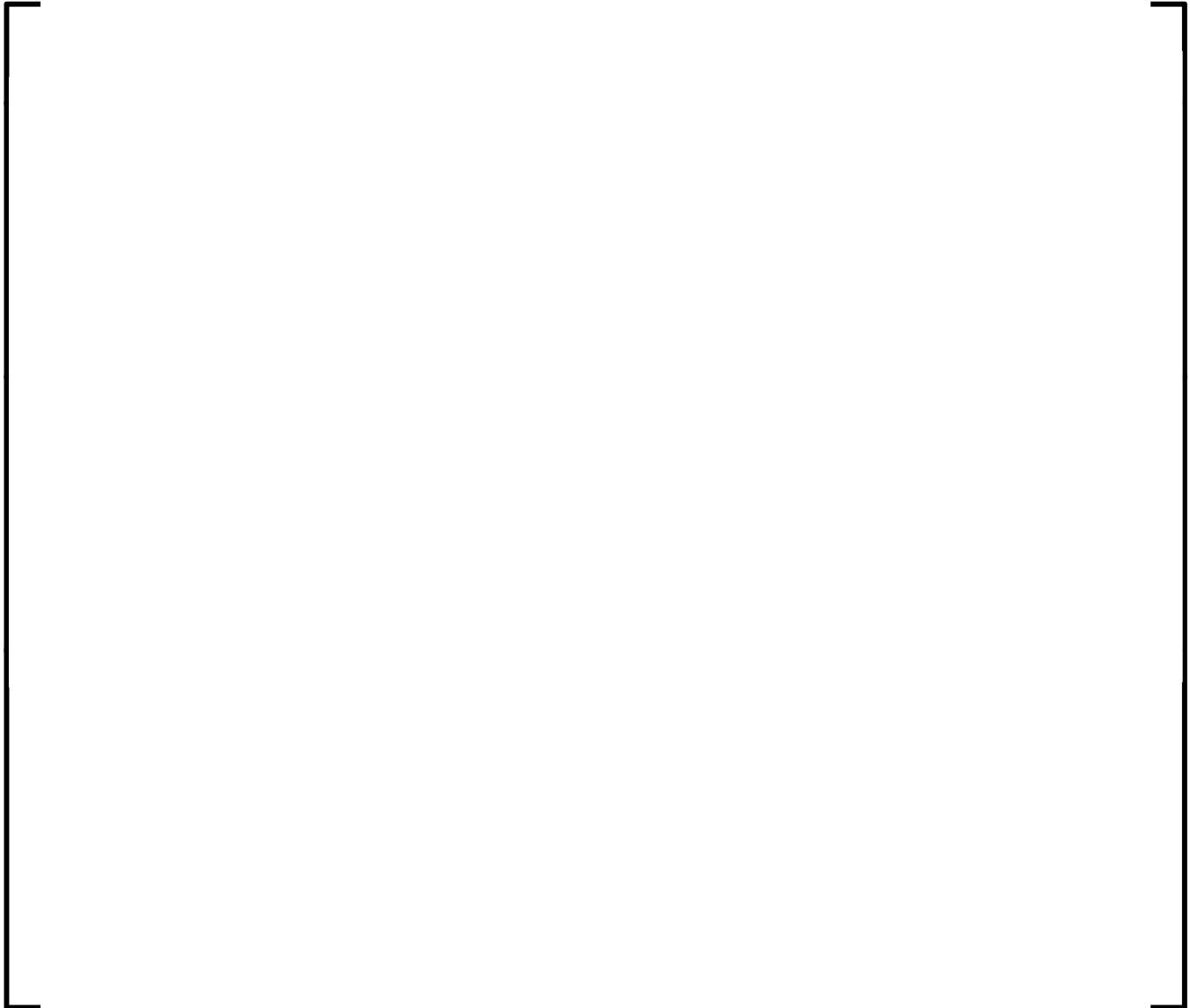
The HFP ARO critical boron concentration as a function of fractional cycle length is shown in Appendix C Figure C 5.3.3-1 to Figure C 5.3.3-9. A summary plot of the boron differences are provided in Appendix C Figure C 5.3.3-10 as a function of absolute burnup. Assembly power distribution comparisons are presented in Appendix C Figure C 5.3.3-11 to Figure C 5.3.3-25. Axial power distributions are shown in Appendix C Figure C 5.3.3-26 to Figure C 5.3.3-40.

Comparisons between the boron differences supplied in Reference 5.5-1, Section 10.4.3 and those provided in this supplement are shown in Figure 5-23.

Comparisons between the RMS values for the assembly average and axial power distributions supplied in Reference 5.5-1, Section 10.4.3 and those provided in this supplement are given in Table 5-26. For Reference 5.5-1, the INPAX-CE methodology with no spacer grid model was used for the power distribution comparisons. For this supplement, the power distribution comparisons are performed with the MEDIAN methodology and include the spacer grid model.

**Table 5-26**  
**Plant C Comparison of (C-M) RMS Differences for Assembly Average**  
**Radial and Core Average Axial Power Distributions**

**Figure 5-23**  
**Plant C Cycles 10-18 Comparison of Critical Boron Concentration**  
**Differences**



### **5.3.4 Plant E Cycles 12-17**

For Plant E, there are some intervals that exceeded the once per 30 EFPD intervals for boron concentration comparisons. All available measured data were used. Results for Plant E Cycles 12-17 are within the applicable Section 5.3 acceptance criteria for HFP measured boron concentrations, core-average axial power distributions, and radial power distributions.

The HFP ARO critical boron concentration as a function of fractional cycle length is shown in Appendix E Figure E 5.3.4-1 to Figure E 5.3.4-6. A summary plot of the boron differences are provided in Appendix E Figure E 5.3.4-7 as a function of absolute burnup. Assembly power distribution comparisons are presented in Appendix E Figure E 5.3.4-8 to Figure E 5.3.4-25. Axial power distributions are shown in Appendix E Figure E 5.3.4-26 to Figure E 5.3.4-43.

The results of this plant are new to Supplement 1. Therefore, no comparisons to Reference 5.5-1 can be made.

### **5.3.5 Plant G1 Cycles 26-30**

Results for Plant G1 Cycles 26-30 are within the applicable Section 5.3 acceptance criteria for HFP measured boron concentrations, core-average axial power distributions, and radial power distributions.

The HFP ARO critical boron concentration as a function of fractional cycle length is shown in Appendix G1 Figure G1 5.3.5-1 to Figure G1 5.3.5-5. A summary plot of the boron differences are provided in Appendix G1 Figure G1 5.3.5-6 as a function of absolute burnup. Assembly power distribution comparisons are presented in Appendix G1 Figure G1 5.3.5-7 to Figure G1 5.3.5-21. Axial power distributions are shown in Appendix G1 Figure G1 5.3.5-22 to Figure G1 5.3.5-36.

Comparisons between the boron differences supplied in Reference 5.5-1, Section 10.4.4 and those provided in this supplement are shown in Figure 5-24.

Comparisons between the RMS values for the assembly average and axial power distributions supplied in Reference 5.5-1, Section 10.4.4 and those provided in this supplement are given in Table 5-27. For Reference 5.5-1, the MEDIAN methodology was used; no spacer grid model was included. For this supplement, the power distribution comparisons are performed with the MEDIAN methodology and include the spacer grid model.

**Table 5-27**  
**Plant G1 Comparison of (C-M) RMS Differences for Assembly**  
**Average Radial and Core Average Axial Power Distributions**

**Figure 5-24**  
**Plant G1 Cycles 26-30 Comparison of Critical Boron Concentration**  
**Differences**



### 5.3.6 Plant G2 Cycles 1-5

During the first half of Cycle 1, Plant G2 was operated in load-follow mode, averaging around 80% of full load. Therefore, measured HFP critical boron concentration is only available close to BOC and for the second half of Cycle 1.

Results for Plant G2 Cycles 1-5 are within the applicable Section 5.3 acceptance criteria for HFP measured boron concentrations and the assembly average power distributions.

For the core-average axial power distributions, one point (BOC 1), the RMS value exceeds the criteria. This is similar to the results given in Reference 5.5-1 and is attributed to the operation mode of plant. The first half of Cycle 1, the plant was operated in load follow mode. Thus, it was not possible to exactly model the reactor state at BOC for this point. All other axial power distribution maps are within the acceptance criteria. The axial power distribution map for BOC 1 will thus be considered an anomaly which does not influence the applicability of the ARCADIA<sup>®</sup> power distribution calculations.

The HFP ARO critical boron concentration as a function of fractional cycle length is shown in Appendix G2 Figure G2 5.3.6-1 to Figure G2 5.3.6-5. A summary plot of the boron differences are provided in Appendix G2 Figure G2 5.3.6-6 as a function of absolute burnup. Assembly power distribution comparisons are presented in Appendix G2 Figure G2 5.3.6-7 to Figure G2 5.3.6-21. Axial power distributions are shown in Appendix G2 Figure G2 5.3.6-22 to Figure G2 5.3.6-36.

Comparisons between the boron differences supplied in Reference 5.5-1, Section 10.4.5 and those provided in this supplement are shown in Figure 5-25.



Comparisons between the RMS values for the assembly average and axial power distributions supplied in Reference 5.5-1, Section 10.4.5 and those provided in this supplement are given in Table 5-28. For Reference 5.5-1, the MEDIAN methodology was used; no spacer grid model was included. For this supplement, the power distribution comparisons are performed with the MEDIAN methodology and include the spacer grid model.

**Table 5-28**  
**Plant G2 Comparison of (C-M) RMS Differences for Assembly**  
**Average Radial and Core Average Axial Power Distributions**

**Figure 5-25**  
**Plant G2 Cycles 1-5 Comparison of Critical Boron Concentration**  
**Differences**



### **5.3.7 Plant S1 Cycles 12-14**

Results for Plant S1 Cycles 12-14 are within the applicable Section 5.3 acceptance criteria for HFP measured boron concentrations, core-average axial power distributions, and radial power distributions.

The HFP ARO critical boron concentration as a function of fractional cycle length is shown in Appendix S1 Figure S1 5.3.7-1 to Figure S1 5.3.7-3. A summary plot of the boron differences are provided in Appendix S1 Figure S1 5.3.7-4 as a function of absolute burnup. Assembly power distribution comparisons are presented in Appendix S1 Figure S1 5.3.7-5 to Figure S1 5.3.7-13. Axial power distributions are shown in Appendix S1 Figure S1 5.3.7-14 to Figure S1 5.3.7-22.

Comparisons between the boron differences supplied in Reference 5.5-1, Section 10.4.6 and those provided in this supplement are shown in Figure 5-26.

Comparisons between the RMS values for the assembly average and axial power distributions supplied in Reference 5.5-1, Section 10.4.6 and those provided in this supplement are given in Table 5-29. For Reference 5.5-1, the INPAX-W methodology with no spacer grid model was used for the power distribution comparisons. For this supplement, the power distribution comparisons are performed with the MEDIAN methodology and include the spacer grid model.

**Table 5-29**  
**Plant S1 Comparison of (C-M) RMS Differences for Assembly**  
**Average Radial and Core Average Axial Power Distributions**



**Figure 5-26**  
**Plant S1 Cycles 12-14 Comparison of Critical Boron Concentration**  
**Differences**



### **5.3.8 Plant S2 Cycles 12-14**

Results for Plant S2 Cycles 12-14 are within the applicable Section 5.3 acceptance criteria for HFP measured boron concentrations, core-average axial power distributions, and radial power distributions.

The HFP ARO critical boron concentration as a function of fractional cycle length is shown in Appendix S2 Figure S2 5.3.8-1 to Figure S2 5.3.8-3. A summary plot of the boron differences are provided in Appendix S2 Figure S2 5.3.8-4 as a function of absolute burnup. Assembly power distribution comparisons are presented in Appendix S2 Figure S2 5.3.8-5 to Figure S2 5.3.8-13. Axial power distributions are shown in Appendix S2 Figure S2 5.3.8-14 to Figure S2 5.3.8-22.

Comparisons between the boron differences supplied in Reference 5.5-1, Section 10.4.7 and those provided in this supplement are shown in Figure 5-27.

Comparisons between the RMS values for the assembly average and axial power distributions supplied in Reference 5.5-1, Section 10.4.7 and those provided in this supplement are given in Table 5-30. For Reference 5.5-1, the INPAX-W methodology with no spacer grid model was used for the power distribution comparisons. For this supplement, the power distribution comparisons are performed with the MEDIAN methodology and include the spacer grid model.

**Table 5-30**  
**Plant S2 Comparison of (C-M) RMS Differences for Assembly**  
**Average Radial and Core Average Axial Power Distributions**



**Figure 5-27**  
**Plant S2 Cycles 12-14 Comparison of Critical Boron Concentration**  
**Differences**





### **5.3.9 Plant T1 Cycles 9-15**

Results for Plant T1 Cycles 9-15 are within the applicable Section 5.3 acceptance criteria for HFP measured boron concentrations, core-average axial power distributions, and radial power distributions.

The HFP ARO critical boron concentration as a function of fractional cycle length is shown in Appendix T1 Figure T1 5.3.9-1 to Figure T1 5.3.9-7. A summary plot of the boron differences are provided in Appendix T1 Figure T1 5.3.9-8 as a function of absolute burnup. Assembly power distribution comparisons are presented in Appendix T1 Figure T1 5.3.9-9 to Figure T1 5.3.9-20. Axial power distributions are shown in Appendix T1 Figure T1 5.3.9-21 to Figure T1 5.3.9-32.

Comparisons between the boron differences supplied in Reference 5.5-1, Section 10.4.8 and those provided in this supplement are shown in Figure 5-28.

Comparisons between the RMS values for the assembly average and axial power distributions supplied in Reference 5.5-1, Section 10.4.8 and those provided in this supplement are given in Table 5-31. For Reference 5.5-1, the power distribution comparisons were calculated using methodology similar to INPAX-CE and no spacer grid model. For this supplement, the power distribution comparisons are performed with the MEDIAN methodology and include the spacer grid model.

**Table 5-31**  
**Plant T1 Comparison of (C-M) RMS Differences for Assembly**  
**Average Radial and Core Average Axial Power Distributions**

**Figure 5-28**  
**Plant T1 Cycles 9-15 Comparison of Critical Boron Concentration**  
**Differences**



### **5.3.10 Plant V1 Cycles 18-22**

Results for Plant V1 Cycles 18-22 are within the applicable Section 5.3 acceptance criteria for HFP measured boron concentrations, core-average axial power distributions, and radial power distributions.

The HFP ARO critical boron concentration as a function of fractional cycle length is shown in Appendix V1 Figure V1 5.3.10-1 to Figure V1 5.3.10-5. A summary plot of the boron differences are provided in Appendix V1 Figure V1 5.3.10-6 as a function of absolute burnup. Assembly power distribution comparisons are presented in Appendix V1 Figure V1 5.3.10-7 to Figure V1 5.3.10-21. Axial power distributions are shown in Appendix V1 Figure V1 5.3.10-22 to Figure V1 5.3.10-36.

Comparisons between the boron differences supplied in Reference 5.5-1, Section 10.4.9 and those provided in this supplement are shown in Figure 5-29.

Comparisons between the RMS values for the assembly average and axial power distributions supplied in Reference 5.5-1, Section 10.4.9 and those provided in this supplement are given in Table 5-32. For Reference 5.5-1, the INPAX-W methodology with no spacer grid model was used for the power distribution comparisons. For this supplement, the power distribution comparisons are performed with the MEDIAN methodology and include the spacer grid model.

**Table 5-32**  
**Plant V1 Comparison of (C-M) RMS Differences for Assembly**  
**Average Radial and Core Average Axial Power Distributions**

**Figure 5-29**  
**Plant V1 Cycles 18-22 Comparison of Critical Boron Concentration**  
**Differences**



## **5.4      *Conclusions***

A summary of the core benchmark results are presented in Table 5-33 through Table 5-35. Results of the benchmarks support the conclusion that the ARCADIA<sup>®</sup> code system is applicable to all PWR fuel types and for in-core detector systems that are fixed, moveable or Aeroball, full length or axially segmented.

**Table 5-33**  
**Summary of ARCADIA<sup>®</sup> Validation and Results**

**Table 5-34**  
**Results of ARCADIA<sup>®</sup> Calculations with Startup Physics Test**  
**Measurements**



**Table 5-35**  
**Results of ARCADIA<sup>®</sup> Calculations with Core Follow Measurements**

## **5.5      *References***

- 5.5-1    ANP-10297P-A, Revision 0, The ARCADIA<sup>®</sup> Reactor Analysis System for PWRs Methodology Description and Benchmarking Results Topical Report, February 2013.
- 5.5-2    ANSI/ANS-19.6.1-2011, "Reload Startup Physics Tests for Pressurized Water Reactors," American Nuclear Society, January 13, 2011.

## 6.0 ADDITIONAL PARAMETER BENCHMARKS

### 6.1 *Cold Critical Benchmarks*

Comparisons of ARCADIA<sup>®</sup> to measurements made at cold conditions are performed to support the validation of the code system at these conditions.

A set of nine critical boron concentration measurements were performed in the Plant G2 reactor at the end of cycle 8. Plant G2 is a Siemens – KONVOI reactor containing 193 18x18 fuel assemblies. The measurements were performed for various temperatures between approximately [ ] and for different control rod positions.

A cycle calculation was performed to reach the initial conditions and burnup [ ] at which the measurement program was started. Each calculation considered the xenon concentration at the time of measurement. Critical boron concentrations were calculated at the reported control rod configuration, moderator temperature and pressure. The reported conditions are presented in Table 6-1. [ ]

[ ] Table 6-1 along with the calculated boron concentration and the calculated-to-measured (C-M) difference in ppm.

**Table 6-1**  
**Cold Critical Benchmark Conditions and Critical Boron**  
**Concentration Comparisons**

Additional measurements for boron worth and isothermal temperature coefficient were made as part of the cold critical benchmarks. The calculations were performed at Case 9 in Table 6-1. [

].

**Table 6-2**  
**Cold Critical Benchmark Boron Worth and ITC Comparisons**

The critical boron concentrations obtained for the cold critical benchmark are in good agreement with the measured values, with a maximum absolute deviation of

[         ] . The boron worth and ITC calculated values are also in good agreement with the measured values. The ITC for the cold condition is similar to what is seen on average for ITCs measured at HZP condition. Likewise, the differences in boron concentration are consistent to what is seen at HZP conditions (see Section 5.2 of this supplement). This supports the conclusion that ARCADIA<sup>®</sup> is capable of modeling configurations at cold conditions.

## **6.2         *Pseudo-Ejected Rod Worth Benchmarks***

An additional validation of the ARCADIA<sup>®</sup> code package with respect to control rod worth is provided by comparison of calculated pseudo-ejected rod worth with measured values. Four measurements were available for 3 plants: Plant D1, Plant T1 and Plant S1. Plants D1 and S1 are both Westinghouse reactors containing 193 17x17 fuel assemblies. Plant T1 is a Babcock & Wilcox reactor containing 177 15x15 fuel assemblies.

Measurements for Plants D1 and T1 were performed by withdrawing a single rod during boration from a steady state condition (critical boron and equilibrium xenon with all rods inserted at an initial position). The Plant S1 measurement as well as a second Plant T1 measurement were conducted using the rod drop technique in which a single rod worth was measured during boron dilution. The initial conditions for these tests were critical boron and equilibrium xenon for an initial rod configuration with the selected single rod fully withdrawn. All measurements were made during hot zero power (HZP) physics testing during Cycle 1 startup.

Calculations for the pseudo-ejected rod worth were made by modeling each core at the initial conditions of the measurement as indicated in Table 6-3. The critical boron concentration was calculated for the initial conditions and then held constant. For the Plant D1 and T1 boron swap measurements, the selected ejected rod was withdrawn from the core to the final position and the reactivity change was calculated in pcm. For the Plant S1 and T1 rod drop measurements, the selected rod was fully inserted into the core and the reactivity change was calculated in pcm.

Measured and calculated rod worth values as well as comparisons are provided in Table 6-4.

The ARCADIA<sup>®</sup> calculated pseudo-ejected rod worth values are in good agreement with the measured values, all differences fall within the [ -0.0015, 0.0015 ] . The results support the validation of ARCADIA<sup>®</sup> for calculating individual rod worths.

**Table 6-3**  
**Cycle 1 HZP Pseudo-Ejected Rod Worth Measurement Conditions**

Case	Initial Bank Configurations	Core Location of Selected Rod	Rod Final Position
Plant D1	Bank B: 166 steps w/d Bank C: 51 steps w/d Bank D: 0 steps w/d Core location D-12: 0 steps w/d	D-12	190 steps w/d
Plant T1, boron swap	Groups 1-4: 100% w/d Group 5: 6% w/d Groups 6-7: 0% w/d Group 8: 27.5% w/d Core location F-2: 0% w/d	F-2	100% w/d
Plant T1, rod drop	Groups 1-4: 100% w/d Group 5: 13% w/d Groups 6-7: 0% w/d Group 8: 27.5% w/d Core location F-2: 100% w/d	F-2	0% w/d
Plant S1	Bank C: 81/82 steps w/d All other banks: 228 steps w/d Core Location D-12: 228 steps w/d	D-12	0 steps w/d

## **Table 6-4**

### **Cycle 1 HZP Pseudo-Ejected Rod Worth Comparisons**

## **6.3      *Doppler Benchmarks***

### **6.3.1      Introduction**

This ARCADIA® supplement adds Doppler benchmarks to demonstrate the adequacy of the added upscatter model (see Section 2.2 of this supplement), to extend the range of validation, and to provide a baseline for future development.

A key parameter in Safety analyses is the Doppler Temperature Coefficient (DTC). A DTC cannot be measured directly in commercial plants. The measured tests that come closest to measuring a DTC are the Doppler Power (DPC) and Power Coefficient (PC) tests. The difference between a DTC and a DPC is that the DPC contains the fuel temperature change due to a power change without moderator temperature changes. Hence, a DPC inherently contains the thermal fuel response functions to power and a DTC does not. The difference between a DPC and a PC is that the PC contains the moderator reactivity differences with power. Both contain the fuel temperature effects with power. An Isothermal Temperature Coefficient (ITC) test is performed at most plants and includes both the effects of an MTC and DTC. The ITC test cannot separate these effects and the error of the test is too large to estimate the error of a DTC.

DPC and/or PC tests are typically performed during Cycle 1 startups and typically are not performed thereafter so only a limited amount of data is available. The results from startup tests from six plants are presented in this supplement. The tests are very similar; the core temperature is changed to measure the power response. Three different test procedures are referenced. For three of the plants (Plants D1, S1, and S2), the temperature effect was reversed. The increase/decrease of the temperature was repeated multiple times for each test. The test results were reported differently. For Plant D1 the DPC is reported and for Plants S1 and S2 the PC was reported. For both tests, some testing results are available but it is not in sufficient detail to reprocess. The third test procedure used for Plants F1, P1, and P2 employs one core temperature change with detailed measurements of power and temperature versus time. The time of the test is significantly long so that xenon buildup occurs and can be used to infer both the measured ITC and DPC. The test and predicted results are shown in Table 6-5, Table 6-6, and Table 6-7, respectively.



**Table 6-5**  
**DPC Comparisons with Multiple Power Swings**

Plant	Power %	Doppler Power Coefficient		Difference (A-M)/M %
		Measured pcm/%	ARTEMIS™ pcm/%	
D1	30	-13.57		
D1	50	-12.75		
D1	75	-11.59		

**Table 6-6**  
**PC Comparisons with Multiple Power Swings**

Plant	Power %	Power Coefficient		Difference (A-M)/M %
		Measured pcm/%	ARTEMIS™ pcm/%	
S1	30%	-15.17		
S1	50%	-14.39		
S1	75%	-12.33		
S1	90%	-14.97		
S2	30%	-15.50		
S2	50%	-14.60		

**Table 6-7**  
**DPC Comparisons with Single Power Swing**

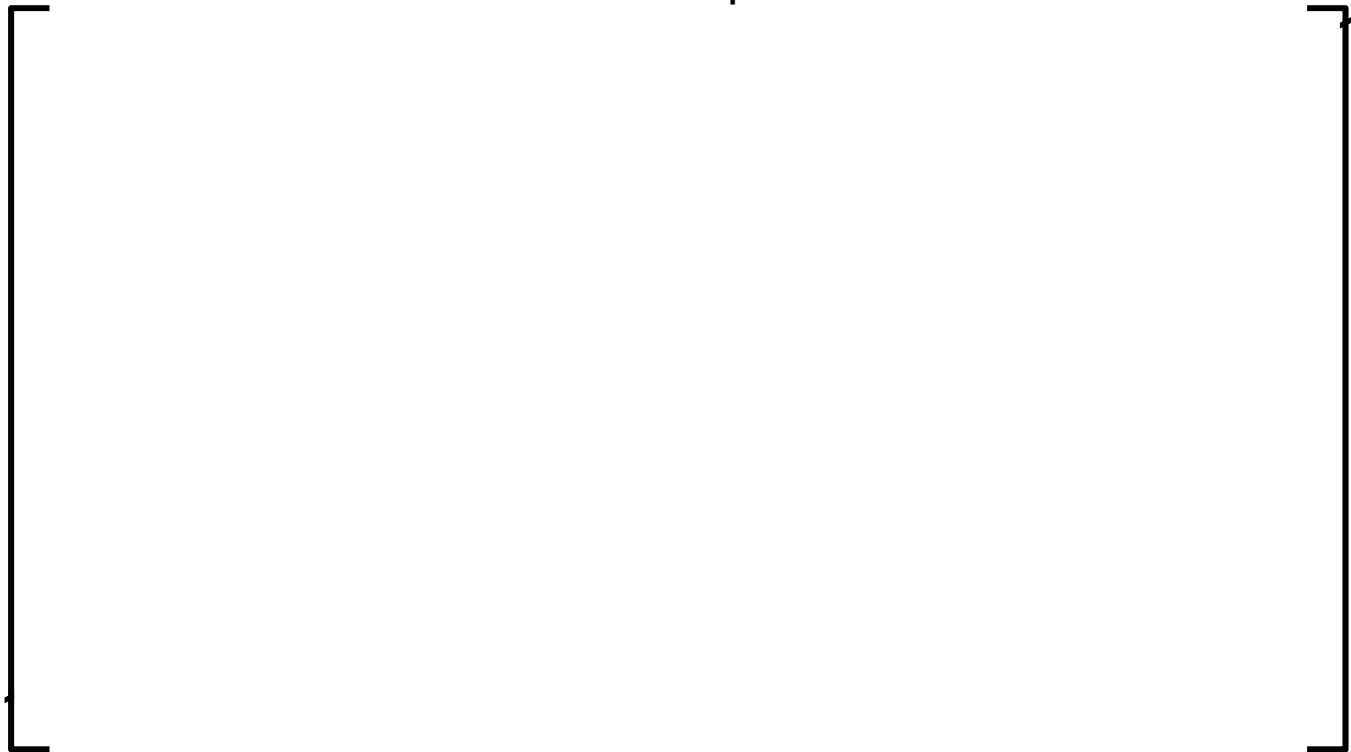
Plant	Power %	Doppler Power Coefficient		Difference (A-M)/M %
		Measured pcm/%	ARTEMIS™ pcm/%	
F1	100	-10.39		
P1	45	-10.88		
P1	50	-11.65		
P1	75	-9.36		
P1	76	-7.89		
P1	92	-9.35		
P1	92	-8.18		
P1	102	-9.23		
P2	50	-11.53		
P2	50	-9.31		
P2	74	-8.20		
P2	90	-8.48		

### 6.3.2 Doppler Benchmark Conclusions

The behavior of the data from all the tests has consistent trends as shown in Figure 6-1.

The mean and standard deviation of the comparisons are [                      ]  
respectively. The data implies that ARCADIA<sup>®</sup> is underpredicting the magnitude of the  
DTC, which is consistent with a previous code system (Reference 6.4-2). This also  
demonstrates that the upscatter model was an improvement over the referenced code  
system and that the Doppler effects are not over-compensated.

**Figure 6-1**  
**Test Data Comparisons**



## 6.4 References

- 6.4-1 ANP-10297P-A, Revision 0, The ARCADIA<sup>®</sup> Reactor Analysis System for PWRs Methodology Description and Benchmarking Results Topical Report, February 2013.
- 6.4-2 BAW-10180-A, Revision 1, “NEMO – Nodal Expansion Method Optimized,” March 1993.

## 7.0 VALIDATION FOR TRANSIENT MODEL

Validation of the ARTEMIS<sup>TM</sup> transient model was provided in Reference 7.5-1, Section 11.0 by comparison of ARTEMIS<sup>TM</sup> calculated results to reference or measured results for the TWIGL-2D benchmarks, the NEACRP reference rod ejection benchmarks and the Rod Drop Tests.

Some of the changes incorporated into ARTEMIS<sup>TM</sup> have a potential impact on the results of the transient benchmarks presented in Reference 7.5-1. In addition, inclusion of the up-scatter treatment in the cross sections has a potential impact on power levels in dropped rod predictions. Therefore, the NEACRP reference rod ejection benchmarks along with the Rod Drop tests were re-analyzed to capture the impact of these changes. Results for the NEACRP and Rod Drop benchmarks are presented below in Sections 7.1 and 7.2, respectively. Furthermore, evaluation of two rod ejection experiments from the SPERT III E-core REA Benchmark program is included for additional validation. These experiments are discussed in Section 7.3.

### 7.1 *NEACRP Reference Rod Ejection Benchmarks*

The NEACRP benchmarks are a set of analytical control rod ejection benchmarks. The specification document for these benchmarks is Reference 7.5-2. This reference defines the core configurations, inputs, and conditions to be used for each transient modeled with ARTEMIS<sup>TM</sup>. The core modeled in the PWR transient is a 157 fuel assembly core. The nuclear data and its dependence on boron, moderator density, moderator temperature, fuel temperature, and control rods are defined in Reference 7.5-2. The reference also defines clad and fuel thermal properties.

### 7.1.1 NEACRP Case Description

There are six cases (A1, A2, B1, B2, C1, and C2) in the NEACRP benchmark problem. These cases represent control rod ejections from three different configurations (A, B, and C) and from both zero power (1) and full power (2) conditions. In the Case A transients, the center rod is ejected. In the Case B transients, a set of four periphery rods are ejected. Finally, the Case C transients eject a single periphery rod in the core. The zero power cases eject a fully inserted control rod and the full power cases eject a partially inserted control rod. The NEACRP cases provide a range of reactivity insertions and core conditions resulting in an effective test of the coupled neutronics, fuel rod, and thermal-hydraulics transient responses.

A summary of results for several industry codes (Reference 7.5-3) used to model the NEACRP control rod ejections was compiled. The results from the PANTHER code (Reference 7.5-4) are typically used as the reference solution for the NEACRP control rod ejection benchmark cases. The reference results are included for comparison to ARTEMIS™.

### 7.1.2 NEACRP Results

Comparisons of important steady-state parameters between ARTEMIS™ and the reference case are provided in Table 7-1. These conditions define the starting point prior to the transient. Boron concentrations are within [            ]. Full power effective Doppler fuel temperatures are within [            ]. The initial local peak is within [            ]. The reactivity release for each case is within [            ]. The reactivity release is the worth of the ejected rod with feedbacks on, at the initial power level. The steady state comparisons verify that the input data is correct and that the static calculations using that data are consistent with the reference data. Therefore, the initialization of the two codes is equivalent.

Table 7-2 provides a summary of kinetics results for ARTEMIS™ and the reference cases. These comparisons include the power level at the time of peak power and at 5 seconds, and the core average Doppler fuel temperature at the point of maximum power and at 5 seconds. The Case A1 power distributions for axial plane 6 (0.34 fraction of core height) are presented in Figure 7-1, Figure 7-2, and Figure 7-3. These comparisons respectively represent the initial conditions, the point of peak power, and the conditions at 5 seconds. Note that the power distributions are normalized to 1.0 for the peak assembly. The time dependence of the core power, Doppler average fuel temperature, and core exit temperature for selected cases A1, B2, and C1 are provided in Figure 7-4 through Figure 7-12. The time dependent data for the reference case were extracted from the plots in Reference 7.5-3.

The ARTEMIS™ peak power for [ ].

The time to peak power for the zero power cases are within [ ], and the time to peak power for the full power cases are within [ ]. The average Doppler temperatures differences are within [ ] at the time of peak power and within [ ] throughout the transient. The core exit temperatures are within [ ] throughout the transient. Comparison of the power distributions between ARTEMIS™ and the reference case show a maximum difference of [ ]


[ ] and a maximum difference of [ ]. The comparisons from Figure 7-4 through Figure 7-12 show that ARTEMIS™ and the reference case comparisons are consistent throughout the transient.

These results show that the ARTEMIS™ code with the time dependent neutronics solutions coupled with the time dependent thermal-hydraulics and thermal-mechanical solutions appropriately model the time dependent phenomena.

**Table 7-1**  
**Steady State Results for the NEACRP Benchmark**



**Table 7-2**  
**Transient Results for the NEACRP Benchmark**



**Figure 7-1**  
**Power Distribution at Initial Conditions (Plane 6) - Case A1**





**Figure 7-2**  
**Power Distribution at time of Maximum Power**  
**(Plane 6) - Case A1**



**Figure 7-3**  
**Power Distribution at 5 sec (Plane 6) - Case A1**



**Figure 7-4**  
**Core Power Fraction – Case A1**



**Figure 7-5**  
**Core Average Fuel Temperature – Case A1**



**Figure 7-6**  
**Core Exit Moderator Temperature – Case A1**



**Figure 7-7**  
**Core Power Fraction – Case B2**

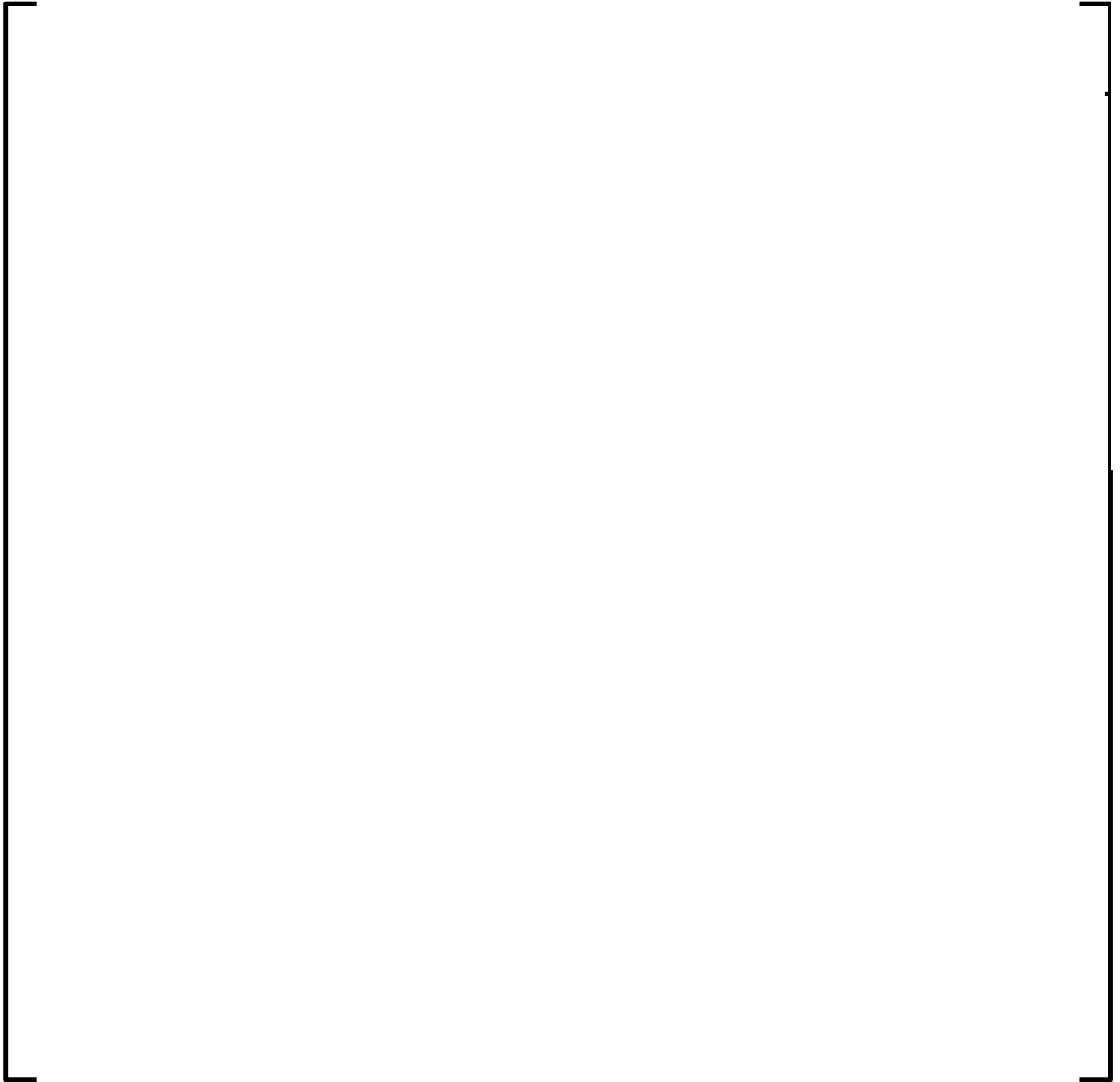


**Figure 7-8**  
**Core Average Fuel Temperature – Case B2**



**Figure 7-9**  
**Core Exit Moderator Temperature – Case B2**





**Figure 7-10**  
**Core Power Fraction – Case C1**



**Figure 7-11**  
**Core Average Fuel Temperature – Case C1**



**Figure 7-12**  
**Core Exit Moderator Temperature – Case C1**



## **7.2      *ROD DROP TESTS***

### **7.2.1      Rod Drop Test Description**

Section 11.3 of Reference 7.5-1 discusses five rod drop tests that were performed for three plants with 193 fuel assemblies:

- Test 1: Two, interior, half core symmetric rods dropped near beginning of cycle, 50% power
- Tests 2-4: Two, interior, half core symmetric rods dropped near middle of cycle, 50.7% power
- Test 5: Two, interior, half core symmetric rods dropped near end of cycle, 50.1% power

Additional details of these tests including core layout and operating conditions were provided in Reference 7.5-1.

### **7.2.2      Calculational Model**

The cross sections for the rod drop test calculations were generated with APOLLO2-A. The core was depleted with ARTEMIS<sup>TM</sup>. The radial and axial reaction rate distributions of the core (measured channels) were compared. The kinetic input data (precursor information and neutron velocity) were extracted from APOLLO2-A for the assembly types that make up the core in the three plants considered in the rod drop evaluation. These values were averaged based on the enrichment of different assembly types. Excore responses were simulated in ARTEMIS<sup>TM</sup> using the peripheral assembly powers and the associated weighting factors. The weighting factors were provided in Table 11.3-2 of Reference 7.5-1.

### 7.2.3 Results

The ARTEMIS™ results are compared to the measured values in Figure 7-13 to Figure 7-17 for each of the five rod drop tests. The first graphic of each figure shows the evolution of the nuclear flux (normalized to the core power) versus time. The second graphic of each figure shows the derivative of the nuclear flux  $dP/dt$  calculated with the Laplace transform function implemented in the measured system of the studied reactors. Comparisons between measured and calculation show consistent behavior prior to reaching the minimum nuclear flux and its derivative. In the last case (near End of Cycle), a [ ] was observed. In this test, an increased noise level was observed due to differences in the response between detector 1 and detector 2. The half core symmetric positions show [ ]. During the second part of the rod drop test where there is an increase in the nuclear flux and its derivative, the predicted values are within [ ] of the measured results in the cases near Beginning and Middle of Cycle and within [ ] in the case near End of Cycle.

The two parameters analyzed for the rod drop tests are as follows:

- The time to reach the minimum  $dP/dt$  (maximum absolute value of  $dP/dt$ ) – the maximum difference between predicted and measured values is [ ].  
The average difference is [ ] with a standard deviation of [ ].
- The minimum  $dP/dt$  – the maximum difference between predicted and measured values is [ ]. The average difference is [ ] with a standard deviation of 0.26%NP/s. By considering [ ], the maximum deviation on minimum  $dP/dt$  will be [ ].

Results of the rod drop tests are presented in Table 7-3 and in Figure 7-18. The data in Figure 7-18 shows the absolute difference between the calculated-to-measured data for the minimal  $dP/dt$  (in %NP/s) for each of the four excore detectors for each test. These differences are shown versus the measured value of the minimal  $dP/dt$ .

Table 7-4 presents a summary of the results over all the transients. Table 7-4 also shows results from Reference 7.5-1, Table 11.3-3 for comparison to the supplement values.

The graphs provided in Figure 7-13 through Figure 7-18 are similar to those provided in Reference 7.5-1, Figure 11.3-2 through Figure 11.3-7.

**Table 7-3**  
**Rod Drop Transient Results**

--	--

**Table 7-4**  
**Results of Rod Drop - Synthesis**

(a) Comparison (Prediction – Measurement) – Time of the minimal  $dP/dt$

--	--

(b) Comparison (Prediction – Measurement) – Minimal  $dP/dt$

--	--

**Figure 7-13**  
**Results of Rod Drop Test 1 – 0.7 GWd/mtU, F6K10 (SD bank)**

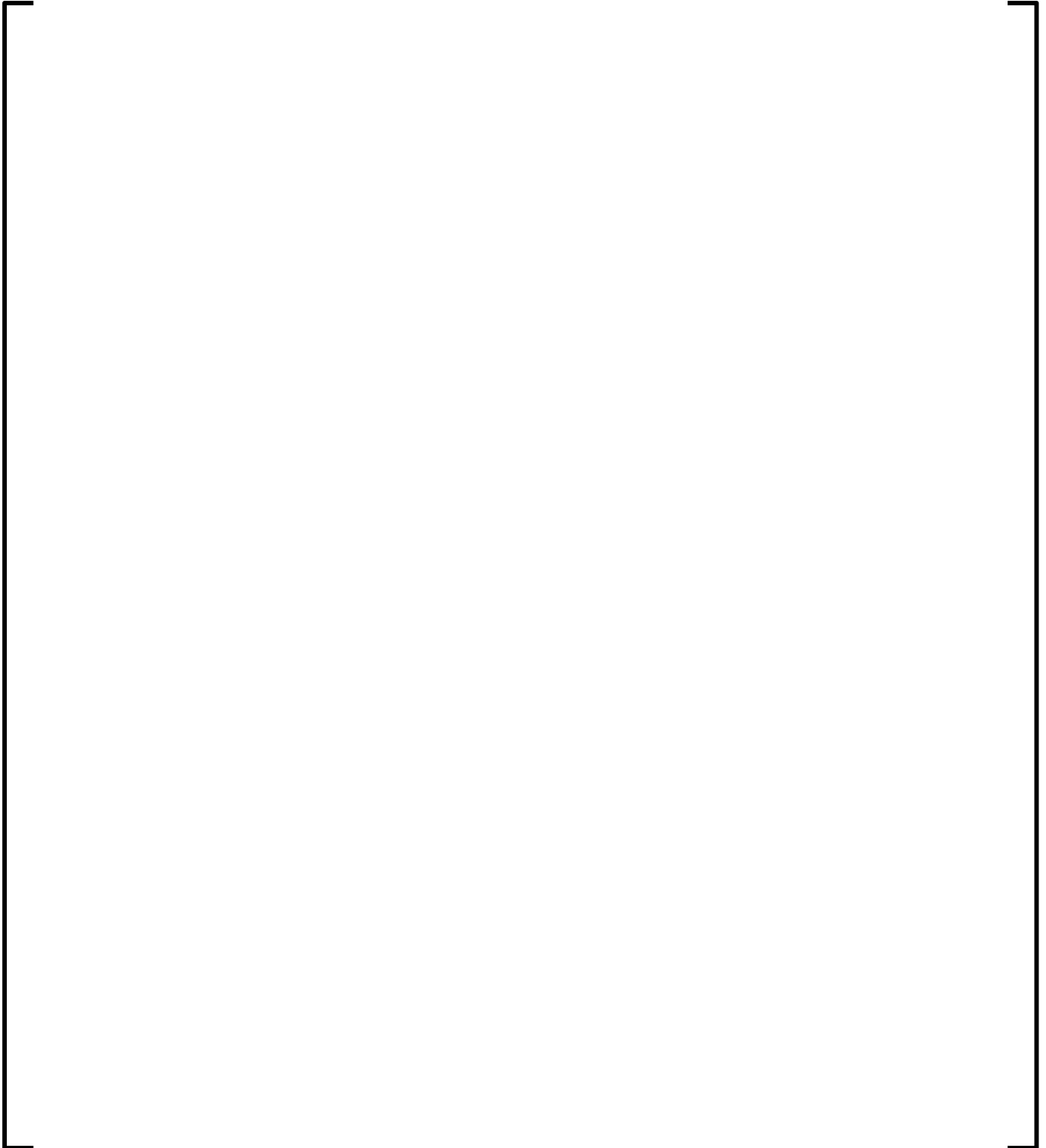




**Figure 7-14**  
**Results of Rod Drop Test 2 – 4.34 GWd/mtU, K6F10 (SD bank)**

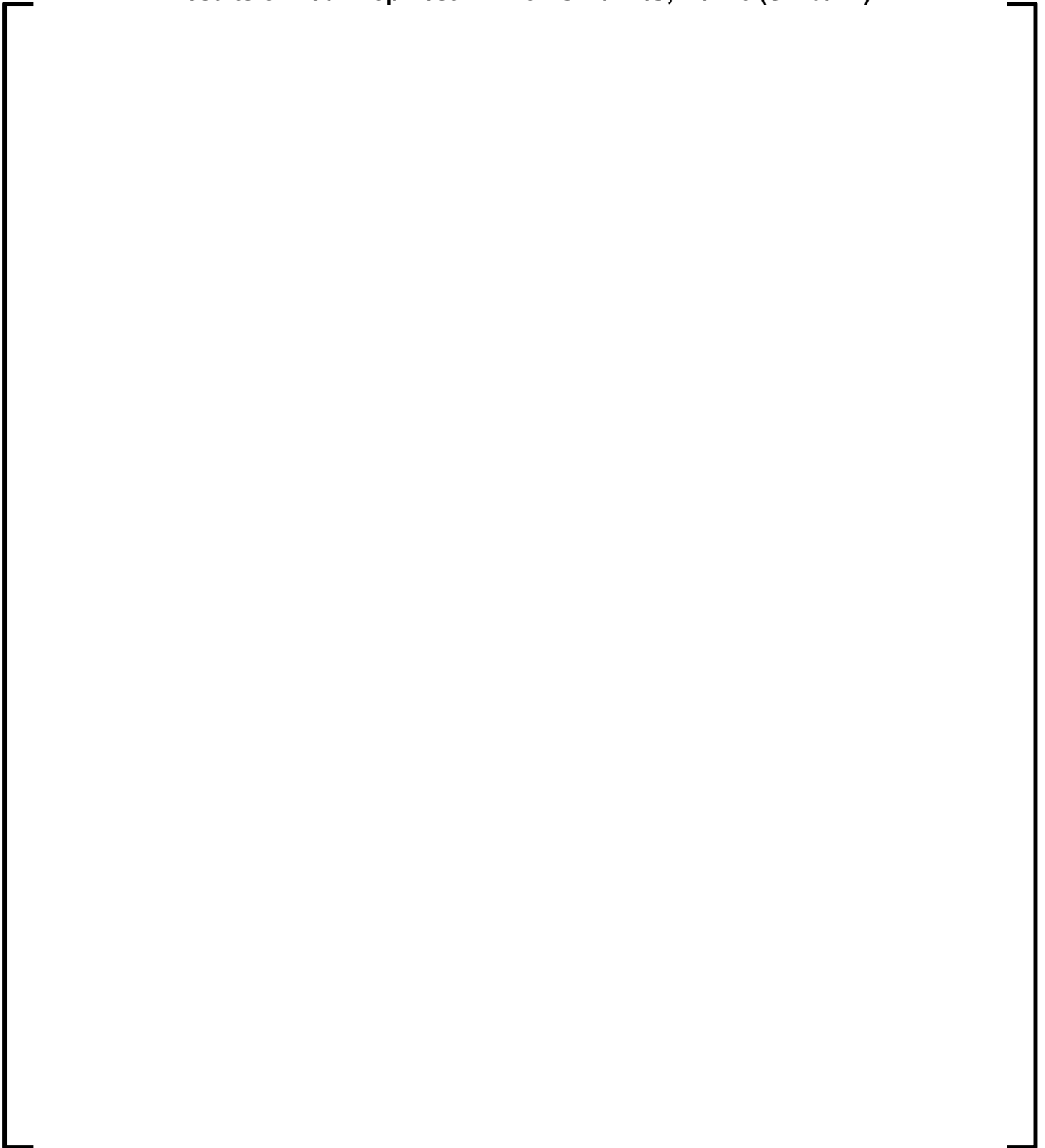


**Figure 7-15**  
**Results of Rod Drop Test 3 – 4.34 GWd/mtU, K4F12 (SC bank)**

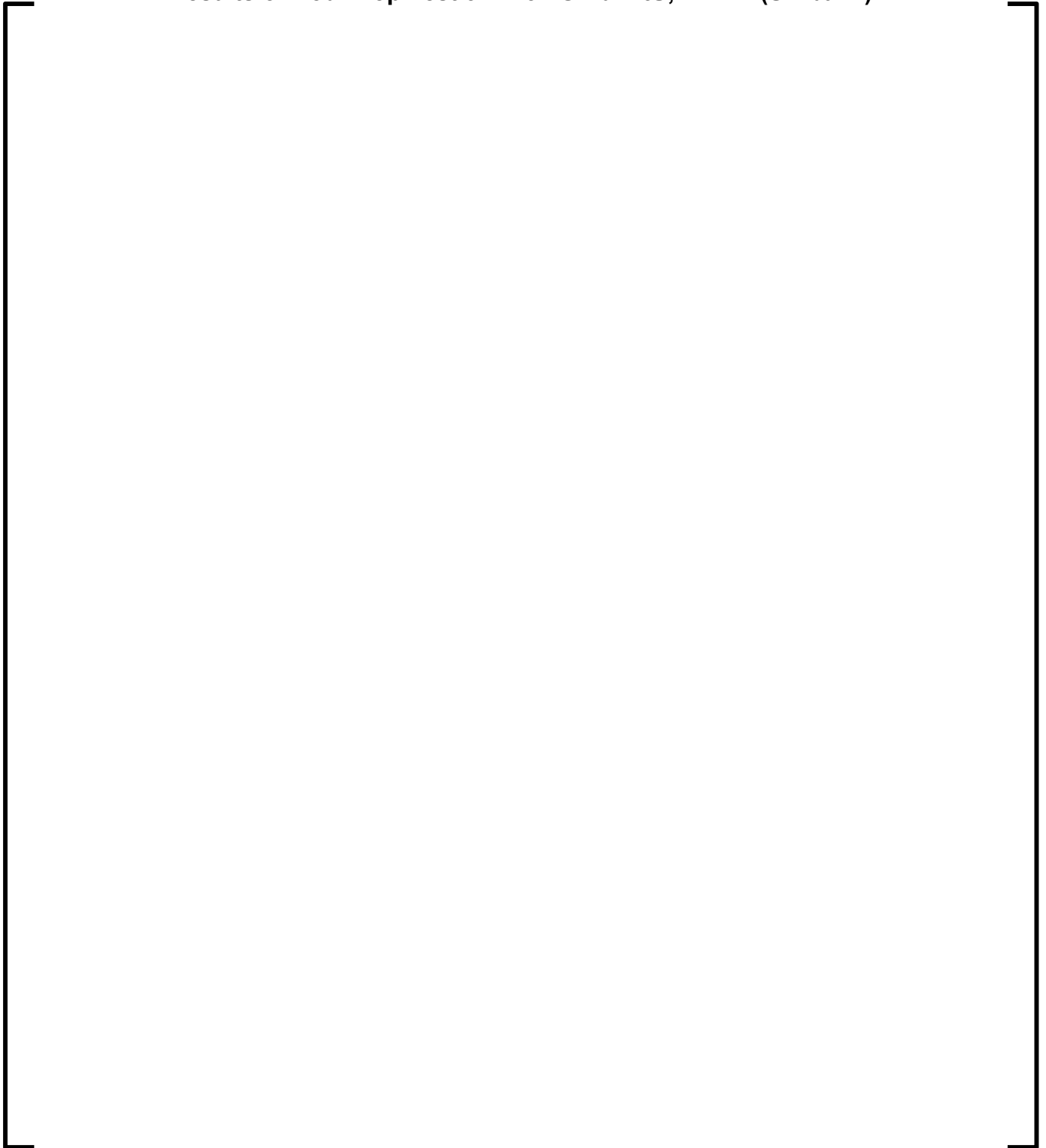


**Figure 7-16**  
**Results of Rod Drop Test 4 – 4.34 GWd/mtU, E5L11 (R bank)**

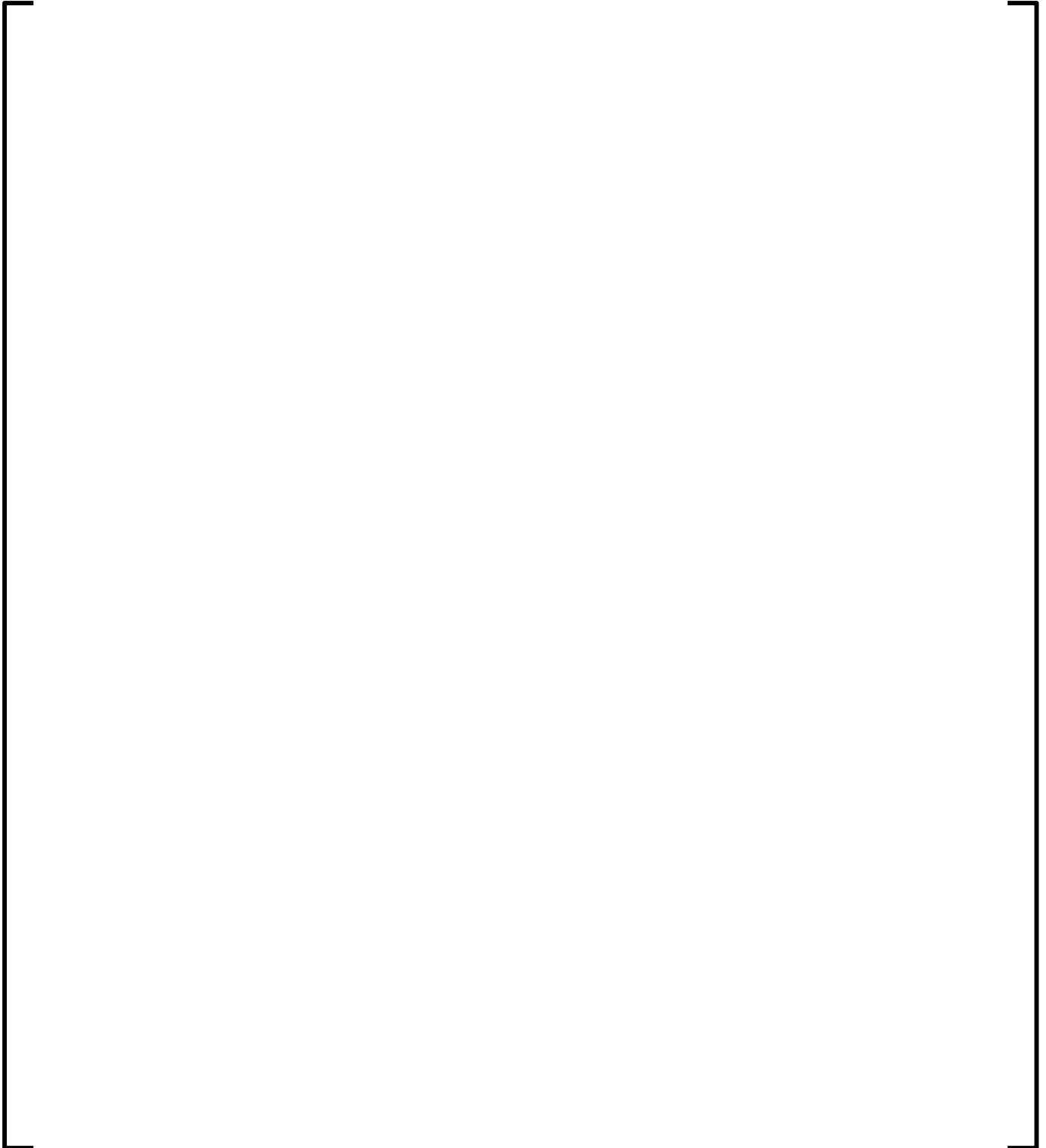


**Figure 7-17**  
**Results of Rod Drop Test 5 – 11.575 GWd/mtU, F6K10 (SD bank)**

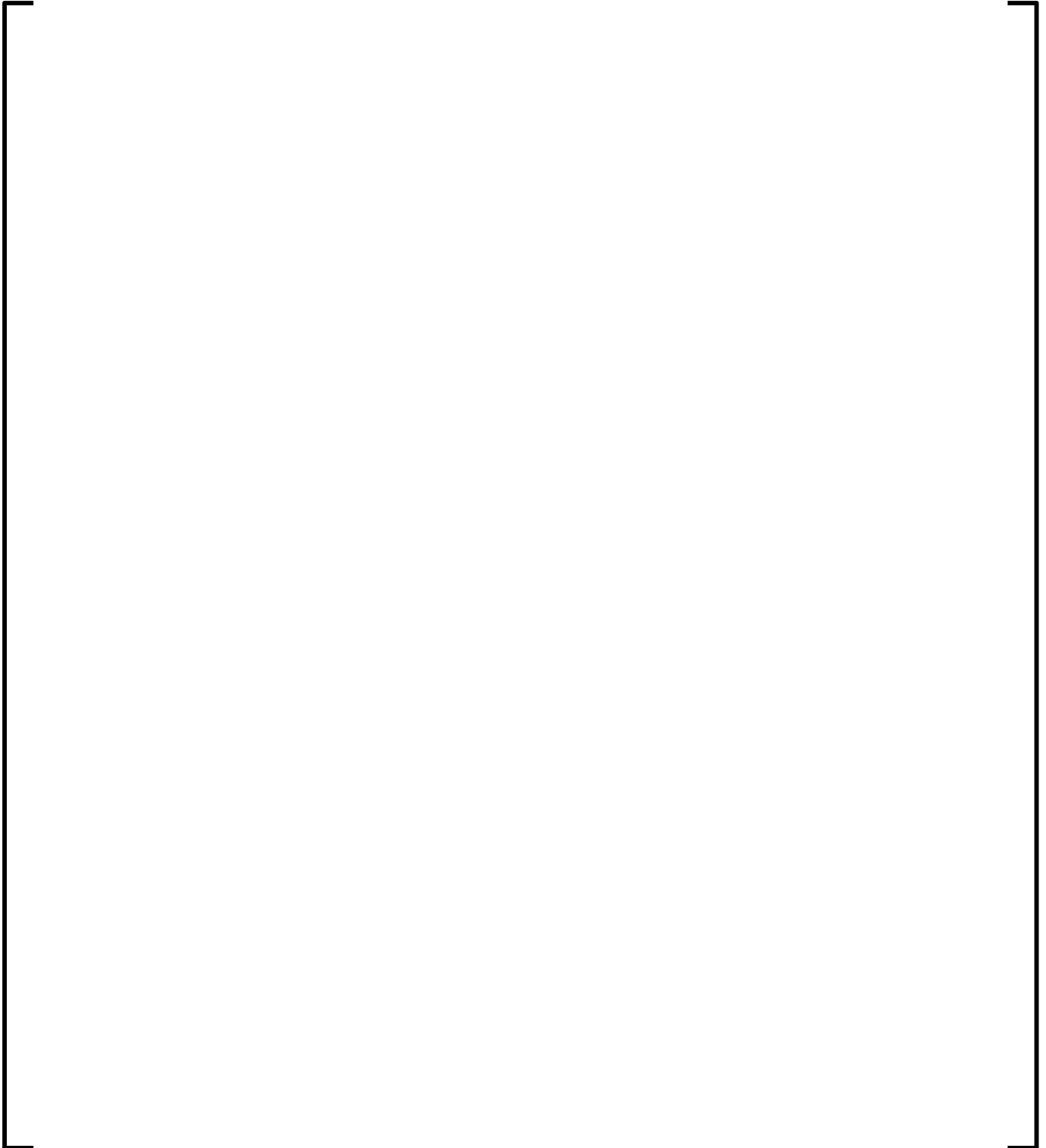


**Figure 7-18**  
**Results of Rod Drop Tests – Synthesis of Deviation on Minimal**  
**Derivative of the Nuclear Flux  $dP/dt$**



### **7.3 SPERT III E-Core REA Benchmarks**

Two rod ejection experiments from the SPERT III E-Core facility (Reference 7.5-5) were selected for evaluation against the test results described in Reference 7.5-6. Test 60 was selected for a hot zero power (HZIP) initial condition and Test 86 was selected for a hot full power (HFP) initial condition. Both tests are simulated using ARTEMIS™, but with cross-section and delayed neutron precursor data provided by the NRC. The cross-sections were converted to ARTEMIS™ XSLIB-type input files for each of the various fuel compositions. A majority of the required design information and measured results were obtained from References 7.5-5 and 7.5-6, or as noted in the text.

Reasonable approximations were made where the design information was not readily available. Several modeling approximations were required to perform these benchmarks due to unavailability of reference information for modeling, or due to the unique design of the experimental facility. Several key modeling approximations are summarized below:



The base neutronic model is validated with two static comparisons. First, the HZP static control rod worth of the transient rod at [ ] was calculated and compared to measured data obtained from Reference 7.5-6; this comparison is shown in Figure 7-19. Second, the HZP moderator temperature coefficient (MTC) calculated by ARTEMIS™ is [ ] and the measured value is cited as  $-4.0 \text{ } \phi/\text{ }^{\circ}\text{F}$ . The agreement with the measured results is good and indicates that the modeling assumptions are reasonable. In addition, the HZP excess reactivity worth of [ ], calculated by the ARTEMIS™ model, compares favorably with the [ ], from Reference 7.5-6.

### 7.3.1 Test 60 - HZP

Test 60 is an ejected control rod test initiated from a core power of 50 watts and an isothermal temperature of [ ]. In Test 60, the initial transient control rod position was set to yield an ejected worth of [ ], which is equal to the measured worth.

Test 60 power pulse response versus time results, as-measured and as-calculated by ARTEMIS<sup>™</sup>, are shown in Figure 7-20. The calculated peak power is [ ] and the measured value is cited as  $410 \pm 41$  MW. The calculated integrated power at the peak is [ ] and the measured value is reported as  $8.5 \pm 1.1$  MW-s. Both calculated values are well within the measurement uncertainty of the test. The enthalpy rise at one pulse-width past the peak was calculated as [ ], not including any radial-local effect; the experimental value is not known.

### 7.3.2 Test 86 - HFP

Test 86 is a prompt critical rod ejection initiated from a core power of 19 MW with a measured ejected rod worth of [ ]

[ ]. Reference 7.5-6 states that the ejected control rod worth cannot be measured directly at power and its uncertainty is higher because the feedback is immediate and a stable reactor period cannot be established. [ ]

].

[

].



For Test 86, the power pulse response versus time, measured and calculated (ARTEMIS™), are shown in Figure 7-21. The calculated peak power response is in agreement with the measured response yielding a calculated peak power of

[ ] compared with the measured value of  $610 \pm 60$  MW. The calculated time integrated power at the peak is [ ] and the measured value is reported as  $17 \pm 2$  MW-s.

The enthalpy rise at one pulse-width past the peak was calculated as [ ], not including any radial-local effect; the experimental value is not known.

### 7.3.3 Conclusion

ARTEMIS™ has been benchmarked against the experimental SPERT III E-Core test results and comparisons of the results demonstrate the adequacy of ARTEMIS™ to simulate a control rod ejection transient.

The calculated cal/g for both Test 60 and Test 86 are within the range of applicability to PWR reactors. Therefore, the benchmark of the SPERT III E-core is valid to qualify ARTEMIS™ for use in performing rod ejection analyses.

**Figure 7-19**  
**SPERT III E-Core Transient Control Rod Worth**



**Figure 7-20**  
**SPERT III E-Core Test 60 Power Response**



**Figure 7-21**  
**SPERT III E-Core Test 86 Power Response**



## **7.4 Conclusions for Transient Benchmarks**

Comparisons made for the NEACRP rod ejection accident, the Rod Drop Tests and the SPERT III E-core show the capability of the coupled (Neutronics/Thermal-hydraulics/Thermal-mechanics) ARTEMIS<sup>™</sup> code in analyzing transient events. This capability has been shown for multiple core designs and control rod types. SPERT provided an additional challenge because the design is not a typical PWR. ARTEMIS<sup>™</sup> was able to accurately predict the behavior of the rod ejection event for this unique configuration.

## **7.5 References**

- 7.5-1 ANP-10297P-A, Revision 0, The ARCADIA<sup>®</sup> Reactor Analysis System for PWRs Methodology Description and Benchmarking Results Topical Report, February 2013.
- 7.5-2 H. Finnemann and A. G. Galati, "NEACRP 3D LWR Core Transient Benchmark," Final Specifications, NEACRP-L-335 (Rev. 1), October 1991 (January 1992).
- 7.5-3 H. Finnemann, H. Bauer, A. G. Galati, and R. Martinelli, "Results of LWR Core Transient Benchmarks," NEA/NSC/DOC(93)25, October 1993.
- 7.5-4 P. K. Hutt, and M. P. Knight, "The Development of a Transient Neutron Flux Solution in the PANTHER Code," Transactions, American Nuclear Society, 61, 348 (1990).
- 7.5-5 J. Dugone, "SPERT III Reactor Facility: E-Core Revision," IDO-17036, U.S. Atomic Energy Commission, November 1965.
- 7.5-6 "Reactivity Accident Test Results and Analyses for the SPERT III E-Core – A Small, Oxide-Fueled, Pressurized Water Reactor," IDO-17281, U.S. Atomic Energy Commission, March 1969.
- 7.5-7 Anthony P. Ulses, "Assessment of the TRACE code against SPERT III E-Core Reactivity Insertion Accident Data," US NRC, June 9, 2009.

## 8.0 POWER DISTRIBUTION UNCERTAINTIES

### 8.1 *Introduction*

For licensing applications, uncertainties need to be applied to local peaking factors such as  $F_{\Delta H}$  and  $F_Q$ . Two types of peaking uncertainties were discussed in Reference 8.6-1, Section 12: an inferred uncertainty and a calculation uncertainty (Nuclear Reliability Factors).

The ability of ARCADIA<sup>®</sup> to provide inferred and predicted power distributions is dependent upon both local (pin to pin) and global (assembly to assembly) power predictions. ARCADIA<sup>®</sup> comparisons to measured fission rates for fuel pins in critical experiments and comparisons to higher order calculations are used to determine the local power component which is identical for both types of uncertainties. The local power comparisons and results are presented in Section 8.2.

Both types of uncertainties depend upon comparisons to measured data at commercial nuclear power plants to determine the global error term. This type of error is different for the inferred and calculated uncertainties because the inferred error is based upon the ability of the simulator to predict the powers in uninstrumented assemblies using the measurements and the calculation uncertainty is based upon comparisons between predicted and measured values. The global component of the inferred uncertainty is calculated for each plant type and combined with the local uncertainty to obtain an inferred uncertainty (Section 8.3). The comparisons of ARTEMIS<sup>™</sup> predictions to measured values and derivation of the calculational uncertainties are presented in Section 8.4. A summary of the estimated uncertainties is provided in Section 8.5.

In Supplement 1, the application of the MEDIAN reconstruction methodology for the inferred uncertainty is extended to include movable fission and fixed rhodium incore detector systems. MEDIAN is described in Section 3.15 of this supplement. The data sets used have been expanded by incorporating data from an additional plant (Plant E) in addition to data used previously in the Reference 8.6-1 uncertainty analysis.

The estimated uncertainties are 95/95 tolerance limits. They are first calculated assuming the populations for the error components are normally distributed which is referred to as a “Normal Uncertainty.” Also, Monte Carlo simulations are performed on the actual distributions to obtain a 95/95 tolerance limit which does not require the data to be normally distributed and is referred to as a “Non-Parametric Uncertainty”.

On page 28 of the NRC’s Safety Evaluation Report for the ARCADIA<sup>®</sup> Code System Topical Report (ANP-10297P-A), the following limitation is imposed:

“The ARCADIA<sup>®</sup> code system is limited to fuel types with non-Inconel grids unless additional verification of uncertainties is conducted to account for any peaking biases due to grid type or other plant effects. Verification of uncertainties must be quantified and accounted for in the uncertainties and/or peaking allowances in the licensing calculations on plant specific basis.”

This limitation was made in response to a statement on pages 12-12 and 12-13 of Reference 8.6-1, stating that assemblies containing Alloy-718 (Inconel) grids were not included in the peak statistics. A letter of clarification was incorporated into ANP-10297P-A, which notes that Alloy-718 is present in most grid designs used by AREVA and that the original statement referred only to grids in the active fuel region that were comprised solely of Alloy 718. Bi-metallic grids that had both Alloy-718 and Zircaloy were considered in the peak statistics.

In this supplement the uncertainty analysis documented in Section 8.0 is performed using data for assemblies with all Alloy-718 grids, bi-metallic grids and all Zircaloy or M5 grids. The peak statistics presented in Table 8-24 of this supplement include the Alloy-718 grids and show that the uncertainties remain well within limits. Thus, the impact of the presence of the all-Alloy-718 spacers are included in the uncertainty analysis results. Therefore, AREVA requests that the limitation, as stated above, be removed.

## **8.2 LOCAL PEAKING UNCERTAINTY**

The local peaking uncertainty analysis is composed of two parts: comparisons of predicted and measured pin fission rate results from critical experiments and comparisons of ARTEMIS<sup>TM</sup> calculated pin powers to APOLLO2-A calculated results for several multi-assembly configurations (i.e., colorsets). Comparisons of critical experiments determine the accuracy of the APOLLO2-A methodology to calculate the local pin power distribution within a fuel assembly. The ARTEMIS<sup>TM</sup> to APOLLO2-A comparisons estimates the error of the ARTEMIS<sup>TM</sup> dehomogenization without and with burnup compared to an explicit pin model in APOLLO2-A. The local peaking uncertainty analysis tests the methodology with twenty-four different multi-assembly problems.

### **8.2.1 Critical Core Configurations**

Six critical experiments performed by the B&W Lynchburg Research Center as part of the DOE Gadolinia project were used for comparisons of predicted and measured pin fission rate to estimate the pin power uncertainty. These criticals were the same as those used for Reference 8.6-1, Section 12.2.1: four experiments using a 15x15 lattice of fuel pins resembling the AREVA Mark B fuel assembly and two experiments representing a CE 16x16 lattice with five larger water holes per assembly. These experiments are the 1980s B&W experiments from Section 4.1. The fission rate distribution comparisons of the calculated and measured data for these six critical experiments are shown in Figure 4-5 through Figure 4-10 of this supplement. These fission rate distributions are relative to an average assembly fission rate of 1.0 for the center assembly. These critical geometries are representative of typical assemblies that could exist in a power reactor and show the power distribution within an assembly. No biases are observed around water holes or poisons.



Percent differences for pin powers greater than [ ] are used to calculate the mean and standard deviation for each experiment. The measurement uncertainty for local pin power distributions is obtained for each critical experiment. The calculated variance is estimated by subtracting measured variance from observed variance for each experiment. Resultant calculated standard deviations for each experiment are between [ ] and no significant differences are noted between cores with or without Gadolinia rods. The calculated error for each set is combined to obtain the total estimated calculational error. These results are shown in Table 8-1 of this supplement.

For comparison, Table 8-2 of this supplement provides the estimated calculated deviation results from Reference 8.6-1, Table 12.2.1-2 and the supplement.

**Table 8-1**  
**Summary of Results of Percent Difference:**  
**Observed = (Calc/Meas – 1)\*100%**

Core	Number of Samples	Observed Mean	Observed Deviation	Measured Deviation	Estimated Calculated Deviation
Core 1	32				
Core 12	32				
Core 18	32				
All Non-Gad	96				
Core 5	29				
Core 14	29				
Core 20	29				
All Gad-Cores	87				
All Cores	183				

**Table 8-2**  
**Comparison of Results for Critical Experiments for Local Peaking**  
**Uncertainty**

### 8.2.2 Multi-Assembly Calculations with APOLLO2-A and ARTEMIS™

Multi-assembly calculations (e.g., colorsets) are used to define the errors from the use of single assembly APOLLO2-A generated nuclear data in ARTEMIS™. The colorset calculations compare pin power distribution from the ARTEMIS™ dehomogenization model to the fine mesh, higher order calculation in APOLLO2-A.

Twenty multi-assembly depletion problems were analyzed with APOLLO2-A and ARTEMIS™ for Reference 8.6-1, Section 12.2.2. Each problem consisted of two different fuel assembly types from actual or planned core designs loaded in a checkerboard 4 x ¼ fuel assembly patterns. Variations between assemblies include enrichment loadings, burnable poison loadings and rod insertion.

An additional four configurations using ERU fuel assemblies are included in the current analysis: colorsets 23-26. A description of these configurations is given in Table 8-3.

Table 8-4 provides a summary of the results of the local pin powers from each multi-assembly problem. All power producing pins in unrodded assemblies with relative powers > [ ] are considered in the statistical results including Gadolinia pins. The maximum peak to peak relative difference for all the problems is [ ]. The standard deviation of the local pin powers is at or below [ ] for each of these cases. The mean and standard deviation for the entire set of cases are [ ], respectively with [ ].

Pin power relative percent differences are provided for colorsets 4, 9 and 24 at 0.1, 10.0 and 20.0 GWd/mtU in Figure 8-1 through Figure 8-9. Some of the peak-to-peak differences are significantly larger than the standard deviation would imply. In these cases the peak is in the corner pin or on the periphery of the assembly. To be conservative in the uncertainty determination, the statistics are taken from the peripheral pins which tend to have higher differences. The mean and standard deviation for the peripheral pins are [ ], respectively with [ ].

For comparison, Table 8-5 provides the estimated calculated deviation results from Reference 8.6-1, Section 12.2.2 and the supplement results.

The multi-assembly benchmark demonstrates the ability of ARTEMIS™ to predict pin powers with burnup effects using the coarse mesh solution (4 nodes per assembly) with its dehomogenization model.

**Table 8-3**  
**Multi-Assembly Descriptions Using ERU Fuel**

Set #	Plant lattice <sup>a</sup>   wt% <sup>235</sup> U + Gad Loading (wt%)	Initial BU	Plant lattice <sup>a</sup>   wt% <sup>235</sup> U + Gad Loading (wt%)	Initial BU
23	(3) W 17x17   ERU 4.75 none	0	(1) W 17x17   4.95 none	40±5
24	(3) W 17x17   ERU 4.75 none	0	(1) W 17x17   4.95 24 Gad 6.0 / 12 Gad 2.0	40±5
25	(2) W 17x17   ERU 4.75 none	20±5	(2) W 17x17   4.95 none	0
26	(3) W 17x17   4.95 none	0	(1) W 17x17   ERU 4.75 none	40±5

<sup>a</sup> (x) indicates the number of assemblies of this type in the 4 x ¼ problem.

**Table 8-4**  
**Multi-Assembly Results**

Set #	Maximum Absolute Relative Difference at BOC (%)	Maximum Absolute Relative Difference Over Entire Depletion (%)	Maximum Absolute Relative Peak to Peak Difference Over Entire Depletion (%)	Standard Deviation of Relative Differences of Each Pin Over Entire Depletion (%)
1				
2				
3				
4				
6				
7				
8				
9				
10				
11				
12				
13				
14				
15				
16				
17				
19				
20				
21				
22				
23				
24				
25				
26				

**Table 8-5**  
**Comparison of Multi-Assembly Statistics**

	ANP-10297P-A	Supplement 1
Maximum Peak to Peak Relative (%)		
Standard Deviation of Local Pin Powers (%)		
Number of Data Points		
Mean for All Cases (%)		
Standard Deviation for All Cases (%)		
Peripheral Pins		
Number of Data Points		
Mean for All Cases (%)		
Standard Deviation for All Cases (%)		

**Figure 8-1**  
**Colorset 4 at 0.1 GWd/MTU, Pin Power Relative Percent Difference**

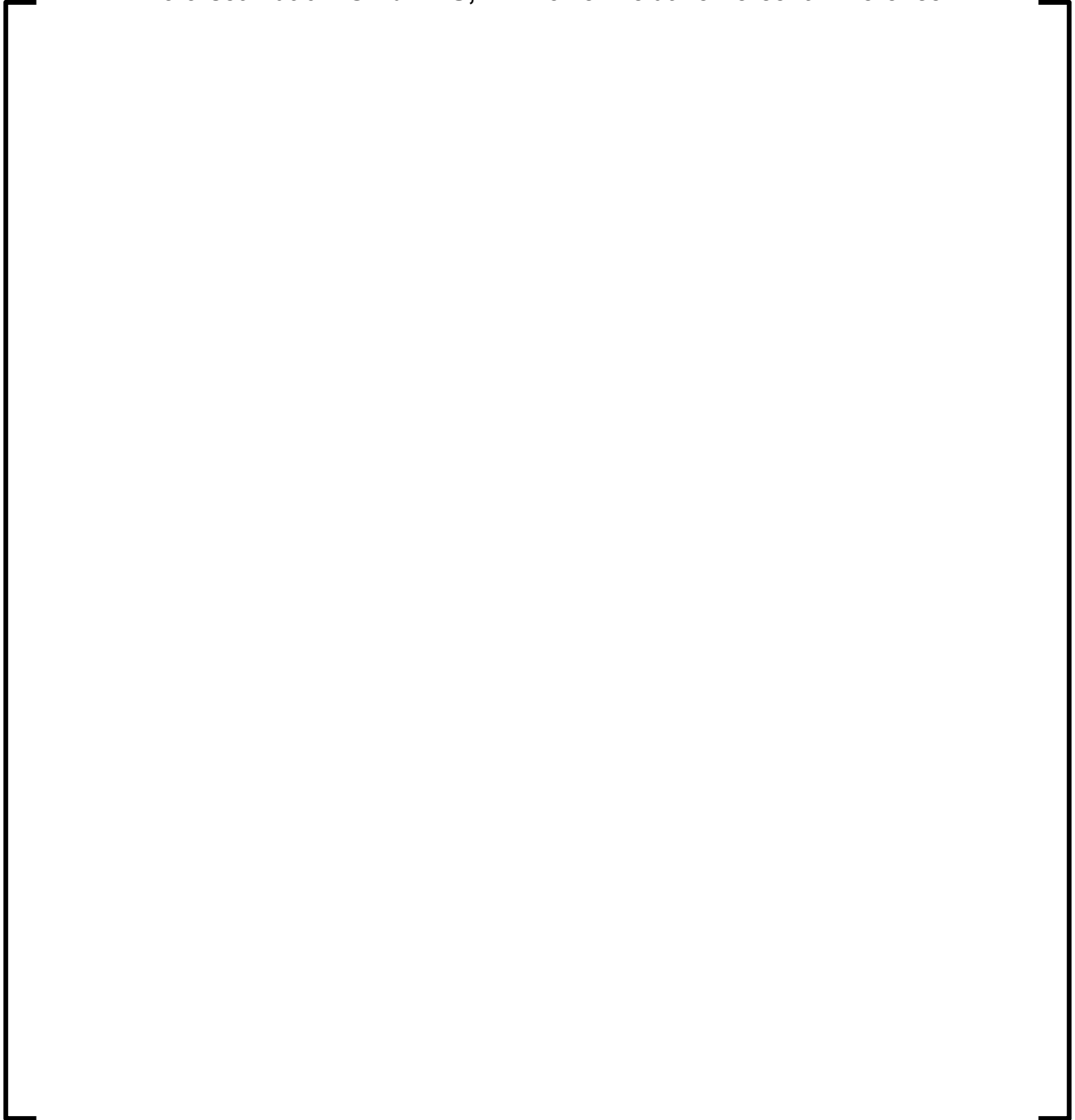




**Figure 8-2**  
**Colorset 4 at 10.0 GWd/MTU, Pin Power Relative Percent Difference**

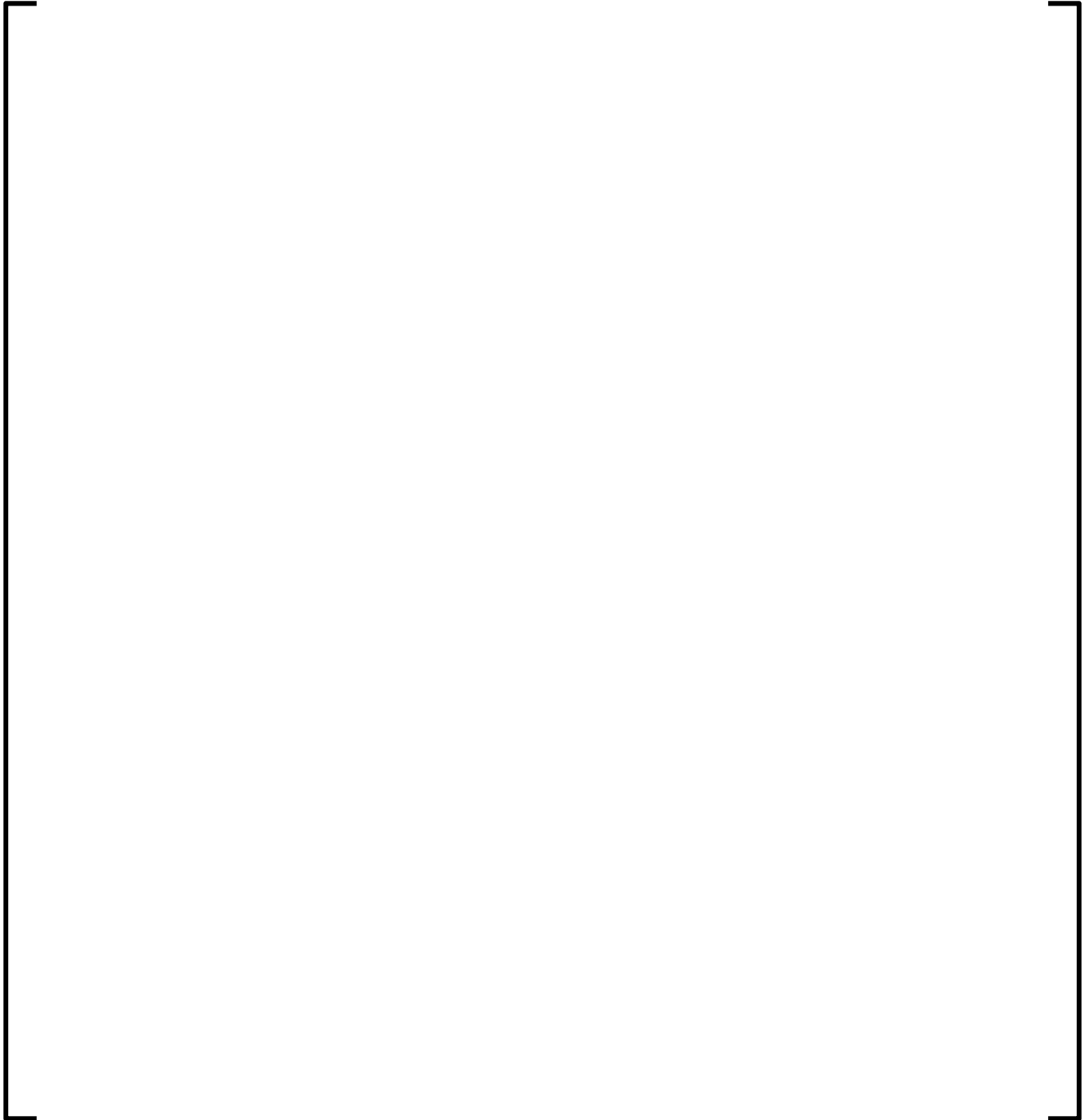


**Figure 8-3**  
**Colorset 4 at 20.0 GWd/MTU, Pin Power Relative Percent Difference**

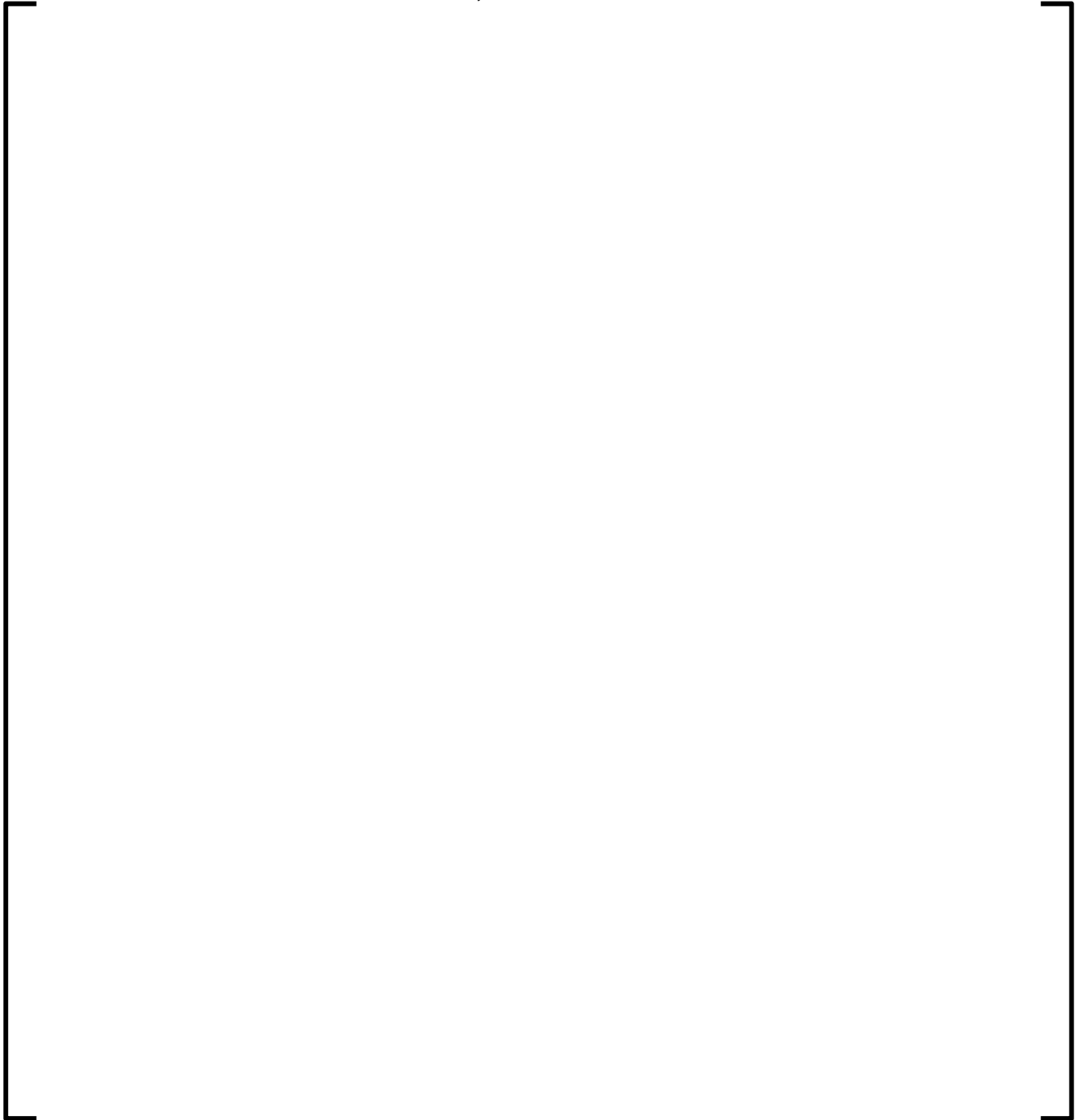


**Figure 8-4**  
**Colorset 9 at 0.1 GWd/MTU, Pin Power Relative Percent Difference**

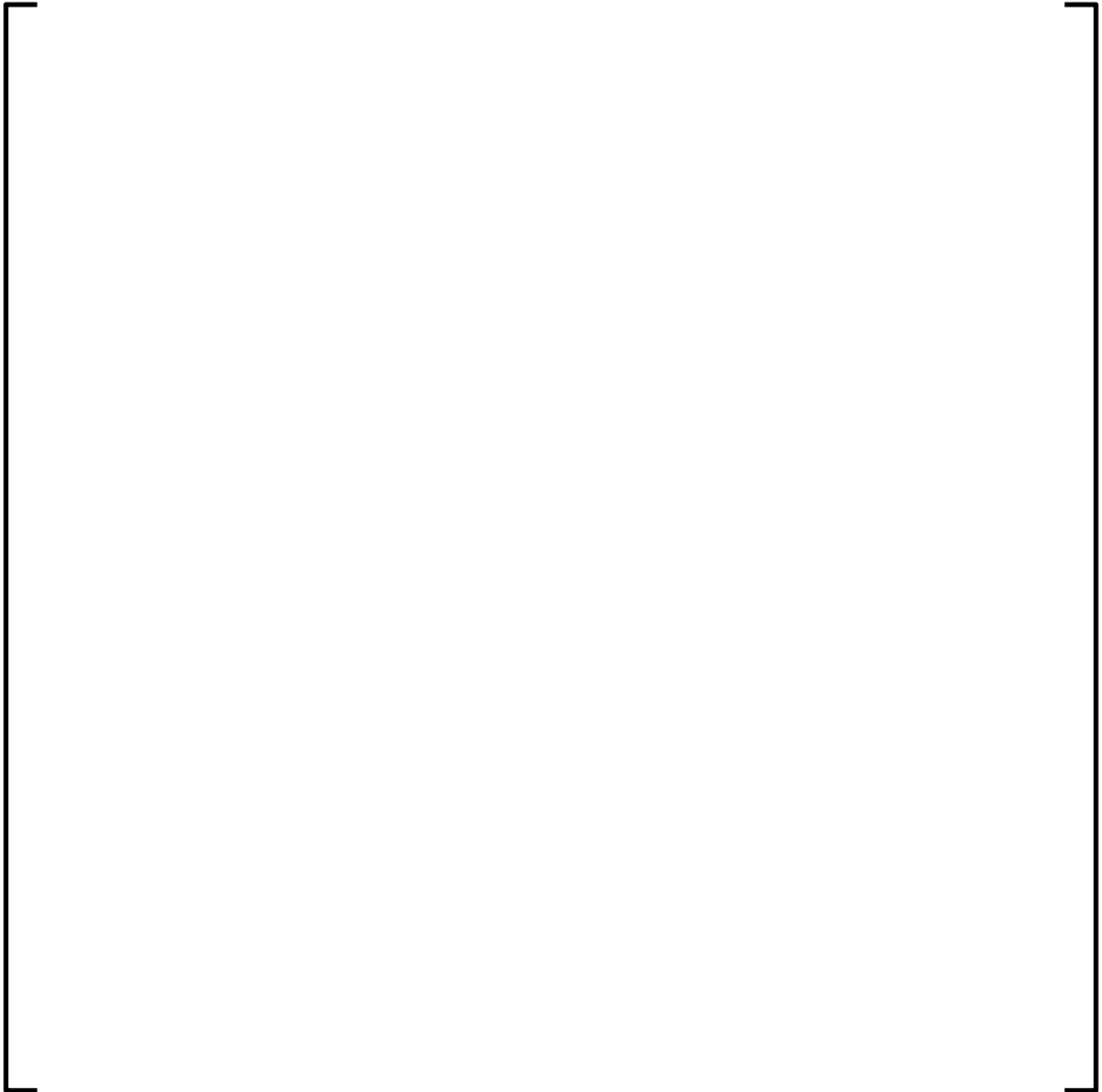


**Figure 8-5**  
**Colorset 9 at 10.0 GWd/MTU, Pin Power Relative Percent Difference**

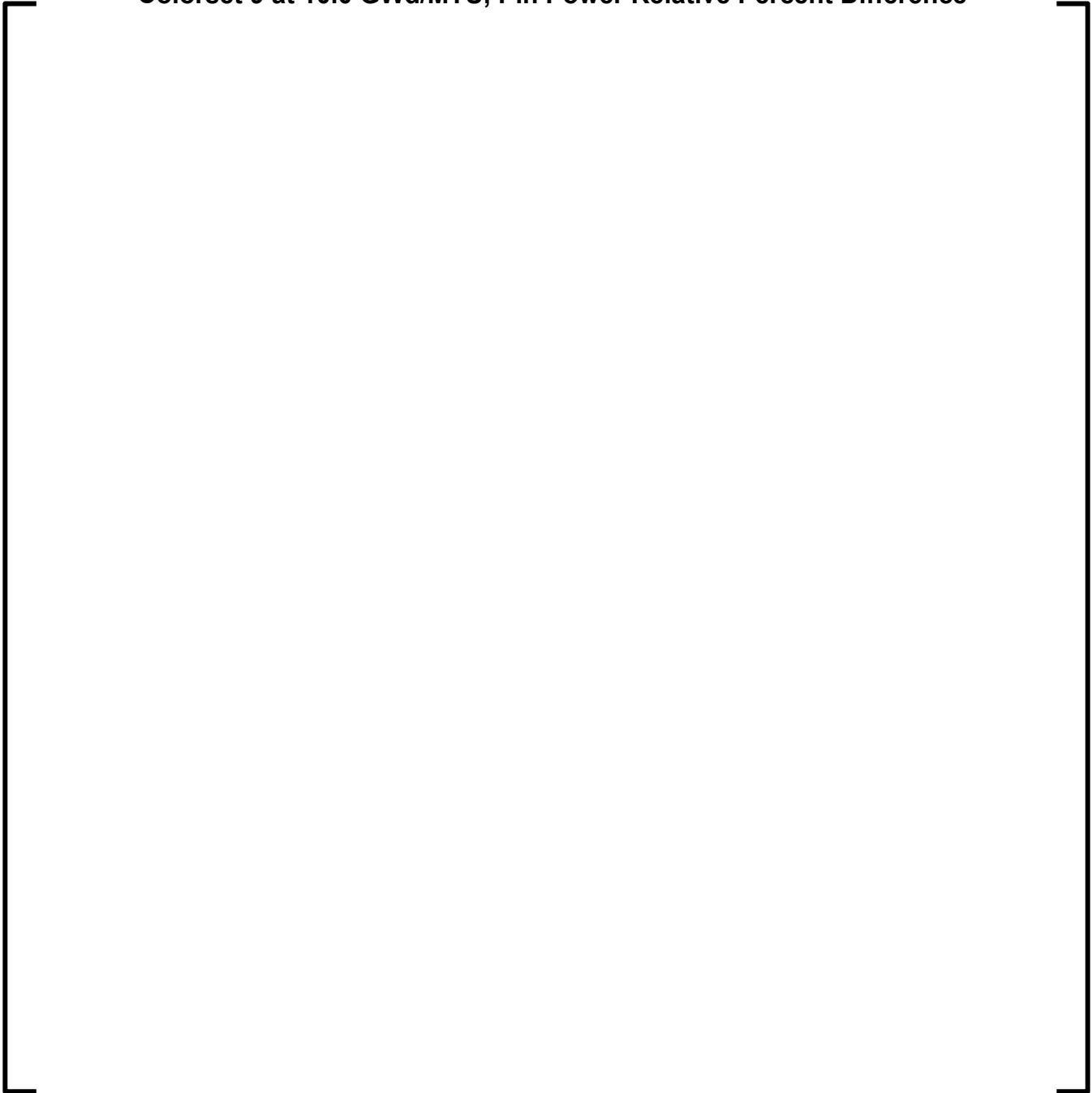


**Figure 8-6**  
**Colorset 9 at 20.0 GWd/MTU, Pin Power Relative Percent Difference**

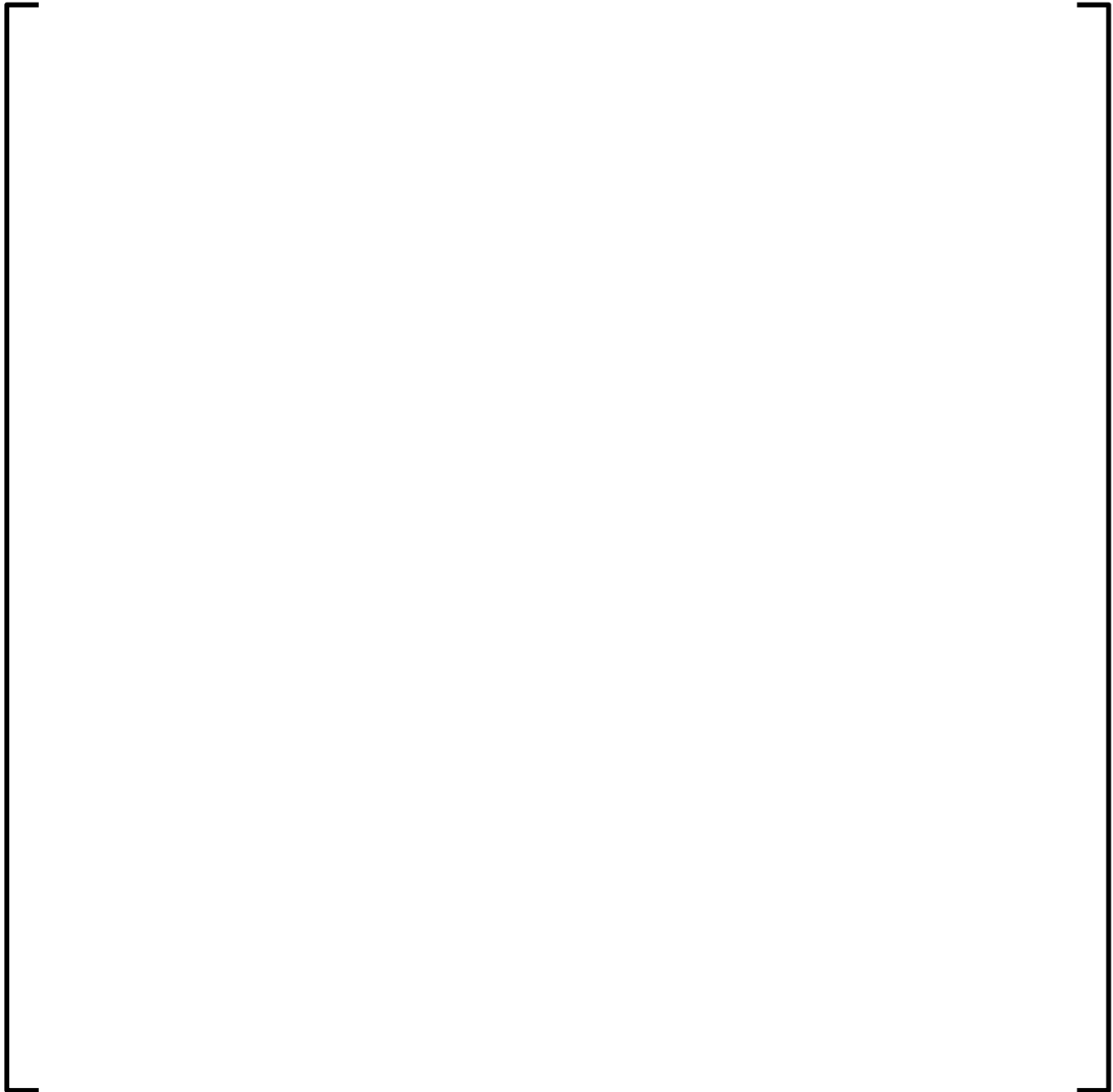


**Figure 8-7**  
**Colorset 24 at 0.1 GWd/MTU, Pin Power Relative Percent Difference**



**Figure 8-8**  
**Colorset 24 at 10 GWd/MTU, Pin Power Relative Percent Difference**



**Figure 8-9**  
**Colorset 24 at 20 GWd/MTU, Pin Power Relative Percent Difference**





### **8.2.3 Local Peaking Uncertainty**

Comparison to the critical experiments provides the error of APOLLO2-A when predicting intra-assembly peaking. The multi-assembly benchmark calculations provide any additional error which occurs due to the flux/power gradients and depletion effects that occur in a PWR core with ARTEMIS™ compared to APOLLO2-A. Frequency plots for the data used from the critical configurations and multi-assembly results are shown in Figure 8-10 and Figure 8-11, respectively. No unusual behavior is observed in these figures. The data for the critical experiments is tested for normality using the Chi<sup>2</sup> test and the hypothesis that the data is normally distributed is not rejected. This test verifies that the assumption of normality used in the statistical removal of the measurement error in Section 8.2.1 is valid. The uncertainties calculated in Sections 8.3 and 8.4 use the local peaking information as inputs to the Normal Uncertainty and Non-Parametric Uncertainty which addresses both normal and non-normal distributions.

**Figure 8-10**  
**Critical Experiments Frequency Distribution versus Normal**  
**Distribution**



**Figure 8-11**  
**Multi-Assembly Problem Frequency Distribution versus Normal**  
**Distribution**



### **8.3      *INFERRED POWER DISTRIBUTION UNCERTAINTY ANALYSES***

The methodology used to derive inferred relative power distribution uncertainties is essentially the same as the MEDIAN methodology used in Reference 8.6-1, Section 12.3. For plant surveillance, peaking information is needed for all locations in the core; however, not all locations in the core have detectors. To obtain the “measured” values in uninstrumented locations, a core simulator and core monitoring algorithms are used to infer the power in uninstrumented locations using both the measured and predicted values. Hence, the inferred uncertainty includes the effects of both calculated and measured powers and results in an uncertainty that can be compared to the measurement system uncertainty. This section presents inferred uncertainty results with ARCADIA<sup>®</sup> for different detector systems supported by AREVA.

For a given parameter of interest, e.g.,  $F_{\Delta H}$  or  $F_Q$ , the methodology estimates the error of the power in uninstrumented assembly locations and is summarized as follows:

1. For a given measured map of signals for the core, the power distribution is constructed with all available operable detectors. Values in the instrumented locations represent the “measured” or reference values.
2. For each detector location with measured axial signals, the signals for this detector location are assumed not to exist and the power distribution is reconstructed without this location. This is similar to setting the signal to inoperable or “failed”. The calculated value in the “failed” location is called the “inferred” value. This step is repeated for each detector location. For a given map with N detector measurements, N relative difference values (inferred minus measured) are generated.
3. This process is repeated for multiple burnup points throughout a cycle, for multiple cycles, and multiple plants where available.
4. The cumulative database forms the basis for the measured global uncertainty that is combined with the local calculational uncertainties to obtain the overall system uncertainty for the measurement system.

The inferred uncertainties for the power distribution peaking factors  $F_{\Delta H}$  and  $F_Q$  are derived for each of 3 different incore measurement systems. Data reduction and statistical treatment techniques are used to derive one-sided 95/95 relative uncertainties. The sampling techniques used in this analysis are:

- All pin powers > [ ] from critical experiments (excludes low powered Gad Pins).
- All pin powers > [ ] from the 4 by 1/4 multi-assembly calculations.
- Relative assembly powers > [ ] for the assembly power distribution uncertainty component for  $F_{\Delta H}$ .
- Relative nodal powers > [ ] in assemblies w/ relative assembly power > [ ] for the nodal power distribution uncertainty component for  $F_Q$ .

The minimum threshold is used because the uncertainty is applied to the core limiting values which are significantly higher than the excluded values.

Note that the application of the MEDIAN reconstruction methodology augments the INPAX-W and INPAX-CE reconstruction methodologies which have been approved in the Reference 8.6-1, Section 12.3 topical report.

### 8.3.1 MEDIAN with Moveable Fission Detector System

The application of the MEDIAN reconstruction methodology is extended for moveable fission detector systems in Supplement 1. The methodology for moveable fission detector systems is essentially the same as the methodology used in Reference 8.6-1, Section 12.3, except that MEDIAN is used for power reconstruction. Plants S1, S2, A, B, E and V1 are used for the uncertainty analysis for this system. Results for each cycle and plant are shown in Table 8-6. For  $F_{\Delta H}$  the mean and standard deviation for the entire sample are [ ], respectively, with [ ].

For  $F_Q$  the mean and standard deviation for the entire sample are [ ], respectively with [ ]. The reconstruction uncertainty is combined with the local uncertainty components from Section 8.2 assuming both normality and non-parametric distributions to obtain estimations of the combined uncertainties. Combined frequency distributions are shown in Figure 8-12 and Figure 8-13 for the global peaking component of the  $F_{\Delta H}$  and  $F_Q$  uncertainties, respectively. No atypical behavior is seen in these figures.

The global uncertainty is combined with the local uncertainty components from Section 8.2 to estimate the Normal Uncertainty and Non-Parametric Uncertainty and is shown in Table 8-7 and Table 8-8 for  $F_{\Delta H}$  and  $F_Q$ , respectively. Both inferred power distribution uncertainty simulations are less than the typical measurement system uncertainty for  $F_{\Delta H}$  and  $F_Q$  of [ ], respectively.

**Table 8-6**  
**Global Statistics for MEDIAN with Moveable Fission Detector**

Plant	Cycle	$F_{\Delta H}$		$F_Q$	
		mean	s.d.	mean	s.d.
S1	12				
S1	13				
S1	14				
S1	12 to 14				
S2	12				
S2	13				
S2	14				
S2	12 to 14				
A	11				
A	12				
A	13				
A	14				
A	11 to 14				
B	1				
E	12				
E	13				
E	14				
E	15				
E	16				
E	17				
E	12 to 17				
V1	18				
V1	19				
V1	20				
V1	21				
V1	22				
V1	18 to 22				
Total	All				

**Table 8-7**  
**F<sub>ΔH</sub> Summary Statistics for MEDIAN with Moveable Fission Detector**

	mean*	Standard deviation	# of points	degrees of freedom	uncertainty %
Criticals Colorsets Radial					
Normal Non-Parametric					

\* For normal analysis, bias is conservatively ignored if mean is > 0.0 (overprediction)

**Table 8-8**  
**Summary Statistics for MEDIAN with Moveable Fission Detector**

	mean*	standard deviation	# of points	degrees of freedom	uncertainty %
Criticals Colorsets Peak					
Normal Non-Parametric					

\* For normal analysis, bias is conservatively ignored if mean is > 0.0 (overprediction)



**Figure 8-12**  
**MEDIAN Moveable Fission Detector Radial Frequency Distribution**  
**versus Normal Distribution**



**Figure 8-13**  
**MEDIAN Moveable Fission Detector Frequency Distribution versus**  
**Normal Distribution**



### 8.3.2 MEDIAN WITH CE Fixed Rhodium Detector System

The MEDIAN reconstruction methodology is applied for Combustion Engineering Plants using fixed rhodium incore detectors. Due to the nature of the fixed incore detector system additional components of the total uncertainties need to be evaluated. The methodology is the same as the methodology used in Reference 8.6-1, Section 12.3, except that MEDIAN is used for power reconstruction. For the  $F_{\Delta H}$  ( $F_R$  is the label of this term for CE plants) and  $F_Q$  uncertainty analyses, these values are equivalent to the 2 equations shown below:

The data from Plant C is used to derive the FSA component of the uncertainty analysis for this system. The results for each cycle are shown in Table 8-9. The mean and standard deviation for the entire sample are [ ], respectively with [ ].

Results for each cycle and plant are shown in Table 8-10. For FR the mean and standard deviation for the entire sample are [ ], respectively with [ ]. For FZ the mean and standard deviation for the entire sample are [ ], respectively with [ ]. Combined frequency distributions for FSA, FR, and FZ are shown in Figure 8-14, Figure 8-15, and Figure 8-16, respectively, for the global peaking component of the  $F_R$  and  $F_Q$  uncertainties. No atypical behavior is seen in these figures.

The global reconstruction uncertainty is combined with the local uncertainty components from Section 8.2 to estimate the Normal Uncertainty and Non-Parametric Uncertainty and is shown in Table 8-11 and Table 8-12 for  $F_R$  and  $F_Q$ , respectively. Both inferred power distribution uncertainty simulations are less than the typical measurement system uncertainty for  $F_R$  and  $F_Q$  of [ ], respectively.

For CE plants with rhodium fixed incore detectors, the MEDIAN reconstruction uncertainty needs to be combined with detector signal conditioning uncertainties (such as detector depletion effects on various uncertainty components) to provide the uncertainty of the monitoring system. This uncertainty will be generated during implementation since it is plant type dependent.

**Table 8-9**  
**FSA Statistics for MEDIAN with CE Fixed Rhodium Detector**

Plant	Cycle	FSA	
		mean	s.d.
C	14		
C	15		
C	16		
C	17		
C	18		
C	14 to 18		

**Table 8-10**  
**FR and FZ Statistics for MEDIAN with CE Fixed Rhodium Detector**

Plant	Cycle	FR		FZ	
		mean	s.d.	mean	s.d.
S1	12				
S1	13				
S1	14				
S1	12 to 14				
S2	12				
S2	13				
S2	14				
S2	12 to 14				
A	11				
A	12				
A	13				
A	14				
A	11 to 14				
Total	All				

**Table 8-11**  
**F<sub>R</sub> Summary Statistics for MEDIAN with CE Fixed Rhodium Detector**

	mean*	standard deviation	# of points	degrees of freedom	uncertainty %
Criticals					
Colorsets					
FSA					
FR					
Normal					
Non-Parametric					

\* For normal analysis, bias is conservatively ignored if mean is > 0.0 (overprediction)

**Table 8-12**  
**F<sub>Q</sub> Summary Statistics for MEDIAN with CE Fixed Rhodium Detector**

	mean*	standard deviation	# of points	degrees of freedom	uncertainty %
Criticals					
Colorsets					
FSA					
FR					
FZ					
Normal					
Non-Parametric					

\* For normal analysis, bias is conservatively ignored if mean is > 0.0 (overprediction)

**Figure 8-14**  
**MEDIAN with CE Fixed Rhodium Detector FSA Frequency**  
**Distribution versus Normal Distribution**



**Figure 8-15**  
**MEDIAN with CE Fixed Rhodium FR Frequency Distribution versus**  
**Normal Distribution**





**Figure 8-16**  
**MEDIAN with CE Fixed Rhodium FZ Frequency Distribution versus**  
**Normal Distribution**



### 8.3.3 MEDIAN AMS Reconstruction Methodology

The MEDIAN AMS (Aeroball Measurement System) is being used in German reactors and is planned to be implemented in U.S. EPR plants. Plants G1 and G2 are used for the uncertainty analysis of this system. Results for each cycle and plant are shown in Table 8-13. For  $F_{\Delta H}$  the mean and standard deviation for the entire sample are

[                      ], respectively with [                      ]. For  $F_Q$  the mean and

standard deviation for the entire sample are [                      ], respectively with

[                      ]. Combined frequency distributions are shown in Figure 8-17 and

Figure 8-18 for the global peaking component of the  $F_{\Delta H}$  and  $F_Q$  uncertainties,

respectively. No atypical behavior is seen in these figures.

The inferred component from above is combined with the local uncertainty components from Section 8.2 to estimate the Normal Uncertainty and Non-Parametric Uncertainty and is shown in Table 8-14 and Table 8-15 for  $F_{\Delta H}$  and  $F_Q$ , respectively. Both inferred power distribution uncertainty simulations are less than the inferred power distribution uncertainty for  $F_{\Delta H}$  and  $F_Q$  of [                      ], respectively.

**Table 8-13**  
**Statistics for MEDIAN AMS Detector System**

Plant	Cycle	$F_{\Delta H}$		$F_Q$	
		mean	s.d.	mean	s.d.
G1	26				
G1	27				
G1	28				
G1	29				
G1	30				
G1	26 to 30				
G2	1				
G2	2				
G2	3				
G2	4				
G2	5				
G2	1 to 5				
Total	All				

**Table 8-14**  
**F<sub>ΔH</sub> Summary Statistics for MEDIAN AMS Detector System**

	mean*	standard deviation	# of points	degrees of freedom	uncertainty %
Criticals Colorsets Radial					
Normal Non-Parametric					

\* For normal analysis, bias is conservatively ignored if mean is > 0.0 (overprediction)

**Table 8-15**  
**F<sub>Q</sub> Summary Statistics for MEDIAN AMS Detector System**

	mean*	standard deviation	# of points	degrees of freedom	uncertainty %
Criticals Colorsets Peak					
Normal Non-Parametric					

\* For normal analysis, bias is conservatively ignored if mean is > 0.0 (overprediction)

**Figure 8-17**  
**MEDIAN AMS Radial Frequency Distribution versus Normal**  
**Distribution**



**Figure 8-18**  
**MEDIAN AMS Peak Frequency Distribution versus Normal**  
**Distribution**



### 8.3.4 MEDIAN WITH B&W Fixed Rhodium Detector System

The MEDIAN reconstruction methodology is applied for B&W plants using fixed rhodium incore detectors. As in Section 8.3.2, due to the nature of the fixed incore detector system additional components of the total uncertainties need to be evaluated. The methodology is an extension of the methodology used for CE Fixed Rhodium detector system, discussed in Section 8.3.2.

The data from Plant T1 is used to derive the FSA component of the uncertainty analysis for this system. The results for each cycle are shown in Table 8-16. The mean and standard deviation for the entire sample are [ ], respectively with

[ ].

Results for each cycle and plant are shown in Table 8-17. For FR the mean and standard deviation for the entire sample are [ ], respectively with [ ]. For FZ the mean and standard deviation for the entire samples are [ ], respectively with [ ]. Combined frequency distributions for FSA, FR, and FZ are shown in Figure 8-19, Figure 8-20, and Figure 8-21, respectively, for the global peaking component of the  $F_{\Delta H}$  and  $F_Q$  uncertainties, respectively. No atypical behavior is seen in these figures.

The global reconstruction uncertainty is combined with the local uncertainty components from Section 8.2 to estimate the Normal Uncertainty and Non-Parametric Uncertainty and is shown in Table 8-18 and Table 8-19 for  $F_{\Delta H}$  and  $F_Q$ , respectively. Both inferred power distribution uncertainty simulations are less than what is reported for CE fixed Rhodium incore system in Section 8.3.2, which is expected since there are more axial detectors in the B&W fixed Rhodium incore system. The values are also lower than the typical Measurement Uncertainty used for B&W reactors which are [ ] for  $F_{\Delta H}$  and  $F_Q$  respectively.

For B&W plants with rhodium fixed incore detectors, the MEDIAN reconstruction uncertainty needs to be combined with detector signal conditioning uncertainties (such as detector depletion effects on various uncertainty components) to provide the uncertainty of the monitoring system. This uncertainty will be generated during implementation since it is plant type dependent.

**Table 8-16**  
**FSA Statistics for MEDIAN with B&W Fixed Rhodium Detector**

Plant	Cycle	FSA	
		mean	s.d.
T1	12		
T1	13		
T1	14		
T1	15		
T1	12 to 15		

**Table 8-17**  
**FR and FZ Statistics for MEDIAN with B&W Fixed Rhodium**  
**Detector**

Plant	Cycle	FR		FZ	
		mean	s.d.	mean	s.d.
S1	12				
S1	13				
S1	14				
S1	12 to 14				
S2	12				
S2	13				
S2	14				
S2	12 to 14				
A	11				
A	12				
A	13				
A	14				
A	11 to 14				
Total	All				

**Table 8-18**  
**F<sub>ΔH</sub> Summary Statistics for MEDIAN with B&W Fixed Rhodium**  
**Detector**

	mean*	standard deviation	# of points	degrees of freedom	uncertainty %
Criticals Colorsets FSA FR					
Normal Non-Parametric					

\* For normal analysis, bias is conservatively ignored if mean is > 0.0 (overprediction)



**Table 8-19**  
**F<sub>Q</sub> Summary Statistics for MEDIAN with B&W Fixed Rhodium**  
**Detector**

	mean*	standard deviation	# of points	degrees of freedom	uncertainty %
Criticals Colorsets FSA FR FZ  Normal Non-Parametric					

\* For normal analysis, bias is conservatively ignored if mean is > 0.0  
(overprediction)

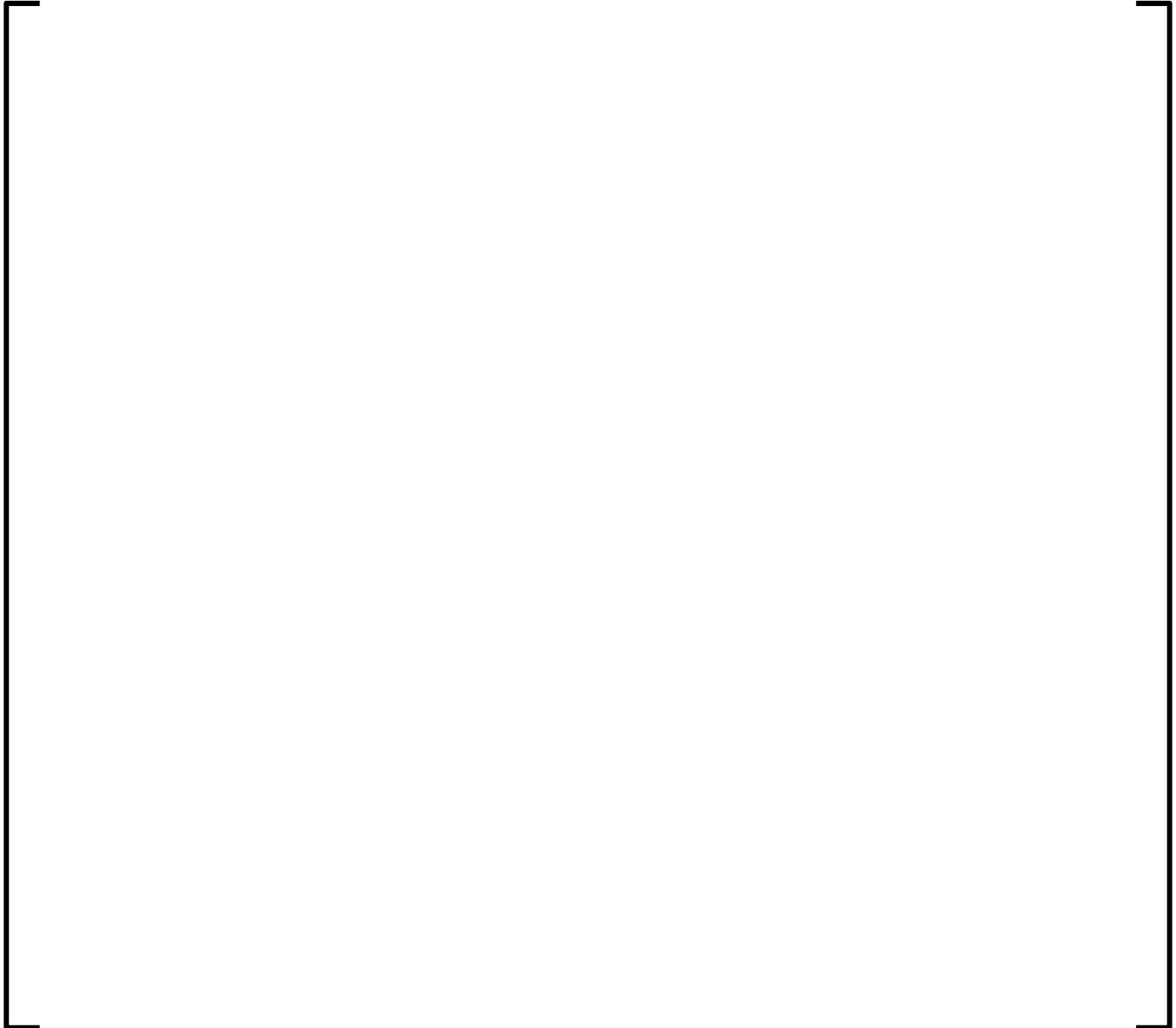
**Figure 8-19**  
**MEDIAN with B&W Fixed Rhodium Detector FSA Frequency**  
**Distribution versus Normal Distribution**



**Figure 8-20**  
**MEDIAN with B&W Fixed Rhodium FR Frequency Distribution versus**  
**Normal Distribution**



**Figure 8-21**  
**MEDIAN with B&W Fixed Rhodium FZ Frequency Distribution versus**  
**Normal Distribution**



## **8.4      *Calculated Power Distribution Uncertainty Analyses (Nuclear Reliability Factors)***

The Nuclear Reliability Factors (NRF) for ARCADIA<sup>®</sup> are determined for the hot pin power ( $F_{\Delta H}$ ) and the hot pellet power ( $F_Q$ ). Each NRF is composed of two error terms, one for the global power prediction and the other for the local prediction (Section 8.2). The ARTEMIS<sup>™</sup> core global power distributions are compared to measured data to determine the global error term. The results of the global comparisons presented in this section are combined with the uncertainties defined in Section 8.2 to derive the NRFs for the ARCADIA<sup>®</sup> system.


All plants modeled in Section 5.0 (Description of Benchmarks) of this Supplement are used to obtain the global calculational uncertainties. This database is representative of the PWR cores supported by AREVA and is sufficient to derive NRFs for ARCADIA<sup>®</sup>. In the following sections, the statistical results (Section 8.4.1) are presented for the global power distributions and the NRFs (Section 8.4.2) are calculated for ARCADIA<sup>®</sup>.

### **8.4.1      Global Results**

The sample mean and standard deviation of the relative difference between predicted and reference can be calculated for each of the comparisons by using the following formulas.



Alternatively, the results could be compiled as an absolute difference as in the following equation.



In general, statistical information is computed for [ ]. A frequency plot is used as a means of examining the database. The measured and predicted reaction rates are compared to estimate the global uncertainty in the powers. For cores with fixed incore detectors, the four detector locations with the highest predicted powers for each of the instrumented assembly locations are used for the peak statistics. The four highest mid-grid values are used to determine the peak values for detector systems that contain a more continuous axial measurement. The statistical summaries for each of the analyzed plant cycles for the global uncertainties are shown in Table 8-20 and Table 8-21 for the assembly radial powers and peak assembly powers, respectively. For the radial powers, the mean and standard deviation for the entire sample are [ ], respectively with [ ].

The mean and standard deviation for the peak power comparisons are [ ], respectively with [ ].

Frequency distributions are shown for the radial and peak power comparisons in Figure 8-22 and Figure 8-23, respectively. No atypical behavior is seen in these distributions.

**Table 8-20**  
**Global Radial Power Statistics**

Plant	Cycle	RADIAL	
		mean	s.d.
S1	12		
S1	13		
S1	14		
S1	12 to 14		
S2	12		
S2	13		
S2	14		
S2	12 to 14		
A	11		
A	12		
A	13		
A	14		
A	11 to 14		
B	1		
T1	12		
T1	13		
T1	14		
T1	15		
T1	12 to 15		
C	14		
C	15		
C	16		
C	17		
C	18		
C	14 to 18		
G1	26		
G1	27		
G1	28		
G1	29		
G1	30		
G1	26 to 30		
G2	1		
G2	2		
G2	3		
G2	4		
G2	5		
G2	1 to 5		
V1	18		
V1	19		
V1	20		
V1	21		
V1	22		
V1	18 to 22		
E	12		
E	13		
E	14		
E	15		
E	16		
E	17		
E	12 to 17		
ALL	ALL		

**Table 8-21**  
**Global Peak Power Statistics**

Plant	Cycle	PEAK	
		mean	s.d.
S1	12		
S1	13		
S1	14		
S1	12 to 14		
S2	12		
S2	13		
S2	14		
S2	12 to 14		
A	11		
A	12		
A	13		
A	14		
A	11 to 14		
B	1		
T1	12		
T1	13		
T1	14		
T1	15		
T1	12 to 15		
C	14		
C	15		
C	16		
C	17		
C	18		
C	14 to 18		
G1	26		
G1	27		
G1	28		
G1	29		
G1	30		
G1	26 to 30		
G2	1		
G2	2		
G2	3		
G2	4		
G2	5		
G2	1 to 5		
V1	18		
V1	19		
V1	20		
V1	21		
V1	22		
V1	18 to 22		
E	12		
E	13		
E	14		
E	15		
E	16		
E	17		
E	12 to 17		
ALL	ALL		



**Figure 8-22**  
**All Plants Radial Power Frequency Distribution versus Normal**  
**Distribution**



**Figure 8-23**  
**All Plants Peak Power Frequency Distribution versus Normal**  
**Distribution**



### 8.4.2 NRF Determination

The NRF is calculated with both normal assumptions and with non-parametric methods. The most conservative of the two methods is used as the uncertainty. The uncertainty is defined as a one-sided 95/95 tolerance limit.

The NRFs for  $F_{\Delta H}$  and  $F_Q$  are determined from three components representing the global and local peaking variations. The two local components are described in Section 8.2. The reference value for the global power distributions is the measured data. A Monte Carlo method is utilized to combine the uncertainties. The same non-parametric tolerance method applied in Reference 8.6-1, Section 12.4.2 is used with the Monte Carlo simulation to calculate the NRF.

The Monte Carlo simulation randomly samples the data from each of the three components of the error terms for both the predicted value and reference value. These three components are the global assembly values and the two local components. The three predicted values are multiplied together to simulate an actual ARCADIA® calculation (predicted). Similarly, the resultant reference value is obtained and divided into the predicted value. The 95/95 tolerance limit of the resulting ratio is then obtained based on the order statistics. In this process, the Satterthwaite's approximation is used to determine the equivalent degrees of freedom for the number of samples to be used in the Monte Carlo simulation. The resultant tolerance limit is then inverted to give the NRF.

Calculated uncertainties are combined with the local uncertainty components from Section 8.2 to estimate the Normal Uncertainty and Non-Parametric Uncertainty and are shown in Table 8-22 and Table 8-23 for  $F_{\Delta H}$  and  $F_Q$ , respectively. The largest NRFs for either method for  $F_{\Delta H}$  and  $F_Q$  are [ ], respectively. These values are less than the values of [ ] for  $F_{\Delta H}$  and  $F_Q$  respectively, calculated in Reference 8.6-1 Section 12.4.2.

**Table 8-22**  
**Summary  $F_{\Delta H}$  Statistics**

	mean*	standard deviation	# of points	degrees of freedom	uncertainty %
Criticals Colorsets Radial  Normal Non-Parametric					

\* For normal analysis, bias is conservatively ignored if mean is > 0.0 (overprediction)

**Table 8-23**  
**Summary  $F_Q$  Statistics**

	mean*	standard deviation	# of points	degrees of freedom	uncertainty %
Criticals Colorsets Peak  Normal Non-Parametric					

\* For normal analysis, bias is conservatively ignored if mean is > 0.0 (overprediction)

## 8.5 *Power Distribution Uncertainty Summary*

The uncertainties for ARCADIA<sup>®</sup> are calculated for both the inferred power distribution uncertainties and calculational uncertainties and are summarized in Table 8-24 with both the ARCADIA<sup>®</sup> calculated values and the current licensing values. As shown in Table 8-24, all calculated values for ARCADIA<sup>®</sup> are less than the current licensing values used for the criteria.

**Table 8-24**  
**Power Distribution Uncertainty Summary**

Type of Uncertainty	$F_{\Delta H}$ ( $F_R$ for CE)		$F_Q$	
	Estimated*	Criteria	Estimated*	Criteria
Inferred Moveable fission				
Inferred CE Rhodium				
Inferred B&W Rhodium				
Inferred AMS				
Calculational				

\*Uncertainties have been rounded up to the digits displayed.

## 8.6 *References*

- 8.6-1 ANP-10297P-A, Revision 0, The ARCADIA<sup>®</sup> Reactor Analysis System for PWRs Methodology Description and Benchmarking Results Topical Report, February 2013.

## **9.0 SAFETY PARAMETER UNCERTAINTIES**

### **9.1 *Introduction***

Total rod worth and Isothermal Temperature Coefficients (ITC) are typically measured and calculated as part of reactor startup physics testing. Comparisons of these parameters are included in the validation of neutronics models. In Section 5.2, these data were provided for nearly 50 cycles as part of the benchmarking of core calculations.

Total rod worth and ITC values are also used in safety analyses. Uncertainties are applied to these parameters to assure that a conservative analysis is performed.

This supplement includes a statistical analysis of the total rod worth and ITC comparisons to generate uncertainty values for these parameters that can be applied when evaluating cores during the safety analyses using the ARCADIA<sup>®</sup> package. Data provided in Section 5.2 for the core benchmarks as well as data from an additional 14 cycles are used in the analysis. The additional cycles are from Plant A (Cycles 15-18), Plant S1 (Cycles 15-20) and Plant S2 (Cycles 15-20). Total rod worth and ITC differences are shown in Table 9-1 for the additional cycles.

The statistical method approach for both the total rod worth and ITC uncertainties was the same. Data from eight different plants were used. For one plant, there was only one data point for each parameter (Plant B, Cycle 1). This point was combined with a similar plant type for statistical purposes (Plant A). Since Plants S1 and S2 are the same plant type/fuel type, these data were also combined as one group.

The mean ( $\overline{\mu_i}$ ) and variance ( $s_i^2$ ) of the data were calculated for plant type  $i$  with  $n_i$

data points. [

]

Use of the weighting function in determining the combined mean ( $\mu$ ) captures the effects due to different plant types and amount of data available for each plant. The combined mean ( $\mu$ ) and variance ( $s^2$ ) for all sets of data is calculated as:

where,

$(n_i - 1)$  is the degrees of freedom (DOF) for the plant type.

For each parameter, an upper and lower bound for a 95/95 uncertainty is calculated as:

The parameter uncertainty value is determined by considering both upper and lower bounds calculated above.

The above method assumes that the data is normally distributed. The D'Agostinio (D') test as discussed in Reference 9.4-2, Section 11.10 is used to test the normality of the data.

**Table 9-1**  
**Additional Data for Total Rod Worth and ITC used in Determining**  
**Safety Parameter Uncertainties**

--	--



## 9.2 *Total Rod Worth*

The data needed to determine the total rod worth uncertainty is summarized in Table 9-2. The D' test was used to test the normality of the total rod worth data. The statistics associated with this test are found in Table 9-3.

A histogram showing a visual representation of normality test is shown in Figure 9-1. Using the D' test, the assumption of normality for the total rod worth data is not rejected.

Using the methodology in Section 9.1, the uncertainty associated with the total rod worth is [      ].

**Table 9-2**  
**Total Rod Worth Uncertainty Statistics**

--	--

**Table 9-3**  
**D' Normality Test Statistics for Total Rod Worth Data**



**Figure 9-1**  
**Total Rod Worth Difference Frequency Distribution versus Normal**  
**Distribution**



### **9.3      *Isothermal Temperature Coefficient***

Data needed to determine the ITC uncertainty is summarized in Table 9-4. The D' test was used to test the normality of the ITC data. The statistics associated with this test are found in Table 9-5. A histogram showing a visual representation of normality test is shown in Figure 9-2. Using the D' test, the assumption of normality for ITC data is not rejected.

Using the methodology in Section 9.1, the uncertainty associated with the ITC is

[            ].

**Table 9-4**  
**ITC Uncertainty Statistics**

--	--

**Table 9-5**  
**D' Normality Test Statistics for ITC Data**



**Figure 9-2**  
**ITC Difference Frequency Distribution versus Normal Distribution**



**9.4      *References***

- 9.4-1   P.G. Hoel, S. C. Port, and C. J. Stone, "Introduction to Statistical Theory", Houghton Mifflin Company, 1971.
- 9.4-2   D. Lurie, L. Abramson, and J. Vail, "Applying Statistics", NUREG-1475, Revision 1, March 2011.

## 10.0 SUMMARY AND QUALIFICATION METHOD

This section summarizes the results presented in this document and provides the process that AREVA will use when incorporating future changes into the ARCADIA<sup>®</sup> code system. The data presented in this report provides a qualification base for the ARCADIA<sup>®</sup> code system. Comparisons to results from Reference 10.6-1 show that the modifications made to the ARCADIA<sup>®</sup> code system subsequent to the NRC approval of Reference 10.6-1 provide results that are within the established criteria without introducing biases and provides validation of the change process presented in Section 13.4 of Reference 10.6-1.

Future modifications to the equations, algorithms and methods to the ARCADIA<sup>®</sup> code system as defined in Reference 10.6-1 and Sections 2.0 and 3.0 of this document can be used for licensing applications as long as it has been shown that the criteria specified in Table 10-2 remain valid.

The range of applicability for the application of the ARCADIA<sup>®</sup> code system is provided below along with a change process that ensures that the code system remains valid over the specified range when modifications are incorporated. A summary is provided in Section 10.5.

### 10.1 *Range of Applicability*

The chosen benchmarks in this topical include a wide range of plant designs, fuel types and operating histories. Benchmarks have been provided for both static and transient conditions in order to qualify ARCADIA<sup>®</sup> for licensing applications. The benchmarks include the following:

- critical k and fission rate measurements from critical experiments,
- measured isotopic concentrations from spent fuel rods,
- measured parameters from operating commercial reactors at startup and during cycle operations,

- measured parameters from cold conditions,
- reference analytical static and kinetic solutions, and
- measured power responses from dropped rod tests and rod ejection tests.

The benchmarks provide evidence that ARCADIA® is capable of modeling diverse plant types, lattice types and operating conditions. Plant benchmarks include comparisons to Westinghouse, Combustion Engineering, Babcock and Wilcox, Siemens and Framatome designed reactors. The benchmarks include uncertainty verification for plants that use moveable incore fission detectors, fixed Rhodium SPNDs and Aeroball incore detectors. The breadth of the ARCADIA® validation suite is demonstrated in Table 10-1. From this table the diversity and extensive nature of the validation suite are shown. The typical plant types, plant sizes, and lattice types are considered. Typical burnable absorber types and control rod absorber types are also considered. Several cycles use combinations of burnable absorber types which are also shown in Table 10-1. This validation establishes the ability to predict core designs with enrichments up to 5.0 wt% <sup>235</sup>U and ERU enrichments up to 4.01 wt% <sup>235</sup>U and for cycle lengths ranging from annual cycles to 24 month cycles.

**Table 10-1**  
**Operating Cycle Benchmarks**

Plant Type	Core Size	Fuel	# of Cycles	Lattice	Burnable Absorbers	Control Rod Absorbers	Detectors
W	157	UO <sub>2</sub>	14	17x17	Pyrex, WABA, IFBA, Gd	Hf, AIC	TIP
W	157	UO <sub>2</sub>	1	17x17	Pyrex + Gd	AIC	TIP
CE	217	UO <sub>2</sub>	9	14x14	Gd	B <sub>4</sub> C	SPND
S	177	UO <sub>2</sub>	5	15x15	Gd	AIC	AMS
S	193	UO <sub>2</sub>	5	18x18	Gd	AIC	AMS
W	193	UO <sub>2</sub>	3	17x17	B <sub>4</sub> C, B <sub>4</sub> C + Gd	AIC	TIP
W	193	UO <sub>2</sub>	3	17x17	B <sub>4</sub> C, B <sub>4</sub> C + Gd	AIC	TIP
B&W	177	UO <sub>2</sub>	7	15x15	B <sub>4</sub> C, B <sub>4</sub> C + Gd, Gd	AIC	SPND
W	157	UO <sub>2</sub>	5	15x15	Gd (up to 10 wt%)	AIC	TIP
W	157	ERU	6	17x17	None	AIC	TIP

Total Number of Cycles      58



The comparisons provided in this report demonstrate the flexibility of ARCADIA<sup>®</sup> for a diverse set of plants. Therefore, ARCADIA<sup>®</sup> is applicable to all PWR plant types, square lattice designs, burnable absorbers and control rod types.

## **10.2      *Methods and Qualifications***

Criteria established to qualify the ARCADIA<sup>®</sup> code system for use in reactor calculations are provided in Table 10-2. These criteria are consistent with ANSI/ANS Reload Startup Physics standard (Reference 10.6-2).

The qualification method for the ARCADIA<sup>®</sup> code system remains the same as that presented in Section 13.2 of Reference 10.6-1. The neutronics code qualification is based on the ability of the code system to predict several key neutronics parameters. The key parameters are critical boron or critical k-effective from cold to hot conditions, individual bank/rod worths, total bank worths, isothermal temperature coefficients, and power uncertainties. These predicted parameters will be compared to measured results and the differences will be compared to the established criteria. For the comparisons performed in this document, the acceptance criteria presented in Table 13.2-1 of Reference 10.6-1 are used in order to remain consistent with the data presented in that report.

For application of the ARCADIA<sup>®</sup> code system, the criteria presented in Table 10-2 will be used. These criteria are consistent with ANSI/ANS Reload Startup Physics standard (Reference 10.6-2) with the exception of the total control rod worth and the ITC. Total control rod worth and ITC uncertainties were developed in Section 9.0 of this supplement.

**Table 10-2**  
**Methods Qualification Criteria**

Parameter	Criteria
Core Physics Testing	
ARO, HZP Critical Boron Concentration	±50 ppm or ±500 pcm equivalent
Control Rod Worth	
Individual group or specified group	±15% <sup>1</sup> or ±100 pcm, whichever is greater
Reference Bank (rod swap)	±10% <sup>1</sup>
Total Worth (95/95 limit) <sup>2</sup>	[      ]
Isothermal Temperature Coefficient (95/95 limit) <sup>3</sup>	[                      ]
Core Follow Measurements	
HFP Critical Boron Concentration	±50 ppm or ±500 pcm equivalent
Assembly Average Power Distribution	Maximum RMS <sup>4</sup> * 100 < 5
Axial Average Power Distribution	Maximum RMS <sup>4</sup> * 100 < 5

1) Percent difference is defined as (predicted – measured)/measured \* 100

2) Limit defined in Section 9.2

3) Limit defined in Section 9.3

4) RMS is defined as

$$\sqrt{\sum_{i=1}^N \frac{\Delta RPD_i^2}{N}}$$

Table 10-1 demonstrates the extensive range of the ARCADIA® code system validation suite. The ARCADIA® code system is applicable to all PWR types with any square lattice geometry, burnable absorber or control rod types. Benchmarks can be performed to show that the criteria specified in Table 10-2 are satisfied demonstrating that ARCADIA® is qualified for use in performing reactor analyses. This extension process applies only to incore detector systems listed in Table 10-1. A different detector system requires a new uncertainty analysis that must be reviewed and approved by the NRC.

APOLLO2-A was validated against critical experiments for both reactivity and fission rates. Calculated results were consistent with measured values. With respect to spent fuel isotopics, APOLLO2-A shows the ability to accurately predict changes in isotopic concentrations for varying irradiation times. The reactivity, fission rate and isotopic comparisons show the flexibility of APOLLO2-A in modeling various lattice types, fuel materials, control rod materials and burnable absorbers. APOLLO2-A can be used to model any PWR square lattice with any control rod or burnable absorber. It is also capable of predicting fuel isotopics for any typical PWR fuel rod.

### **10.3      *Plant Application***

AREVA will continue to monitor its methods with respect to current cycle designs for licensing applications. AREVA will evaluate at least three full cycles of data against the Table 10-2 criteria prior to first use of ARCADIA<sup>®</sup> at a plant. This includes verification of the power measurement uncertainties and/or calculational uncertainties by using the appropriate method presented in either Section 12 of Reference 10.6-1 or Section 8.0 of this document.

Continuous comparisons will be made to measured plant data to ensure that there is no drift in the ARCADIA<sup>®</sup> models used in plant calculations. Validity of the uncertainty analysis will be checked by ensuring the RMS for the axial and radial power distribution comparisons remain within the criteria in Table 10-2.

### **10.4      *Code Modification Change Process***

There are many situations that might require a change to codes or libraries. Some of the reasons include:

- Improved computer capabilities allowing first principle models rather than empirical models.
- Changes to models to handle unique features of a plant
- A change to the number of energy groups to analyze for a particular phenomena

- Input parameter changes may be required to account for a change to another approved code used in generation of the inputs
- Incorporate an improvement in the input or output data structure (these types of changes have no impact on the numerics of the codes and should not require NRC review).
- Changes to or use of new data libraries (e.g., cross section library)
- Improvements in pin power dehomogenization process to provide more consistency between the nodal and lattice code
- Incorporation of new history effects to improve behavior with exposure

Anytime code modifications are made an internal change process is followed. This change process includes documentation of the changes, execution of test cases which include regression testing, and updated documentation for theory and users manuals. Additional cases will be run that include a subset of the original validation suite presented in Table 10-1. This test suite will be sufficient to capture the effect of the changes made and will include documentation showing adherence to the acceptance criteria in Table 10-2. This analysis will also show that power distributions remain within the uncertainties of Section 8.0. A summary report will be generated annually documenting all changes made within the year and provided to the NRC.

The change process ensures that there is no loss of quality in comparisons to criteria and examines the changes with regards to the limitations specified in the NRC's Safety Evaluation Report. If changes result in improvements outside of SER limitations, then one of the following actions will be taken:

1. No credit taken for change
2. Change documented in a new supplement to ANP-10297P-A for approval
3. Include change into a License Amendment Request for site specific approval
4. Change documented and presented to the NRC for acceptance under the change process defined in this supplement.

## 10.5 **Summary**

ARCADIA<sup>®</sup> is an integrated code package that includes a neutronic spectral/lattice code APOLLO2-A and a core simulator, ARTEMIS<sup>™</sup> that has direct inline coupling with the state-of-the-art thermal hydraulics code COBRA-FLX<sup>™</sup> and an explicit fuel rod module.

The benchmarks of APOLLO2-A to measurements demonstrate that the code is capable of producing accurate results for pin powers, critical eigenvalues, and spent fuels isotopic concentrations. ARTEMIS<sup>™</sup> comparisons to measured rod worths, critical boron concentrations, isothermal temperature coefficients and assembly power distributions were made for several operating PWRs. The key ARCADIA<sup>®</sup> results from these comparisons are summarized in Table 10-3 and are an example of meeting the qualification method criteria outlined in this section. In addition, the validation of the coupling with the Thermal Hydraulic Module (COBRA-FLX<sup>™</sup>) and the Fuel Rod Module remains valid as shown with the comparisons to plant operating data and the comparisons in the transient benchmarks with ARTEMIS<sup>™</sup>.

Results presented in Table 10-3 demonstrate that the ARCADIA<sup>®</sup> code system is an accurate tool for predicting both local and global core neutronic static and kinetic behavior. ARCADIA<sup>®</sup> can be used to perform neutronic calculations for the reload designs of pressurized water reactors, to analyze spent fuel isotopics, reactivity and power distributions, perform transient calculations and to make startup predictions.

**Table 10-3**  
**Summary of Results**

Parameter - (% relative difference or difference between predicted and measured values)	Criteria	Results
HFP Critical k-effective	Within $\pm 50$ ppm or $\pm 500$ pcm	Maximum absolute difference $< 50$ ppm or $< 500$ pcm equivalent
HZP Critical k-effective	Within $\pm 50$ ppm or $\pm 500$ pcm	Maximum absolute difference of [       ]
Single Bank Worth, %	With $\pm 15\%$ or $\pm 100$ pcm	Maximum absolute difference of [       ]
Total Bank Worth, %	$\pm 10\%$ <sup>b</sup>	Maximum absolute difference of [       ]
HZP Isothermal Temperature Coefficient, pcm/°F	$\pm 2$ pcm/°F <sup>b</sup>	Maximum absolute difference of [       ]
F <sub>ΔH</sub> Calculation Uncertainty	$< 3.8\%$	
F <sub>Q</sub> Calculation Uncertainty	$< 4.8\%$	
Inferred Power Distribution Uncertainty F <sub>ΔH</sub> F <sub>Q</sub>	Westinghouse  F <sub>ΔH</sub> $\leq 4\%$ F <sub>Q</sub> $\leq 5\%$	
Inferred Power Distribution Uncertainty F <sub>R</sub> F <sub>Q</sub>	CE  F <sub>ΔH</sub> $\leq 6\%$ F <sub>Q</sub> $\leq 7\%$	
Inferred Power Distribution Uncertainty F <sub>R</sub> F <sub>Q</sub>	B&W  F <sub>ΔH</sub> $\leq 5\%$ F <sub>Q</sub> $\leq 7.5\%$	
Inferred Power Distribution Uncertainty F <sub>ΔH</sub> F <sub>Q</sub>	AMS  F <sub>ΔH</sub> $\leq 4.1\%$ F <sub>Q</sub> $\leq 5.1\%$	

## **10.6      *References***

- 10.6-1 ANP-10297P-A, Revision 0, The ARCADIA<sup>®</sup> Reactor Analysis System for PWRs Methodology Description and Benchmarking Results Topical Report, February 2013.
- 10.6-2 ANSI/ANS-19.6.1-2011, Reload Startup Physics Tests for Pressurized Water Reactors, January 13, 2011.

## **11.0 QA PROGRAM**

This supplement and its supporting analyses were generated in accordance with AREVA's 10 CFR 50 Appendix B Quality Assurance program documented in AREVA's Fuel Section Management Manual (FMM), current revision.



## APPENDIX A

**Table A 5.2.1-1**  
**Plant A Hot Zero Power All Rods Out Critical Boron Concentrations**  
**for Cycles 1-14**

--	--

**Table A 5.2.1-2**  
**Plant A Cycle 1 Hot Zero Power Individual Rod Bank Worth**

--	--

**Table A 5.2.1-3**  
**Plant A Cycle 2 Hot Zero Power Individual Rod Bank Worth**

--	--

**Table A 5.2.1-4**  
**Plant A Cycle 3 Hot Zero Power Individual Rod Bank Worth**

--	--

**Table A 5.2.1-5**  
**Plant A Cycle 4 Hot Zero Power Individual Rod Bank Worth**

--	--

**Table A 5.2.1-6**  
**Plant A Cycle 5 Hot Zero Power Individual Rod Bank Worth**

--	--

**Table A 5.2.1-7**  
**Plant A Cycle 6 Hot Zero Power Individual Rod Bank Worth**

--	--

**Table A 5.2.1-8**  
**Plant A Cycle 7 Hot Zero Power Individual Rod Bank Worth**

--	--



**Table A 5.2.1-9**  
**Plant A Cycle 8 Hot Zero Power Individual Rod Bank Worth**

--	--

**Table A 5.2.1-10**  
**Plant A Cycle 9 Hot Zero Power Individual Rod Bank Worth**

--	--

**Table A 5.2.1-11**  
**Plant A Cycle 10 Hot Zero Power Individual Rod Bank Worth**

--	--

**Table A 5.2.1-12**  
**Plant A Cycle 11 Hot Zero Power Individual Rod Bank Worth**

--	--

**Table A 5.2.1-13**  
**Plant A Cycle 12 Hot Zero Power Individual Rod Bank Worth**

--	--

**Table A 5.2.1-14**  
**Plant A Cycle 13 Hot Zero Power Individual Rod Bank Worth**

[illegible]

**Table A 5.2.1-15**  
**Plant A Cycle 14 Hot Zero Power Individual Rod Bank Worth**

--	--

**Table A 5.2.1-16**  
**Plant A Summary of Total Bank Worths**

--	--



**Table A 5.2.1-17**  
**Plant A Hot Zero Power All Rods Out Isothermal Temperature**  
**Coefficient for Cycles 1-14**

--	--

**Figure A 5.3.1-1**  
**Plant A Cycle 1 Critical Boron Concentration vs. Burnup**



**Figure A 5.3.1-2**  
**Plant A Cycle 2 Critical Boron Concentration vs. Burnup**



**Figure A 5.3.1-3**  
**Plant A Cycle 3 Critical Boron Concentration vs. Burnup**



**Figure A 5.3.1-4**  
**Plant A Cycle 4 Critical Boron Concentration vs. Burnup**



**Figure A 5.3.1-5**  
**Plant A Cycle 5 Critical Boron Concentration vs. Burnup**



**Figure A 5.3.1-6**  
**Plant A Cycle 6 Critical Boron Concentration vs. Burnup**

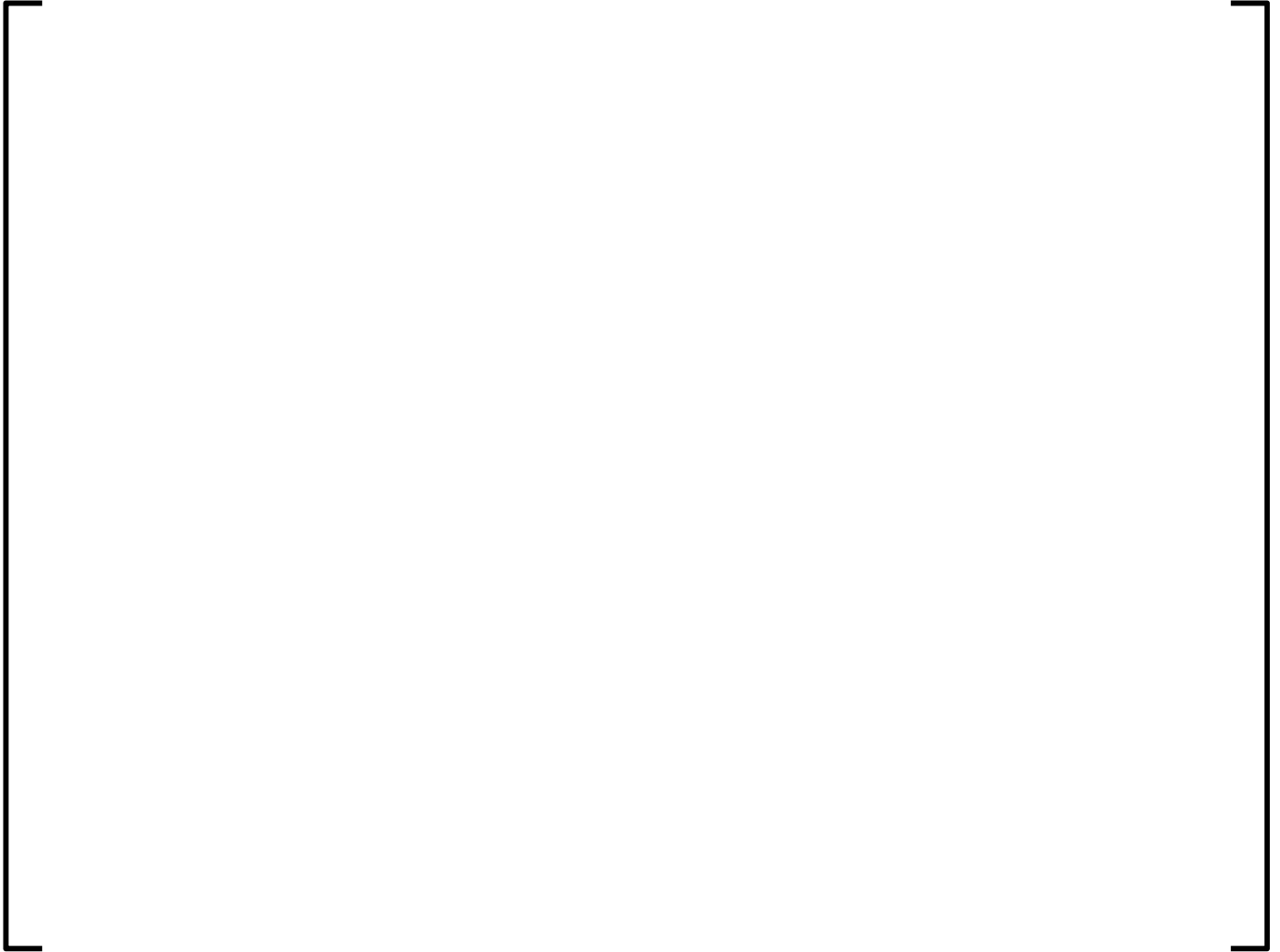


**Figure A 5.3.1-7**  
**Plant A Cycle 7 Critical Boron Concentration vs. Burnup**





**Figure A 5.3.1-8**  
**Plant A Cycle 8 Critical Boron Concentration vs. Burnup**



**Figure A 5.3.1-9**  
**Plant A Cycle 9 Critical Boron Concentration vs. Burnup**



**Figure A 5.3.1-10**  
**Plant A Cycle 10 Critical Boron Concentration vs. Burnup**



**Figure A 5.3.1-11**  
**Plant A Cycle 11 Critical Boron Concentration vs. Burnup**



**Figure A 5.3.1-12**  
**Plant A Cycle 12 Critical Boron Concentration vs. Burnup**



**Figure A 5.3.1-13**  
**Plant A Cycle 13 Critical Boron Concentration vs. Burnup**



**Figure A 5.3.1-14**  
**Plant A Cycle 14 Critical Boron Concentration vs. Burnup**

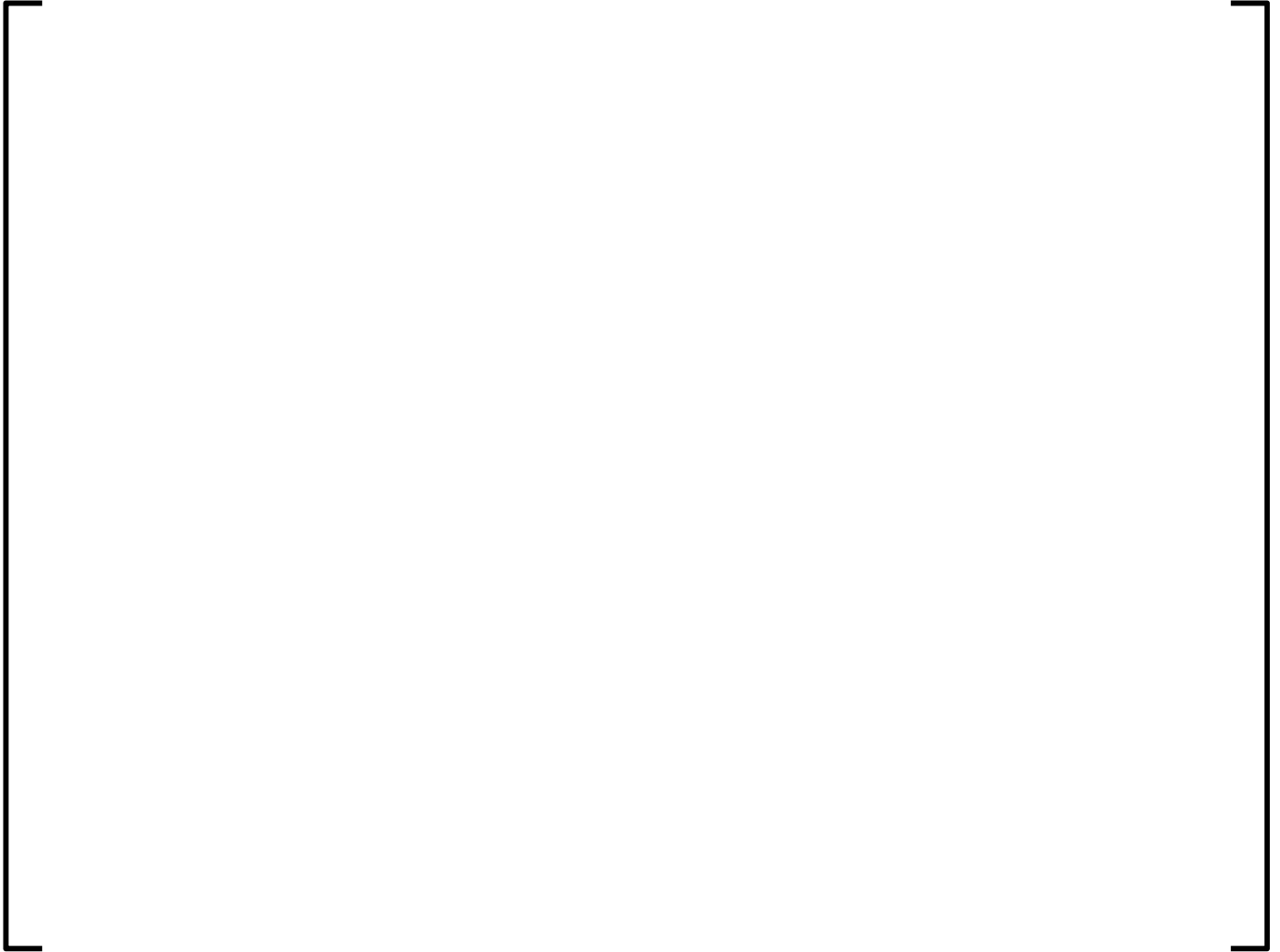


**Figure A 5.3.1-15**  
**Plant A Cycles 1-14 Boron Differences**





**Figure A 5.3.1-16**  
**Plant A BOC 11 Assembly Average Radial Power Distribution**

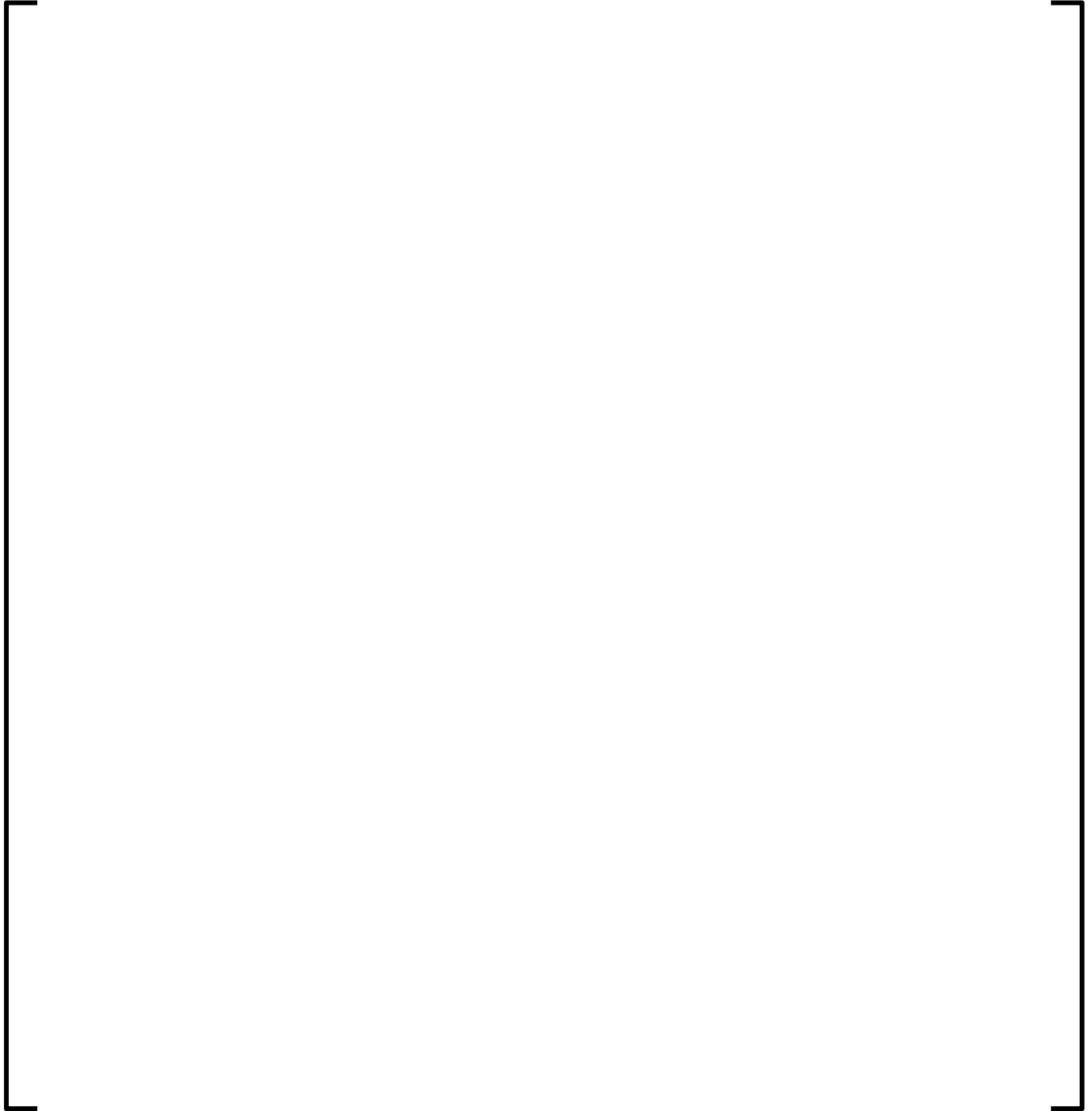


**Figure A 5.3.1-17**  
**Plant A MOC 11 Assembly Average Radial Power Distribution**

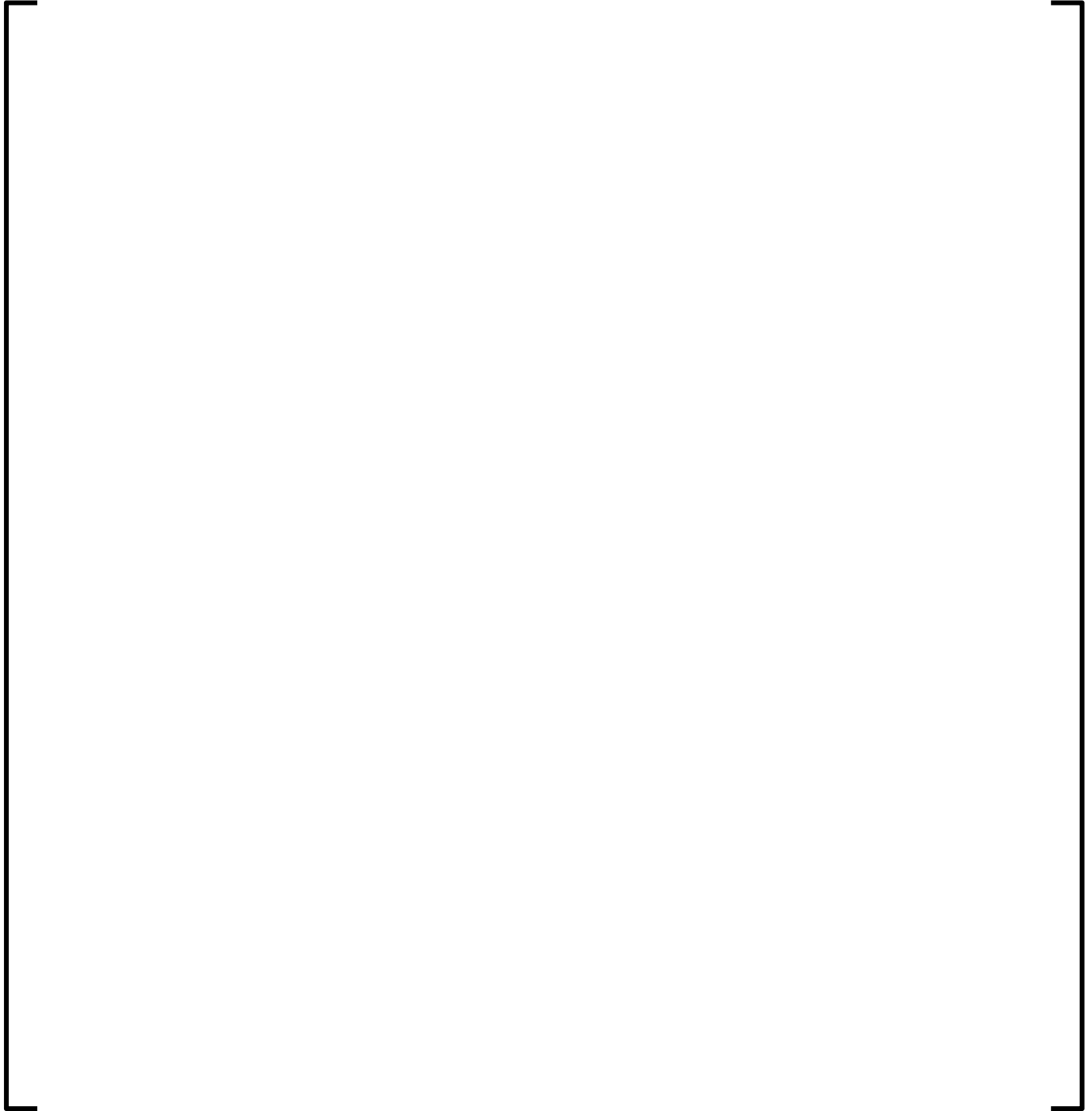


**Figure A 5.3.1-18**  
**Plant A EOC 11 Assembly Average Radial Power Distribution**

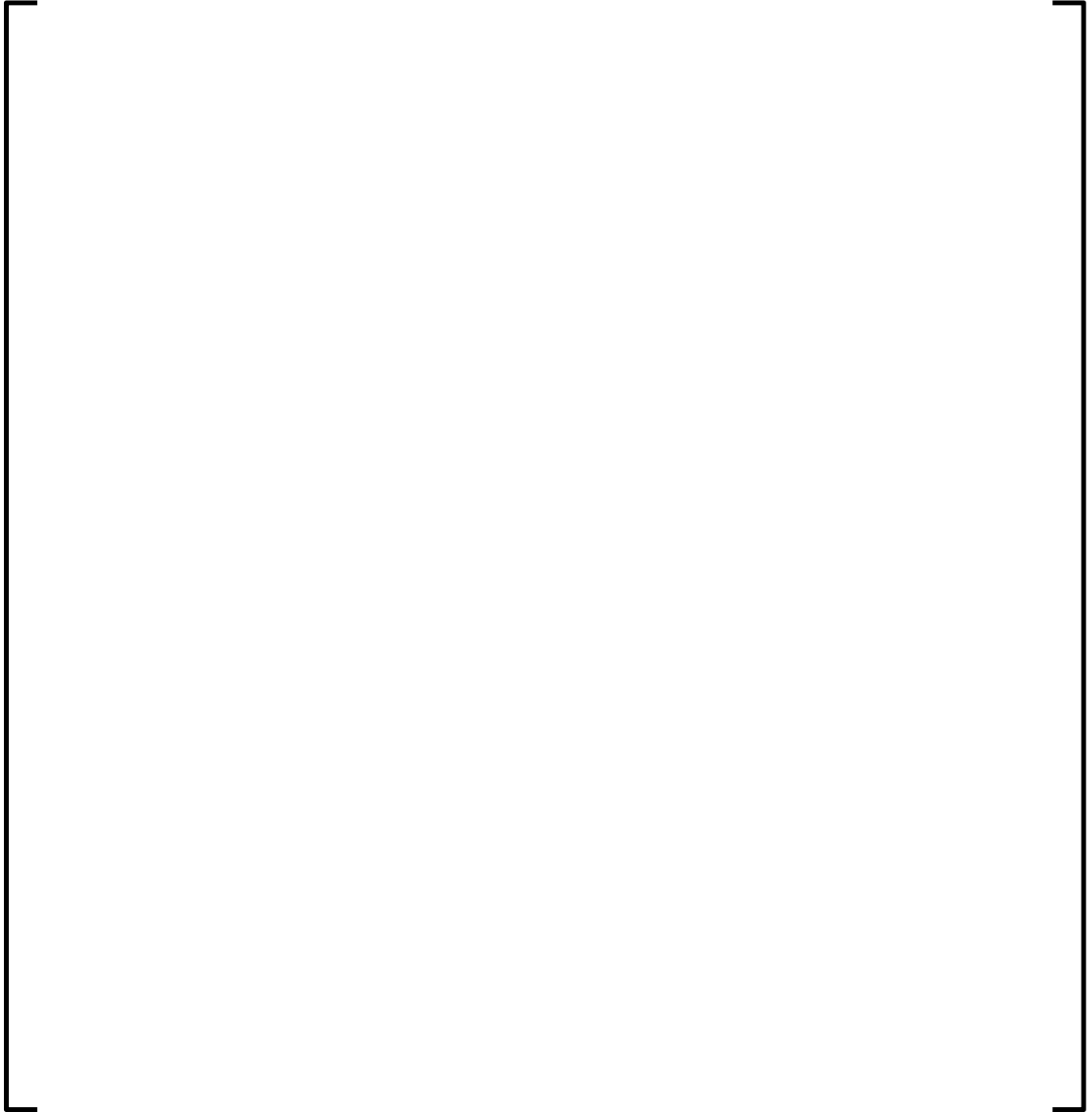


**Figure A 5.3.1-19**  
**Plant A BOC 12 Assembly Average Radial Power Distribution**

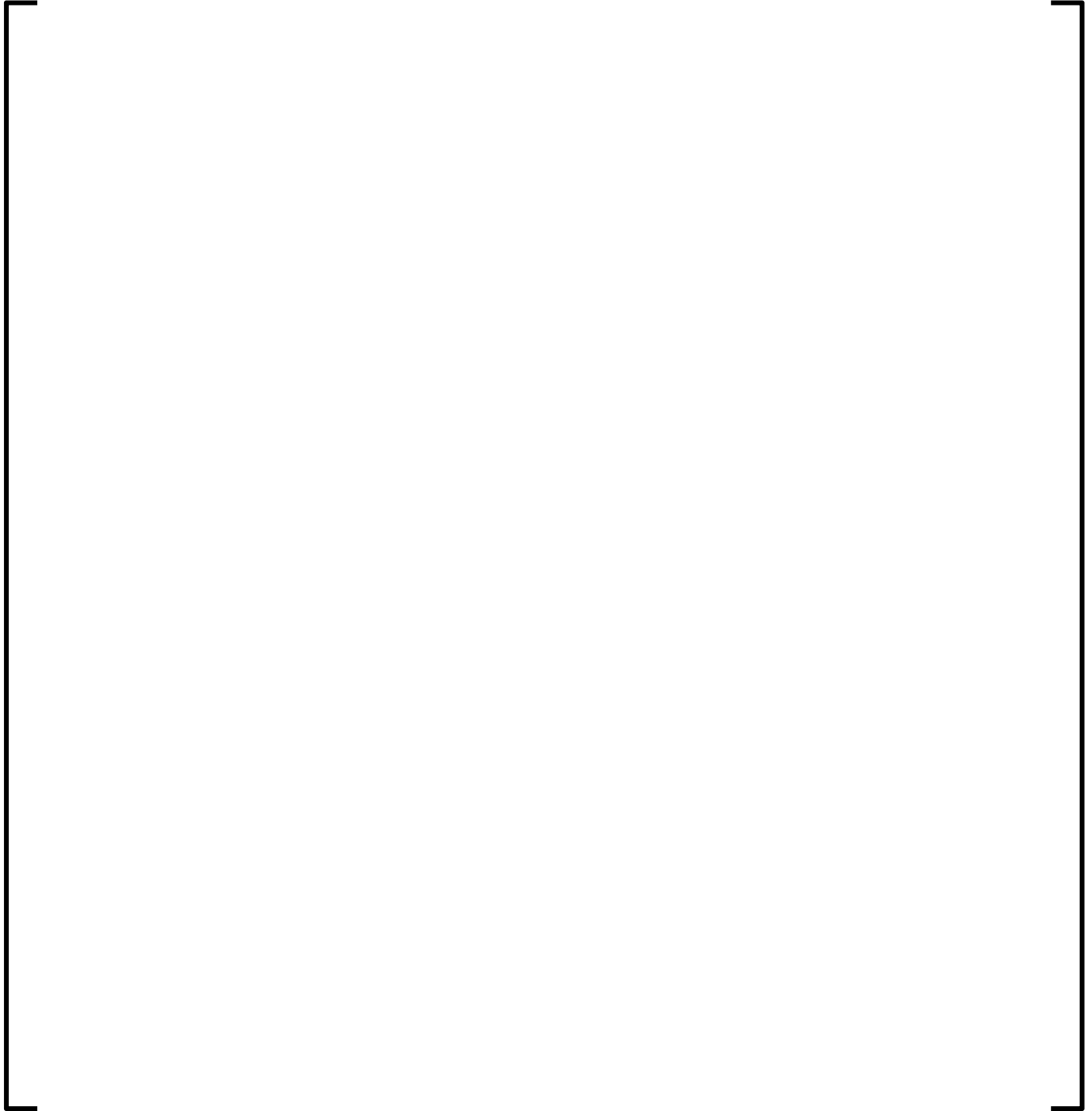


**Figure A 5.3.1-20**  
**Plant A MOC 12 Assembly Average Radial Power Distribution**

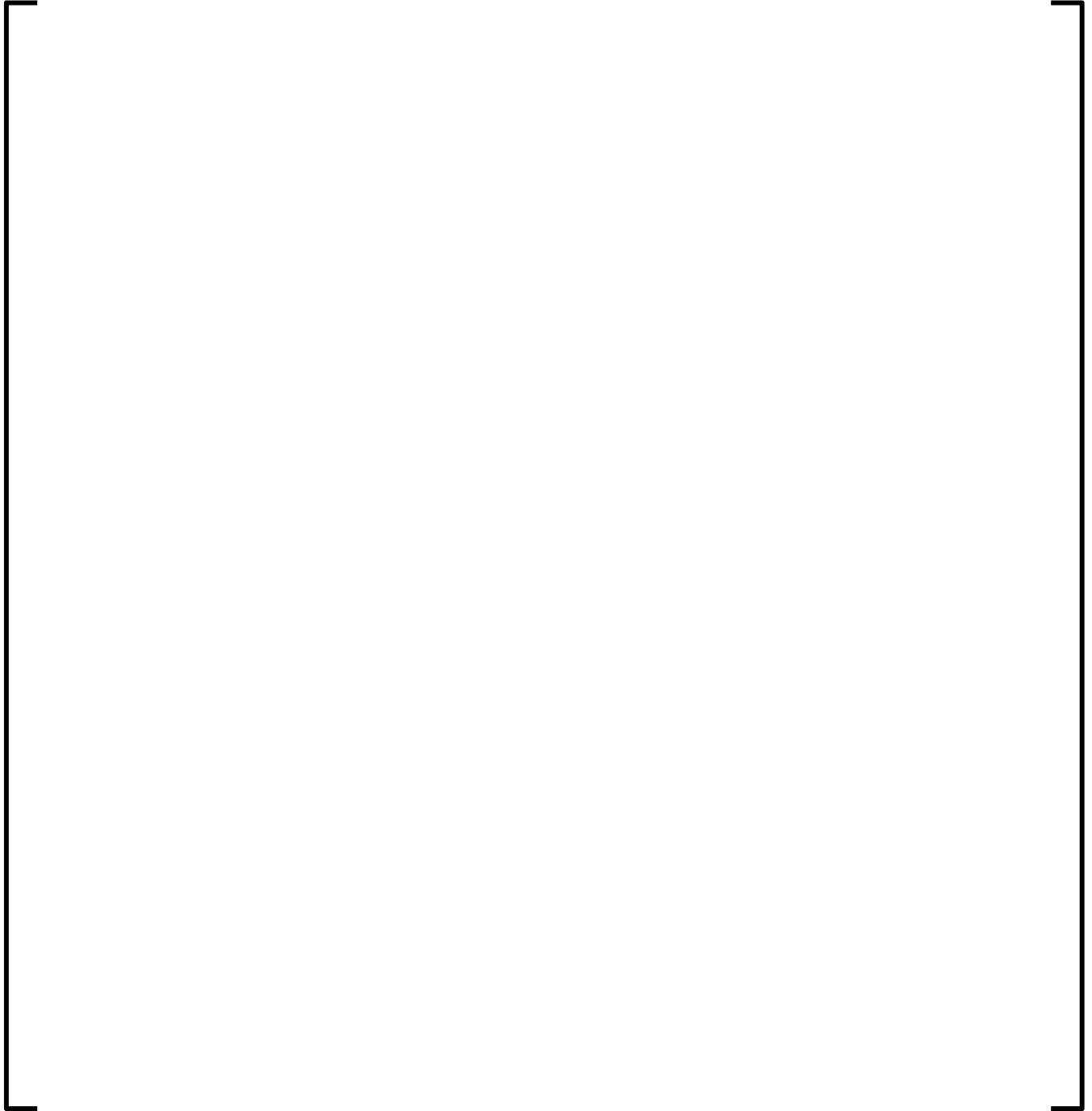


**Figure A 5.3.1-21**  
**Plant A EOC 12 Assembly Average Radial Power Distribution**

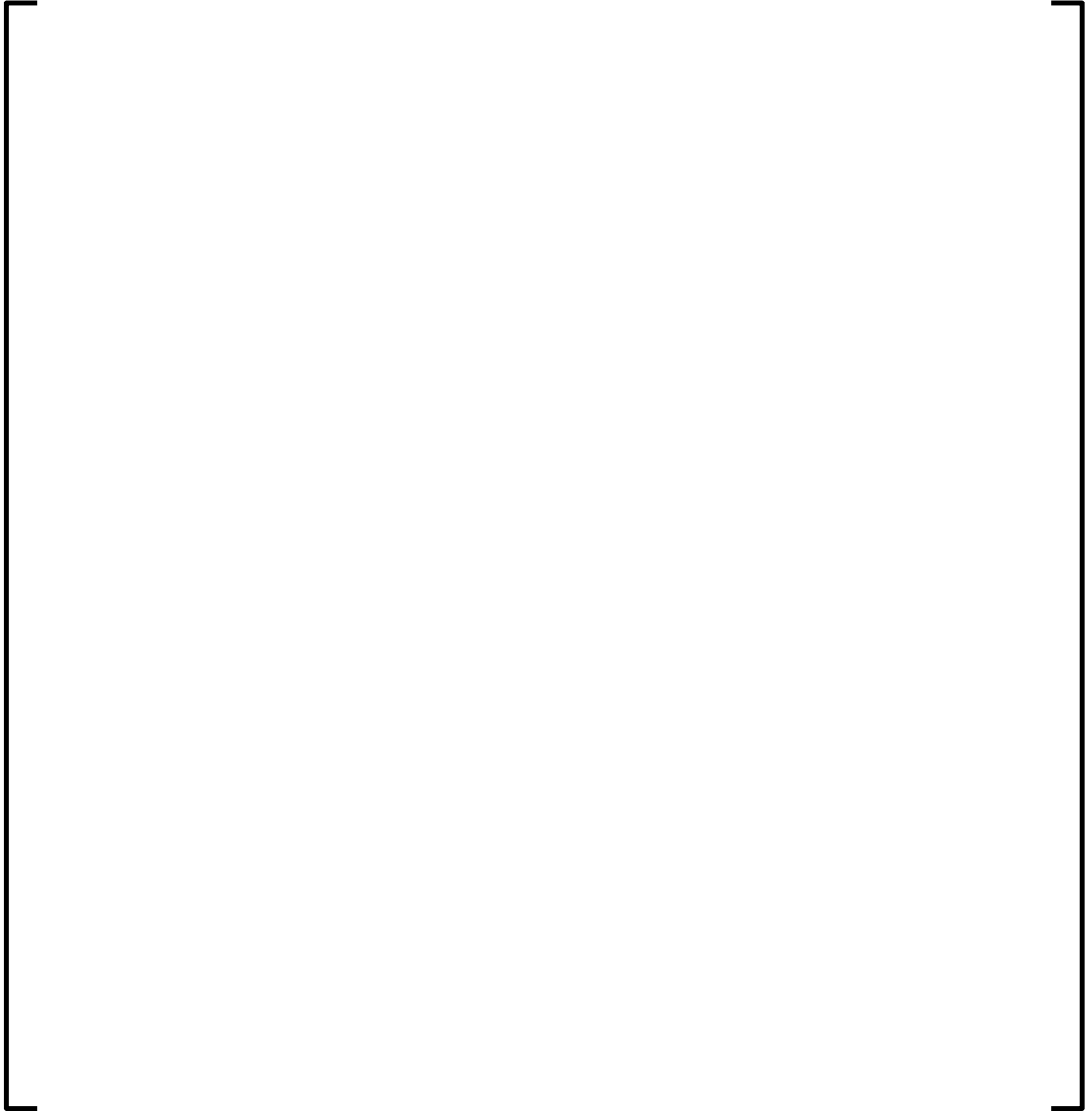


**Figure A 5.3.1-22**  
**Plant A BOC 13 Assembly Average Radial Power Distribution**

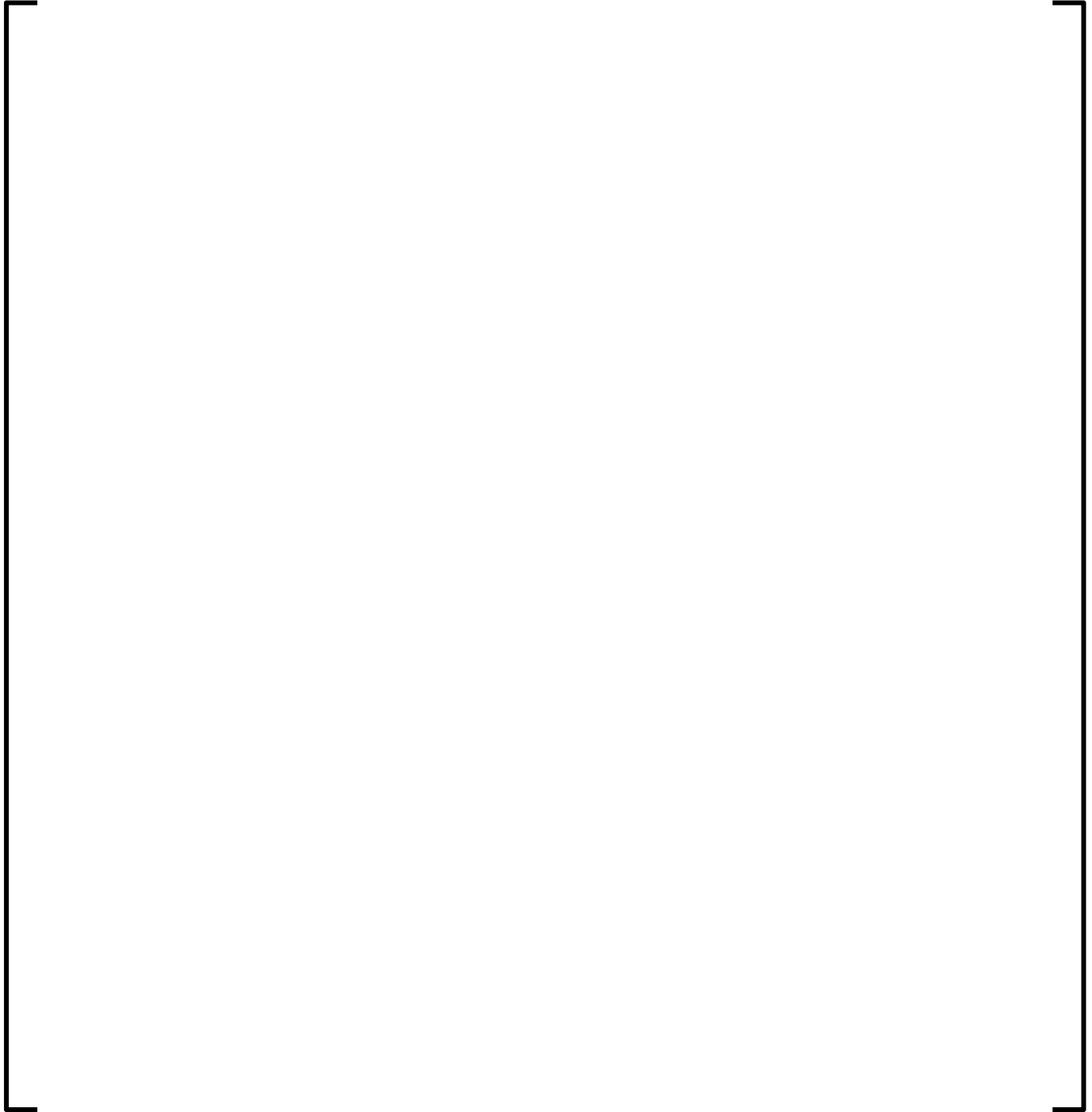


**Figure A 5.3.1-23**  
**Plant A MOC 13 Assembly Average Radial Power Distribution**

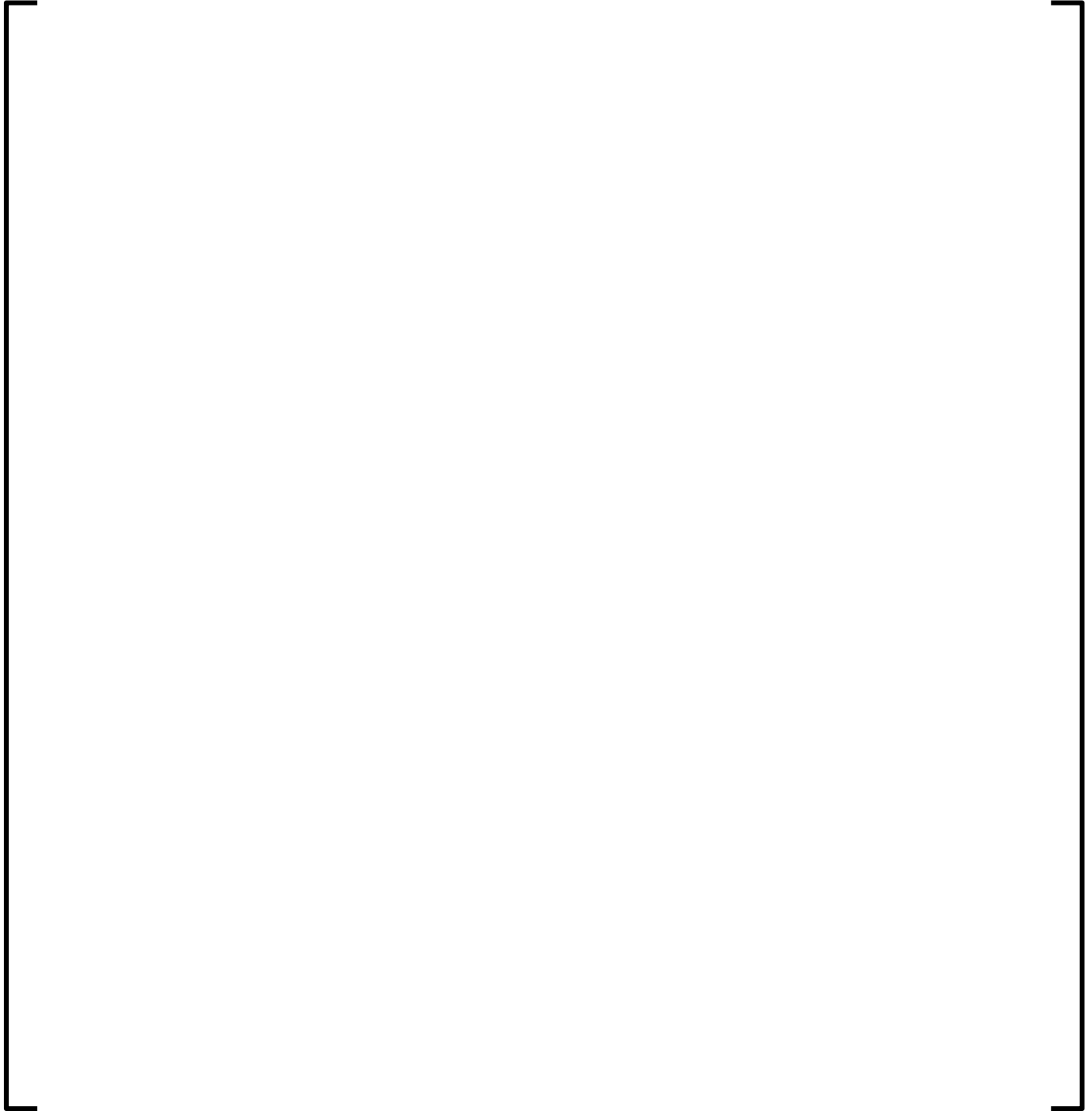




**Figure A 5.3.1-24**  
**Plant A EOC 13 Assembly Average Radial Power Distribution**

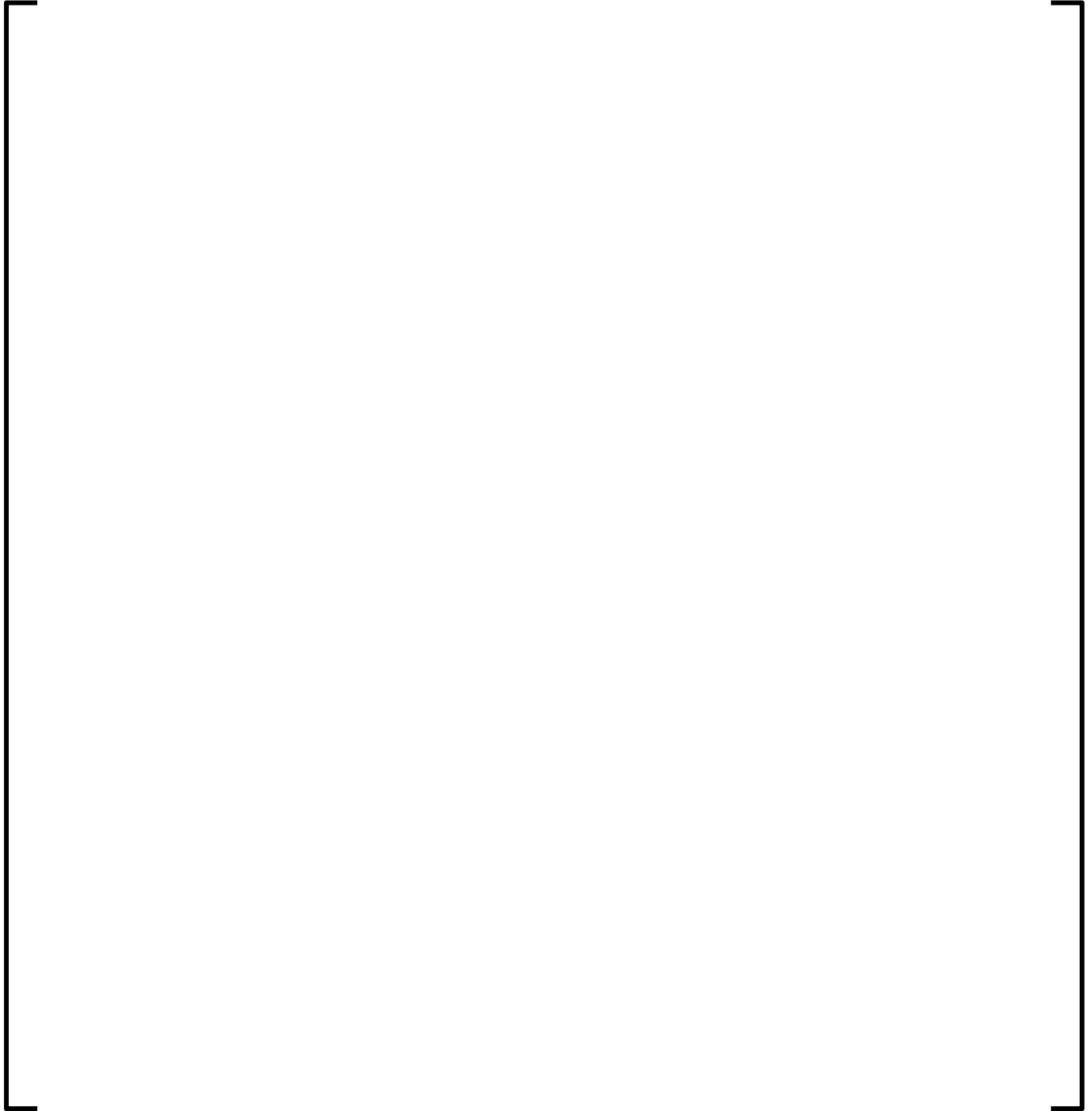


**Figure A 5.3.1-25**  
**Plant A BOC 14 Assembly Average Radial Power Distribution**

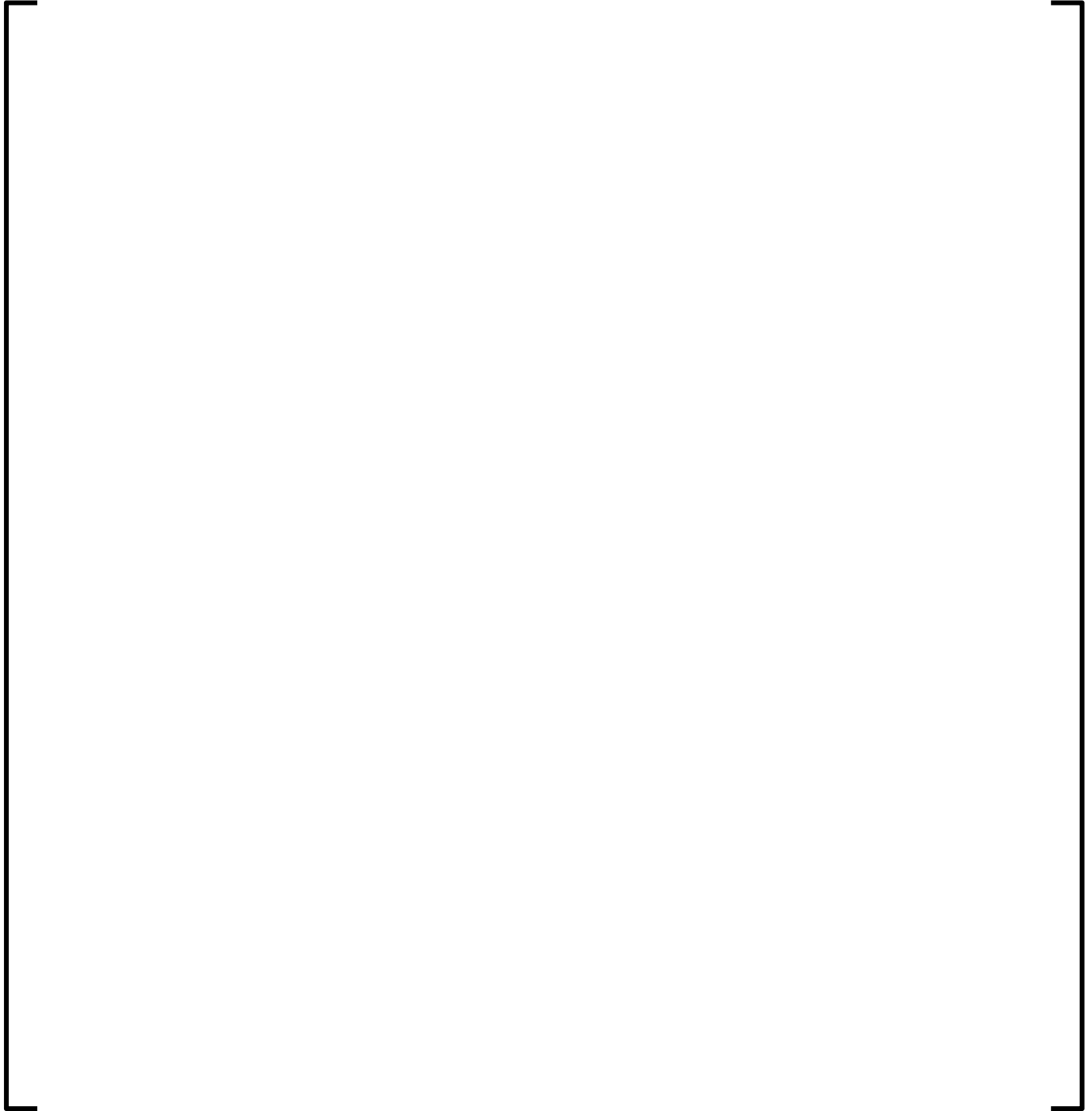


**Figure A 5.3.1-26**  
**Plant A MOC 14 Assembly Average Radial Power Distribution**

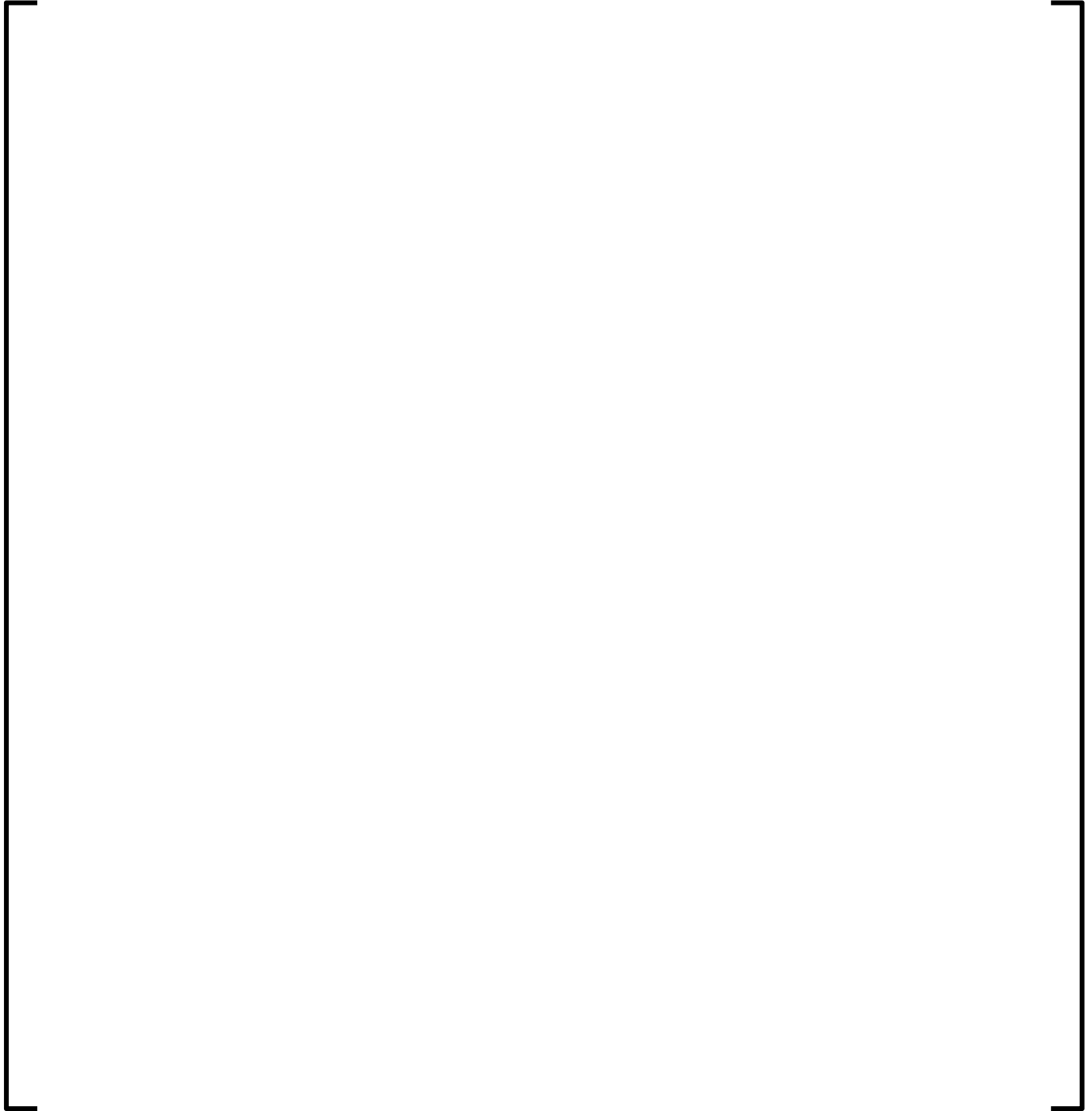


**Figure A 5.3.1-27**  
**Plant A EOC 14 Assembly Average Radial Power Distribution**

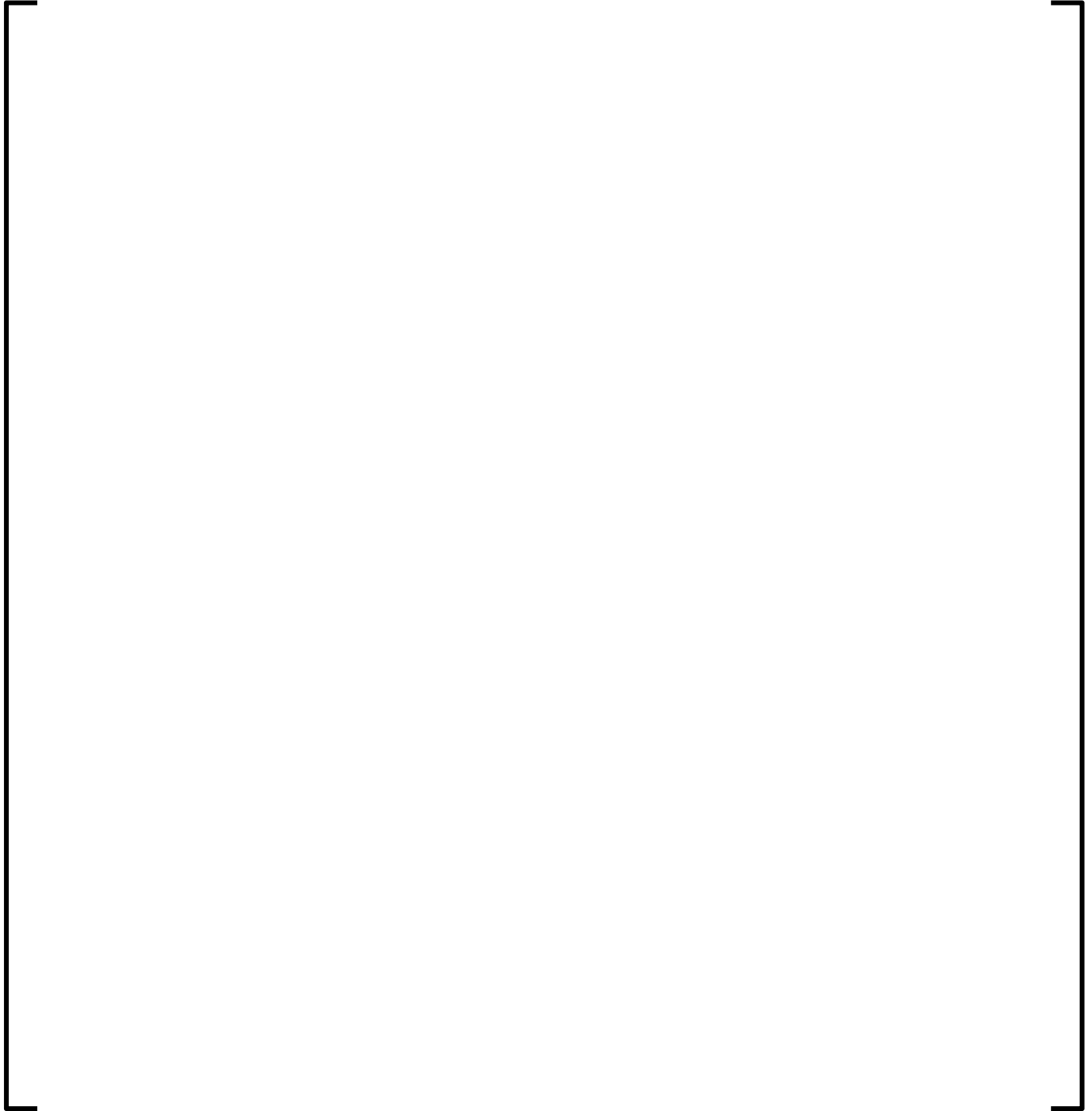


**Figure A 5.3.1-28**  
**Plant A BOC 11 Core Average Axial Power Distribution**



**Figure A 5.3.1-29**  
**Plant A MOC 11 Core Average Axial Power Distribution**



**Figure A 5.3.1-30**  
**Plant A EOC 11 Core Average Axial Power Distribution**

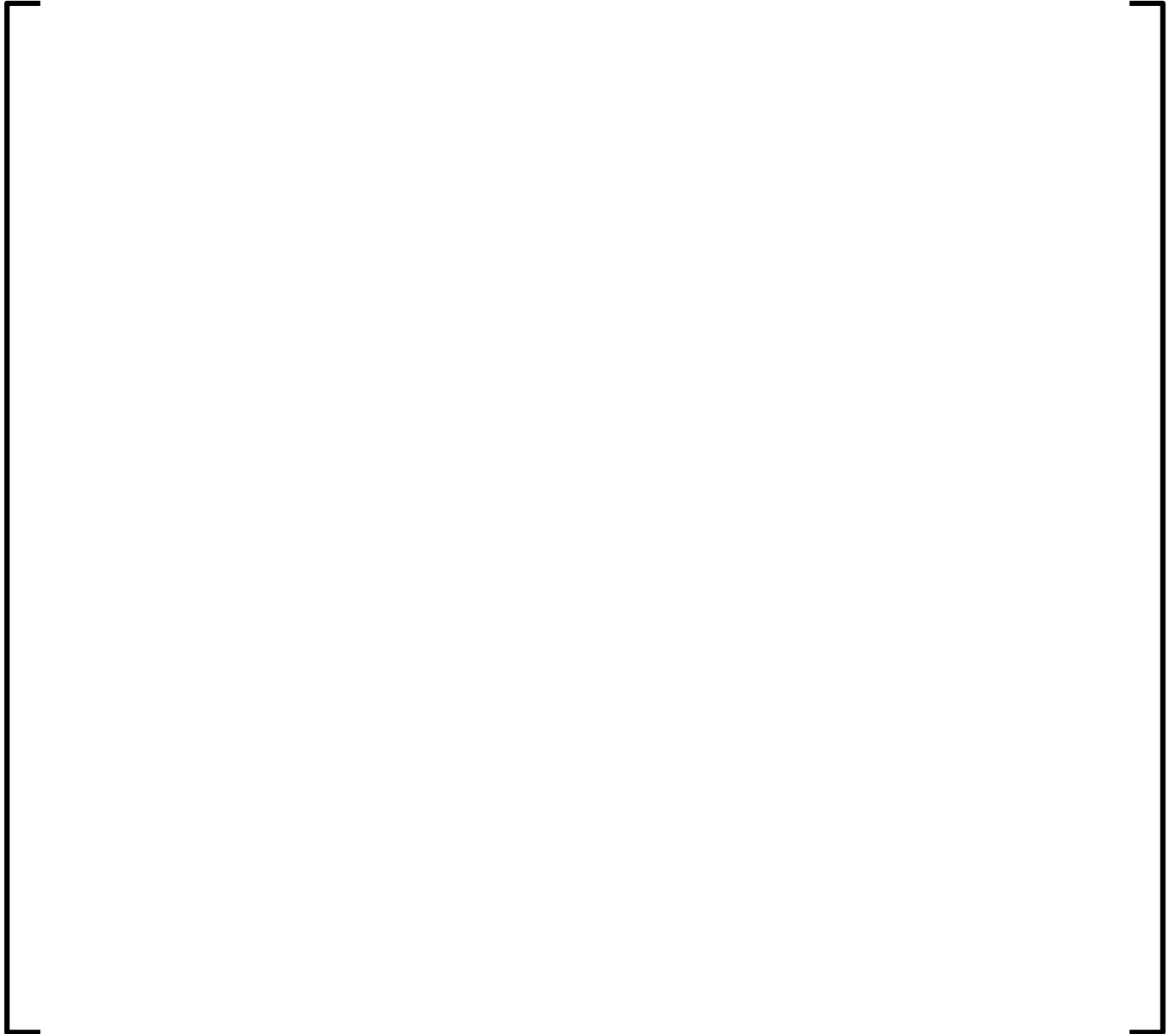


**Figure A 5.3.1-31**  
**Plant A BOC 12 Core Average Axial Power Distribution**





**Figure A 5.3.1-32**  
**Plant A MOC 12 Core Average Axial Power Distribution**



**Figure A 5.3.1-33**  
**Plant A EOC 12 Core Average Axial Power Distribution**



**Figure A 5.3.1-34**  
**Plant A BOC 13 Core Average Axial Power Distribution**



**Figure A 5.3.1-35**  
**Plant A MOC 13 Core Average Axial Power Distribution**



**Figure A 5.3.1-36**  
**Plant A EOC 13 Core Average Axial Power Distribution**



**Figure A 5.3.1-37**  
**Plant A BOC 14 Core Average Axial Power Distribution**



**Figure A 5.3.1-38**  
**Plant A MOC 14 Core Average Axial Power Distribution**

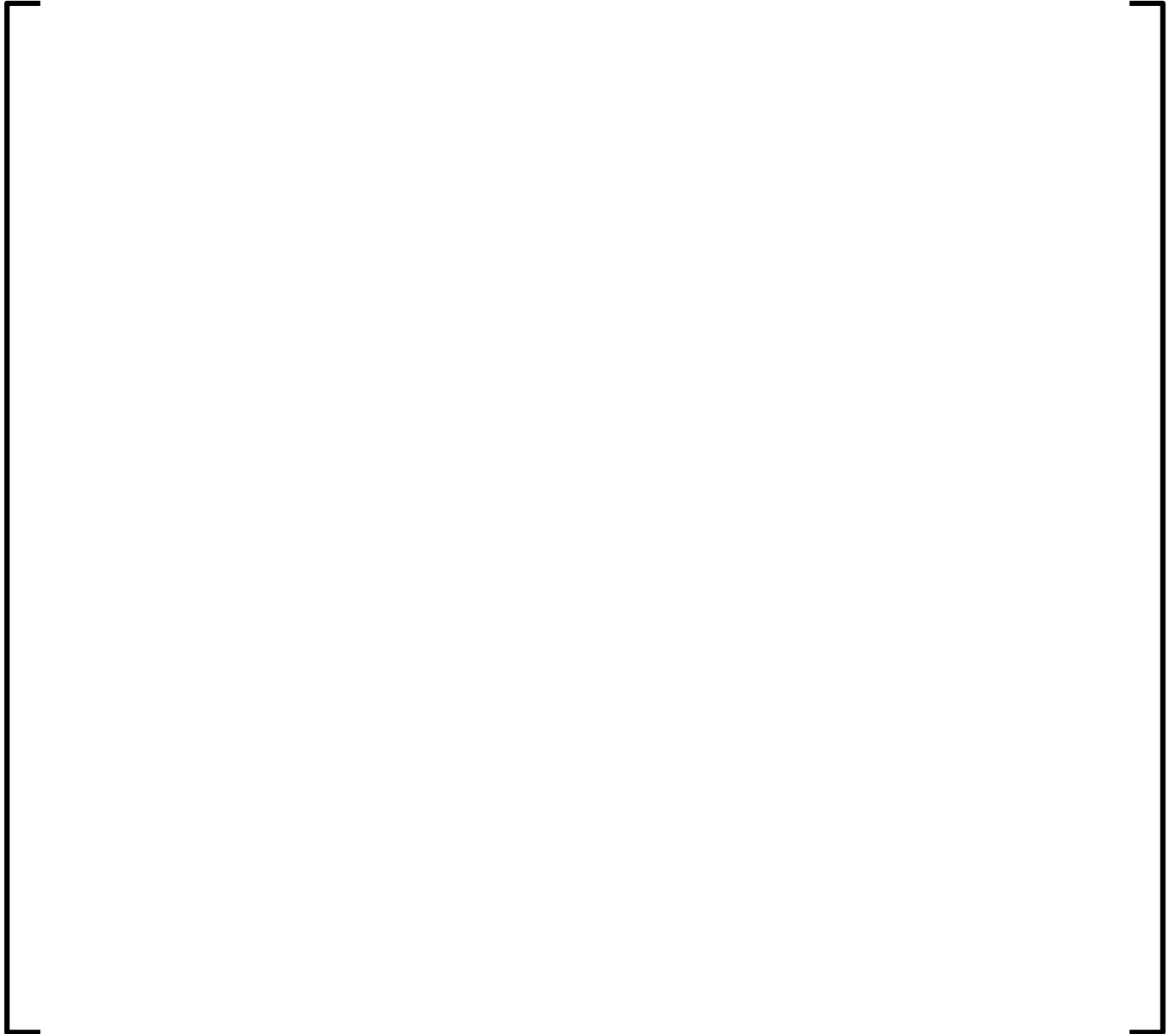


**Figure A 5.3.1-39**  
**Plant A EOC 14 Core Average Axial Power Distribution**





## **APPENDIX B**

**Table B 5.2.2-1**  
**Plant B Hot Zero Power All Rods Out Critical Boron Concentrations**  
**for Cycle 1**

--	--

**Table B 5.2.2-2**  
**Plant B Cycle 1 Hot Zero Power Individual Rod Bank Worth**

--	--

**Table B 5.2.2-3**  
**Plant B Summary of Total Bank Worths**

--	--

**Table B 5.2.2-4**  
**Plant B Hot Zero Power All Rods Out Isothermal Temperature**  
**Coefficient for Cycle 1**

--	--

**Figure B 5.3.2-1**  
**Plant B Cycle 1 Critical Boron Concentration vs. Burnup**



**Figure B 5.3.2-2**  
**Plant B Cycle 1 Boron Differences**



**Figure B 5.3.2-3**  
**Plant B BOC 1 Assembly Average Radial Power Distribution**

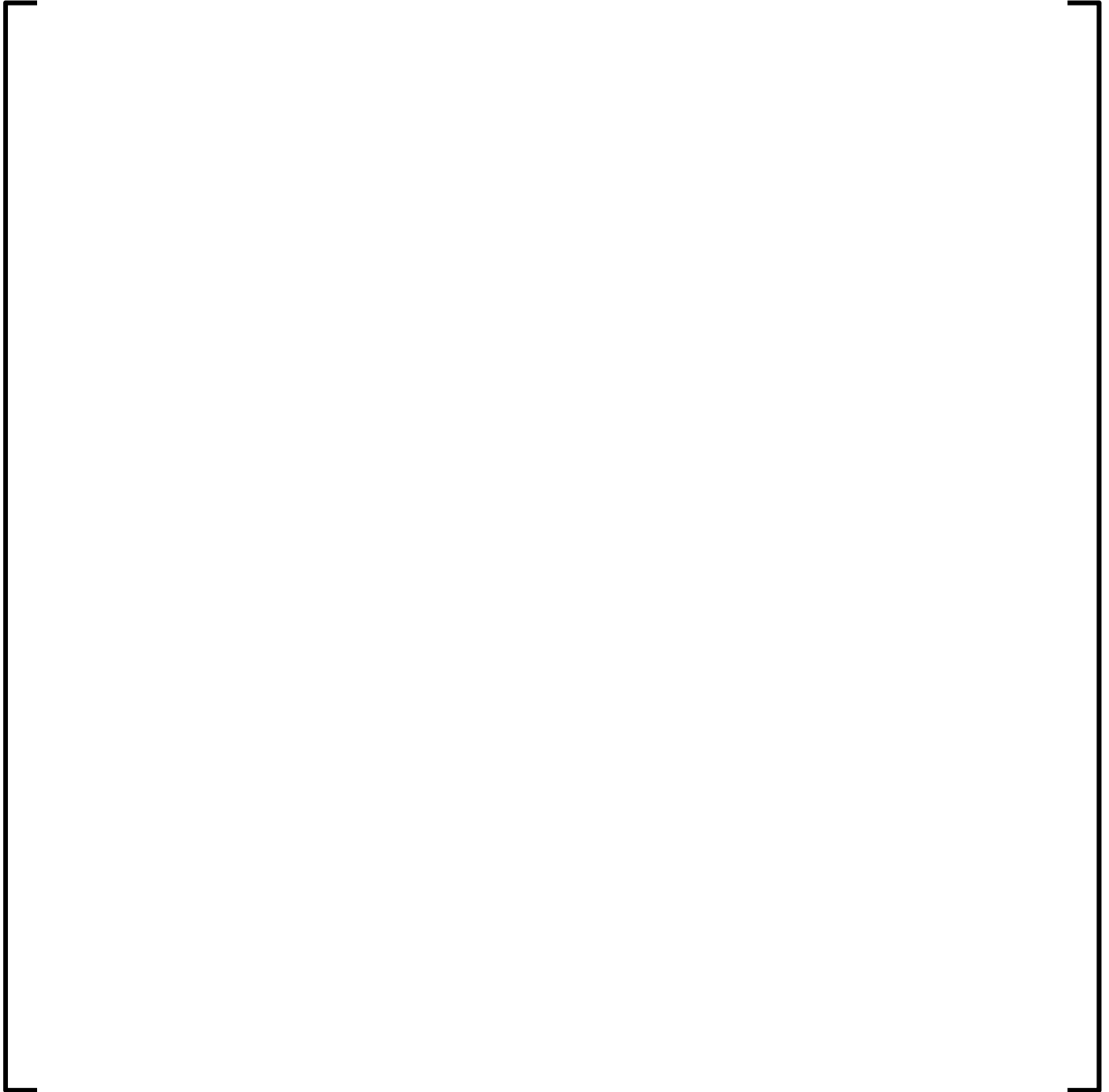


**Figure B 5.3.2-4**  
**Plant B MOC 1 Assembly Average Radial Power Distribution**

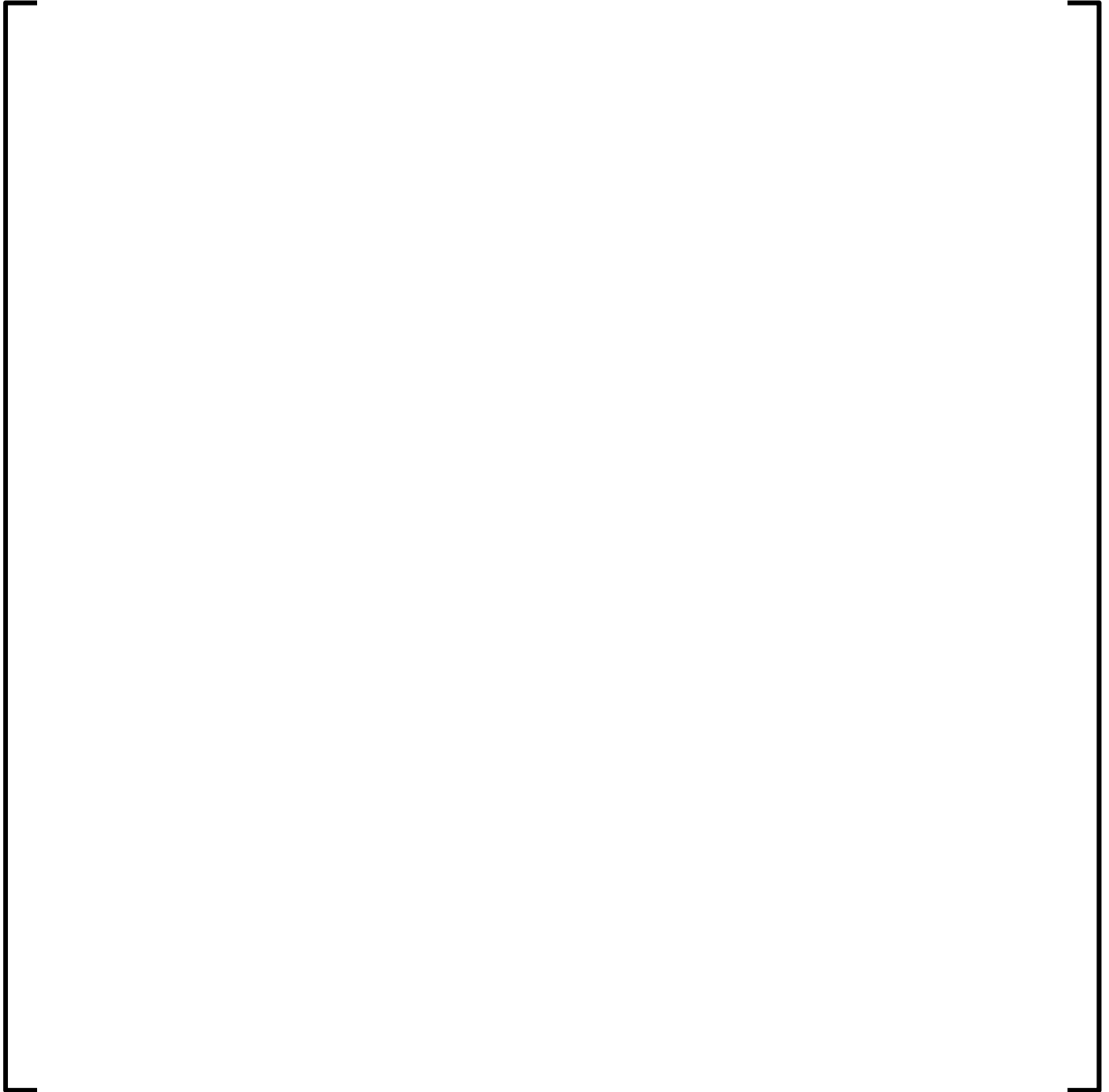




**Figure B 5.3.2-5**  
**Plant B EOC 1 Assembly Average Radial Power Distribution**

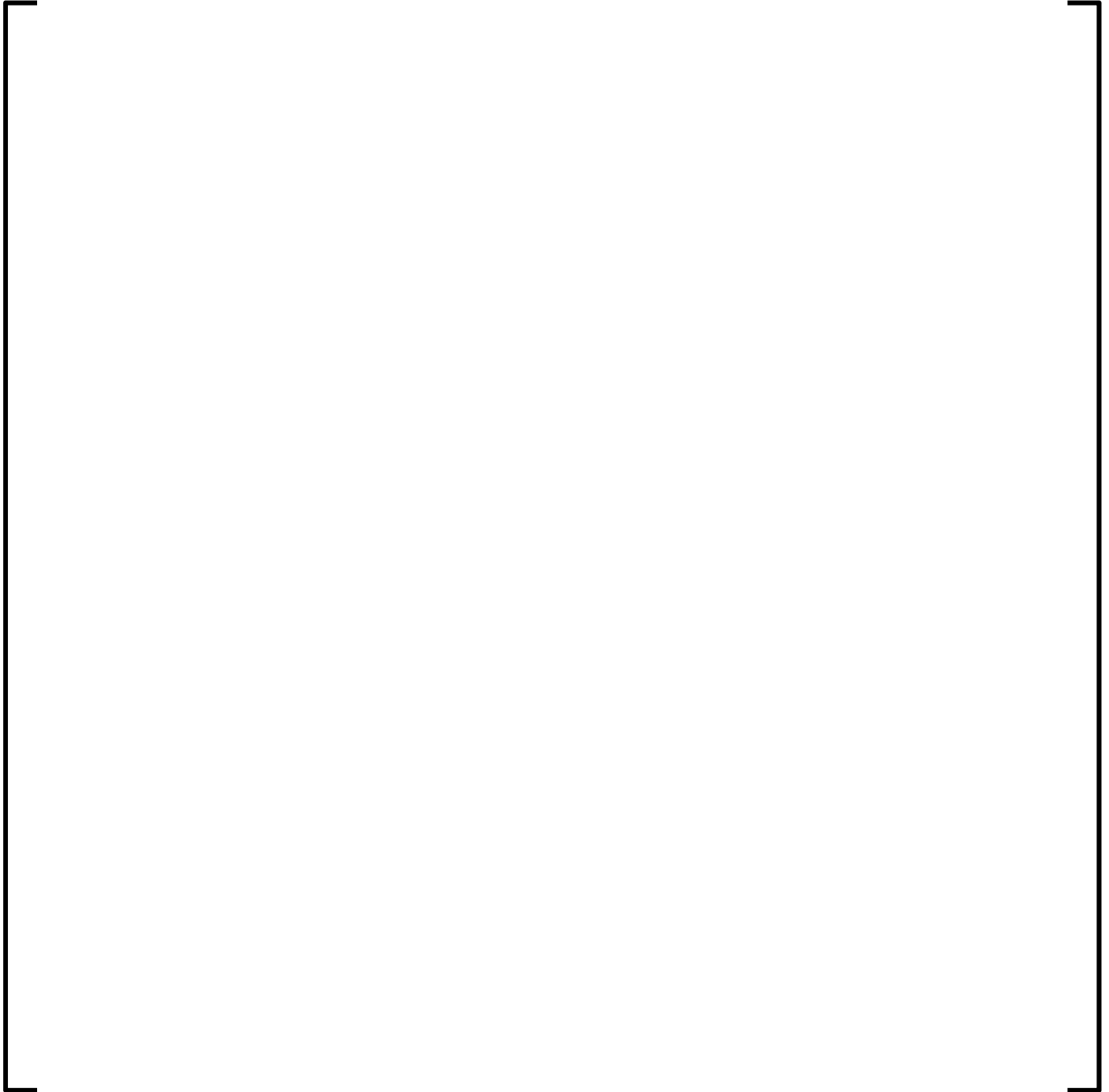


**Figure B 5.3.2-6**  
**Plant B BOC 1 Core Average Axial Power Distribution**



**Figure B 5.3.2-7**  
**Plant B MOC 1 Core Average Axial Power Distribution**



**Figure B 5.3.2-8**  
**Plant B EOC 1 Core Average Axial Power Distribution**



## **APPENDIX C**

**Table C 5.2.3-1**  
**Plant C Hot Zero Power All Rods Out Critical Boron Concentrations**  
**for Cycles 10-18**

--	--

**Table C 5.2.3-2**  
**Plant C Cycle 10 Hot Zero Power Individual Rod Bank Worth**

--	--

**Table C 5.2.3-3**  
**Plant C Cycle 11 Hot Zero Power Individual Rod Bank Worth**

--	--

**Table C 5.2.3-4**  
**Plant C Cycle 12 Hot Zero Power Individual Rod Bank Worth**

--	--



**Table C 5.2.3-5**  
**Plant C Cycle 13 Hot Zero Power Individual Rod Bank Worth**

--	--

**Table C 5.2.3-6**  
**Plant C Cycle 14 Hot Zero Power Individual Rod Bank Worth**

--	--

**Table C 5.2.3-7**  
**Plant C Cycle 15 Hot Zero Power Individual Rod Bank Worth**

--	--

**Table C 5.2.3-8**  
**Plant C Cycle 16 Hot Zero Power Individual Rod Bank Worth**

--	--

**Table C 5.2.3-9**  
**Plant C Cycle 17 Hot Zero Power Individual Rod Bank Worth**

--	--

**Table C 5.2.3-10**  
**Plant C Summary of Total Bank Worths**

--	--

**Table C 5.2.3-11**  
**Plant C Hot Zero Power All Rods Out Isothermal Temperature**  
**Coefficient for Cycles 10-18**

--	--

**Figure C 5.3.3-1**  
**Plant C Cycle 10 Critical Boron Concentration vs. Burnup**





**Figure C 5.3.3-2**  
**Plant C Cycle 11 Critical Boron Concentration vs. Burnup**



**Figure C 5.3.3-3**  
**Plant C Cycle 12 Critical Boron Concentration vs. Burnup**



**Figure C 5.3.3-4**  
**Plant C Cycle 13 Critical Boron Concentration vs. Burnup**



**Figure C 5.3.3-5**  
**Plant C Cycle 14 Critical Boron Concentration vs. Burnup**



**Figure C 5.3.3-6**  
**Plant C Cycle 15 Critical Boron Concentration vs. Burnup**



**Figure C 5.3.3-7**  
**Plant C Cycle 16 Critical Boron Concentration vs. Burnup**

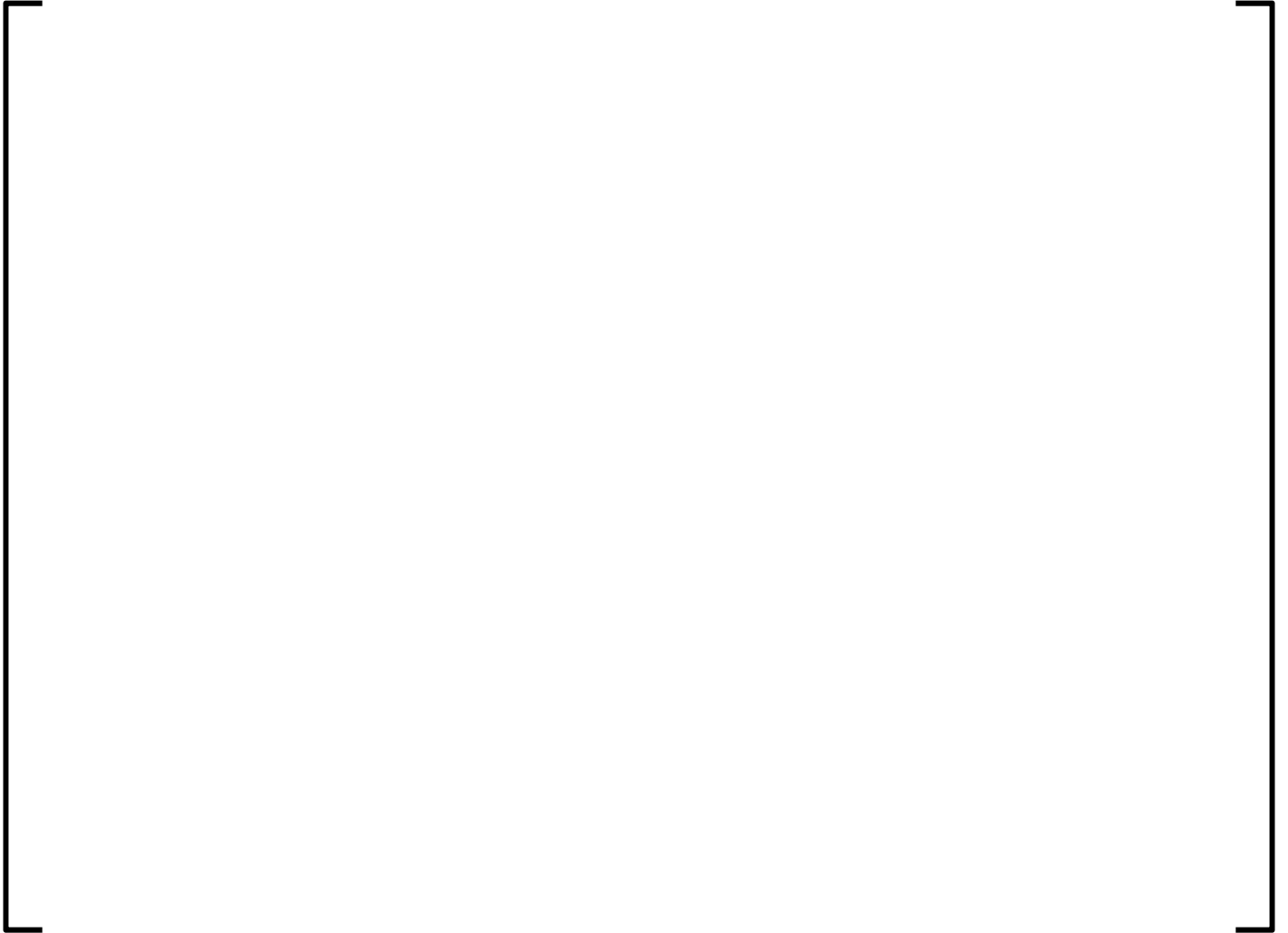


**Figure C 5.3.3-8**  
**Plant C Cycle 17 Critical Boron Concentration vs. Burnup**



**Figure C 5.3.3-9**  
**Plant C Cycle 18 Critical Boron Concentration vs. Burnup**





**Figure C 5.3.3-10**  
**Plant C Cycles 10-18 Boron Differences**



**Figure C 5.3.3-11**  
**Plant C BOC 14 Assembly Average Radial Power Distribution**

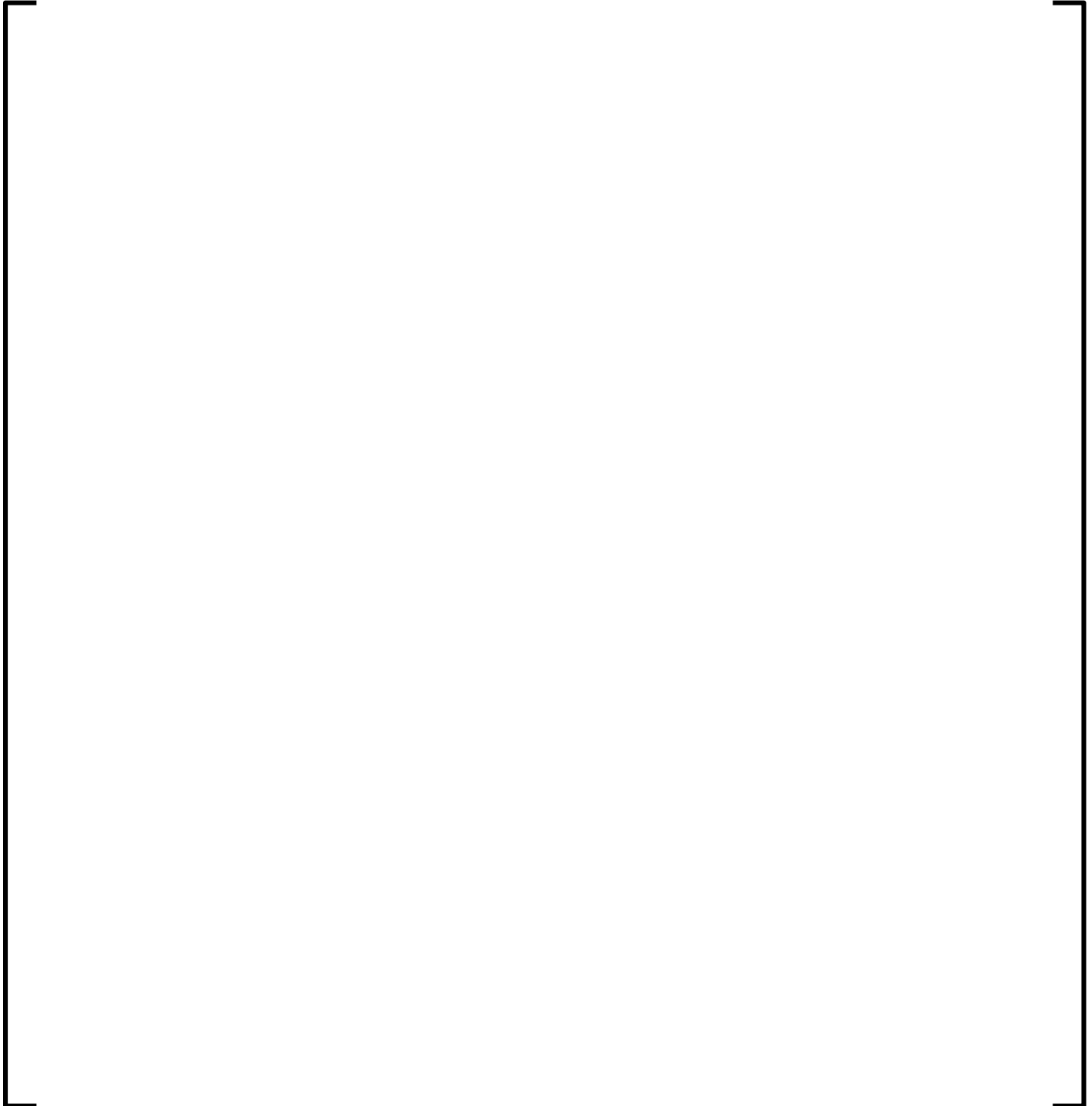


**Figure C 5.3.3-12**  
**Plant C MOC 14 Assembly Average Radial Power Distribution**

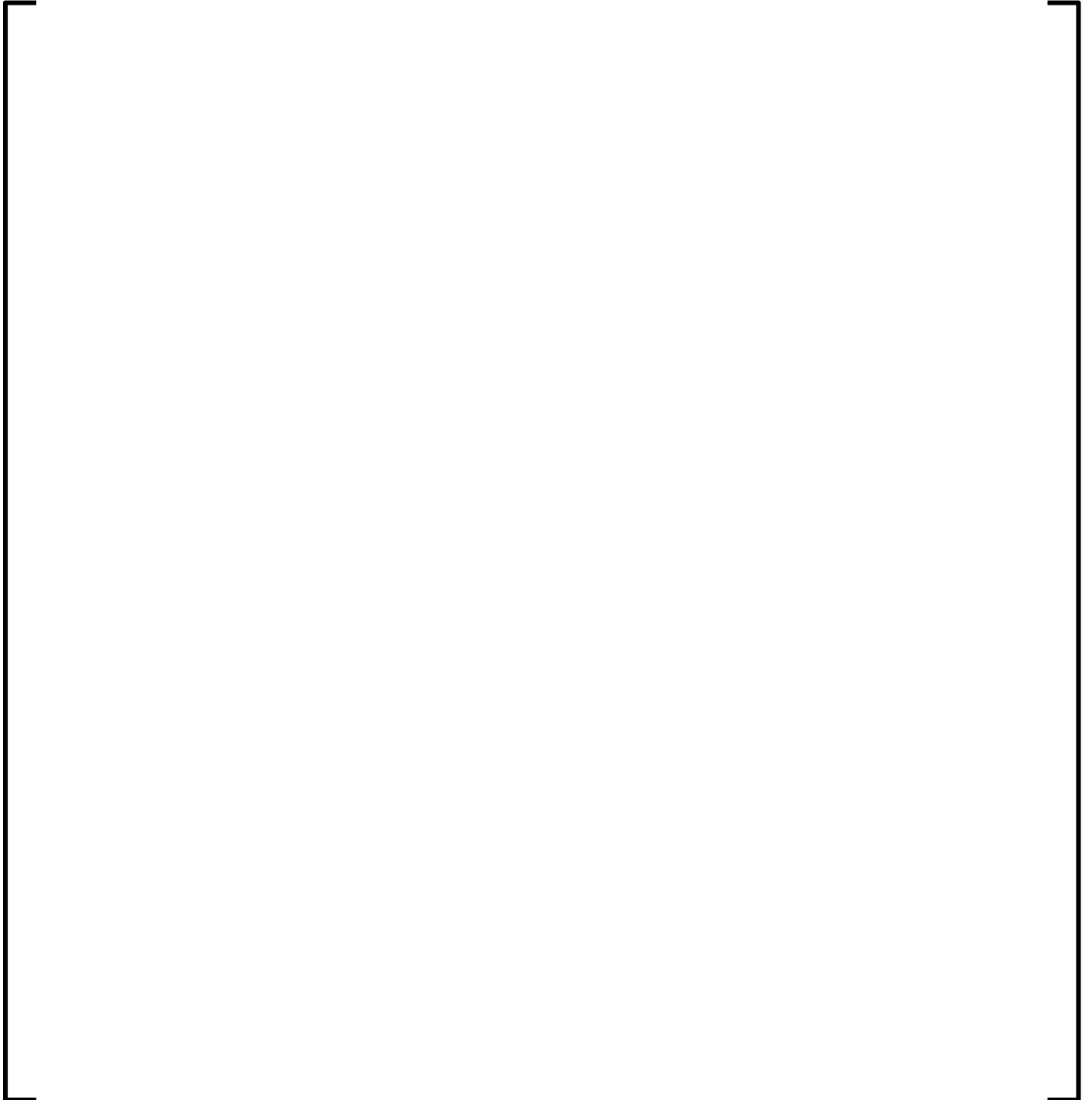


**Figure C 5.3.3-13**  
**Plant C EOC 14 Assembly Average Radial Power Distribution**

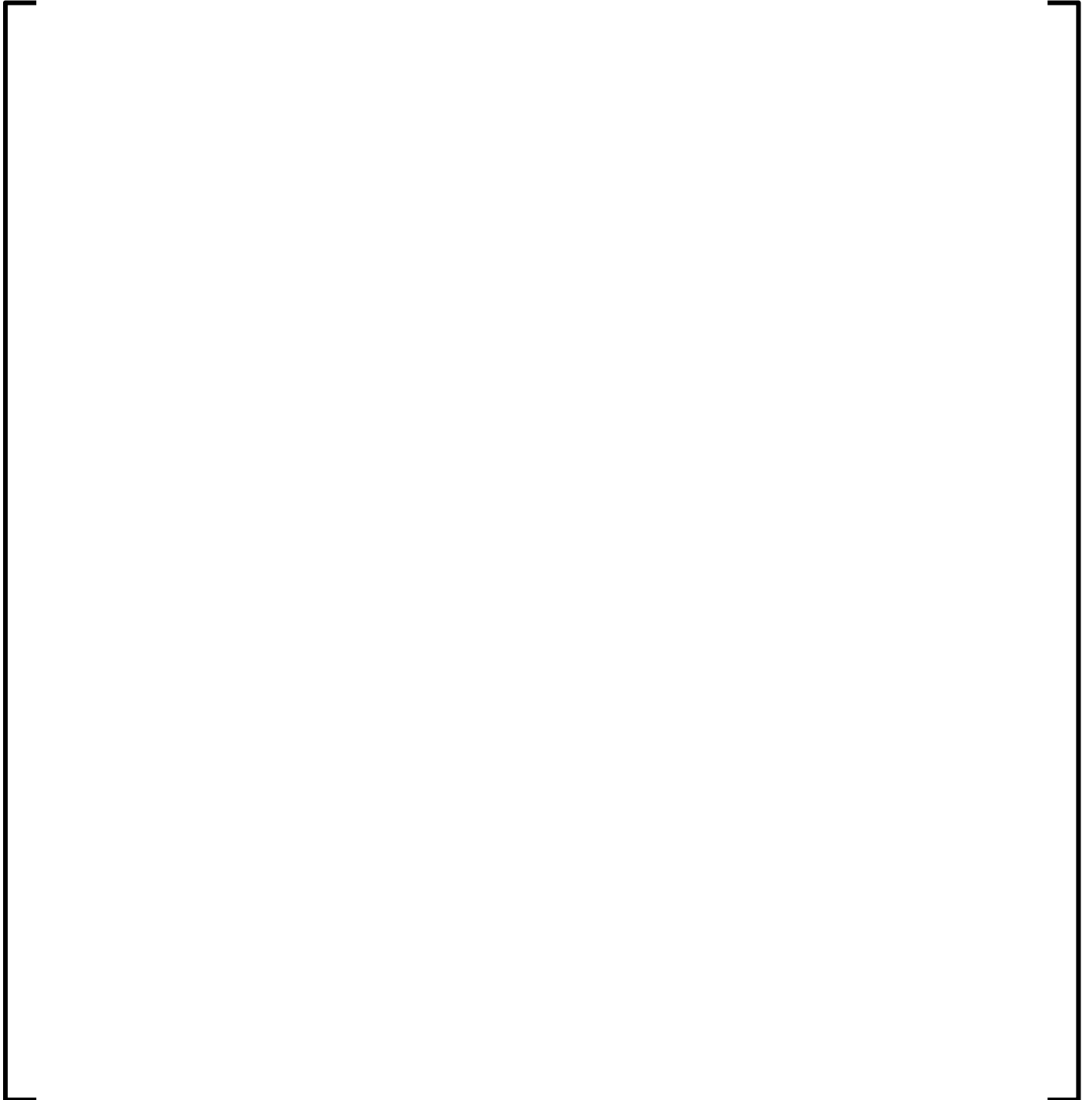


**Figure C 5.3.3-14**  
**Plant C BOC 15 Assembly Average Radial Power Distribution**

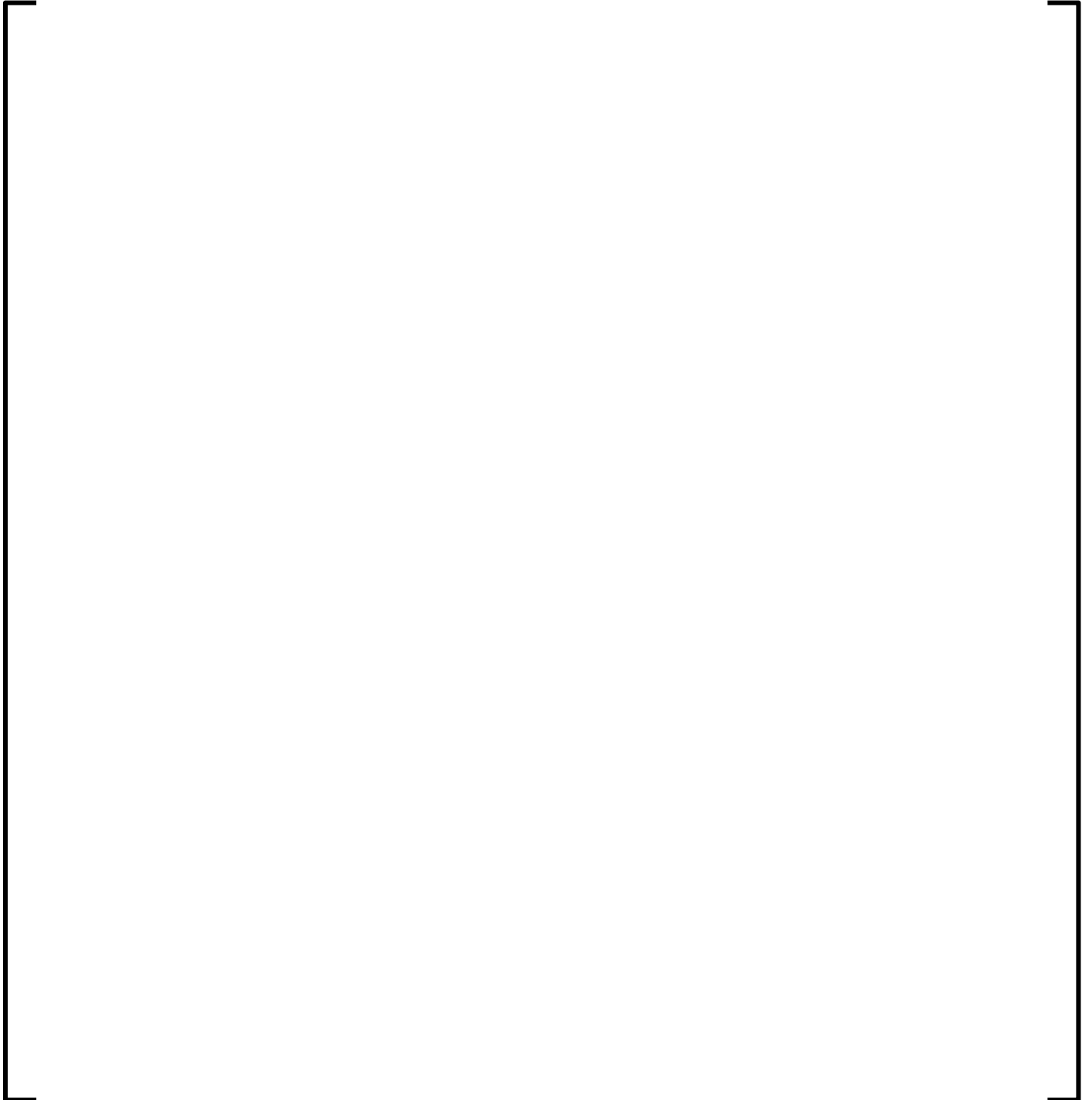


**Figure C 5.3.3-15**  
**Plant C MOC 15 Assembly Average Radial Power Distribution**

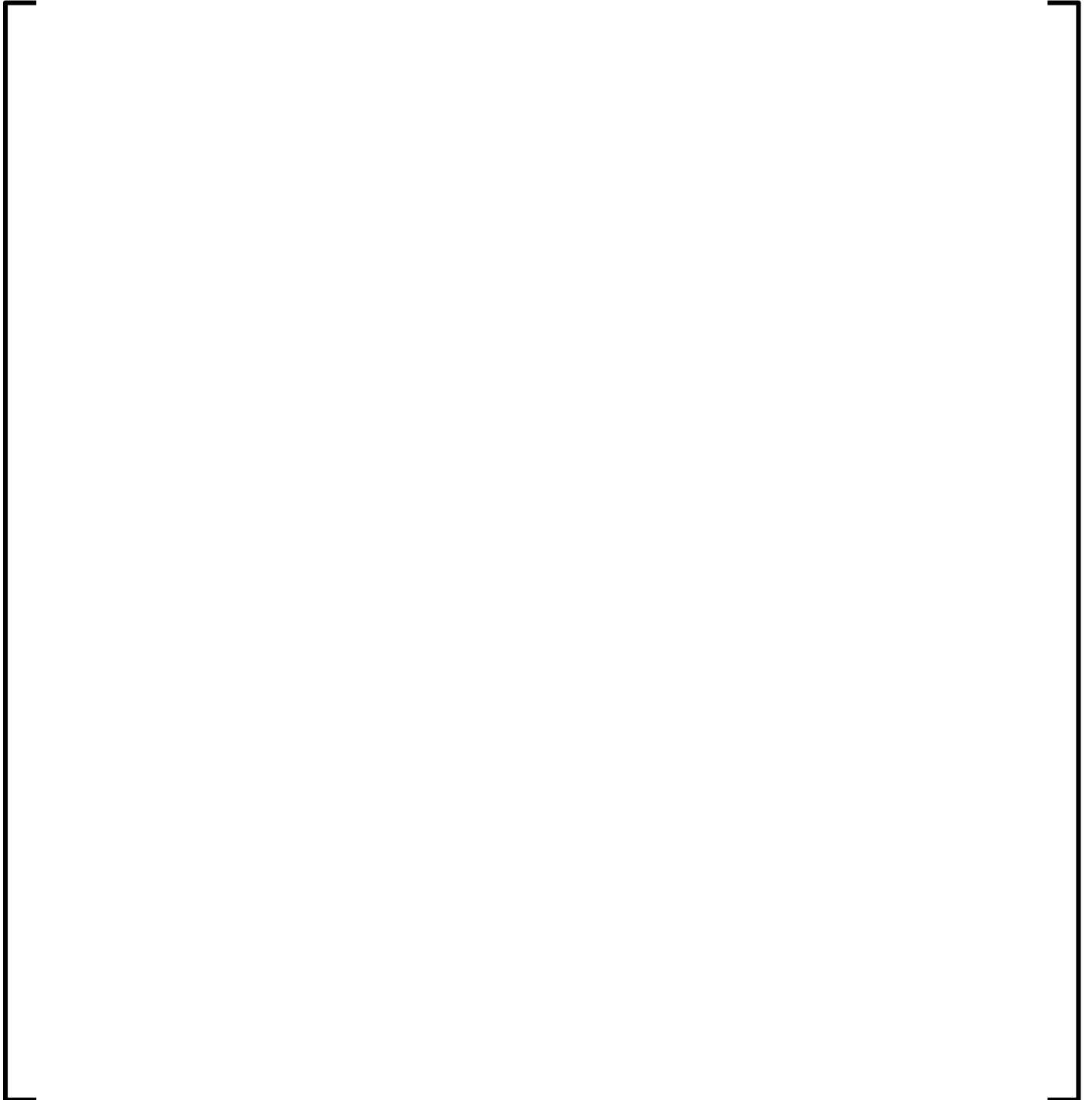


**Figure C 5.3.3-16**  
**Plant C EOC 15 Assembly Average Radial Power Distribution**

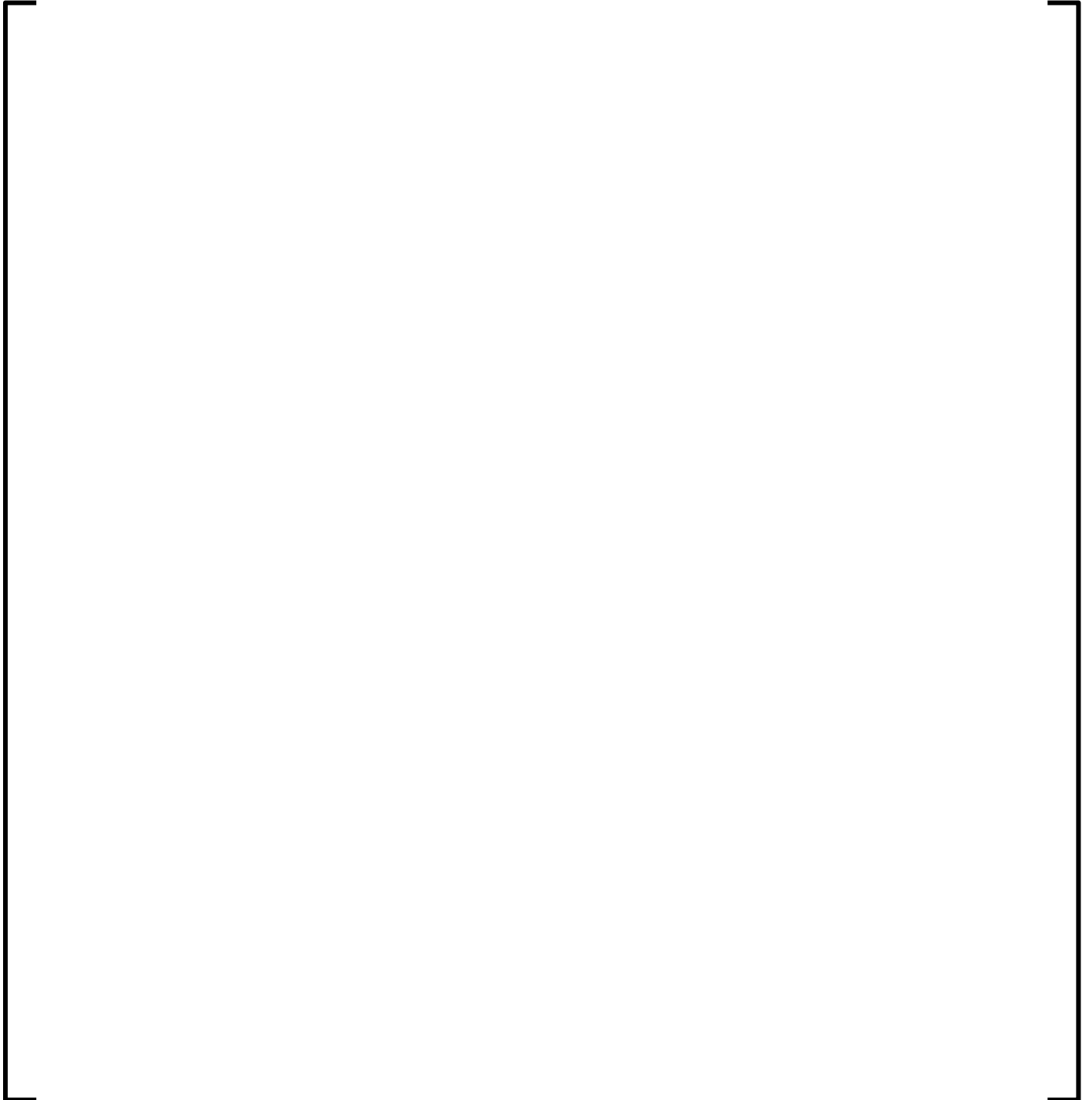


**Figure C 5.3.3-17**  
**Plant C BOC 16 Assembly Average Radial Power Distribution**

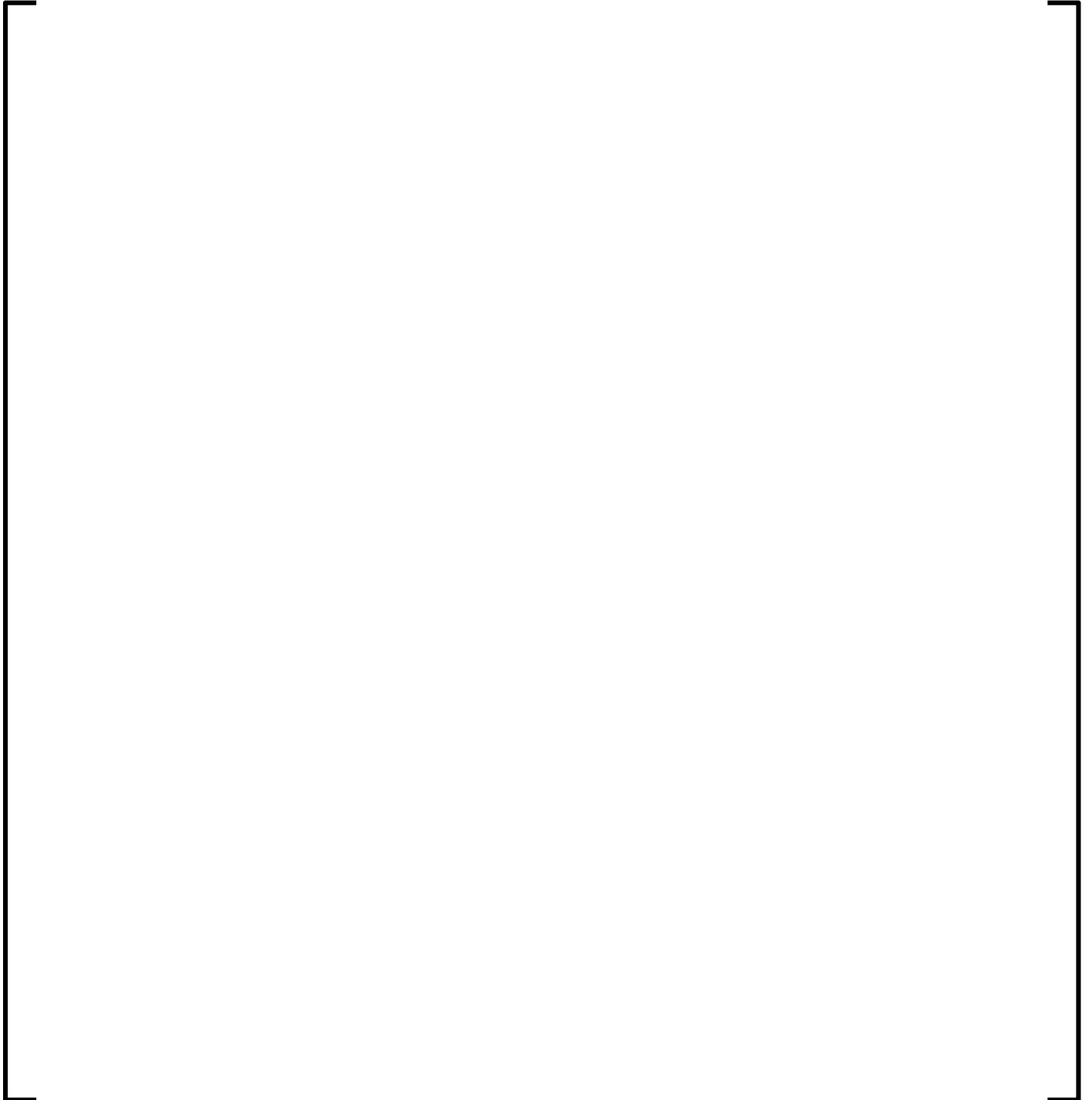




**Figure C 5.3.3-18**  
**Plant C MOC 16 Assembly Average Radial Power Distribution**

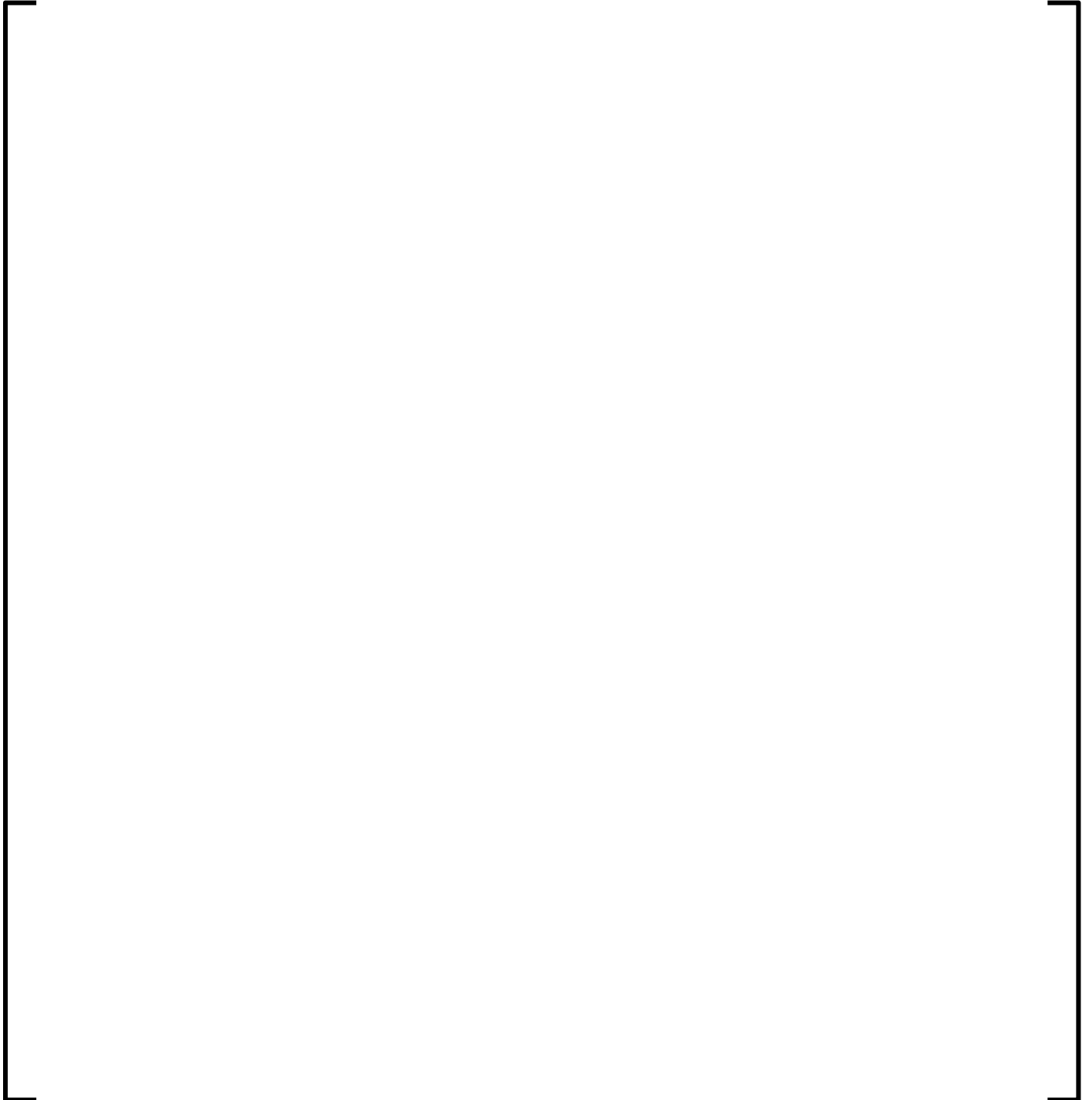


**Figure C 5.3.3-19**  
**Plant C EOC 16 Assembly Average Radial Power Distribution**

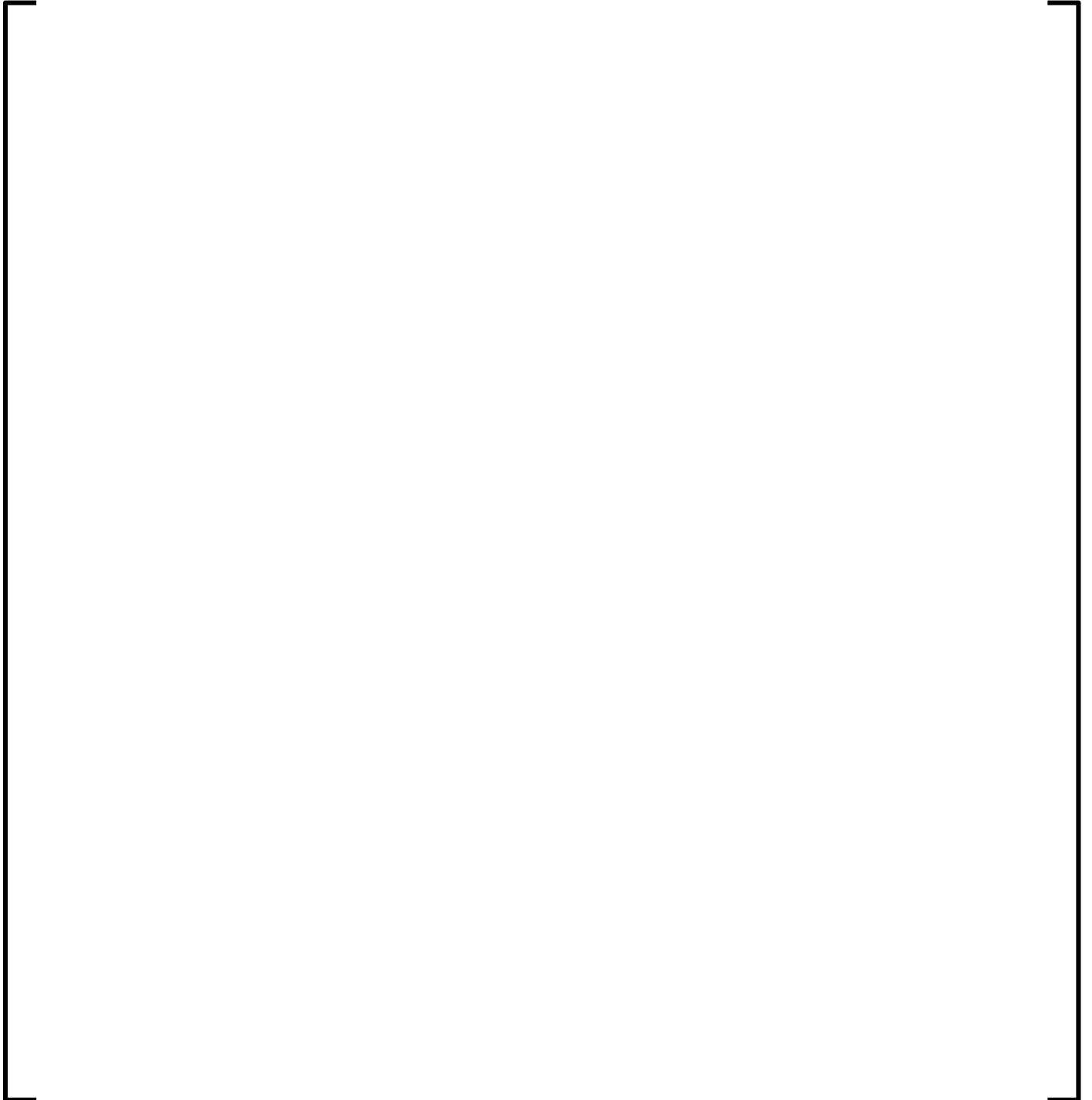


**Figure C 5.3.3-20**  
**Plant C BOC 17 Assembly Average Radial Power Distribution**

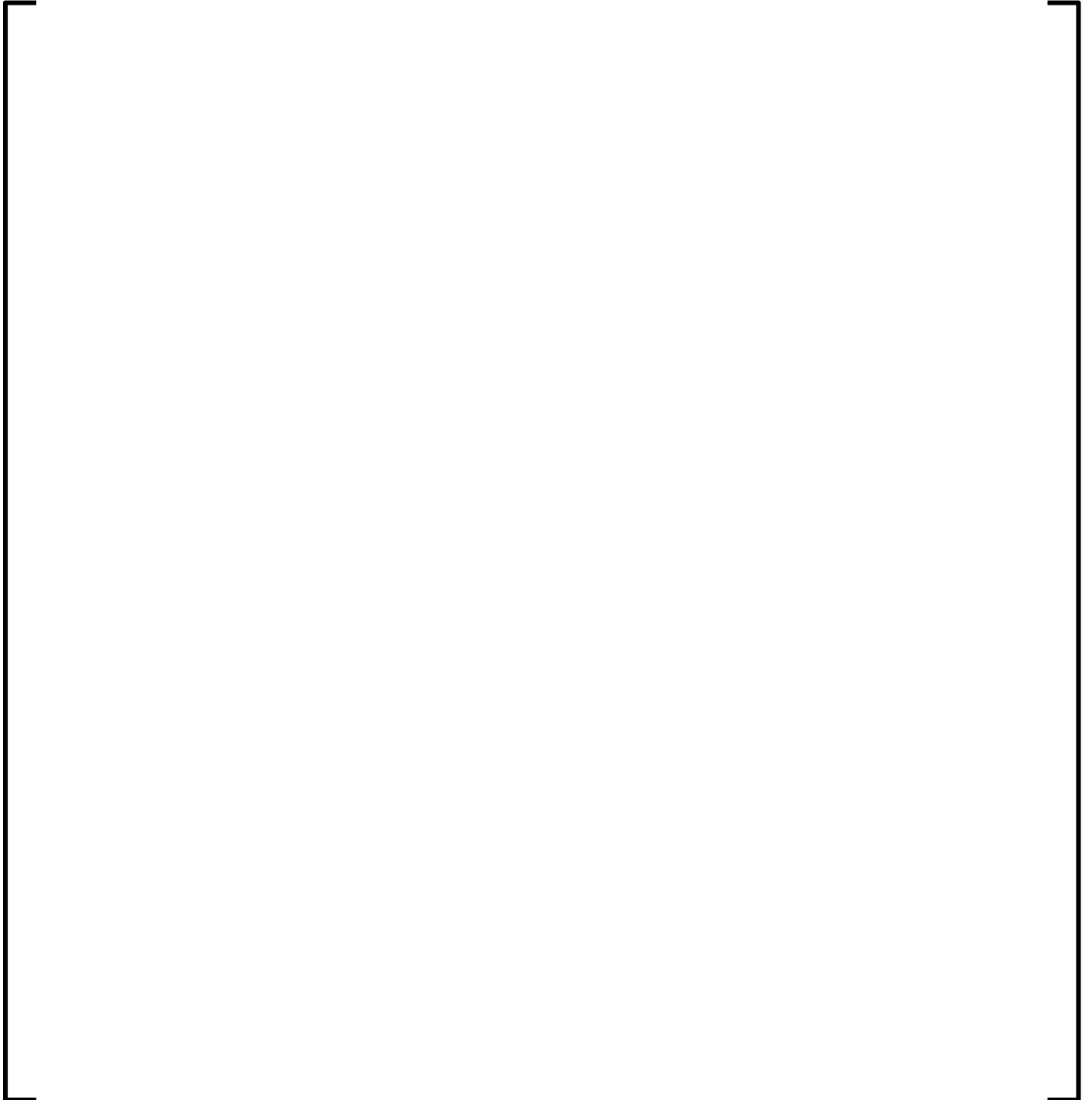


**Figure C 5.3.3-21**  
**Plant C MOC 17 Assembly Average Radial Power Distribution**

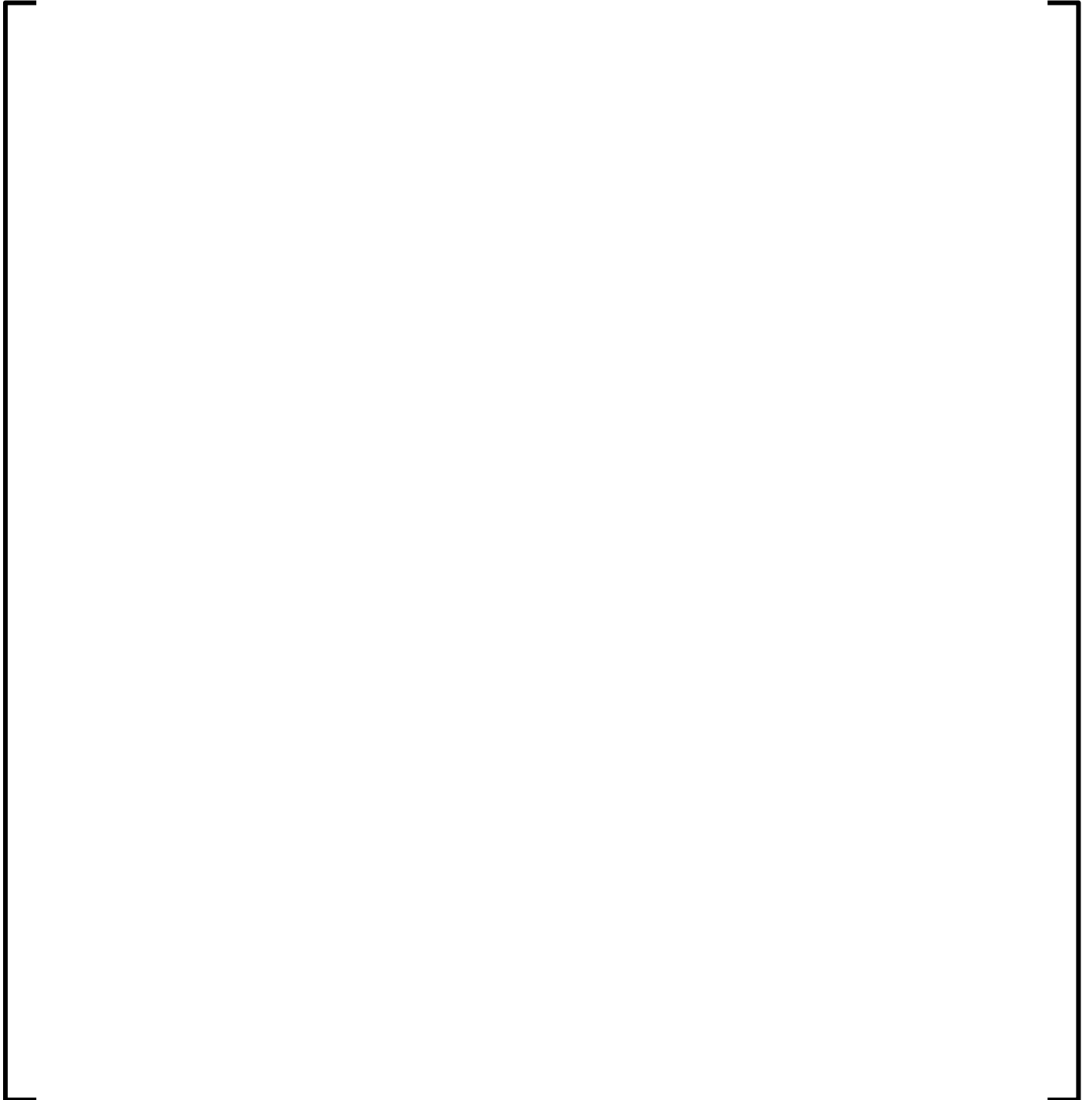


**Figure C 5.3.3-22**  
**Plant C EOC 17 Assembly Average Radial Power Distribution**

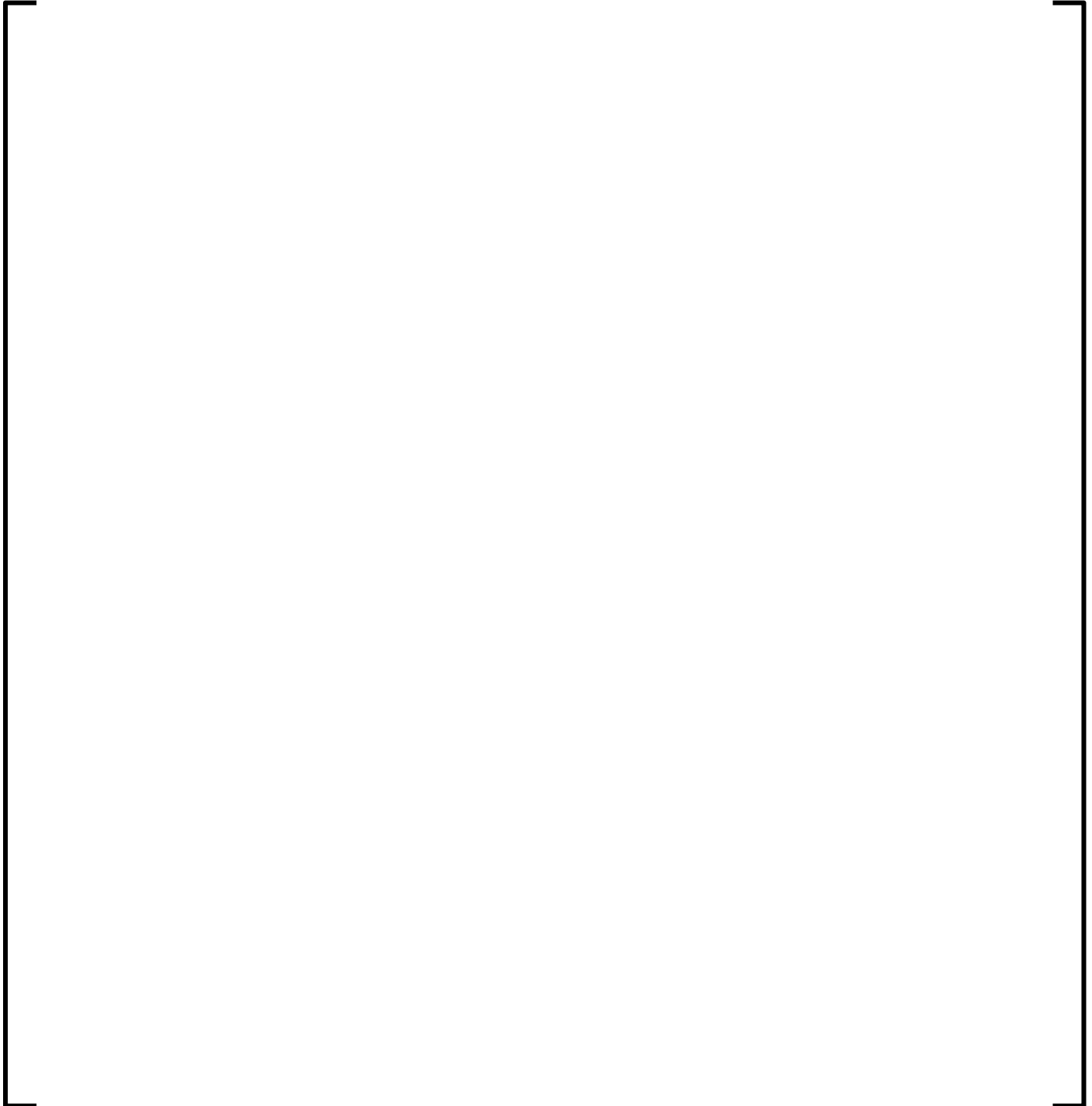


**Figure C 5.3.3-23**  
**Plant C BOC 18 Assembly Average Radial Power Distribution**

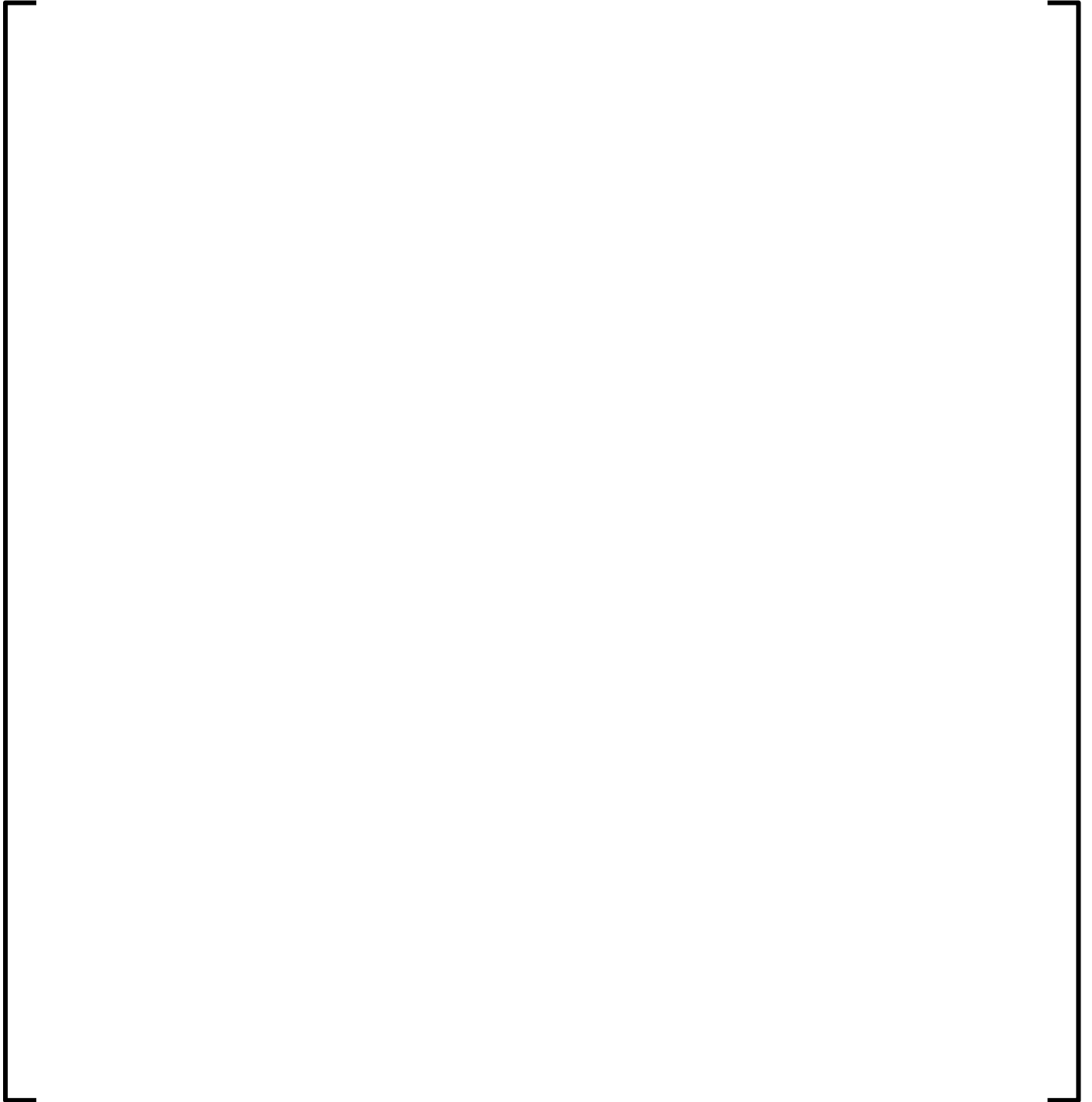


**Figure C 5.3.3-24**  
**Plant C MOC 18 Assembly Average Radial Power Distribution**

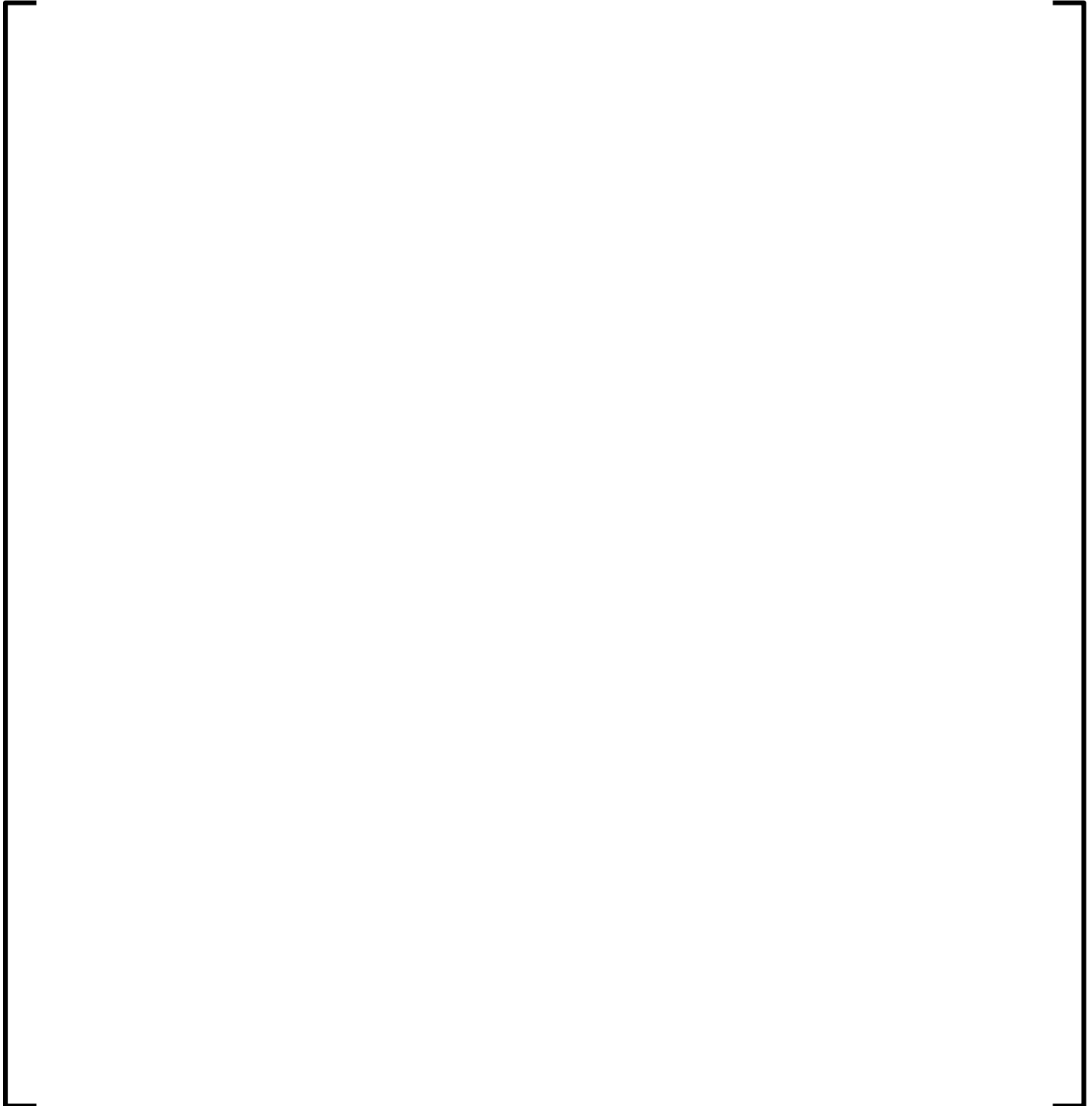


**Figure C 5.3.3-25**  
**Plant C EOC 18 Assembly Average Radial Power Distribution**

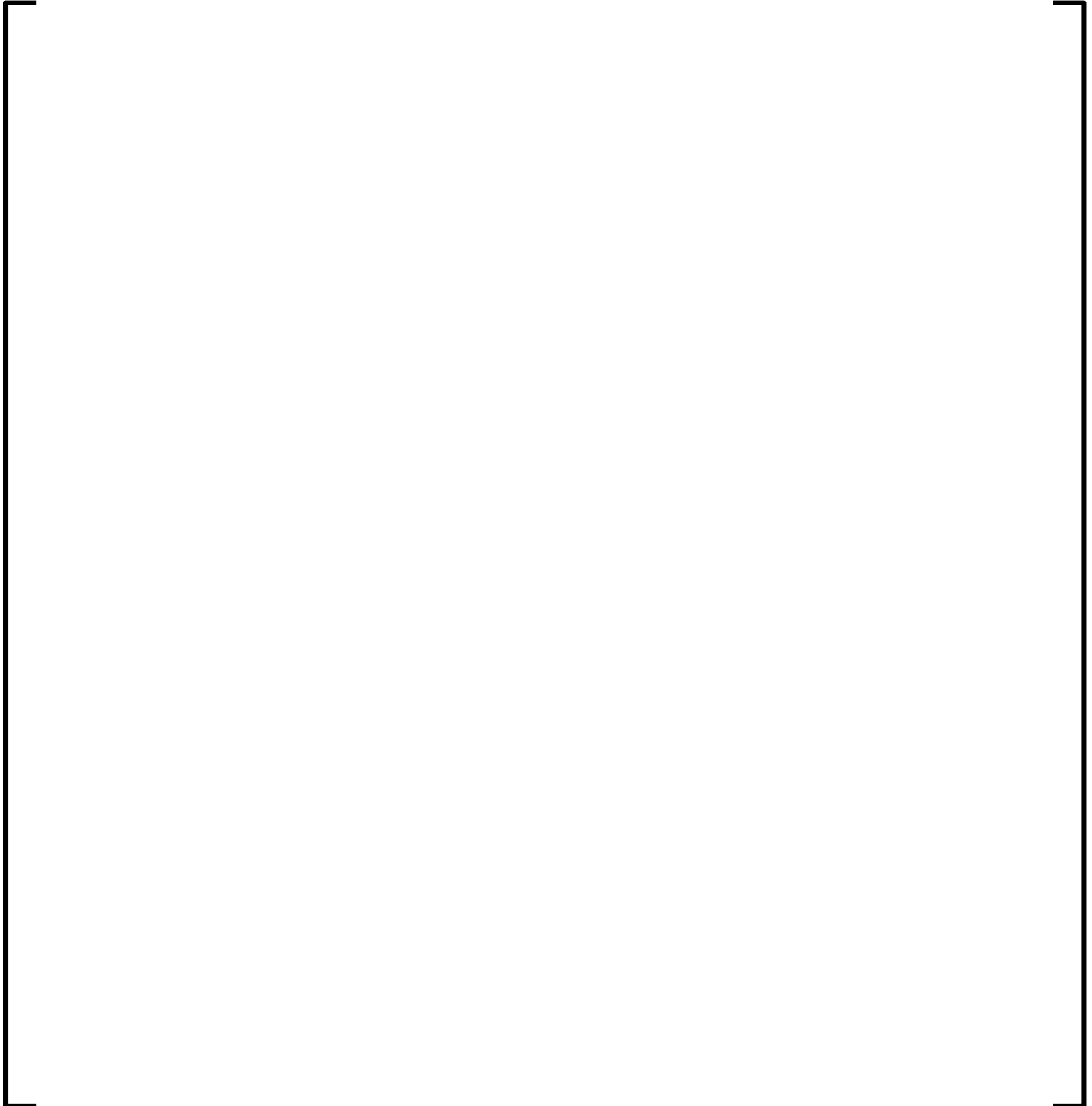




**Figure C 5.3.3-26**  
**Plant C BOC 14 Core Average Axial Power Distribution**



**Figure C 5.3.3-27**  
**Plant C MOC 14 Core Average Axial Power Distribution**



**Figure C 5.3.3-28**  
**Plant C EOC 14 Core Average Axial Power Distribution**



**Figure C 5.3.3-29**  
**Plant C BOC 15 Core Average Axial Power Distribution**



**Figure C 5.3.3-30**  
**Plant C MOC 15 Core Average Axial Power Distribution**



**Figure C 5.3.3-31**  
**Plant C EOC 15 Core Average Axial Power Distribution**



**Figure C 5.3.3-32**  
**Plant C BOC 16 Core Average Axial Power Distribution**



**Figure C 5.3.3-33**  
**Plant C MOC 16 Core Average Axial Power Distribution**

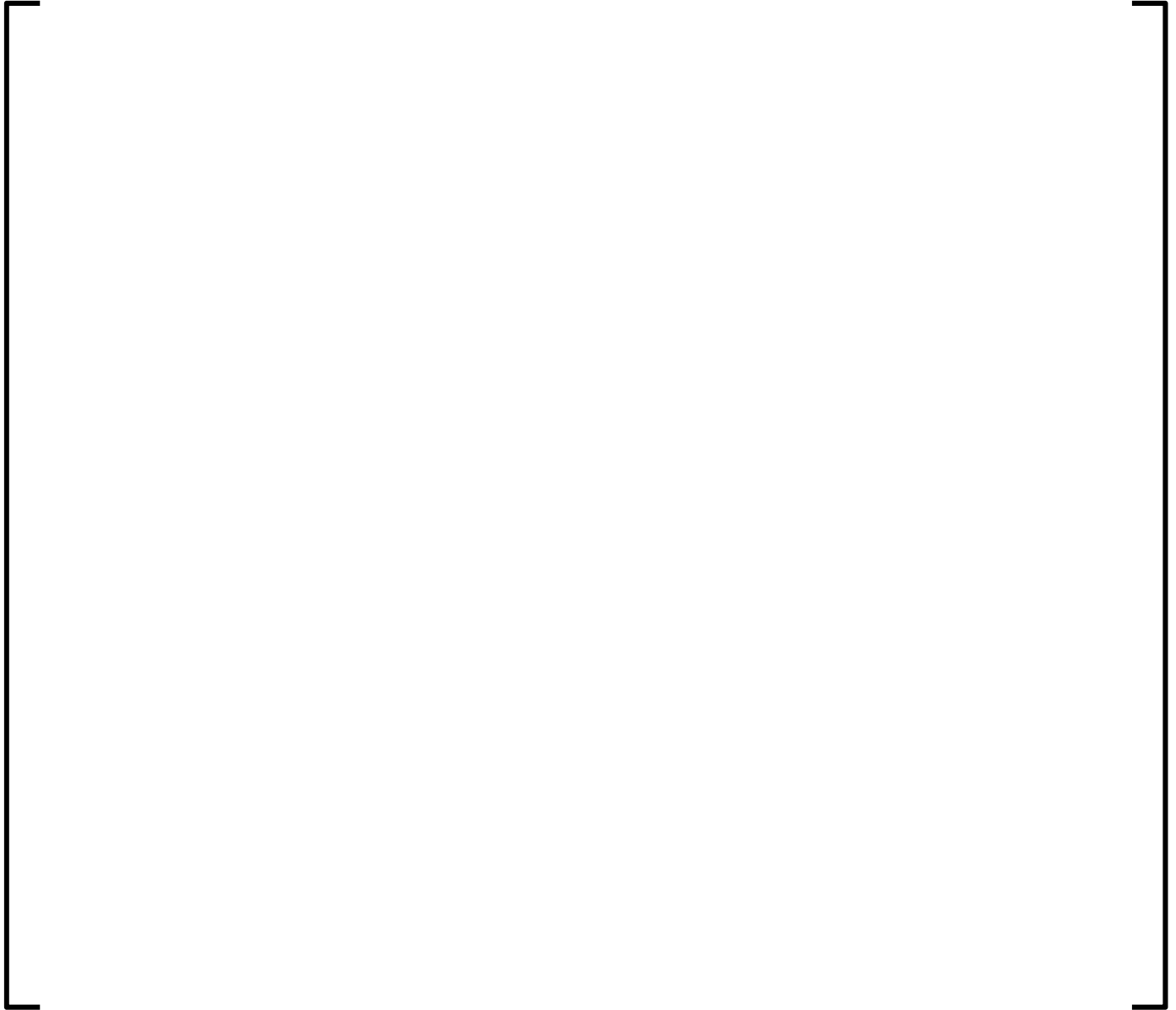




**Figure C 5.3.3-34**  
**Plant C EOC 16 Core Average Axial Power Distribution**



**Figure C 5.3.3-35**  
**Plant C BOC 17 Core Average Axial Power Distribution**



**Figure C 5.3.3-36**  
**Plant C MOC 17 Core Average Axial Power Distribution**



**Figure C 5.3.3-37**  
**Plant C EOC 17 Core Average Axial Power Distribution**



**Figure C 5.3.3-38**  
**Plant C BOC 18 Core Average Axial Power Distribution**



**Figure C 5.3.3-39**  
**Plant C MOC 18 Core Average Axial Power Distribution**



**Figure C 5.3.3-40**  
**Plant C EOC 18 Core Average Axial Power Distribution**



## APPENDIX E

**Table E 5.2.4-1**  
**Plant E Hot Zero Power All Rods Out Critical Boron Concentrations**  
**for Cycles 12-17**

--	--



**Table E 5.2.4-2**  
**Plant E Cycle 12 Hot Zero Power Individual Rod Bank Worth**

--	--

**Table E 5.2.4-3**  
**Plant E Cycle 13 Hot Zero Power Individual Rod Bank Worth**

--	--

**Table E 5.2.4-4**  
**Plant E Cycle 14 Hot Zero Power Individual Rod Bank Worth**

--	--

**Table E 5.2.4-5**  
**Plant E Cycle 15 Hot Zero Power Individual Rod Bank Worth**

--	--

**Table E 5.2.4-6**  
**Plant E Cycle 16 Hot Zero Power Individual Rod Bank Worth**

--	--

**Table E 5.2.4-7**  
**Plant E Cycle 17 Hot Zero Power Individual Rod Bank Worth**

--	--

**Table E 5.2.4-8**  
**Plant E Summary of Total Bank Worths**

--	--

**Table E 5.2.4-9**  
**Plant E Hot Zero Power All Rods Out Isothermal Temperature**  
**Coefficient for Cycles 12-17**

--	--



**Figure E 5.1-1**  
**Plant E Fuel Assembly Guide Tube Configuration**

3	3	3	3	3	3	3	3	3	3	3	3	3	3	3	3	3
3	3	3	3	3	3	3	3	3	3	3	3	3	3	3	3	3
3	3	3	3	3	1	3	3	1	3	3	1	3	3	3	3	3
3	3	3	1	3	3	3	3	3	3	3	3	3	1	3	3	3
3	3	3	3	3	3	3	3	3	3	3	3	3	3	3	3	3
3	3	1	3	3	1	3	3	1	3	3	1	3	3	1	3	3
3	3	3	3	3	3	3	3	3	3	3	3	3	3	3	3	3
3	3	3	3	3	3	3	3	3	3	3	3	3	3	3	3	3
3	3	1	3	3	1	3	3	2	3	3	1	3	3	1	3	3
3	3	3	3	3	3	3	3	3	3	3	3	3	3	3	3	3
3	3	3	3	3	3	3	3	3	3	3	3	3	3	3	3	3
3	3	1	3	3	1	3	3	1	3	3	1	3	3	1	3	3
3	3	3	3	3	3	3	3	3	3	3	3	3	3	3	3	3
3	3	3	1	3	3	3	3	3	3	3	3	3	1	3	3	3
3	3	3	3	3	1	3	3	1	3	3	1	3	3	3	3	3
3	3	3	3	3	3	3	3	3	3	3	3	3	3	3	3	3
3	3	3	3	3	3	3	3	3	3	3	3	3	3	3	3	3



Guide tube



Guide tube with instrument

UO<sub>2</sub> Rod

**Figure E 5.3.4-1**  
**Plant E Cycle 12 Critical Boron Concentration vs. Burnup**

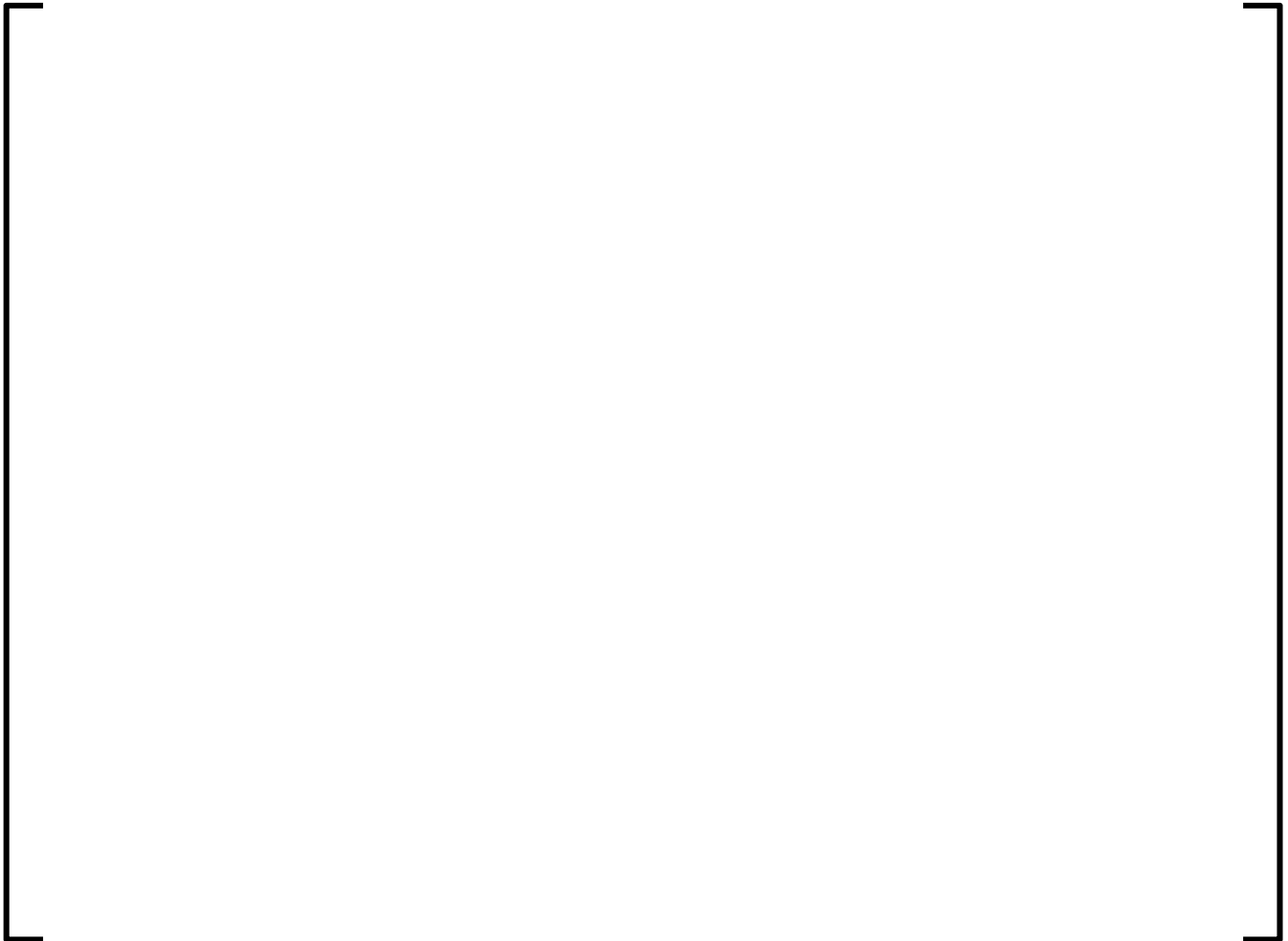


**Figure E 5.3.4-2**  
**Plant E Cycle 13 Critical Boron Concentration vs. Burnup**



**Figure E 5.3.4-3**  
**Plant E Cycle 14 Critical Boron Concentration vs. Burnup**



**Figure E 5.3.4-4**  
**Plant E Cycle 15 Critical Boron Concentration vs. Burnup**



**Figure E 5.3.4-5**  
**Plant E Cycle 16 Critical Boron Concentration vs. Burnup**



**Figure E 5.3.4-6**  
**Plant E Cycle 17 Critical Boron Concentration vs. Burnup**



**Figure E 5.3.4-7**  
**Plant E Cycles 12-17 Boron Differences**





**Figure E 5.3.4-8**  
**Plant E BOC 12 Assembly Average Radial Power Distribution**

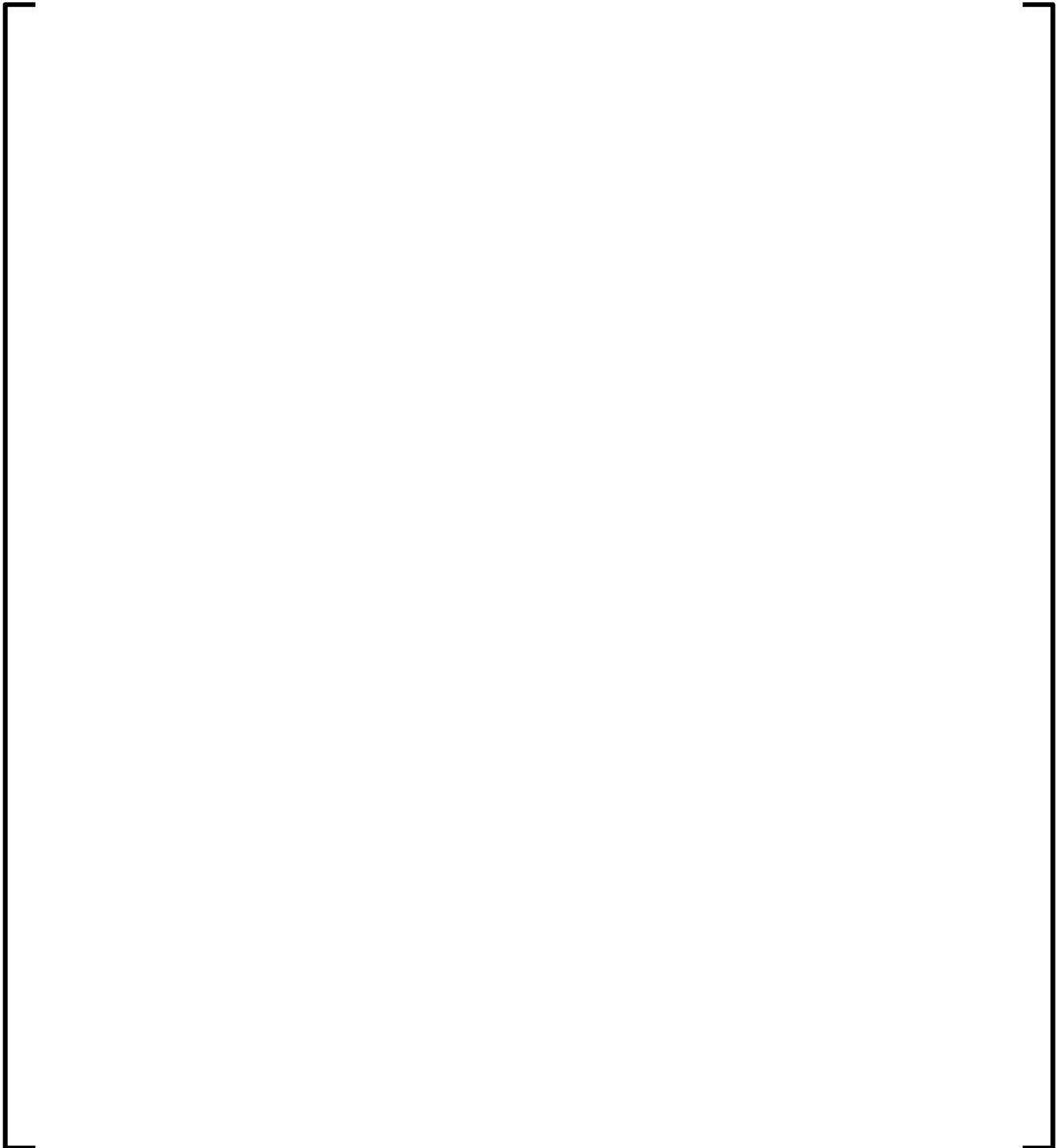


**Figure E 5.3.4-9**  
**Plant E MOC 12 Assembly Average Radial Power Distribution**

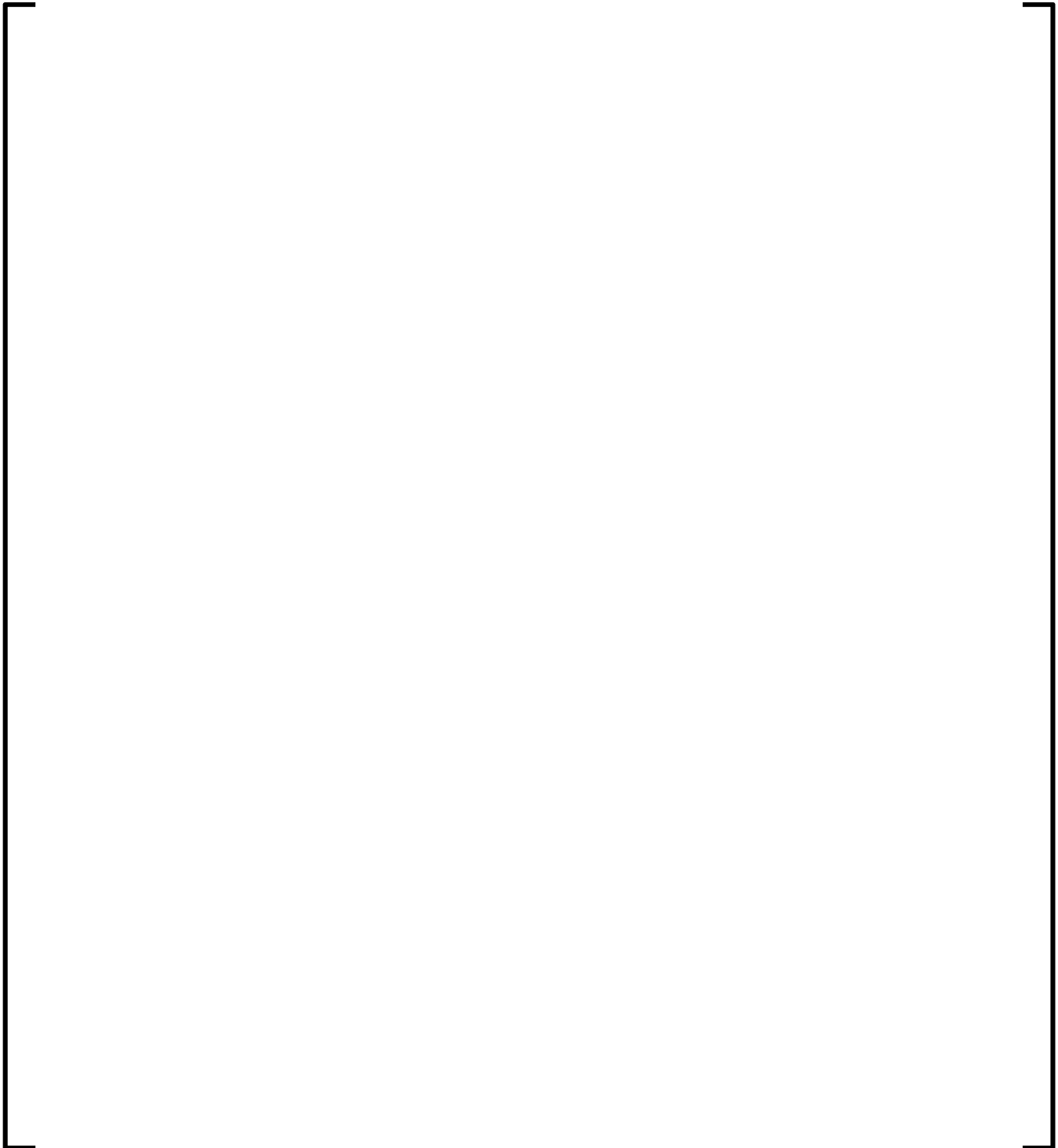


**Figure E 5.3.4-10**  
**Plant E EOC 12 Assembly Average Radial Power Distribution**

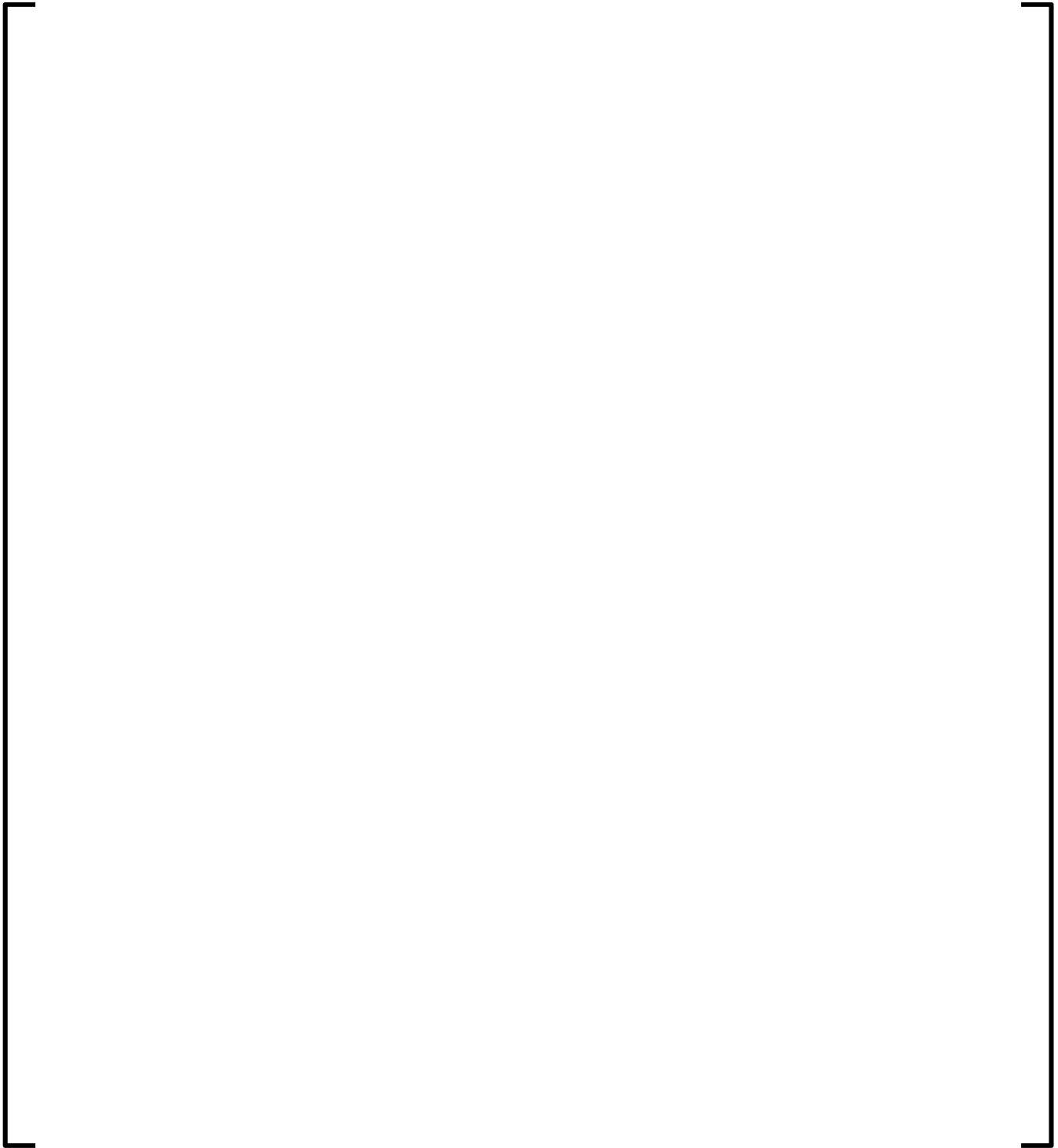


**Figure E 5.3.4-11**  
**Plant E BOC 13 Assembly Average Radial Power Distribution**

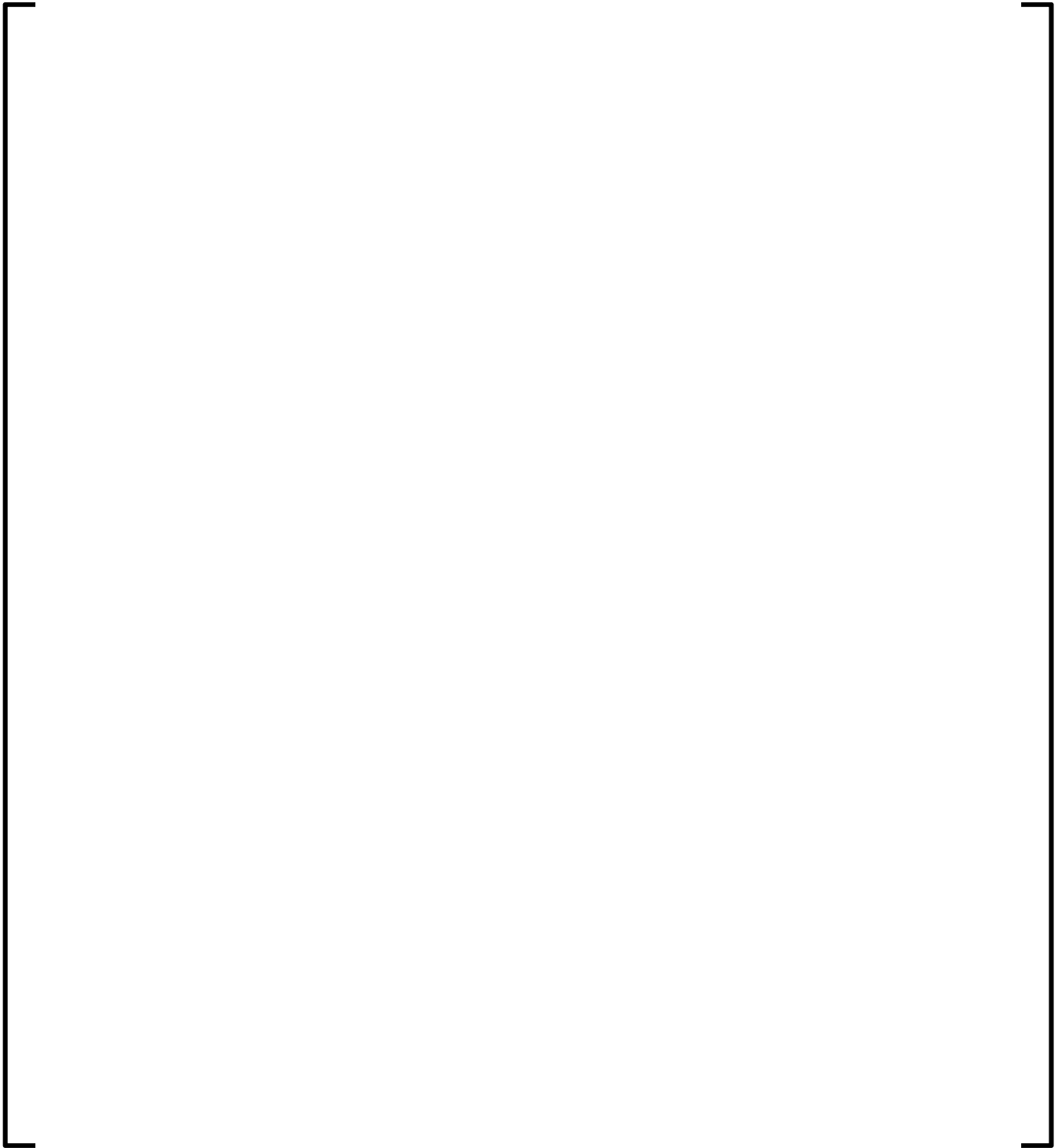


**Figure E 5.3.4-12**  
**Plant E MOC 13 Assembly Average Radial Power Distribution**

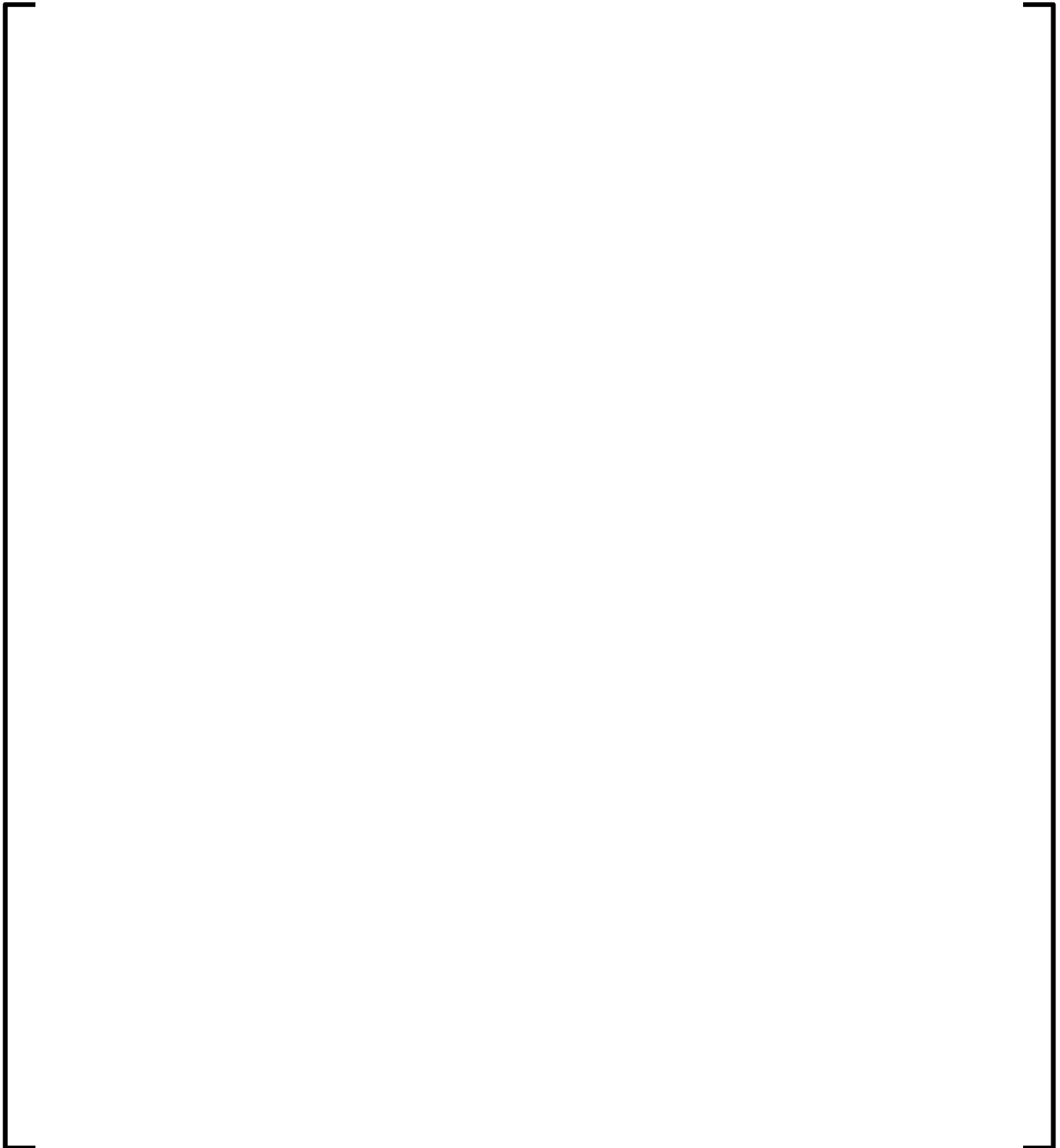


**Figure E 5.3.4-13**  
**Plant E EOC 13 Assembly Average Radial Power Distribution**

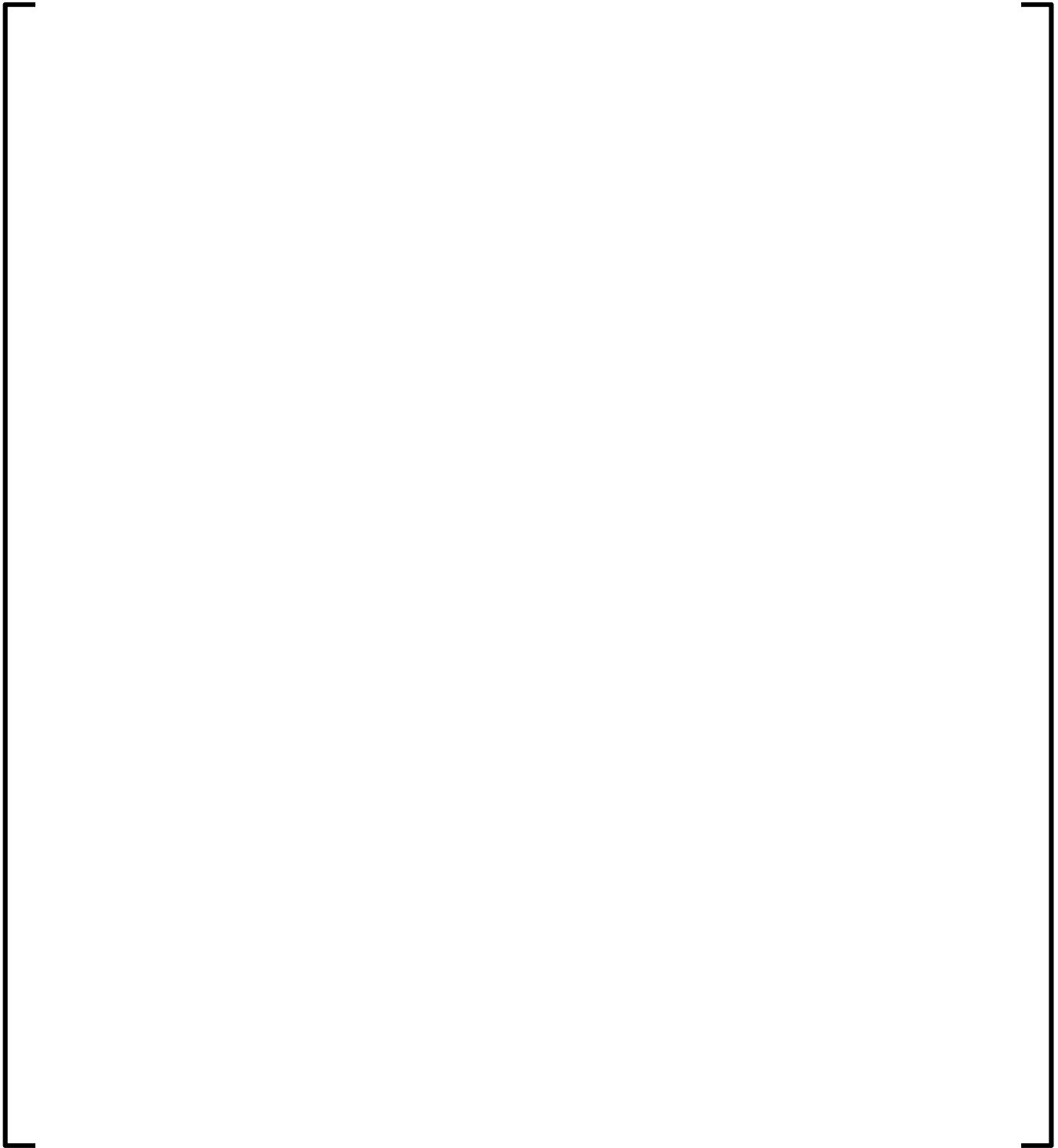


**Figure E 5.3.4-14**  
**Plant E BOC 14 Assembly Average Radial Power Distribution**

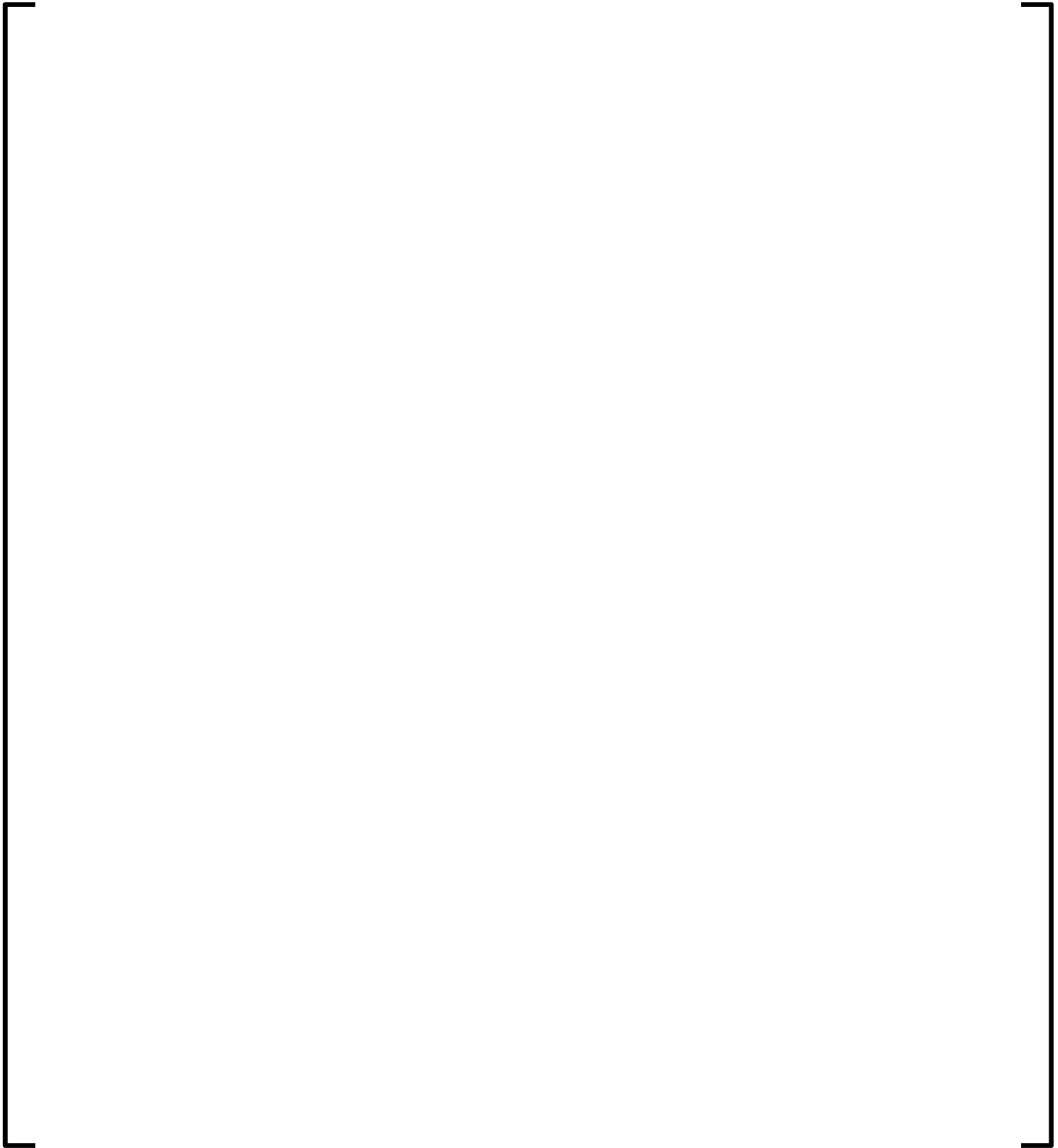


**Figure E 5.3.4-15**  
**Plant E MOC 14 Assembly Average Radial Power Distribution**

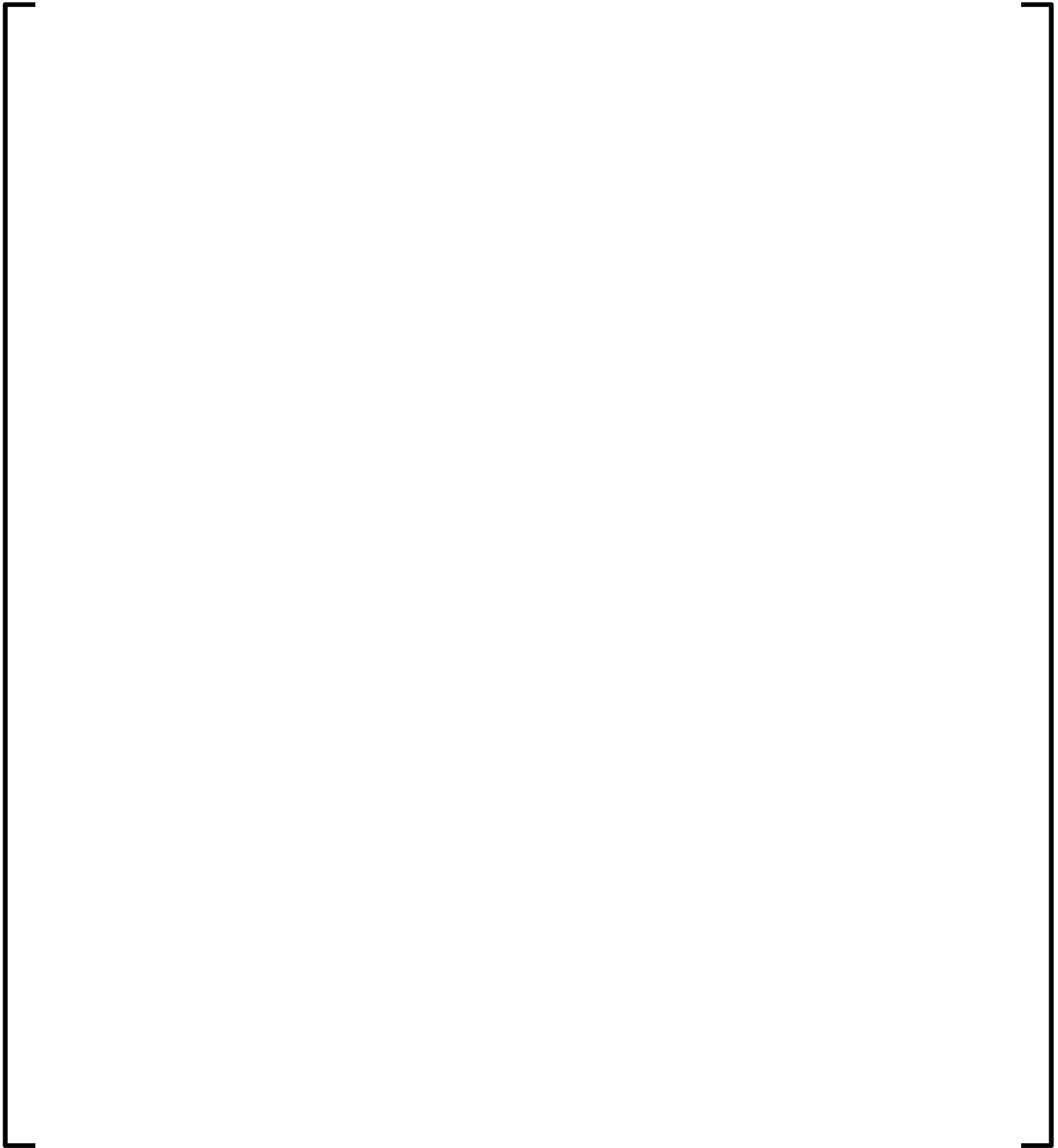




**Figure E 5.3.4-16**  
**Plant E EOC 14 Assembly Average Radial Power Distribution**

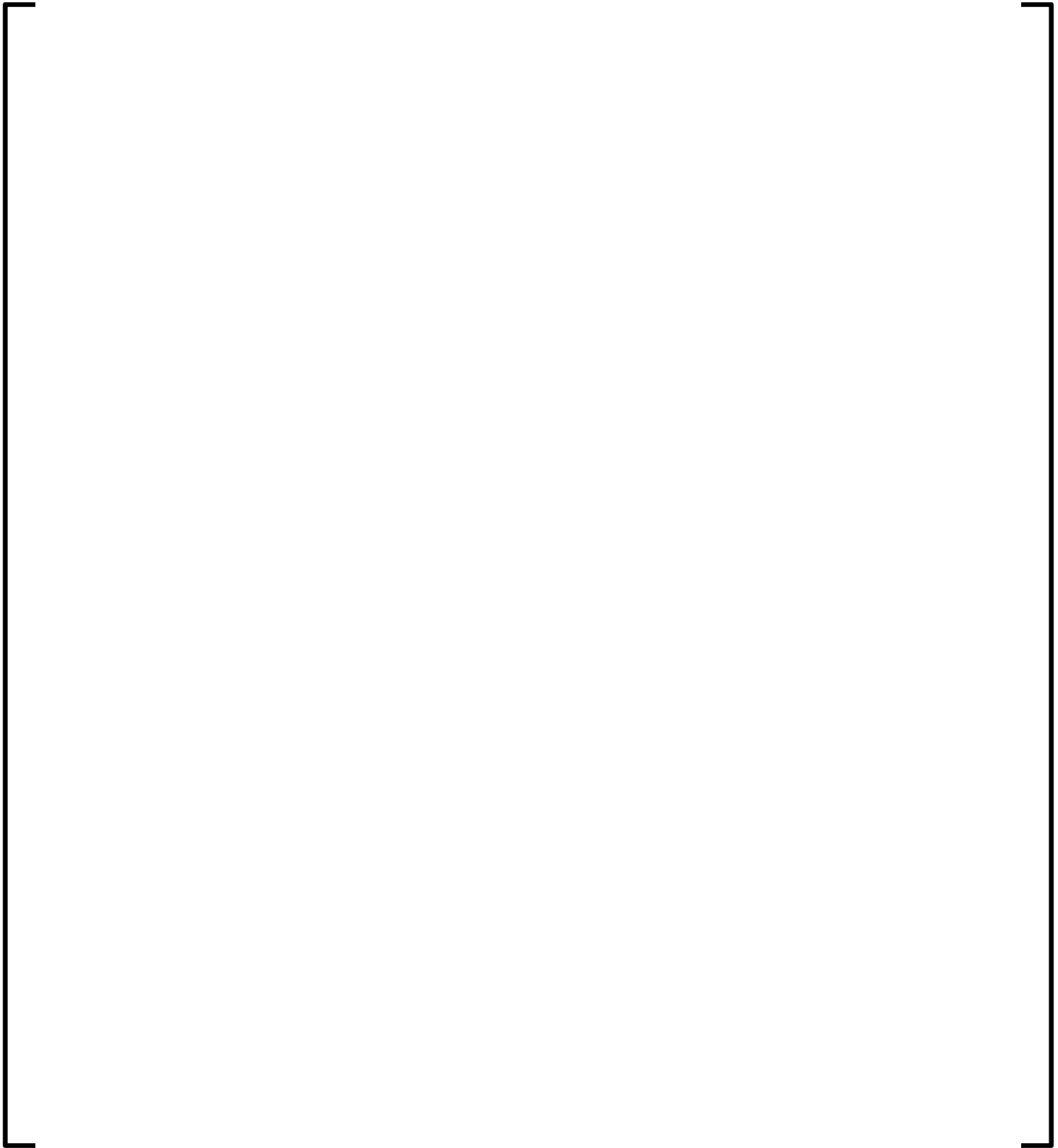


**Figure E 5.3.4-17**  
**Plant E BOC 15 Assembly Average Radial Power Distribution**

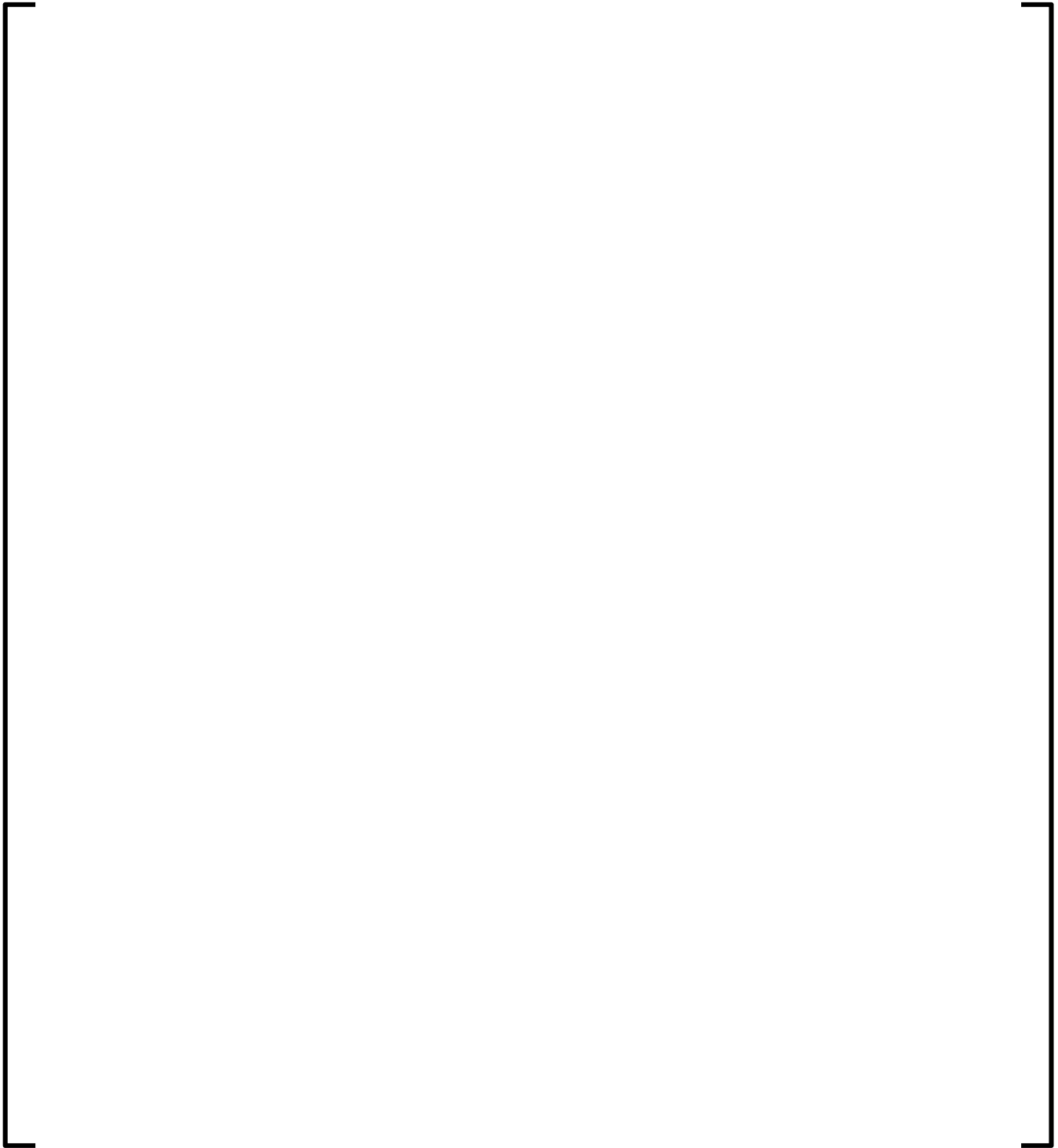


**Figure E 5.3.4-18**  
**Plant E MOC 15 Assembly Average Radial Power Distribution**

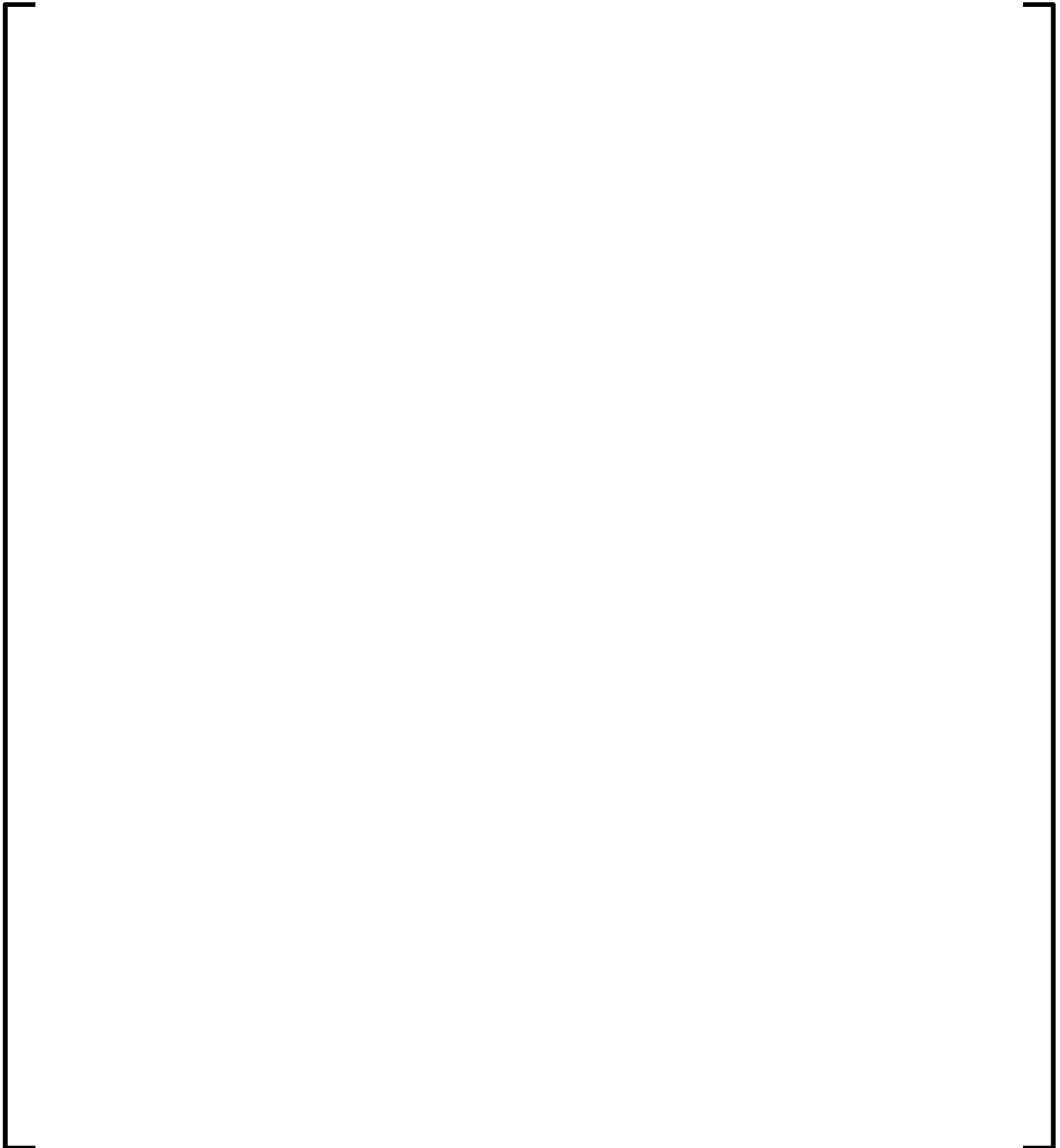


**Figure E 5.3.4-19**  
**Plant E EOC 15 Assembly Average Radial Power Distribution**

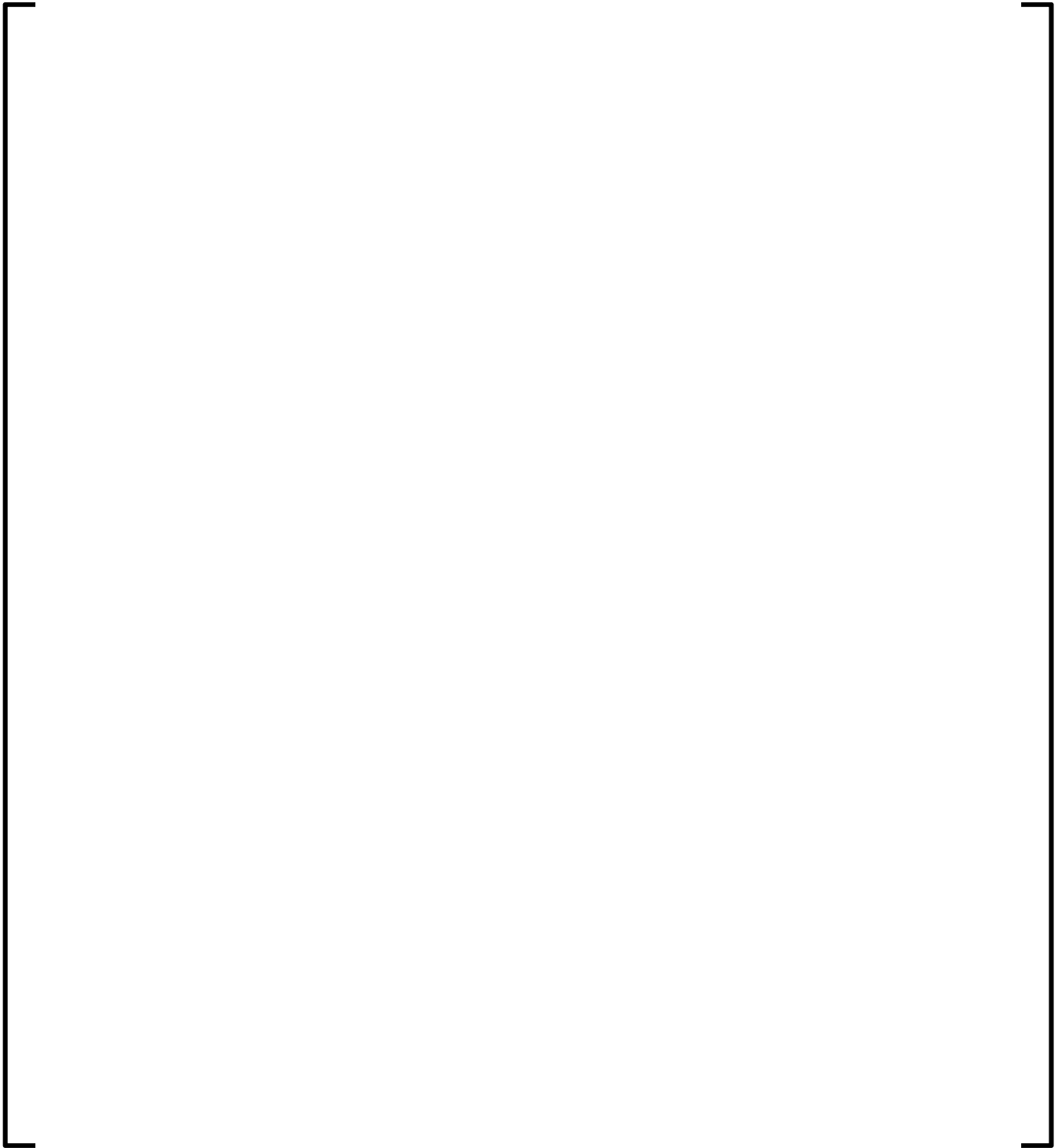


**Figure E 5.3.4-20**  
**Plant E BOC 16 Assembly Average Radial Power Distribution**

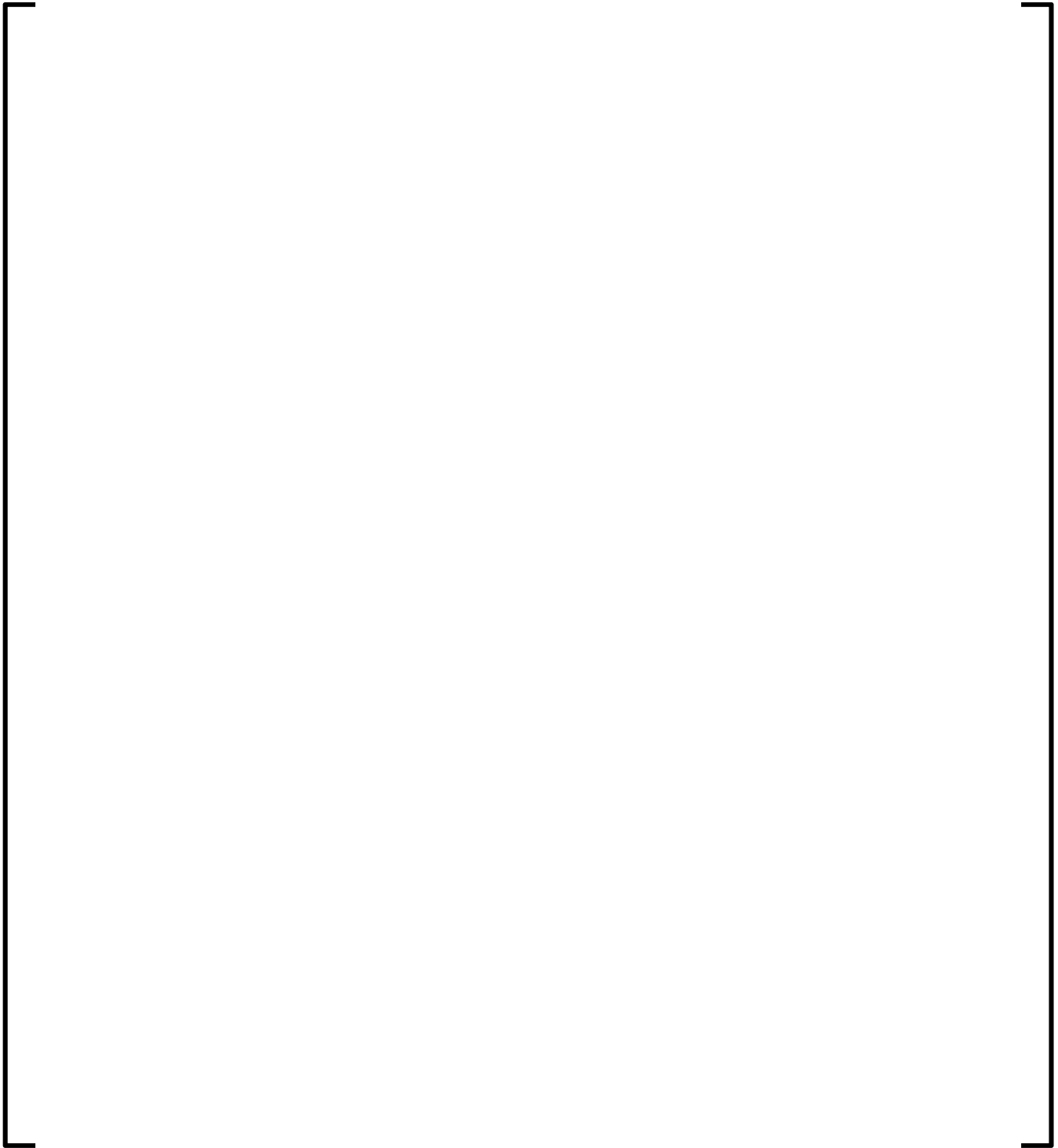


**Figure E 5.3.4-21**  
**Plant E MOC 16 Assembly Average Radial Power Distribution**

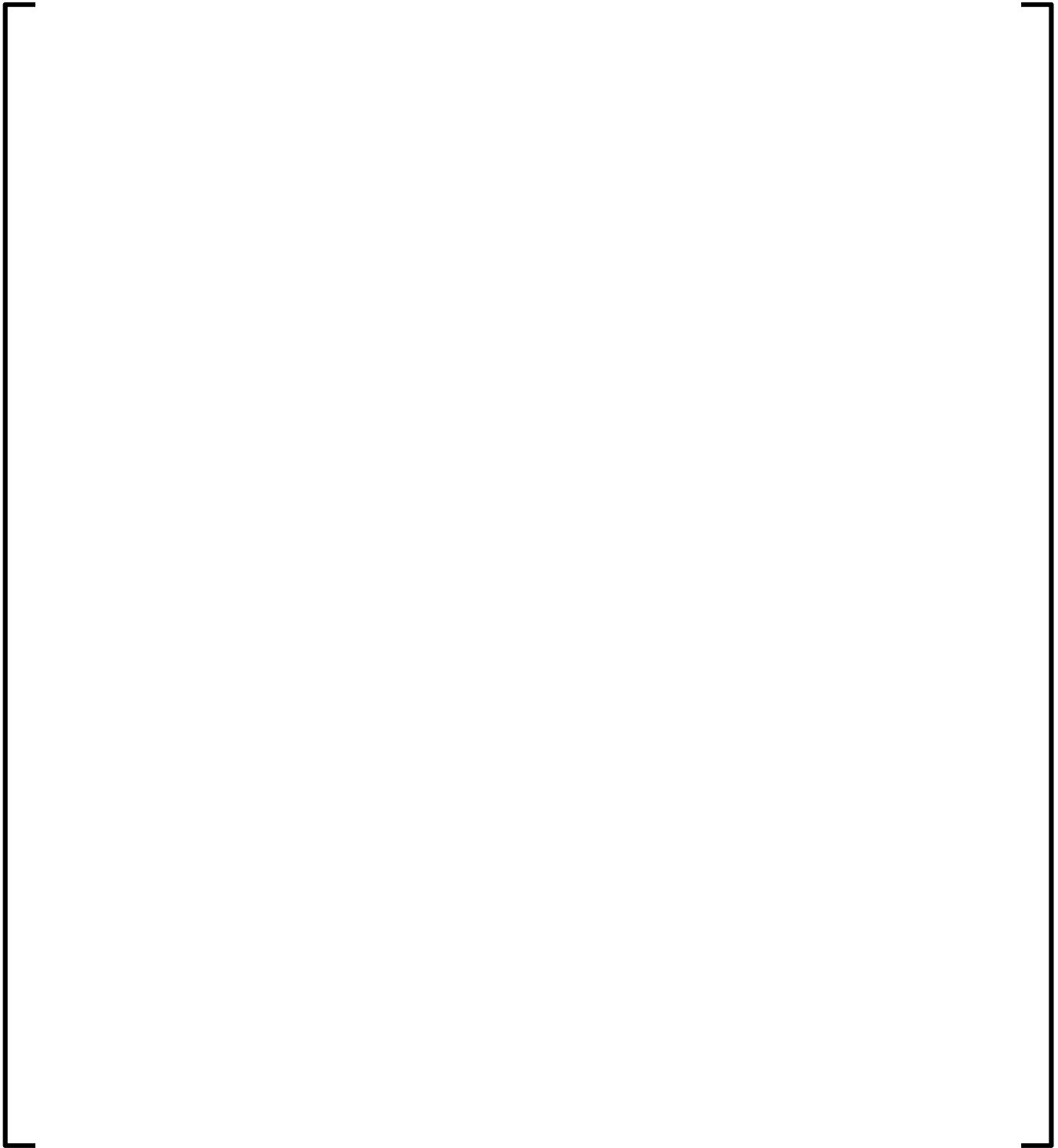


**Figure E 5.3.4-22**  
**Plant E EOC 16 Assembly Average Radial Power Distribution**

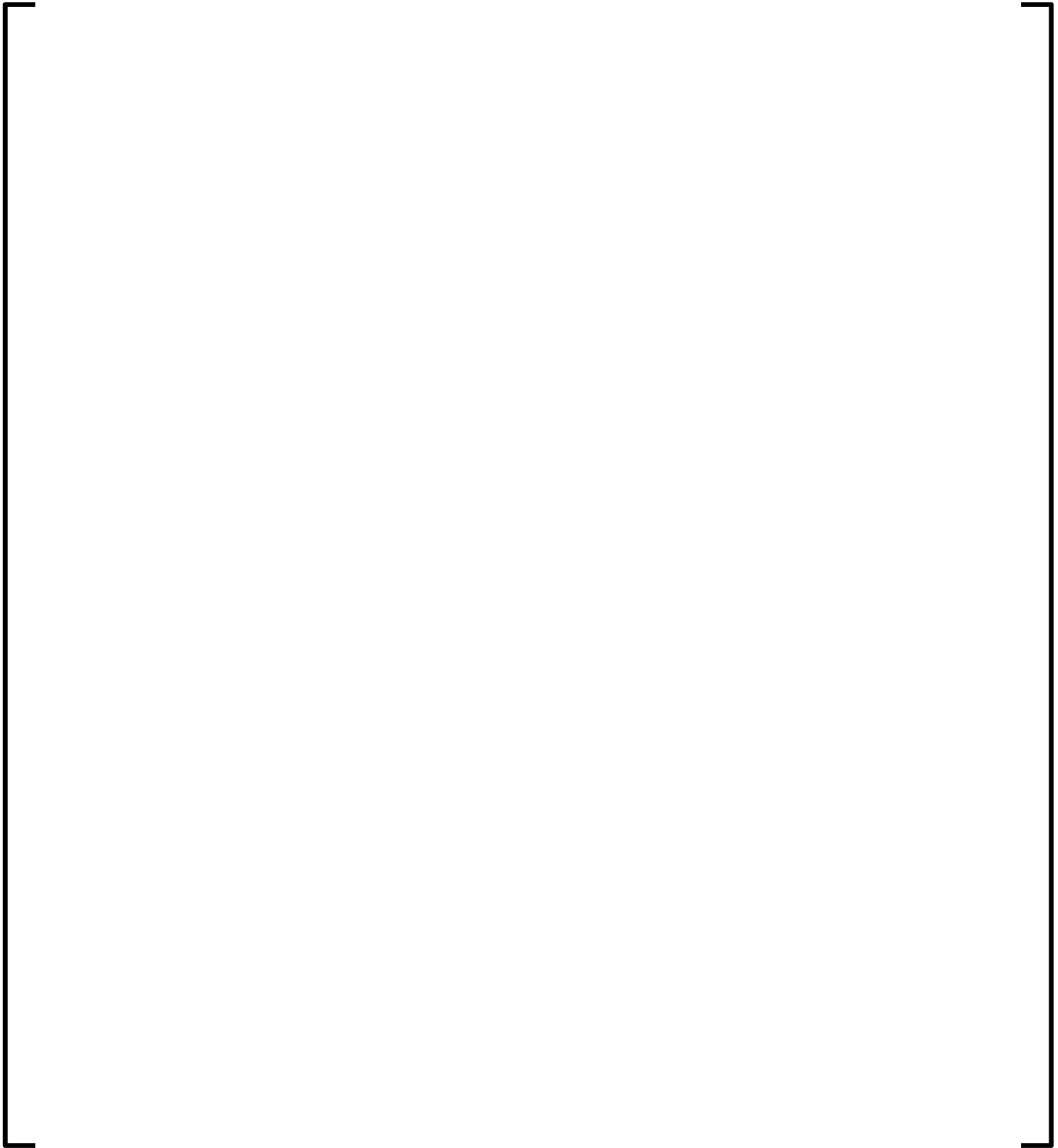


**Figure E 5.3.4-23**  
**Plant E BOC 17 Assembly Average Radial Power Distribution**

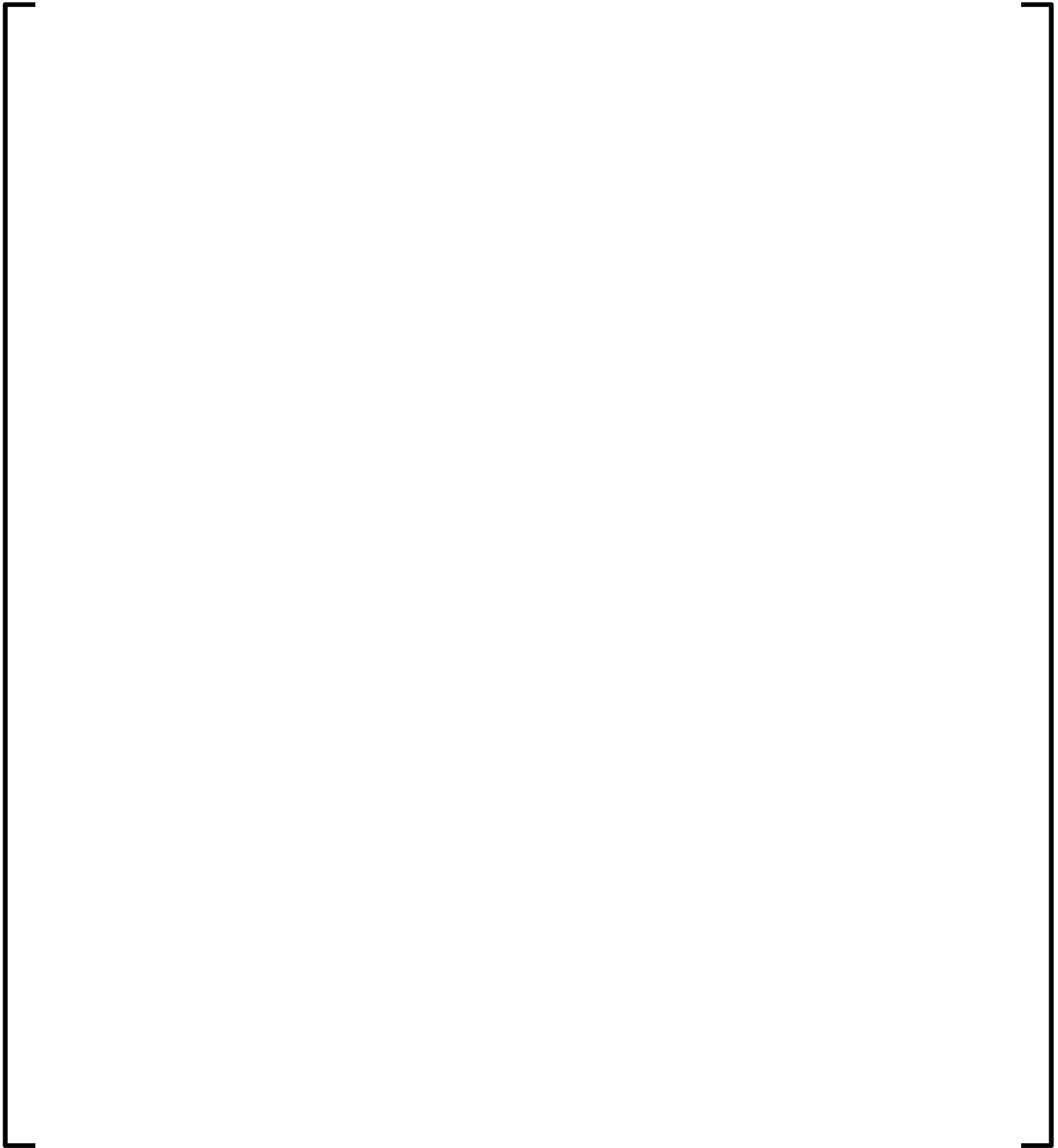




**Figure E 5.3.4-24**  
**Plant E MOC 17 Assembly Average Radial Power Distribution**

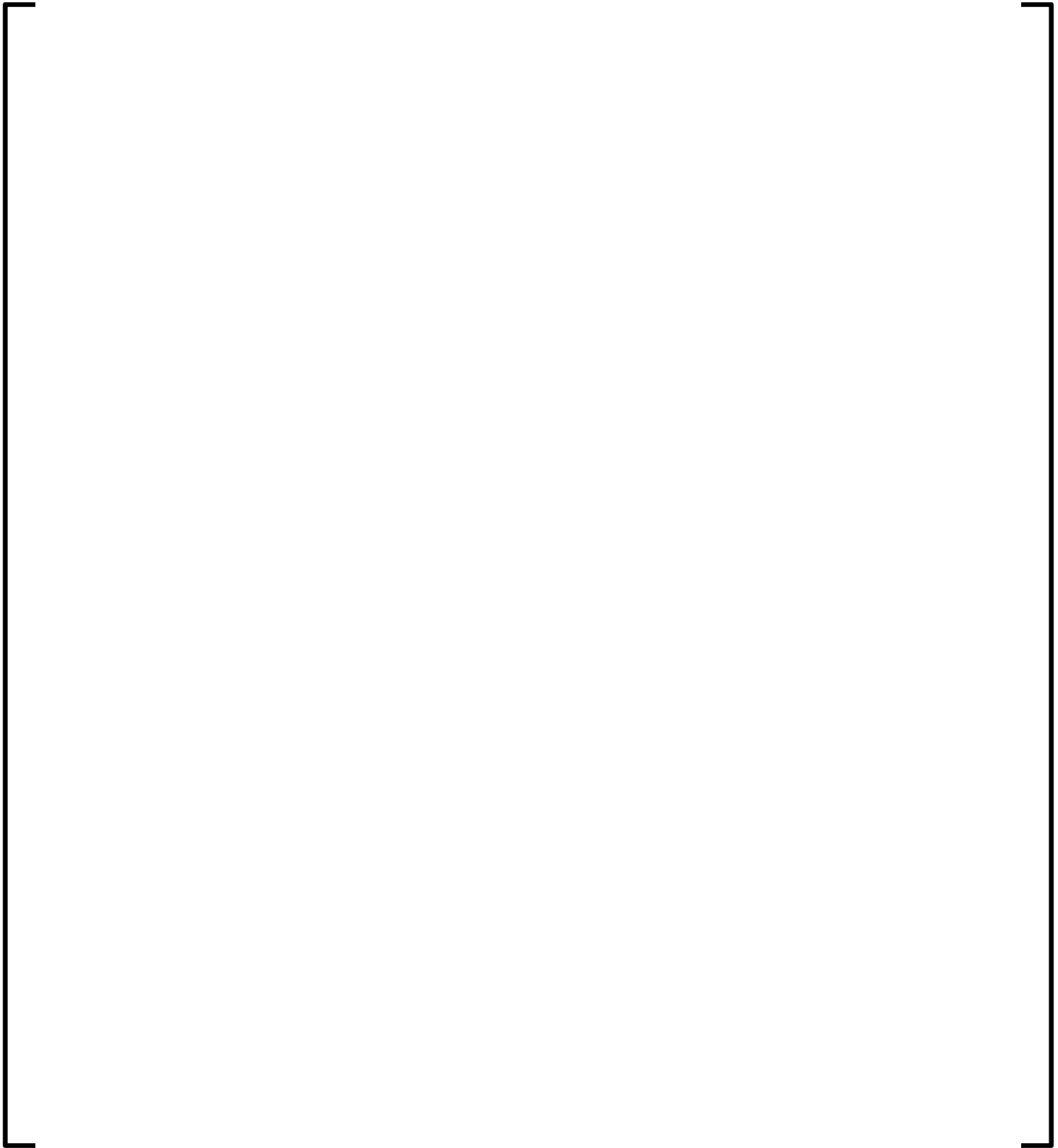


**Figure E 5.3.4-25**  
**Plant E EOC 17 Assembly Average Radial Power Distribution**

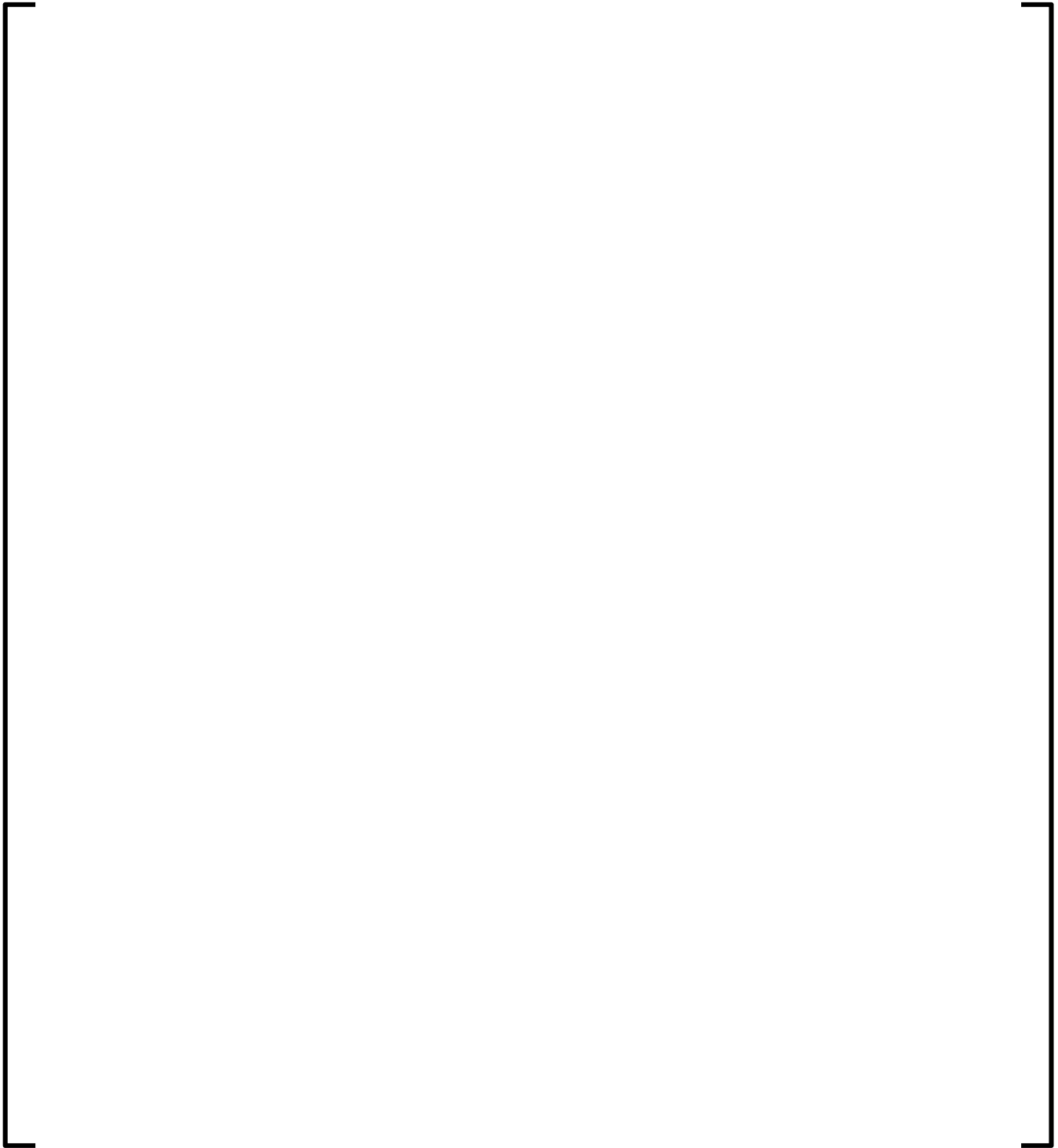


**Figure E 5.3.4-26**  
**Plant E BOC 12 Core Average Axial Power Distribution**



**Figure E 5.3.4-27**  
**Plant E MOC 12 Core Average Axial Power Distribution**



**Figure E 5.3.4-28**  
**Plant E EOC 12 Core Average Axial Power Distribution**



**Figure E 5.3.4-29**  
**Plant E BOC 13 Core Average Axial Power Distribution**



**Figure E 5.3.4-30**  
**Plant E MOC 13 Core Average Axial Power Distribution**



**Figure E 5.3.4-31**  
**Plant E EOC 13 Core Average Axial Power Distribution**





**Figure E 5.3.4-32**  
**Plant E BOC 14 Core Average Axial Power Distribution**



**Figure E 5.3.4-33**  
**Plant E MOC 14 Core Average Axial Power Distribution**



**Figure E 5.3.4-34**  
**Plant E EOC 14 Core Average Axial Power Distribution**



**Figure E 5.3.4-35**  
**Plant E BOC 15 Core Average Axial Power Distribution**



**Figure E 5.3.4-36**  
**Plant E MOC 15 Core Average Axial Power Distribution**



**Figure E 5.3.4-37**  
**Plant E EOC 15 Core Average Axial Power Distribution**



**Figure E 5.3.4-38**  
**Plant E BOC 16 Core Average Axial Power Distribution**



**Figure E 5.3.4-39**  
**Plant E MOC 16 Core Average Axial Power Distribution**





**Figure E 5.3.4-40**  
**Plant E EOC 16 Core Average Axial Power Distribution**



**Figure E 5.3.4-41**  
**Plant E BOC 17 Core Average Axial Power Distribution**



**Figure E 5.3.4-42**  
**Plant E MOC 17 Core Average Axial Power Distribution**



**Figure E 5.3.4-43**  
**Plant E EOC 17 Core Average Axial Power Distribution**



## APPENDIX G1

**Table G1 5.2.5-1**  
**Plant G1 Hot Zero Power All Rods Out Critical Boron Concentrations**  
**for Cycles 26-30**

--	--

**Figure G1 5.3.5-1**  
**Plant G1 Cycle 26 Critical Boron Concentration vs. Burnup**



**Figure G1 5.3.5-2**  
**Plant G1 Cycle 27 Critical Boron Concentration vs. Burnup**



**Figure G1 5.3.5-3**  
**Plant G1 Cycle 28 Critical Boron Concentration vs. Burnup**





**Figure G1 5.3.5-4**  
**Plant G1 Cycle 29 Critical Boron Concentration vs. Burnup**



**Figure G1 5.3.5-5**  
**Plant G1 Cycle 30 Critical Boron Concentration vs. Burnup**



**Figure G1 5.3.5-6**  
**Plant G1 Cycles 26-30 Boron Differences**



**Figure G1 5.3.5-7**  
**Plant G1 BOC 26 Assembly Average Radial Power Distribution**

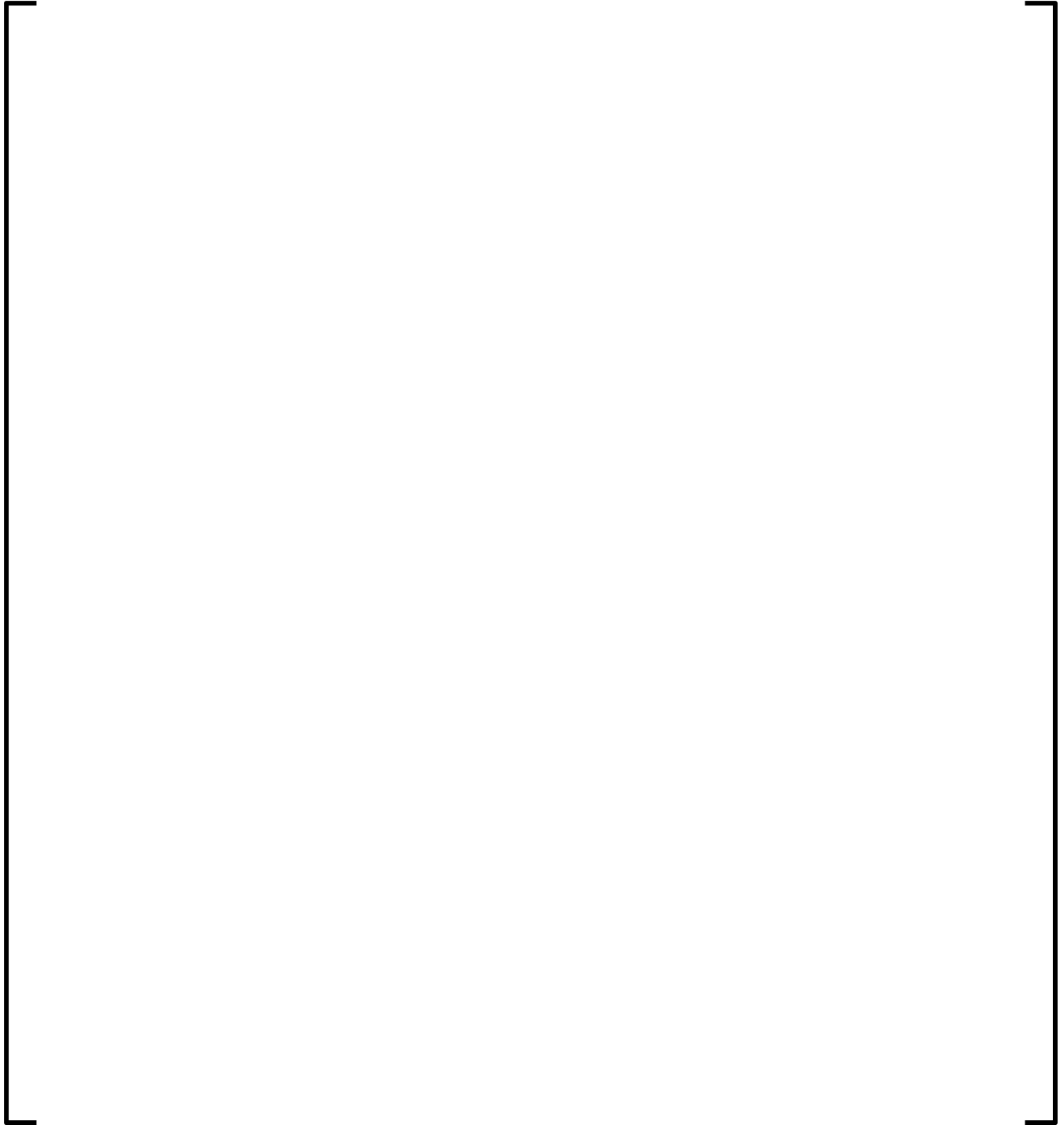


**Figure G1 5.3.5-8**  
**Plant G1 MOC 26 Assembly Average Radial Power Distribution**

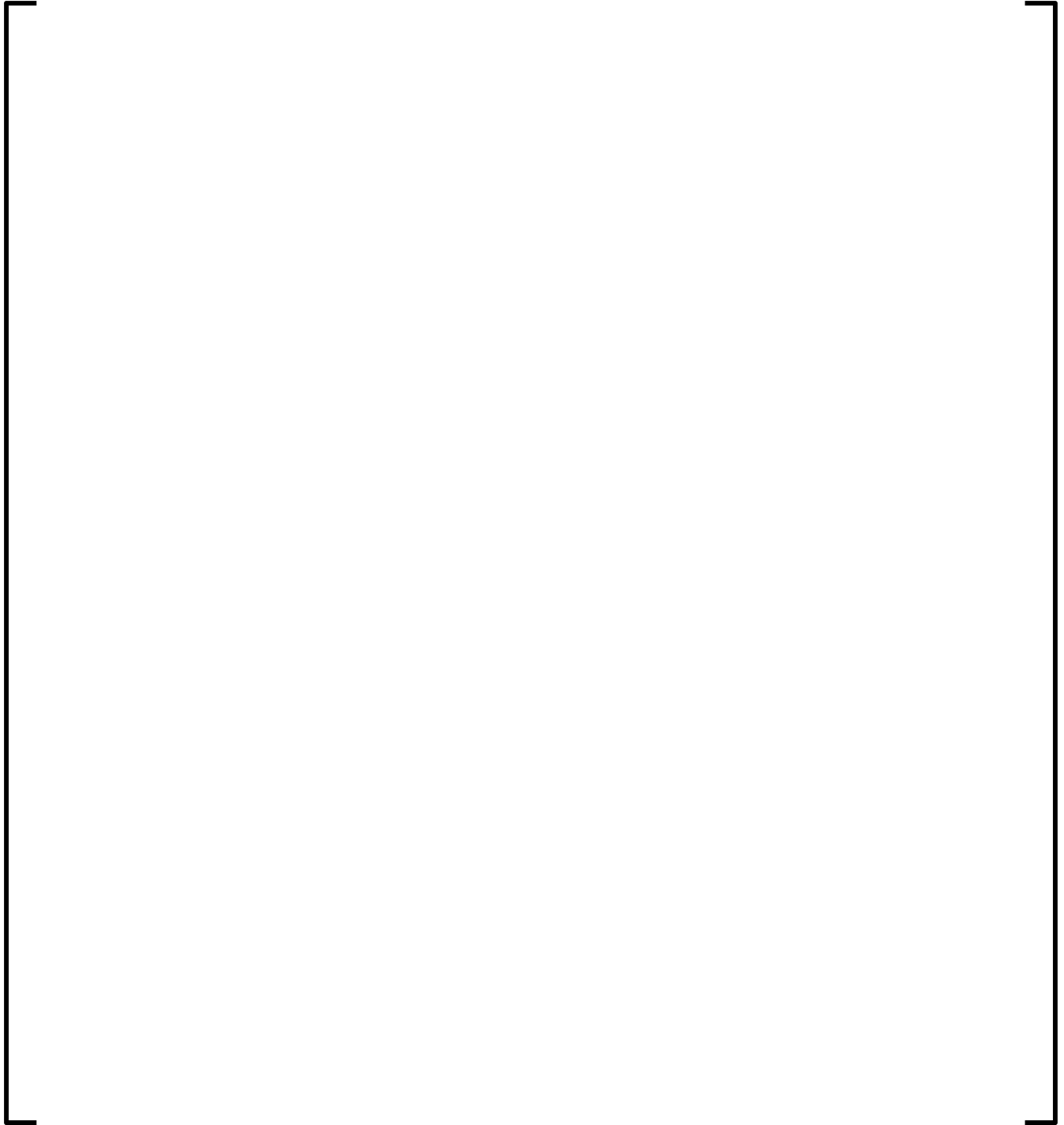


**Figure G1 5.3.5-9**  
**Plant G1 EOC 26 Assembly Average Radial Power Distribution**

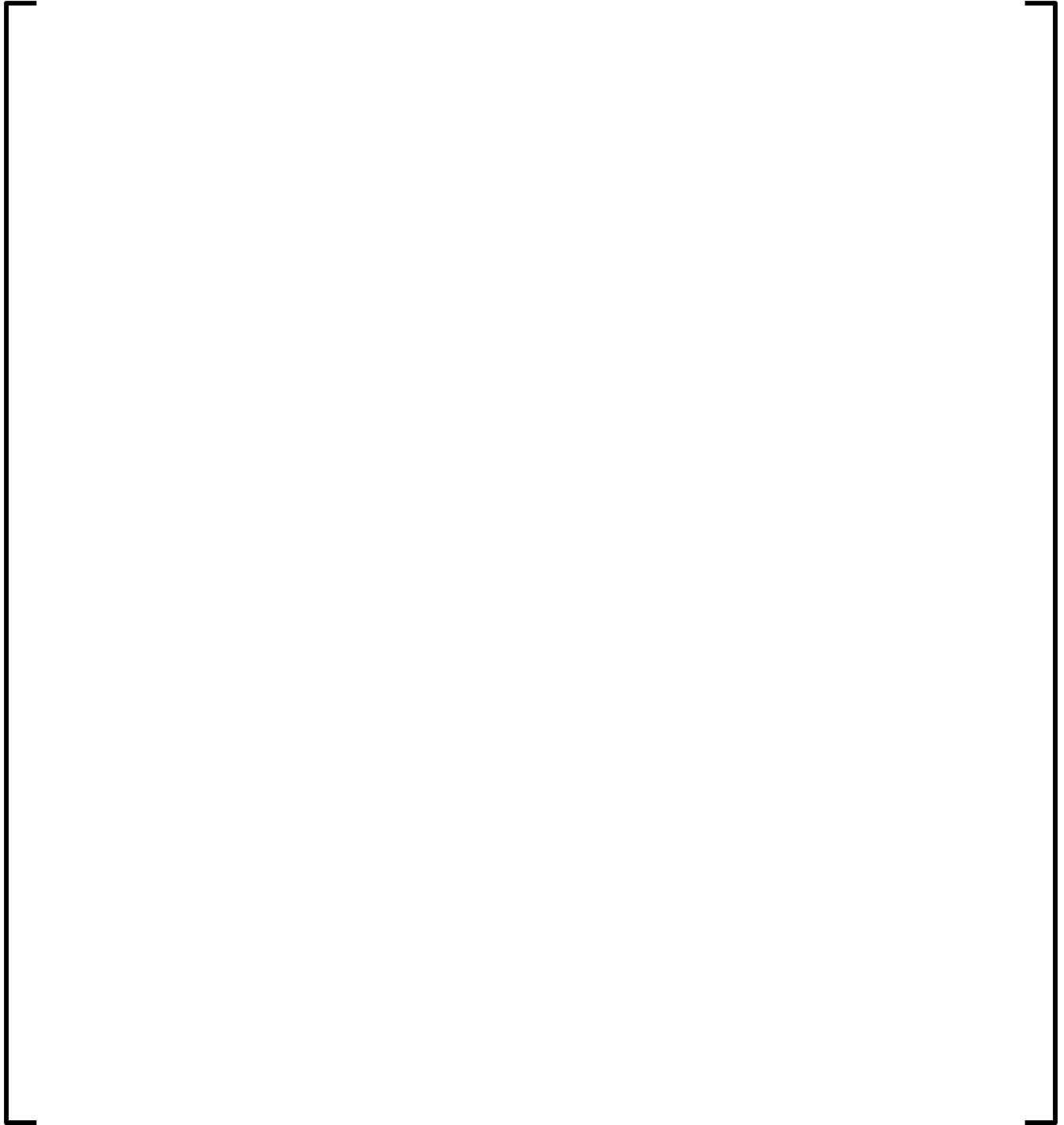


**Figure G1 5.3.5-10**  
**Plant G1 BOC 27 Assembly Average Radial Power Distribution**

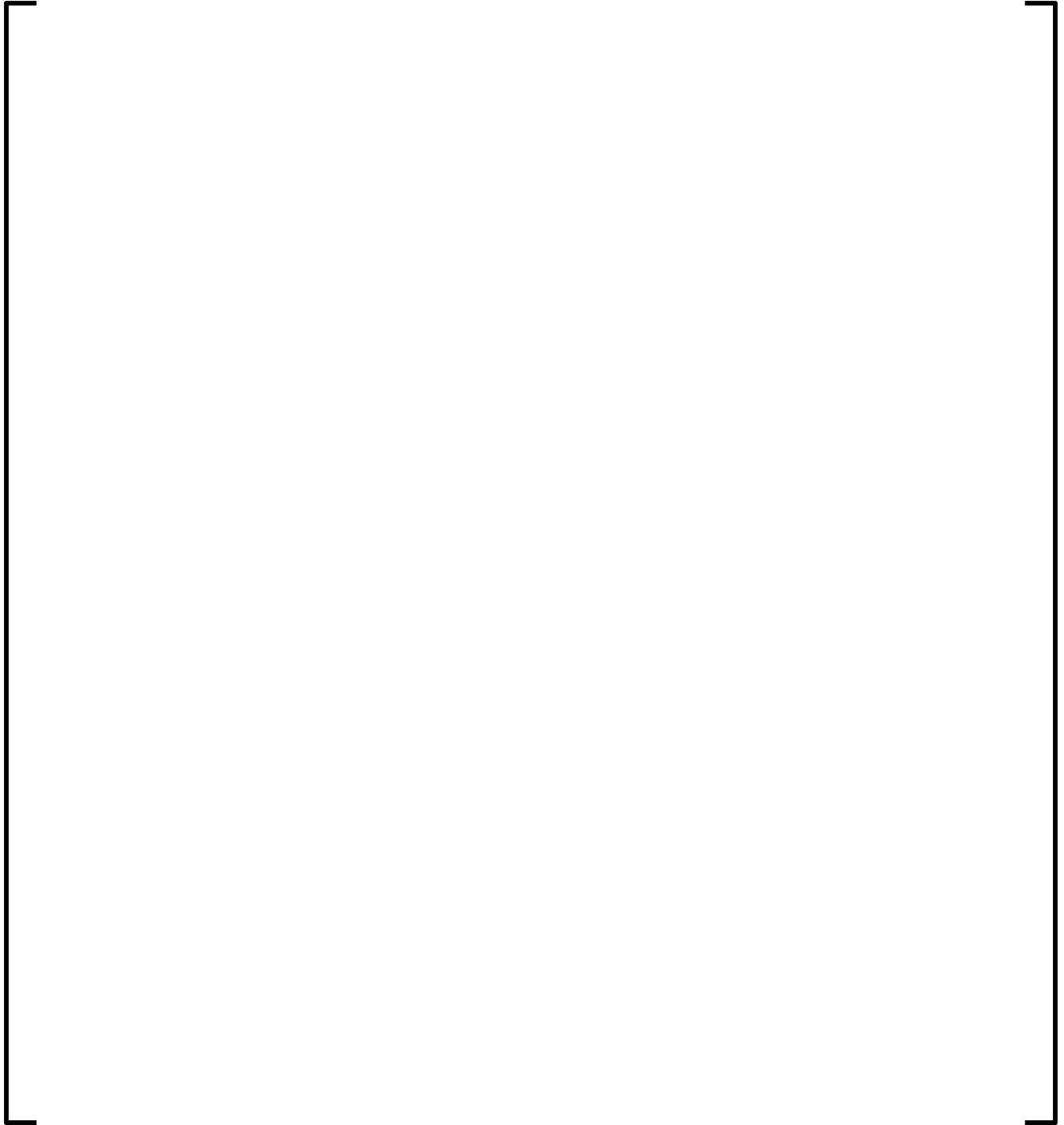


**Figure G1 5.3.5-11**  
**Plant G1 MOC 27 Assembly Average Radial Power Distribution**

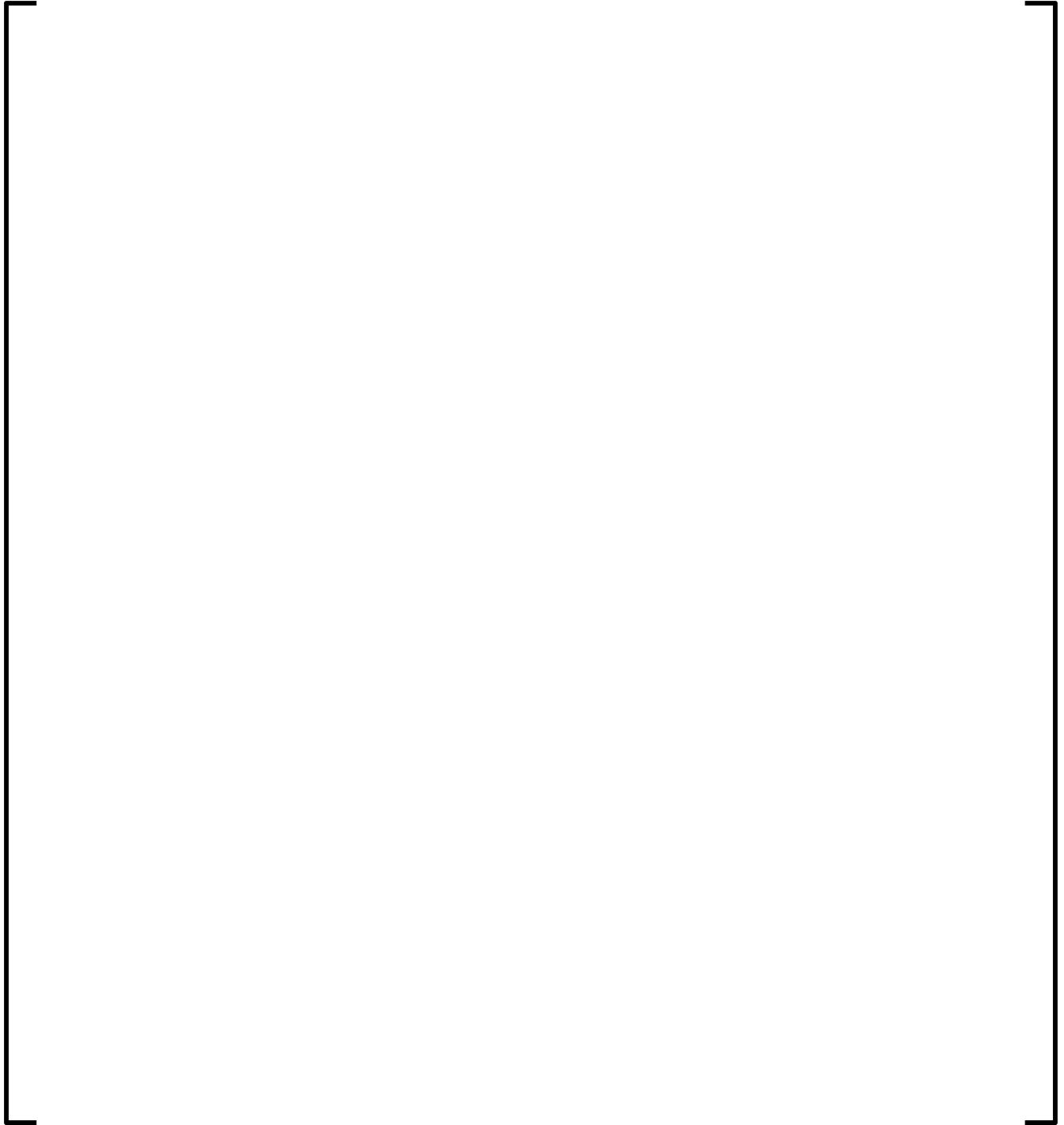




**Figure G1 5.3.5-12**  
**Plant G1 EOC 27 Assembly Average Radial Power Distribution**

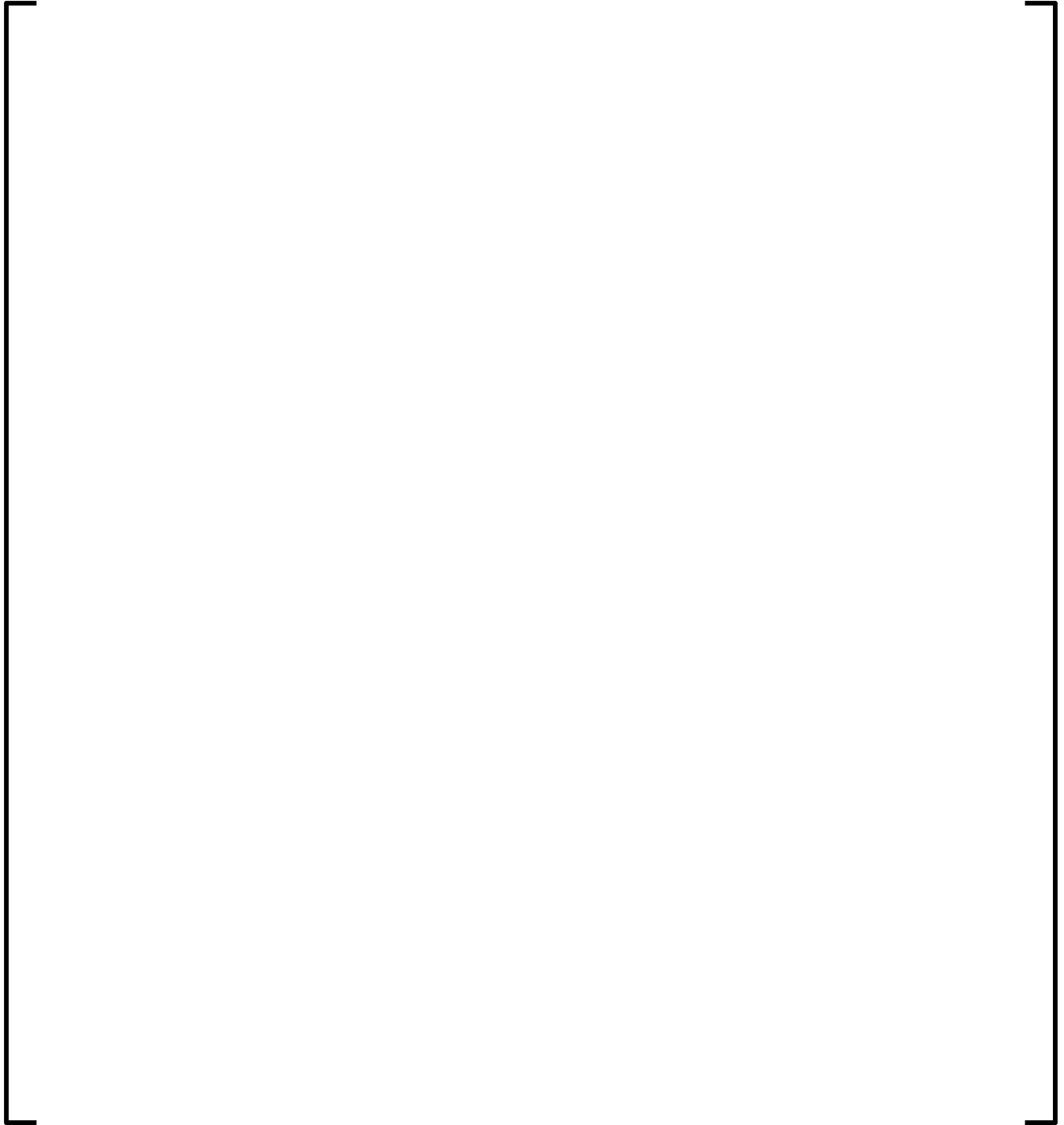


**Figure G1 5.3.5-13**  
**Plant G1 BOC 28 Assembly Average Radial Power Distribution**

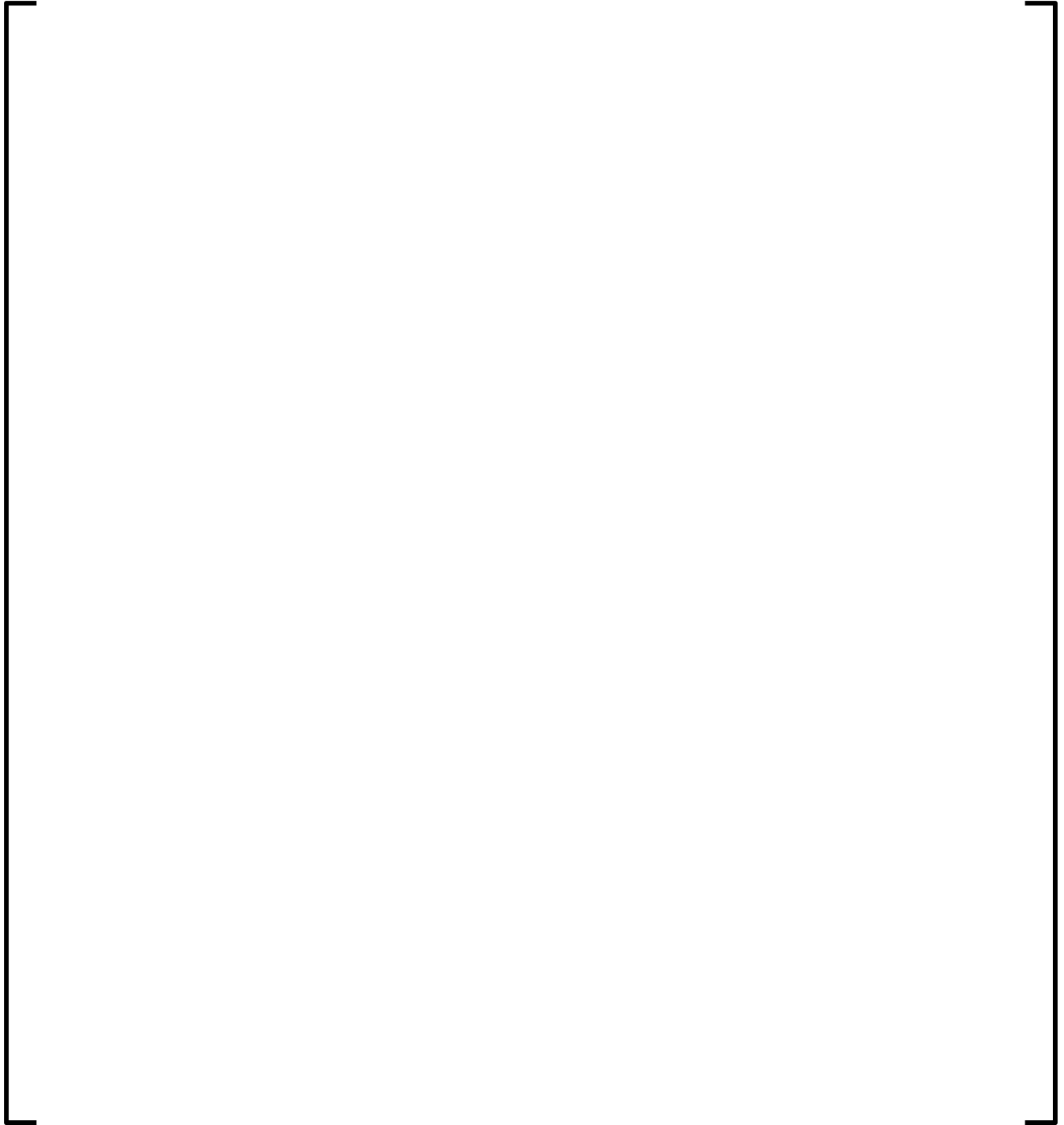


**Figure G1 5.3.5-14**  
**Plant G1 MOC 28 Assembly Average Radial Power Distribution**

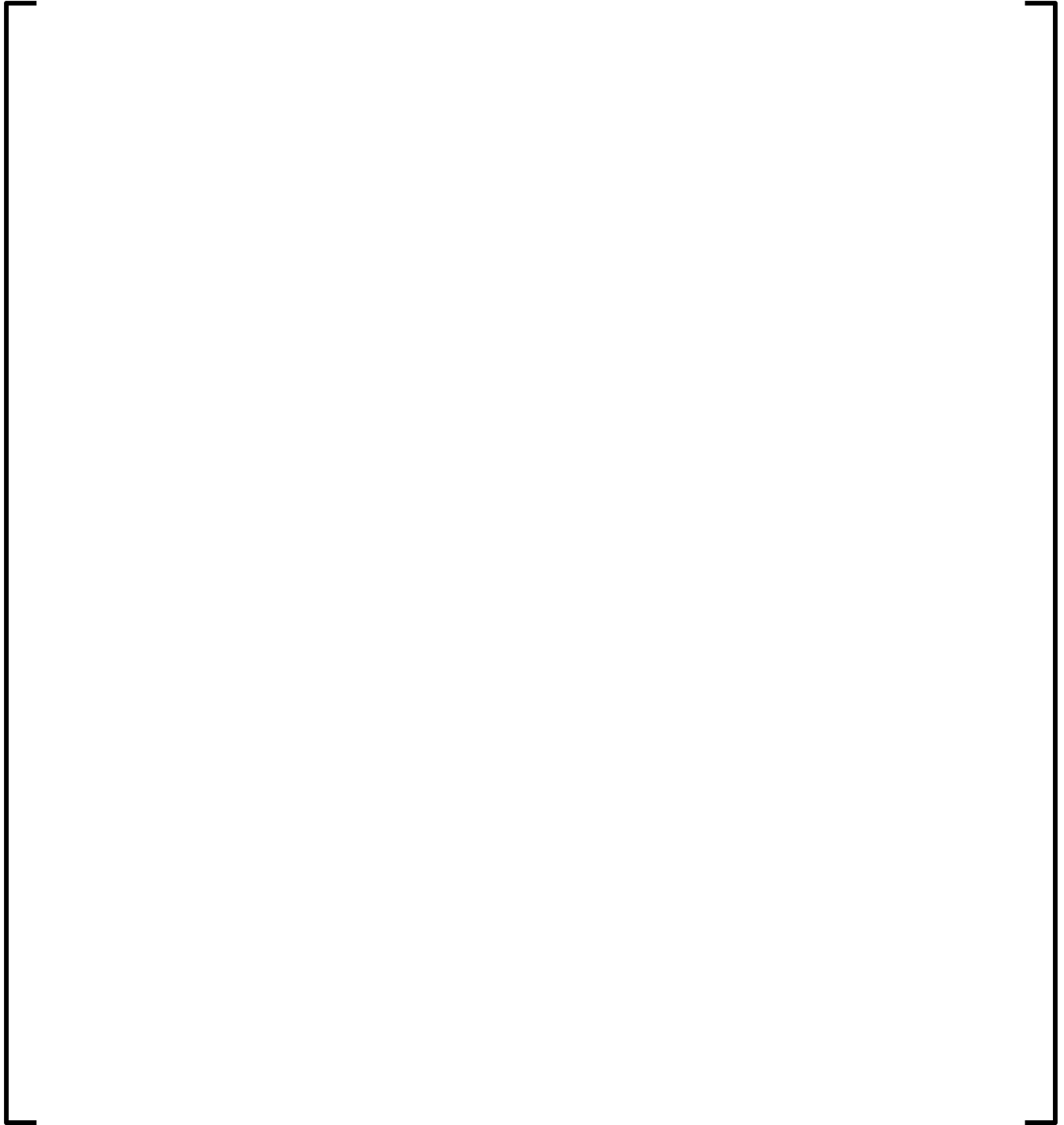


**Figure G1 5.3.5-15**  
**Plant G1 EOC 28 Assembly Average Radial Power Distribution**

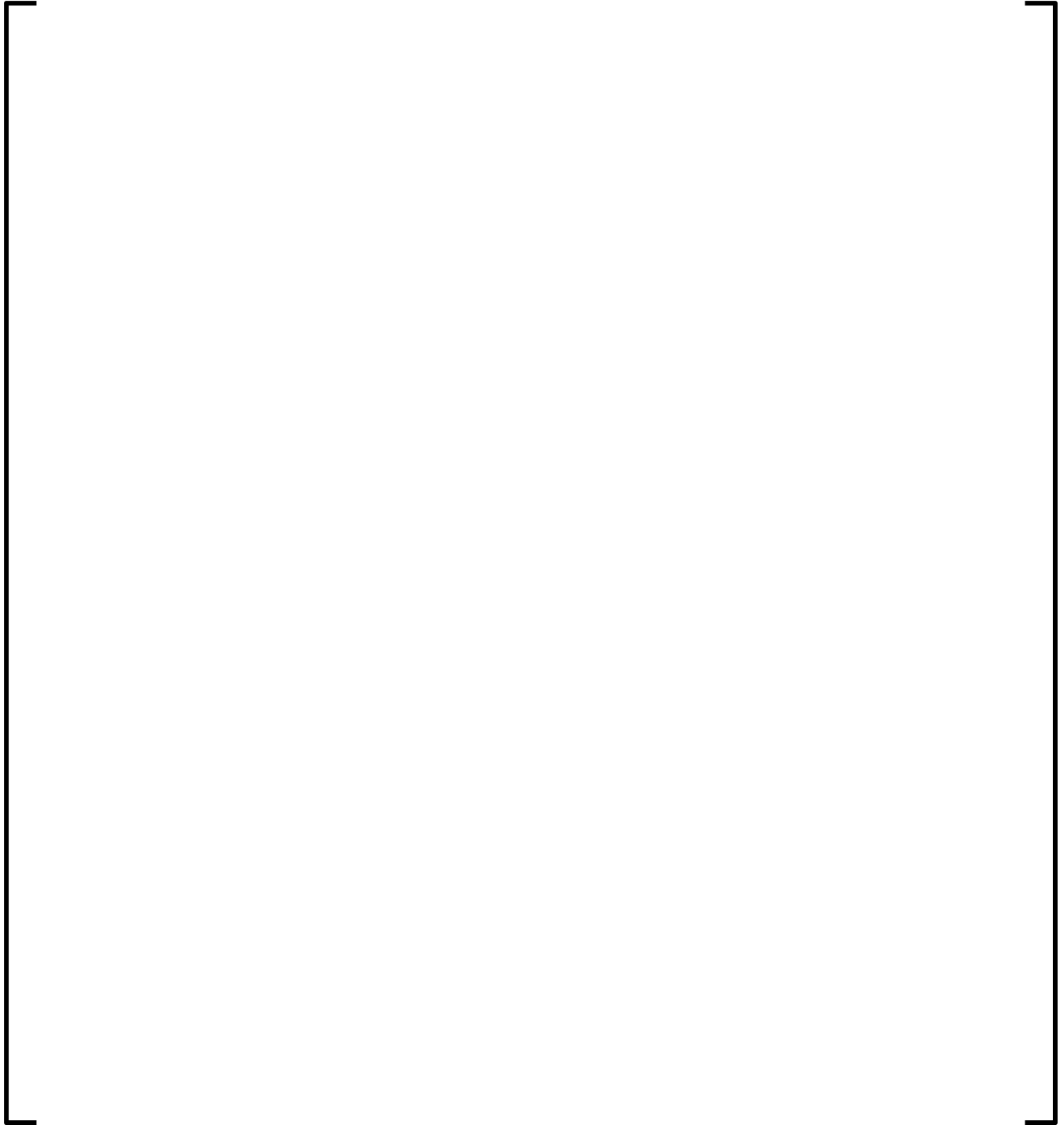


**Figure G1 5.3.5-16**  
**Plant G1 BOC 29 Assembly Average Radial Power Distribution**

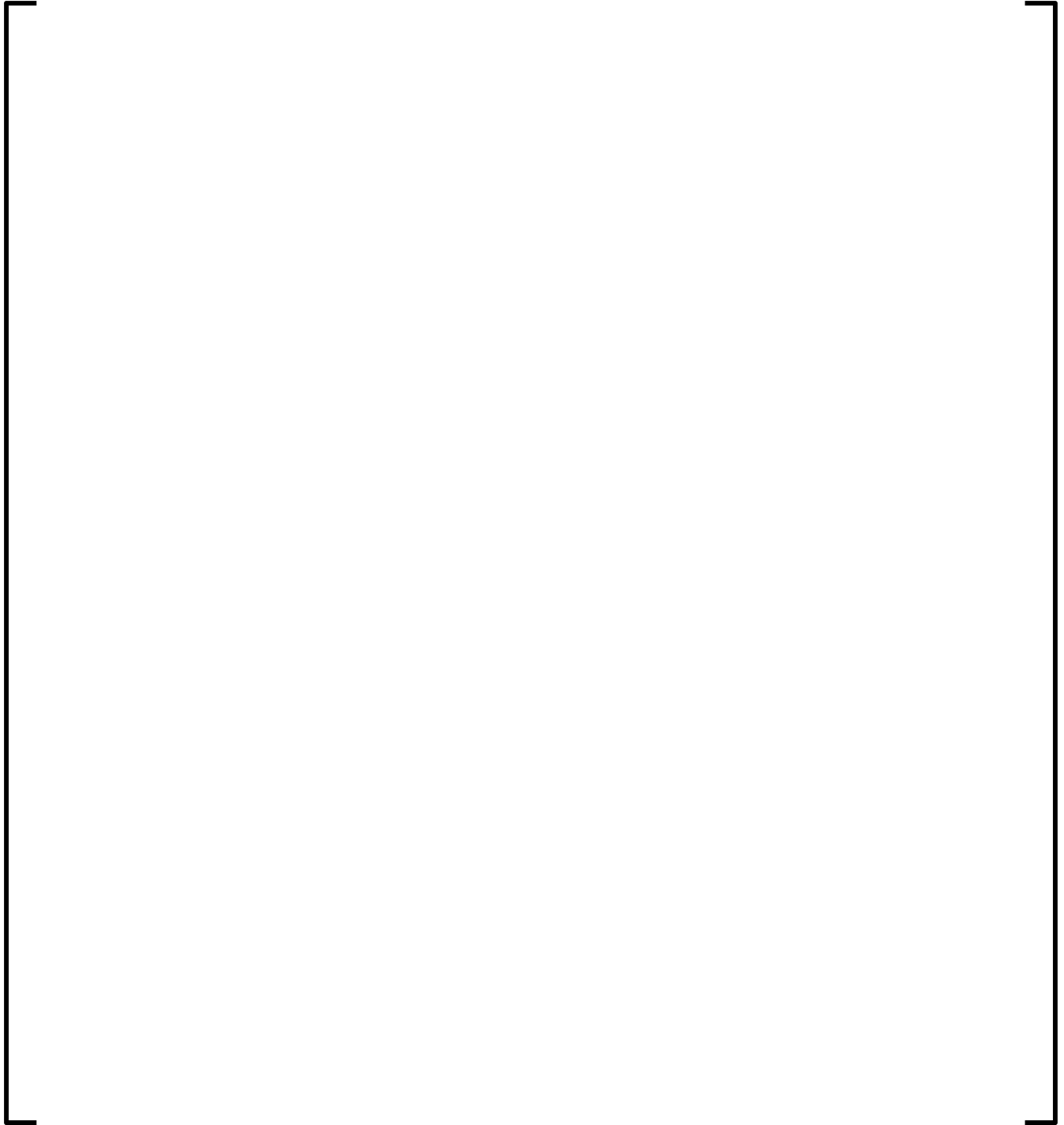


**Figure G1 5.3.5-17**  
**Plant G1 MOC 29 Assembly Average Radial Power Distribution**

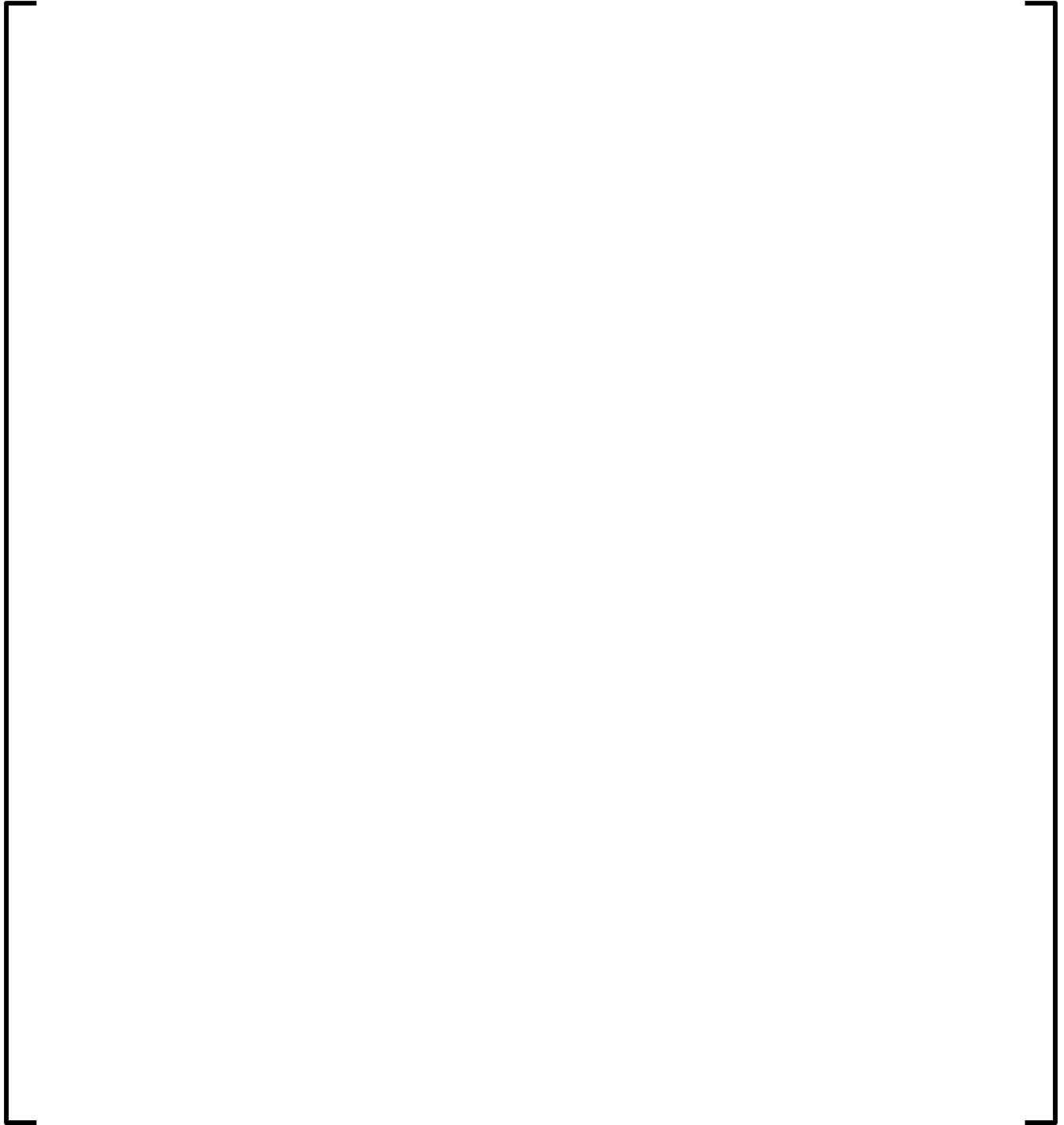


**Figure G1 5.3.5-18**  
**Plant G1 EOC 29 Assembly Average Radial Power Distribution**

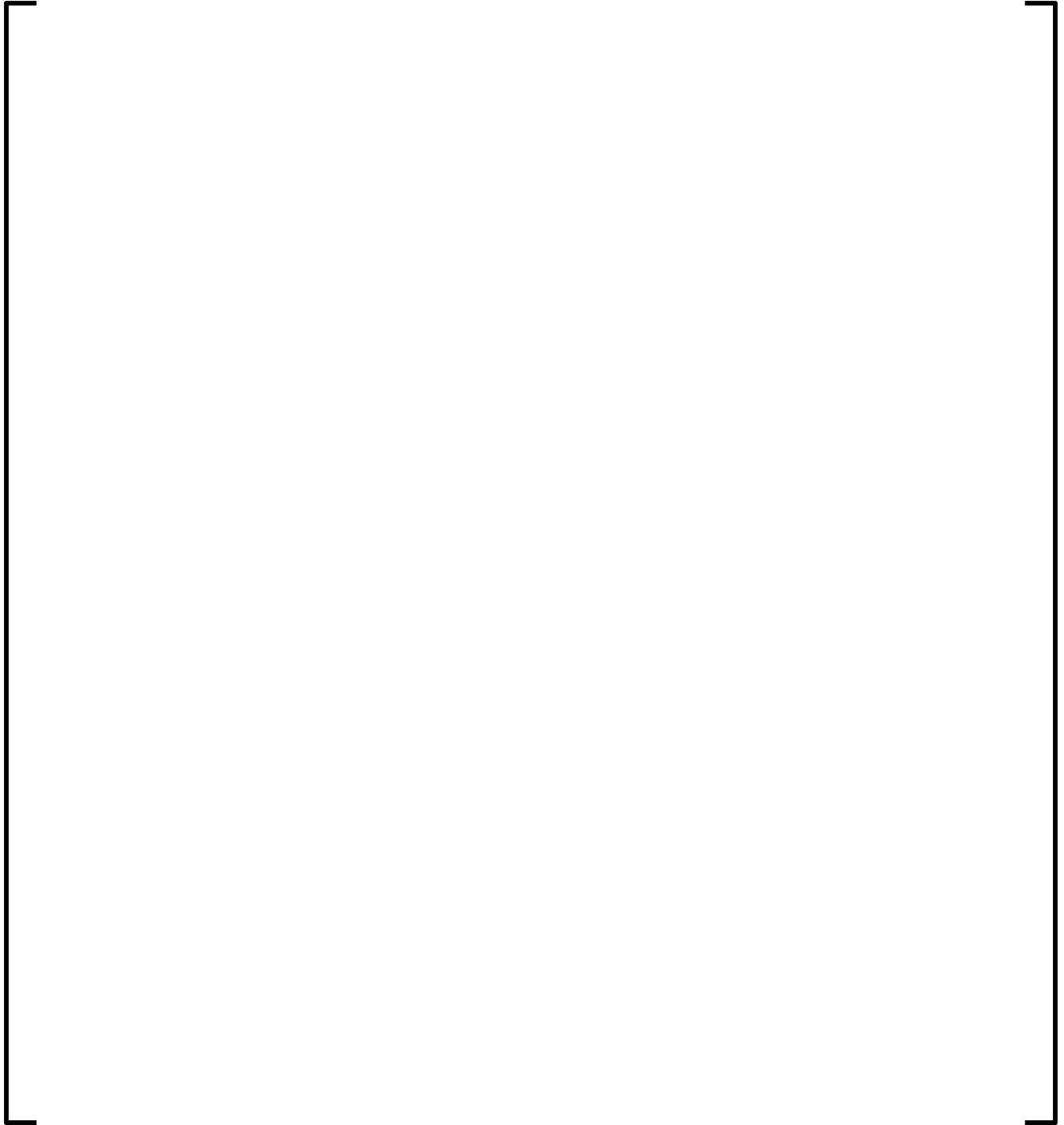


**Figure G1 5.3.5-19**  
**Plant G1 BOC 30 Assembly Average Radial Power Distribution**

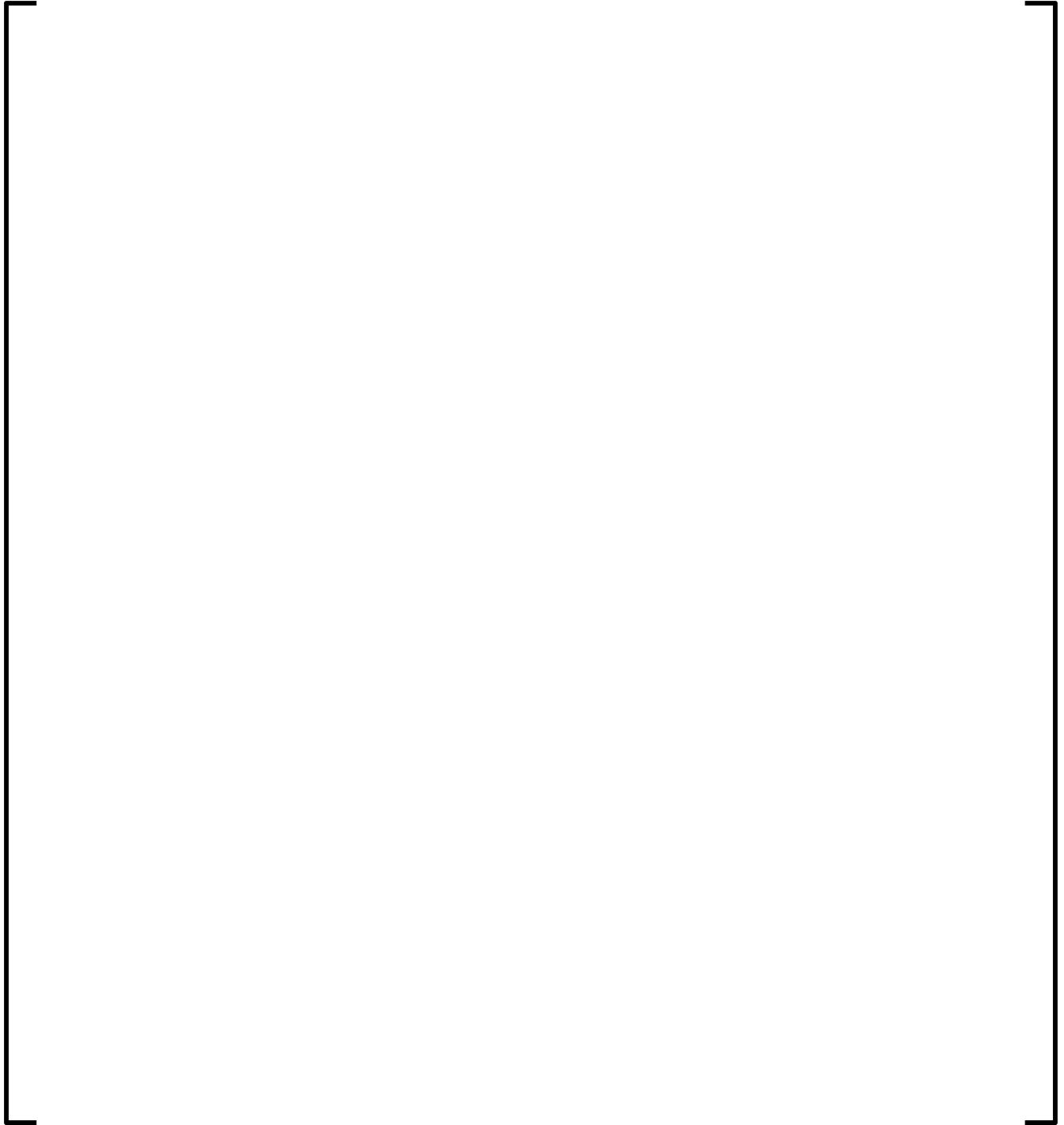




**Figure G1 5.3.5-20**  
**Plant G1 MOC 30 Assembly Average Radial Power Distribution**

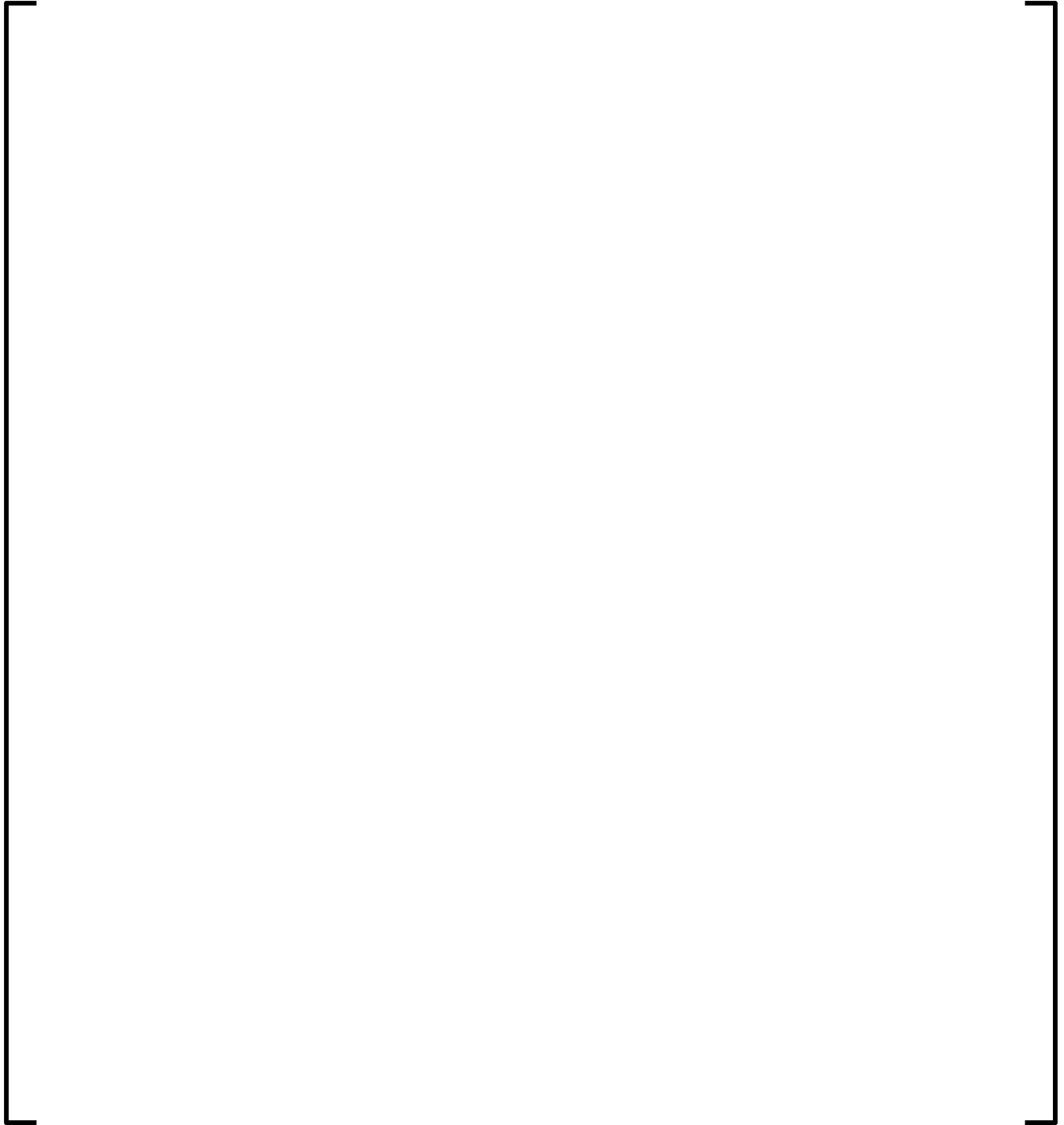


**Figure G1 5.3.5-21**  
**Plant G1 EOC 30 Assembly Average Radial Power Distribution**

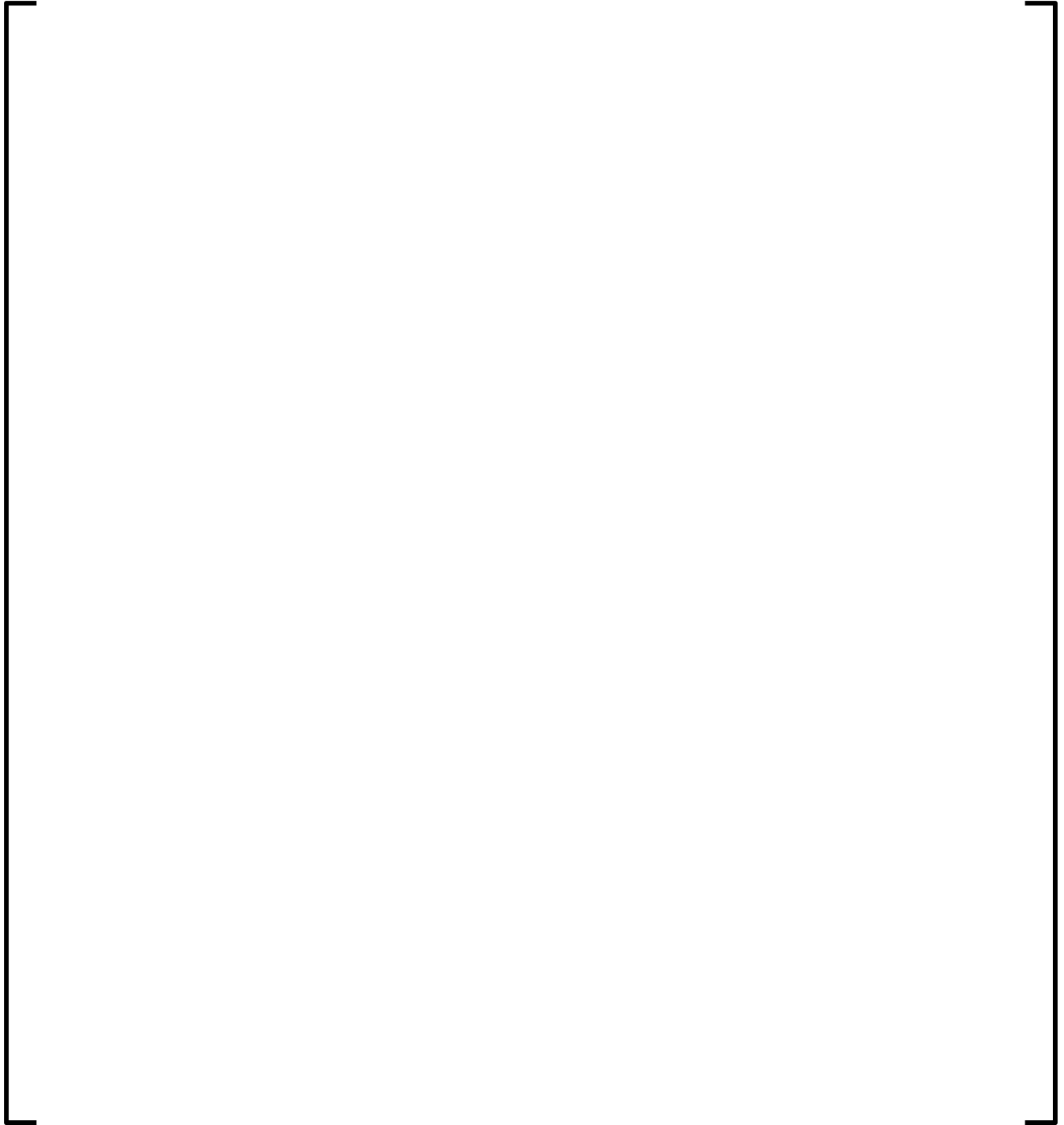


**Figure G1 5.3.5-22**  
**Plant G1 BOC 26 Core Average Axial Power Distribution**



**Figure G1 5.3.5-23**  
**Plant G1 MOC 26 Core Average Axial Power Distribution**



**Figure G1 5.3.5-24**  
**Plant G1 EOC 26 Core Average Axial Power Distribution**



**Figure G1 5.3.5-25**  
**Plant G1 BOC 27 Core Average Axial Power Distribution**



**Figure G1 5.3.5-26**  
**Plant G1 MOC 27 Core Average Axial Power Distribution**



**Figure G1 5.3.5-27**  
**Plant G1 EOC 27 Core Average Axial Power Distribution**





**Figure G1 5.3.5-28**  
**Plant G1 BOC 28 Core Average Axial Power Distribution**

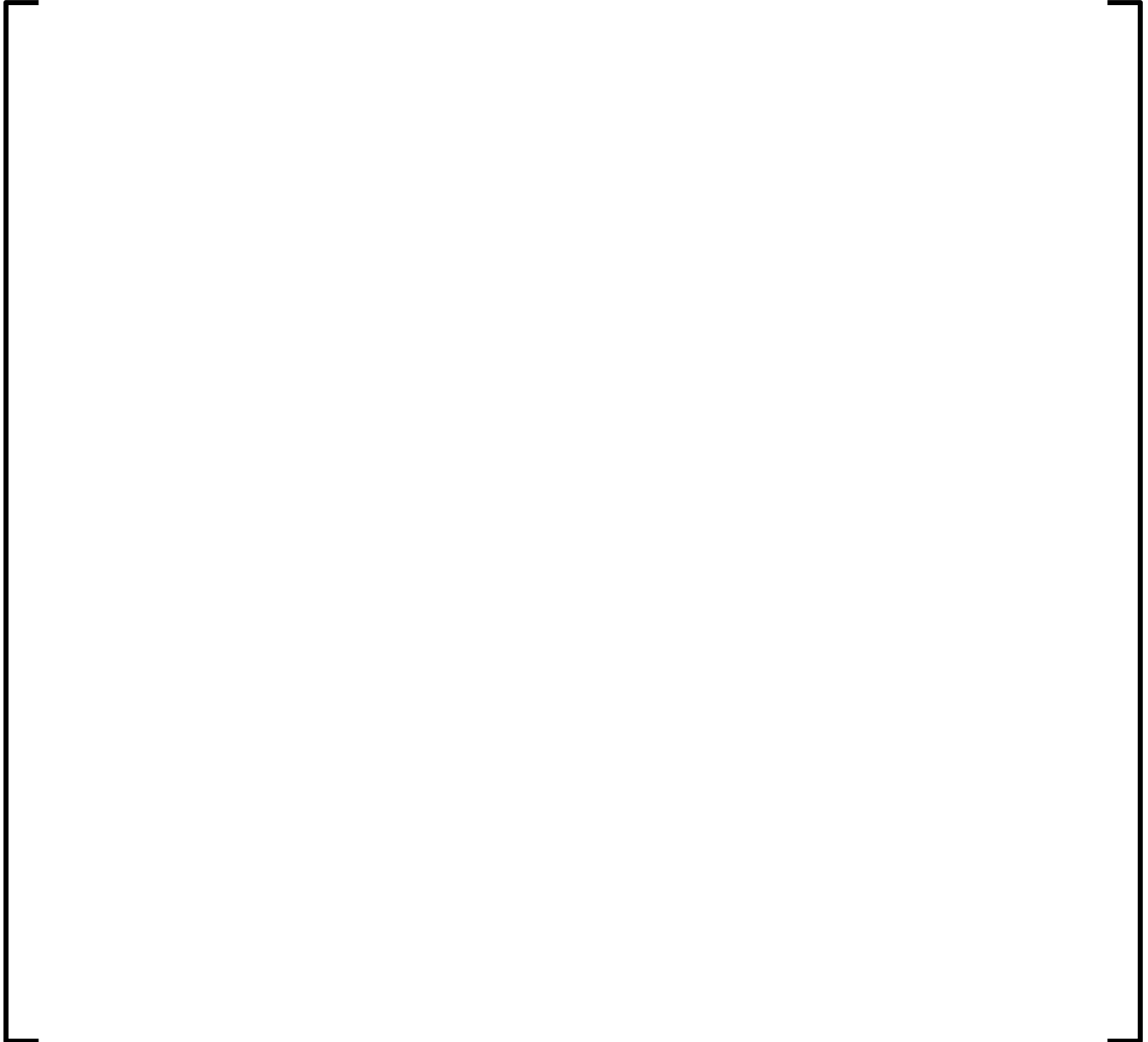


**Figure G1 5.3.5-29**  
**Plant G1 MOC 28 Core Average Axial Power Distribution**



**Figure G1 5.3.5-30**  
**Plant G1 EOC 28 Core Average Axial Power Distribution**



**Figure G1 5.3.5-31**  
**Plant G1 BOC 29 Core Average Axial Power Distribution**



**Figure G1 5.3.5-32**  
**Plant G1 MOC 29 Core Average Axial Power Distribution**



**Figure G1 5.3.5-33**  
**Plant G1 EOC 29 Core Average Axial Power Distribution**



**Figure G1 5.3.5-34**  
**Plant G1 BOC 30 Core Average Axial Power Distribution**

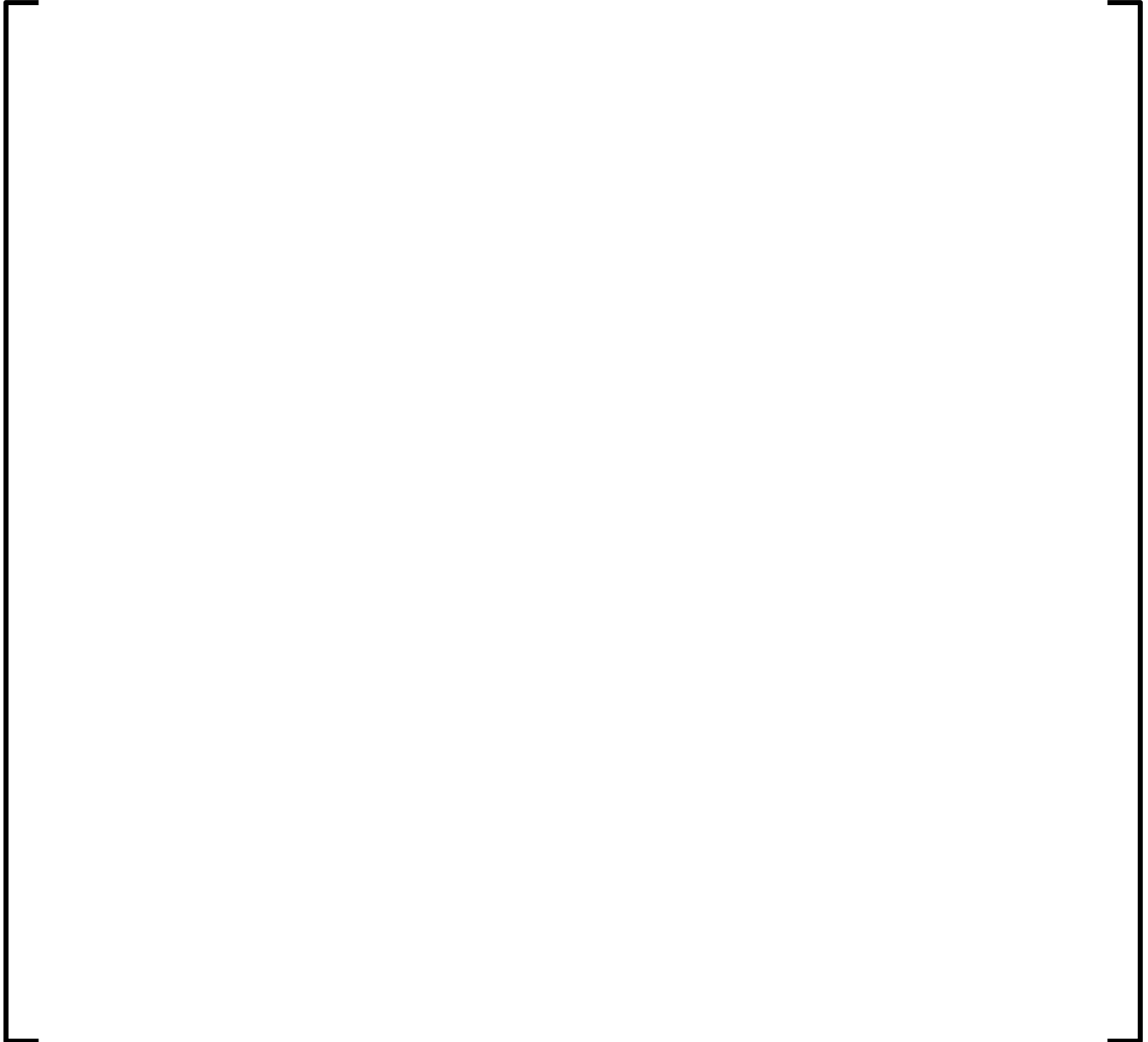


**Figure G1 5.3.5-35**  
**Plant G1 MOC 30 Core Average Axial Power Distribution**





**Figure G1 5.3.5-36**  
**Plant G1 EOC 30 Core Average Axial Power Distribution**



## APPENDIX G2

**Table G2 5.2.6-1**  
**Plant G2 Hot Zero Power All Rods Out Critical Boron Concentrations**  
**for Cycles 1-5**

--	--

**Figure G2 5.3.6-1**  
**Plant G2 Cycle 1 Critical Boron Concentration vs. Burnup**



**Figure G2 5.3.6-2**  
**Plant G2 Cycle 2 Critical Boron Concentration vs. Burnup**



**Figure G2 5.3.6-3**  
**Plant G2 Cycle 3 Critical Boron Concentration vs. Burnup**



**Figure G2 5.3.6-4**  
**Plant G2 Cycle 4 Critical Boron Concentration vs. Burnup**



**Figure G2 5.3.6-5**  
**Plant G2 Cycle 5 Critical Boron Concentration vs. Burnup**



**Figure G2 5.3.6-6**  
**Plant G2 Cycles 1-5 Boron Differences**





**Figure G2 5.3.6-7**  
**Plant G2 BOC 1 Assembly Average Radial Power Distribution**

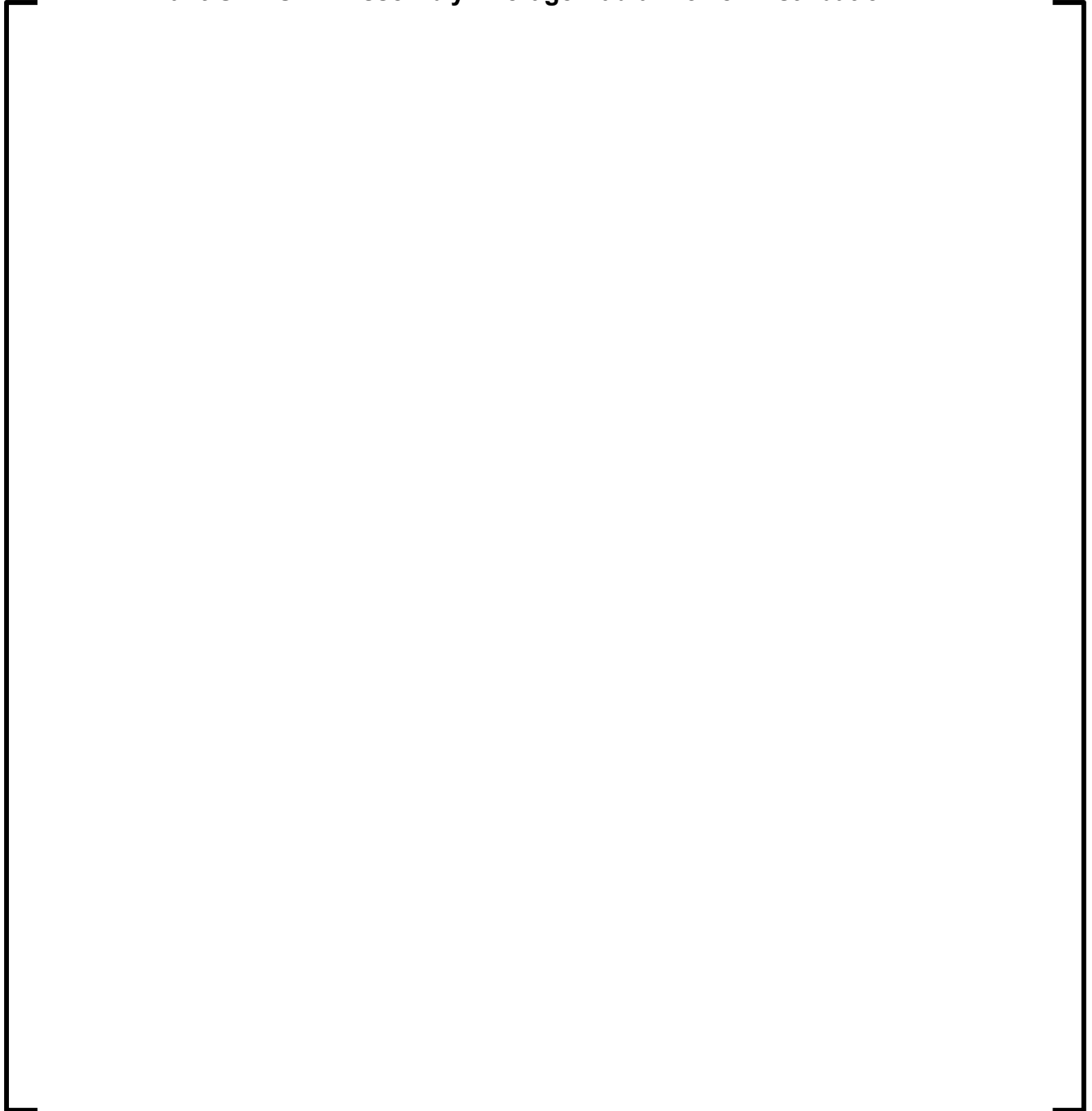


**Figure G2 5.3.6-8**  
**Plant G2 MOC 1 Assembly Average Radial Power Distribution**

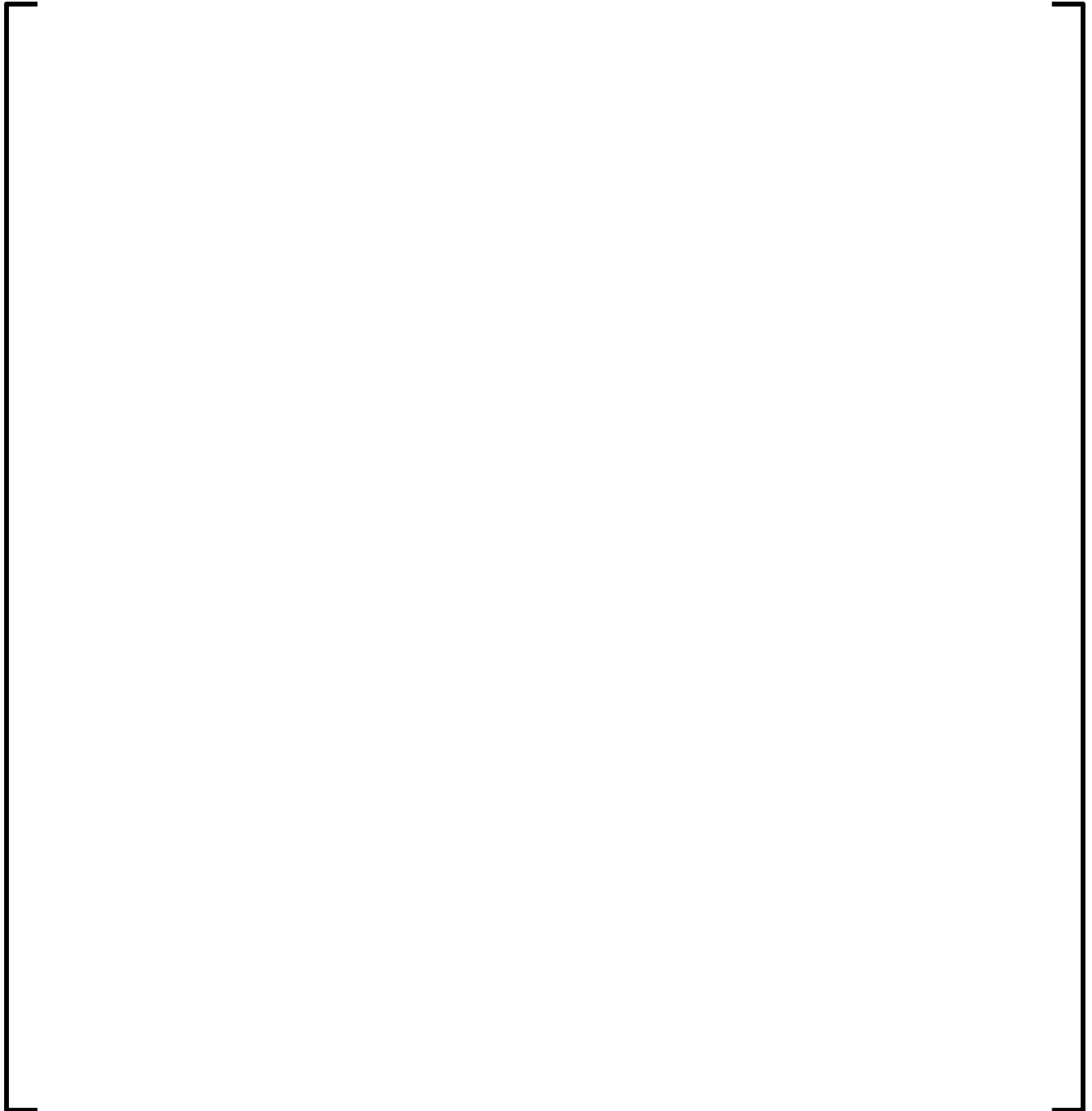


**Figure G2 5.3.6-9**  
**Plant G2 EOC 1 Assembly Average Radial Power Distribution**

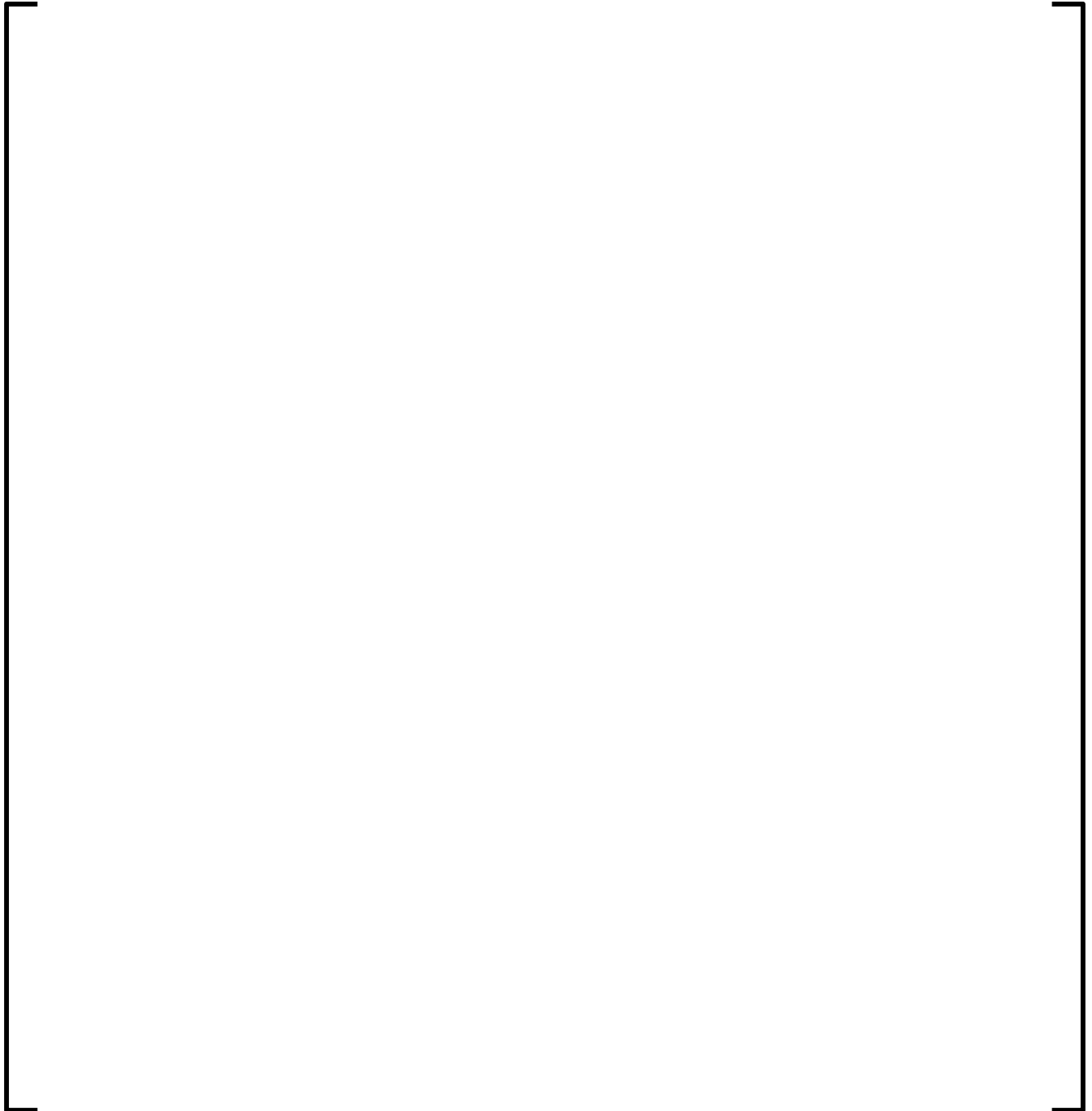


**Figure G2 5.3.6-10**  
**Plant G2 BOC 2 Assembly Average Radial Power Distribution**

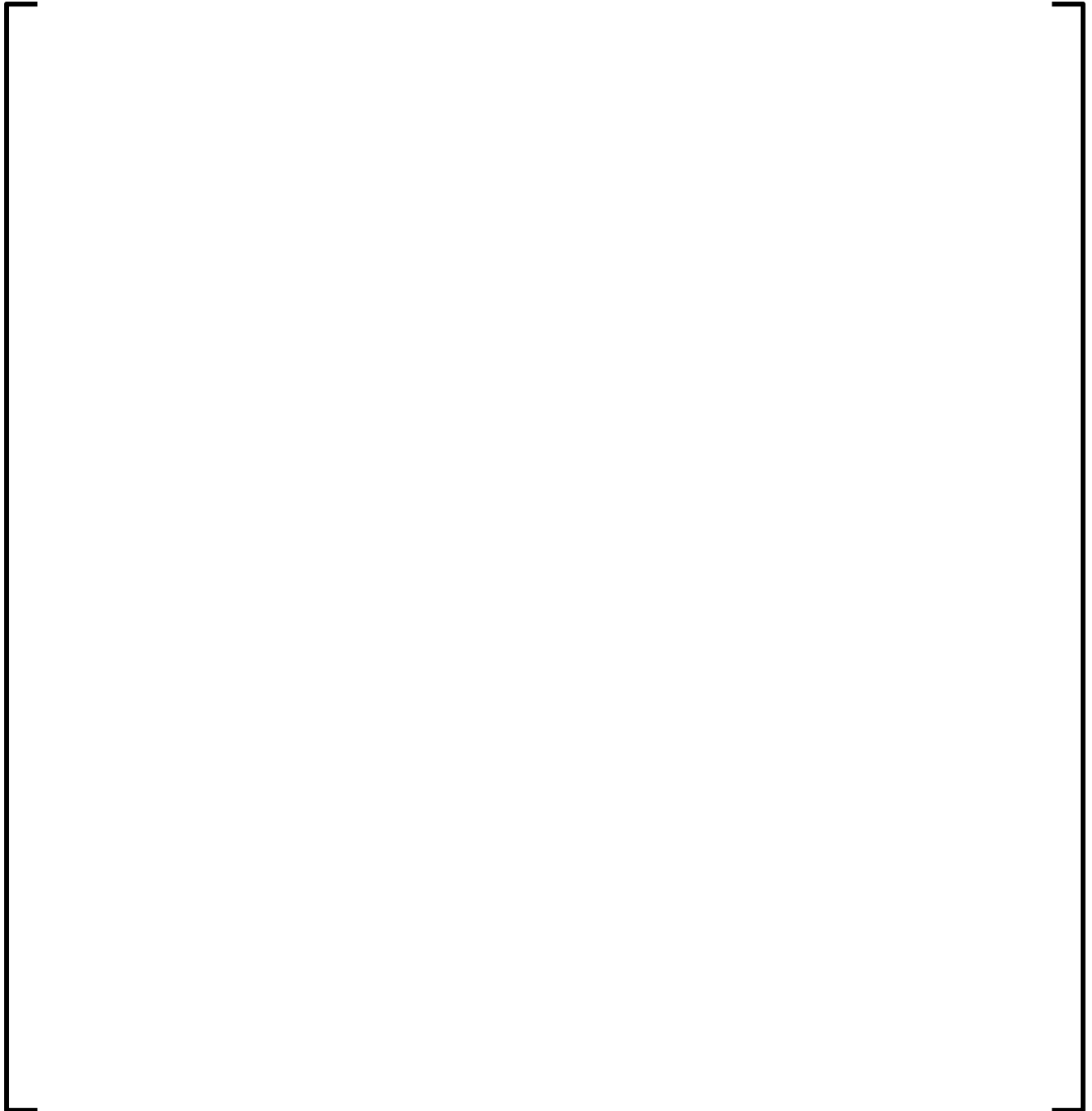


**Figure G2 5.3.6-11**  
**Plant G2 MOC 2 Assembly Average Radial Power Distribution**

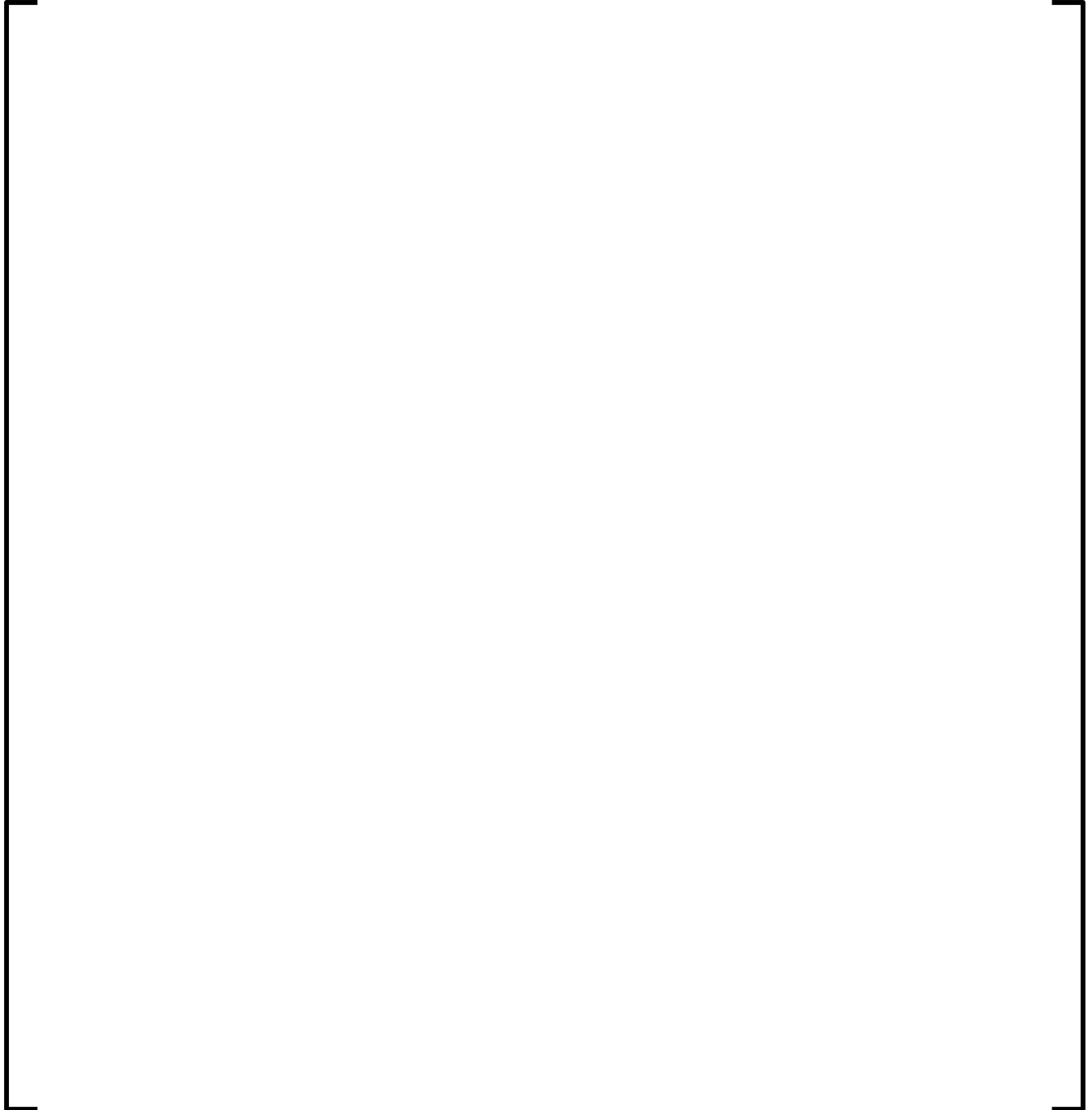


**Figure G2 5.3.6-12**  
**Plant G2 EOC 2 Assembly Average Radial Power Distribution**

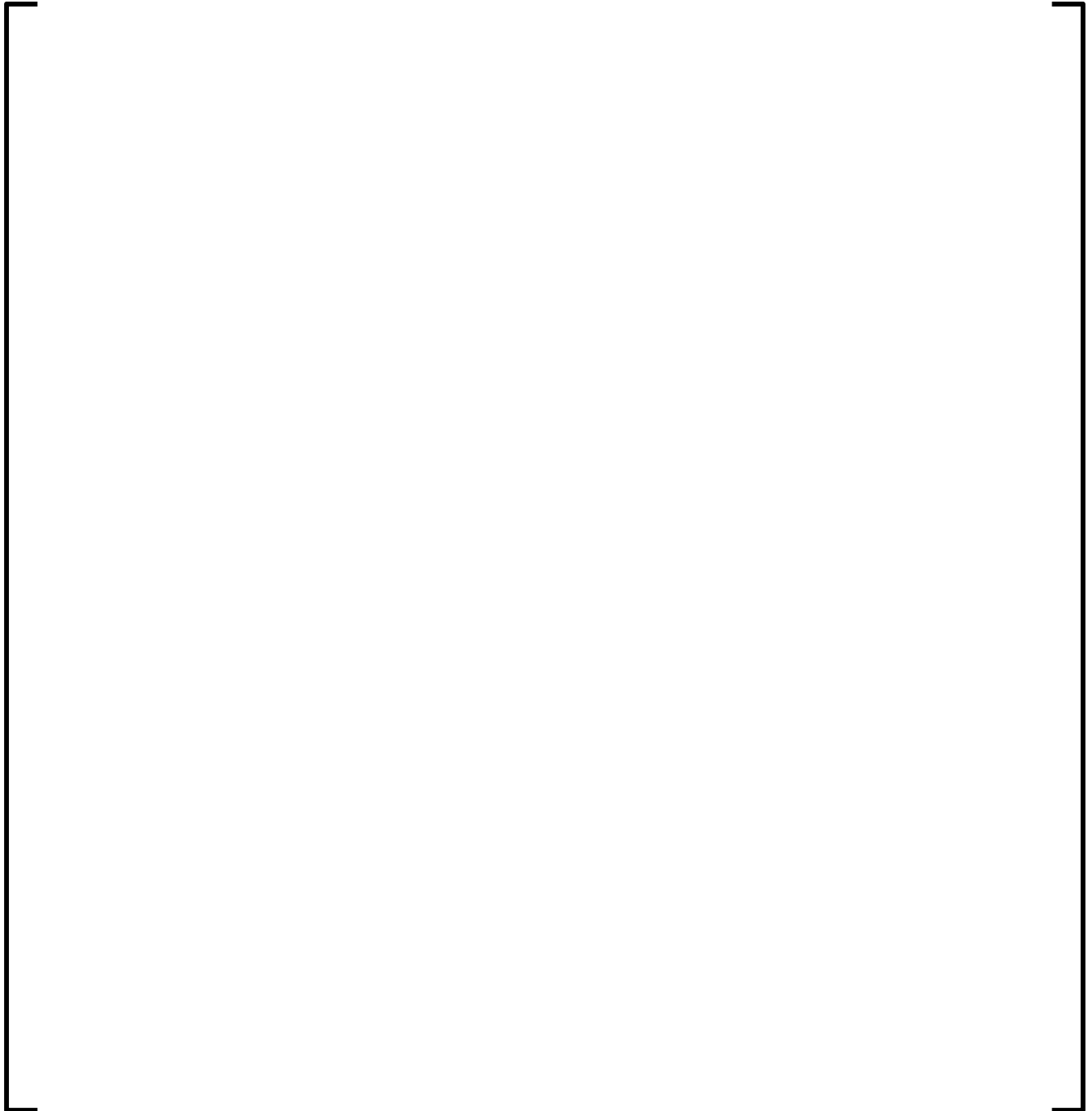


**Figure G2 5.3.6-13**  
**Plant G2 BOC 3 Assembly Average Radial Power Distribution**

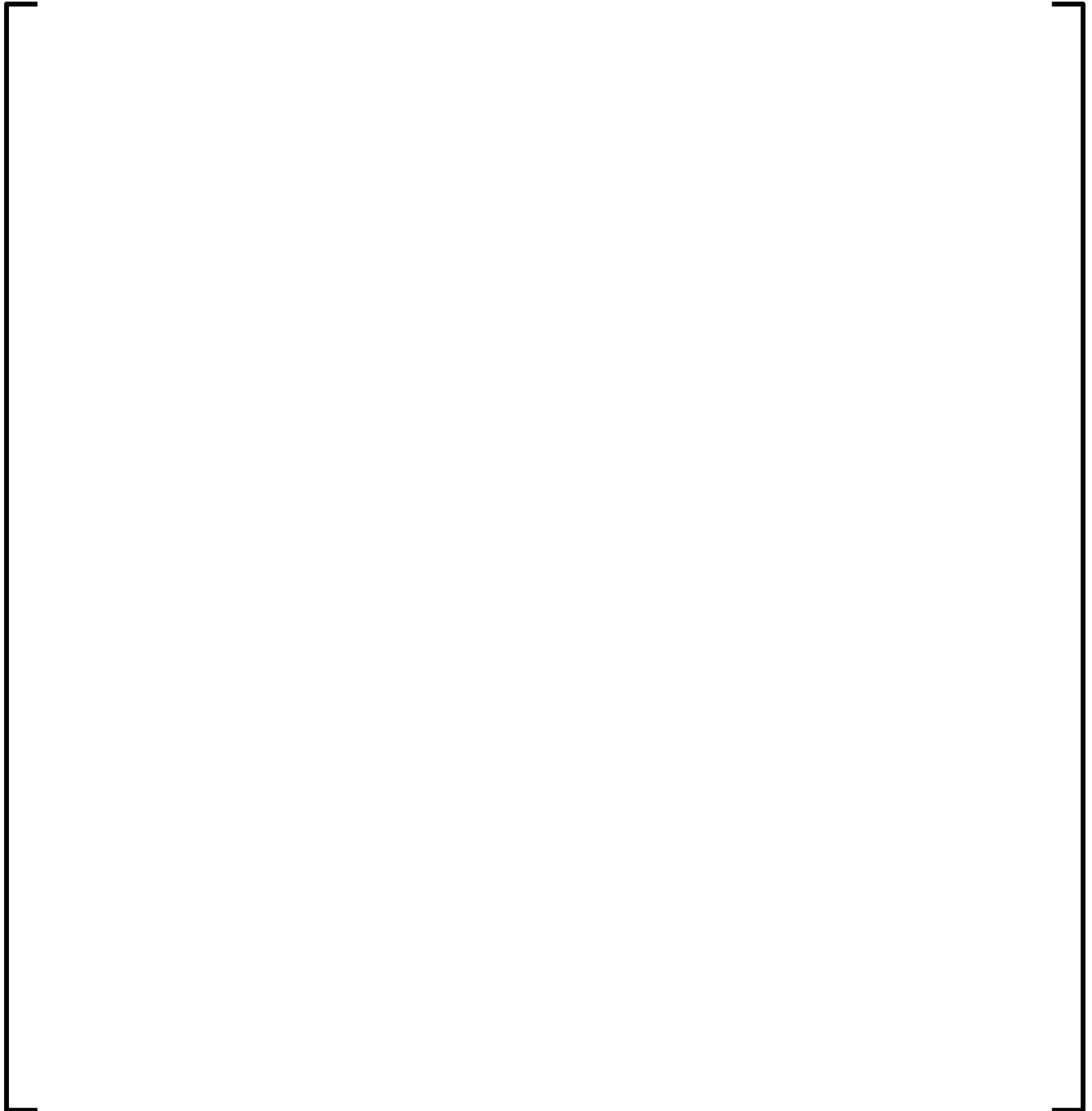


**Figure G2 5.3.6-14**  
**Plant G2 MOC 3 Assembly Average Radial Power Distribution**

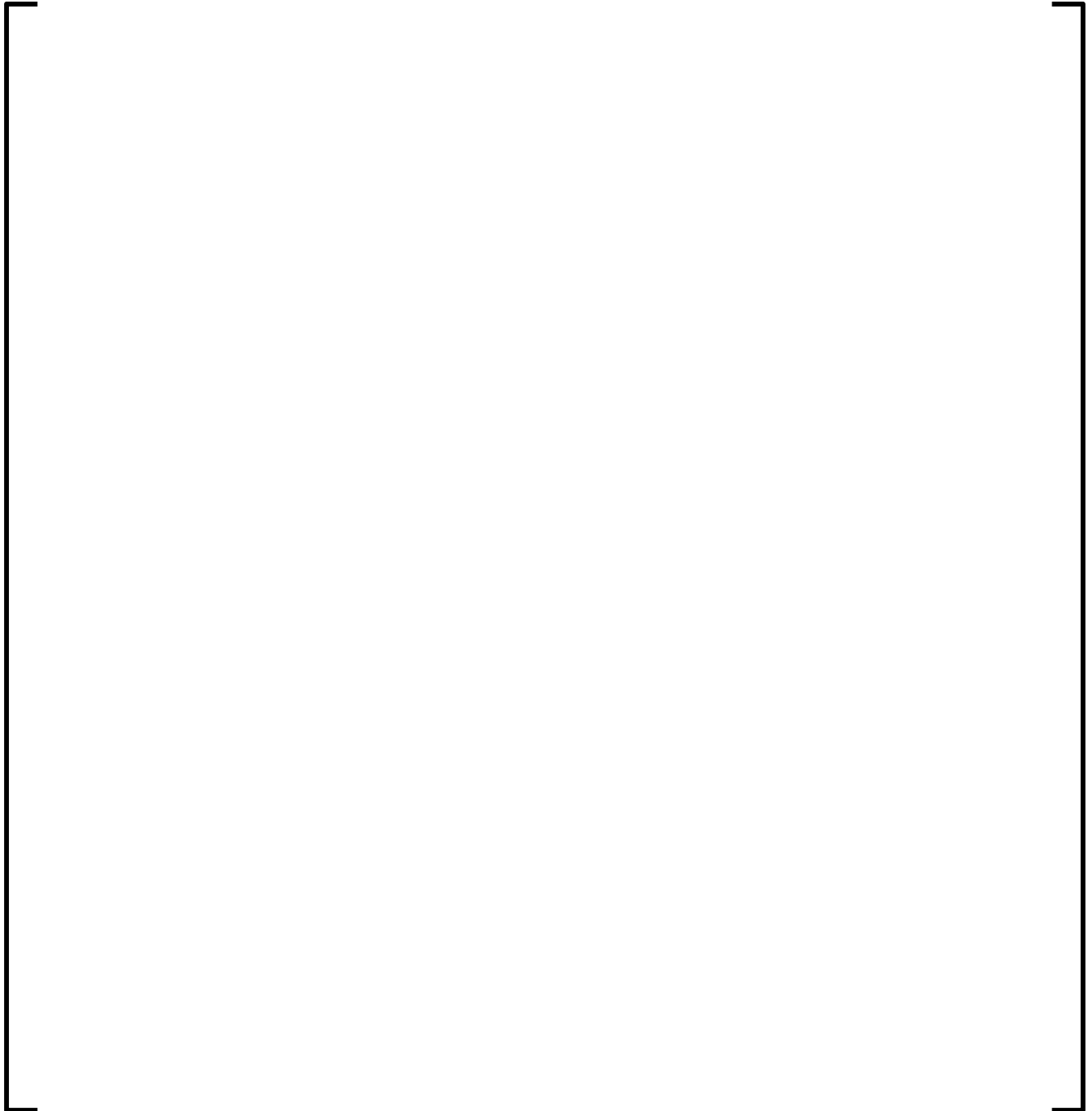




**Figure G2 5.3.6-15**  
**Plant G2 EOC 3 Assembly Average Radial Power Distribution**

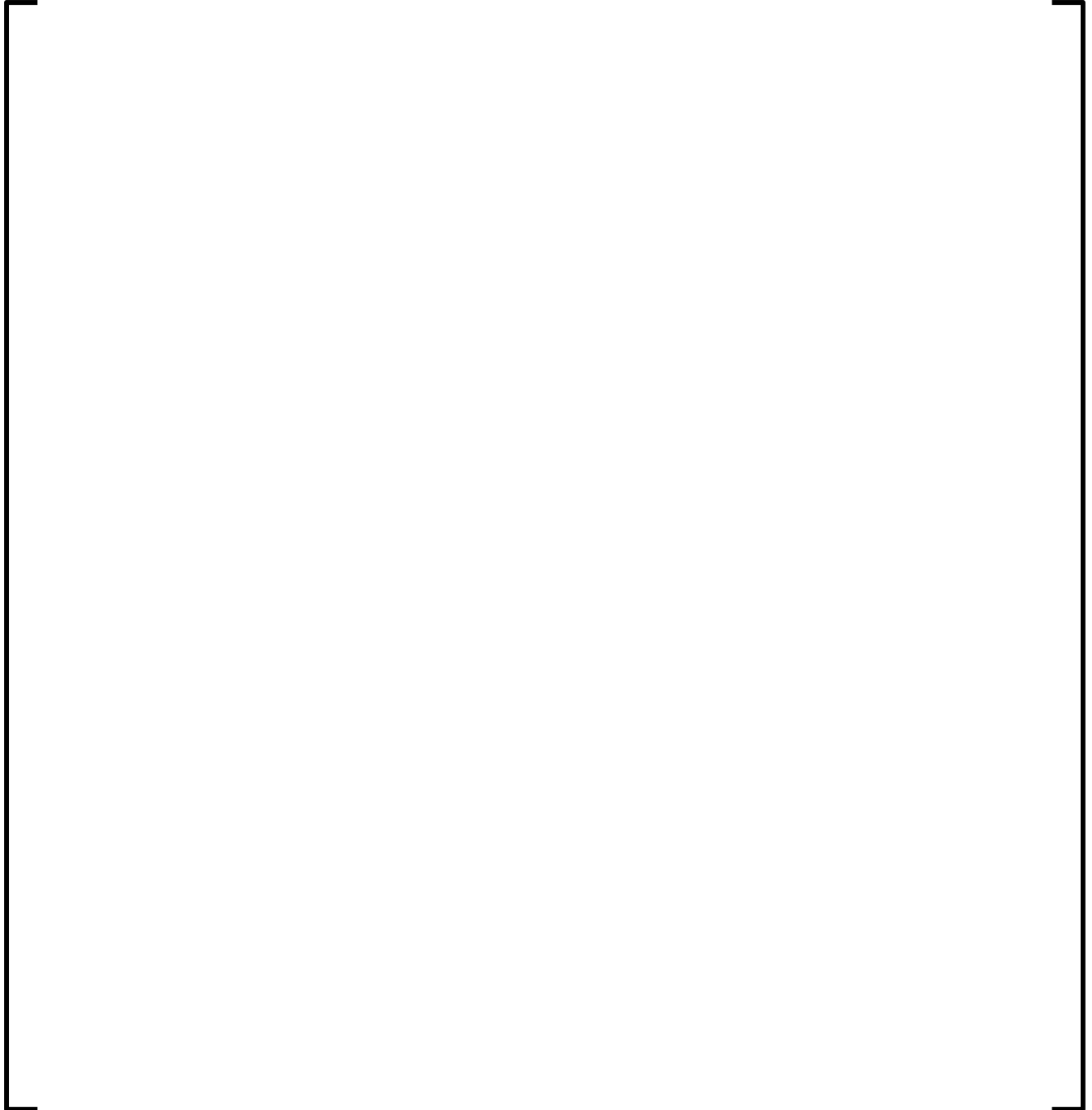


**Figure G2 5.3.6-16**  
**Plant G2 BOC 4 Assembly Average Radial Power Distribution**

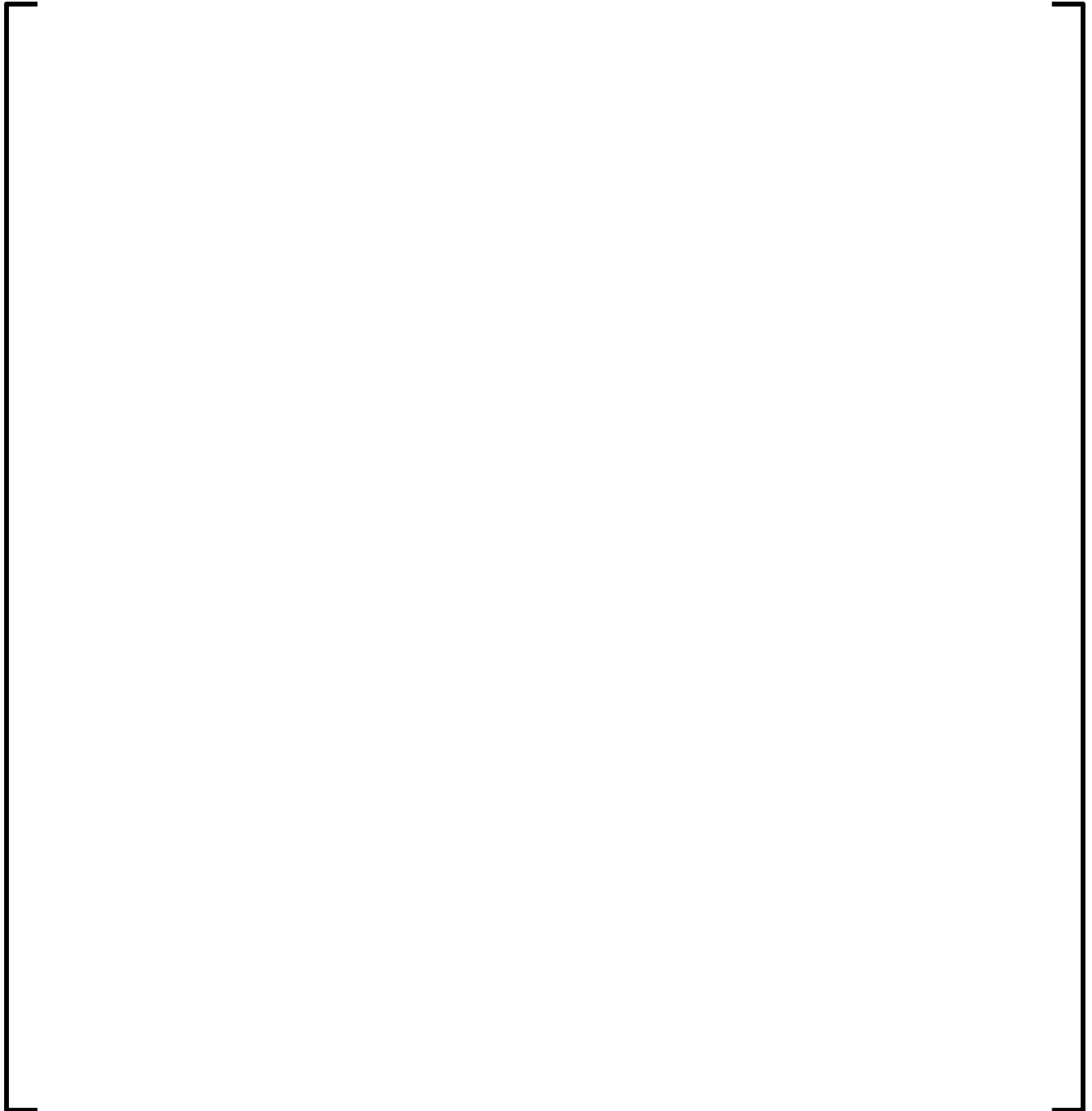


**Figure G2 5.3.6-17**  
**Plant G2 MOC 4 Assembly Average Radial Power Distribution**

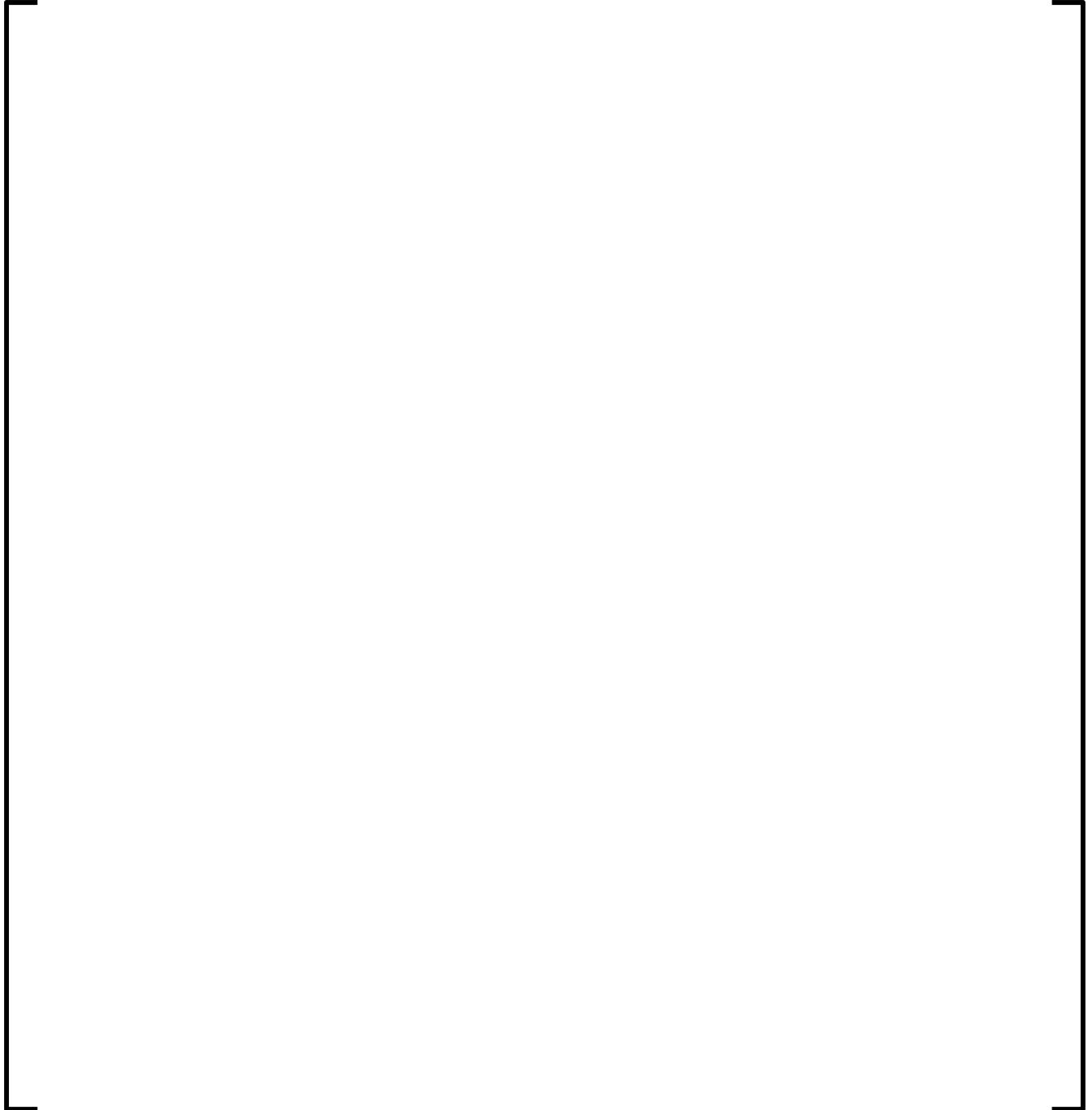


**Figure G2 5.3.6-18**  
**Plant G2 EOC 4 Assembly Average Radial Power Distribution**

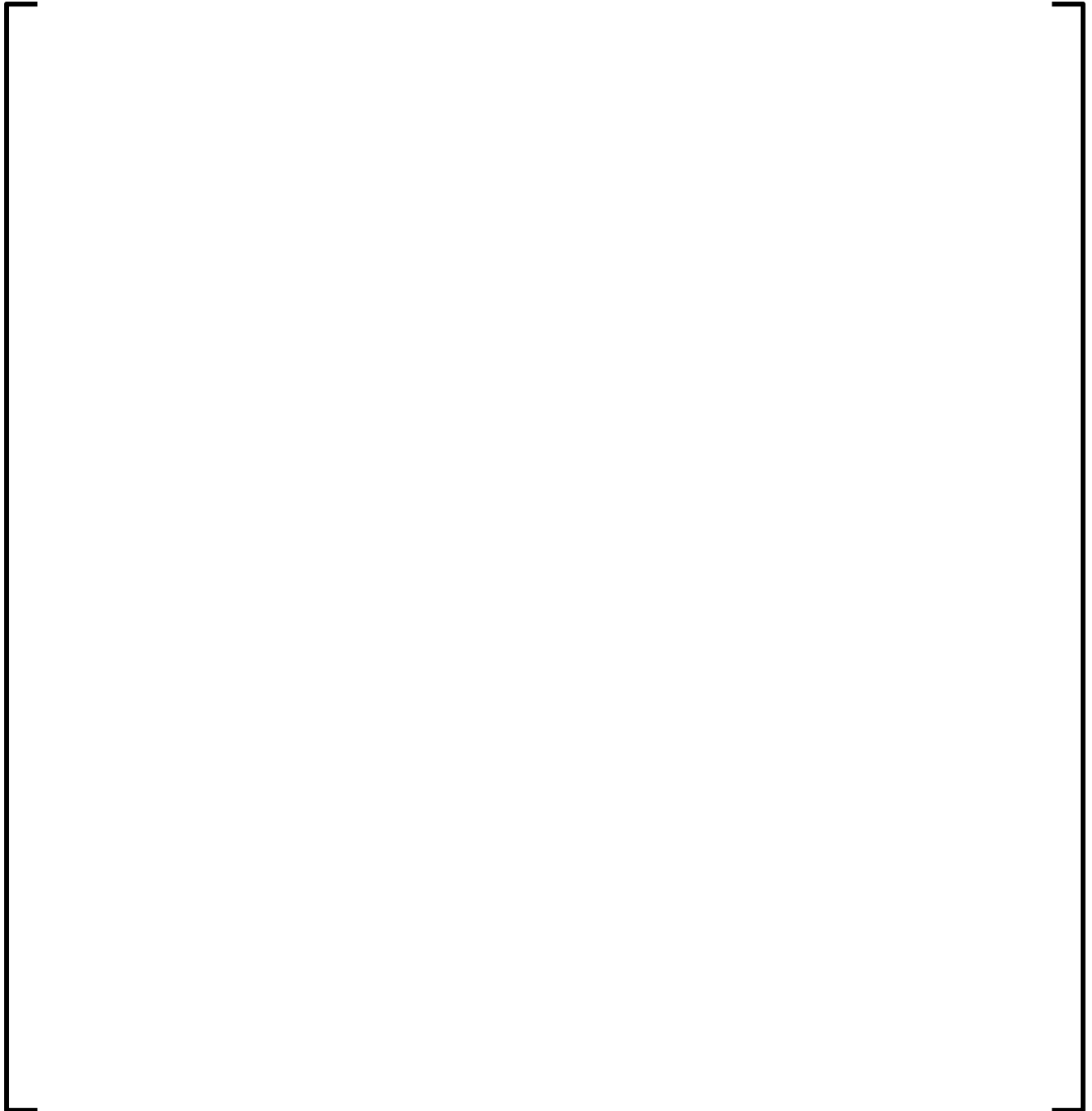


**Figure G2 5.3.6-19**  
**Plant G2 BOC 5 Assembly Average Radial Power Distribution**

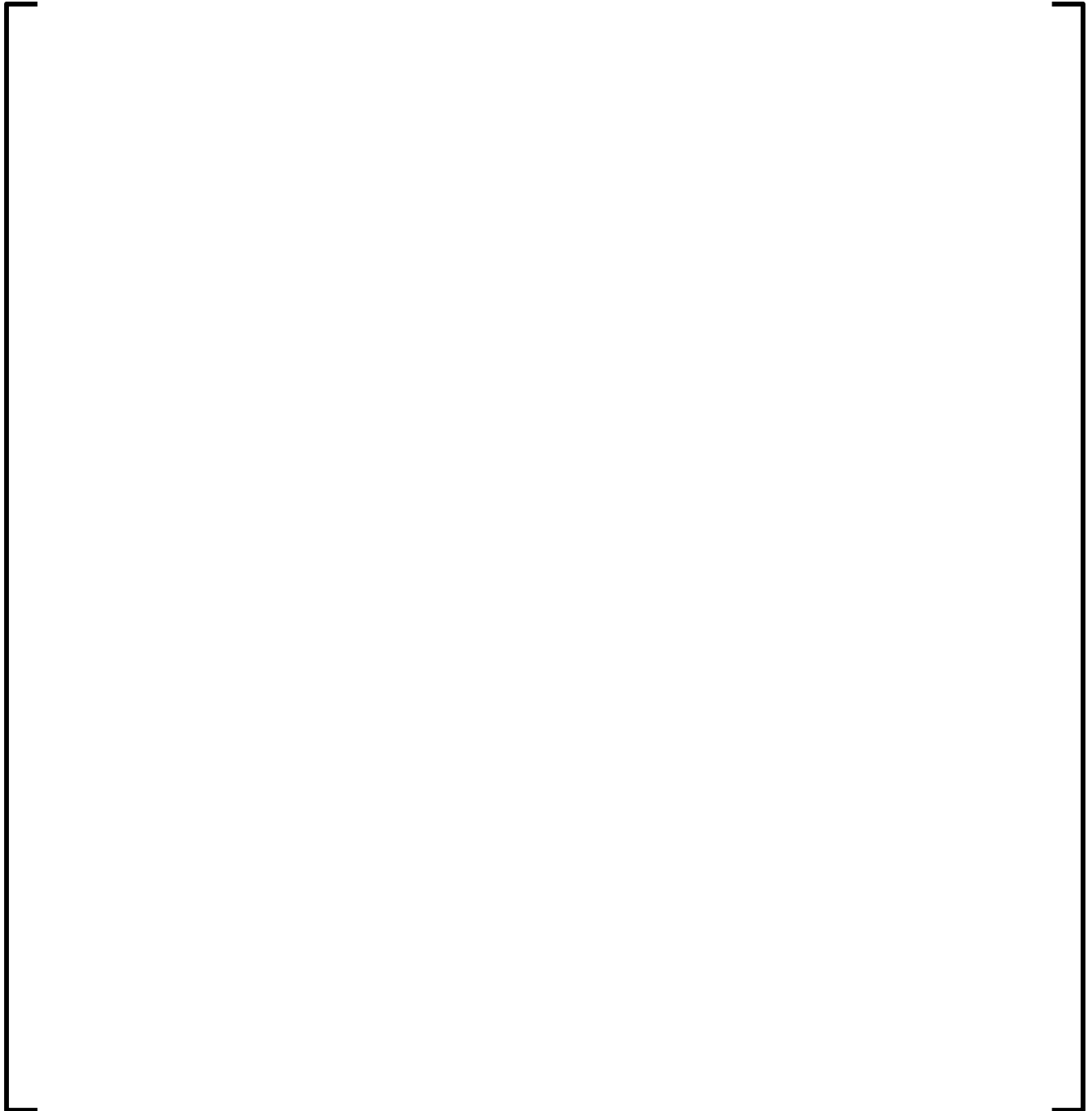


**Figure G2 5.3.6-20**  
**Plant G2 MOC 5 Assembly Average Radial Power Distribution**

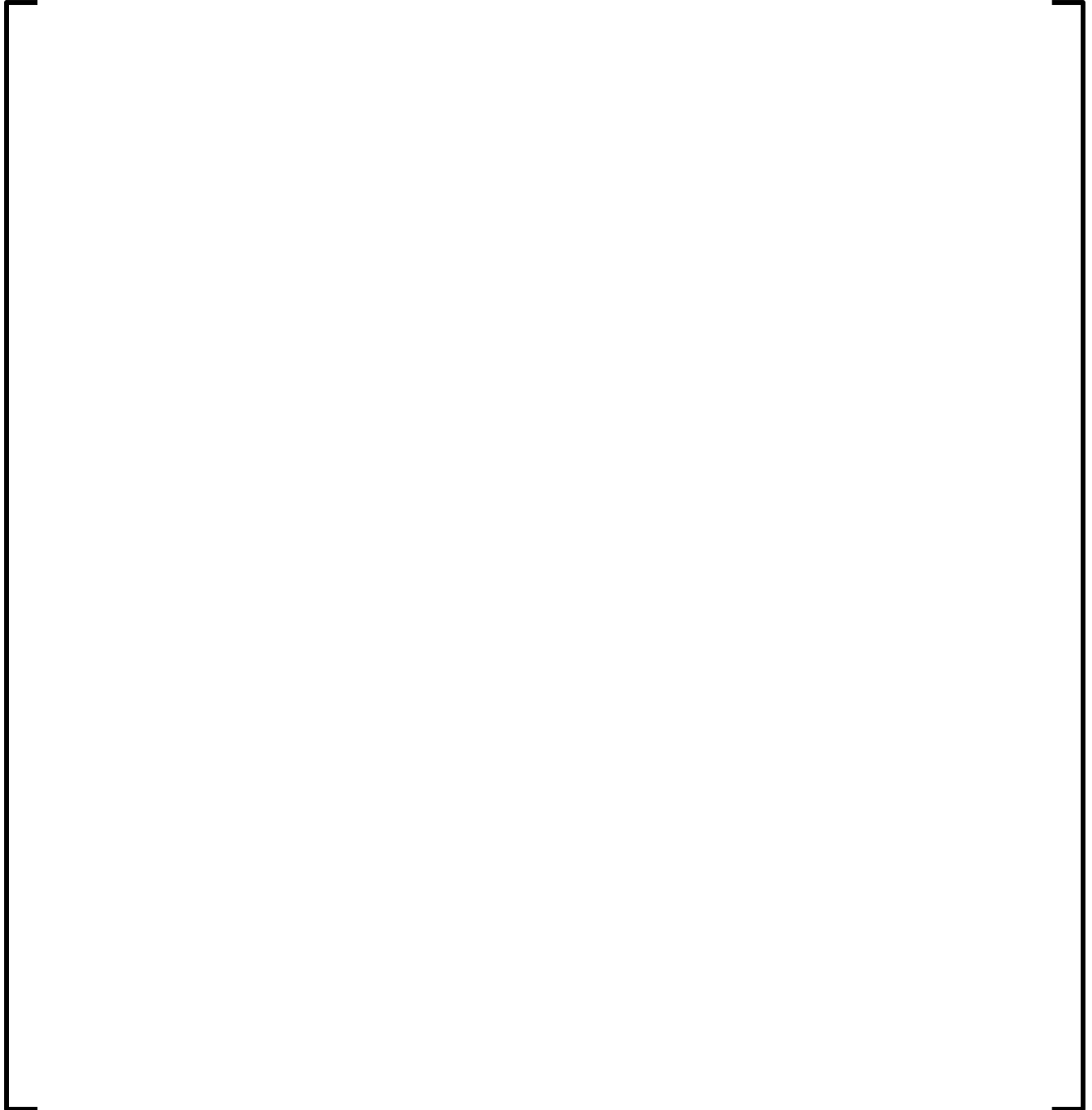


**Figure G2 5.3.6-21**  
**Plant G2 EOC 5 Assembly Average Radial Power Distribution**

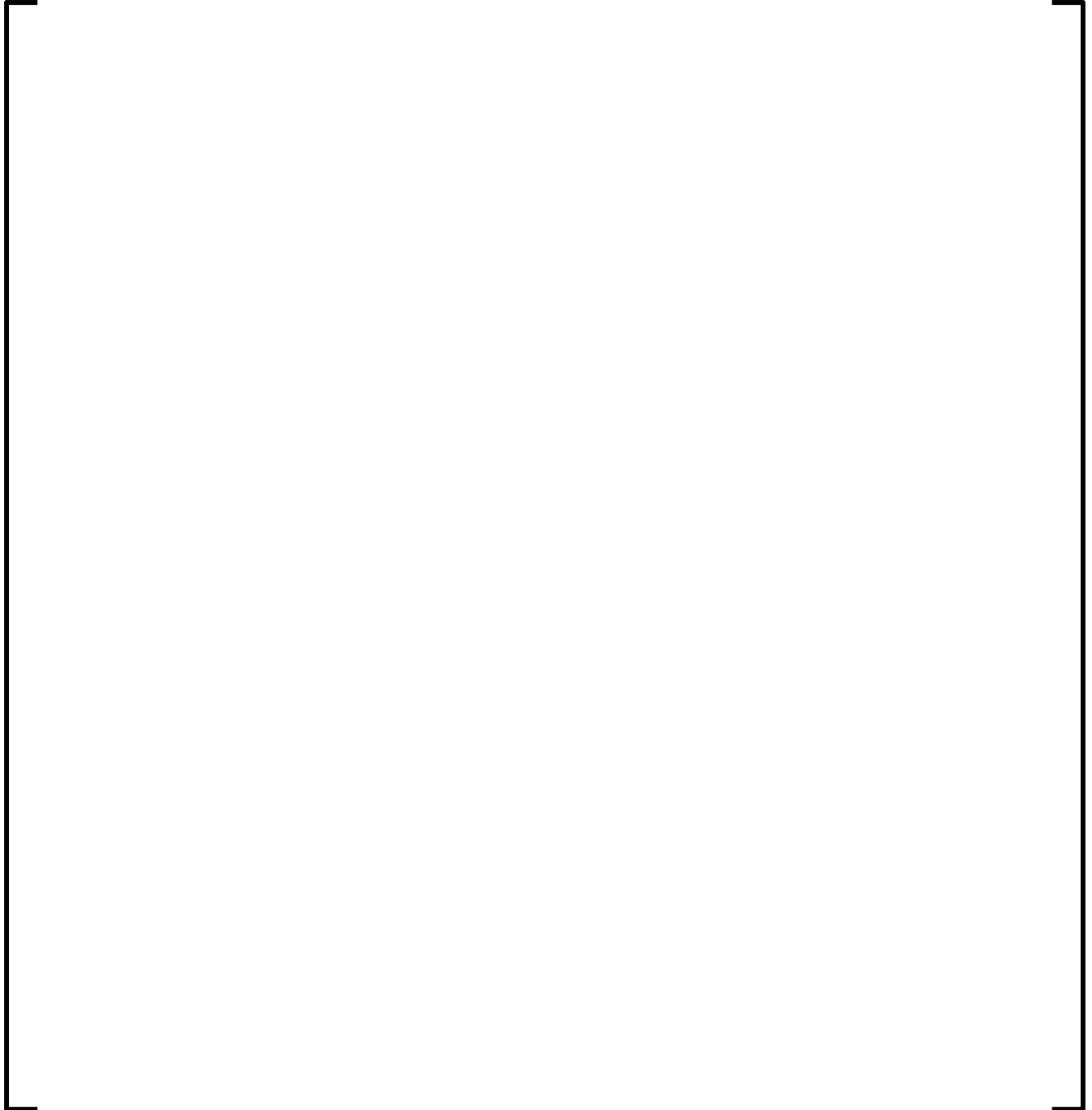


**Figure G2 5.3.6-22**  
**Plant G2 BOC 1 Core Average Axial Power Distribution**

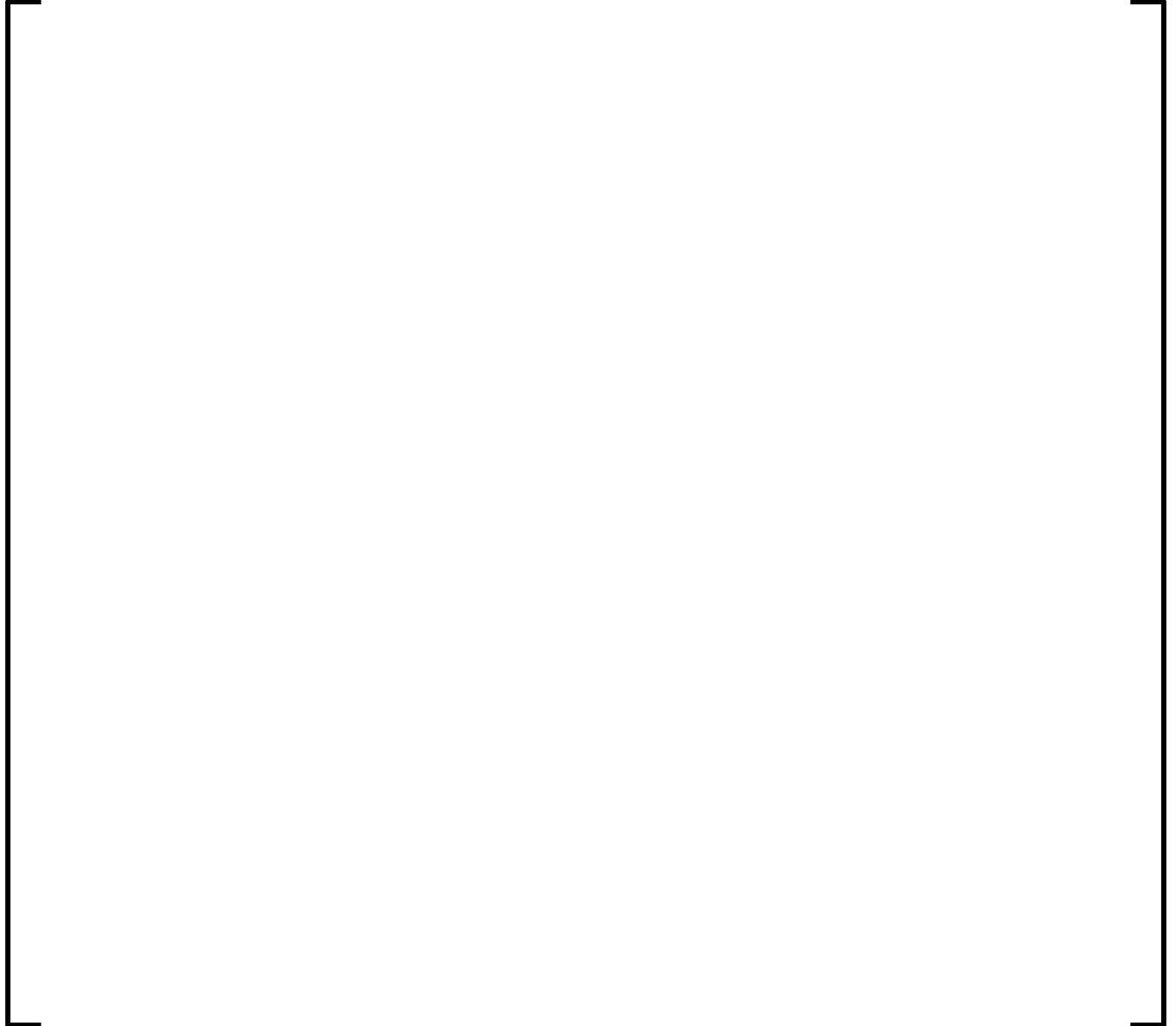




**Figure G2 5.3.6-23**  
**Plant G2 MOC 1 Core Average Axial Power Distribution**



**Figure G2 5.3.6-24**  
**Plant G2 EOC 1 Core Average Axial Power Distribution**



**Figure G2 5.3.6-25**  
**Plant G2 BOC 2 Core Average Axial Power Distribution**



**Figure G2 5.3.6-26**  
**Plant G2 MOC 2 Core Average Axial Power Distribution**



**Figure G2 5.3.6-27**  
**Plant G2 EOC 2 Core Average Axial Power Distribution**



**Figure G2 5.3.6-28**  
**Plant G2 BOC 3 Core Average Axial Power Distribution**



**Figure G2 5.3.6-29**  
**Plant G2 MOC 3 Core Average Axial Power Distribution**



**Figure G2 5.3.6-30**  
**Plant G2 EOC 3 Core Average Axial Power Distribution**

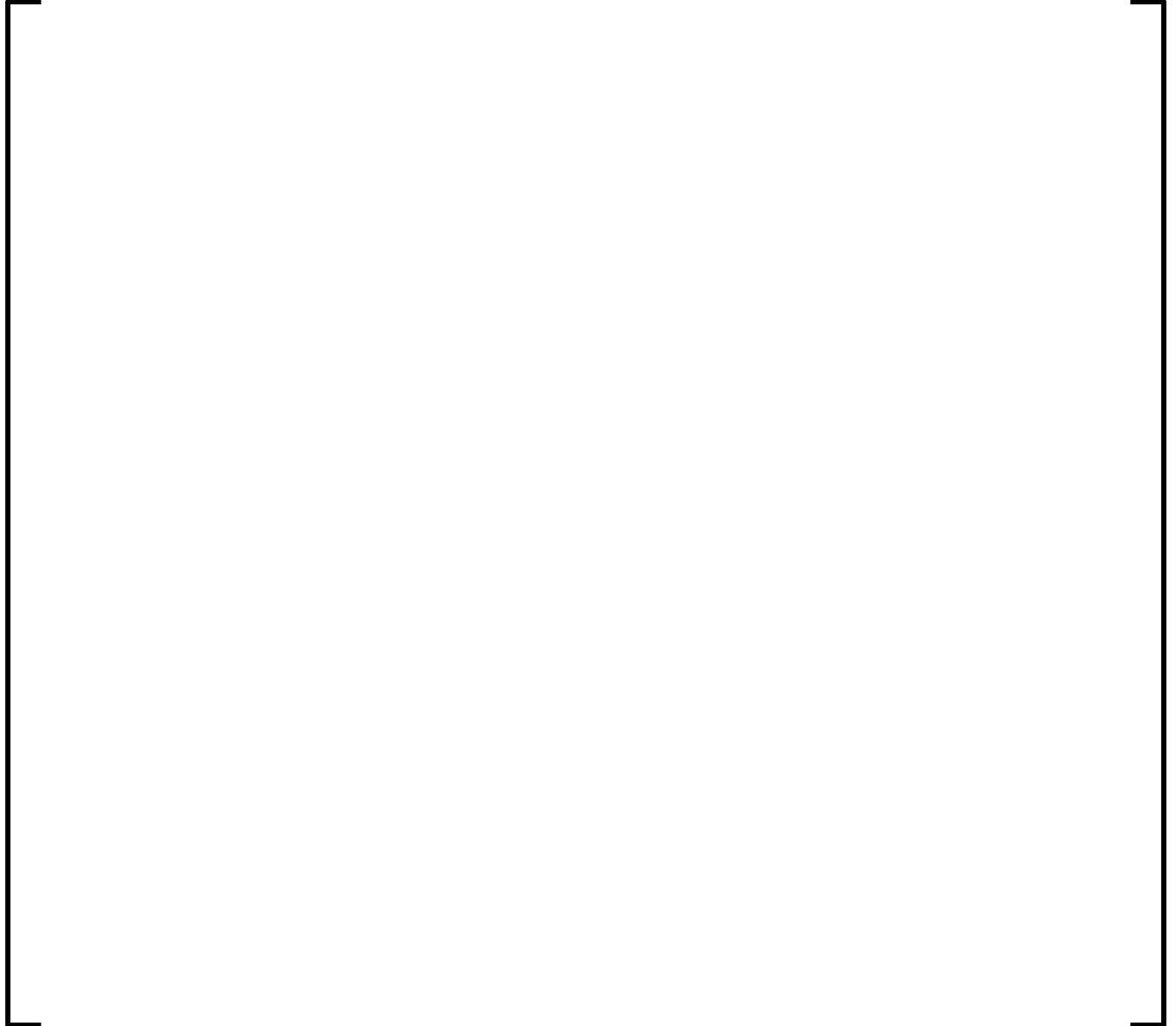




**Figure G2 5.3.6-31**  
**Plant G2 BOC 4 Core Average Axial Power Distribution**



**Figure G2 5.3.6-32**  
**Plant G2 MOC 4 Core Average Axial Power Distribution**



**Figure G2 5.3.6-33**  
**Plant G2 EOC 4 Core Average Axial Power Distribution**



**Figure G2 5.3.6-34**  
**Plant G2 BOC 5 Core Average Axial Power Distribution**



**Figure G2 5.3.6-35**  
**Plant G2 MOC 5 Core Average Axial Power Distribution**



**Figure G2 5.3.6-36**  
**Plant G2 EOC 5 Core Average Axial Power Distribution**



## **APPENDIX S1**

**Table S1 5.2.7-1**  
**Plant S1 Hot Zero Power All Rods Out Critical Boron Concentrations**  
**for Cycles 12-14**

[

]

**Table S1 5.2.7-2**  
**Plant S1 Cycle 12 Hot Zero Power Individual Rod Bank Worth**

--	--



**Table S1 5.2.7-3**  
**Plant S1 Cycle 13 Hot Zero Power Individual Rod Bank Worth**

--	--

**Table S1 5.2.7-4**  
**Plant S1 Cycle 14 Hot Zero Power Individual Rod Bank Worth**

--	--

**Table S1 5.2.7-5**  
**Plant S1 Summary of Total Bank Worths**

--	--

**Table S1 5.2.7-6**  
**Plant S1 Hot Zero Power All Rods Out Isothermal Temperature**  
**Coefficient for Cycles 12-14**

--	--

**Figure S1 5.3.7-1**  
**Plant S1 Cycle 12 Critical Boron Concentration vs. Burnup**



**Figure S1 5.3.7-2**  
**Plant S1 Cycle 13 Critical Boron Concentration vs. Burnup**



**Figure S1 5.3.7-3**  
**Plant S1 Cycle 14 Critical Boron Concentration vs. Burnup**



**Figure S1 5.3.7-4**  
**Plant S1 Cycles 12-14 Boron Differences**





**Figure S1 5.3.7-5**  
**Plant S1 BOC 12 Assembly Average Radial Power Distribution**

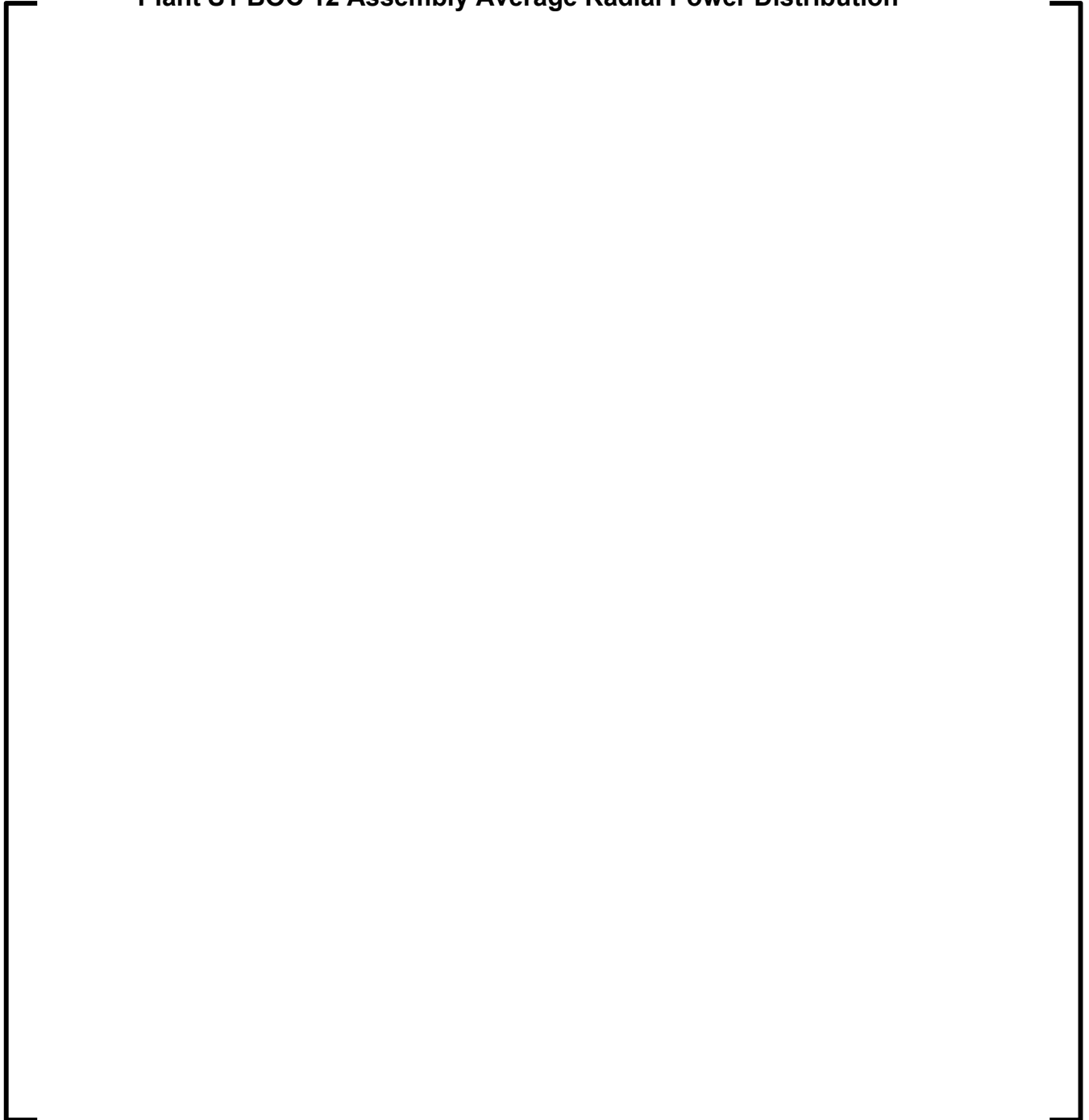


**Figure S1 5.3.7-6**  
**Plant S1 MOC 12 Assembly Average Radial Power Distribution**

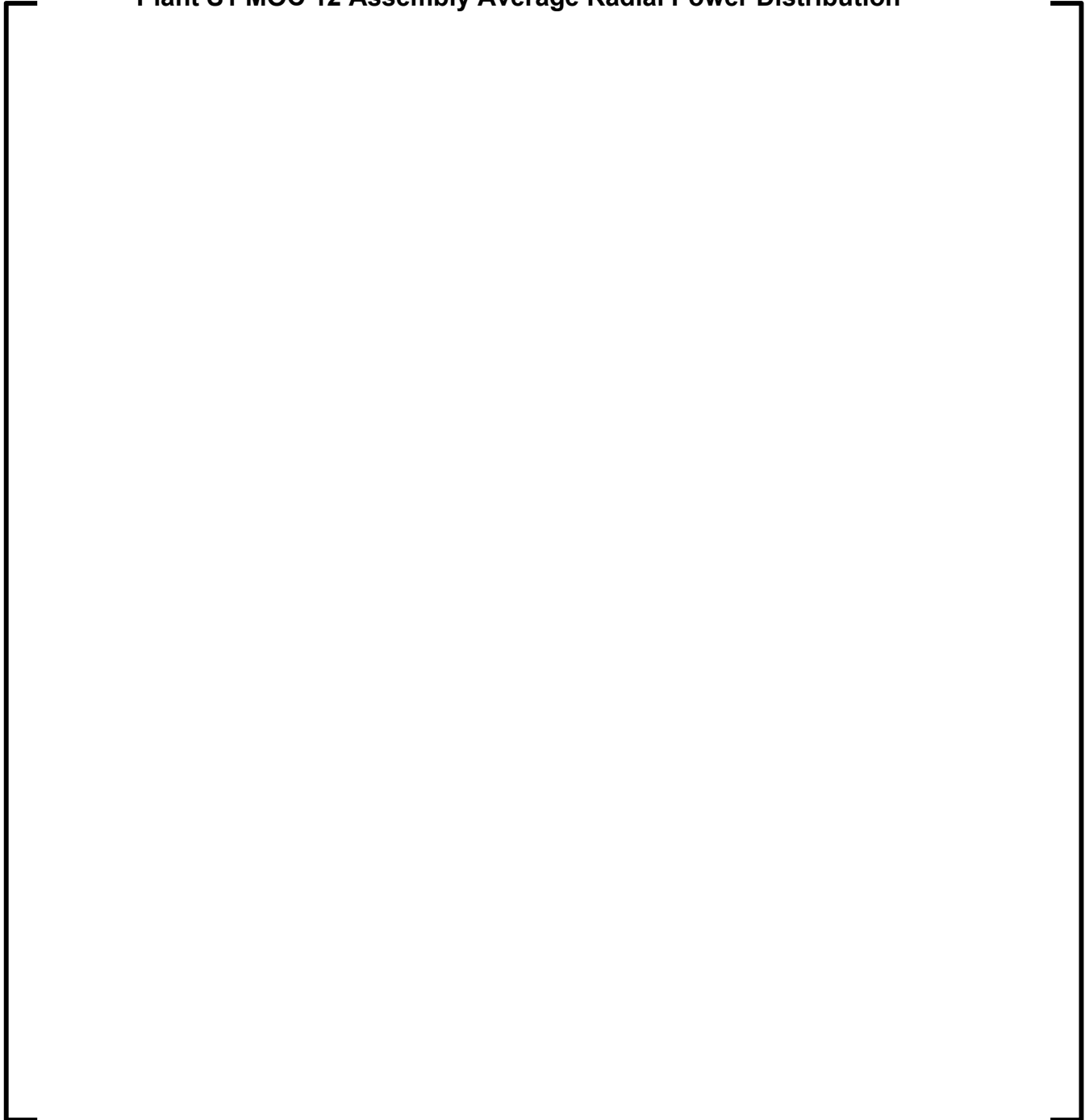


**Figure S1 5.3.7-7**  
**Plant S1 EOC 12 Assembly Average Radial Power Distribution**

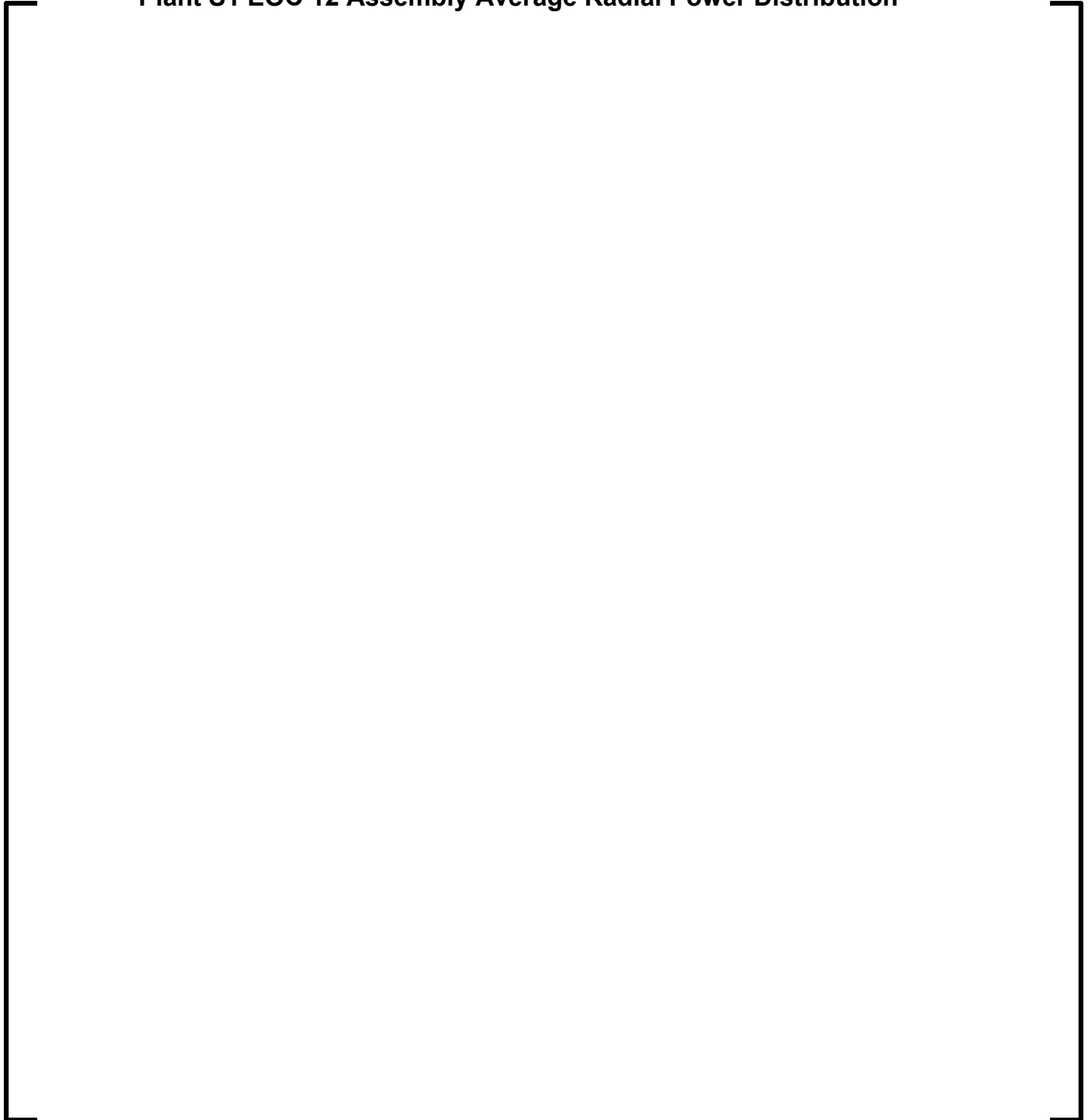


**Figure S1 5.3.7-8**  
**Plant S1 BOC 13 Assembly Average Radial Power Distribution**

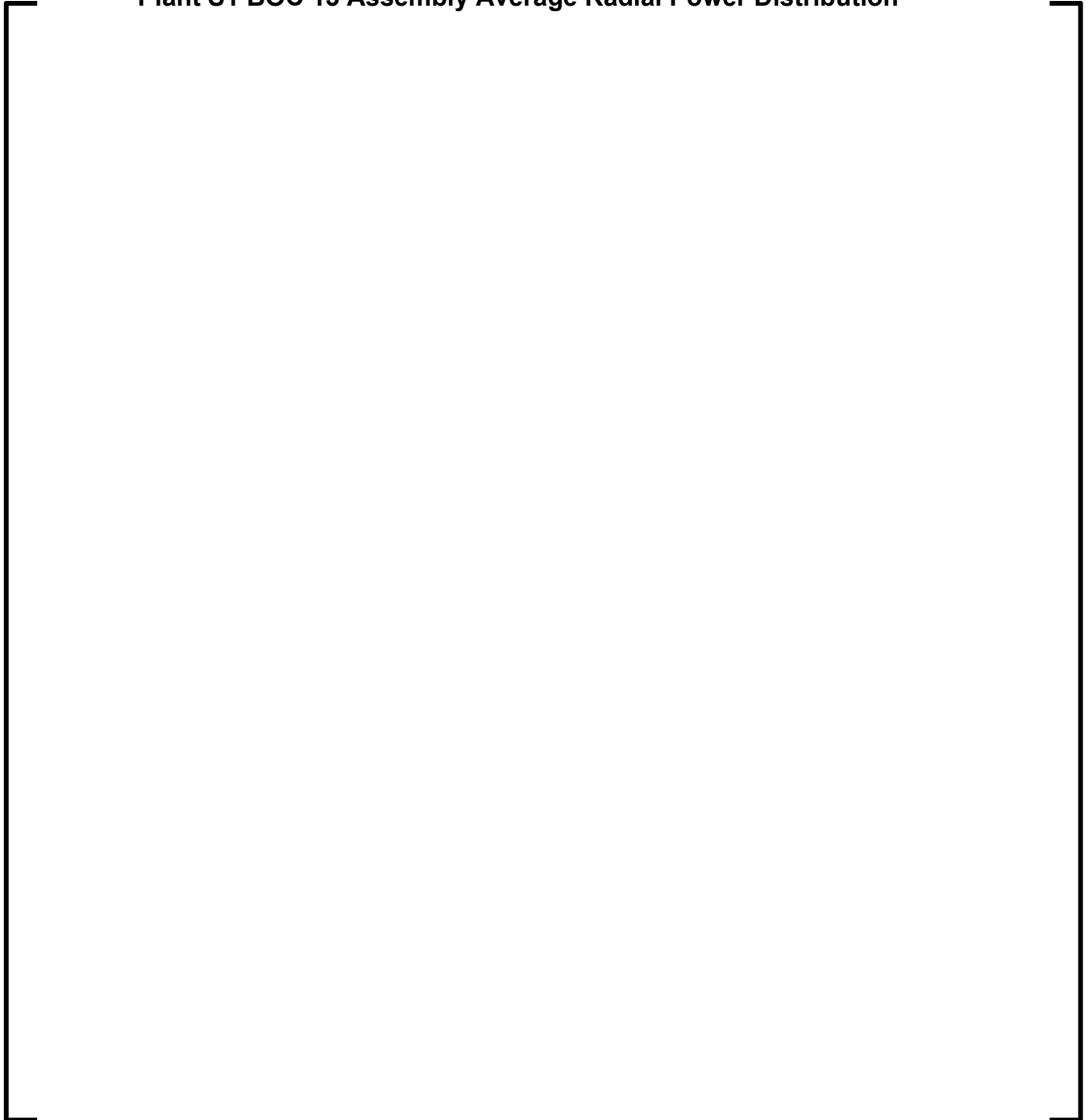


**Figure S1 5.3.7-9**  
**Plant S1 MOC 13 Assembly Average Radial Power Distribution**

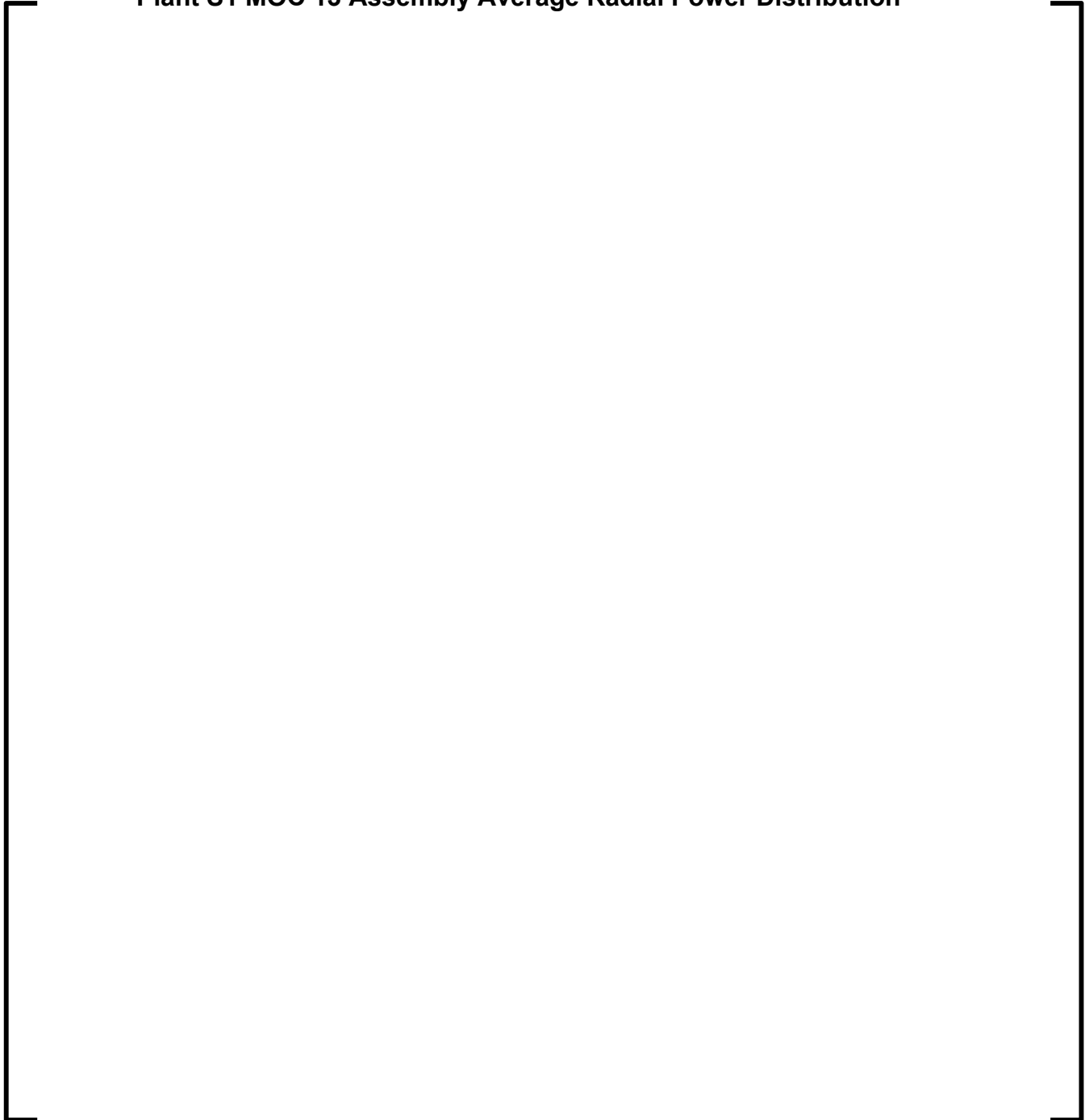


**Figure S1 5.3.7-10**  
**Plant S1 EOC 13 Assembly Average Radial Power Distribution**

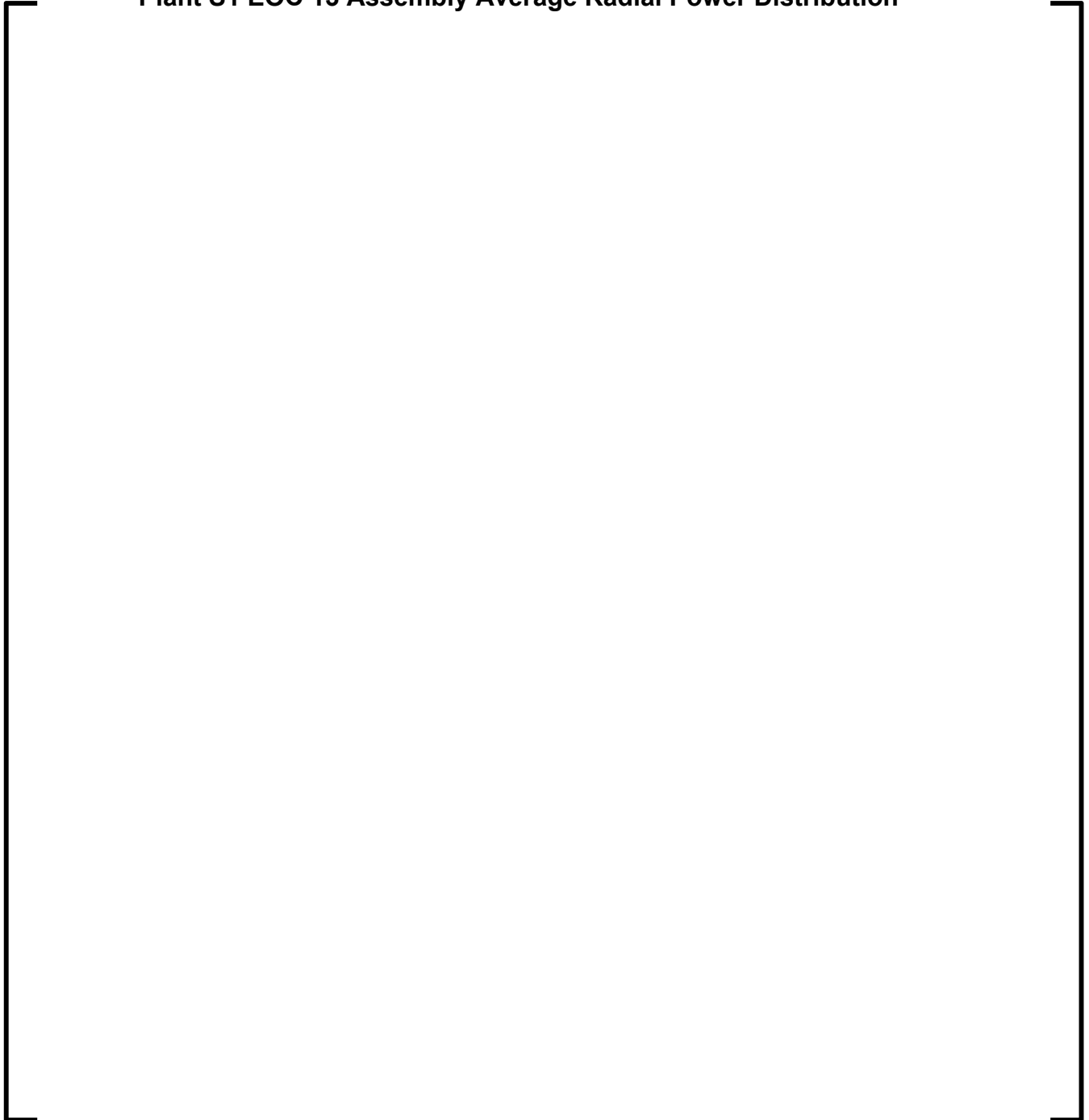


**Figure S1 5.3.7-11**  
**Plant S1 BOC 14 Assembly Average Radial Power Distribution**

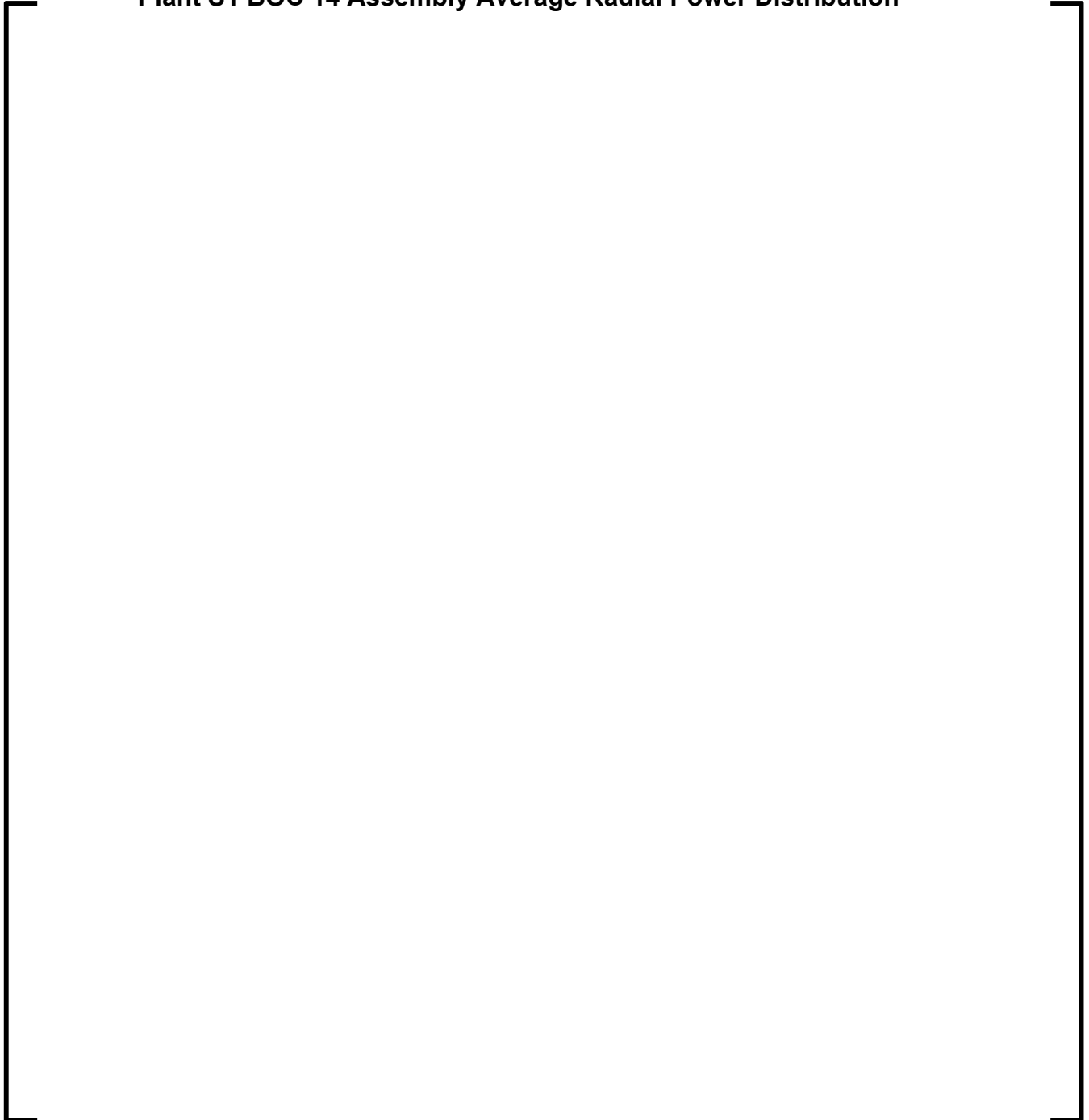


**Figure S1 5.3.7-12**  
**Plant S1 MOC 14 Assembly Average Radial Power Distribution**

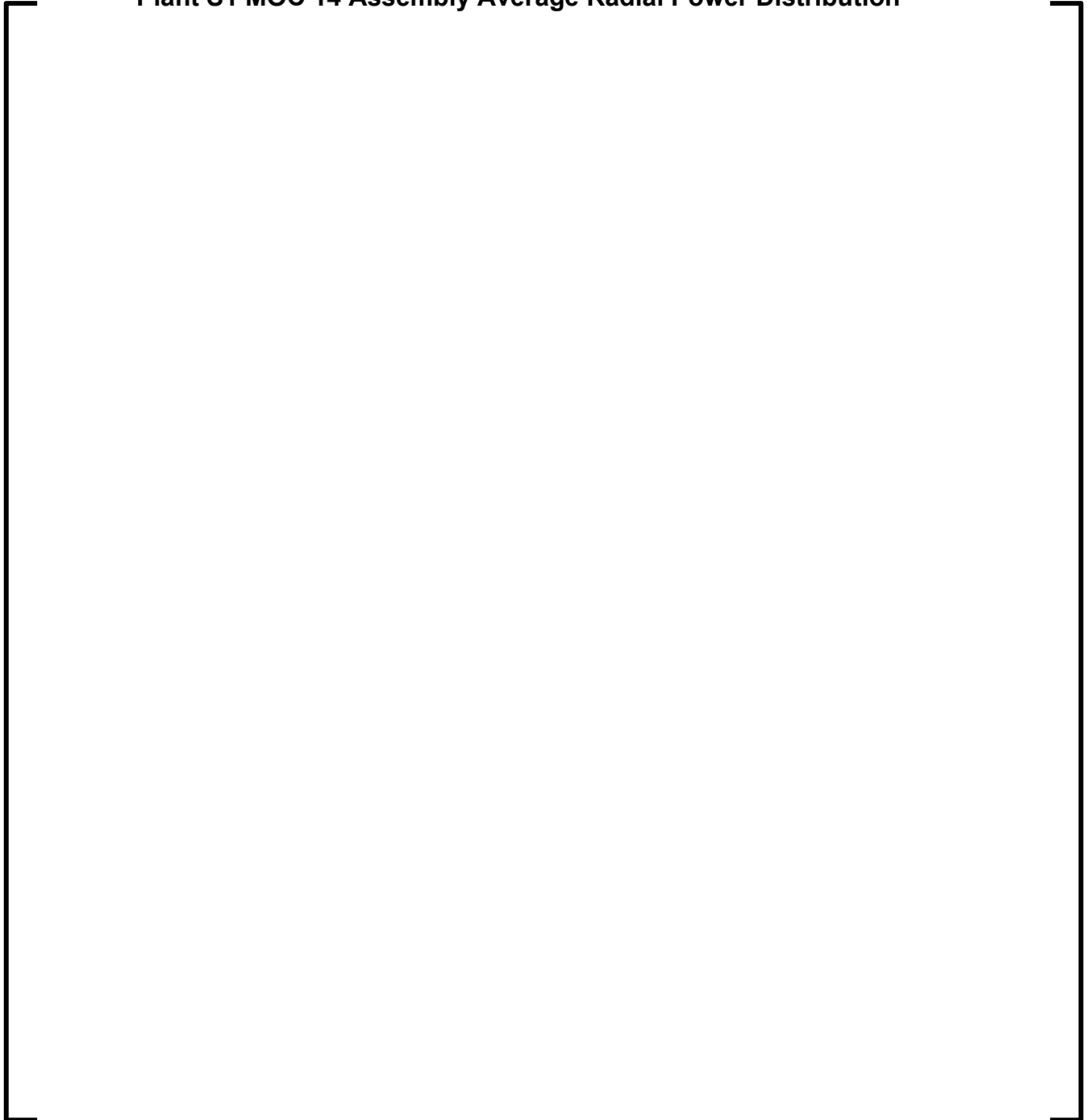




**Figure S1 5.3.7-13**  
**Plant S1 EOC 14 Assembly Average Radial Power Distribution**

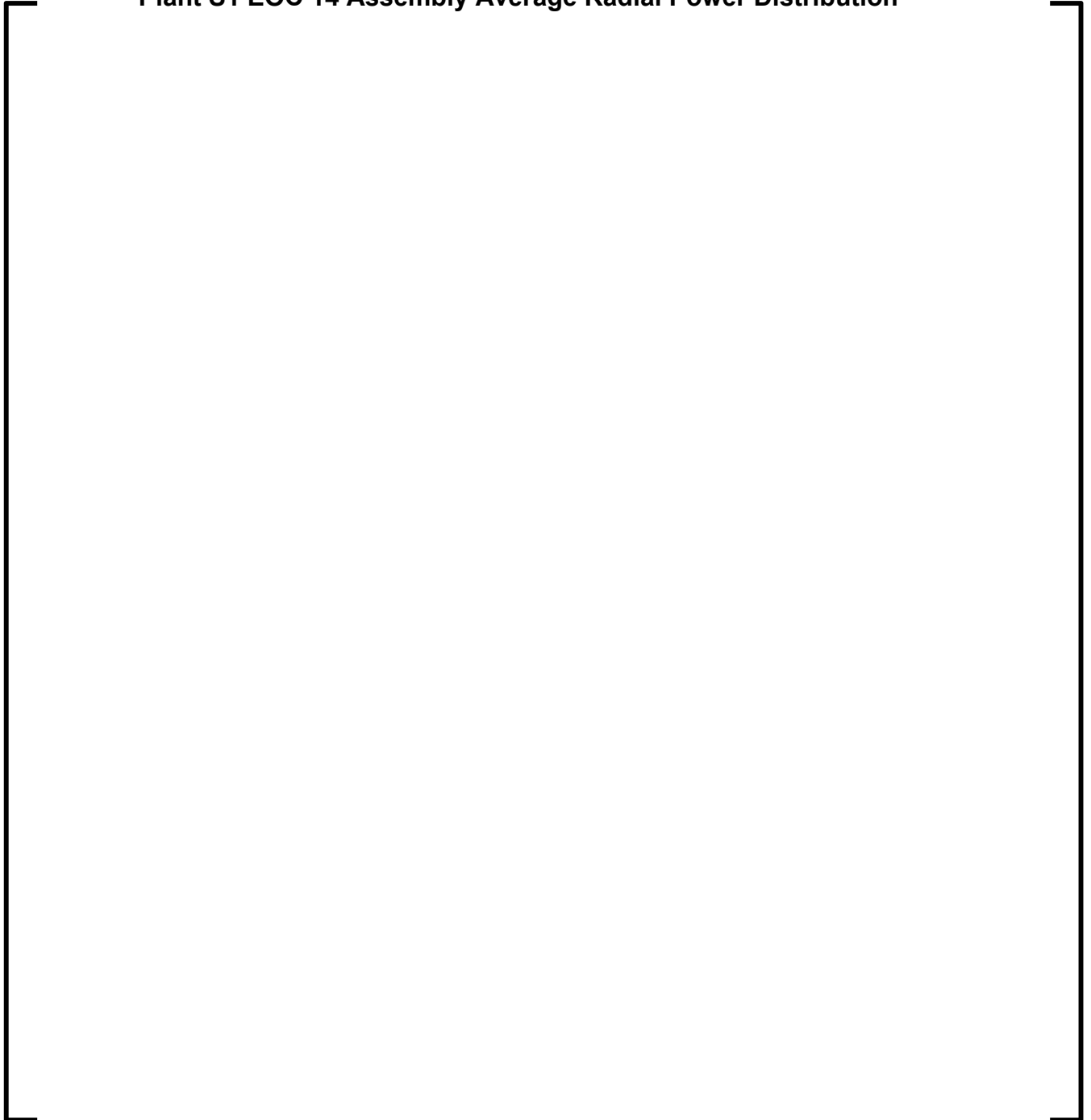


**Figure S1 5.3.7-14**  
**Plant S1 BOC 12 Core Average Axial Power Distribution**



**Figure S1 5.3.7-15**  
**Plant S1 MOC 12 Core Average Axial Power Distribution**



**Figure S1 5.3.7-16**  
**Plant S1 EOC 12 Core Average Axial Power Distribution**



**Figure S1 5.3.7-17**  
**Plant S1 BOC 13 Core Average Axial Power Distribution**



**Figure S1 5.3.7-18**  
**Plant S1 MOC 13 Core Average Axial Power Distribution**



**Figure S1 5.3.7-19**  
**Plant S1 EOC 13 Core Average Axial Power Distribution**



**Figure S1 5.3.7-20**  
**Plant S1 BOC 14 Core Average Axial Power Distribution**





**Figure S1 5.3.7-21**  
**Plant S1 MOC 14 Core Average Axial Power Distribution**



**Figure S1 5.3.7-22**  
**Plant S1 EOC 14 Core Average Axial Power Distribution**



## **APPENDIX S2**

### **Table S2 5.2.8-1**

#### **Plant S2 Hot Zero Power All Rods Out Critical Boron Concentrations for Cycles 12-14**



**Table S2 5.2.8-2**  
**Plant S2 Cycle 12 Hot Zero Power Individual Rod Bank Worth**

--	--

**Table S2 5.2.8-3**  
**Plant S2 Cycle 13 Hot Zero Power Individual Rod Bank Worth**

--	--

**Table S2 5.2.8-4**  
**Plant S2 Cycle 14 Hot Zero Power Individual Rod Bank Worth**

--	--

**Table S2 5.2.8-5**  
**Plant S2 Summary of Total Bank Worths**

--	--

**Table S2 5.2.8-6**  
**Plant S2 Hot Zero Power All Rods Out Isothermal Temperature**  
**Coefficient for Cycles 12-14**





**Figure S2 5.3.8-1**  
**Plant S2 Cycle 12 Critical Boron Concentration vs. Burnup**



**Figure S2 5.3.8-2**  
**Plant S2 Cycle 13 Critical Boron Concentration vs. Burnup**



**Figure S2 5.3.8-3**  
**Plant S2 Cycle 14 Critical Boron Concentration vs. Burnup**



**Figure S2 5.3.8-4**  
**Plant S2 Cycles 12-14 Boron Differences**



**Figure S2 5.3.8-5**  
**Plant S2 BOC 12 Assembly Average Radial Power Distribution**

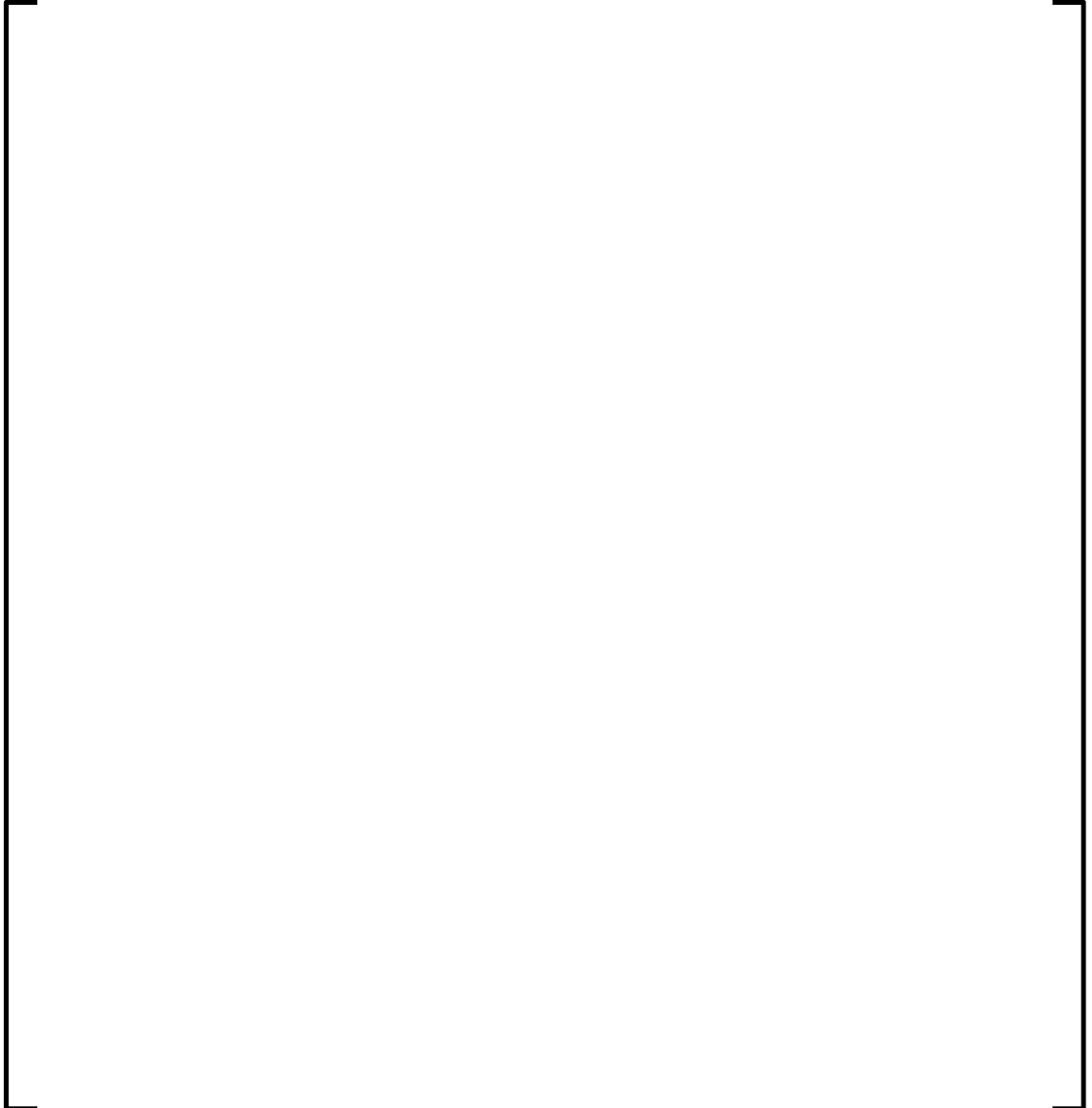


**Figure S2 5.3.8-6**  
**Plant S2 MOC 12 Assembly Average Radial Power Distribution**

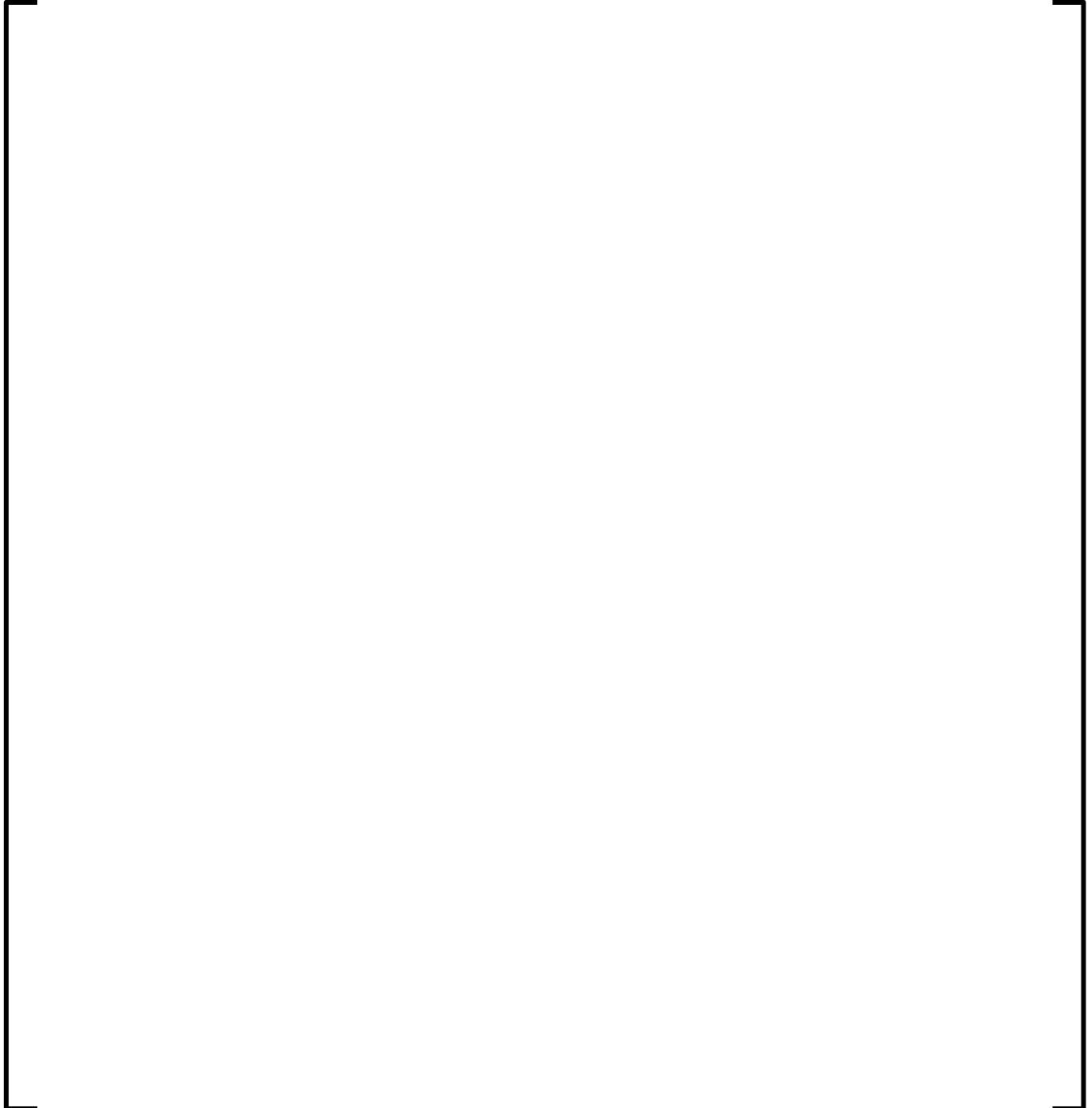


**Figure S2 5.3.8-7**  
**Plant S2 EOC 12 Assembly Average Radial Power Distribution**

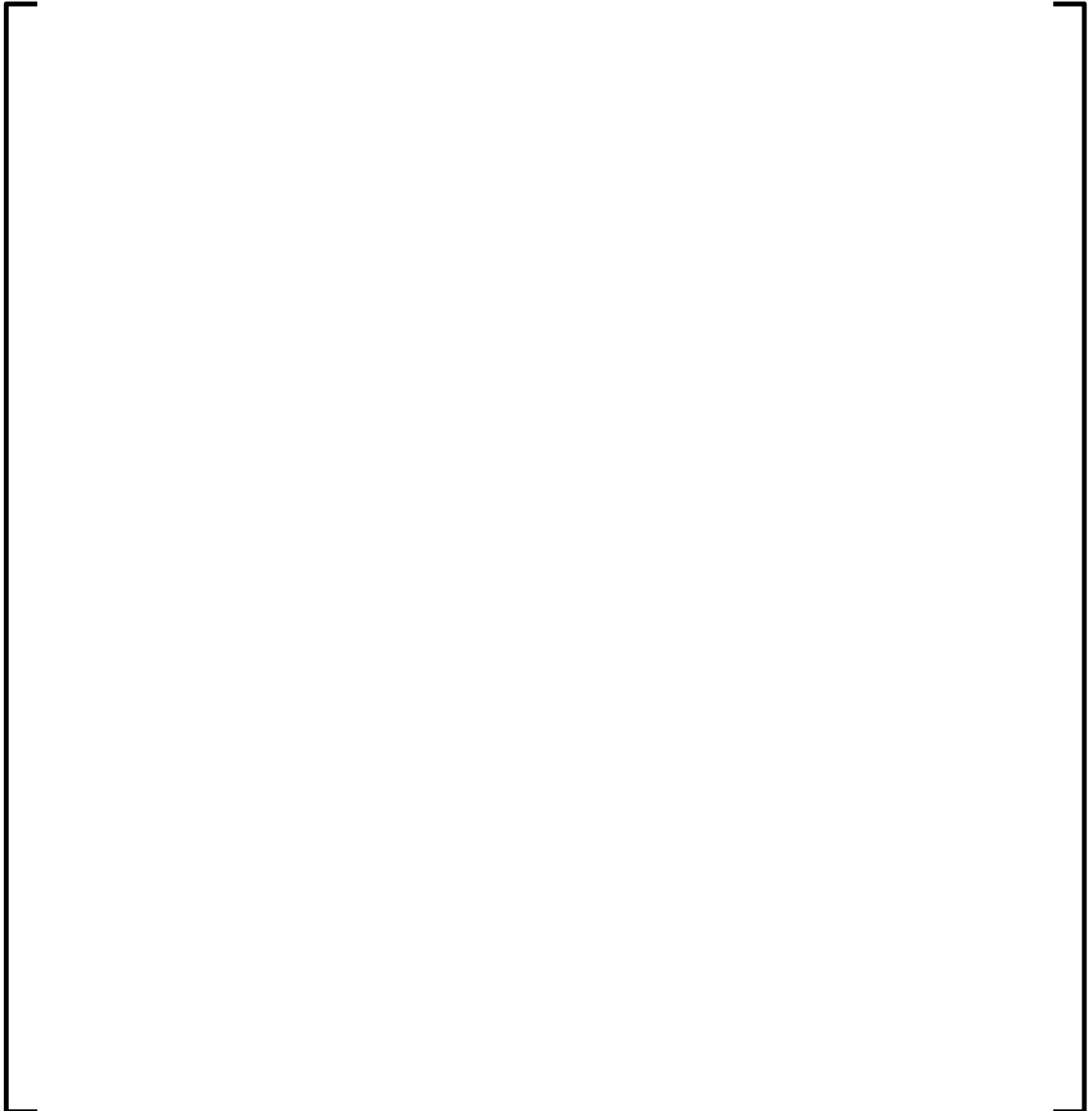


**Figure S2 5.3.8-8**  
**Plant S2 BOC 13 Assembly Average Radial Power Distribution**

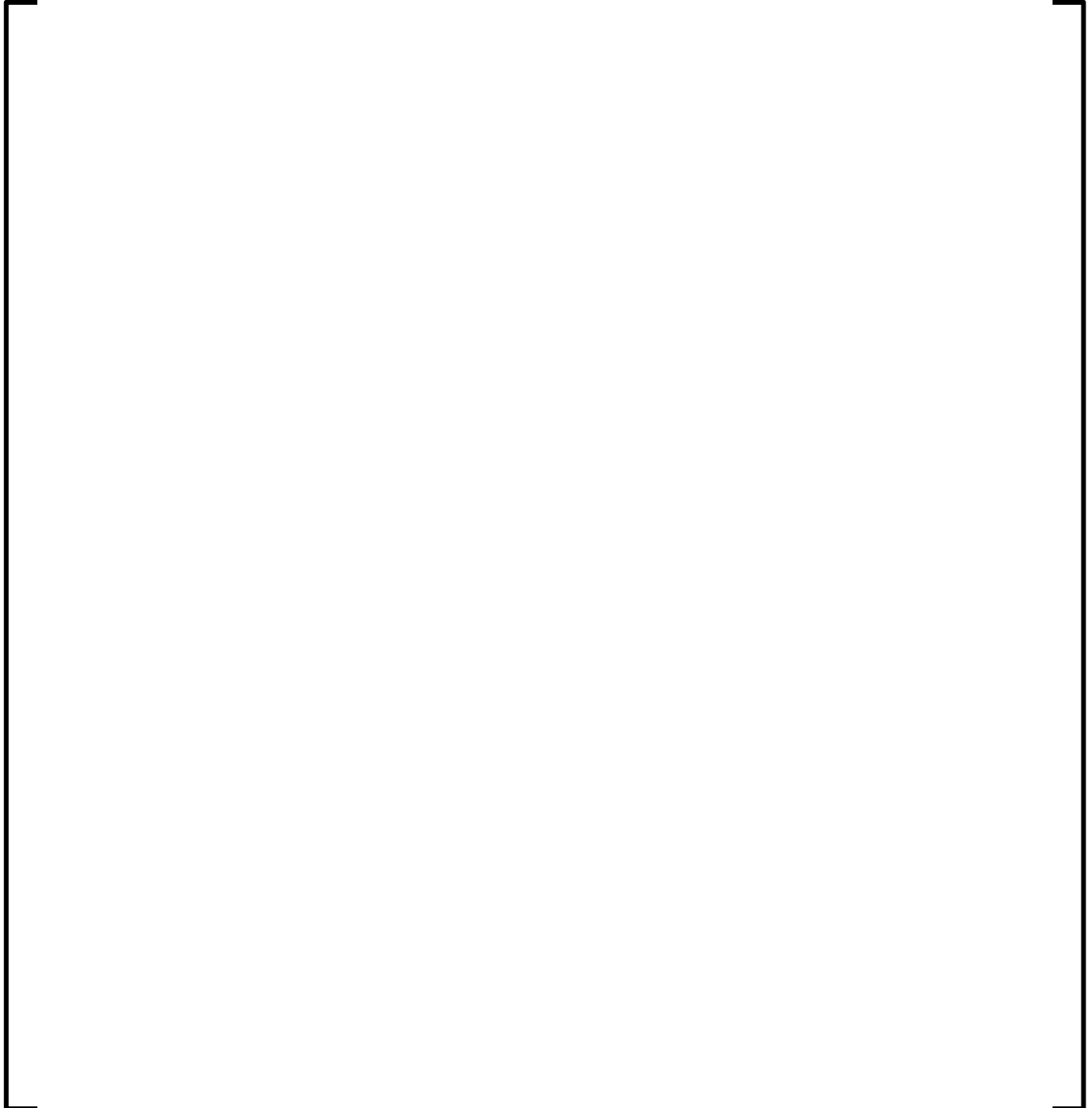




**Figure S2 5.3.8-9**  
**Plant S2 MOC 13 Assembly Average Radial Power Distribution**

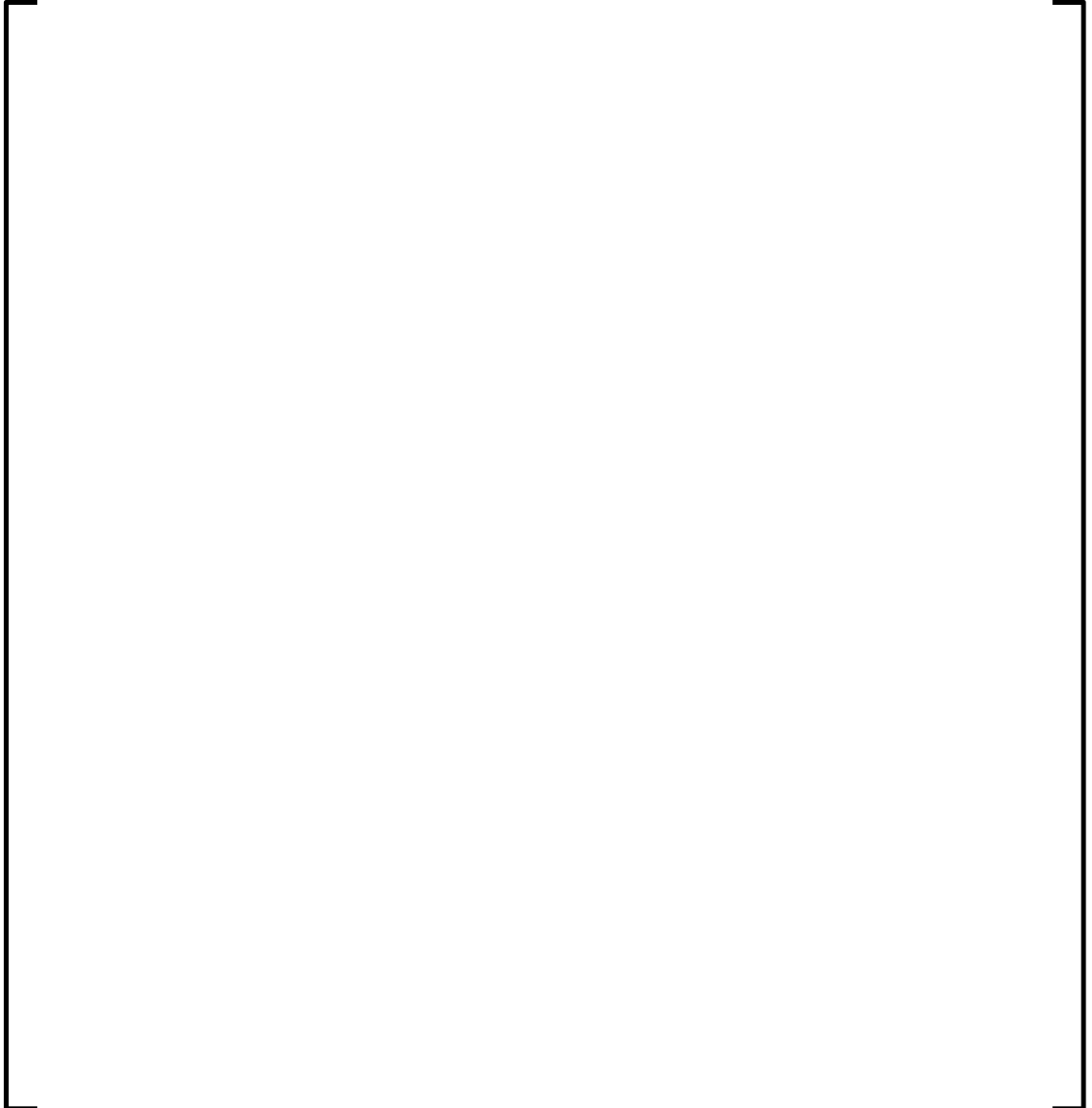


**Figure S2 5.3.8-10**  
**Plant S2 EOC 13 Assembly Average Radial Power Distribution**

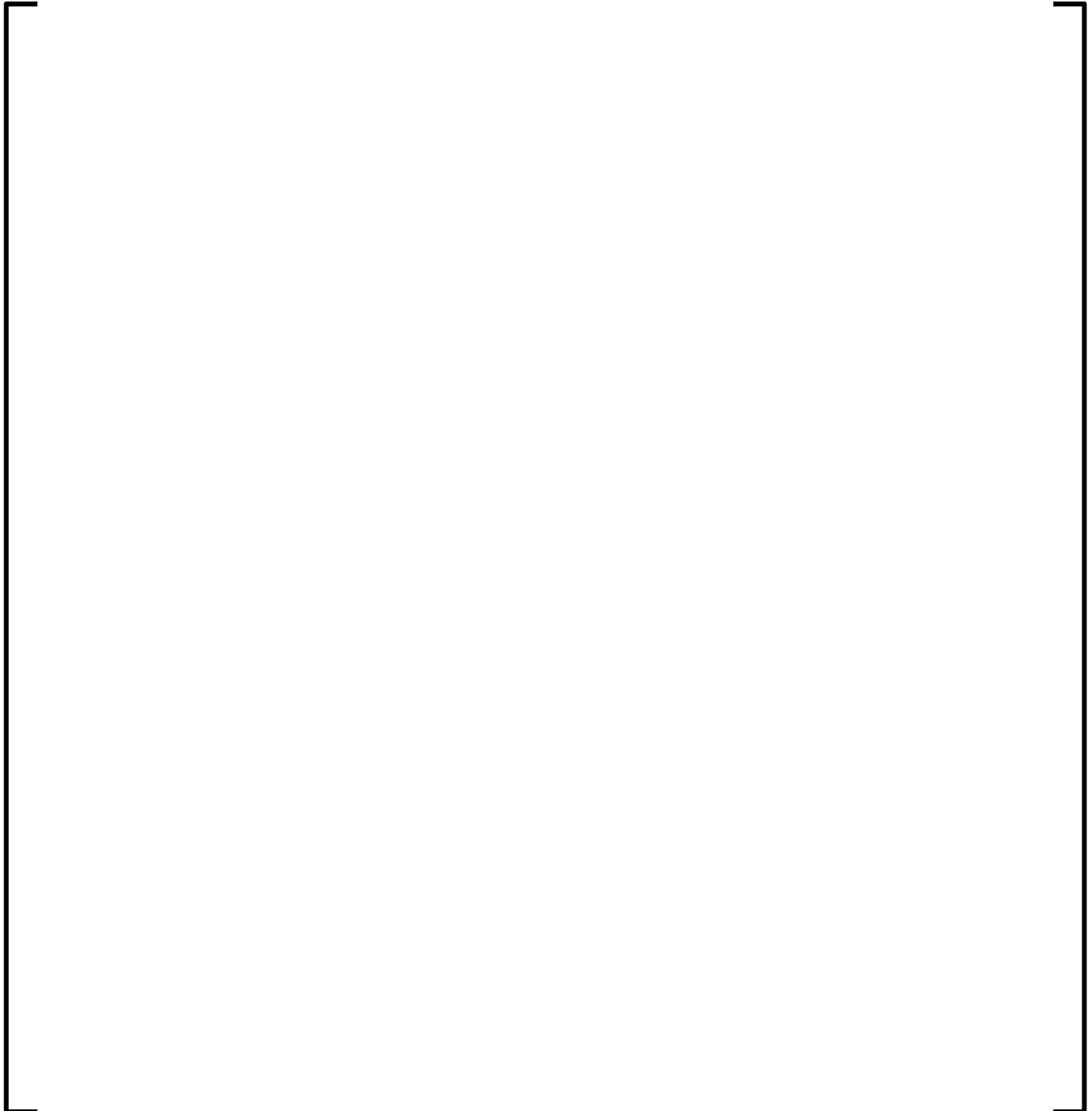


**Figure S2 5.3.8-11**  
**Plant S2 BOC 14 Assembly Average Radial Power Distribution**

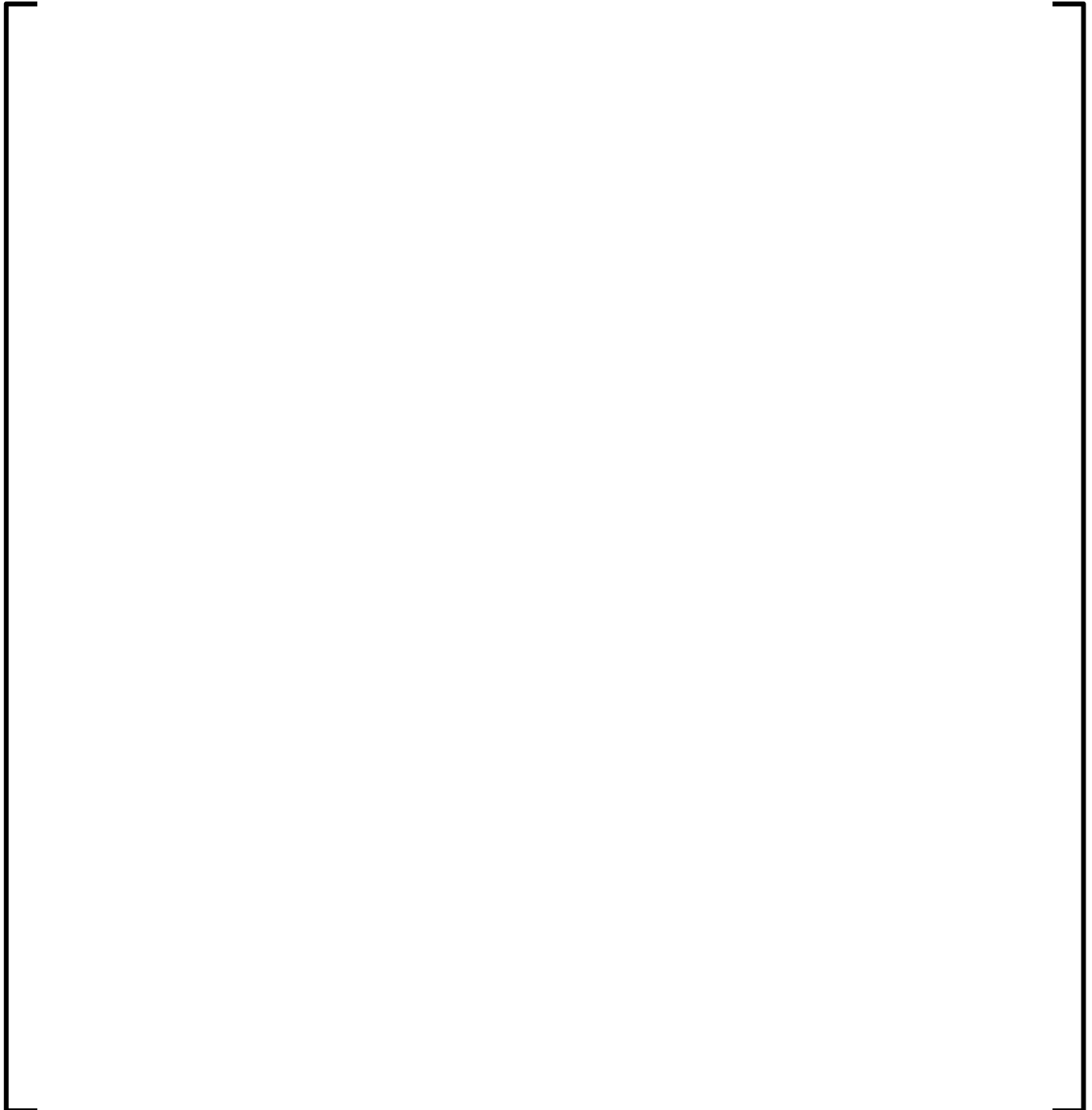


**Figure S2 5.3.8-12**  
**Plant S2 MOC 14 Assembly Average Radial Power Distribution**

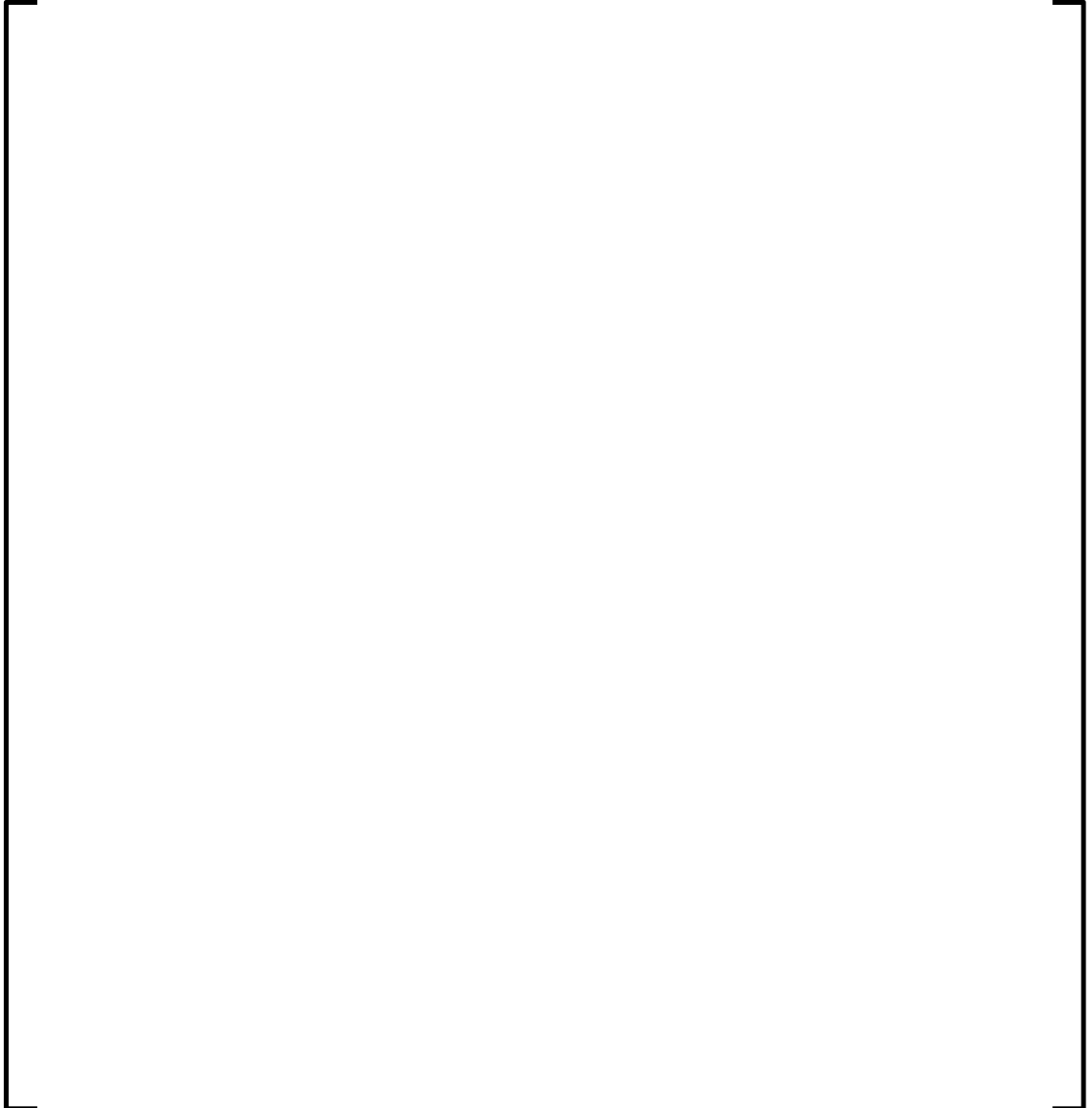


**Figure S2 5.3.8-13**  
**Plant S2 EOC 14 Assembly Average Radial Power Distribution**

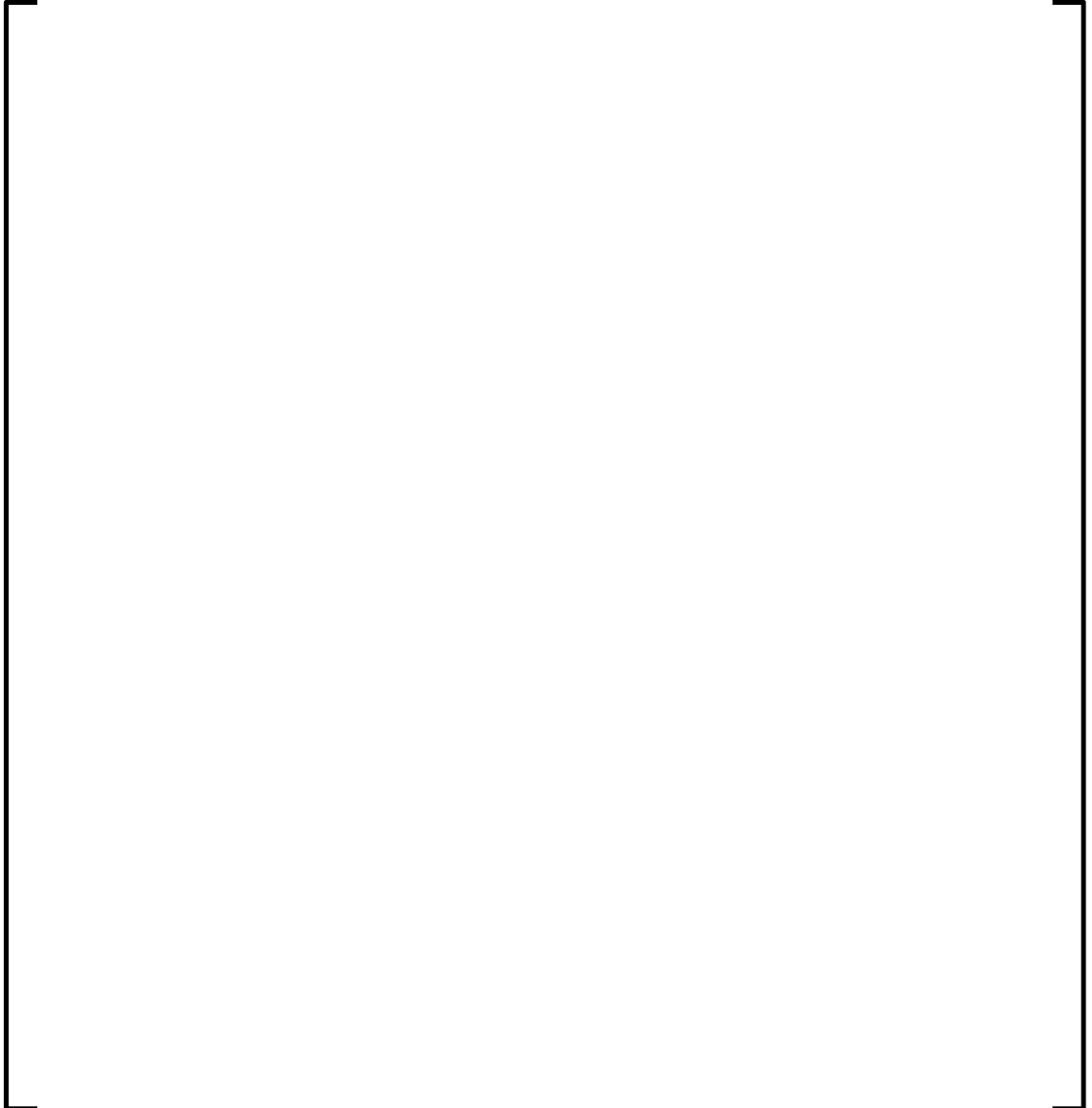


**Figure S2 5.3.8-14**  
**Plant S2 BOC 12 Core Average Axial Power Distribution**



**Figure S2 5.3.8-15**  
**Plant S2 MOC 12 Core Average Axial Power Distribution**



**Figure S2 5.3.8-16**  
**Plant S2 EOC 12 Core Average Axial Power Distribution**





**Figure S2 5.3.8-17**  
**Plant S2 BOC 13 Core Average Axial Power Distribution**



**Figure S2 5.3.8-18**  
**Plant S2 MOC 13 Core Average Axial Power Distribution**



**Figure S2 5.3.8-19**  
**Plant S2 EOC 13 Core Average Axial Power Distribution**



**Figure S2 5.3.8-20**  
**Plant S2 BOC 14 Core Average Axial Power Distribution**



**Figure S2 5.3.8-21**  
**Plant S2 MOC 14 Core Average Axial Power Distribution**



**Figure S2 5.3.8-22**  
**Plant S2 EOC 14 Core Average Axial Power Distribution**



## **APPENDIX T1**

### **Table T1 5.2.9-1**

#### **Plant T1 Hot Zero Power All Rods Out Critical Boron Concentrations for Cycles 9-15**



**Table T1 5.2.9-2**  
**Plant T1 Cycle 9 Hot Zero Power Individual Rod Bank Worth**

--	--



**Table T1 5.2.9-3**  
**Plant T1 Cycle 10 Hot Zero Power Individual Rod Bank Worth**

--	--

**Table T1 5.2.9-4**  
**Plant T1 Cycle 11 Hot Zero Power Individual Rod Bank Worth**

--	--

**Table T1 5.2.9-5**  
**Plant T1 Cycle 12 Hot Zero Power Individual Rod Bank Worth**

--	--

**Table T1 5.2.9-6**  
**Plant T1 Cycle 13 Hot Zero Power Individual Rod Bank Worth**

--	--

**Table T1 5.2.9-7**  
**Plant T1 Cycle 14 Hot Zero Power Individual Rod Bank Worth**

--	--

**Table T1 5.2.9-8**  
**Plant T1 Cycle 15 Hot Zero Power Individual Rod Bank Worth**

--	--

**Table T1 5.2.9-9**  
**Plant T1 Summary of Total Bank Worths**

--	--

**Table T1 5.2.9-10**  
**Plant T1 Hot Zero Power All Rods Out Isothermal Temperature**  
**Coefficient for Cycles 9-15**





**Figure T1 5.3.9-1**  
**Plant T1 Cycle 9 Critical Boron Concentration vs. Burnup**

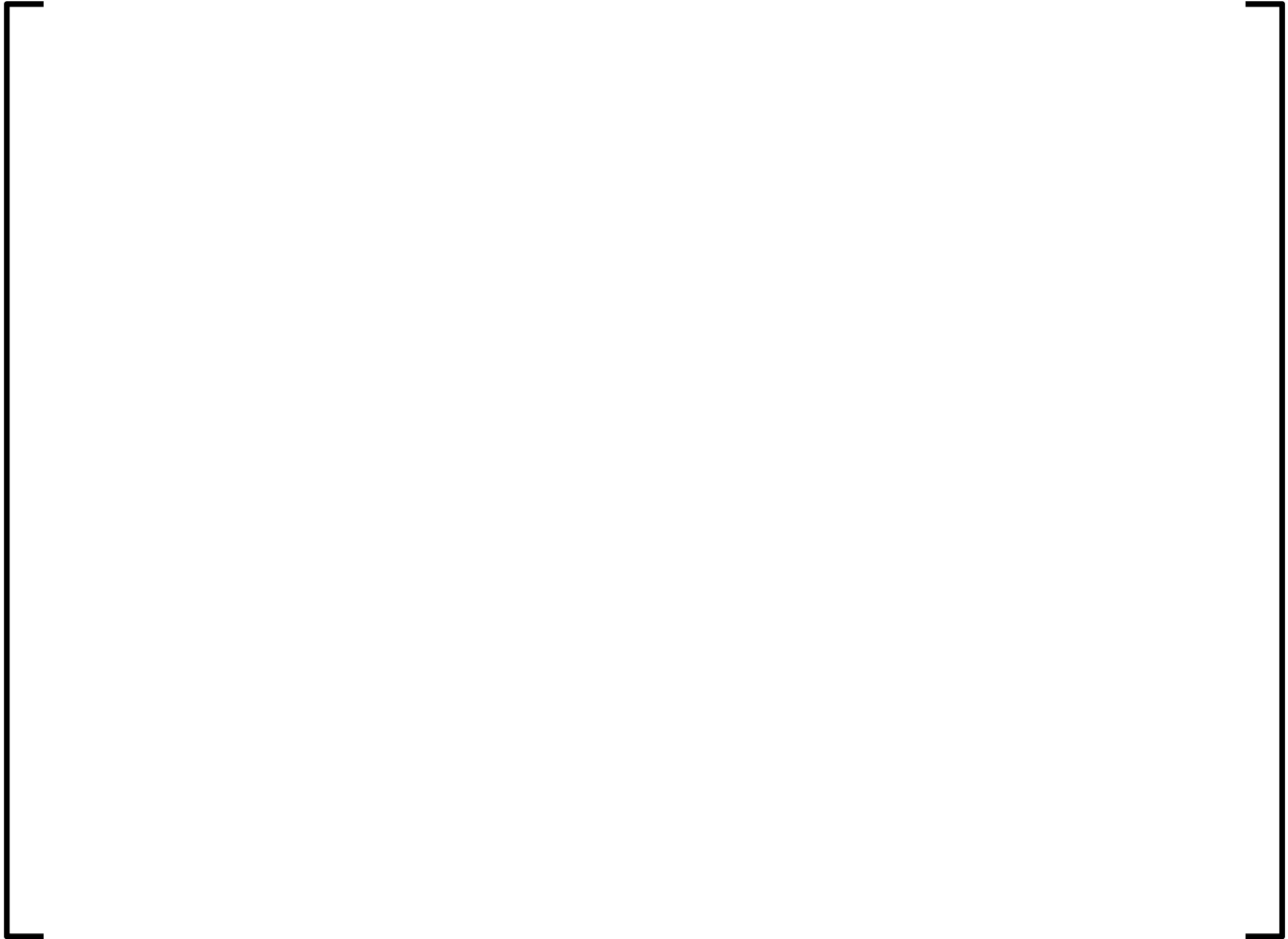


**Figure T1 5.3.9-2**  
**Plant T1 Cycle 10 Critical Boron Concentration vs. Burnup**



**Figure T1 5.3.9-3**  
**Plant T1 Cycle 11 Critical Boron Concentration vs. Burnup**



**Figure T1 5.3.9-4**  
**Plant T1 Cycle 12 Critical Boron Concentration vs. Burnup**



**Figure T1 5.3.9-5**  
**Plant T1 Cycle 13 Critical Boron Concentration vs. Burnup**



**Figure T1 5.3.9-6**  
**Plant T1 Cycle 14 Critical Boron Concentration vs. Burnup**



**Figure T1 5.3.9-7**  
**Plant T1 Cycle 15 Critical Boron Concentration vs. Burnup**



**Figure T1 5.3.9-8**  
**Plant T1 Cycles 9-15 Boron Differences**





**Figure T1 5.3.9-9**  
**Plant T1 BOC 12 Assembly Average Radial Power Distribution**

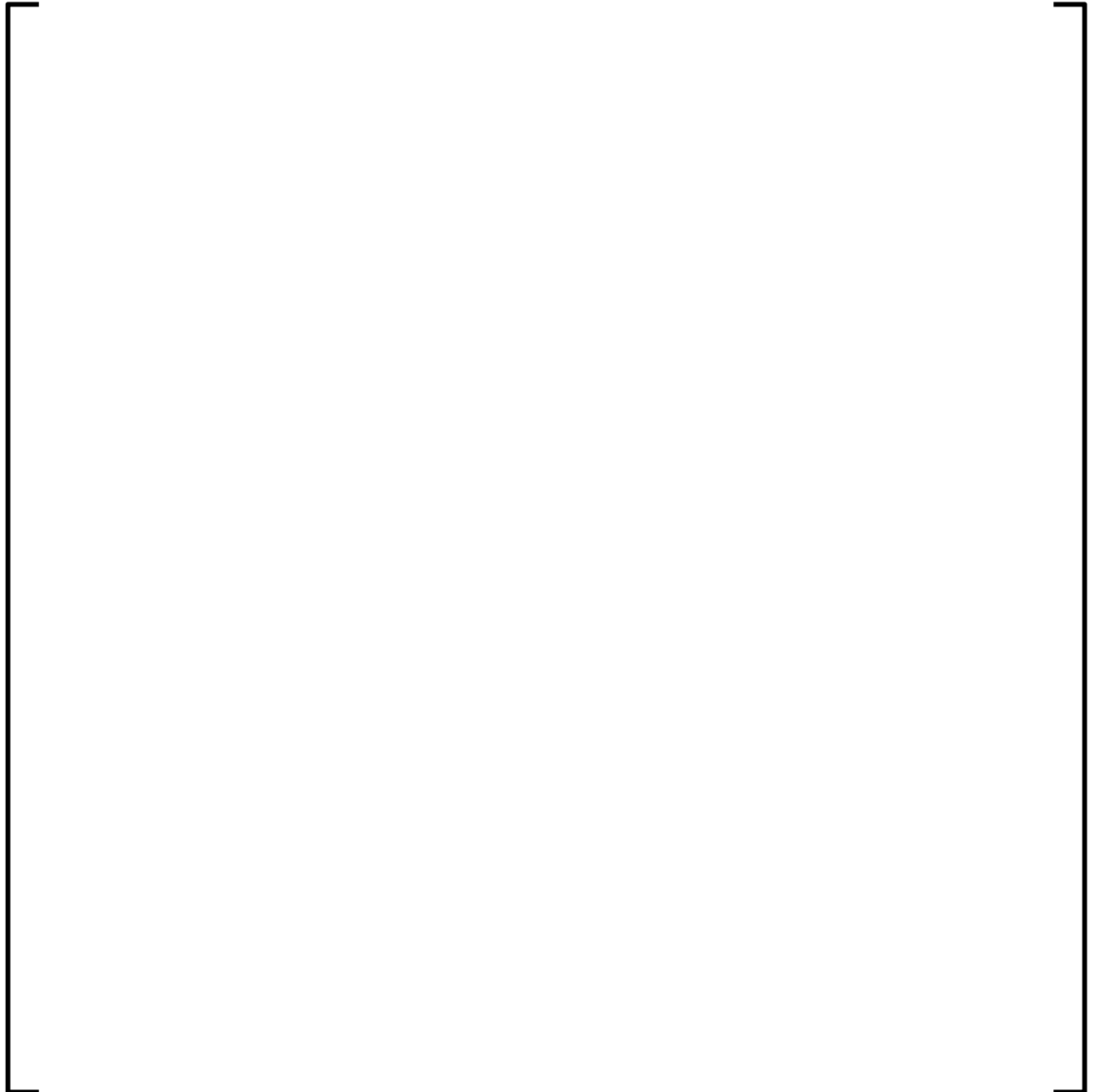


**Figure T1 5.3.9-10**  
**Plant T1 MOC 12 Assembly Average Radial Power Distribution**

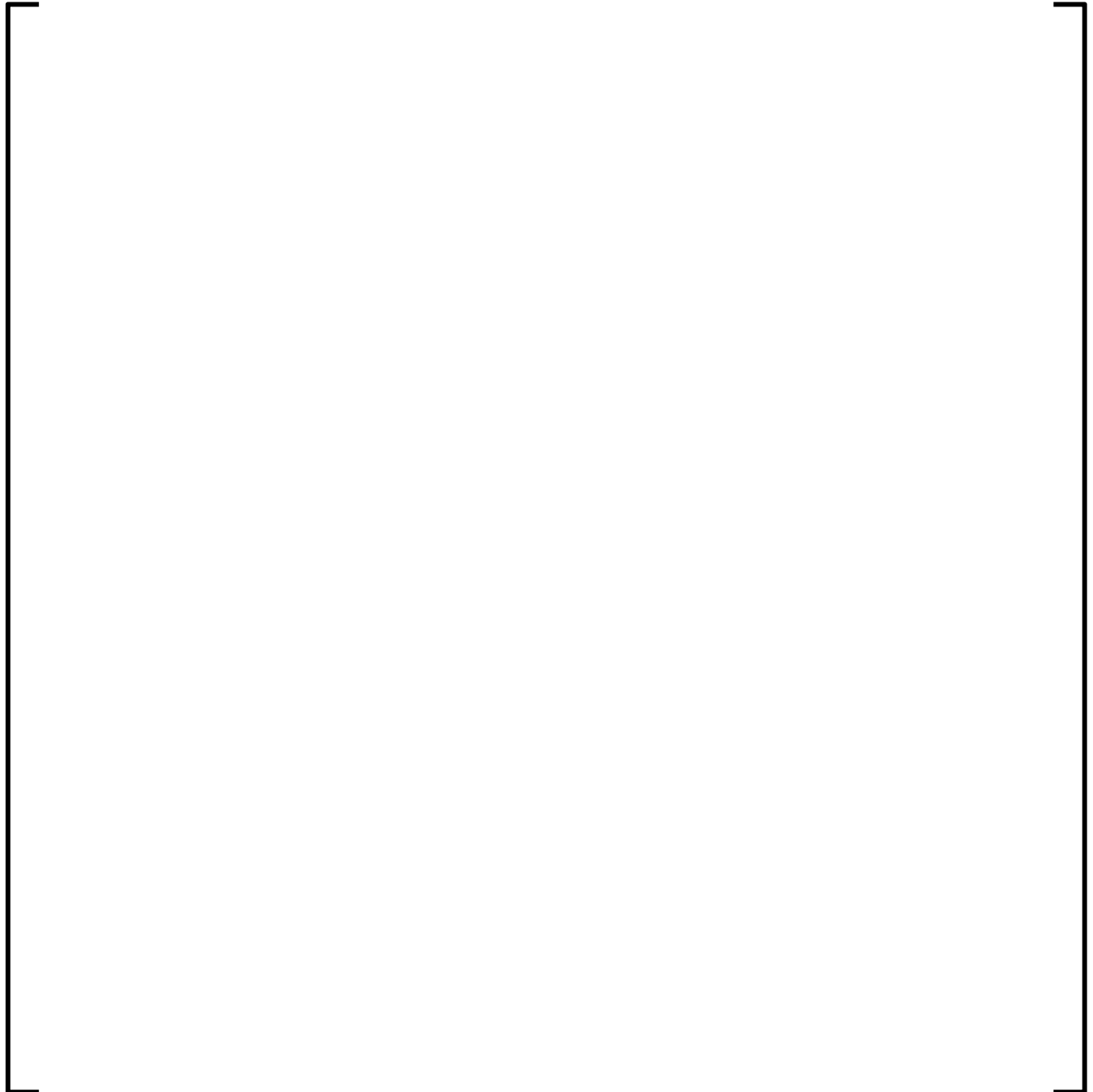


**Figure T1 5.3.9-11**  
**Plant T1 EOC 12 Assembly Average Radial Power Distribution**

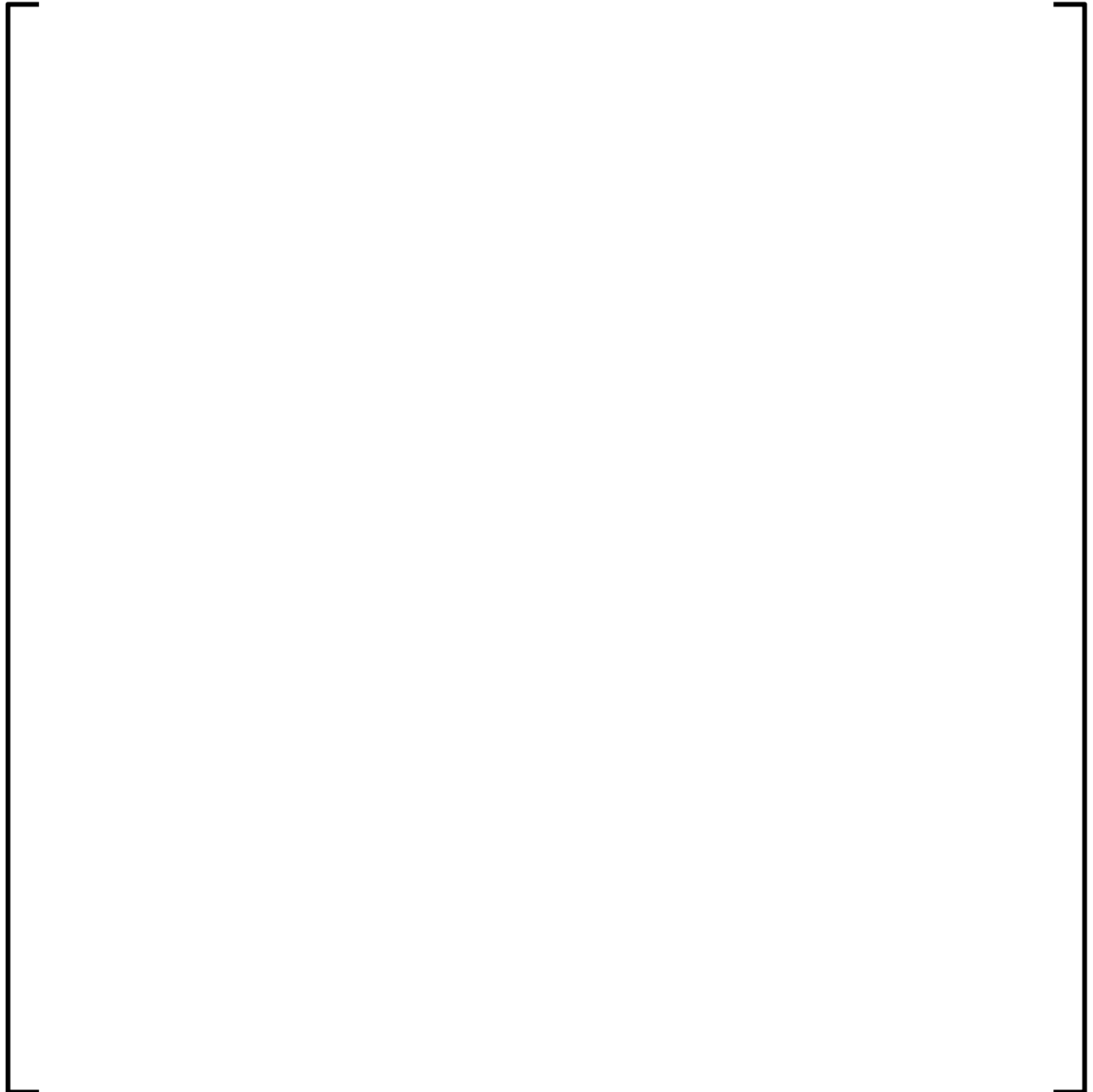


**Figure T1 5.3.9-12**  
**Plant T1 BOC 13 Assembly Average Radial Power Distribution**

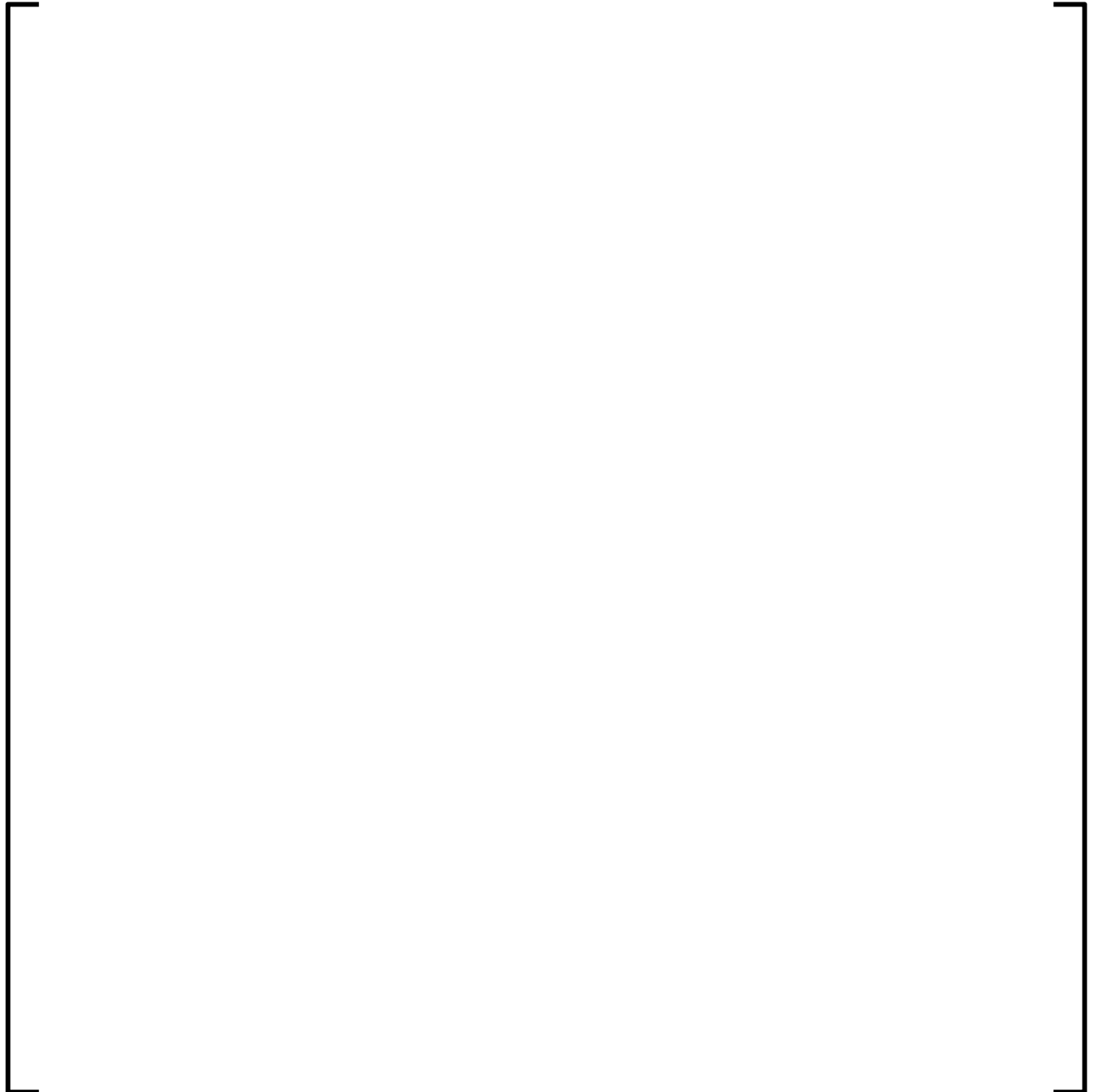


**Figure T1 5.3.9-13**  
**Plant T1 MOC 13 Assembly Average Radial Power Distribution**

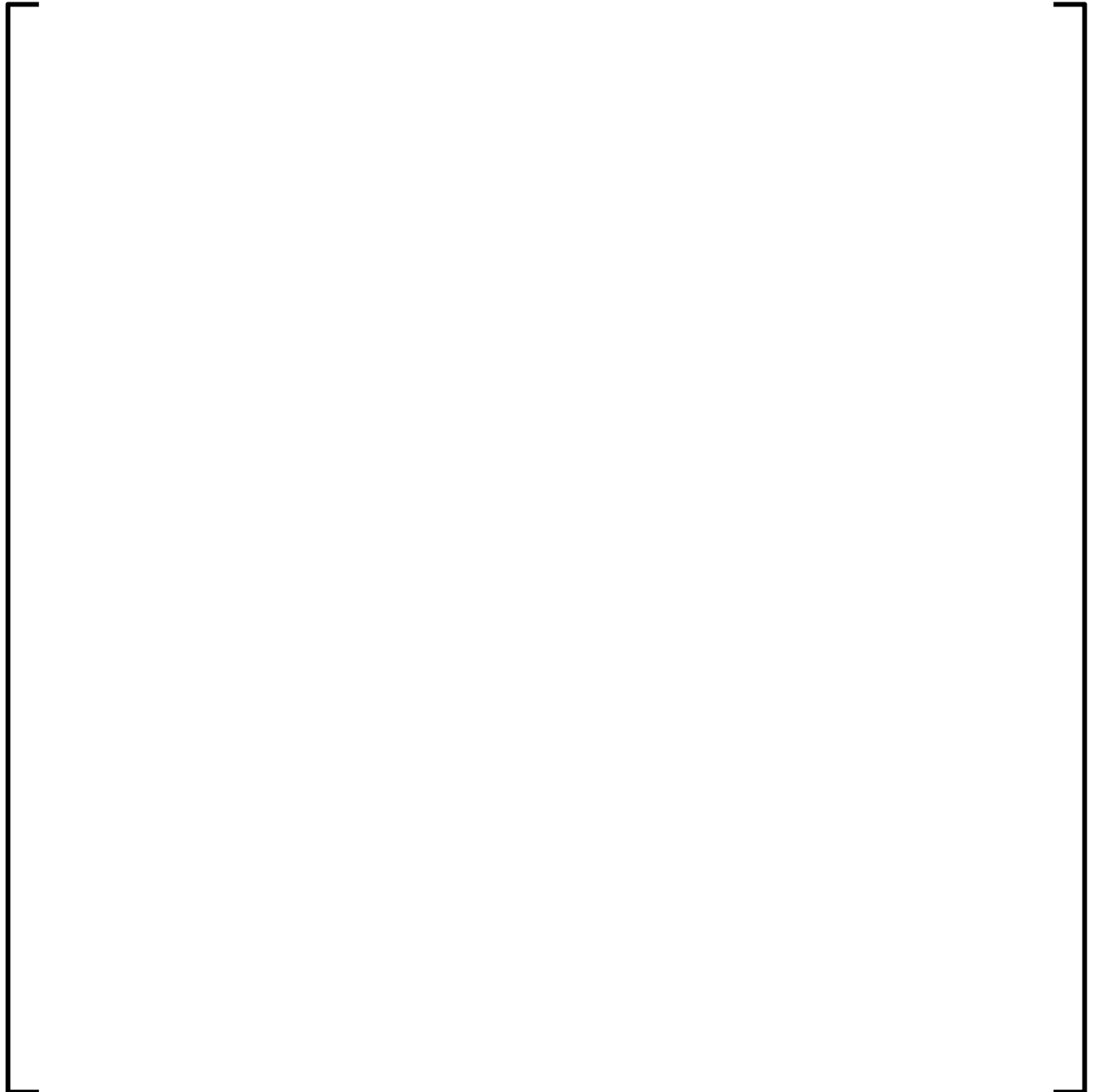


**Figure T1 5.3.9-14**  
**Plant T1 EOC 13 Assembly Average Radial Power Distribution**

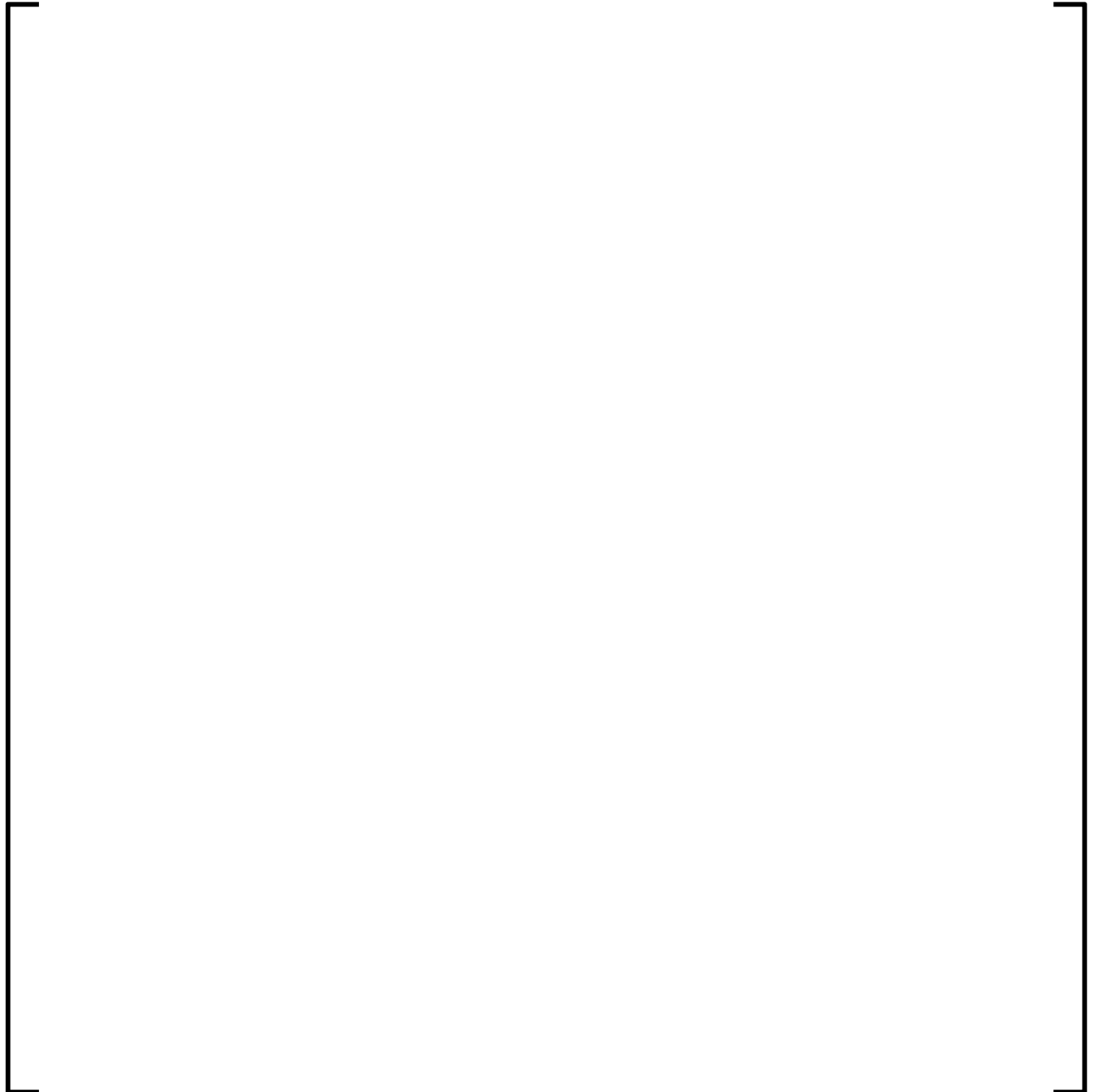


**Figure T1 5.3.9-15**  
**Plant T1 BOC 14 Assembly Average Radial Power Distribution**

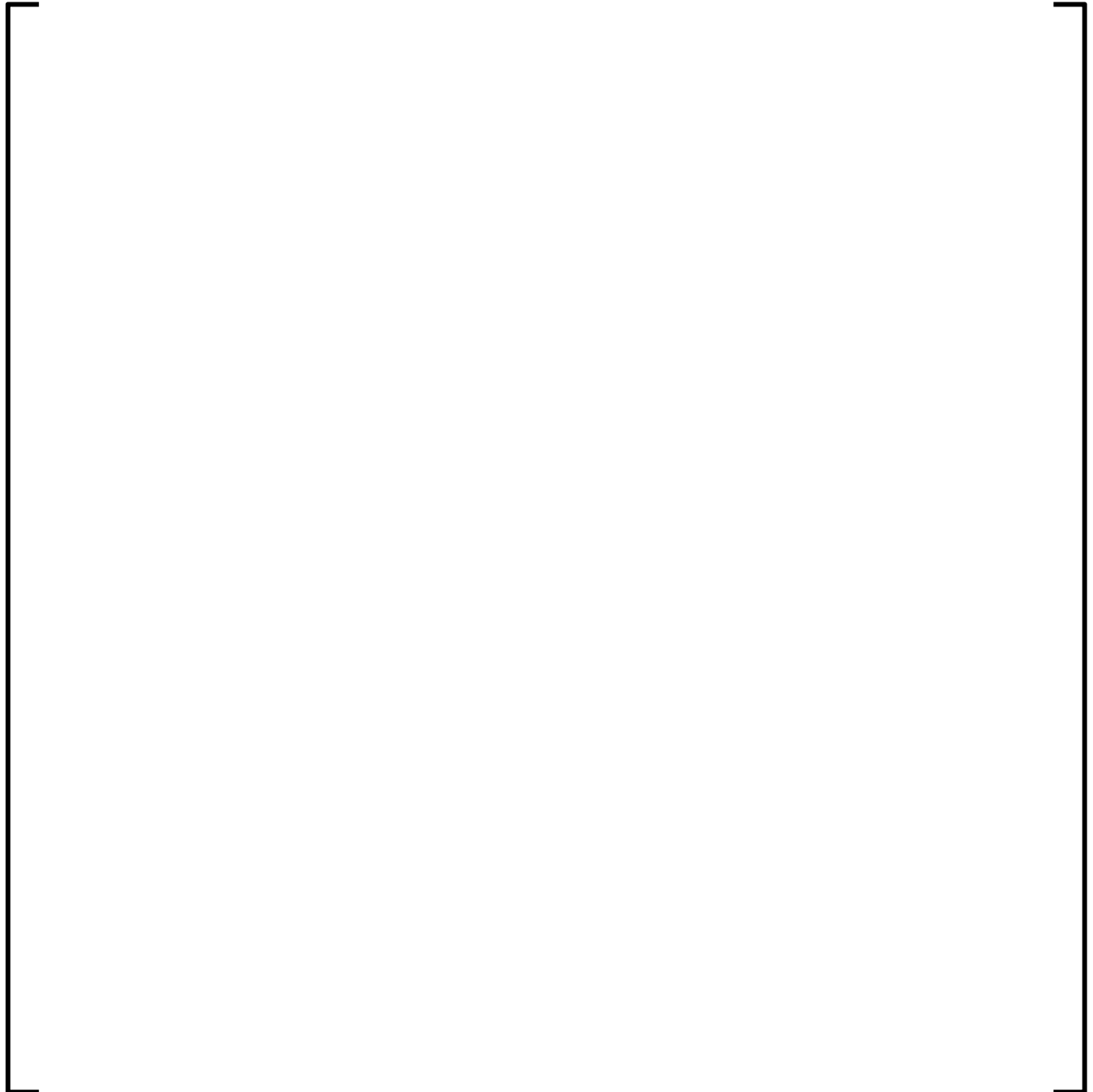


**Figure T1 5.3.9-16**  
**Plant T1 MOC 14 Assembly Average Radial Power Distribution**

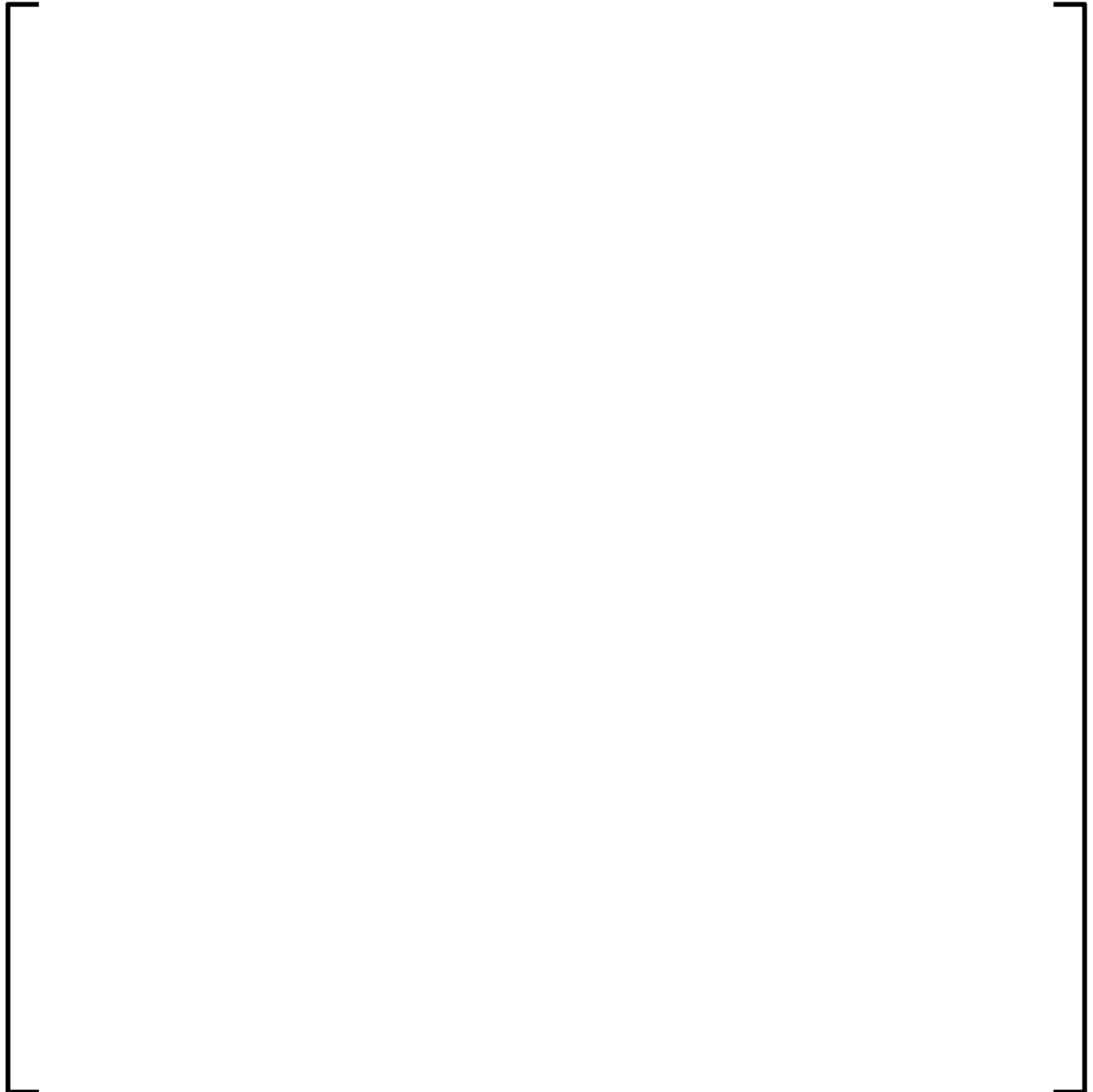




**Figure T1 5.3.9-17**  
**Plant T1 EOC 14 Assembly Average Radial Power Distribution**

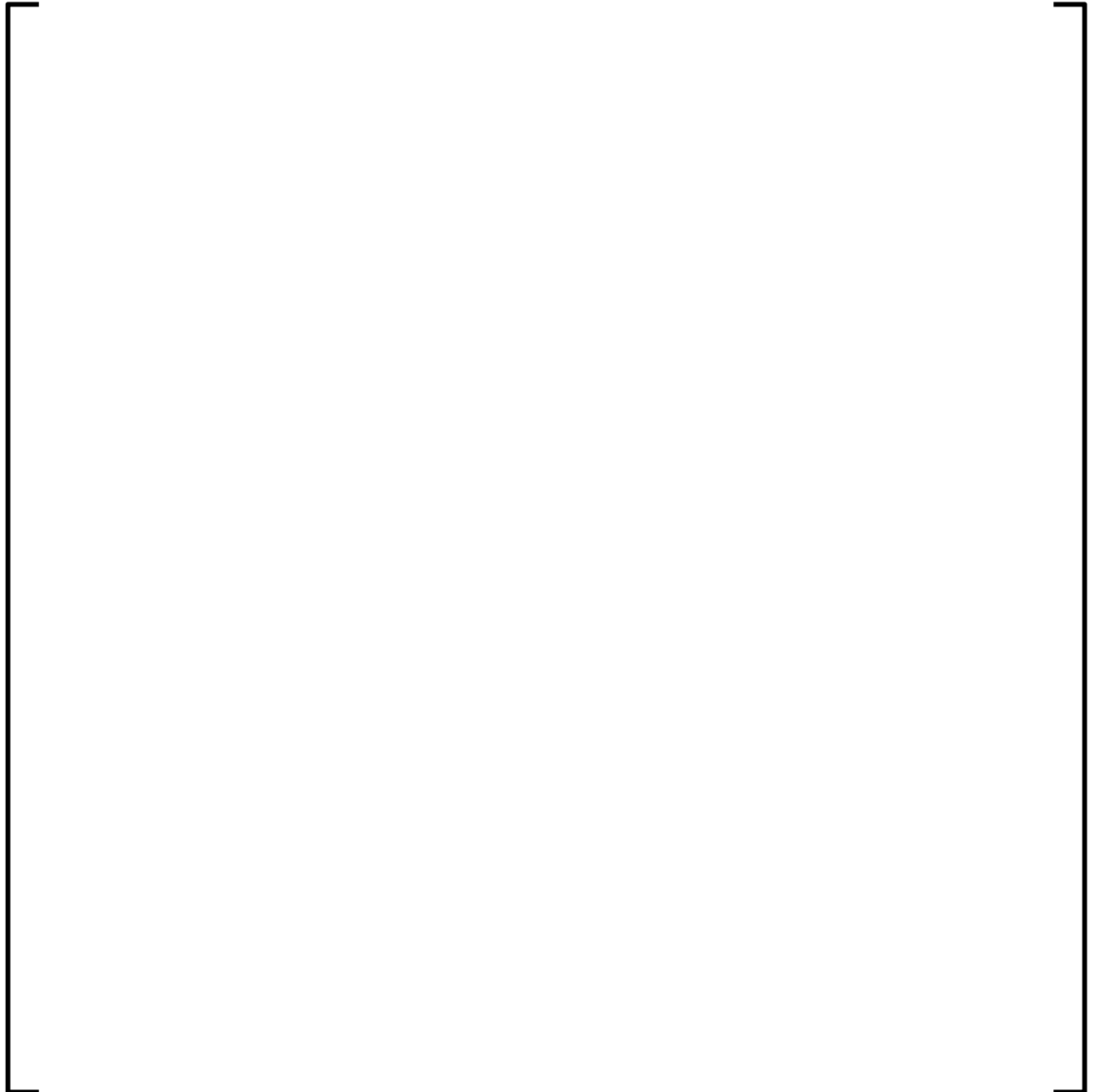


**Figure T1 5.3.9-18**  
**Plant T1 BOC 15 Assembly Average Radial Power Distribution**

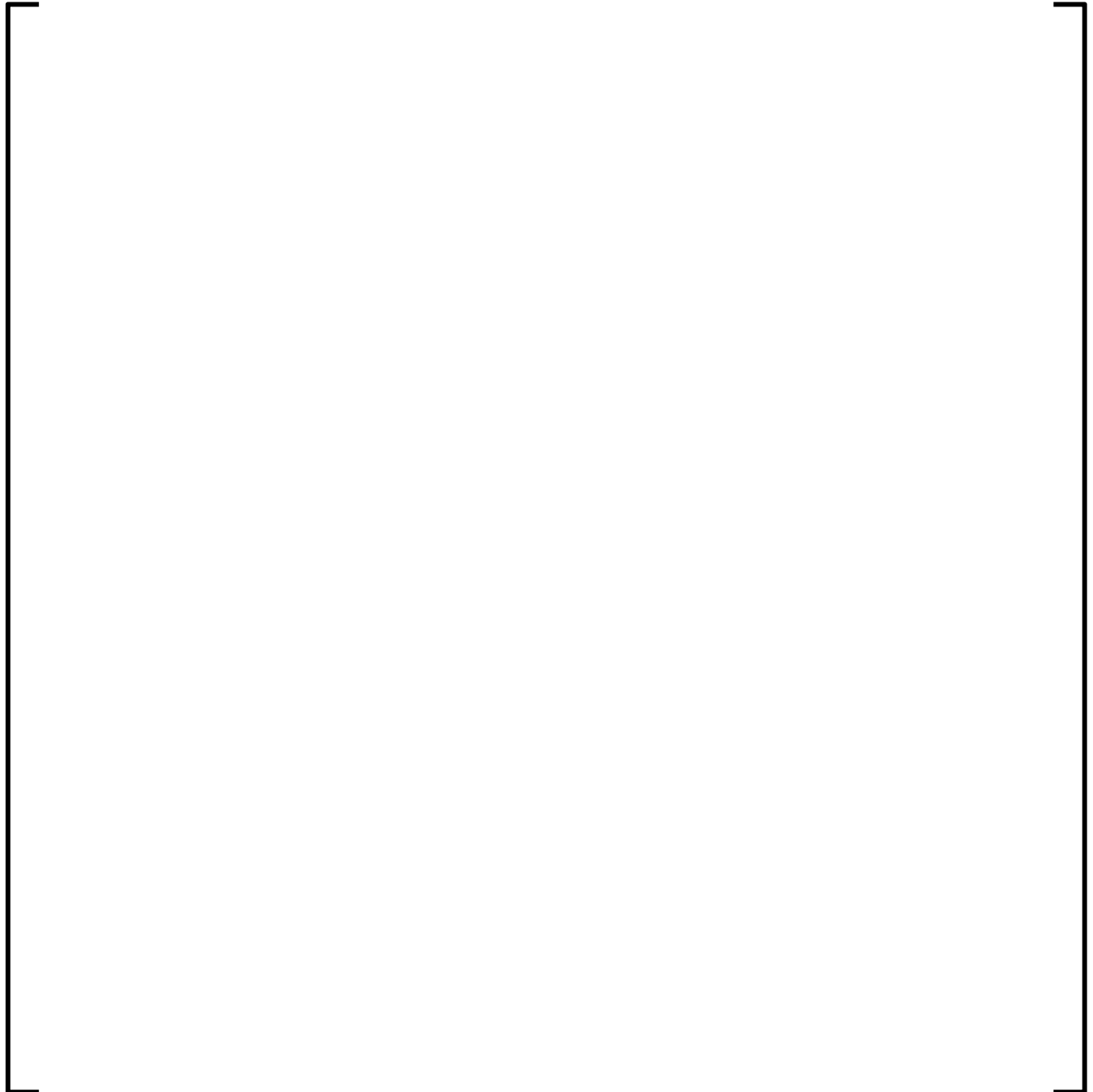


**Figure T1 5.3.9-19**  
**Plant T1 MOC 15 Assembly Average Radial Power Distribution**

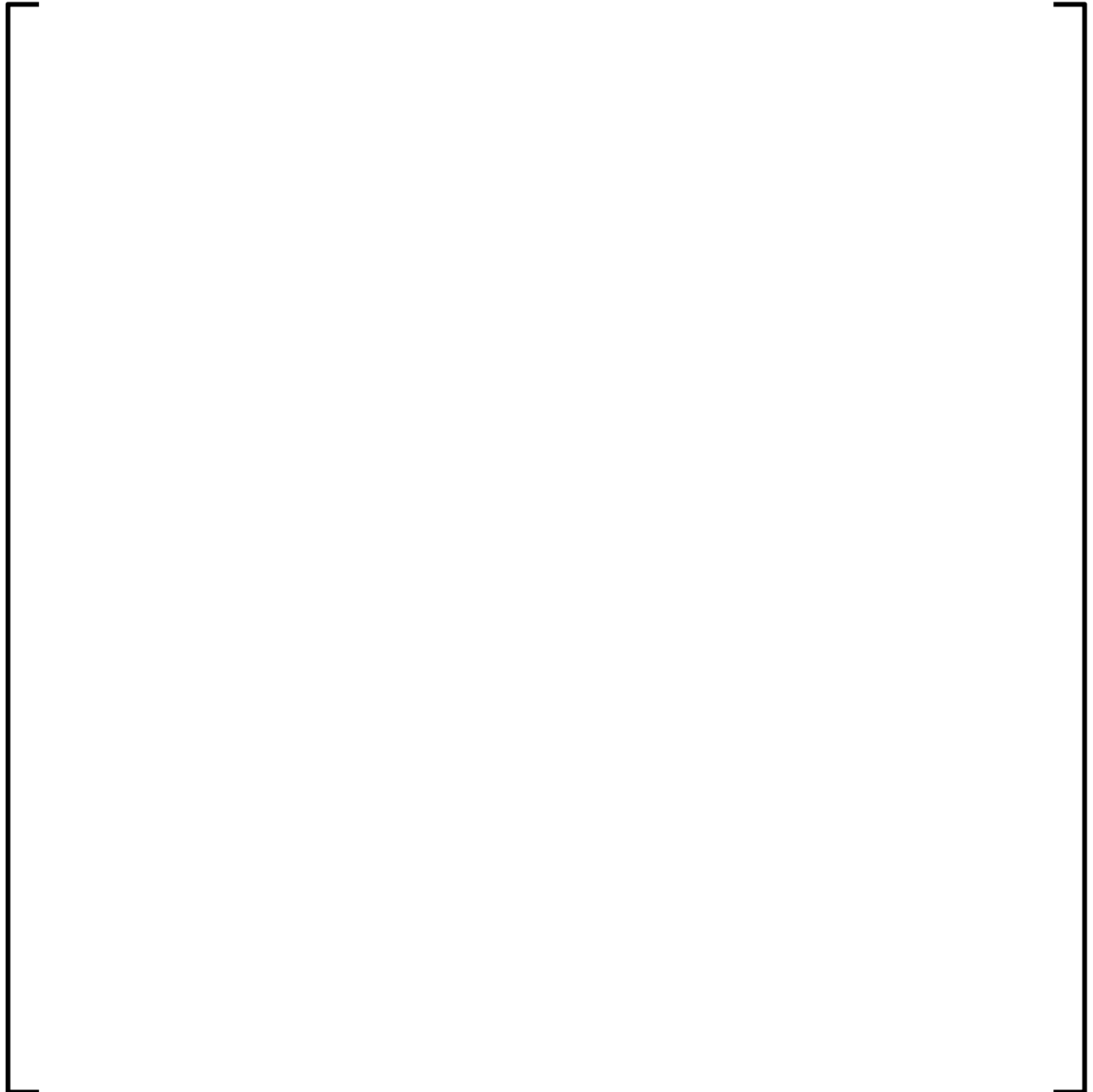


**Figure T1 5.3.9-20**  
**Plant T1 EOC 15 Assembly Average Radial Power Distribution**

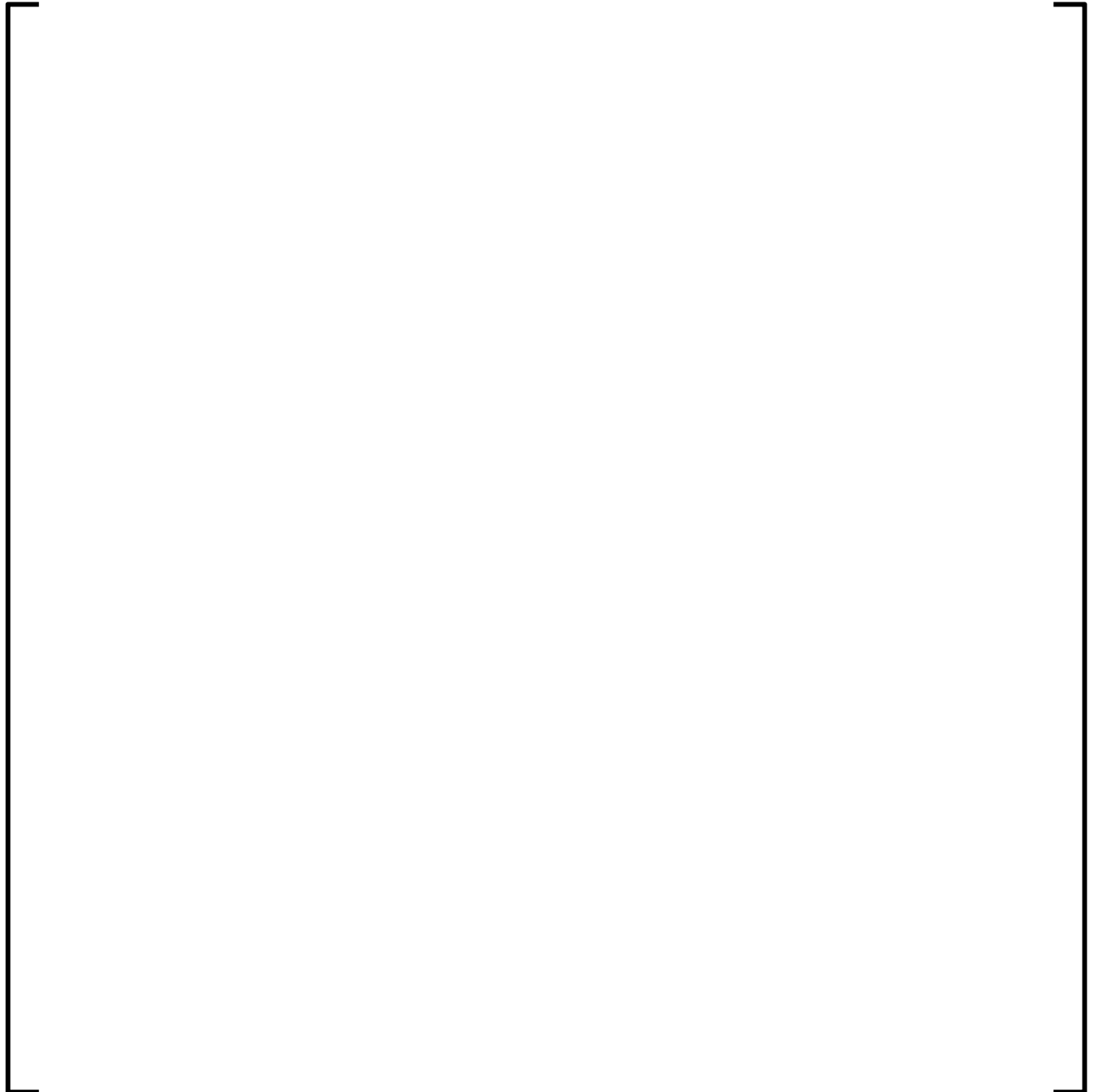


**Figure T1 5.3.9-21**  
**Plant T1 BOC 12 Core Average Axial Power Distribution**



**Figure T1 5.3.9-22**  
**Plant T1 MOC 12 Core Average Axial Power Distribution**

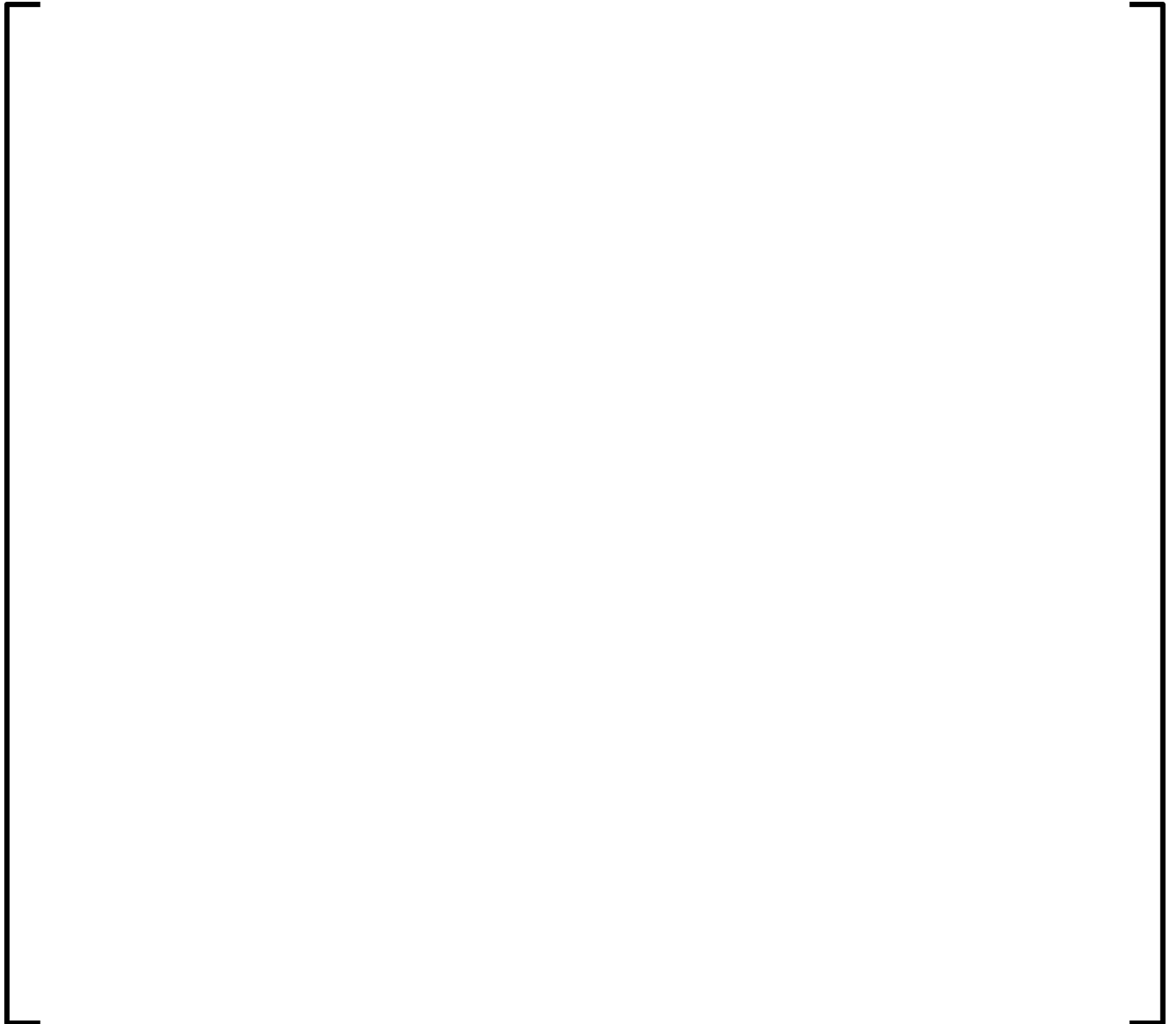


**Figure T1 5.3.9-23**  
**Plant T1 EOC 12 Core Average Axial Power Distribution**



**Figure T1 5.3.9-24**  
**Plant T1 BOC 13 Core Average Axial Power Distribution**





**Figure T1 5.3.9-25**  
**Plant T1 MOC 13 Core Average Axial Power Distribution**



**Figure T1 5.3.9-26**  
**Plant T1 EOC 13 Core Average Axial Power Distribution**



**Figure T1 5.3.9-27**  
**Plant T1 BOC 14 Core Average Axial Power Distribution**



**Figure T1 5.3.9-28**  
**Plant T1 MOC 14 Core Average Axial Power Distribution**



**Figure T1 5.3.9-29**  
**Plant T1 EOC 14 Core Average Axial Power Distribution**



**Figure T1 5.3.9-30**  
**Plant T1 BOC 15 Core Average Axial Power Distribution**

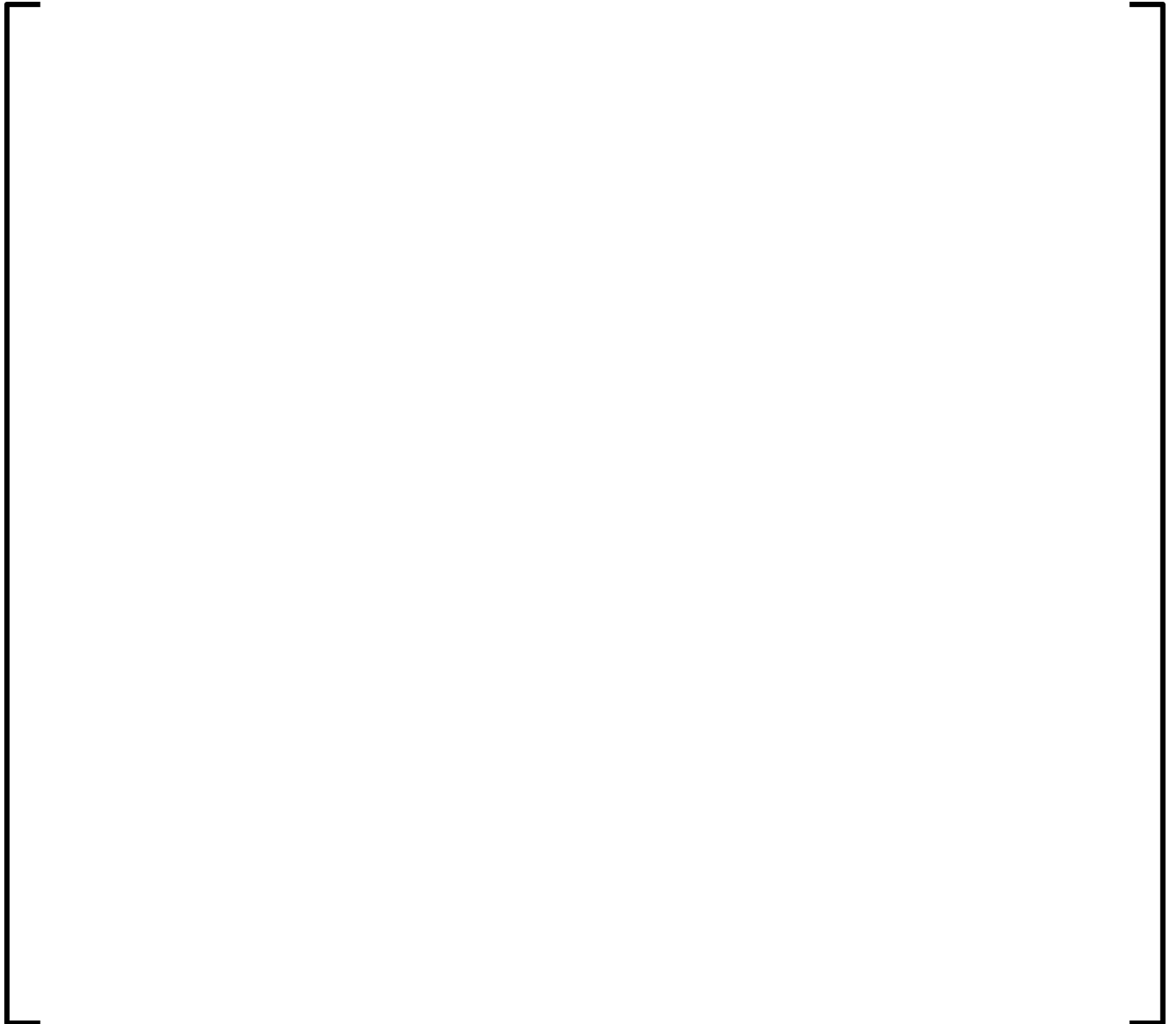


**Figure T1 5.3.9-31**  
**Plant T1 MOC 15 Core Average Axial Power Distribution**



**Figure T1 5.3.9-32**  
**Plant T1 EOC 15 Core Average Axial Power Distribution**





## **APPENDIX V1**

**Table V1 5.2.10-1**  
**Plant V1 Hot Zero Power All Rods Out Critical Boron Concentrations**  
**for Cycles 18-22**



**Table V1 5.2.10-2**  
**Plant V1 Cycle 18 Hot Zero Power Individual Rod Bank Worth**

--	--

**Table V1 5.2.10-3**  
**Plant V1 Cycle 19 Hot Zero Power Individual Rod Bank Worth**

--	--

**Table V1 5.2.10-4**  
**Plant V1 Cycle 20 Hot Zero Power Individual Rod Bank Worth**

--	--

**Table V1 5.2.10-5**  
**Plant V1 Cycle 21 Hot Zero Power Individual Rod Bank Worth**

--	--

**Table V1 5.2.10-6**  
**Plant V1 Cycle 22 Hot Zero Power Individual Rod Bank Worth**

--	--

**Table V1 5.2.10-7**  
**Plant V1 Summary of Total Bank Worths**

--	--

**Table V1 5.2.10-8**  
**Plant V1 Hot Zero Power All Rods Out Isothermal Temperature**  
**Coefficient for Cycles 18-22**





**Figure V1 5.3.10-1**  
**Plant V1 Cycle 18 Critical Boron Concentration vs. Burnup**

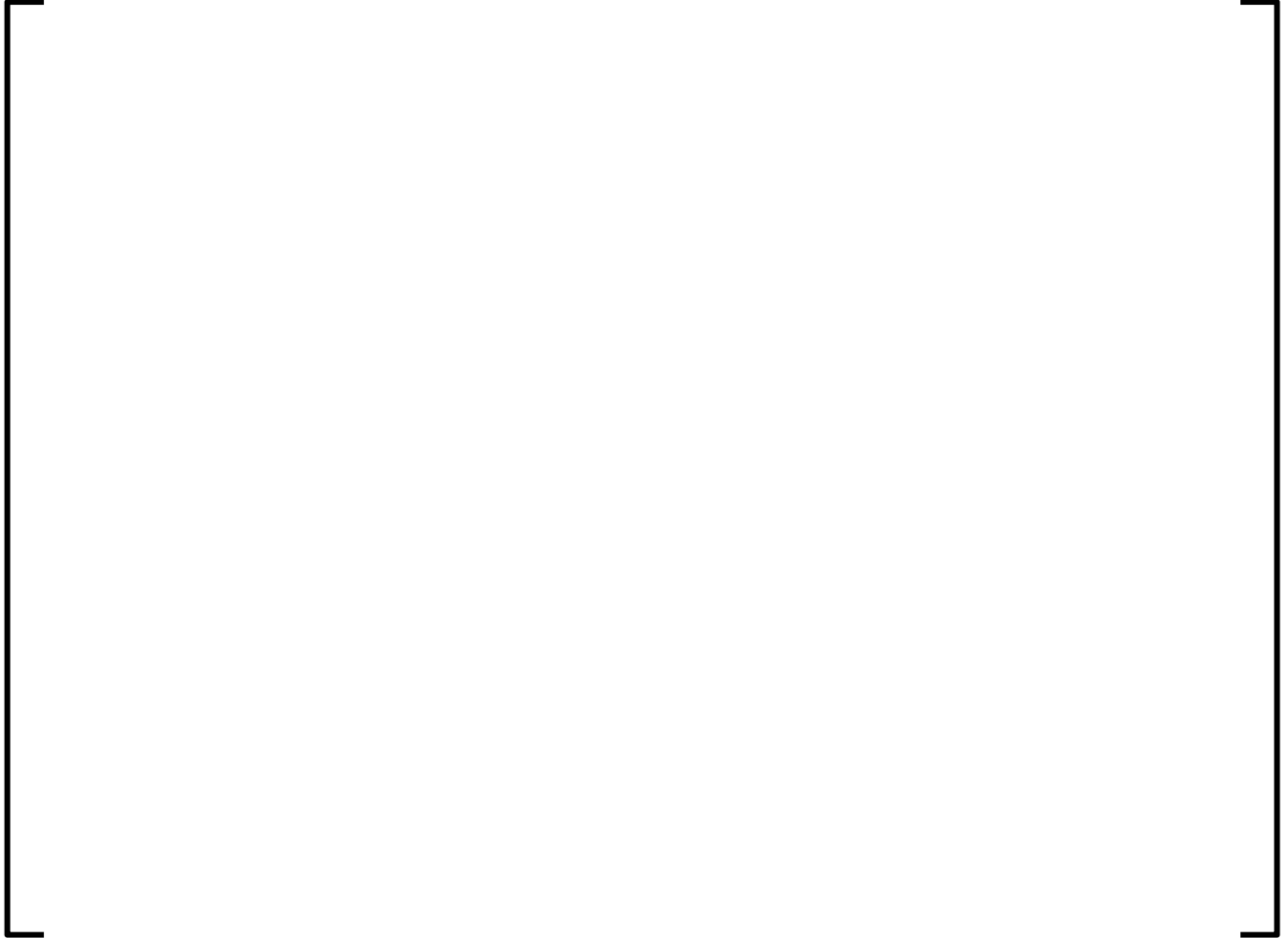


**Figure V1 5.3.10-2**  
**Plant V1 Cycle 19 Critical Boron Concentration vs. Burnup**



**Figure V1 5.3.10-3**  
**Plant V1 Cycle 20 Critical Boron Concentration vs. Burnup**



**Figure V1 5.3.10-4**  
**Plant V1 Cycle 21 Critical Boron Concentration vs. Burnup**

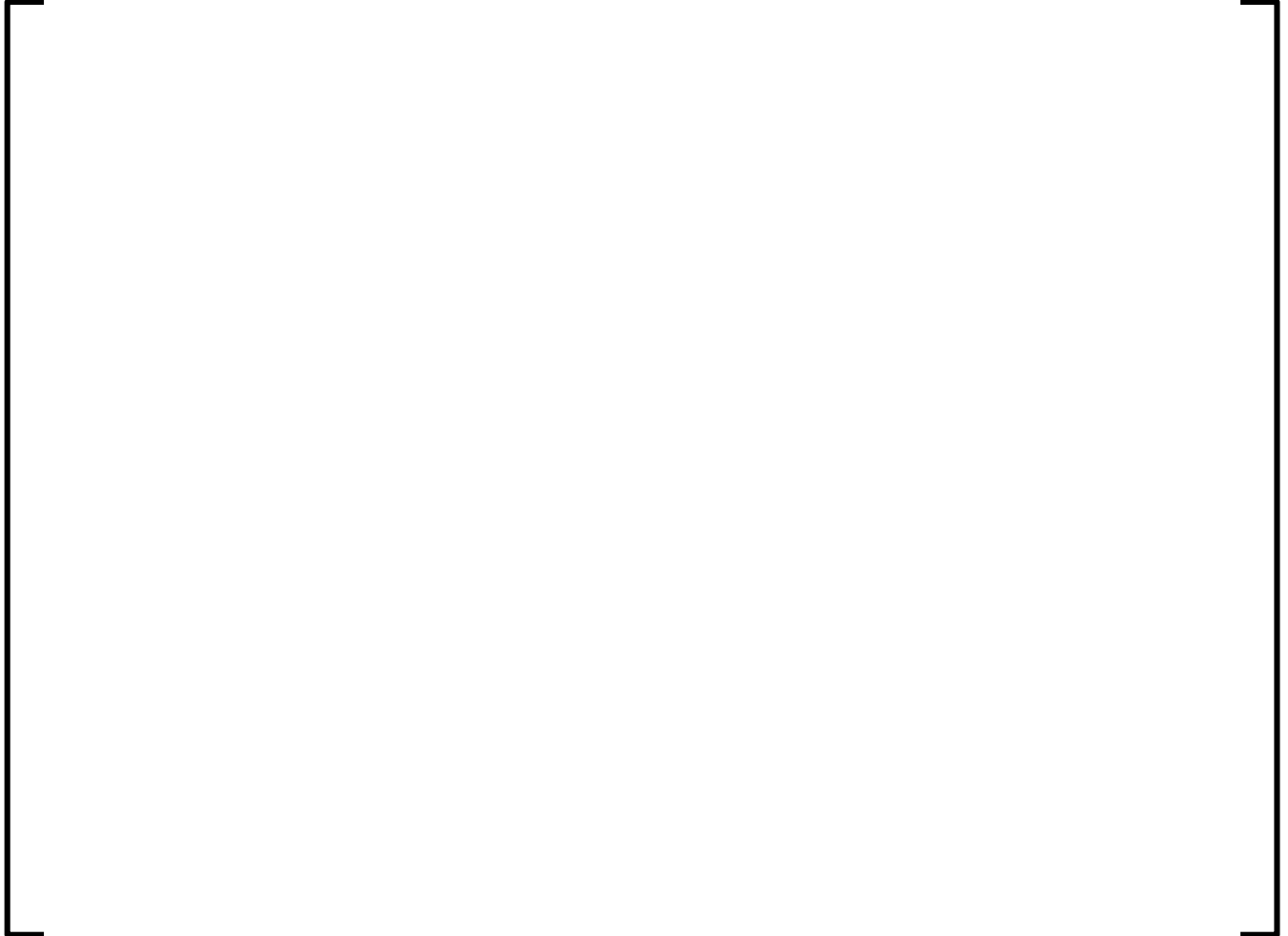


**Figure V1 5.3.10-5**  
**Plant V1 Cycle 22 Critical Boron Concentration vs. Burnup**

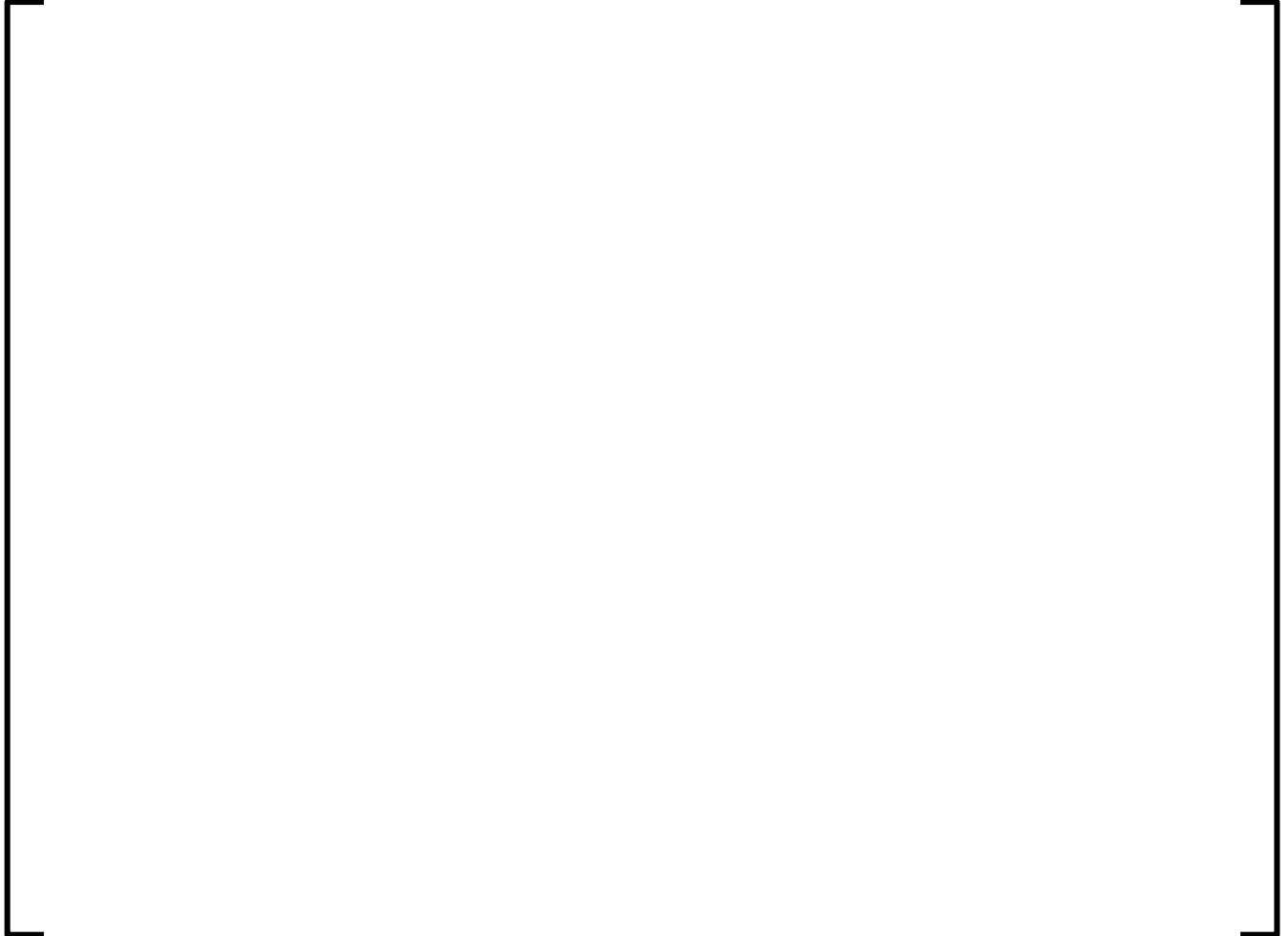


**Figure V1 5.3.10-6**  
**Plant V1 Cycles 18-22 Boron Differences**

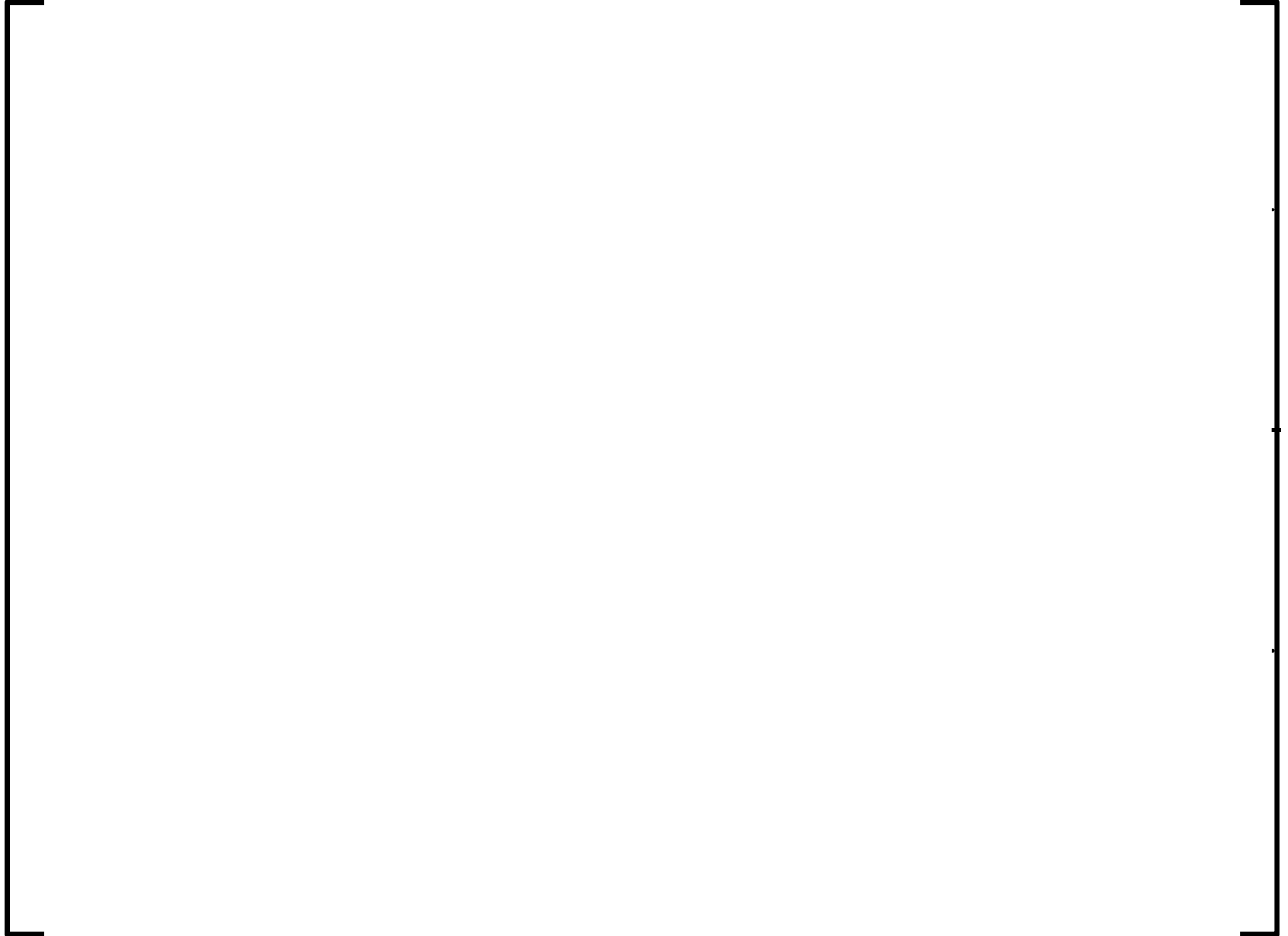


**Figure V1 5.3.10-7**  
**Plant V1 BOC 18 Assembly Average Radial Power Distribution**

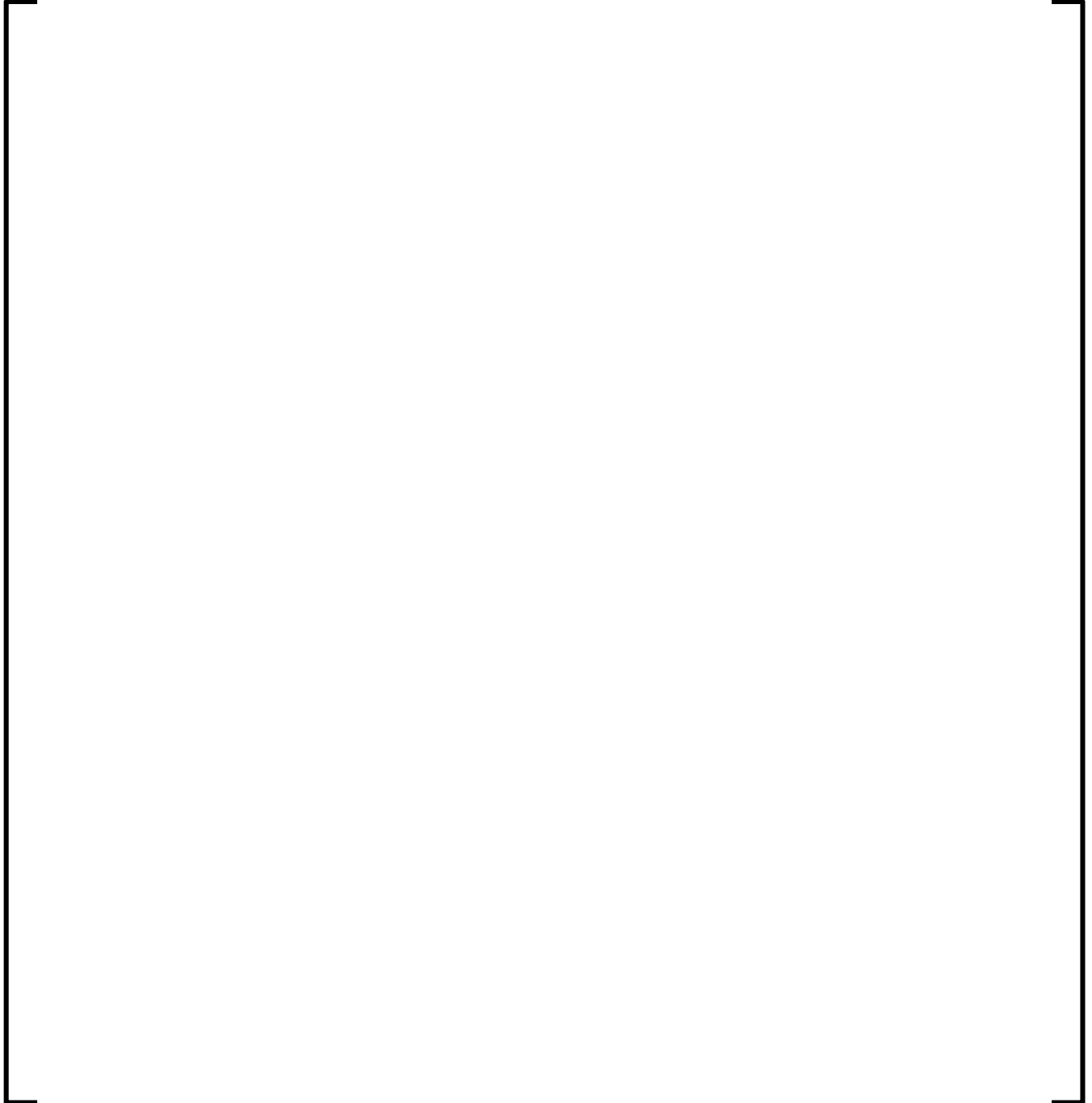


**Figure V1 5.3.10-8**  
**Plant V1 MOC 18 Assembly Average Radial Power Distribution**

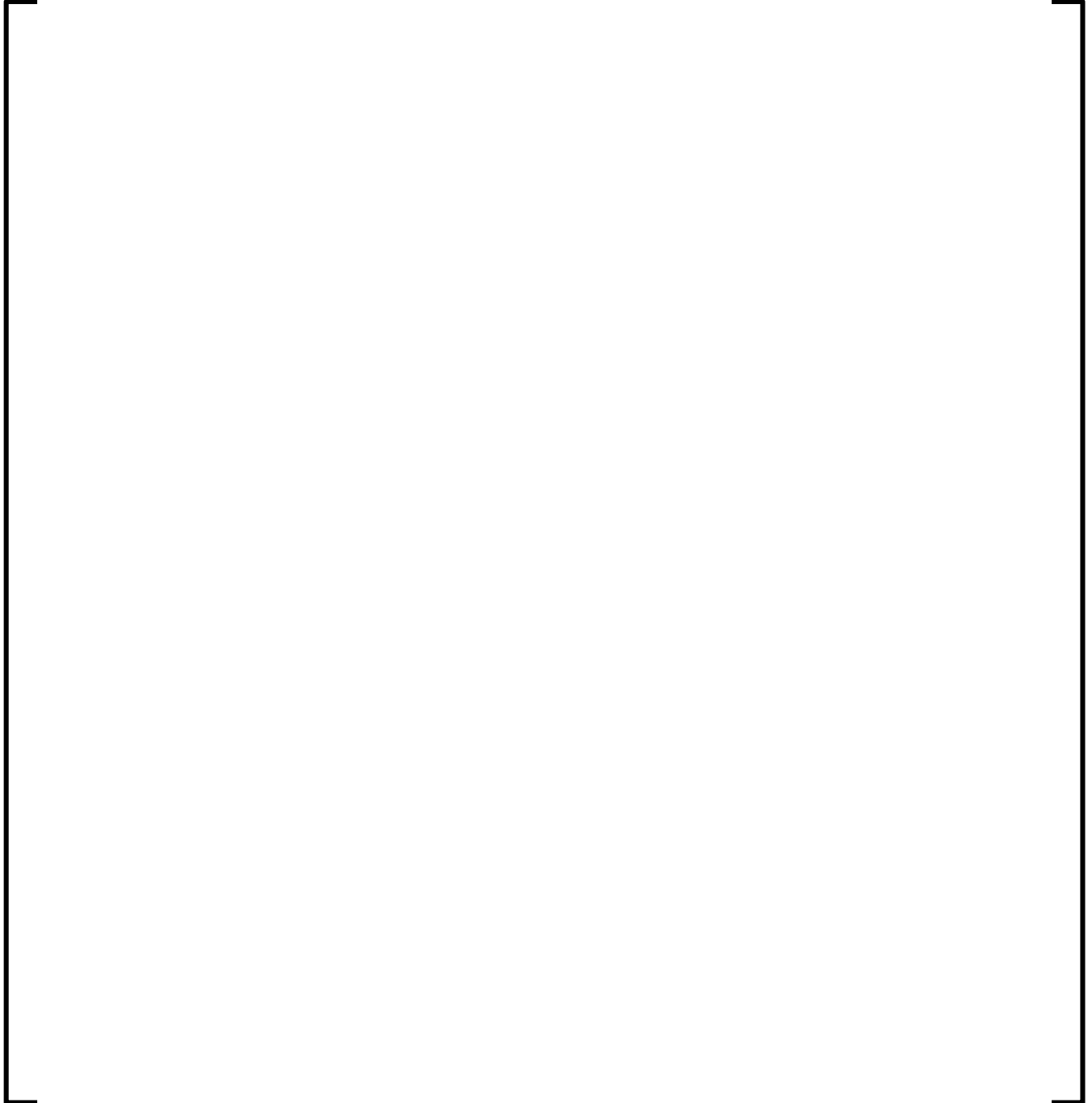




**Figure V1 5.3.10-9**  
**Plant V1 EOC 18 Assembly Average Radial Power Distribution**

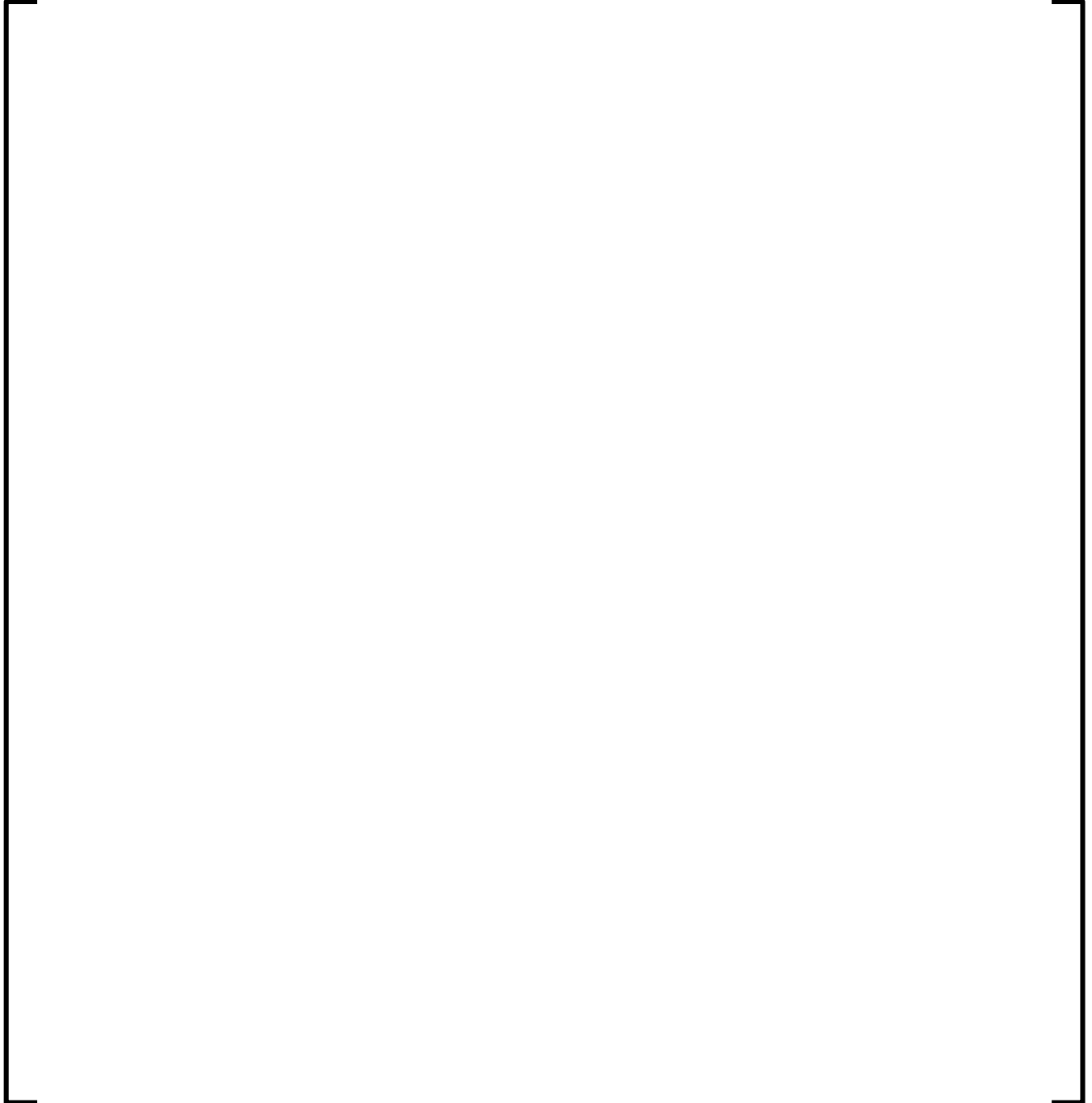


**Figure V1 5.3.10-10**  
**Plant V1 BOC 19 Assembly Average Radial Power Distribution**

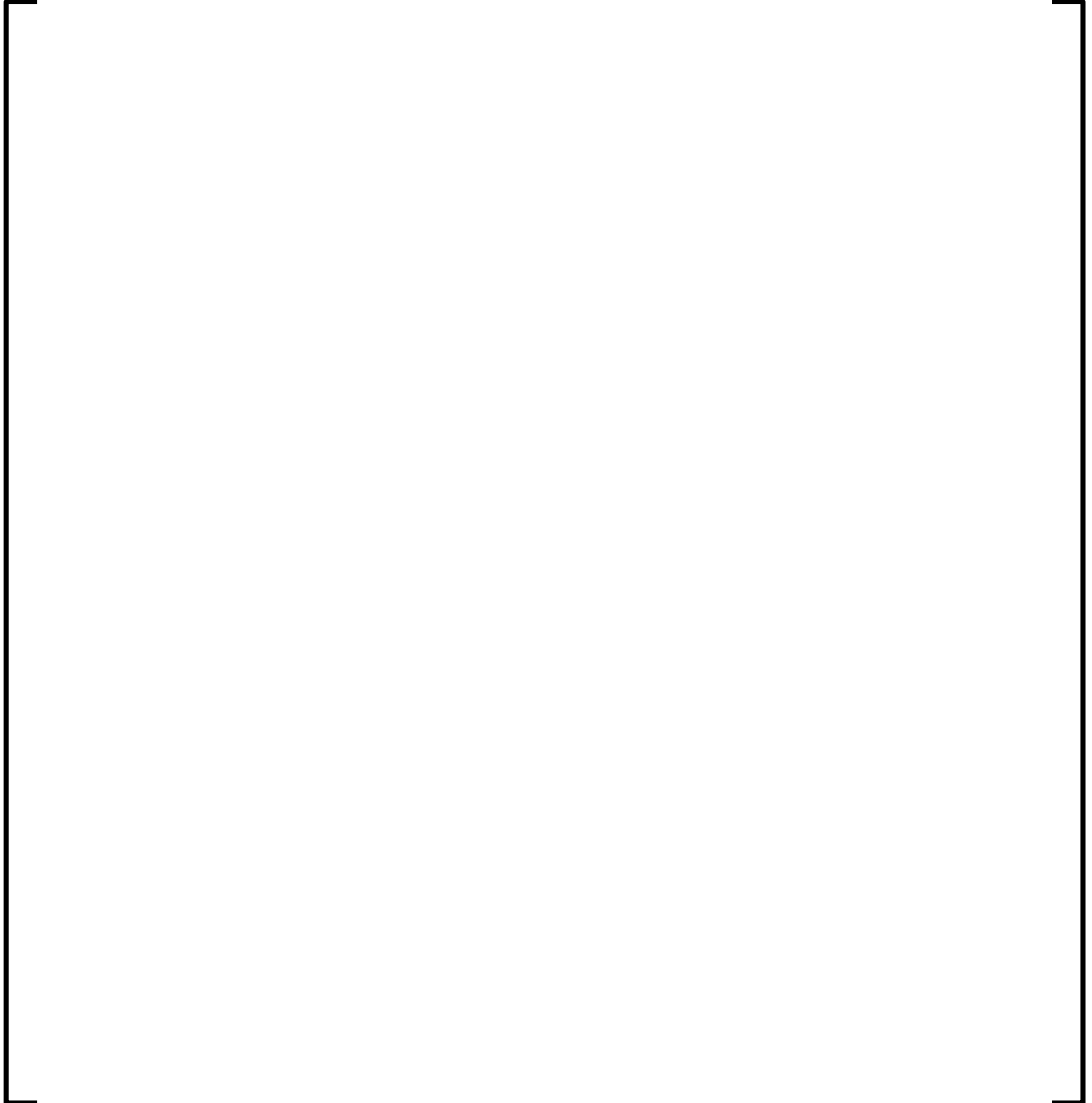


**Figure V1 5.3.10-11**  
**Plant V1 MOC 19 Assembly Average Radial Power Distribution**

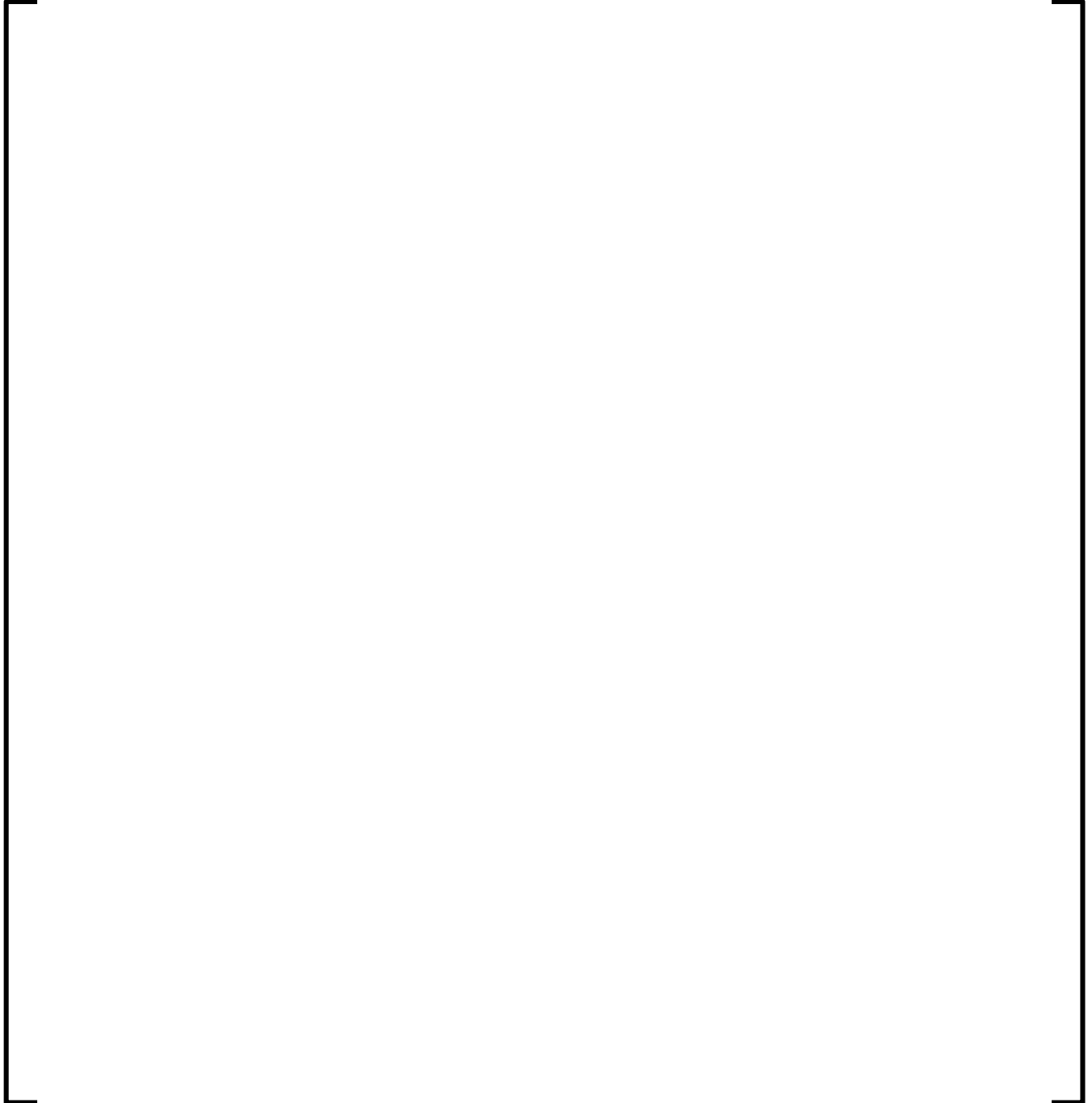


**Figure V1 5.3.10-12**  
**Plant V1 EOC 19 Assembly Average Radial Power Distribution**

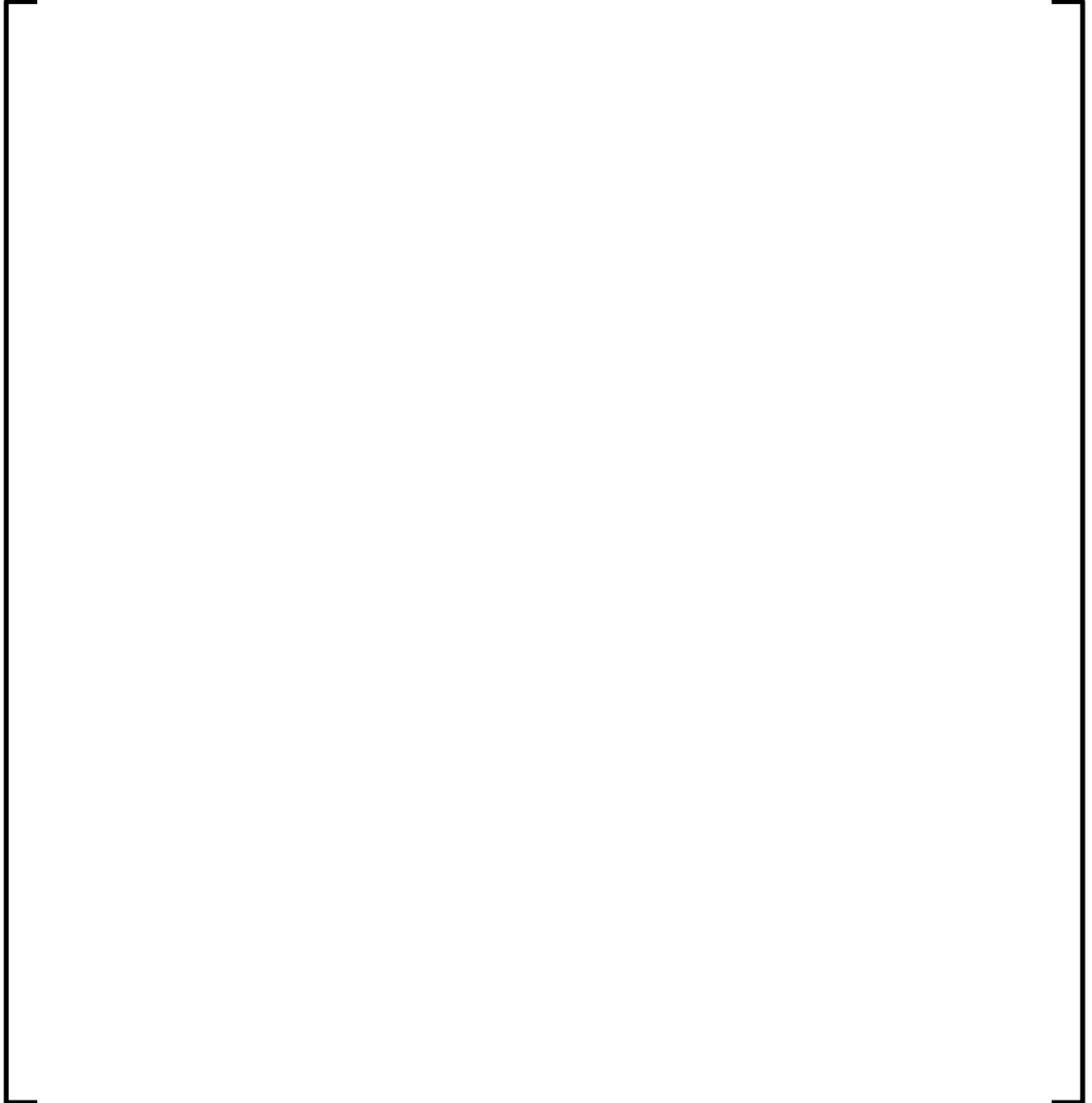


**Figure V1 5.3.10-13**  
**Plant V1 BOC 20 Assembly Average Radial Power Distribution**

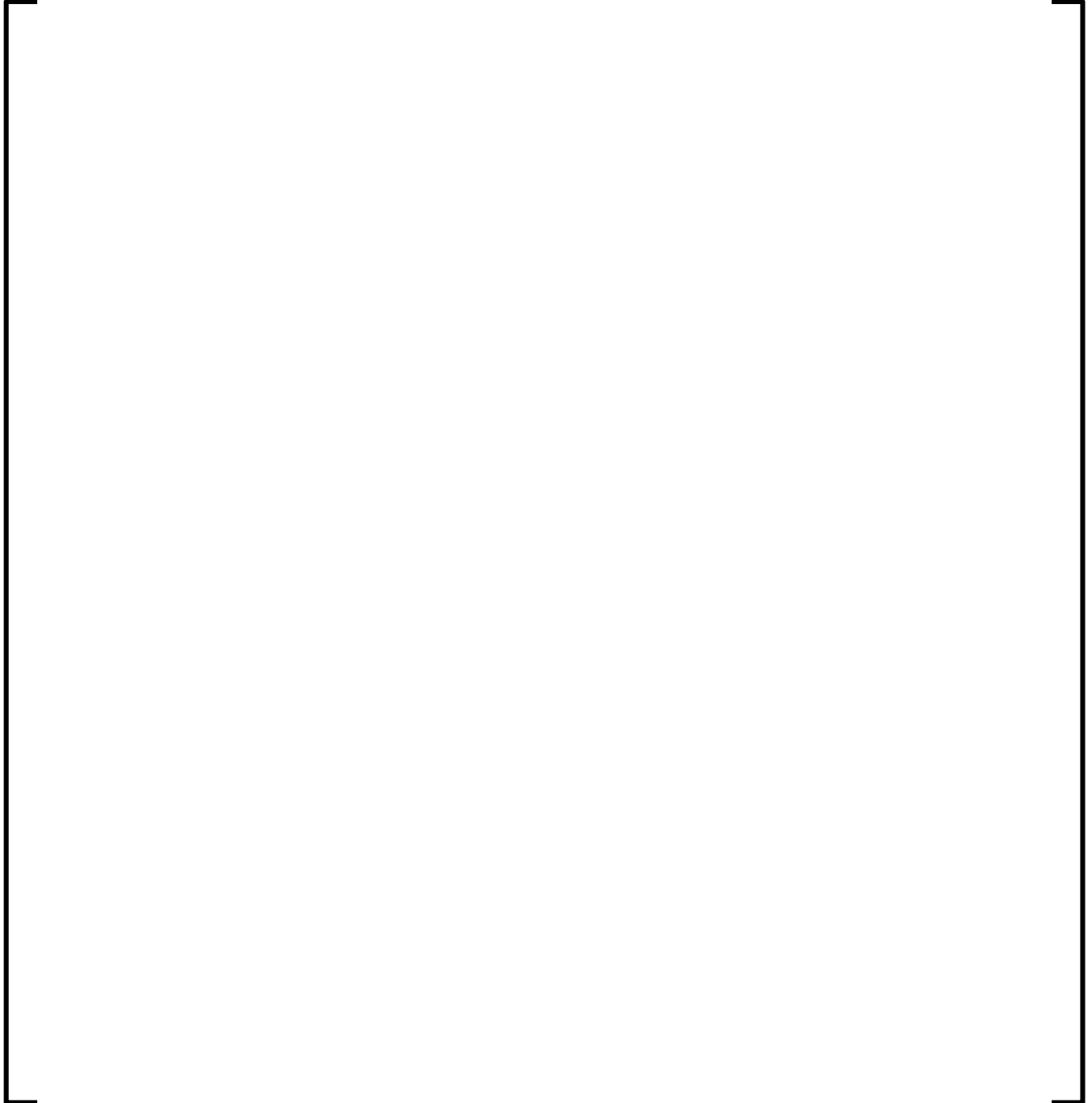


**Figure V1 5.3.10-14**  
**Plant V1 MOC 20 Assembly Average Radial Power Distribution**

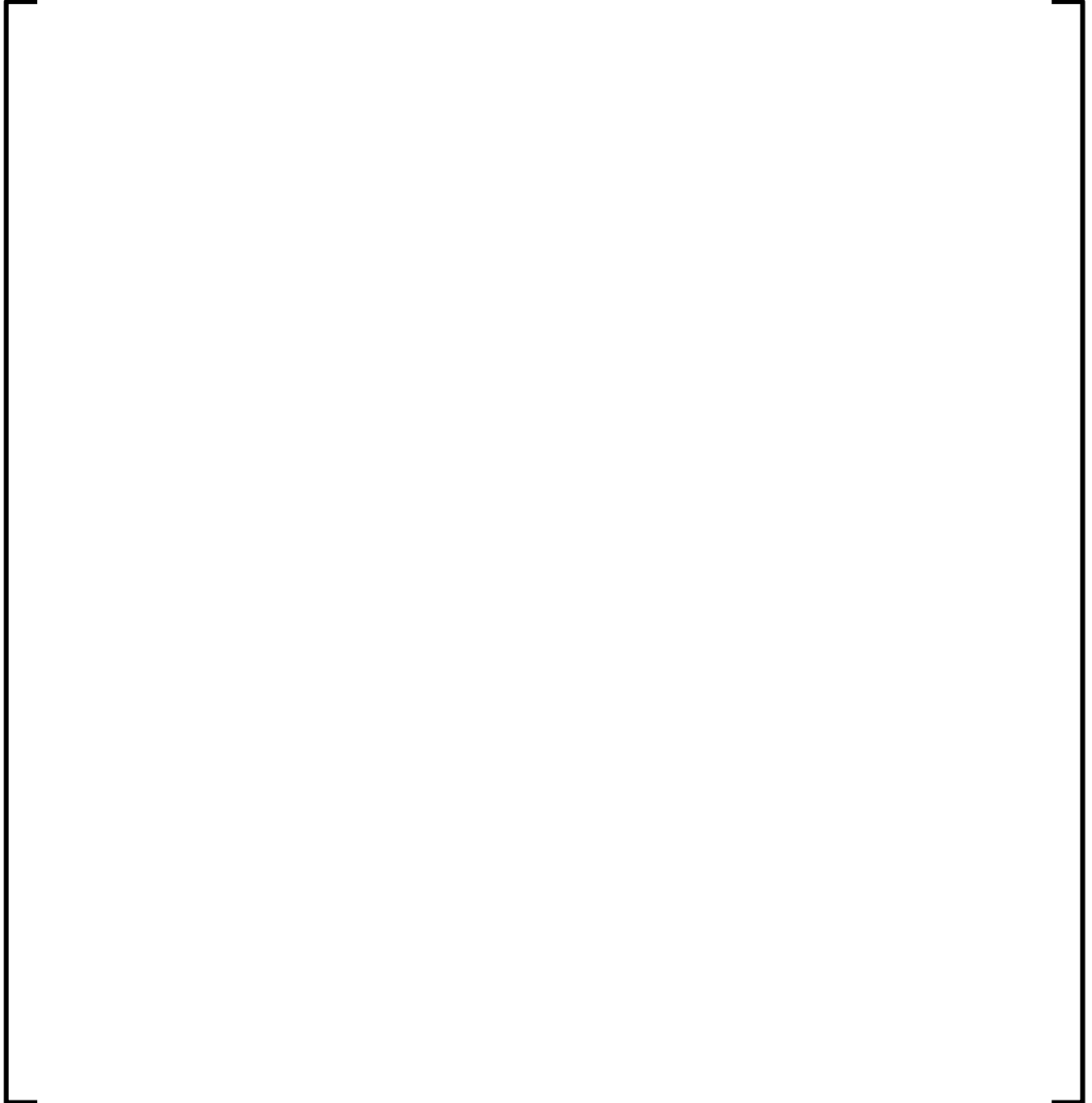


**Figure V1 5.3.10-15**  
**Plant V1 EOC 20 Assembly Average Radial Power Distribution**

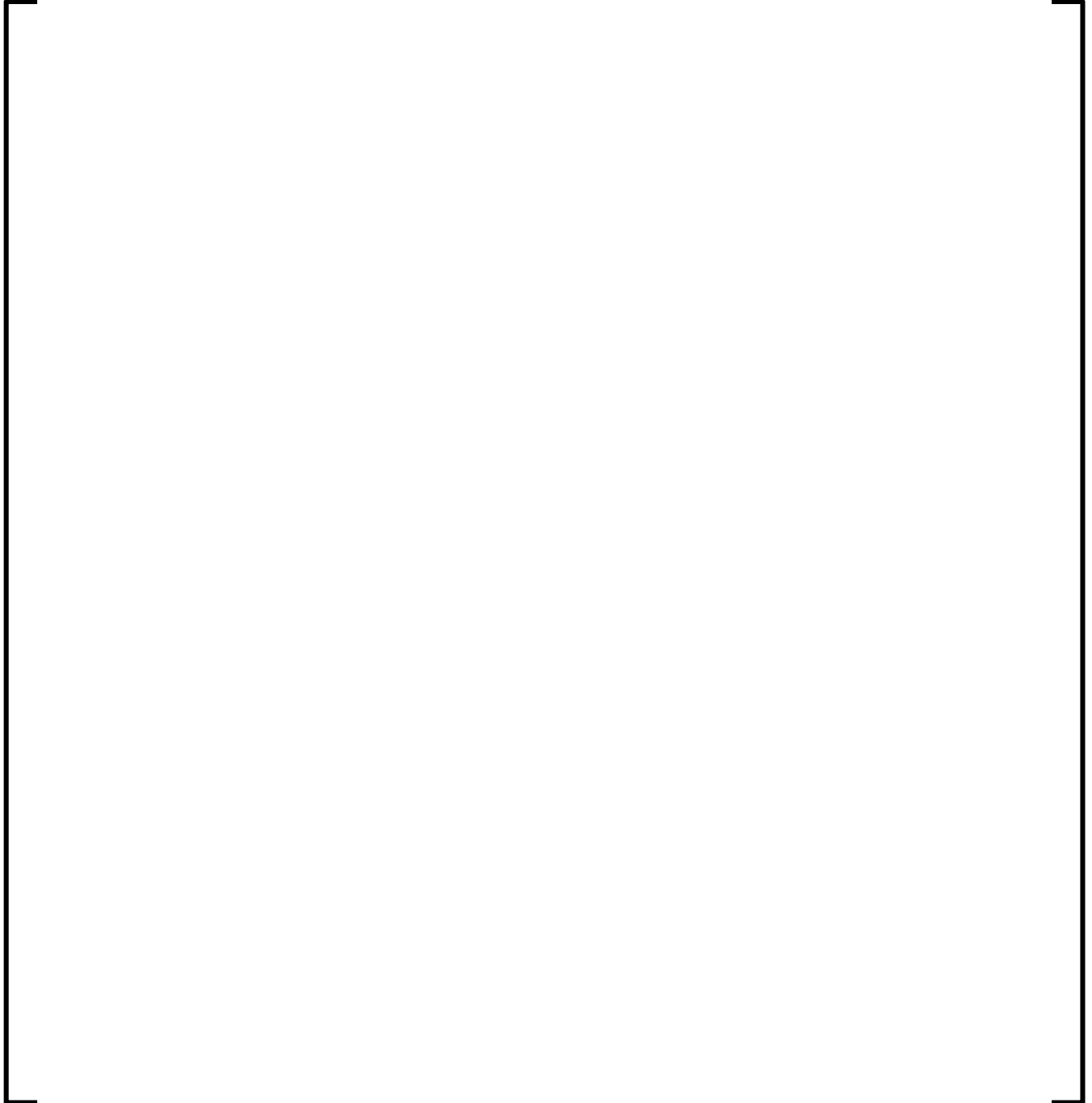


**Figure V1 5.3.10-16**  
**Plant V1 BOC 21 Assembly Average Radial Power Distribution**

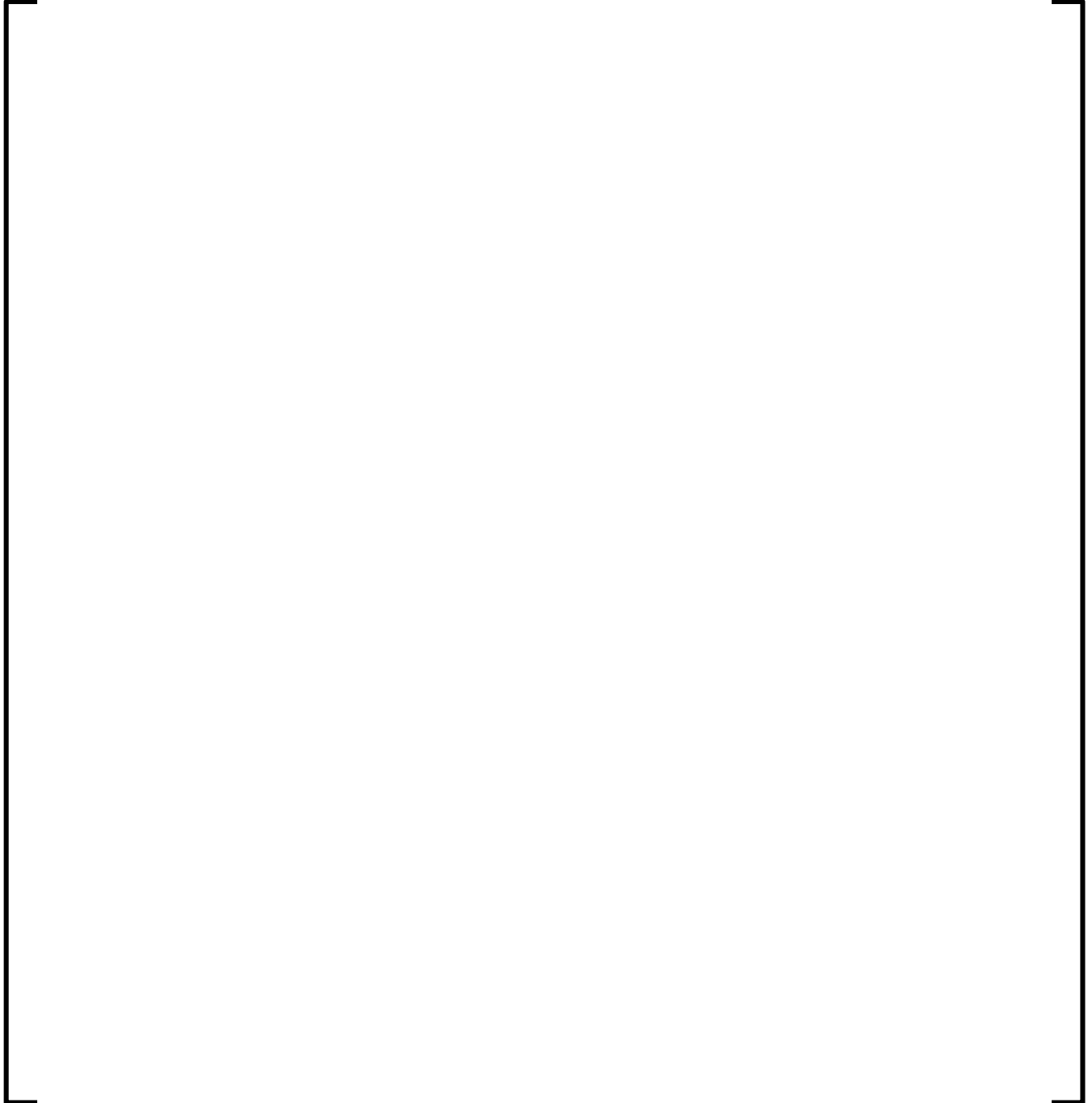




**Figure V1 5.3.10-17**  
**Plant V1 MOC 21 Assembly Average Radial Power Distribution**

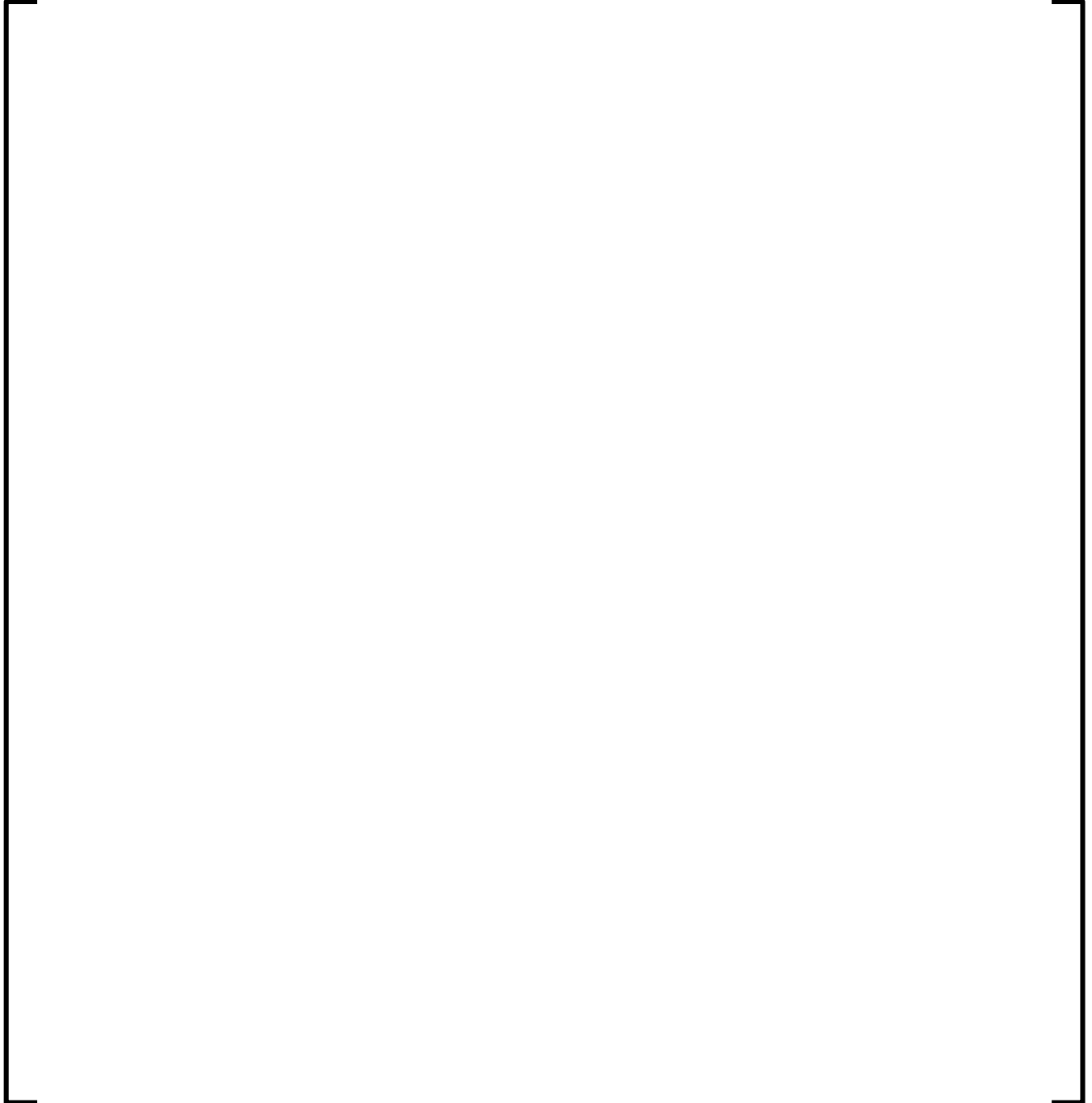


**Figure V1 5.3.10-18**  
**Plant V1 EOC 21 Assembly Average Radial Power Distribution**

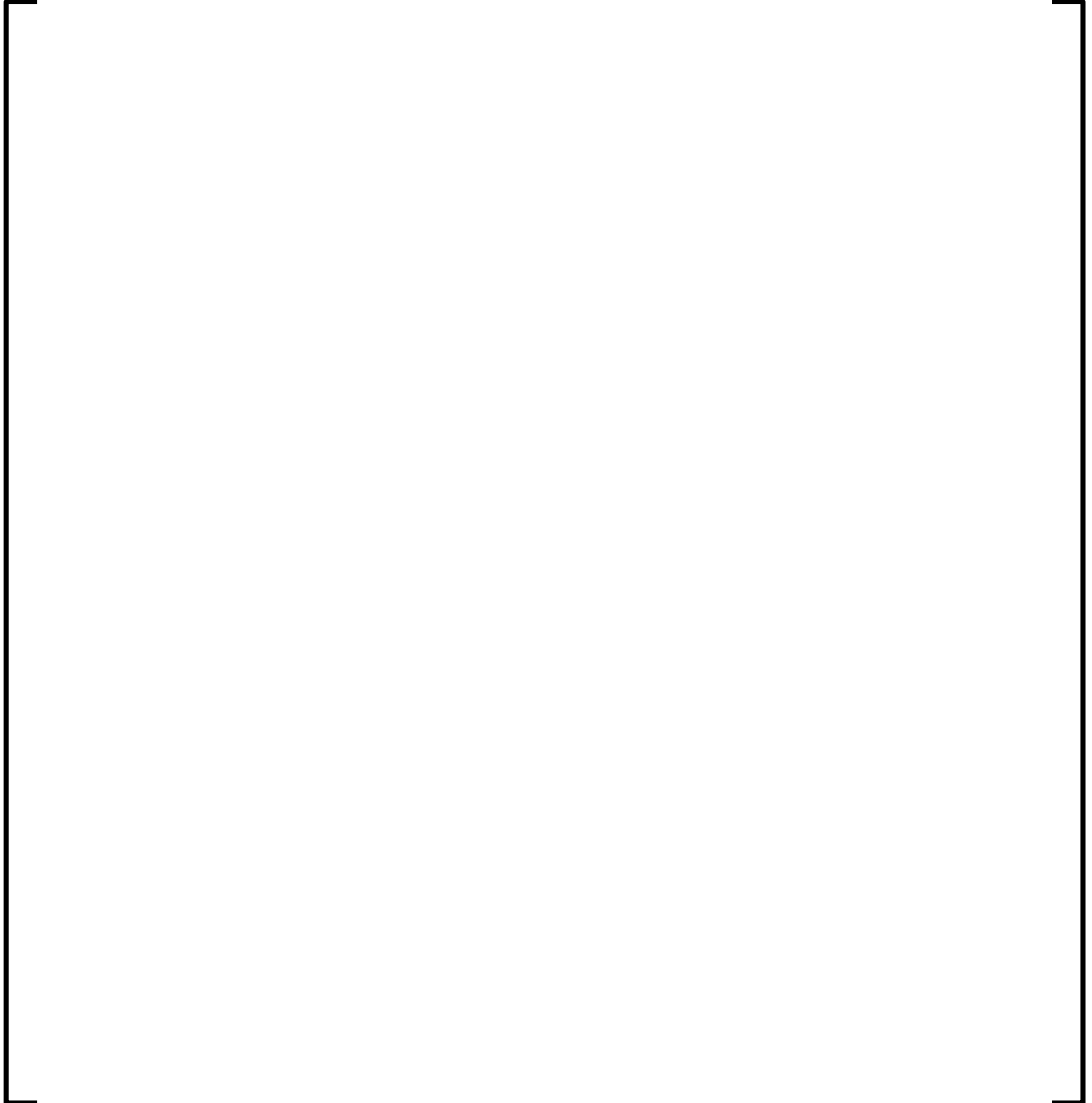


**Figure V1 5.3.10-19**  
**Plant V1 BOC 22 Assembly Average Radial Power Distribution**

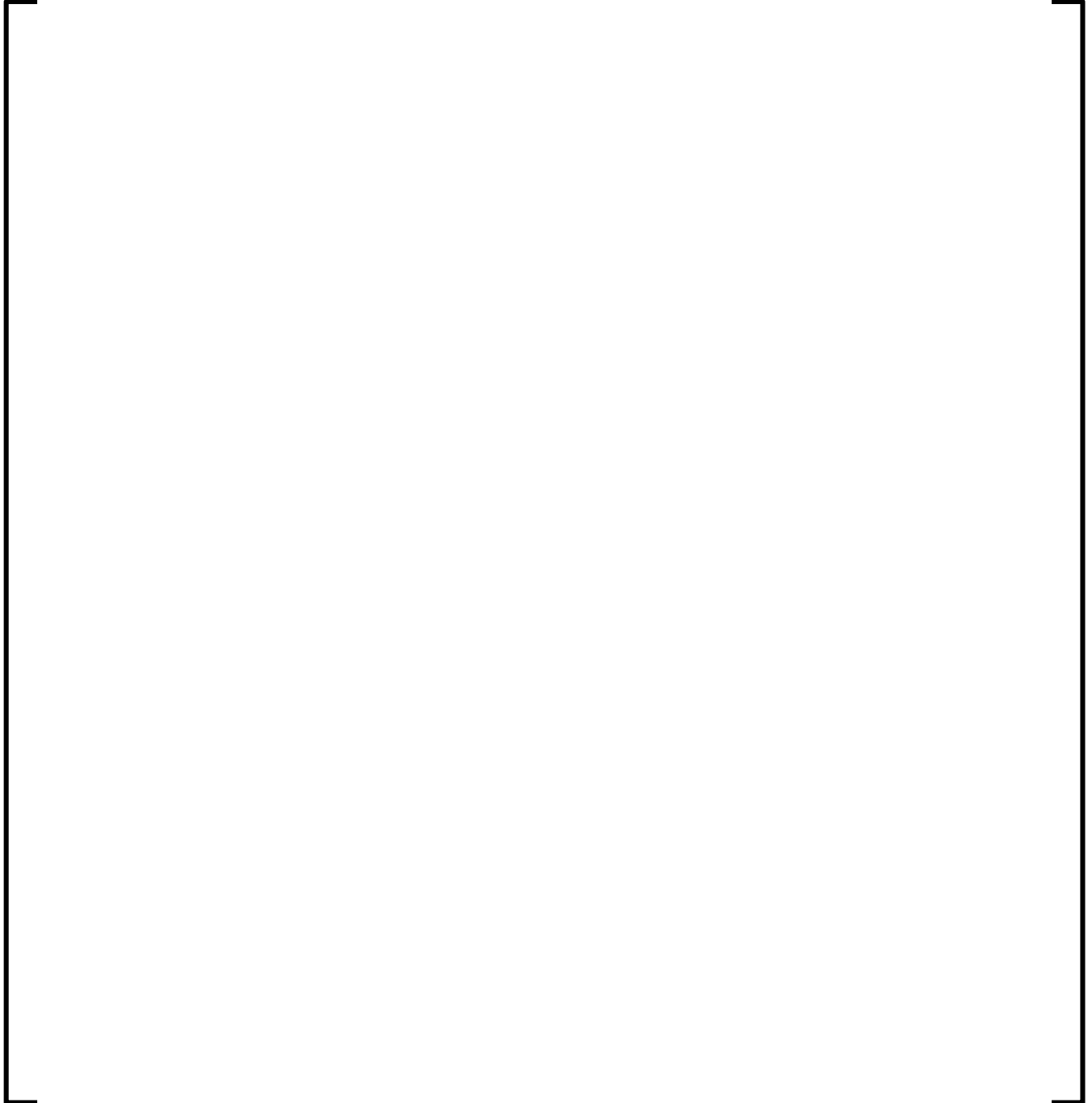


**Figure V1 5.3.10-20**  
**Plant V1 MOC 22 Assembly Average Radial Power Distribution**

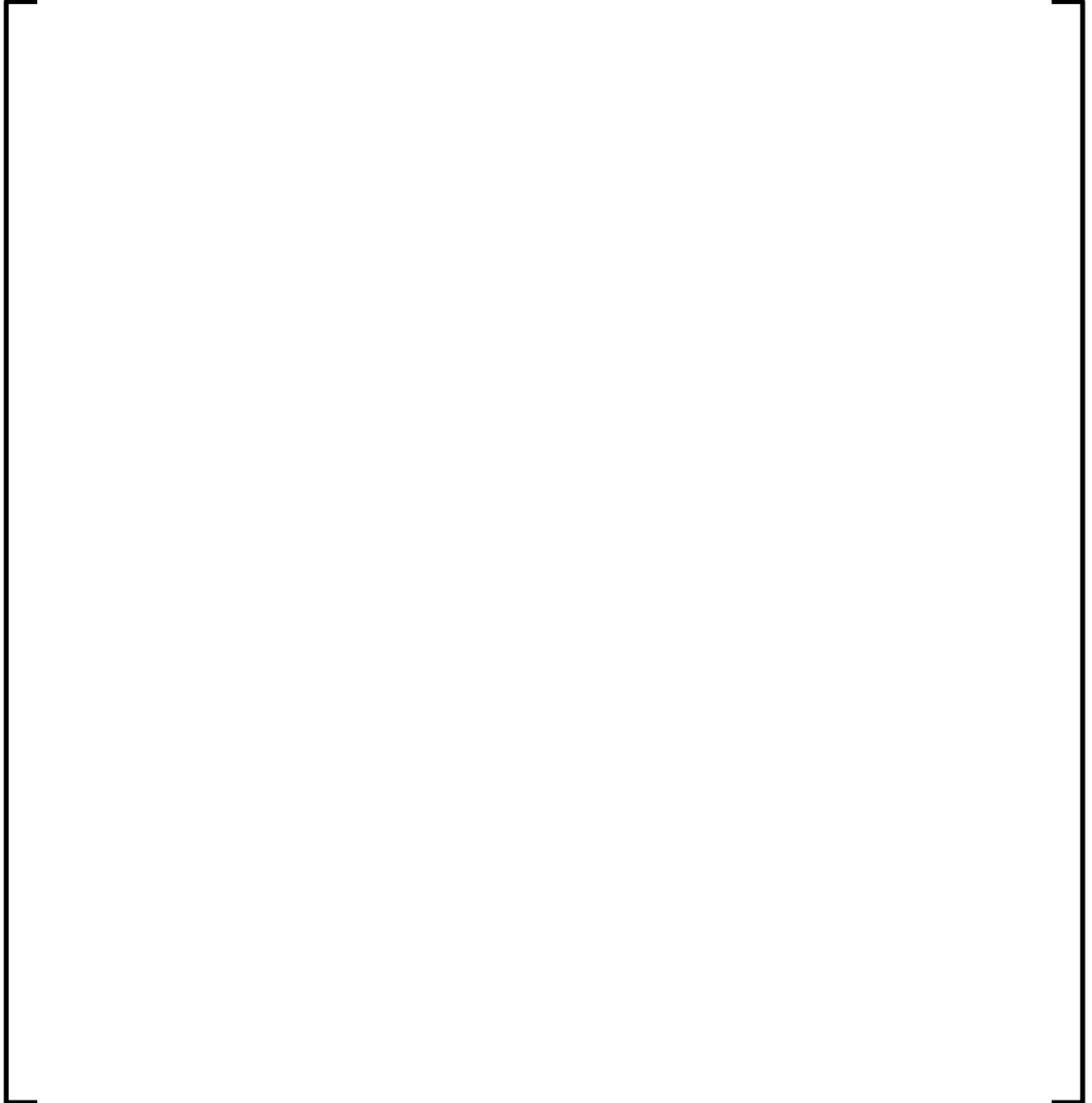


**Figure V1 5.3.10-21**  
**Plant V1 EOC 22 Assembly Average Radial Power Distribution**

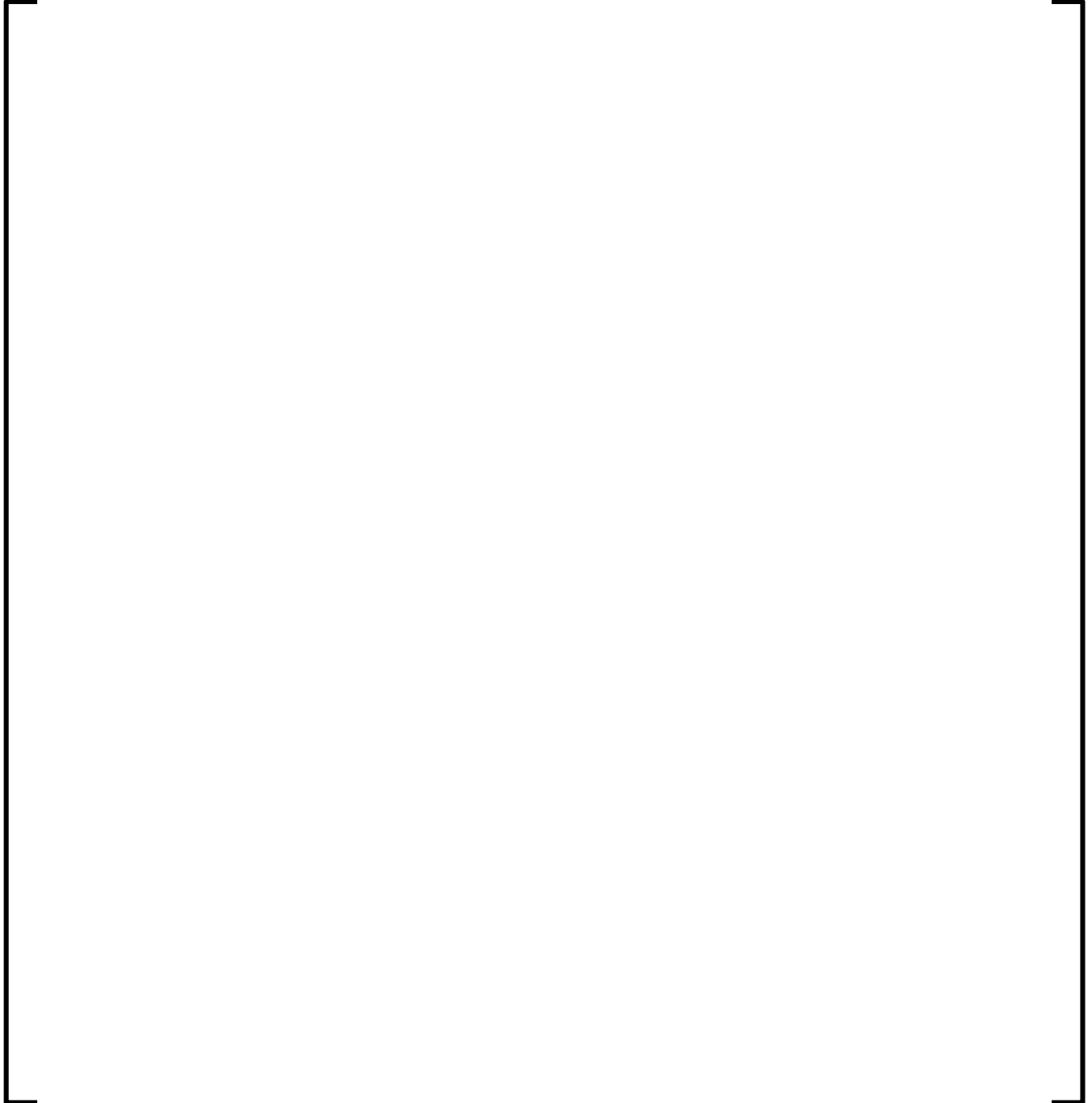


**Figure V1 5.3.10-22**  
**Plant V1 BOC 18 Core Average Axial Power Distribution**



**Figure V1 5.3.10-23**  
**Plant V1 MOC 18 Core Average Axial Power Distribution**



**Figure V1 5.3.10-24**  
**Plant V1 EOC 18 Core Average Axial Power Distribution**





**Figure V1 5.3.10-25**  
**Plant V1 BOC 19 Core Average Axial Power Distribution**



**Figure V1 5.3.10-26**  
**Plant V1 MOC 19 Core Average Axial Power Distribution**

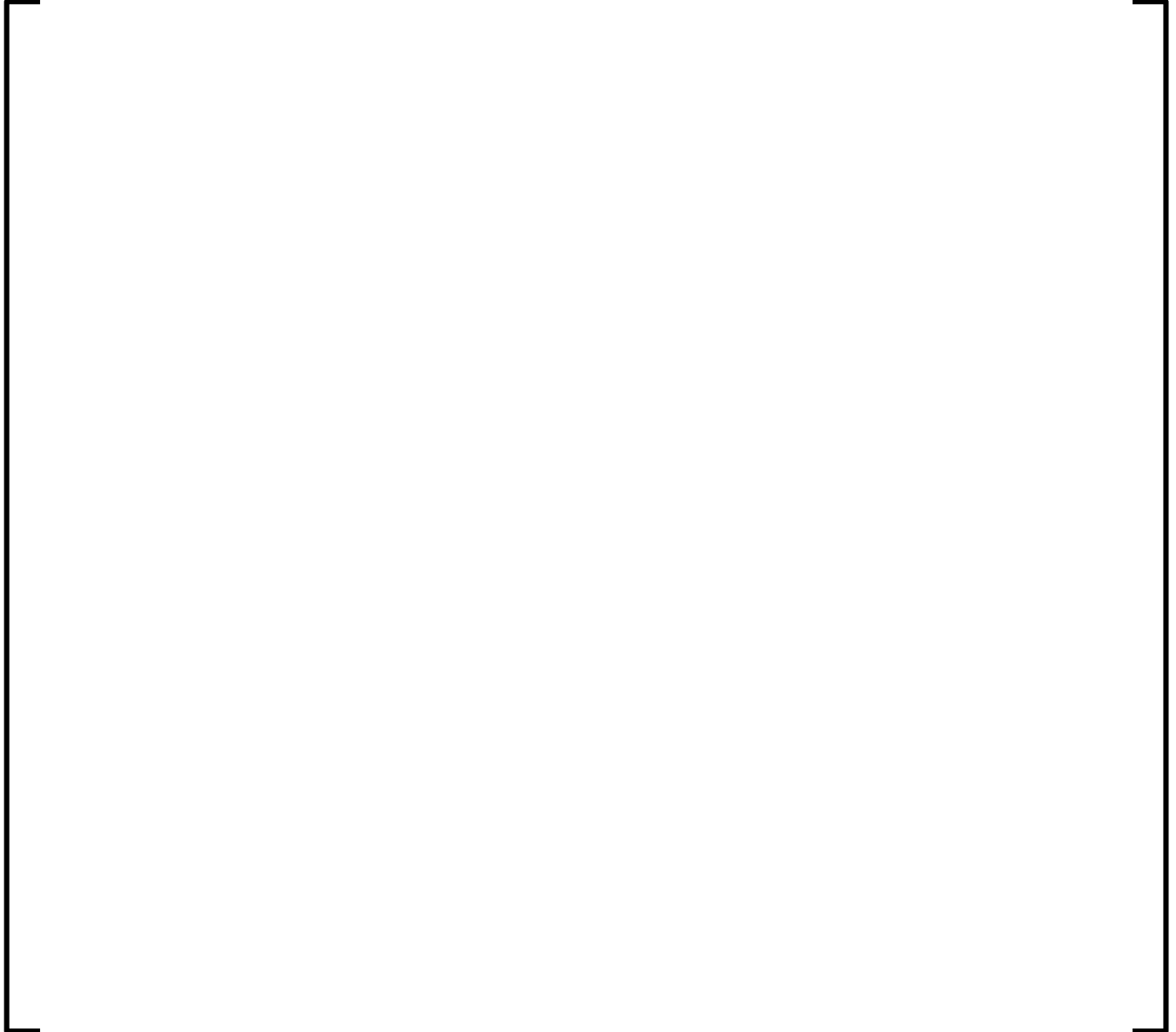


**Figure V1 5.3.10-27**  
**Plant V1 EOC 19 Core Average Axial Power Distribution**



**Figure V1 5.3.10-28**  
**Plant V1 BOC 20 Core Average Axial Power Distribution**



**Figure V1 5.3.10-29**  
**Plant V1 MOC 20 Core Average Axial Power Distribution**



**Figure V1 5.3.10-30**  
**Plant V1 EOC 20 Core Average Axial Power Distribution**



**Figure V1 5.3.10-31**  
**Plant V1 BOC 21 Core Average Axial Power Distribution**



**Figure V1 5.3.10-32**  
**Plant V1 MOC 21 Core Average Axial Power Distribution**





**Figure V1 5.3.10-33**  
**Plant V1 EOC 21 Core Average Axial Power Distribution**



**Figure V1 5.3.10-34**  
**Plant V1 BOC 22 Core Average Axial Power Distribution**

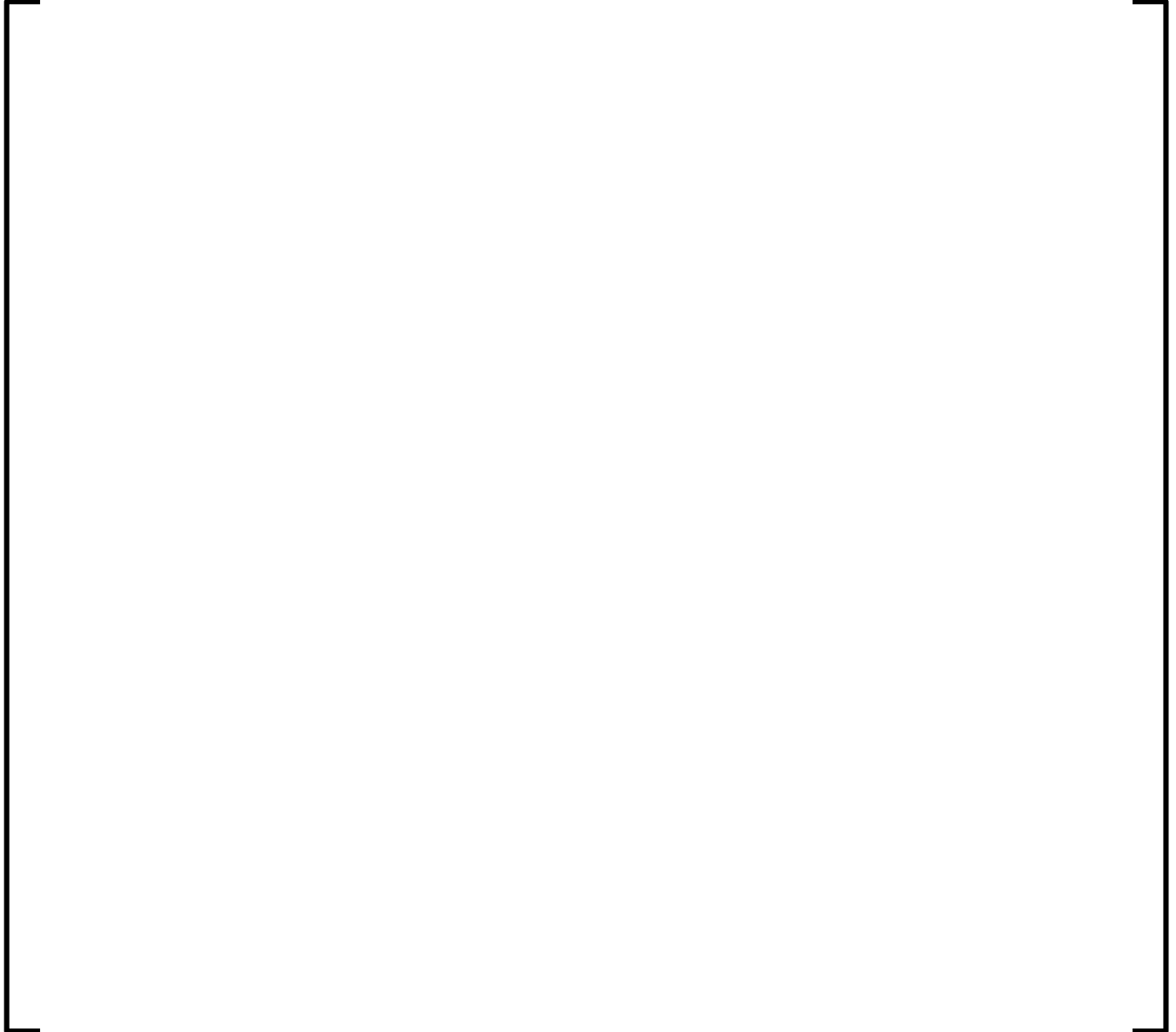


**Figure V1 5.3.10-35**  
**Plant V1 MOC 22 Core Average Axial Power Distribution**



**Figure V1 5.3.10-36**  
**Plant V1 EOC 22 Core Average Axial Power Distribution**

